Book of Abstracts

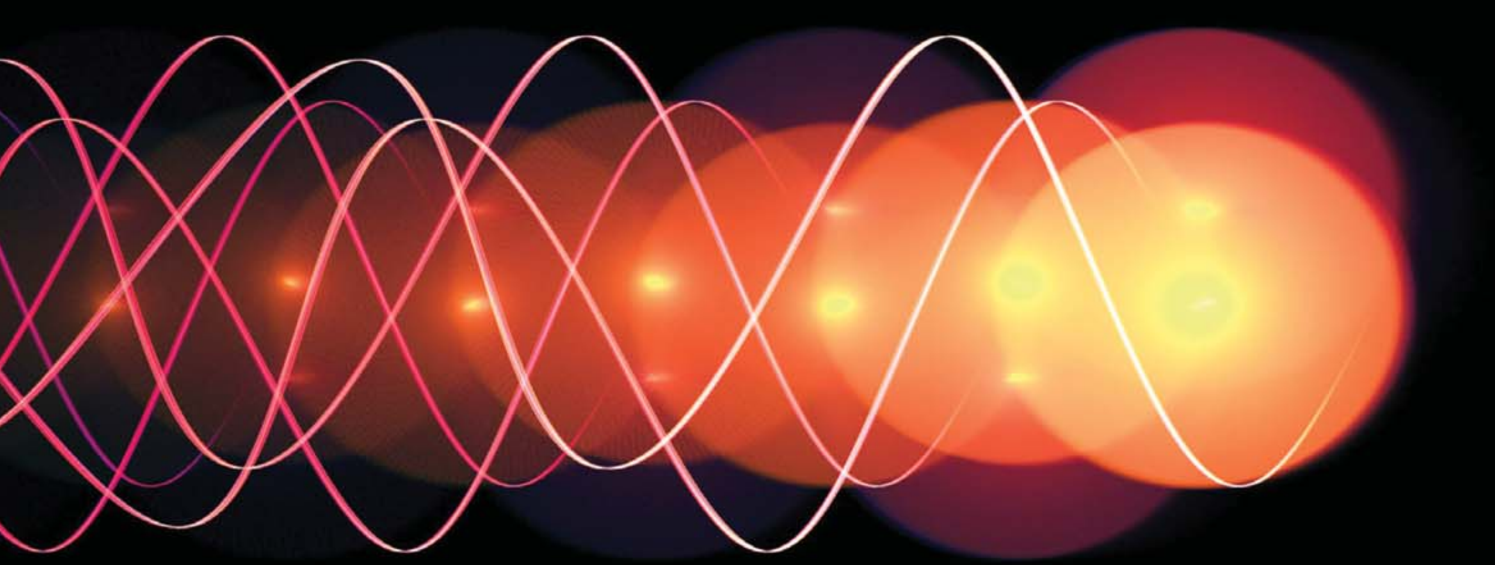

SPW 2019

# SINGLE PHOTON WORKSHOP

Politecnico di Milano
Milan, 21-25 October 2019

Event organized by

POLITECNICO
MILANO 1863

In cooperation with

Fondazione Politecnico di Milano

# Table of Contents

## Single Photon Workshop 2019

Single Photon Workshop 2019 is the ninth installment in a series of workshops on SINGLE-PHOTON TECHNOLOGIES AND APPLICATIONS. SPW 2019 is intended to bring together a broad range of people with interests in single-photon sources, single-photon detectors, photon entanglement, and their use in scientific and industrial applications. It is an exciting opportunity for those interested in these technologies to learn about the state of the art and to foster continuing partnerships with others seeking to advance the capabilities of such technologies.

The four main areas of the single-photon scientific research and industrial applications are covered by the workshop:

- **Single-Photon Detectors**
  Devices, circuits and systems to achieve single-photon sensitivity
- **Single-Photon Sources**
  Materials, schemes and architectures to generate and control light emission at single photon level
- **Applications**
  Single-photon technologies for scientific and industrial applications, from ground to space, from life science to quantum information processing
- **Metrology**
  Validation techniques and instrumentation to prove single-photon generation and acquisition.

## About Politecnico di Milano

Politecnico di Milano is a scientific-technological university which trains engineers, architects and industrial designers.

The University has always focused on the quality and innovation of its teaching and research, developing a fruitful relationship with business and productive world by means of experimental research and technological transfer.

Research has always been linked to didactics and it is a priority commitment which has allowed Politecnico Milano to achieve high quality results at an international level as to join the university to the business world. Research constitutes a parallel path to that formed by cooperation and alliances with the industrial system.

Knowing the world in which you are going to work is a vital requirement for training students. By referring back to the needs of the industrial world and public administration, research is facilitated in following new paths and dealing with the need for constant and rapid innovation. The alliance with the industrial world, in many cases favored by Fondazione Politecnico and by consortiums to which Politecnico belong, allows the university to follow the vocation of the territories in which it operates and to be a stimulus for their development.

The challenge which is being met today projects this tradition which is strongly rooted in the territory beyond the borders of the country, in a relationship which is developing first of all at the European level with the objective of contributing to the creation of a single professional training market. Politecnico takes part in several research, sites and training projects collaborating with the most qualified European universities. Politecnico's contribution is increasingly being extended to other countries: from North America to Southeast Asia to Eastern Europe. Today the drive to internationalization sees Politecnico Milano taking part into the European and world network of leading technical universities and it offers several courses beside many which are entirely taught in English.

## Scientific Committee

Félix Bussières (University of Geneva, Switzerland)
Jessica Cheung (NPL, UK)
Christopher Chunnilall (NPL, UK)
Ivo Pietro Degiovanni (INRIM, Italy)
Warren Grice (Qubitekk, USA)
Thomas Gerrits (NIST, USA)
Stefan Kueck (PTB, Germany)
John H. Lehman (NIST, USA)
Alan L. Migdall (NIST, USA)
Alberto Tosi (Politecnico di Milano, Italy)
Hugo Zbinden (University of Geneva, Switzerland)

## Program Committee

Giulia Acconcia (Politecnico di Milano, Italy)
Félix Bussières (University of Geneva, Switzerland)
Jessica Cheung (NPL, UK)
Christopher Chunnilall (NPL, UK)
Ivo Pietro Degiovanni (INRIM, Italy)
Warren Grice (Qubitekk, USA)
Thomas Gerrits (NIST, USA)
Massimo Ghioni (Politecnico di Milano, Italy)
Angelo Gulinatti (Politecnico di Milano, Italy)
Stefan Kueck (PTB, Germany)
John H. Lehman (NIST, USA)
Alan L. Migdall (NIST, USA)
Ivan Rech (Politecnico di Milano, Italy)
Alberto Tosi (Politecnico di Milano, Italy)
Federica Villa (Politecnico di Milano, Italy)
Franco Zappa (Politecnico di Milano, Italy)
Hugo Zbinden (University of Geneva, Switzerland)

## Local Committee

Alberto Tosi (Politecnico di Milano, Italy) - Workshop general chair
Angelo Gulinatti (Politecnico di Milano, Italy)
Ivan Rech (Politecnico di Milano, Italy)
Federica Villa (Politecnico di Milano, Italy)
Franco Zappa (Politecnico di Milano, Italy)
Massimo Ghioni (Politecnico di Milano, Italy)

## Platinum Sponsors

## Gold Sponsors

## Silver Sponsors

# Venue

## Workshop venue

Aula Magna Carassa e Dadda
Politecnico di Milano, Campus Bovisa,
Building BL28,
Via Lambruschini 4, 20156 Milano (MI), Italy

## Welcome cocktail

*Monday 21st October 2019*

Rectorate building at "Leonardo Campus" of Politecnico di Milano.
Piazza Leonardo da Vinci 32, 20133 Milano. Building 1.

How to reach Leonardo Campus
Take Line 2 of the underground railway: MM2 green line.
Get off the train at the PIOLA station.
Take the left-hand exit from Piola station; walk along Via D'Ovidio, keeping to the left and cross Via Bonardi: you will arrive in Piazza Leonardo da Vinci. Politecnico di Milano is facing you.

## Conference dinner

*Wednesday 23rd October 2019*

Castello Sforzesco, Milano.
Castello Sforzesco, Piazza Castello, Milano.

How to reach Castello Sforzesco
From SPW 2019 workshop venue
Walk to "Milano Nord Bovisa" train station and take a train to "Cadorna" station (travel time is 6 minutes).
You need the Biglietto ordinario" of ATM (2 euro).
When exiting the Cadorna station, turn left and walk along Via Marco Minghetti to get to the castle.

## Guided tours

Before the conference dinner, guided tours of Castello Sforzesco will be organized (free of charge), including Leonardo's Special.
The year 2019 marks the 500th anniversary of Leonardo da Vinci's death. Milano is the city where Leonardo da Vinci stayed the longest. Here Leonardo arrived in 1482, at the service of Duke Ludovico Sforza, and his presence has left an indelible mark in the history and artistic production of the City and in the entire region of Lombardy.
For this reason, Milano and Lombardy will dedicate a whole year to the Maestro.

More info on SPW website (https://spw2019.polimi.it).

## Wireless access

- Guest users members of an Eduroam federated entity can access the "eduroam" Wi-Fi network using the credentials provided by their institution of affiliation. The connection will be permanent and encrypted.

- Other guest users will be provided with other Wi-Fi credentials on site.

## Important contacts

| | |
|---|---|
| Emergency telephone number: | 112 |
| POLIMI emergency call center: | +39 02 2399 9399 (only 9399 from internal phones) |

| | |
|---|---|
| e-mails: | spw2019@polimi.it (generic needs) |
| | spw2019-reg@fondazione.polimi.it (registration) |

## About Milano

With a population of about 1.3 million, Milan, the capital of Lombardy, is located in the Po Valley, not far from the Alps with the great lakes (Lake Como, Lake Maggiore, Lake Lugano) to the North. Milan is considered the Italian economic and finance center, with the headquarters of the Stock Exchange and of many of the most important industrial and financial businesses of the Country. The city hosted the Universal Exposition in 2015 under the theme "Feeding the planet, energy for life".

It is also the Italian symbol of fashion and design: it hosts many of the main Italian fashion maisons and international design fairs, such as "Settimana della Moda" (Milan Fashion Week) and the "Salone Internazionale del Mobile" (Milan Furniture Fair); also, a Design School operates at Politecnico di Milano.
Milan hosts the "Teatro alla Scala", considered the temple of lyrics all over the world, and several prose theatres such as the "Piccolo Teatro" founded by Giorgio Strehler.
In Milan are located the headquarters of the main daily newspapers (Il Corriere della Sera, Il Sole 24 Ore) and many of the main Italian publishers (Mondadori, Feltrinelli, Garzanti, Rizzoli).
The city offers to visitors the possibility to admire a wide range of monuments, museums and buildings reflecting the vestiges of history and culture left by many people who lived here. The ancient Roman remains are preserved at the Colonne di San Lorenzo, whereas the Romanesque can be admired at Sant'Ambrogio, Sant'Eustorgio or San Simpliciano Basilicas. The Duomo is one of the largest cathedrals in the world and the most important example of Gothic architecture in Italy. The Castello Sforzesco, built on the wishes of the Duke Francesco Sforza, nowadays hosts the Michelangelo's "Pietà Rondanini" and several museums. The church of Santa Maria delle Grazie hosts the famous masterpiece "The Last Supper" by Leonardo da Vinci – declared part of the World Heritage by UNESCO.
The city has always participated actively to the National History since its origins, contributing to the purposes and the aims that led to reunification of Italy in the 18th century. Some distinguished people, who gave a significant contribution to Italian culture, lived in Milan, such as Leonardo da Vinci (who lived in Milan from 1482 to 1500), the poet and novelist Alessandro Manzoni, the musician Arturo Toscanini, the writer Carlo Emilio Gadda, the film director Luchino Visconti. Two Nobel prizes operated in Milan: Giulio Natta (1963, in chemistry) and Dario Fo (1997, in literature).

The year 2019 marks the 500th anniversary of Leonardo da Vinci's death: Milano is the city where Leonardo da Vinci stayed the longest. Here Leonardo arrived in 1482, at the service of Duke Ludovico Sforza, and his presence has left an indelible mark in the history and artistic production of the City and in the entire region of Lombardy. For this reason, Milano and Lombardy will dedicate a whole year to the Maestro: visit the Social Program page for additional information on dedicated events.

More info on SPW website (https://spw2019.polimi.it).

# Local transportation

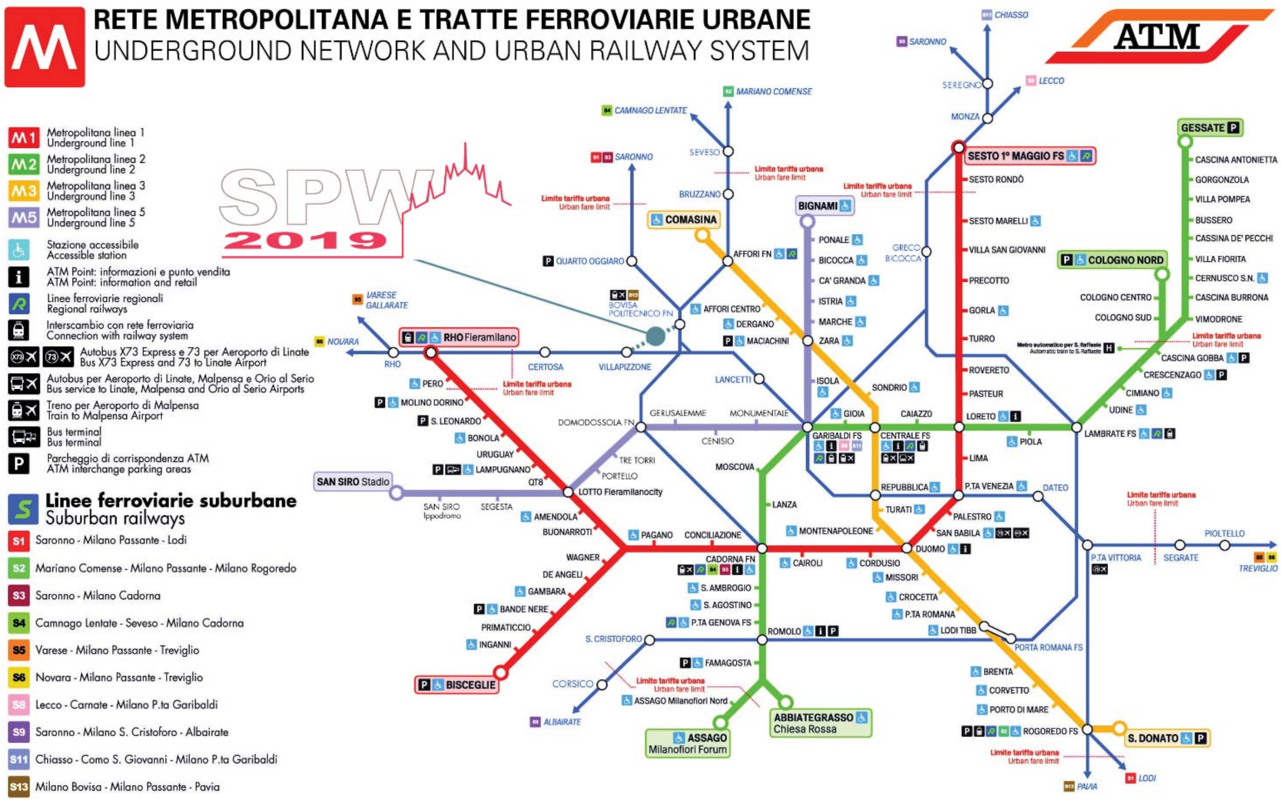


**Ordinary Ticket** (or **Biglietto Ordinario**) – Price: € 2.00
Valid for 90 minutes after stamping, gives you unrestricted travels for all the Milan Municipality area, including the area where SPW 2019 is located.
The ticket is valid for a single journey on the underground or rail network, including the urban rail lines of Trenord and the 'Passante Ferroviario' (Urban Railway Network).

**One Day Ticket** – Price: € 7.00
Valid for 24 hours after stamping, gives you unrestricted travels for all the Milan Municipality area.

**3 Days Ticket** – Price: € 12.00
Valid for 3 consecutive days from the day of the first validation until the end of the service on the third day, without limit to the number of journeys within the Milan Municipality area.

**Carnet 10 tickets** – Price: € 18.00
A block of 10 ordinary tickets. The trips cannot be used on road services managed by operators other than ATM and Trenord; it cannot be used by more than one person at the same time.

**Weekly pass** – Price: € 17.00
Valid from Monday to Sunday of the same week until the end of the service of Sunday, without limit to the number of journeys within the territory defined by the zones purchased.

You can also travel on the metro by paying at the ticket gate with your **contactless card** (Mastercard, Visa, Maestro and VPay).
Or you can download the **ATM Milano official** app and purchase tickets there.

## Program Overview

| Monday, October 21, 2019 | |
|---|---|
| 08:00 | Registration opening |
| 09:00 | Welcome |
| 09:10 | Session 1 - Sources I |
| 10:40 | Coffee break |
| 11:10 | Session 2 - Applications I |
| 13:00 | Platinum sponsor presentation |
| 13:05 | Lunch |
| 14:20 | Session 3 - Detectors I |
| 15:50 | Coffee break |
| 16:20 | Session 4 - Metrology I |
| 18:30 | Welcome reception@Leonardo |

| Tuesday, October 22, 2019 | |
|---|---|
| 09:00 | Historical perspective by S. Cova |
| 09:15 | Session 5 - Detectors II |
| 10:45 | Coffee break |
| 11:15 | Session 6 - Metrology II |
| 12:35 | Platinum sponsor presentation |
| 12:40 | Lunch |
| 13:55 | Session 7 - Applications II |
| 15:45 | Platinum sponsor presentation |
| 15:50 | Coffee break |
| 16:20 | Session 8 - Applications III |
| 18:10 | Poster session I |

| Wednesday, October 23, 2019 | |
|---|---|
| 09:00 | Session 9 - Applications IV |
| 10:50 | Coffee break |
| 11:20 | Session 10 - Metrology III |
| 12:50 | Platinum sponsor presentation |
| 12:55 | Lunch |
| 14:10 | Session 11 - Detectors III |
| 16:00 | Coffee break |
| 16:30 | Session 12 - Sources II |
| 18:30 | Guided tours of Castello Sforzesco |
| 20:00 | Dinner at Castello Sforzesco |

| Thursday, October 24, 2019 | |
|---|---|
| 09:00 | Session 13 - Sources III |
| 10:50 | Coffee break |
| 11:20 | Session 14 - Applications V |
| 12:50 | Platinum sponsor presentation |
| 12:55 | Lunch |
| 14:10 | Session 15 - Detectors IV |
| 16:00 | Coffee break |
| 16:30 | Session 16 - Applications VI |
| 18:20 | Poster session II |

| Friday, October 25, 2019 | |
|---|---|
| 09:00 | Session 17 - Detectors V |
| 10:50 | Coffee break |
| 11:20 | Session 18 - Sources IV |
| 13:10 | Lunch |
| 14:15 | Session 19 - Applications VII |
| 16:05 | Concluding remarks |
| 16:15 | Farewell coffee |

Lunches, coffee breaks, welcome reception, dinner and guided tour at Castello Sforzesco are included in the registration fee.

# Monday, October 21, 2019

| | | |
|---|---|---|
| 08:00 | Registration opening | |
| 09:00 | Welcome | |
| 09:10 | Session 1<br>Sources I<br><br>Chair: A. Migdall | **S. Reitzenstein - Deterministically fabricated quantum dot – waveguide systems for on-chip quantum optics** |
| 09:40 | | F. Graffitti - Direct generation of tailored ultrafast entanglement |
| 10:00 | | S. Haffouz - InAsP quantum dot nanowires for telecom single photon emission |
| 10:20 | | T. Mueller - Quantum teleportation using highly coherent emission from telecom C-band quantum dots |
| 10:40 | Coffee break | |
| 11:10 | Session 2<br>Applications I<br><br>Chair: M. Lucamarini | **E. Diamanti - Demonstrating quantum advantage with practical photonic systems** |
| 11:40 | | F. Xu - Experimental Quantum Switching for Exponentially Superior Quantum Communication Complexity |
| 12:00 | | D. Cozzolino - Hybrid entanglement distribution through an air-core fiber |
| 12:20 | | C. Vigliar - High-Dimensional Chip-to-Chip Entanglement Distribution through Multicore Fibres |
| 12:40 | | J. Chiles - Nanowire Detection of Photons from the Dark Side |
| 13:00 | Platinum sponsor presentation: ID Quantique | |
| 13:05 | Lunch | |
| 14:20 | Session 3<br>Detectors I<br><br>Chair: A. Gulinatti | **E. Charbon - Massively parallel, three-dimensional photon counting: a versatile tool for quantum experimentalists and consumers** |
| 14:50 | | E. Conca - Wide-area fast-gated single-photon detector with integrated TDC for near-infrared spectroscopy applications |
| 15:10 | | F. Acerbi - Silicon photomultipliers optimized for cryogenic temperatures |
| 15:30 | | S. Grosse - Single-Photon Detectors based on CSPAD technology |
| 15:50 | Coffee break (sponsored by Excelitas) | |
| 16:20 | Session 4<br>Metrology I<br><br>Chair: E. Diamanti | F. Piacentini - New Frontiers in Quantum Measurement: Protective Measurement, Genetic Quantum Measurement and Robust Weak Measurement |
| 16:40 | | L. Shalm - Certified Randomness Expansion using a Loophole-Free Bell Test |
| 17:00 | | C. Chunnilall - Investigations towards transmitting time and QKD signals over the same optical fibre |
| 17:20 | | M. Lasota - Reliable estimation of the statistics of photons emitted from an unknown source of light |
| 17:40 | Transfer to Leonardo campus | |
| 18:30 | Welcome reception @ Leonardo campus | |
| 20:30 | End | |

## Tuesday, October 22, 2019

| | | |
|---|---|---|
| 09:00 | Historical perspective by Sergio Cova | |
| 09:15 | Session 5 Detectors II<br>Chair: H. Zbinden | **B. Korzh - Advances in superconducting nanowire single photon detectors and related applications** |
| 09:45 | | V. Verma - Kilopixel arrays of superconducting nanowire single-photon detectors |
| 10:05 | | D.H. Smith - Multiplexed Superconducting Nanowire Single-Photon Detectors on UV-Written Silica Waveguides |
| 10:25 | | F. Martini - SNSPD readout using the amplitude multiplexing approach |
| 10:45 | Coffee break (offered by PicoQuant) | |
| 11:15 | Session 6 Metrology II<br>Chair: C. Chunnilall | S. Polyakov - First quantum-measurement-inspired, scalable communication protocol and its experimental demonstration |
| 11:35 | | S. Schwarz - Reconstructing ultrafast energy-time entangled two-photon pulses |
| 11:55 | | D. Fuster - Development of a plug&play single photon source using electro-optical pumping schemes |
| 12:15 | | H. Ollivier - Quantum dot based single photon sources: performance reproducibility |
| 12:35 | Platinum sponsor presentation: attocube / Quandela | |
| 12:40 | Lunch | |
| 13:55 | Session 7 Applications II<br>Chair: J. Matthews | **M. Lucamarini - Measurement Device Independent Quantum Cryptography** |
| 14:25 | | M. Minder - Experimental quantum key distribution beyond the repeaterless secret key capacity |
| 14:45 | | M. Avesani - Practical Source-Device-Independent Quantum random number generators |
| 15:05 | | S. Wengerowsky - In-field entanglement distribution over a 96 km and a 192 km submarine optical fibre |
| 15:25 | | S. Wengerowsky - An entanglement-based wavelength-multiplexed Quantum Communication Network |
| 15:45 | Platinum sponsor presentation: MPD /OEC | |
| 15:50 | Coffee break | |
| 16:20 | Session 8 Applications III<br>Chair: M. Ghioni | **K. Suhling - Time-correlated single photon counting wide-field Fluorescence Lifetime Imaging Microscopy** |
| 16:50 | | D. Tabakaev - Entangled two-photon absorption and the quantum advantage in sensing |
| 17:10 | | A. Ingle - Towards General-Purpose Passive Imaging with Single-Photon Sensors |
| 17:30 | | D. Lindell - Efficient Confocal Non-Line-of-Sight Imaging |
| 17:50 | | A. White - Realtime photon-number resolution & Imaging via photon counting |
| 18:10 | Poster session I | |
| 19:30 | End | |

# Wednesday, October 23, 2019

| | | |
|---|---|---|
| 09:00 | Session 9<br>Applications IV<br><br>Chair: F. Bussieres | **J. Matthews - Integrated Homodyne Detection for Large Scale Silicon Quantum Photonics** |
| 09:30 | | F. Ceccarelli - Low-power reconfigurable photonic integrated circuits fabricated by femtosecond laser micromachining |
| 09:50 | | P. Connolly - Multispectral single-photon imaging using high efficiency plasmonic metasurface filters |
| 10:10 | | S. Olivier - Towards an integrated quantum photonics platform on silicon for secured communications |
| 10:30 | | J. Renema - Imperfect Gaussian Boson Sampling is Classically Simulable |
| 10:50 | Coffee break (offered by ID Quantique) | |
| 11:20 | Session 10<br>Metrology III<br><br>Chair: S. Kueck | **I. Degiovanni - Light sources characterisation and optical modes reconstruction** |
| 11:50 | | Y.-L. Mao - Error-Disturbance Trade-off in Sequential Quantum Measurements |
| 12:10 | | A. Paterova - Infrared metrology with visible light |
| 12:30 | | K. Laiho - Characterizing heralded single photons from a Bragg-reflection waveguide loss-tolerantly via moment generating function |
| 12:50 | Platinum sponsor presentation: PicoQuant | |
| 12:55 | Lunch | |
| 14:10 | Session 11<br>Detectors III<br><br>Chair: A. Tosi | **B. Aull - Large-Format Image Sensors Based on Integration of Custom Geiger-Mode Avalanche Photodiode Arrays with All-Digital CMOS Circuits** |
| 14:40 | | C.-Y. Park - Room temperature operation of InP/InGaAs single photon avalanche diode |
| 15:00 | | G. Buller - Planar Geometry Ge-on-Si Single-Photon Avalanche Diode Detectors for the Short-Wave Infrared |
| 15:20 | | G. Acconcia - Fully integrated electronics for high-performance and high-speed acquisition with Single Photon Avalanche Diodes |
| 15:40 | | M. Salomoni - Future perspective of SiPM technology |
| 16:00 | Coffee break | |
| 16:30 | Session 12<br>Sources II<br><br>Chair: C. Toninelli | C.A. Solanas - Scalable interfacing of quantum photonic platforms: solid-state single-photon sources and reconfigurable photonic circuits |
| 16:50 | | T. Heindel - Single-Photon QKD using Engineered Solid-State Quantum-Light Sources |
| 17:10 | | S.D. Tchernij - Electrical control of Nitrogen – Vacancy centers in diamond |
| 17:30 | | S. Ecker - Overcoming noise in entanglement distribution through high-dimensional encoding |
| 17:50 | Transfer to Castello Sforzesco | |
| 18:30 | Guided tours of Castello Sforzesco | |
| 20:00 | Dinner at Castello Sforzesco | |
| 23:00 | End | |

## Thursday, October 24, 2019

| | | |
|---|---|---|
| 09:00 | Session 13<br>Sources III<br><br>Chair: T. Gerrits | **C. Toninelli - Single-molecule based single photon sources** |
| 09:30 | | R. Schofield - Nanophotonic waveguide coupling to organic molecules in micro-capillaries |
| 09:50 | | H. Abudayyeh - Quantum light manipulation: A path towards efficient pure room-temperature single photon sources |
| 10:10 | | H. Wang - Single photons for quantum technologies |
| 10:30 | | G. Solomon - Filter-free single-photon emission in an integrated cavity-waveguide device |
| 10:50 | Coffee break (offered by attocube / Quandela) | |
| 11:20 | Session 14<br>Applications V<br><br>Chair: S. W. Nam | **K. Srinivasan - Quantum source and frequency conversion technologies based on integrated nanophotonics** |
| 11:50 | | J. Adcock - Programmable mutliphoton graph states on a silicon chip |
| 12:10 | | G. Kavuri - Towards a loophole-free Bell experiment on a tabletop |
| 12:30 | | Z.-H. Xiang - Network Integration of Quantum Dot Device and Entanglement in Cambridge Fiber Network |
| 12:50 | Platinum sponsor presentation: Excelitas | |
| 12:55 | Lunch | |
| 14:10 | Session 15<br>Detectors IV<br><br>Chair: I. Rech | **S. W. Nam - From dark matter detection to artificial intelligence: applications of superconducting nanowire single photon detectors** |
| 14:40 | | M. Perrenoud - High detection rate and high efficiency with parallel SNSPDs |
| 15:00 | | S. Buckley - Progress in superconducting optoelectronic networks for neuromorphic computing |
| 15:20 | | T. Takumi - Time-resolved measurement of a single-photon wave packet with an optical Kerr effect |
| 15:40 | | E. Fossum - Quanta Image Sensor Progress Review |
| 16:00 | Coffee break | |
| 16:30 | Session 16<br>Applications VI<br><br>Chair: F. Zappa | **S. Verghese - Self-driving cars and lidar** |
| 17:00 | | G. Musarra - Single-photon, single-pixel intelligent Lidar |
| 17:20 | | A. Maccarone - Three dimensional imaging of dynamic underwater scenes using single photon detection |
| 17:40 | | R. Tobin - Depth imaging through obscurants using single photon detection in the short-wave infrared |
| 18:00 | | M. Laurenzis - Computational imaging with SPADs at SWIR wavelengths |
| 18:20 | Poster session II | |
| 19:40 | End | |

# Friday, October 25, 2019

| | | |
|---|---|---|
| 09:00 | Session 17<br>Detectors V<br><br>Chair: F. Villa | **J. Rothman - Reaching for GHz single photon detection rates with HgCdTe APD detectors** |
| 09:30 | | L. Gasparini - CMOS-SPAD arrays for Quantum Imaging Applications |
| 09:50 | | M. Zarghami - A Novel Approach to High Dynamic Range Imaging with CMOS-SPADs |
| 10:10 | | G. Jegannathan - Current-assisted single photon avalanche diode(CASPAD) in 350 nm CMOS |
| 10:30 | | G. Tortarolo - Towards Single-Photon Microscopy: Exploiting Extra Spatio-Temporal Information Provided by SPAD Array Detectors in Laser Scanning Microscopy |
| 10:50 | Coffee break (offered by MPD /OEC) | |
| 11:20 | Session 18<br>Sources IV<br><br>Chair: F. Piacentini | **P. Michler - Quantum dots at telecom wavelengths for single- and entangled photon sources** |
| 11:50 | | S. Francesconi - Engineering two-photon wavefunction and exchange statistics in a semiconductor chip |
| 12:10 | | C. P. Lualdi - High-Efficiency Time-Multiplexed Single-Photon Source |
| 12:30 | | C. Marvinney - Toward control of the quantum state of hBN single-photon emitters |
| 12:50 | | J. Grim - Three-Quantum-Dot Superradiance in a Photonic Crystal Waveguide Enabled by Scalable Strain Tuning |
| 13:10 | Lunch | |
| 14:15 | Session 19<br>Applications VII<br><br>Chair: I. Degiovanni | **Q. Zhang - Single photon technology in Long Distance Quantum Communication** |
| 14:45 | | F. Xu - Experimental quantum repeater without quantum memory |
| 15:05 | | A. Scriminich - Hong-Ou-Mandel interference of polarization qubits stored in independent room-temperature quantum memories |
| 15:25 | | S. Grandi - Towards long distance entanglement between a photon and a solid-state quantum memory |
| 15:45 | | M. F. Askarani - Entanglement and non-locality between disparate solid-state quantum memories mediated by photons |
| 16:05 | Concluding remarks | |
| 16:15 | Farewell coffee | |
| 16:45 | End | |

# Abstracts of oral presentations

# Monday, October 21, 2019

| | | |
|---|---|---|
| 08:00 | Registration opening | |
| 09:00 | Welcome | |
| 09:10 | Session 1<br>Sources I<br><br>Chair: A. Migdall | **S. Reitzenstein - Deterministically fabricated quantum dot – waveguide systems for on-chip quantum optics** |
| 09:40 | | F. Graffitti - Direct generation of tailored ultrafast entanglement |
| 10:00 | | S. Haffouz - InAsP quantum dot nanowires for telecom single photon emission |
| 10:20 | | T. Mueller - Quantum teleportation using highly coherent emission from telecom C-band quantum dots |
| 10:40 | Coffee break | |
| 11:10 | Session 2<br>Applications I<br><br>Chair: M. Lucamarini | **E. Diamanti - Demonstrating quantum advantage with practical photonic systems** |
| 11:40 | | F. Xu - Experimental Quantum Switching for Exponentially Superior Quantum Communication Complexity |
| 12:00 | | D. Cozzolino - Hybrid entanglement distribution through an air-core fiber |
| 12:20 | | C. Vigliar - High-Dimensional Chip-to-Chip Entanglement Distribution through Multicore Fibres |
| 12:40 | | J. Chiles - Nanowire Detection of Photons from the Dark Side |
| 13:00 | Platinum sponsor presentation: ID Quantique | |
| 13:05 | Lunch | |
| 14:20 | Session 3<br>Detectors I<br><br>Chair: A. Gulinatti | **E. Charbon - Massively parallel, three-dimensional photon counting: a versatile tool for quantum experimentalists and consumers** |
| 14:50 | | E. Conca - Wide-area fast-gated single-photon detector with integrated TDC for near-infrared spectroscopy applications |
| 15:10 | | F. Acerbi - Silicon photomultipliers optimized for cryogenic temperatures |
| 15:30 | | S. Grosse - Single-Photon Detectors based on CSPAD technology |
| 15:50 | Coffee break (offered by Excelitas) | |
| 16:20 | Session 4<br>Metrology I<br><br>Chair: E. Diamanti | F. Piacentini - New Frontiers in Quantum Measurement: Protective Measurement, Genetic Quantum Measurement and Robust Weak Measurement |
| 16:40 | | L. Shalm - Certified Randomness Expansion using a Loophole-Free Bell Test |
| 17:00 | | C. Chunnilall - Investigations towards transmitting time and QKD signals over the same optical fibre |
| 17:20 | | M. Lasota - Reliable estimation of the statistics of photons emitted from an unknown source of light |
| 17:40 | Transfer to Leonardo campus | |
| 18:30 | Welcome reception @ Leonardo campus | |
| 20:30 | End | |

# Deterministically fabricated quantum dot – waveguide systems for on-chip quantum optics

**P. Schnauber[1], J. Schall[1], S. Bounouar[1], T. Höhne[2], A. Singh[3], K. Sirinvasan[3], M. Davanco[3], J.-D. Song[4], S. Burger[2], S. Rodt[1], S. Reitzenstein[1]**

[1] *Institute of Solid-State Physics, Technische Universität Berlin, Berlin, Germany*

[2] *Zuse Institut Berlin, Berlin, Germany*

[3] *National Institute of Standards and Technology, Gaithersburg, MD, USA*

[4] *Center for Opto-Electronic Convergence Systems, KIST, Seoul, South Korea*

The deterministic integration of quantum emitters into on-chip photonic elements is crucial for the implementation of scalable on-chip quantum circuits. Recent activities in this field include hybrid QD-waveguides for enhanced photon in-coupling [1] and the controlled integration of QDs using multistep-lithography as well as AFM tip transfer [2][3]. Here, we report on the deterministic integration of single quantum dots (QD) into on-chip beam splitters using in-situ electron beam lithography (EBL) [4]. In this advanced single-step technique, photonic building blocks are patterned on top of chosen QDs immediately after spatial and spectral pre-characterization via cathodoluminescence mapping at 10 K. To realize 50/50 coupling elements, we chose tapered multimode interference (MMI) splitters which feature relaxed fabrication tolerances and robust 50/50 splitting ratio. We demonstrate the functionality of the deterministic QD-waveguide structures by µPL spectroscopy and by studying the photon cross-correlation between the two MMI output ports. The latter confirms single-photon emission and on-chip splitting associated with $g^{(2)}(0) \ll 0.5$ [5]. Moreover, the deterministic integration of QDs enables the demonstration and controlled study of chiral light-matter effects and directional emission in QD-WGs [6], as well as the realization of low loss heterogenous QD-WG systems with excellent quantum optical properties in terms of high photon purity and high photon indistinguishability [7].

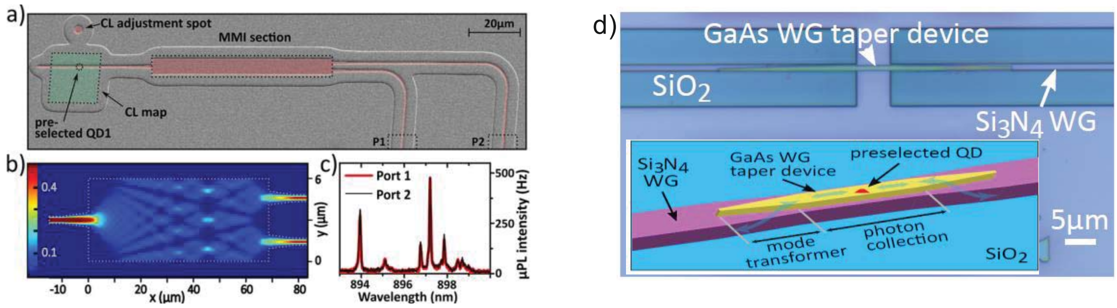


Fig. 1 (a) False-color SEM image of a QD integrated into a 1 × 2 MMI coupler via in-situ EBL. (b) Simulated electric field intensity distribution of the MMI and taper device. (c) µPL spectra of QD1 taken from port 1 and port 2 of the device shown in part a. A 50/50 splitting over the whole spectrum is observed. (d) Optical image of a fully fabricated heterogeneous QD waveguide device. Inset: Schematic of the heterogeneous GaAs-Si3N4 device design.

**References**

[1] A. Davanco et al., Nature Communications 8, 889 (2017)
[2] R. J. Coles et al., Nature Communications 7, 11183 (2016)
[3] Kim J.-H. et al., Nano Letters 17, 7394 (2017)
[4] M. Gschrey et al., Nature Communications 6, 7662 (2015)
[5] P. Schnauber et al., Nano Letters 18, 2336-2342 (2018)
[6] P. Mrowiński et al. ACS Photonics, doi.org/10.1021/acsphotonics.9b00369, (2019); arxiv:1902.01905
[7] P. Schnauber et al., Nano Letters, in press (2019); arXiv:1905.12030

# Direct generation of tailored ultrafast entanglement

Francesco Graffitti,[1] Peter Barrow,[1] Alexander Pickston,[1] Massimiliano Proietti,[1] Dmytro Kundys,[1] Agata M. Brańczyk,[2] and Alessandro Fedrizzi[1]

[1] *Institute of Photonics and Quantum Sciences, School of Engineering and Physical Sciences, Heriot-Watt University, Edinburgh EH14 4AS, UK*

[2] *Perimeter Institute for Theoretical Physics, Waterloo, Ontario, Canada, N2L 2Y5*

Photonic quantum technologies rely on the generation of high-quality single-photons. A key open challenge is to encode as much information as possible into a single photon to enhance the efficiency of quantum protocols. For this reason, the last few years have seen increasing interest in going beyond polarisation encoding exploiting different degrees of freedom (DoF) of light, such as orbital angular momentum, time and frequency.

Here we present a new scheme for generating spectral-mode entanglement in PDC photon pairs, based on sub-coherence length domain engineering of nonlinear reshape its phase-matching function (PMF) to generate PDC photons spectrally-entangled in an arbitrarily high-dimensional Hilbert space, complementing the temporal-mode framework developed in [3]. We experimentally benchmark our technique in group-velocity-matched KTP crystals at telecom wavelengths. The crystal's PMF is designed to generate maximally entangled singlet states in the pulsed spectral-mode space: $|\psi^-\rangle = \frac{1}{\sqrt{2}}\left(|\frown\rangle\,|\backsim\rangle - |\backsim\rangle\,|\frown\rangle\right)$. This can be verified with two-photon interference and joint-spectrum (JSI) reconstruction via dispersive fibre time-of-flight spectroscopy. We measure a nearly-unity visibility of the antibunching interference that, combined with the characteristic shape of the interference pattern and the joint-spectrum, represents an unequivocal signature of the biphoton wavefunction's antisymmetry (see fig. 1). We finally demonstrate the scalability of our technique to multiphoton scenarios by implementing a pulsed spectral-mode entanglement swapping scheme between two photon-pairs produced in two different crystals.

Our technique can be easily implemented as it consists in a standard single-pass PDC setup, achieves high biphoton rates (> 4KHz detected-pairs/mW, 60% symmetric heralding), is compatible with other DoF encodings and can be adapted with small overhead to waveguide sources for integrated quantum photonics applications.

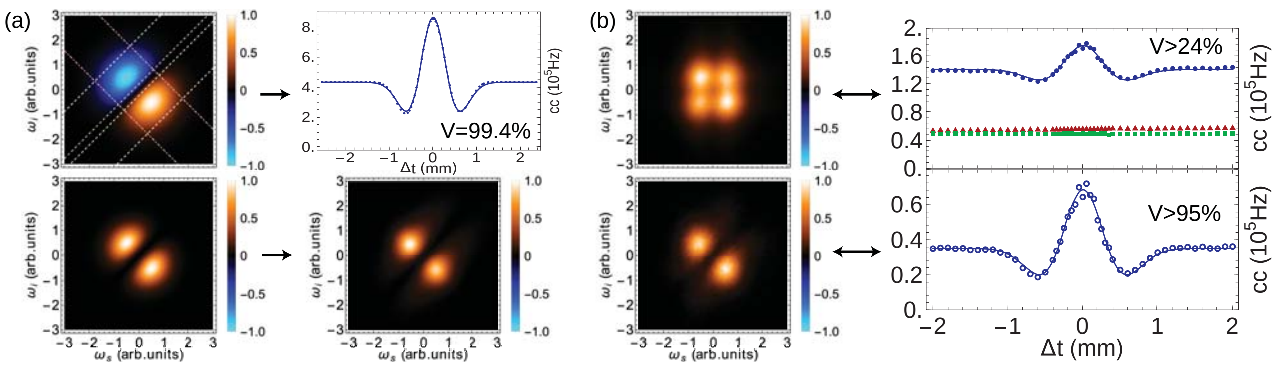


FIG. 1. **(a)** Theoretical joint spetral amplitude and JSI (left) with corresponding experimental interference pattern and JSI (right). **(b)** Experimental JSIs and corresponding interference patterns non-postselected (top) and postselected (bottom) on fourfold coincidences: we measure a protocol success rate higher than 95%

[1] F. Graffitti, D. Kundys, D. T. Reid, A. M. Brańczyk, and A. Fedrizzi, Quantum Science and Technology **2**, 035001 (2017).
[2] F. Graffitti, P. Barrow, M. Proietti, D. Kundys, and A. Fedrizzi, Optica **5**, 514 (2018).
[3] B. Brecht, D. V. Reddy, C. Silberhorn, and M. Raymer, Physical Review X **5**, 041017 (2015).

# InAsP quantum dot nanowires for telecom single photon emission

**S. Haffouz[1], P. J. Poole[1], K. D. Zeuner[2], D. Dalacu[1], J. Jin[1], L. Giner[1], X. Wu[1], K. Mnaymneh[1], J. Lapointe[1], V. Zwiller[2], and R. L. Williams[1].**

[1]*National Research Council of Canada, Ottawa, Canada*
[2]*KTH Royal Institute of Technology, Stockholm, Sweden*

Quantum dots embedded in III-V semiconductor nanowires have shown great promise for fabrication of efficient single photon sources that can be used for quantum information applications[1]. The bottom-up approach allows the precise growth of a single quantum dot along the axis of a photonic waveguide resulting in high photon collection efficiency. The spontaneous emission rate of the quantum dot is controlled by the photonic waveguide diameter through modification of the available optical density of states, i.e., by dictating the overlap of the waveguide mode with the dipole field of the emitter. The demonstration of efficient non-classical emitters that can produce single photons in the telecom band, capable of traveling long distances over optical fibers, is of great interest for long-haul quantum communications.

In this contribution, we report on the site-selected growth of single InAsP quantum dots embedded within InP photonic nanowires using a selective-area vapor-liquid-solid epitaxial growth process[2]. We first review our recent results[3] on the growth of bright single quantum dot nanowires with the unprecedented tuning range from 880 nm to 1550 nm by modifying the quantum dot growth conditions (arsine flux, dot thickness). As an example, a high purity single photon source at 1310 nm with low multiphoton emission probability is demonstrated. We then establish an alternative approach to achieve light emission in the telecom band where we grow the single $InAs_xP_{1-x}$ quantum dot in an $InAs_yP_{1-y}$ quantum rod, all embedded in the InP nanowire waveguide. Using this approach the emission wavelength can be shifted from 950 nm without the InAsP rod to 1310 nm with the rod without changing the growth parameters of the dot. With this dot-in-a-rod configuration (DROD), the emitter emission intensity was increased from 275,000 cps to 613,000 cps. Carrier generation localized to the dot could be achieved by optically pumping the rod below the InP bandgap, and resulted in a narrowing of the dot emission linewidth.

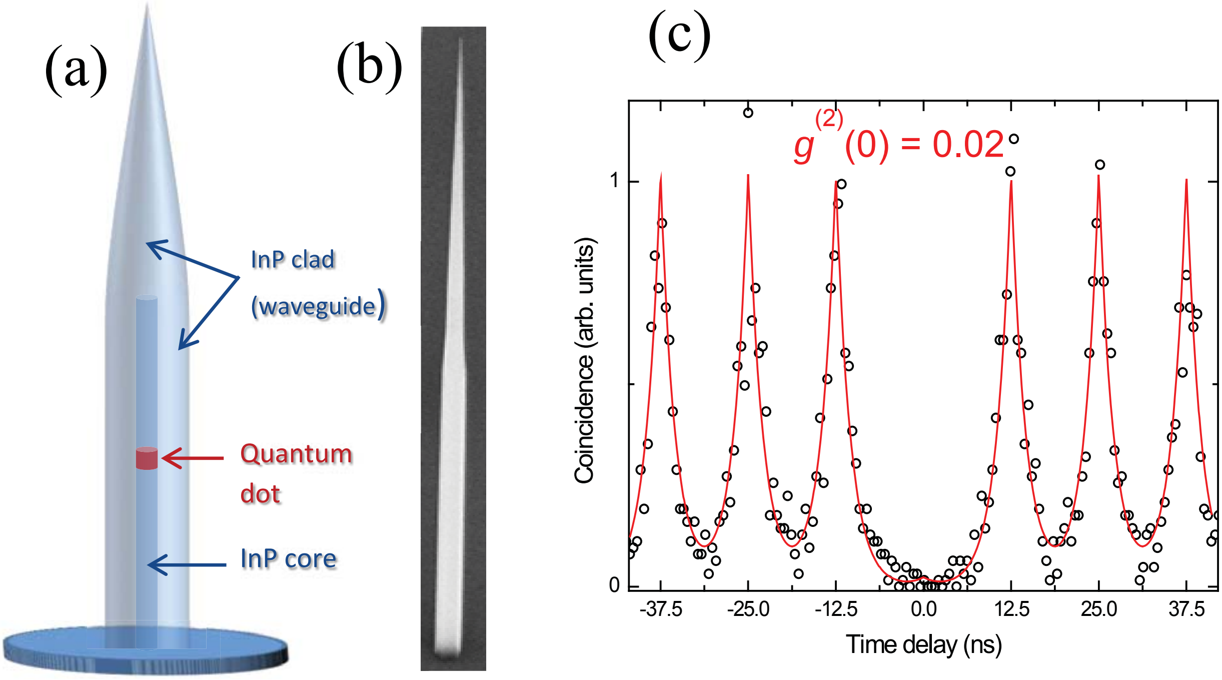


Fig. 1 . (a) Schematic and (b) Scanning electron microscope image of the quantum dot nanowire source. The diameter of the nanowire base is about 350 nm. (c) Second-order correlation measurements of an emitter at 1310 nm.

**References**

[1] D. Dalacu *et al*, Nanotechnology 30 (23), 232001 (2019).
[2] D. Dalacu *et al*, Nano Letters, 12, 5919 (2012).
[3] S. Haffouz *et al*, Nano Letters, **12**, 2888 (2018).

# Quantum teleportation using highly coherent emission from telecom C-band quantum dots

**T. Müller[1], M. Anderson[1,2], J. Huwer[1], J. Skiba-Szymanska[1], A. Krysa[3], R. M. Stevenson[1], J. Heffernan[4], D. A. Ritchie[2] and A. J. Shields[1]**

[1]*Toshiba Research Europe Limited, Cambridge CB4 0GZ, UK*
[2]*Cavendish Laboratory, University of Cambridge, Cambridge CB3 0HE, UK*
[3]*EPSRC National Epitaxy Facility, University of Sheffield, Sheffield S1 3JD, UK*
[4]*Department of Electronic and Electrical Engineering, University of Sheffield, Sheffield S1 3JD, UK*

Quantum network technologies [1], ranging from teleportation and its applications in quantum communication to quantum computing, rely on interference of indistinguishable photons, and demand sources of highly coherent photons with sub-Poissonian statistics. Fibre-based technologies also require photon sources at the minimum loss wavelength of around 1550 nm. Recently, emission of single and entangled photons from semiconductor sources in that band has been reported [2,3], but sufficiently long coherence times have yet to be demonstrated.

Here, we show that droplet epitaxy InAs/InP quantum dots emitting in the telecom C-band can provide photons with coherence times exceeding 1 ns, by using power-dependent single photon interference on a fibre based Michelson interferomenter. A spectrum of such a dot is given in Figure 1 (a). These values enable near-optimal interference of quantum dot emission with a C-band laser qubit, the signature of which is shown in Figure 1(b). Using entangled photons we further demonstrate high fidelity teleportation of such qubits in the horizontal-vertical (HV) basis as well as in the superposition bases DA (diagonal/antidiagonal) and RL (right-hand/left-hand circular). Figure 1 (c) shows the individual fidelities as well as the mean, where the reached value of 83.6±2.2% exceeds the classical limit of 2/3 by 7.8 standard deviations. Beyond direct applications in long-distance quantum communication, the high degree of coherence in these quantum dots is promising for future spin based telecom quantum network applications.

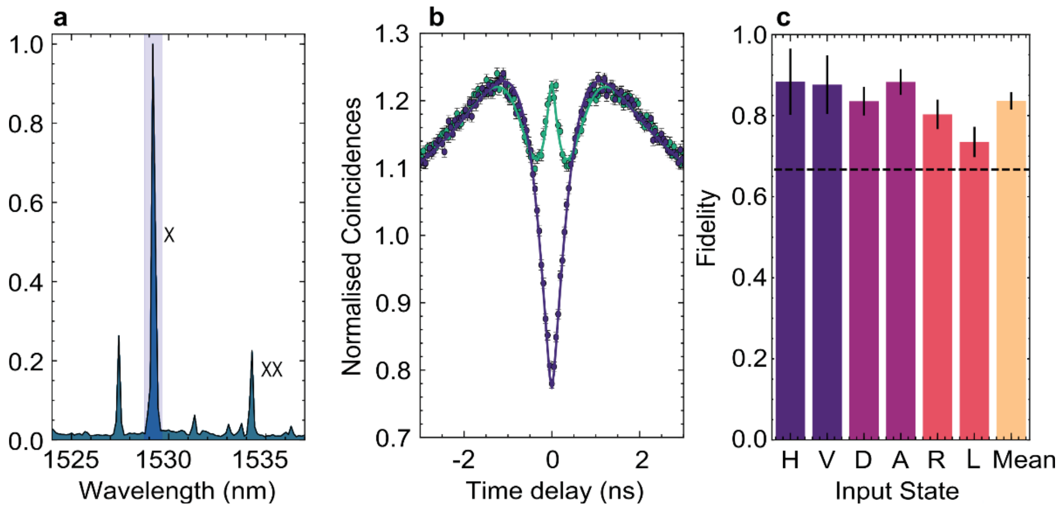


Fig. 1 (a) Spectrum of a representative QD, with X and XX transitions marked. (c) Two-photon interference correlation measurements, with co-polarised correlations in green and cross-polarised photons in purple. The bunching peak for co-polarised photons is the signature of the Hong-Ou-Mandel effect in our setup. (d) Individual fidelities for the 6 input polarization states and the corresponding mean fidelity, with the classical limit of 2/3 given by the dotted line.

**References**

[1] Kimble, H. J. The quantum internet. Nature 453, 1023–1030 (2008).
[2] Olbrich, F. et al. Polarization-entangled photons from an InGaAs-based quantum dot emitting in the telecom C-band. Appl. Phys. Lett. 111, 133106 (2017).
[3] Müller, T. et al. A quantum light-emitting diode for the standard telecom window around 1,550 nm. Nat. Commun. 9, 862 (2018)

# Demonstrating quantum advantage with practical photonic systems

**Eleni Diamanti**

*Sorbonne Université, CNRS, LIP6, F-75005, Paris, France*

The goal of demonstrating a quantum advantage with currently available technology is an outstanding challenge in quantum information science. Here we discuss examples of such rigorous demonstration of advantage in security and communication efficiency due to the use of quantum resources for useful applications in the context of quantum networks, including quantum cryptographic tasks beyond key distribution [1] and quantum communication complexity [2]. This requires devising novel protocols amenable to experimental implementations, which typically involve encoding in properties of coherent states of light, linear optic circuits and single-photon detection. We further discuss the extension of our results in quantum communication complexity to the efficient verification of NP-complete problems with small proofs [3].

.

**References**

[1] M. Bozzio, A. Orieux, L. Trigo Vidarte, I. Zaquine, I. Kerenidis, E. Diamanti, "Experimental investigation of unforgeable quantum money", npj Quantum Information 4, 5 (2018).

[2] N. Kumar, I. Kerenidis, E. Diamanti, "Experimental demonstration of quantum advantage for one-way communication complexity", Nature Communications (2019).

[3] J.-M. Arrazola, E. Diamanti, I. Kerenidis, "Quantum superiority for verifying NP-complete problems with linear optics", npj Quantum Information 4, 56 (2018).

# Experimental Quantum Switching for Exponentially Superior Quantum Communication Complexity

Kejin Wei,[1,2] Nora Tischler,[3] Si-Ran Zhao,[1,2] Yu-Huai Li,[1,2] Juan Miguel Arrazola,[4,5] Yang Liu,[1,2] Weijun Zhang,[6] Hao Li,[6] Lixing You,[6] Zhen Wang,[6] Yu-Ao Chen,[1,2] Barry C. Sanders,[1,7,8] Qiang Zhang,[1,2] Geoff J. Pryde,[3] Feihu Xu,[1,2] and Jian-Wei Pan[1,2]

[1] *Shanghai Branch, Hefei National Laboratory for Physical Sciences at Microscale and Department of Modern Physics, University of Science and Technology of China, Shanghai, 201315, China*

[2] *CAS Center for Excellence and Synergetic Innovation Center in Quantum Information and Quantum Physics, University of Science and Technology of China, Shanghai 201315, P. R. China*

[3] *Centre for Quantum Dynamics, Griffith University, Brisbane, QLD 4111, Australia*

[4] *Xanadu, 372 Richmond Street W, Toronto, Ontario M5V 1X6, Canada*

[5] *Centre for Quantum Technologies, National University of Singapore, 3 Science Drive 2, Singapore 117543*

[6] *State Key Laboratory of Functional Materials for Informatics, Shanghai Institute of Microsystem and Information Technology, Chinese Academy of Sciences, Shanghai 200050, China*

[7] *Institute for Quantum Science and Technology, University of Calgary, Alberta T2N 1N4, Canada*

[8] *Program in Quantum Information Science, Canadian Institute for Advanced Research, Toronto, Ontario M5G 1M1, Canada*

Finding exponential separation between quantum and classical information tasks is like striking gold in quantum information research. Such an advantage is believed to hold for quantum computing but is proven for quantum communication complexity. Recently, a novel quantum resource called the quantum switch—which creates a coherent superposition of the causal order of events, known as quantum causality—has been harnessed theoretically in a new protocol providing provable exponential separation. We experimentally demonstrate such an advantage by realizing a superposition of communication directions for a two-party distributed computation. Our photonic demonstration employs $d$-dimensional quantum systems, qudits, up to $d = 2^{13}$ dimensions and demonstrates a communication complexity advantage, requiring less than $(0.696 \pm 0.006)$ times the communication of any causally ordered protocol. These results elucidate the crucial role of the coherence of communication direction in achieving the exponential separation for the one-way processing task, and open a new path for experimentally exploring the fundamentals and applications of advanced features of indefinite causal structures.

The communication task that we consider is known as the exchange evaluation (EE) game. Alice and Bob receive inputs $(\boldsymbol{x}, f)$ and $(\boldsymbol{y}, g)$, respectively. There is another party, Charlie, who needs to compute the exchange evaluation function $\mathrm{EE}(\boldsymbol{x}, f, \boldsymbol{y}, g) = f(\boldsymbol{y}) \oplus g(\boldsymbol{x})$. Under the condition of one-way communication, for a causally ordered protocol, Alice and Bob can transmit information either from Alice to Bob, then Charlie or from Bob to Alice, then Charlie. Using a quantum switch, a control qubit in the state $|+\rangle_c = 1/\sqrt{2}\,(|0\rangle_c + |1\rangle_c)$ coherently controls the communication direction of the target system $|0\rangle_t$. Charlie computes the exchange evaluation function by measuring the control qubit. As a result, they solve the game with exponential advantage in the scaling of the required communication compared to any causally ordered protocol.

Figure 1 shows the experimental transmitted information required to complete the task for different system sizes. We compare our protocol with a bound for classical protocols (black solid curve) and a bound for quantum causally definite protocols (blue solid curve). Figure 1 indicates that, with increasing system size $n$, the causally indefinite protocol provides an exponential advantage in the scaling of transmitted information. In particular, for $n = 12$, the experimental results clearly beat all classical protocols as well as all quantum causally definite protocols.

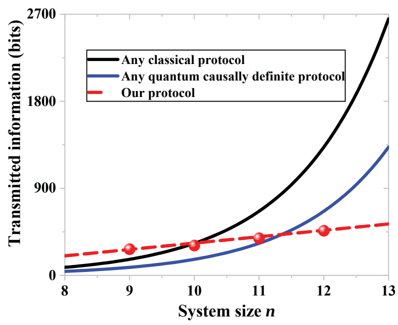


FIG. 1. Comparison of the transmitted information.

Further details of our work can be found in [1].

[1] K. Wei, N. Tischler, S.-R. Zhao, Y.-H. Li, J. M. Arrazola, Y. Liu, W. Zhang, H. Li, L. You, Z. Wang, Y.-A. Chen, B. C. Sanders, Q. Zhang, G. J. Pryde, F. Xu, and J.-W. Pan, Phys. Rev. Lett. **122**, 120504 (2019).

# Hybrid entanglement distribution through an air-core fiber

**Daniele Cozzolino[1], Emanuele Polino[2], Mauro Valeri[2], Gonzalo Carvacho[2], Davide Bacco[1], Nicoló Spagnolo[2], Leif Katsuo Oxenløwe[1] and Fabio Sciarrino[2]**

[1] *CoE SPOC, Dep. Photonics Eng., Technical University of Denmark, Kgs. Lyngby 2800, Denmark*

[2] *Dipartimento di Fisica, Sapienza Universitá di Roma, Piazzale Aldo Moro 5, I-00185 Roma, Italy*

Exploiting optical fiber links to distribute photonic entangled states is fundamental for building the future quantum networks. We exploit a recently developed air-core fiber, supporting OAM modes, to distribute hybrid vector vortex-polarization entangled photon pairs. Polarization entangled photon pairs are generated by a ppKTP crystal in a Sagnac configuration at 1550nm. Photons (1) pass through a polarization analysis stage (QWP, HWP and PBS) and are detected. Photons (2) impinge on a vortex plate which adds an OAM m =+7 to the photons [1]. Depending on the input polarization of photons impinging on the vortex plate (H and V respectively), two vector vortex beam are generated:

$$|r\rangle = \frac{|R,+7\rangle+|L,-7\rangle}{\sqrt{2}} \qquad\qquad |a\rangle = \frac{|R,+7\rangle-|L,-7\rangle}{\sqrt{2}}$$

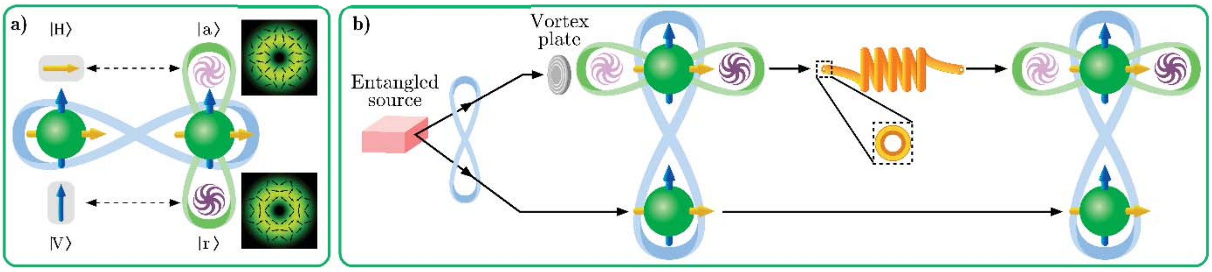


Fig. 1 a) Polarization entanglement of the photon pair (blue ribbon) and entanglement between polarization and OAM of the single photon (green ribbon) are sketched. The inhomogeneous polarization patterns of the VV states are explicitly shown. b) Schematic of the experiment: hybrid VV-polarization entangled state is generated by an initial polarization entangled photon pair. One photon of the pair encodes the VV state by the action of a vortex plate. The VV beam is transmitted through the air-core fiber. Finally, state detection shows that hybrid VV-polarization entanglement (blue and green ribbons) is preserved after fiber transmission.

After the vortex plate, photons are a hybrid entangled state: $|\psi\rangle = (|H\rangle_1|a\rangle_2 - |V\rangle_1|r\rangle_2)/\sqrt{2}$ . Then, photons (2) are coupled to 5m of air-core fiber, transmitted and detected. The quality of the transmitted states and their entanglement are measured through quantum tomography processes and CHSH-like inequality violations respectively. The fidelity of the hybrid entangled state is (97.9 ± 0.02)% with respect to Source entangled state (polarization entangled pair), which in turn has a fidelity of of (93.5 ± 0.02)% with respect to the ideal Bell singlet. The CHSH violation parameters obtained for the hybrid entangled states are $S^{(raw)} = 2.62 \pm 0.03$ and $S = 2.67 \pm 0.03$, subtracting the accidental coincidences. Such values violates by 21 and 22 standard deviations the separable limit S=2, respectively. We finally characterize the hybrid entangled state by considering it as a 3-qubit state. The $2^3$-dimensional Hilbert space is spanned by the polarization bases of both photons and the OAM basis of photon (2). A $2^3$-dimensional quantum state tomography is performed, obtaining a final fidelity of (88.1 ± 0.2)% with respect to the ideal state. Two device independent tests of quantum correlations are performed. Firstly, we test the multipartite Mermin-Ardehali-Belinskii-Klyshko inequality [2] obtaining the values $M^{(raw)} = 3.43 \pm 0.04$ and $M = 3.53 \pm 0.04$, which violates the classical limit $M \leq 2$. Then, we perform a Hardy test by violating the inequality reported in [3] with values $H^{(raw)} = 0.085 \pm 0.08$ and $H = 0.104 \pm 0.08$, where the separable condition is $H \leq 0$. The achieved results demonstrate the capability to perform high fidelity distribution in an OAM supporting fiber of a hybrid VV-polarization entangled state at telecom wavelength, opening new scenarios for quantum applications where correlated complex states can be transmitted by exploiting the vectorial nature of light.

**References**

[1] Marrucci, L., et al., "Optical spin-to-orbital angular momentum conversion in inhomogeneous anisotropic media." *Physical review letters* 96.16 (2006): 163905.

[2] Mermin, N. D. "Extreme quantum entanglement in a superposition of macroscopically distinct states." Physical Review Letters 65.15 (1990): 1838

[3] Jiang, S.-H., et al. "Generalized Hardy's paradox." Physical review letters 120.5 (2018): 050403.

# High-Dimensional Chip-to-Chip Entanglement Distribution through Multicore Fibres

**Caterina Vigliar[1], D. Llewellyn[1], B. Slater[1], B. Da Lio[2, 3], S. Paesani[1], J. Barreto[1], D. Sahin[1], M. Borghi[1], J. G. Rarity[1], L. K. Oxenløwe[2, 3], K. Rottwitt[2, 3], J. Wang[4, 5], Y. Ding[2, 3], M. G. Thompson[1], D. Bacco[2, 3].**

[1] *Quantum Engineering Technology Labs, H. H. Wills Physics Laboratory and Department of Electrical and Electronic Engineering, University of Bristol, BS8 1FD, Bristol, United Kingdom.*

[2] *Department of Photonics Engineering, Technical University of Denmark, 2800 Kgs. Lyngby, Denmark.*

[3] *Center for Silicon Photonics for Optical Communication (SPOC), Technical University of Denmark, 2800 Kgs. Lyngby, Denmark.*

[4] *State Key Laboratory for Mesoscopic Physics and Collaborative Innovation Center of Quantum Matter, School of Physics, Peking University, Beijing 100871, China.*

[5] *Beijing Academy of Quantum Information Sciences, West Bld.3, No.10 Xibeiwang East Rd., Haidian District, Beijing 100193, China.*

The distribution of entangled photons over global networks is of key importance in quantum communication protocols, to establish an unconditional secure key without requiring the presence of trusted nodes, and in distributed quantum computation, in which quantum computers work together to reach larger capacities. Entanglement of multidimensional quantum systems (qudits) constitute an enormous resource for future quantum networks, both in terms of information capacity and in terms of tolerance to noise, exceeding the limitations imposed by qubits [1]. Devices able to generate and manipulate qudits have been demonstrated [2], but the reliable transmission of qudits over optical fibres, a cornerstone of future quantum networks, remains an open challenge.
In this work we report the first chip-to-chip high-dimensional entanglement distribution of path-encoded quantum states of light through multicore fibres. We build a system composed of two integrated silicon chips, a transmitter and a receiver, linked by a five-meter long seven-core fibre (Fig. 1.a). Maximally entangled two- and four-dimensional quantum states, prepared and measured over the two chips, are verified by tomography measurements, with average fidelities of $0.85 \pm 0.04$ and $0.88 \pm 0.01$ respectively.
These results mark a key step towards the development of distributed quantum applications, proving that fibre based spatial mode protocols along with integrated silicon devices can be effectively used for quantum communications in future networks, providing reliable mass-manufacturable and high-performance systems.

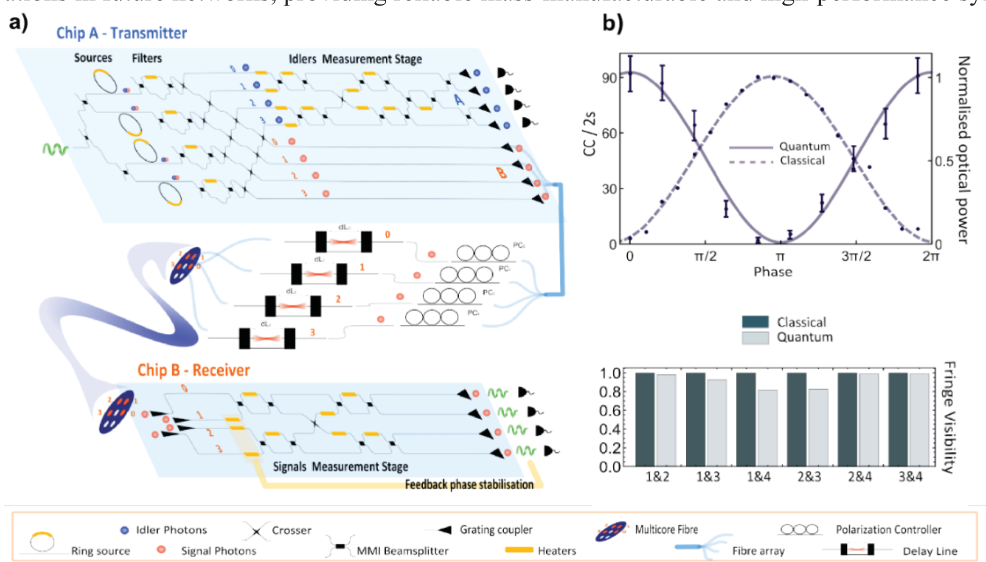


Fig. 1a) Schematic of the setup. The transmitter chip generates a maximally entangled four-dimensional quantum state (two ququarts) and performs on-chip measurements on ququart A. The four modes composing ququart B are coupled in four of the seven cores of the multicore fibre and sent to a receiver chip, which performs arbitrary measurements on B. b) Demonstration of chip-to-chip phase control: interferometric phase scan in a Mach-Zehnder built out of two different chips connected by single mode fibres, polarization controllers, delay lines and a multicore fibre. $2\pi$ phase shift can be obtained with good precision, with active phase stabilisation, both in the classical and in the single-photon regime. Preliminary data showing the visibility of chip-to-chip pairwise interference between each combination of sources.

**References**

[1] N. J. Cerf, et al., “Security of Quantum Key Distribution Using d -Level Systems”, Physical Review Letters 88, 030301(R) (2002).

[2] J. Wang et al., “Multidimensional quantum entanglement with large-scale integrated optics”, Science, 360, 285-291 (2018).

# Nanowire Detection of Photons from the Dark Side

**Asimina Arvanitaki[3], Masha Baryakhtar[4], Karl K. Berggren[1], Ilya Charaev[1], Jeff Chiles[2], Marco Colangelo[1], Andrew E. Dane[1], Junwu Huang[3], Robert Lasenby[6], Sae Woo Nam[2], Ken Van Tilburg[4,5], Varun Verma[2]**

[1] *Massachusetts Institute of Technology, Cambridge, MA, USA*
[2] *National Institute of Standards and Technology, Boulder, CO, USA*
[3] *Perimeter Institute for Theoretical Physics, 31 Caroline Street North, Waterloo, CA*
[4] *New York University, NY, USA*
[5] *Institute for Advanced Studies, Princeton, NJ, USA*
[6] *Stanford University, Stanford, CA, USA*

In recent years, the development of fast and low-dark-count single-photon detectors for photonic quantum information applications promise a radical improvement in our capacity to search for dark matter. The advent of superconducting nanowire detectors, which have fewer than 10 dark counts per day and have demonstrated sensitivity from the mid-infrared to the ultraviolet wavelength band, provides an opportunity to search for bosonic dark matter in the neighborhood of 1 eV. These detectors are simple to fabricate and operate, and can be combined with gas cells, dielectric stacks, or combinations of these structures in cryogenic targets, optimized for dark matter absorption. Furthermore, superconducting nanowires can be used as both target and sensor for direct detection of sub-GeV dark matter [1].

In this work, we will combine resonator systems and large-area single-photon detectors, to establish a novel paradigm to look for dark matter with rest mass energies in the range of meV to 10 eV. Inherently resonant systems at these energies—narrow molecular absorption transitions [2] and periodically layered dielectric stacks [3] — bring with them a range of advantages: selectivity, control, and natural background reduction. We demonstrate a high-performance 400 by 400 μm large-area tungsten-silicide nanowire prototype with 0.8-eV energy threshold with more than 90 thousand seconds of exposure, which showed no dark counts. We also present recent progress on the design, construction and testing of multilayer optical haloscopes serving as the apparatus for resonant detection schemes. Future experiments should enable probing new territory in the dark matter detection landscape, establishing the complementarity of this approach to other existing proposals.

**References**

[1] Y. Hochberg, I. Charaev, S.-W. Nam, V. Verma, M. Colangelo, K. K. Berggren, "Detecting Dark Matter with Superconducting Nanowires," arXiv:1903.05101, 2019.
[2] A. Arvanitaki, S.Dimopoulos, and K. V. Tilburg, "Resonant Absorption of Bosonic Dark Matter in Molecules," Phys. Rev. X **8**, 041001, 2018.
[3] M. Baryakhtar, J. Huang, and Robert Lasenby, "Axion and hidden photon dark matter detection with multilayer optical haloscopes," Phys. Rev. D **98,** 035006, 2018.

# Massively parallel, three-dimensional photon counting: a versatile tool for quantum experimentalists and consumers

**Edoardo Charbon**

*EPFL, Neuchatel, Switzerland*

CMOS SPADs have appeared in 2003 and soon have risen to the status of image sensors with the creation of deep-submicron SPAD technology. The format of these image sensors has expanded from 8x4 pixels of our first LIDAR in 2004 to 512x512 pixels of recent time-resolved cameras, and the applications have literally exploded in the last few years, with the introduction of proximity sensing and portable telemeters. SPAD based sensors are today in almost every smartphone and the promise is that they will be in every car by 2022. The introduction of SPADs in 3D-stacked ICs in 2015 is pushing the potential of this technology even further. The inherently digital nature of SPADs and the increased density of processing and computation over multiple silicon layers will soon enable deep-learning processors, neural networks directly on chip, thus enabling complex processing in situ and reducing the overall power consumption. Another recent trend has been the use of SPADs in qubit readout and control, thus making SPADs amenable to interface with quantum processors, due to SPAD sensitivity and the capability of operating normally at cryogenic temperatures. I will conclude with a technical and economic perspective on SPADs/SPAD imagers and a vision statement for photon counting in CMOS and other cryo-CMOS circuits, including cryo-SPADs in quantum computing.

# Wide-area fast-gated single-photon detector with integrated TDC for near-infrared spectroscopy applications

**Enrico Conca[1], Vincenzo Sesta[1], Federica Villa[1], Mauro Buttafava[1], Simone Tisa[2], Alberto Dalla Mora[3], Davide Contini[3], Alessandro Torricelli[3], Antonio Pifferi[3], Laura Di Sieno[3], Paola Taroni[3], Franco Zappa[1], Alberto Tosi[1]**

*[1]Politecnico di Milano, Dipartimento di Elettronica, Informazione e Bioingegneria. Piazza Leonardo da Vinci, 32 I-20133 Milano, Italy*

*[2]Micro Photon Devices S.r.l. Via Waltraud Gebert Deeg, 3g I-39100 Bolzano, Italy*

*[3]Politecnico di Milano, Dipartimento di Fisica. Piazza Leonardo da Vinci, 32 I-20133 Milano, Italy*

*enrico.conca@polimi.it*

Time-Domain Near-Infrared Spectroscopy (TD-NIRS) is a powerful technique for estimating the composition and microstructure of biological tissues and other highly scattering media, down to a depth of few centimetres, by retrieving the optical absorption and scattering properties. According to TD-NIRS, laser pulses are injected into the sample and the diffused photons are collected by a single-photon detector [1]. TD-NIRS can take advantage of the so-called "fast time-gated acquisition" technique, combined with a short source-detector distance [1]. However, up to now, TD-NIRS instruments have been quite bulky and expensive.

Here, we present a silicon integrated circuit designed for compact and low-cost TD-NIRS systems, combining a fast-gated single-photon detector array (based on SPADs) with 8.6 mm$^2$ active area, a Time-to-Digital Converter (TDC) with 72 ps resolution and integrated histogram builder, a gate window generator and a serial interface (for easy communication with low-cost microcontrollers). The chip has been fabricated in a 0.35 µm CMOS technology and it is designed to fit inside a small standalone module (few cm$^3$ of volume), together with 8 pulsed diode lasers of different wavelengths, in order to build an extremely compact TD-NIRS system with low power consumption. This fully-digital photodetector combines the fast-gating capability of SPAD detectors, previously only demonstrated for single pixels [2], with the large area typically found in detectors like Silicon Photomultipliers (SiPMs). It is therefore called "fast-gated digital SiPM". It allows highly-sensitive time-gated measurements with extended dynamic range (thanks to more than 1700 microcells). Each microcell can be individually disabled either for reducing the overall noise or for adjusting the sensitive area, in order to equalize the signal directly on chip.

Common fast-gating approaches couple a SPAD to a "dummy" device and employ a comparator to extract the avalanche signal while rejecting spurious gating feedthroughs [2]. In this new detector, in order to increase the fill-factor and reduce power consumption, we replaced the dummy structure with a second SPAD and the comparator with a digital XOR gate. We reach a fill-factor of 37% and a maximum gating frequency of 100 MHz. The TDC adopts a Vernier delay line architecture and reaches 72 ps resolution with a Full-Scale Range (FSR) of 9.2 ns, while keeping the conversion time shorter than 100 ns. A 12-bit depth, 128-channel histogram builder accumulates the conversion results and minimizes the bandwidth required for transferring data. The internal gate window generator is used for synchronizing the gate window with the laser pulse. It has adjustable duration with resolution of 1 ns and a range of 24 ns. A low power mode disables the gate generation during TDC conversion.

The detector achieves a temporal response of ~ 300 ps (FWHM) and a dynamic range for gated measurements greater than 50 dB, with a rising edge of the gate window of ~ 300 ps (20% - 80%).

With this solution, TD-NIRS can widen its applications (from labs to hospitals) and even reach mass markets (e.g. in athlete training monitoring and non-destructive assessment of fruit quality).

*This work was supported by the European Union's Horizon 2020 research and innovation programme under G.A. 731877 (SOLUS). SOLUS is an initiative of the Photonics Public Private Partnership.*

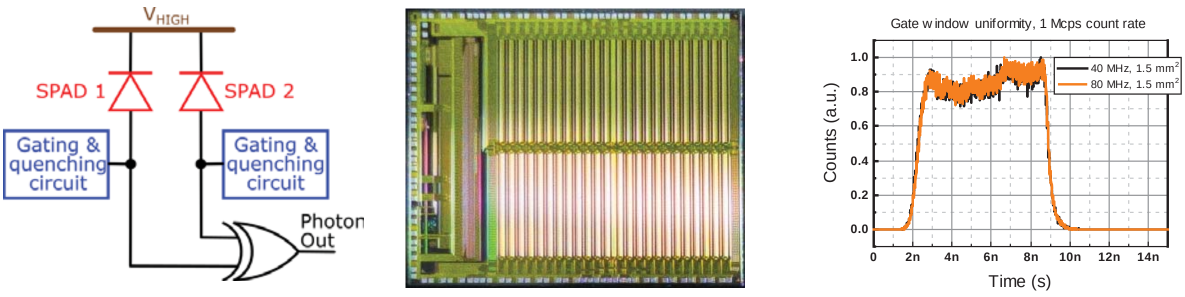


Fig. 1 Left: Microcell block diagram. Center: Fabricated chip. Right: Gate shape when 1.5 mm$^2$ of the active area is ON.

## References

[1] A. Dalla Mora et al., "Towards next-generation time-domain diffuse optics for extreme depth penetration and sensitivity," Biomed. Opt. Express, vol. 6, no. 5, pp. 1749–1760, May 2015.

[2] M. Buttafava et al., "Time-gated single-photon detection module with 110 ps transition time and up to 80 MHz repetition rate," Rev. Sci. Instrum., vol. 85, no. 8, p. 083114, Aug. 2014.

# Silicon photomultipliers optimized for cryogenic temperatures

**Fabio Acerbi[1], Massimo Capasso[1], Alberto Mazzi[1], Giovanni Paternoster[1], Nicola Zorzi[1], Alberto Gola[1]**

*1. Fondazione Bruno Kessler (FBK), via Sommarive 18, Trento, Italy*

Silicon photomultipliers (SiPMs) are arrays of many Single-Photon Avalanche Diodes (SPADs), each one with integrated passive-quenching resistor ("microcell"). All microcells are connected in parallel to common anode and cathode. Each SiPM cell works in Geiger mode and the output current of the SiPM is the sum of all the cells: SiPM is a single-photon detector but the output is proportional to the number of detected photons in a light pulse. SiPMs have obtained growing attention in the last years in the detection of low photon fluxes, thanks to their compactness, ease of use, low operational voltage, insensitivity to magnetic fields and large optical dynamic range. They also have easy scalability, for both the microcell (pixel) size (ranging from 5 µm to 100 µm side) and the overall active area (between less than 1 mm$^2$ and 100 mm$^2$). SiPMs emerged as a promising solution for Light Detection and Ranging (LIDAR), optical spectroscopy [1], fluorescence detection, physics experiments and medical applications. At FBK (Trento, Italy) we developed different technologies for SiPMs and SPADs, optimized for different applications, such as "NUV-HD (near-ultraviolet sensitive, High-Density of cells), NIR-HD (near-infrared sensitive) and VUV-HD (vacuum-ultraviolet sensitive). Examples of spectral PDE can be seen in Fig 1b.

One important recent research topics, where SiPMs are the solution of choice, is the readout of liquid noble gases scintillators such as liquid Xenon [2] and liquid Argon [3], where SiPMs are operated at cryogenic temperatures (between ~80 K and ~160 K). To optimize SiPM performance for such conditions, there have been important studies in the last years. SiPM performance like dark count rate (DCR), afterpulsing, crosstalk, recharge time, etc. have been measured at different temperatures [3]. Given the first results, important enhancements have been demonstrated. In particular reducing the electric field, to reduce the field-enhancement and tunneling generation and limiting the afterpulsing effect that can be dominant at cryogenic temperatures. Fig 1c shows an example of how the correlated noise is limiting the maximum operating bias more and more reducing the temperature, whereas Fig 1d and Fig 1e shows the remarkable reduction of primary DCR reducing the temperature. In "standard" electric field SiPM we reach ~10 cps for 1 mm$^2$ active area (at liquid nitrogen temperature), whereas engineering the electric field we were able to reach ~0.01 cps in 1 mm$^2$ active area.

In this work we will show the performance of different SiPMs, tested at different temperatures, between room temperature down to liquid nitrogen temperature and we will discuss the trends for primary noise, correlated noise, etc. as a function of excess bias and temperature. SiPMs working at low temperatures, e.g. at liquid nitrogen temperature (77K), can have good photon detection efficiency, limited correlated noise and very low dark count rate, of less than 1 cps/mm$^2$ with high dynamic range and with relatively large active areas (up to 100mm$^2$).

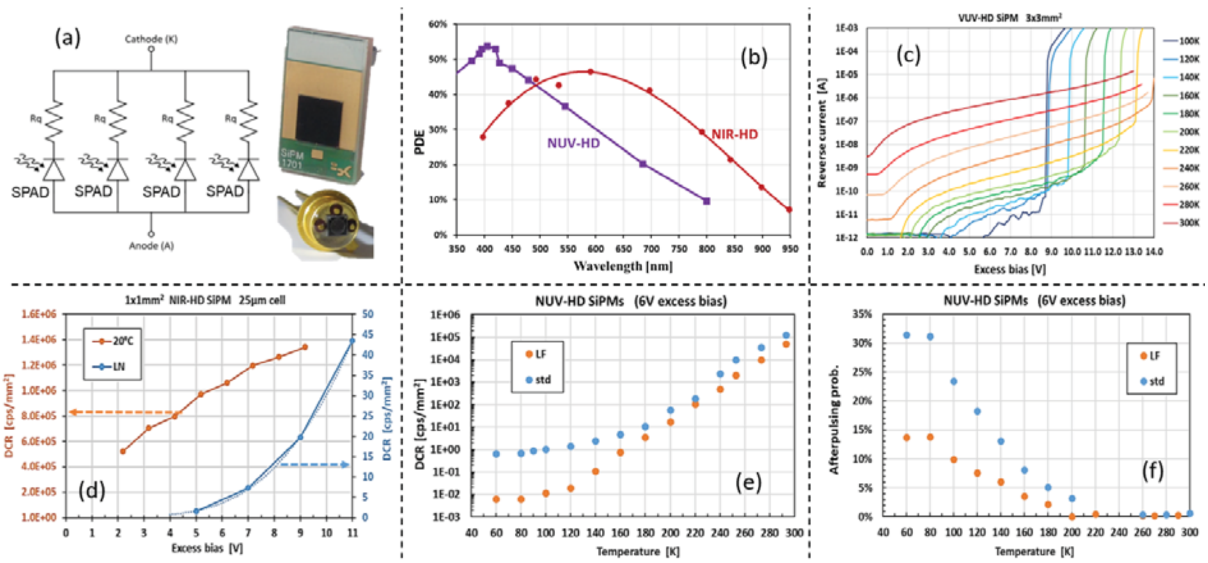


Fig. 1 : Conceptual schematic of SiPM microcells connection and pictures (a), typical photon photon detection efficiency of FBK NUV-HD and NIR-HD technologies (b), example of reverse IV curve at different temperatures of VUV-HD SiPM (c), dark count rate of NIR-HD SiPM measured at 20°C and liquid nitrogen temperature (d), dark count rate of NUV-HD SiPMs std and low-field version, as a function of temperature [3] (e), and afterpulsing for std and low-field version [3] (f).

**References**

[1] A. D. Mora et al., Opt. Exp., vol. 23, no. 11, pp. 13937–13946 (2015)

[2] F. Arneodo, et. al., Nuclear Inst. and Methods in Physics Research, A, 893 (2018) 117–123

[3] F. Acerbi et. al., IEEE trans. On elect. dev., vol. 64, no. 2, p.521 (2017) DOI: 10.1109/TED.2016.2641586

# Single-Photon Detectors based on CSPAD technology

**Simon Grosse, Manuel Ligges, Werner Brockherde**
*Fraunhofer Institute for Microelectronic Circuits and Systems IMS, Duisburg, Germany*

Numerous applications in the fields of LiDAR, quantum imaging, spectroscopy, high energy physics etc. require photon detectors with high sensitivity and time resolution. There are various single-photon detector technologies available to meet these requirements. In comparison to photomultiplier tubes, superconducting nanowire single-photon detectors and electron multiplying CCDs, the SPAD technology can distinguish itself by a high time resolution, a low noise level and low-cost production.

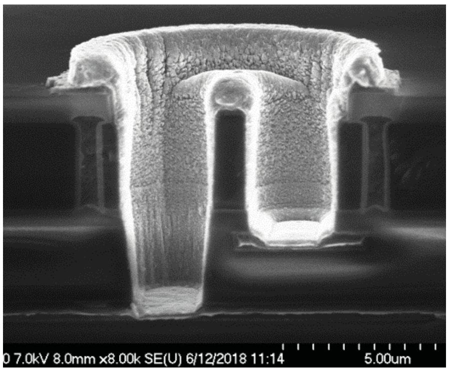


Fig. 1: SEM image of a cross section of a bonded wafer stack (SPAD and ROIC wafer) with etched and filled vias for electrical interconnection.

Being operated above the breakdown voltage (in Geiger mode), SPADs generate a short-duration high current when absorbing an incident photon that can be read-out by a subsequent circuit (ROIC). An active quenching/reset design to restore the SPAD to the operative level leads to a low dead time of below 20 ns and thus a high detection rate. The integration of SPADs into the CMOS process (CSPAD) allows for signal processing close to the active sensor area and high flexibility for custom circuit designs that adapt to various applications.

The Fraunhofer IMS CSPAD detectors provide single-photon sensitivity with a low dark count rate (~10 cps) and a high dynamic range (134 dB) and can be operated in two modes: In *counting mode* the detected photons over a specific time window are counted and can be read-out while the *timing mode* outputs a time stamp of the first detected photon. An adaptive coincidence mechanism provides a more robust measurement and can be applied i.e. for effective background light suppression in LiDAR systems [1].

The CSPAD detectors by IMS are currently used in various applications that require a high sensitivity and time-resolution. The current flash LiDAR system based on Time-of-Flight measurement with a CSPAD detector can achieve a range of 40 m with a distance resolution of ~ 5 cm and a framerate of 25 fps. The implementation of efficient signal processing and algorithms yields a high potential for performance improvement. In the context of the Fraunhofer lighthouse project QUILT the CSPAD linear detector is a pivotal element of an experiment that shows Quantum Ghost Imaging for remote sensing [2]. More current and future applications of the Fraunhofer IMS CSPAD detectors include time-gated Raman spectroscopy, fluorescence lifetime imaging microscopy (FLIM), positron emission tomography (PET) and random number generation for cryptography.

By utilizing a new wafer-to-wafer bonding process with a backside illuminated CSPAD wafer and a ROIC wafer it is possible to achieve a dense 2-dimensional pixel arrangement with a high fill factor. A 64 x 48 pixel SPAD array detector (CSPAD3000) is currently in fabrication and will represent a significant step forward by providing a 2-dimensional focal plane array with 312.5 ps temporal resolution. This bonding technology will also allow the combination of an optimized SPAD process in Fraunhofer IMS with a more advanced technology for the read-out part of the detector. As a result higher temporal and spatial resolution will be achieved, rendering CSPAD detectors even more attractive for a number of applications that require single-photon sensitivity. The implementation of micro-optic arrays and interference filters processed on wafer level is currently being researched and promises a significant increase of the effective fill factor and thus the detector sensitivity.

**References**

[1] Beer, Maik et al. “Background Light Rejection in SPAD-Based LiDAR Sensors by Adaptive Photon Coincidence Detection.” *Sensors (Basel, Switzerland)* vol. 18,12 4338. 8 Dec. 2018, doi:10.3390/s18124338

[2] Fraunhofer-Gesellschaft. (2019). *Quantum Methods for Advanced Imaging Solutions (QUILT)*. [online] Available at: https://www.fraunhofer.de/de/forschung/fraunhofer-initiativen/fraunhofer-leitprojekte/quilt.html [Accessed 5 Jul. 2019].

# New Frontiers in Quantum Measurement: Protective Measurement, Genetic Quantum Measurement and Robust Weak Measurement

**F. Piacentini**[1], **A. Avella**[1], **E. Rebufello**[1,2], **S. Virzì**[1,3], **M. A. de Souza**[4], **R. Lussana**[5], **F. Villa**[5], **A. Tosi**[5], **M. Gramegna**[1], **G. Brida**[1], **M. G. A. Paris**[6], **E. Cohen**[7], **J. Dziewior**[8,9], **L. Vaidman**[10], **I. P. Degiovanni**[1], **M. Genovese**[1]

[1]*Istituto Nazionale di Ricerca Metrologica, Torino, Italy*
[2]*Politecnico di Torino, Torino, Italy*
[3]*Università degli Studi di Torino, Dipartimento di Fisica, Torino, Italy*
[4]*National Institute of Metrology, Quality and Technology – INMETRO, Rio de Janeiro, Brazil*
[5]*Politecnico di Milano, Dipartimento di Elettronica, Informazione e Bioingegneria, Milano, Italy*
[6]*Università degli Studi di Milano, Dipartimento di Fisica, Milano, Italy*
[7]*Faculty of Engineering and the Institute of Nanotechnology and Advanced Materials, Bar Ilan University, Ramat Gan, Israel*
[8]*Max-Planck-Institut für Quantenoptik, Garching, Germany*
[9]*Department für Physik, Ludwig-Maximilians-Universität, München, Germany*
[10]*Raymond and Beverly Sackler School of Physics and Astronomy, Tel-Aviv University, Tel-Aviv, Israel*

Measurement has a crucial role in quantum mechanics, because of features like the wave function collapse (after a "strong" measurement) or the fact that measuring a quantum observable erases the information on its conjugate. Nevertheless, quantum mechanics allows for different measurement paradigms, e.g. weak measurements, i.e. measurements performed with an interaction sufficiently weak not to collapse the original state.
These measurements result in weak values [1-6], exploited for research in fundamental physics [7-13], as well as in applied physics being powerful tools for quantum metrology [14-20].
Another example is given by protective measurements (PMs) [21], a new technique able to extract information on the expectation value of an observable even from a single measurement on a single (protected) particle [22].
In addition, other novel measurement protocols have stemmed from these measurement paradigms. It is the case of genetic quantum measurement (GQM), presenting analogies with the typical mechanisms of genetic algorithms [23] and yielding uncertainties even below the quantum Cramér-Rao bound for prepare-and-measure schemes.
Recently, we have also been exploring a new technique named robust weak value measurement (RWM), able to extract a weak value not as an average on an ensemble of weakly measured particles, but even from a single particle (provided it survives the whole measurement process).
In this talk, we present the first experimental implementation of PM [22], showing unprecedented measurement capability and demonstrating how the expectation value of an observable can be obtained without statistics.
Afterwards, we introduce the GQM paradigm, illustrating its features and advantages, verified by the experimental results obtained in our proof-of-principle demonstration.
Finally, we will present RWM and show the results achieved by our experimental implementation of such protocol.

**References**

[1] A.G. Kofman, S. Ashhab, F. Nori, Phys. Rep. 52, 43 (2012).
[2] B. Tamir and E. Cohen, Quanta 2, 7 (2013).
[3] Y. Aharonov, D.Z. Albert, and L. Vaidman, Phys. Rev. Lett. 60, 1351 (1988).
[4] N.W.M. Ritchie, J.G. Story, and R.G. Hulet, Phys. Rev. Lett. 66, 1107 (1991).
[5] G.J. Pryde, J.L. O'Brien, A.G. White, T.C. Ralph, and H.M. Wiseman, Phys. Rev. Lett. 94, 220405 (2005).
[6] O. Hosten and P. Kwiat, Science 319, 787 (2008).
[7] Y. Aharonov et al., Phys. Lett. A 301, 130 (2002).
[8] H.M. Wiseman, New J. Phys. 9, 165 (2007).
[9] R. Mir et al., New J. Phys. 9, 287 (2007).
[10] N.S. Williams and A.N. Jordan, Phys. Rev. Lett. 100, 026804 (2008).
[11] M.E. Goggin et al., PNAS 108, 1256 (2011).
[12] M. Pusey, Phys. Rev. Lett. 113, 200401 (2014).
[13] F. Piacentini et al., Phys. Rev. Lett. 116, 180401 (2016).
[14] O. Hosten and P. Kwiat, Science 319, 787 (2008).
[15] K.J. Resch, Science 319, 733 (2008).
[16] P.B. Dixon, D.J. Starling, A.N. Jordan, and J.C. Howell, Phys. Rev. Lett. 102, 173601 (2009).
[17] J.M. Hogan et al., Opt. Lett. 36, 1698 (2011).
[18] O.S. Magaña-Loaiza, M. Mirhosseini, B. Rodenburg, and R. W. Boyd, Phys. Rev. Lett. 112, 200401 (2014).
[19] J. Salvail et al., Nature Phot. DOI 10.1038;
[20] J. Lundeen, B. Sutherland, A. Patel, C. Stewart, and C. Bamber, Nature 474, 188 (2011).
[21] Y. Aharonov and L. Vaidman, Phys. Lett. A 178, 38 (1993).
[22] F. Piacentini et al., Nat. Phys. 13, 1191–1194 (2017).
[23] M. Mitchell, An Introduction to Genetic Algorithms, Cambridge, MA: MIT Press (1996).

# Certified Randomness Expansion using a Loophole-Free Bell Test

**L. K. Shalm[1], Y. Zhang[2], M. A. Alhejji[1], M. Mazurek[1], M. Stevens[1], C. Abellán[3], M. W. Mitchell[3], S. W. Nam[1], E. Knill[1]**

[1] *National Institute of Standards and Technology, 325 Broadway, Boulder, Colorado 80305, USA*

[2] *NTT Basic Research Laboratories and NTT Research Center for Theoretical Quantum Physics, NTT Corporation, 3-1 Morinosato-Wakamiya, Atsugi, Kanagawa 243-0198, Japan*

[3] *ICFO-Institut de Ciencies Fotoniques, The Barcelona Institute of Science and Technology, 08860 Castelldefels (Barcelona), Spain*

In 2015 our group performed one of the first loophole-free tests of Bell's inequalities **Error! Reference source not found.**. While this brought to an end the efforts to conclusively rule out local realism as an alternative theory to quantum mechanics, it has heralded the start of a new era of experimental capabilities and techniques in quantum information. Instead of ruling out a local hidden variable model of nature, a loophole-free Bell test can be used to put bounds on how much information a hacker or bad actor can gain about the outcome of Bell-type measurements. The predictive power of a hacker is in fact equivalent to a hidden variable model [2]. This has led to numerous proposals for device-independent cryptographic protocols where a loophole-free Bell test can severely limit the power of an attacker.

In 2017 we were able to use our loophole-free setup to experimentally generate the first randomness that can be certified directly in a device-independent manner [3,4]. In 10 minutes of experimental data, we produce 1024 bits with a bias that deviates from uniform by less than a part in 10^12. To directly verify a bias at this level using any other randomness generation method would require producing on the order of 10^24 bits–a feat that would take hundreds of thousands of years using the fastest random number generators that are currently on the market. However, for this experiment we required on the order of 120 million random input bits to make Alice's and Bob's space-like separated measurement decisions.

In this talk I will discuss our recent work performing the first device-independent randomness expansion, where our experiment is able to produce more certified random output bits than random input bits consumed. These expansion protocols have more demanding requirements compared to regular device-independent randomness generation. Several theoretical and experimental innovations were required in order to realize randomness expansion. After taking 130 hours of data, we have achieved certified randomness expansion. Our work opens the way for other novel device-independent protocols, and has the potential for use in quantum networked applications where entanglement must be distributed over long distances with high success probability.

**References**

[1] L. K. Shalm et al., *Strong loophole-free test of local realism*, PRL **115**, 250402 (2015)
[2] Colbeck, R. & Kent, A. *Private randomness expansion with untrusted devices*. J. Phys. A **44**, 095305 (2011).
[3] Bierhorst et al., *Experimentally generated randomness certified by the impossibility of superluminal signals*, Nature **556**, pp. 223–226 (2018)
*[4]* Y. Zhang et al., *Experimental Low-Latency Device-Independent Quantum Randomness,* arXiv:1812.07786 [quant-ph]

# Investigations towards transmitting time and QKD signals over the same optical fibre


**Christopher Chunnilall[1*], Elizabeth Laier-English[1], Anthony Vaquero-Stainer[1,2], Adrian Wonfor[3]**

[1]*National Physical Laboratory (NPL), Hampton Road, Teddington, TW11 0LW, U.K*

[2]*Department of Physics, University of York, York, YO10 5DD, U.K.*

[3]*Centre for Advanced Photonics and Electronics, Engineering Department, University of Cambridge, CB3 0FA, U.K.*

**christopher.chunnilall@npl.co.uk*


The National Physical Laboratory (NPL) is developing techniques to perform single-photon metrology of the quantum-optical layer in QKD hardware. This capability will contribute to establishing an assurance process for quantum communications in the UK.

The UK Quantum Communications Hub, a collaboration between academia and industry, supported by the UK's National Quantum Technologies Programme, has established the UK's first quantum network to enable the trialling and testing of quantum communications products. NPL is a partner of the Hub, and is working to develop the expertise to test the quantum layers of the systems used in this network.

In a separate endeavour, NPL provides a time signal traceable to UTC(NPL) +/- 1 microsecond to the finance sector via optical fibre to enable the accurate time-stamping of financial transactions; the Precision Time Protocol is currently used, and the White Rabbit protocol is being investigated for future use. NPL also uses fibre links to enable remote frequency comparison between optical clocks. These applications normally use signal powers around 0 dBm (1 mW).

NPL, with the support of the Hub, is investigating the ability to operate QKD over fibres which are also transmitting time signals. Successful implementation would provide additional options for extending these services through their combined fibre networks. A major obstacle to implementing QKD is the significant scattering at the single-photon level which is produced by the time signals.

Initial investigations are being performed on spools of fibre in a laboratory environment, with the aim of subsequently demonstrating this capability over installed fibre links. This presentation will report on our progress towards our objective, and the characterisation of the link and hardware parameters.


*This work is funded by the UK government's Department for Business, Energy and Industrial Strategy (BEIS) and the EPSRC Quantum Communications Hub (grant no: EP/M013472/1).*

# Reliable estimation of the statistics of photons emitted from an unknown source of light

**<u>Mikołaj Lasota</u>, Marta Misiaszek, Piotr Kolenderski**

[1]*Faculty of Physics, Astronomy and Informatics, Nicolaus Copernicus University, Grudziadzka 5, 87-100 Toruń, Poland*

There are many applications of quantum photonics technologies, which require a strictly defined number of photons for their correct working. However, realistic sources of light are imperfect and the number of photons generated by them in a single pulse can be governed by various probability distributions. Precise characterization of a given source is therefore an essential condition for its reliable utilization in practice. Unfortunately, also the detection systems that can be used for this task in realistic situation are imperfect. Due to this fact, the number of photons emitted in a single pulse typically corresponds to the number of clicks registered in a detection system in non-trivial way. In effect, the estimation methods for the probabilities of emitting different number of photons often rely on precise measurement of several quantities and are unstable to the statistical fluctuations. This means that a slight change in the measured values can lead to a dramatic change in the calculated probabilities. Moreover, multipixel detectors, which offer decent photon-number resolution, are usually plagued by significant level of crosstalk, further complicating precise characterization of photon sources [1, 2, 3].

Here we present a novel approach to the problem of estimating the statistics of photons emitted from an unknown source of light by utilizing a detection system based on spatial multiplexing of four on/off single-photon detectors [4]. To this end we derive a set of analytical formulas that can be used to estimate the probabilities of producing up to four photons by the source. We also calculate the error bounds and show that the obtained formulas are relatively stable to the statistical fluctuations. To test it we perform numerical simulations of a spontaneous parametric down-conversion (SPDC) source in realistic situation. Assuming that the relative errors of all the quantities that should be measured in experiment are within 2%, we demonstrate that the expected photon statistic is recreated correctly with errors for the probabilities of emitting one, two and three photons smaller than 3%, 7% and 15% respectively. Furthermore, we show how the relevant parameters of the detection system can be estimated by using a single-mode SPDC source with unknown intensity of the generated light.

The method can be implemented using standard on/off detectors or multipixel ones. The results of our work have several applications including phase estimation utilizing multiphoton interference effects [5] and quantum optical coherence tomography [6]. They may be also used in the analysis of the number of luminescent color centers located in diamonds [7].

**References**

[1] S. Jahanmirinejad, G. Frucci, F. Mattioli, D. Sahin, A. Gaggero, R. Leoni, A. Fiore, *Photon-number resolving detector based on a series array of superconducting nanowires*, Appl. Phys. Lett. **101**, 072602 (2012).

[2] D.A. Kalashnikov, S.H. Tan, L.A. Krivitsky, *Crosstalk calibration of multi-pixel photon counters using coherent states*, Opt. Express **20**, 5044-5051 (2012).

[3] A. Divochiy, F. Marsili, D. Bitauld, A. Gaggero, R. Leoni, F. Mattioli, A. Korneev, V. Seleznev, N. Kaurova, O. Minaeva, G. Gol'tsman, K. G. Lagoudakis, M. Benkhaoul, F. L´evy, A. Fiore, *Superconducting nanowire photon-number-resolving detector at telecommunication wavelengths*, Nat. Photonics **2**, 302-306 (2008).

[4] M. Lasota, P. Kolenderski, in preparation.

[5] S. M. Barnett, J. Jeffers, A. Gatti, R. Loudon, *Quantum optics of lossy beam splitters*, Phys. Rev. A **57**, 2134-2145 (1998).

[6] D. Lopez-Mago, L. Novotny, *Quantum-optical coherence tomography with collinear entangled photons*, Opt. Lett. **37**, 4077-4079 (2012).

[7] M. Berthel, O. Mollet, G. Dantelle, T. Gacoin, S. Huant, A. Drezet, *Photophysics of single nitrogen-vacancy centers in diamond nanocrystals*, Phys. Rev. B **91**, 035308 (2015).

# Tuesday, October 22, 2019

| | | |
|---|---|---|
| 09:00 | Historical perspective by Sergio Cova | |
| 09:15 | Session 5 Detectors II<br><br>Chair: H. Zbinden | **B. Korzh - Advances in superconducting nanowire single photon detectors and related applications** |
| 09:45 | | V. Verma - Kilopixel arrays of superconducting nanowire single-photon detectors |
| 10:05 | | D.H. Smith - Multiplexed Superconducting Nanowire Single-Photon Detectors on UV-Written Silica Waveguides |
| 10:25 | | F. Martini - SNSPD readout using the amplitude multiplexing approach |
| 10:45 | Coffee break (offered by PicoQuant) | |
| 11:15 | Session 6 Metrology II<br><br>Chair: C. Chunnilall | S. Polyakov - First quantum-measurement-inspired, scalable communication protocol and its experimental demonstration |
| 11:35 | | S. Schwarz - Reconstructing ultrafast energy-time entangled two-photon pulses |
| 11:55 | | D. Fuster - Development of a plug&play single photon source using electro-optical pumping schemes |
| 12:15 | | H. Ollivier - Quantum dot based single photon sources: performance reproducibility |
| 12:35 | Platinum sponsor presentation: attocube / Quandela | |
| 12:40 | Lunch | |
| 13:55 | Session 7 Applications II<br><br>Chair: J. Matthews | **M. Lucamarini - Measurement Device Independent Quantum Cryptography** |
| 14:25 | | M. Minder - Experimental quantum key distribution beyond the repeaterless secret key capacity |
| 14:45 | | M. Avesani - Practical Source-Device-Independent Quantum random number generators |
| 15:05 | | S. Wengerowsky - In-field entanglement distribution over a 96 km and a 192 km submarine optical fibre |
| 15:25 | | S. Wengerowsky - An entanglement-based wavelength-multiplexed Quantum Communication Network |
| 15:45 | Platinum sponsor presentation: MPD /OEC | |
| 15:50 | Coffee break | |
| 16:20 | Session 8 Applications III<br><br>Chair: M. Ghioni | **K. Suhling - Time-correlated single photon counting wide-field Fluorescence Lifetime Imaging Microscopy** |
| 16:50 | | D. Tabakaev - Entangled two-photon absorption and the quantum advantage in sensing |
| 17:10 | | A. Ingle - Towards General-Purpose Passive Imaging with Single-Photon Sensors |
| 17:30 | | D. Lindell - Efficient Confocal Non-Line-of-Sight Imaging |
| 17:50 | | A. White - Realtime photon-number resolution & Imaging via photon counting |
| 18:10 | Poster session I | |
| 19:30 | End | |

# Advances in superconducting nanowire single photon detectors and related applications

**Boris Korzh**

*Jet Propulsion Laboratory, California Institute of Technology, Pasadena, 91109 CA, USA*

Given the fast progress made in improvement of superconducting nanowire single photon detectors (SNSPD) in the last decade, renewed effort has focused on understanding the fundamental limits of the detection process. A wide range of experiments have been performed across many groups to push beyond the state of the art in individual metrics, such as dark count rate, efficiency, photon number resolution, long wavelength sensitivity and timing resolution. These results have triggered significant improvements in understanding of the detection mechanism, however, gaps between experiment and theory still remain and leaves the door open for further investigations. Timing resolution in particular can be as good as 2.6±0.2 ps for visible wavelengths and 4.3±0.2 ps at 1550 nm (Fig 1a-d). This has an impact on many applications including classical and quantum communication, higher spatial resolution in laser ranging with fewer photons (Fig 1e), observation of shorter-lived fluorophores in biomedical applications and fast optical waveform capture (Fig 1f). Encouragingly, it is not believed that fundamental limits have been reached yet. The limits of photon energy cut-off are also an ongoing topic of study and single photon response has been observed out to 9.9 µm (Fig 1g) which is promising for a number of applications, including exoplanet transient spectroscopy.

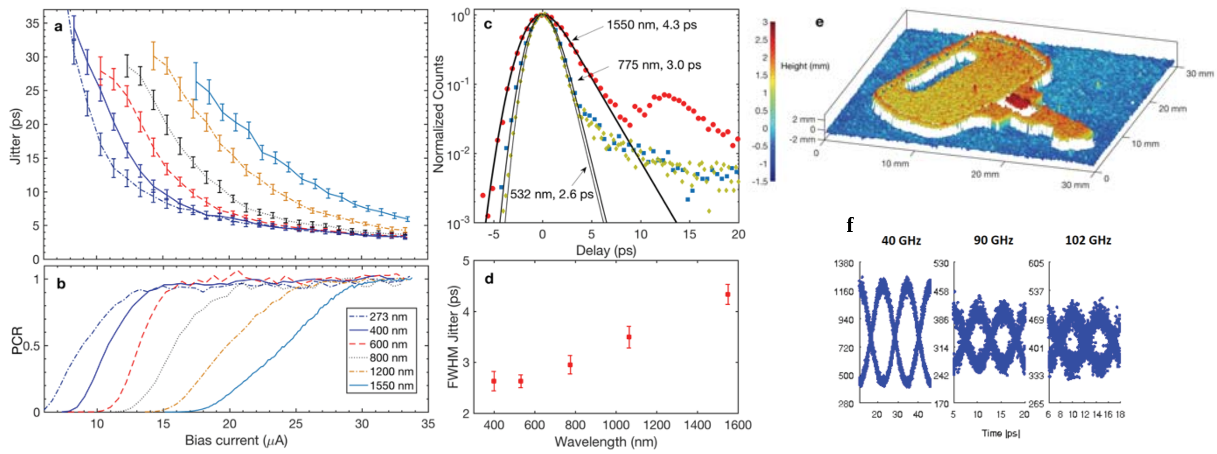


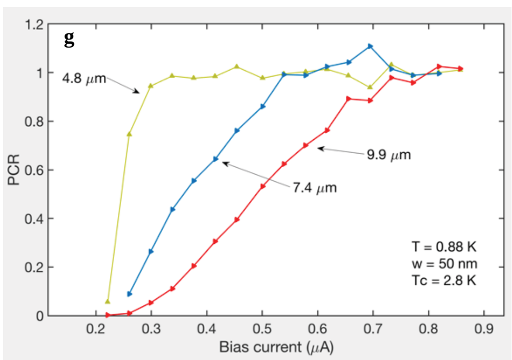


Fig. 1 (a) Jitter and (b) and internal quantum efficiency for an NbN nanowire for different wavelengths. Timing jitter histograms (c) and minimum values of jitter (d) achieved at different wavelengths for a 120 nm wide NbN detector. The saturation of jitter values in (a) and (d) suggest that external instrumental effects might contribute to the minimum values achievable. (e) Reconstructed profile of a small key achieved by scanned laser ranging over a table-top distance, using a low jitter NbN SNSPD and high-speed time-tagging electronics, demonstrating sub-millimeter resolution with as few as tens of photons. (f) The same low jitter SNSPD, allowing for waveforms as fast as 100 GHz to be captured. Small nanowire cross section and low-Tc WSi was used to demonstrate saturated internal efficiency for mid-IR light.

## References

[1] B. Korzh, Q-Y Zhao, et al, “Demonstrating sub-3 ps temporal resolution in a superconducting nanowire single-photon detector.” arxiv:1804.06839.

# Kilopixel arrays of superconducting nanowire single-photon detectors

**V. B. Verma[1], E. E. Wollman[2], A. E. Lita[1], B. Korzh[2], M. D. Shaw[2], R. P. Mirin[1], and S. W. Nam[1]**

[1]*National Institute of Standards and Technology (NIST), Boulder, CO, USA*

[1]*Jet Propulsion Laboratory (JPL), California Institute of Technology, Pasadena, CA, USA*

Superconducting nanowire single-photon detectors (SNSPDs) are a versatile class of superconducting single-photon detector with broadband sensitivity from the UV to the mid-infrared. System detection efficiencies of greater than 90% are typical in the near-infrared [1], with jitters on the order of 100 ps, maximum count rates of ~10 MHz, and dark counts lower than $10^{-4}$ cps [2]. Recently we have begun to develop large arrays of SNSPDs for applications in astronomy and chemical sensing in the mid-infrared (2 – 11 µm wavelength range) [3, 4]. The fabrication of these arrays has been made possible by drastic improvements in yield resulting from the use of amorphous superconducting materials such as WSi and MoSi.

Here we report on the fabrication and characterization of a 32 x 32 SNSPD array (1024 pixels) with an active area of 1.6 mm x 1.6 mm (Fig. 1, left). Detection events from each of the 1024 pixels are read out using the "row-column" architecture on 32 row lines and 32 column lines. This architecture has been demonstrated previously by our group in a smaller 64-pixel array [5]. Each pixel of the array consists of a meandering WSi nanowire covering an area of 30 x 30 µm, with a pixel pitch of 50 µm, yielding a fill factor of 36%. The first array tested functioned as designed with a pixel yield of 99.4%. Measurements of the array were performed at a temperature of 730 mK on a He-3 sorption cooler and illuminated with 1550 nm light using free-space optics. Figure 1 (right) shows an image of a laser spot on the array imaged through a set of three short-pass filters mounted at the 40 K and 4 K radiation shields which block room-temperature blackbody radiation while maintaining high transmission at 1550 nm. Four dead pixels are evident in black, and two "hot" pixels with elevated count rates are evident in yellow in the first and last rows. Hot pixels are indicative of relaxation oscillations likely caused by fabrication defects or "constrictions" in those pixels. The total system detection efficiency is estimated to be 4% at 1550 nm. However, this array was not embedded inside of an optical stack to enhance absorption, which could significantly increase the system efficiency in future designs. A jitter of 250 ps was attained at the highest possible bias current, and the maximum count rate is estimated to be ~ 1 GHz. Although this array has not yet been optimized for the mid-infrared (2 – 11 µm wavelengths), we will also present preliminary results on optimizing single-pixel WSi SNSPDs for this region of the spectrum, demonstrating saturation of the internal detection efficiency up to a wavelength of 10 µm.

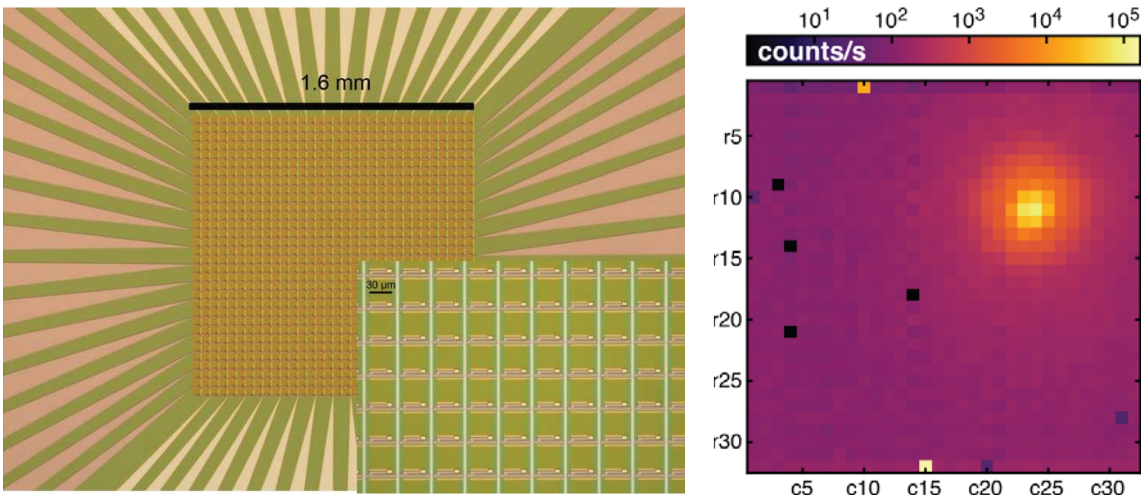


Fig. 1: 32 x 32 row-column array. Left: Magnified optical microscope image of the array active area. Inset in the lower right shows several individual 30 µm pixels, vias, resistors, and wiring layers. Right: Log-scale image of a laser spot produced by the array. 4 dead pixels are evident in black, and 2 hot pixels are seen in the top and bottom rows.

## References

[1] F. Marsili et. al, "Detecting single infrared photons with 93% system efficiency, Nat. Photonics **7**, 2-6 (2013).

[2] Y. Hochberg et. al., "Detecting Dark Matter with Superconducting Nanowires," arXiv :1903.05101 (2019).

[3] Proceedings Volume 10978, Advanced Photon Counting Techniques XIII; 109780N (2019) https://doi.org/10.1117/12.2519474

[4] The OST mission concept study team, "The Origins Space Telescope (OST) Mission Concept Study Interim Report,"arXiv1809.09702 (2018).

[5] M. S. Allman et al., "A near-infrared 64-pixel superconducting nanowire single photon detector array with integrated multiplexed readout," Appl. Phys. Lett. **106**, 192601 (2015).

# Multiplexed Superconducting Nanowire Single-Photon Detectors on UV-Written Silica Waveguides

**Devin Smith[1], David S. Phillips[2], Paolo L. Mennea[1], Varun B. Verma[3], Adriana E. Lita[3], Thomas Gerrits[3], Richard P. Mirin[3], Rex H.S. Bannerman[1], Paul C. Gow[1] Jelmer J. Renema[2,4], Robert J.A. Francis-Jones[2], Raj B. Patel[2], Santiago Sempere-Llagostera[5], Peter G.R. Smith[1], Sae Woo Nam[3], Ian A. Walmsley[2,5], and James C. Gates[1]**

[1] *Optoelectronics Research Centre, University of Southampton, UK*
[2] *Clarendon Laboratory, University of Oxford, UK*
[3] *National Institute of Standards and Technology, Boulder, CO, USA*
[4] *Complex Photonic Systems, University of Twente, Enschende, Netherlands*
[5] *Blackett Laboratory, Imperial College London, UK*

We report the first superconducting nanowire single-photon detectors (SNSPD) on an integrated silica platform. Four WSi detectors were deposited atop each of a set of waveguides inscribed by direct-UV writing, each providing a weak measurement of the guided mode. The detectors operated with a jitter of about 200 ps and a dead time of 180 ns, while the detectors each detected approximately 0.12% of the passing light with a dark count rate of 0.4 s$^{-1}$ operating at 1550 nm.

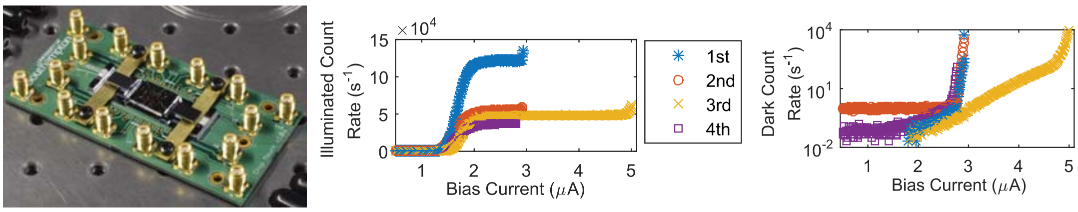


**Fig. 1:** (Left) The chip, as mounted ready for cooldown. Four SNSPDs are mounted on each of four waveguides (Centre) Calibration curves for one waveguide. The plateau on the right is the operating region. (Right) Dark count curves for the same waveguide.

The silica glass was deposited by flame hydrolysis deposition of a waveguiding and photosensitive core layer onto silicon substrate with a thermal oxide layer acting as a bottom clad and an air top clad. A 244 nm laser then inscribes the waveguides. The laser also inscribes Bragg gratings in the sample via computer-controlled two-beam interference. The mode profile of the waveguide was a compromise between coupling to fibre and the nanowires, leading to a theoretical coupling loss between the chip and fibre of 2.9 dB. We intend in future work to deposit a glass top-clad over the nanowire layer, substantially reducing coupling loss, however this was omitted here to reduce risk. In principle the coupling loss to fibre could be reduced to below 0.2 dB.

Atop these silica-glass waveguides SNSPDs can be deposited; these nanowires are identical to NIST's standard fibre-coupled WSi nanowire detectors, leading to a direct comparison of performance. Each nanowire is a 16 µm square meander of WSi deposited with the wires oriented transversely to the waveguide.

One advantage of this geometry is that the detectors can be laid across a waveguide without terminating it as the surface of the chip is flat. This allows multiple detectors to be multiplexed on a single waveguide, as minimally shown here. This can either enhance detection efficiency while providing number resolution—as each nanowire is unlikely to absorb multiple photons—or could be used with cavity enhancement to provide spectral discrimination at several spectral lines of interest. The cavities could be created by Bragg gratings surrounding the nanowire inscribed simultaneously with the waveguide.

1

# SNSPD readout using the amplitude multiplexing approach

**A. Gaggero[1], F. Martini[1], F. Mattioli[1], F. Chiarello[1] R. Cernansky[2], A. Politi[2] and R. Leoni[1]**

[1] *Istituto di Fotonica e Nanotecnologie – CNR, Via Cineto Romano 42, 00156 Roma, Italy*

[2] *Department of Physics and Astronomy, University of Southampton, Southampton SO17 1BJ, UK*

The realization of large quantum-optic experiments carried out in photonic quantum circuits is undergoing a fast development, where the number of modes composing the optical circuit is constantly growing in size. In many applications, the on-chip detection of single photons is desired to avoid the fiber-to-chip coupling losses and to grant the scalability of the platform. In this work, we address the readout of several superconducting single photon detectors (SNSPDs) by proposing a novel multiplexing scheme [1] capable to operate more than one hundred detectors with only an output port.

Fig. 1a) shows the photonic circuit employed for the implementation of the proof-of-principle of this scheme, where the light coupling is controlled by the input and out ports. Fig. 1b) and c) show the fabricated detectors, made of 80nm-wide NbN nanowires, with AuPd resistances in parallel of different values. Upon the absorption of one photon, the bias current is partially diverted in the parallel resistance and therefore the position of the firing detector is encoded in the amplitude height of the pulse generated from the SNSPD. At the output of the readout electronics, three pulses height are clearly visible (Fig. 1d): the pulses due to the firing of SNSPD1 (red squared), the pulses due to SNSPD2 (yellow squares) and finally the pulses due to the simultaneous firing of both detectors (purple squares), attesting a coincidence count. From the analysis of the noise sources in our scheme and the use of a cryogenic amplifier, we estimate that more than one hundred detectors can be read with only one coaxial cable.

This result has a tremendous importance in the field of photonic quantum technologies, where in experiments like Boson Sampling, Quantum Walk and Photonic Quantum Computing, the increasing number of modes requires the readout of arrays of single photon detectors integrated on top of a photonic chip. Differing from previous works, we could implement this scheme directly on top of a photonic circuit thanks to its compactness and simplicity. Furthermore, the work provides a complete discussion of the scalability of the system for different electronic configurations, making the results exploitable for a broad audience with different needs.

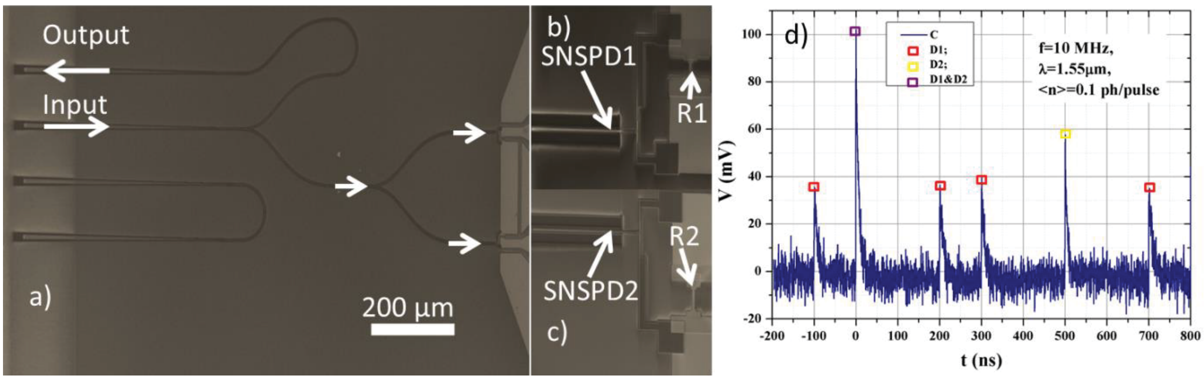


Fig. 1 a) SEM image of the photonic circuit employed for the characterization of the integrated amplitude multiplexing readout; with b) and c) are illustrated the 30um-long NbN SNSPDs with in parallel the on-chip AuPd resistances of different values. d) Oscilloscope trace of the output signals with three different pulse heights.

## References

[1] A. Gaggero, F. Martini, F. Mattioli, F. Chiarello, R. Cernansky, A. Politi, and R. Leoni, "Amplitude-multiplexed readout of single photon detectors based on superconducting nanowires," Optica **6**, 823 (2019).

# First quantum-measurement-inspired, scalable communication protocol and its experimental demonstration

**Ivan A. Burenkov[1,2], M.V. Jabir[1], Abdella Battou[1], and Sergey V. Polyakov[1,2]**

[1]*National Institute of Standards and Technology, Gaithersburg, MD, USA*
[2]*Physics Department, University of Maryland, College Park, MD, USA*

Energy efficiency per communicated bit will have the paramount significance for further advances in communication. Until recently, only classical methods were used for information exchange. Quantum mechanics allows measurements that surpass the fundamental sensitivity limits of classical methods, however it might not be obvious how to take the most advantage of quantum-enabled sensitivity for communication. We present the experimental implementation of the first communication protocol with coherent states of light that was created and optimized for quantum measurement at the receiver, [1].

Particularly, we found an encoding family whose quantum sensitivity limit (Helstrom bound) yields energy efficiency better than that of legacy classical protocols enhanced with quantum measurement for large communication alphabets M>4, i.e. when more than 2 bits are exchanged in one act of measurement. It is based on coherent frequency shift keying (CFSK) with optimized parameters of the alphabet states. The parameter space of CFSK contains frequency, phase shift detunings between the adjacent states. Note that CFSK parameter space includes a phase shift keying (PSK) protocol. PSK is popular for communication with light, because it readily lends itself to a simple, high-sensitivity classical discrimination measurement (homodyne receiver). A quantum measurement is required to improve sensitivity beyond the classical homodyne. A quantum receiver relies on adaptive displacement of the hypothesized most likely input state to vacuum, followed with single-photon detection. Unlike other quantum receivers, the CFSK receiver uses timestamps of photon detections for better sensitivity.

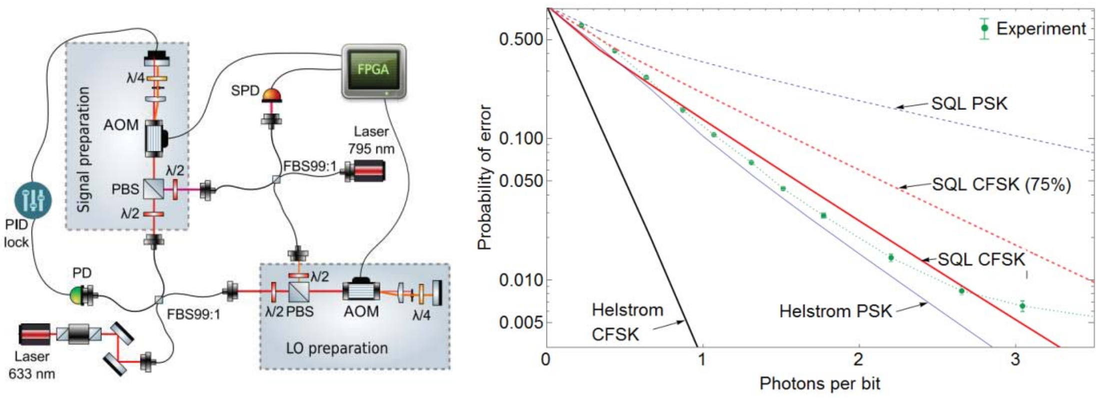


Fig. 1 Left: experimental setup. Right: Experimentally obtained sensitivity of the CFSK M=8 quantum receiver showing sensitivity below the classical SQL for ideal detection (solid red line). The CFSK quantum bound, or Helstrom bound (black solid line). SQL of a classical receiver with the same system efficiency as our receiver, 75%, is shown (dashed red line). For context, theoretical bounds of PSK are also shown: SQL (dashed blue), Helstrom (solid blue).

Classical sensitivity is bound by shot noise, known as standard quantum limit, SQL. For comparison with classical receivers, we find the most sensitive CFSK protocol parameters for idealized, classical receivers with unity system efficiency. Best attainable SQL is shown in Fig. 1 in solid red. We experimentally demonstrate sensitivity below this lowest classical bound for energy-efficient protocols with M=4 (not shown) and M=8 (Fig. 1). It is evident that our prototype receiver beats the best idealized classical receiver over the entire CFSK parameter space with as little as <1 photon per bit inputs. For further context, our CFSK if we compare our measurement to a classical measurement with the equal system efficiency, 75% (dashed red curve), our receiver demonstrates 5 dB improvement. And, obviously, our quantum receiver beats the SQL of PSK by more than 10 dB! However, our experimental results are less sensitive than Helstrom bound of PSK. We note that the difference between PSK and CFSK in sensitivity increases with increasing M. We expect that our receiver will experimentally surpass both classical and quantum sensitivity limits of the PSK.

In conclusion, we present the first experimental implementation of a quantum receiver for the first communication protocol that was designed to maximize sensitivity gain from a quantum measurement.

**References**

[1] I A Burenkov, O V Tikhonova and S V Polyakov, Optica 5, 227 (2018)

# Reconstructing ultrafast energy-time entangled two-photon pulses

**Sacha Schwarz**[1,2], **Jean-Philippe W. MacLean**[1,2], **and Kevin J. Resch**[1,2]

[1]*Institute for Quantum Computing, University of Waterloo, Waterloo, Ontario, Canada N2L 3G1*

[2]*Departement of Physics & Astronomy, Universtiy of Waterloo, Ontario, Canada, N2L 3G1*

In ultrafast optics and laser physics, the ability to measure the amplitude and phase of laser pulses on ultrafast timescales is essential for nonlinear optics and spectroscopy. Optical pulses can be produced on time scales much shorter than any photodetector response time, and consequently, the only thing fast enough to measure an ultrafast laser pulse is another ultrafast pulse. Techniques such as frequency-resolved optical gating [1] make use of nonlinear optical processes to measure and reconstruct ultrafast pulses. However, adapting them to quantum states of light is challenging due to the low power levels of single photons. In addition, the algorithms developed for laser pulses do not account for the possibility that photons can be entangled. New innovations are therefore needed to reconstruct the joint state of entangled ultrafast photon pulses.

Recovering the phase of a field from intensity measurements in Fourier-related domains is known as a phase-retrieval problem. In 1972, Gerchberg and Saxton provided a practical solution to this problem. They introduced an iterative algorithm to extract the complete wavefunction of an electron beam, including its phase, from intensity recordings in the image and diffraction planes [2].

In our work [3], we implement a technique to recover the phase of ultrafast energy-time entangled two-photon pulses based on intensity measurements of the frequency and the arrival time. Inspired by Gerchberg and Saxton, we develop an algorithm based on a method of alternate projections that iterates between the frequency and time domains imposing the measured intensity constraints at each iteration. Measurements in frequency are performed with single-photon spectrometers and measurements in time are implemented via optical gating with an ultrafast optical laser pulse.

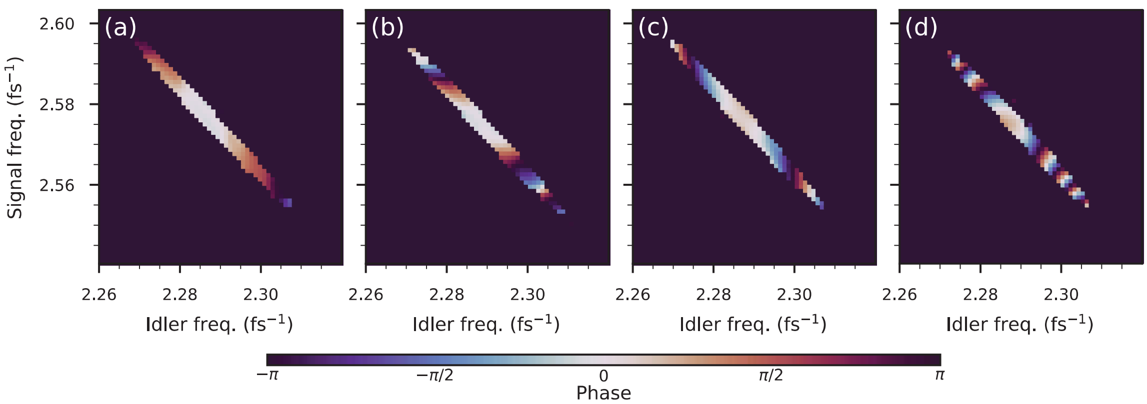


Fig. 1 Phase reconstruction of energy-time entangled states. Reconstructed joint spectral phase for energy-time entangled photon pairs with (a) no added dispersion, (b) positive dispersion on the signal, (c) negative dispersion on the idler, (d) negative dispersion on both the signal and idler. Phase points outside the 2σ intensity contours are removed for clarity. We observe (a) a relatively flat phase variation, (b) a positive quadratic phase variation along the signal axis, (c) a negative quadratic phase variation along the idler axis, (d) and a negative quadratic phase variation along both axes.

**References**

[1] D. J. Kane and R. Trebino, Single-shot measurement of the intensity and phase of an arbitrary ultrashort pulse by using frequency-resolved optical gating, Opt. Lett. 18, 823 (1993).

[2] R. W. Gerchberg and W. Saxton, A practical algorithm for the determination of phase from image and diffraction plane pictures, Optik 35, 237 (1972).

[3] J.-P. W. MacLean, S. Schwarz, and K. J. Resch, Reconstructing ultrafast energy-time entangled two-photon pulses, arXiv:1901.11116.

# Development of a plug&play single photon source using electro-optical pumping schemes

**David Fuster, José M. Llorens, Yolanda González and Benito Alén***

*Instituto de Micro y Nanotecnología, IMN-CNM,CSIC (CEI UAM+CSIC) Isaac Newton, 8, E-28760, Tres Cantos, Madrid, Spain*

Single photon and entangled photon pair sources are an essential component of QKD cryptographic systems. They are also at the heart of linear optical quantum computing integrated devices and distributed quantum computing schemes. For unattended long-life operation in potentially harsh environments, these devices shall contain the minimum number of optomechanical elements and moving parts, thus eliminating the risk of misalignment due to vibrations and/or temperature changes. Most single photon sources rely on the optical pumping of a two level system with a laser and of an accurate and delicate optical coupling between them. Thus, for the development of plug&play single photon sources, which are both alignment-free and vibration resistant, a good start would be to integrate the pumping source and the single photon source in a monolithic design. [1-3]

In this work, we will present our design for such a plug&play device [1]. It is based on a vertical multijunction heterostructure comprising quantum dots and two separated electrical injection and electrical tuning regions in a bi-polar transistor configuration. The connection between them is purely optical and thus, it naturally avoids sheet resistance problems when applied to nanophotonic devices. We will show finite element simulations of different electrical and photonic designs together with results obtained in the first fabricated devices. Our initial prototypes show single photon emission with g2(0)<0.1 at injection currents as low as 100 mA/cm$^2$ and fully linear conversion between electrical power and single photon flux.

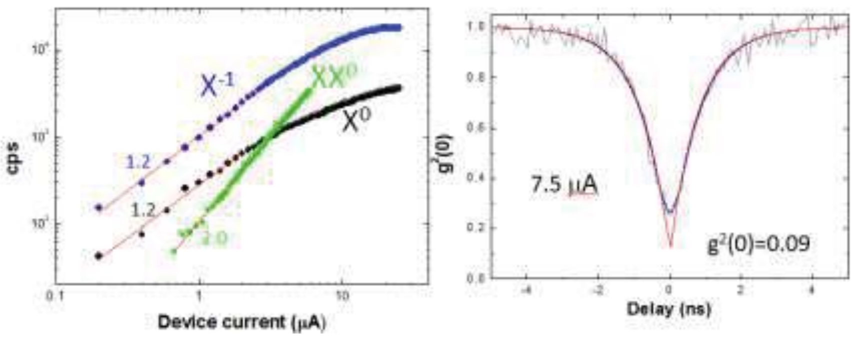


Fig. 1 Left: Single photon count rates for varying current applied to the device. Right: Second order correlation function for the negative trion.

*benito.alen@csic.es

**References**

[1] B. Alén et al "Tunable monolithic quantum light source and quantum circuit thereof" Patent pending EP/17382061.4, PCT/EP2018/052960. Date: Feb 8th 2017

[2] J. P.Murray et al "Electrically Driven and Electrically Tunable Quantum Light Sources". Appl. Phys. Lett. 2017, 110 (7), 071102.

[3]P.Munnelly et al "Electrically Tunable Single-Photon Source Triggered by a Monolithically Integrated Quantum Dot Microlaser". ACS Photonics 2017, 4 (4), 790–794.

# Quantum dot based single photon sources: performance reproducibility

**H. Ollivier[1], I. Maillette[1], G. Coppola[1], S. Wein[2], P. Hilaire[1], A. Harouri[1], A. Lemaître[1], I. Sagnes[1], L. Lanco[1,4], S. Thomas[1], J. Loredo[1], C. Anton[1], N. Somaschi[3], P. Senellart[1]**

[1] *Centre de Nanosciences et Nanotechnologies, CNRS, 91460 Palaiseau, France*

[2] *IQST and Department of Physics and Astronomy, University of Calgary, Canada*

[3] *Quandela, SAS, 86 rue de Paris, 91400 Orsay, France*

[4] *Université Paris Diderot, Paris 7, 75205 Paris CEDEX 13, France*

Quantum dots are promising candidates to generate the single photons needed to implement quantum networks. Although quantum dot indistinguishable single photon sources have already allowed an exponential speedup of quantum optics experiments, such as Boson Sampling, so far only single photons emitted by one quantum dot source have been used. Indeed, it remains to demonstrate that this technology can be reproducibly fabricated for widespread applications, an important challenge since quantum dots show natural inhomogeneity. In this presentation, we show that it is possible to produce multiple sources presenting homogeneous characteristics (operating at similar wavelengths, with comparable temporal shapes, and with consistently high efficiency, single-photon purity and indistinguishability). We benchmark the performances of a dozen sources and highlight the path towards scaling up quantum dot single-photon technology to implement the fundamental blocks for the development of future large-scale quantum networks.

Our sources are composed of quantum dots deterministically embedded in semiconductor micropillar cavities [1]. The quantum dot behaves as an artificial atom producing single photons that are efficiently collected by the cavity. We fabricate them in a deterministic and reproducible way, assuring high single-photon purity, indistinguishability and brightness [2].

We study two types of sources, corresponding to two optical transitions, based on either a neutral or a charged exciton. We discuss the physical phenomena at play rendering differences in single-photon source performance. We also propose new techniques to identify the source type and discuss how to improve their performances [3].

**References**

[1] N. Somaschi et al., Nat. Photon. 10, 340 (2016).
[2] A. Nowak et al., Nat. Commun. 5, 3240 (2014).
[3] H. Ollivier et al., submitted (2019).

# Measurement Device Independent Quantum Cryptography

**Marco Lucamarini, Zhiliang Yuan, James F. Dynes, Andrew J. Shields**
*Toshiba Research Europe Ltd, Cambridge, United Kingdom.*

Since its inception in 2012, Measurement-Device-Independent (MDI) Quantum Key Distribution (QKD) [1] (see also [2]) has grown into a well-established technique that features several remarkable properties: it overcomes all the implementation loopholes related to using sensitive detection apparatuses; it partially removes the restriction of a trusted-node architecture in a quantum network, using a single untrusted node (Charlie) to connect distant users (Alice and Bob); it improves the signal to noise ratio of point-to-point QKD, thus slightly extending its transmission range in the asymptotic scenario.

The practicality of MDI-QKD has been convincingly proven in various experiments. Nevertheless, its overall key rate remains quite modest due to a coincidence detection Charlie has to perform on the two photons sent by Alice and Bob. Moreover, MDI-QKD key rate scales only linearly with the channel transmission $\eta$, similarly to the direct-link QKD, while the presence of an intermediate node could lead, in principle, to a better scaling. Theoretical papers have shown that MDI-QKD endowed with a quantum memory has the potential to approach the scaling law of a single repeater, $O(\sqrt{\eta})$, but the realization of this proposal is still elusive (for a recent attempt see [3]).

Recently, a far more efficient form of MDI-QKD named "Twin-Field" (TF) QKD has been introduced in [4]. This new technique inherits all the security-related benefits of MDI-QKD but, as an extra, it also features the single-repeater scaling law $O(\sqrt{\eta})$ without employing a quantum memory, using only currently available technology. This makes it possible to overcome at long distance the Repeaterless Secret Key Capacity (RSKC) [5] (see also [6]), a bound that is unsurpassable with point-to-point QKD only. Overcoming this bound is the benchmark of a quantum repeater. Therefore, experiments performing TF-QKD beyond the RSKC limit [7]-[10], such as the ones in Fig. 1, are considered the first realizations of an "effective quantum repeater" [11].

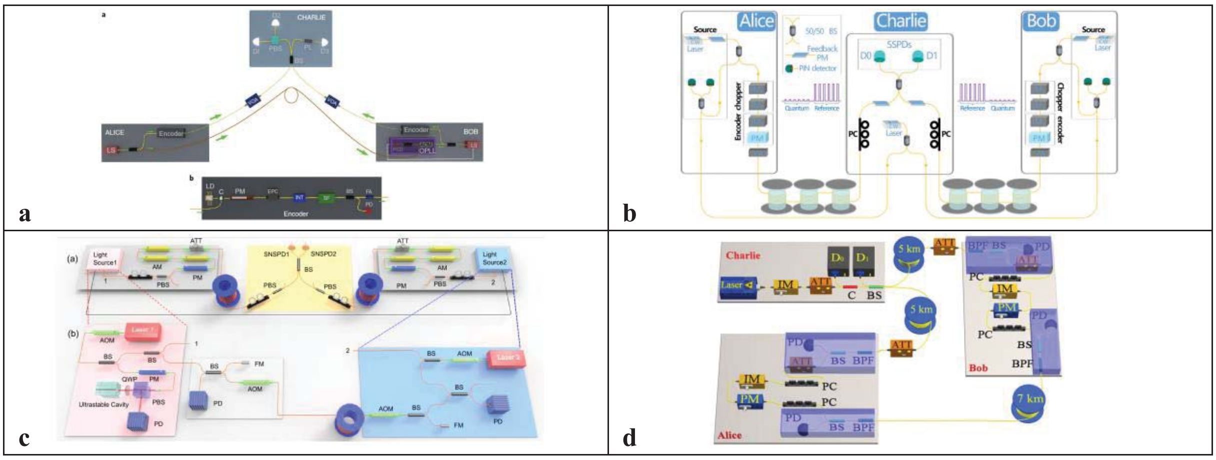


Fig. 1 – Four different experimental realisations of TF-QKD, an efficient form of MDI-QKD, in chronological order: a, Ref. [7] ; b, Ref. [8]; c, Ref. [9]; d, Ref. [10].

In this talk, I will introduce the TF type of MDI-QKD protocols and rationalise the recent literature in this rapidly evolving research area. Starting from observations on the requirements of practical implementation, I will move towards security proofs and experimental results that compose the current landscape of TF quantum cryptography.

**References**

[1] H.-K. Lo *et al*., Phys. Rev. Lett. **108**, 130503 (2012)
[2] S. L. Braunstein and S. Pirandola, Phys. Rev. Lett. **108**, 130502 (2012).
[3] M. K. Bhaskar *et al*., arXiv:1909.01323 (2019).
[4] M. Lucamarini *et al*., Nature **557**, 400 (2018).
[5] S. Pirandola *et al*., Nature Commun. **8**, 15043 (2017).
[6] M. Takeoka *et al*., Nature Commun. **5**, 5235 (2014).
[7] M. Minder, M. Pittaluga *et al*., Nature Photon. **13**, 334 (2019).
[8] S. Wang *et al*., Phys. Rev. X **9**, 021046 (2019).
[9] Y. Liu *et al*., Phys. Rev. Lett. **123,** 100505 (2019).
[10] X. Zhong *et al*., Phys. Rev. Lett. **123,** 100506 (2019).
[11] S. Pirandola *et al*., arXiv:1906.01645 (2019).

# Experimental quantum key distribution beyond the repeaterless rate-loss limit

**Mariella Minder[1,2,†*], Mirko Pittaluga[1,3†], George L. Roberts[1,2], Marco Lucamarini[1], James F. Dynes[1], Zhiliang Yuan[1], Andrew J. Shields[1]**

[1] Toshiba Research Europe, 208 Cambridge, UK

[2] Cambridge University Engineering Department, Cambridge, UK

[3] School of Electronic and Electrical Engineering, University of Leeds, Leeds, UK

† These authors contributed equally to this work.

*mariella.minder@crl.toshiba.co.uk

Quantum key distribution (QKD) allows users to generate shared encryption keys that are guaranteed to be theoretically secure by the laws of quantum mechanics. Due to the use of dim optical pulses and losses in the quantum channel, there is a fundamental rate-distance limit in QKD that was thought to be unsurpassable with current technology [1]. The recent proposal of the Twin-Field QKD (TF-QKD) protocol [2] promises to overcome this limit and predicts the same square root dependence of key rate on channel loss that a quantum repeater offers, using twin light fields to carry quantum information. Here we provide the first experimental validation of this prediction by implementing TF-QKD over channel losses exceeding 90dB. This result was achieved through an interferometric setup where the two users phase encode and randomise light fields which are sent through two quantum channels for interference at a third untrusted node. The mutual phase of the light fields was locked with an optical phase-locked loop distributed between the two users, and the phase fluctuations due to the optical channel were stabilised through an active feedback system. The acquired key rates in the high-loss regime proves for the first time that the repeaterless rate-loss limit [3] can be experimentally surpassed.

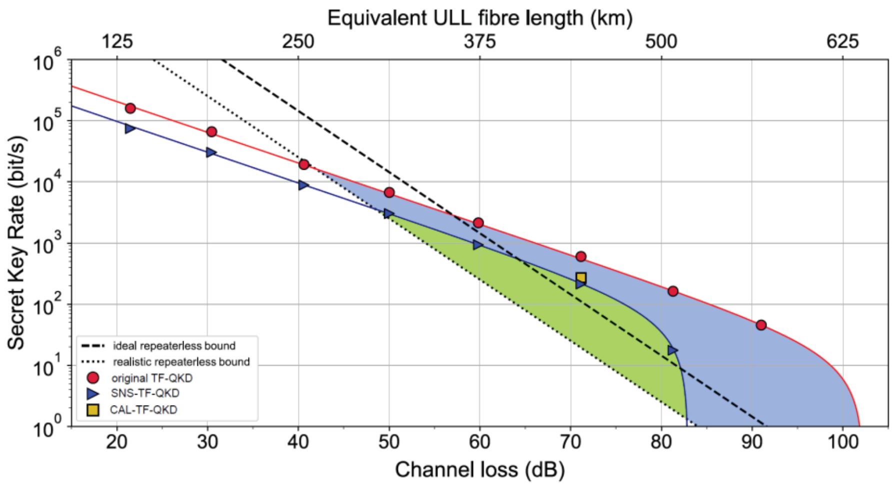


Fig. 1 **TF-QKD key rates:** Secret key rates are plotted against the channel loss (lower horizontal axis) and the corresponding ultra-low loss (ULL) fibre distance (upper horizontal axis). The markers show the acquired experimental data and the solid lines show results from simulations. The ideal repeaterless bound (dashed line) and the realistic one (dotted line) are plotted along with the key rates of the original TF-QKD protocol (red circles), the protocol in ref. [4] (blue triangles) and the protocol in ref. [5] (yellow square). The TF-QKD supremacy region is shaded in purple for conditional security and in green for unconditionally secure keys.

**References**

[1] M. Takeoka, S. Guha, and M. M. Wilde, "Fundamental rate-loss tradeoff for optical quantum key distribution," *Nat. Commun*., vol. 5, p. 5235, oct 2014.

[2] M. Lucamarini, Z. L. Yuan, J. F. Dynes, and A. J. Shields, "Overcoming the rate-distance limit of quantum key distribution without quantum repeaters: Supplementary material," *Nature*, vol. 557, no. 7705, pp. 400-403, 2018.

[3] S. Pirandola, R. Laurenza, C. Ottaviani, and L. Banchi, "Fundamental limits of repeaterless quantum communications," *Nat. Commun*., vol. 8, p. 15043, apr 2017.

[4] X.-B. Wang, Z.-W. Yu, and X.-L. Hu, "Twin-field quantum key distribution with large misalignment error," *Phys. Rev. A,* vol. 98, 062323, 2018.

[5] M. Curty, K. Azuma, and H.-K. Lo, "Simple security proof of twin-field type quantum key distribution protocol," Preprint at http://arxiv.org/abs/1807.07667, 2018.

# Practical Source-Device-Independent Quantum random number generators

**Marco Avesani[1], Davide G. Marangon[1,*], Hamid Tebyanian[1], Giuseppe Vallone[1], Paolo Villoresi[1]**

[1]*Dipartimento di Ingegneria dell'Informazione, Università degli Studi di Padova, Padova, Italia*

[*]*Now at Toshiba CRL*

Random numbers are a fundamental resource for many different applications, ranging from simulations to cryptography and tests of fundamental physics. Quantum random number generators (QRNG) offer a significative advantage over algorithmic and classical generators, where randomness is only apparent due to the determinism of the underlying processes. However, practical QRNG need to trust their internal devices and their security can be fully compromised in case of imperfections or malicious external actions. On the other hand, Device-Independent (DI) QRNG [1] don't assume anything about the devices and offer the highest level of security. Unfortunately, their experimental implementation is highly challenging and their secure generation rate, around hundred of bits/s, is not sufficient in practical scenarios. A promising approach, that combines the speed of commercial QRNG and the security of DI-QRNG, is given by Semi-Device-Independent (Semi-DI) protocols: with respect to common trusted QRNG, they require weaker assumptions on the devices (e.g, only on the source or on the measurement side), but they can achieve a generation rate dramatically larger than DI-QRNG [2].

a)

b)

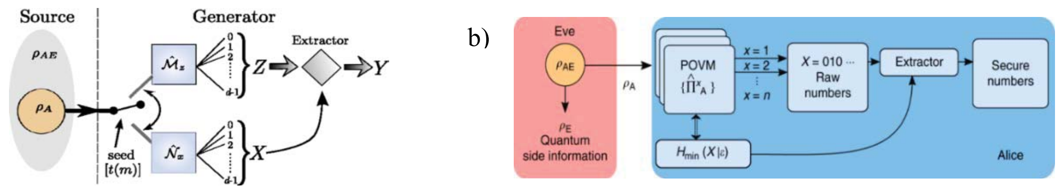


Fig. 1 Schematic representation of the protocols. a) In [3] and [4] the conditional min-entropy is bounded using the EUP and the measurements in two conjugate bases. b) In [2] and [5] the structure of the POVM bounds a priori the secure randomness.

Here, we describe a series of works [2,3,4,5] where different Semi-DI protocols are proposed and experimentally realized using photonic systems. These protocols exploit both discrete and continuous degrees of freedom of light to generate private randomness. In particular, these protocols do not assume anything about the source but require to trust the measurement apparatus. The protocol in [3] exploits the entropic uncertainty principle (EUP) to bound the number of secure random bits, expressed by the quantum conditional min-entropy. By measuring in two conjugate bases, the user can bound the purity of the unknown input state and so the quantum side information that an attacker could gain through purification. We experimentally implemented the protocol for both qubit and quart, encoded in the polarization degree of freedom of single photons. In [4] we extended the previous security proof to continuous degrees of freedom, such as the quadratures of the electromagnetic field, and the infinite-dimensional entropic uncertainty relations. The untrusted incoming state of light was measured with a homodyne receiver, where the phase of the local oscillator was set to be either 0 or $\frac{\pi}{2}$, in order to select the basis. The increased dimension of the underlying Hilbert space, together with the availability of fast homodyne detectors, enabled us to reach a secure rate of 1.7 Gbps. In [2], we employed heterodyne detection in order to measure the two quadratures simultaneously. In this way, no active switching and input randomness was required, increasing both the performance and security respect the previous protocols. We exploited the structure of the POVM implemented by the heterodyne, and their link to the Husimi Q-function, to naturally bound the private extractable randomness. Unlike previous secure QNRG, the amount of extractable randomness did not depend on the data, but only on the structure of the measurement. Thanks to these advantages, we could experimentally demonstrate a secure generation rate higher than 17 Gbps. Finally, in [5] we proposed a new method to generate and certify, in a Source-DI way, an unbounded amount of randomness from a single qubit. In particular, we showed that for particular POVMS the amount of extractable randomness scales with the number of POVM elements. We experimentally implemented the protocol using single photon qubits and POVM with 3,4 and 6 outcomes.

**References**

[1] Y. Liu et al., High-speed device-independent quantum random number generation without a detection loophole, Phys. Rev. Lett., vol. 120 (2018).

[2] M. Avesani, et al. "Source-device-independent heterodyne-based quantum random number generator at 17 Gbps." Nature Communications 9.1, 5365, (2018).

[3] G. Vallone, et al. "Quantum randomness certified by the uncertainty principle." Physical Review A 90.5 052327, (2014).

[4] D. G. Marangon, G.Vallone and P. Villoresi,. Source-device-independent ultrafast quantum random number generation. Physical review letters, 118(6), 060503, (2017).

[5] M. Avesani, et al. "Source-Device-Independent certification of unbounded randomness from a single qubit", in preparation

# In-field entanglement distribution over a 96 km and a 192 km submarine optical fibre

**Sören Wengerowsky[1], Siddarth Koduru Joshi[2], Fabian Steinlechner[3], Julien R. Zichi[4,5], Sergiy. M. Dobrovolskiy[4], René van der Molen[4], Johannes W. N. Los[4], Val Zwiller[4,5], Marijn A. M. Versteegh[5] Alberto Mura[6] Davide Calonico[6], Massimo Inguscio[7], Hannes Hübel[8], Liu Bo[1], Thomas Scheidl[1], Anton Zeilinger[1], André Xuereb[9], and Rupert Ursin[1]**

[1]*Institute for Quantum Optics and Quantum Information - Vienna, Austrian Academy of Sciences, Austria*

[2]*Present Address: Quantum Engineering Technology Labs, H. H. Wills Physics Laboratory, Bristol, UK*

[3]*Present Address: Fraunhofer Institute for Applied Optics and Precision Engineering IOF, Jena, Germany*

[4]*Single Quantum B.V., Delft, The Netherlands*

[5]*Department of Applied Physics, Royal Institute of Technology (KTH), SE-106 91 Stockholm, Sweden*

[6]*I.N.Ri.M.—Istituto Nazionale di Ricerca Metrologica, Turin, Italy*

[7]*CNR - Consiglio Nazionale delle Recerche, Rome, Italy*

[8]*AIT Austrian Institute of Technology, Center for Digital Safety & Security, Vienna, Austria*

[9]*Department of Physics, University of Malta, Msida MSD 2080, Malta*

We present the distribution of polarisation-entangled photons between the two islands Malta and Sicily using a 96 km-long submarine telecommunications fibre as a quantum channel.

The source was based on spontaneous parametric down-conversion in a nonlinear crystal (MgO:ppLN), producing pairs of photons in the telecommunications C-band around 1550.15 nm. The source was located in Malta, where one of the two photons was detected after polarization analysis in an SNSPD system. The detection system used in Sicily was more mobile and was in fact mounted in a vehicle that was moved to the location daily and connected to the submarine fibre. This detection system used SPADs. A schematic of the setup can be seen in figure 1.

We were able to observe around 260 photon pairs per second, with a polarisation visibility above 86%. We verify that polarisation-entanglement of two photons is well preserved over long distances in fibre in a real-world application scenario. Our results thus demonstrate the practicality of polarisation-entanglement-based QKD with long-distance submarine links. This opens up possibilities for future experiments and technological applications using existing infrastructure. A full-length article about this experiment is available in ref. [1].

In a second experiment we send one of the entangled photons through this cable back and forth such that two of the deployed fibres were used consecutively as a loop. Both photons were then detected in the same SNSPD system in Malta. The observed coincidence rate in this case was about 4.3 cps. The visibility of the quantum state was about 85%, mainly due to the deterioration of the signal due to accidentally identified coincident clicks. More details about this experiment can be found in ref. [2].

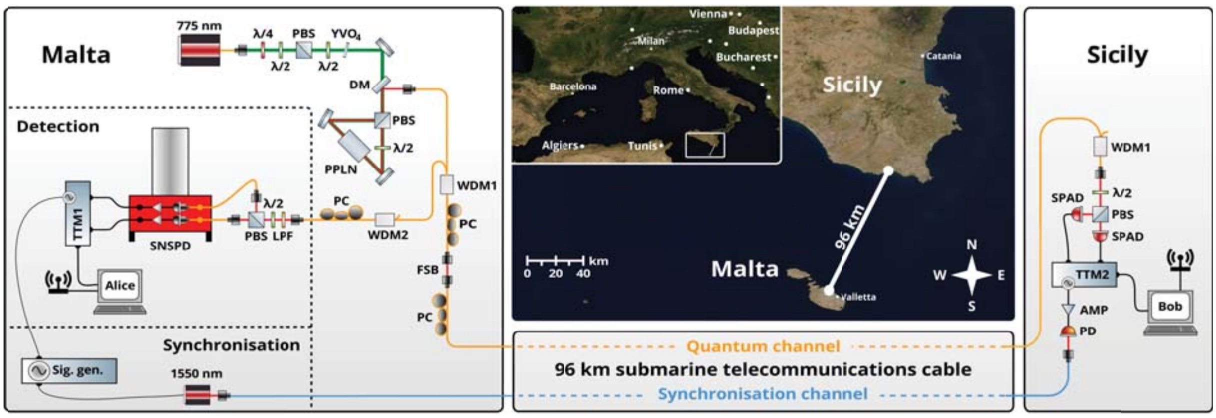


Fig. 1 Set-up and location of the experiment. The cable used here links the Mediterranean islands of Malta and Sicily. Photos courtesy of NASA Worldview. A continuous-wave laser at 775 nm bidirectionally pumped a PPLN crystal and created photon pairs via the process of spontaneous parametric down-conversion, which are entangled in polarisation due to the Sagnac geometry. Signal and idler photons are separated by frequency into two different fibres; one is detected locally in Malta in a polarisation analysis module consisting of a half-wave plate in front of a PBS and two superconducting nanowire detectors (SNSPD), and the other in Sicily after transmission through the 96 km submarine telecommunications fibre.

**References**

[1] Wengerowsky et al. Proceedings of the National Academy of Sciences Apr 2019, 116 (14) 6684-6688.

[2] Wengerowsky et al. arXiv:1907.04864

# An entanglement-based wavelength-multiplexed Quantum Communication Network

**S. Wengerowsky[1] , S. K. Joshi[1,2] , F. Steinlechner[1,3] , H. Hübel[4] , R. Ursin[1]**

[1]*Institute for Quantum Optics and Quantum Information - Vienna, Austrian Academy of Sciences, Vienna, Austria*

[2]*Present Address: Quantum Engineering Technology Labs, H. H. Wills Physics Laboratory, Bristol, UK*

[3]*Present Address: Fraunhofer Institute for Applied Optics and Precision Engineering IOF, Jena, Germany*

[4]*AIT Austrian Institute of Technology, Center for Digital Safety & Security, Vienna, Austria*

We present a proof-of-principle experiment consisting of four users in a novel network architecture which enables scalable quantum communication based on polarization-entangled photon pairs at telecommunications wavelength. Our scheme uses frequency multiplexing to share 6 two-photon entangled states between each pair of clients in a mesh-like network topology using only one fiber per client.

As clients need minimal resources - one polarization detection module and single-mode fiber each, the physical topology of the network outside the source scales linearly if a user is added, while the logical topology scales quadratically with N(N-1) network connections between N users. The quantum correlations and physical topology are illustrated in figure 1.

The source employs type-0 spontaneous parametric down-conversion centered at 1550 nm, pumped by a continuous-wave laser. The resulting 60 nm-wide spectrum is split symmetrically into 6 pairs of wavelength-correlated channels. Each client receives 3 channels which are polarization-entangled with the channels sent to each of the other clients. Every client measures all three channels in a single polarization analyzer in either the HV or DA basis and records the results using a time tagging unit. Results of the measurement of the Bell-state fidelity can be seen in figure 2. Photon pairs were identified by their relative arrival times. More details can be found in the publication [1].

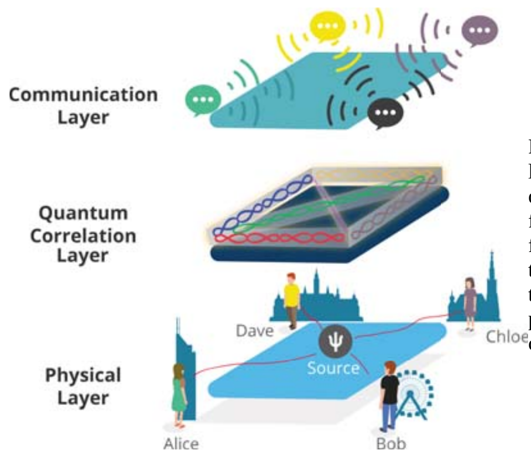


Fig. 1: Scheme of our network architecture: Different layers represent different levels of abstraction. Physical layer: contains all tangible components. Each of the 4 clients receives a combination of 3 channels via a solitary single mode fiber. Thus, the source distributes 6 bi-partite entangled photon states to the four clients Alice, Bob, Chloe and Dave. Quantum Correlation layer: shows the 6 entangled states (each corresponding to a different secure key) that link the 4 clients. Communications Layer: Entanglement-based two-party QKD protocols like E91 can be used to generate secure keys between all pairs of clients.

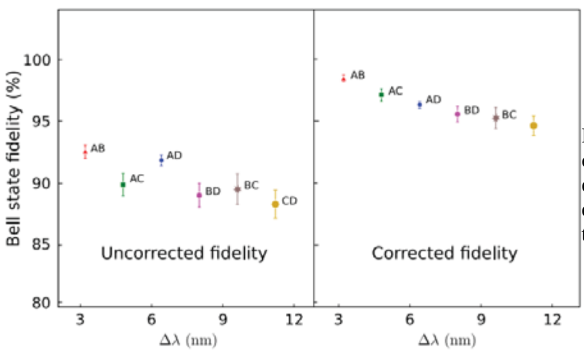


Figure 2: Measured fidelities with and without subtraction of accidental coincidences. Each point corresponds to a connection between two users, for example "AB" is between "Alice" and "Bob". The X-axis represents the difference in wavelength between the respective channels of the respective two partner photons.

**References**

[1] S. Wengerowsky, S. K. Joshi, F. Steinlechner, H. Hübel, R. Ursin, Nature 564, 225-228 (2018)

# Time-correlated single photon counting wide-field Fluorescence Lifetime Imaging Microscopy

**Klaus Suhling[1], Jakub Nedbal[1], Liisa M. Hirvonen[2]**

[1]*Department of Physics, King's College London, Strand, London WC2R 2LS, UK*

[1]*Randall Centre for Cell and Molecular Biophysics, King's College London, Guy's Campus, London SE1 1UL, UK*

Time-correlated single photon counting (TCSPC) is a widely used, sensitive, precise and robust technique to detect photon arrival times in fluorescence spectroscopy and microscopy. In confocal or multiphoton excitation fluorescence microscopy, it is often implemented with beam scanning and single point detectors. However, we have implemented a camera-based wide-field TCSPC method, where the position and the arrival time of the photons are recorded simultaneously. This has some advantages for certain types of microscopy.[1, 2]

We employ a photon counting image intensifier in combination with a 1 MHz frame rate CMOS camera, thus combining an ultra-fast frame rate with single photon sensitivity. Compatibility of this method with live-cell imaging was demonstrated by imaging europium-containing beads with a lifetime of 570 µs in living HeLa cells, as well as decays of ruthenium compound Ru(dpp) with lifetimes from around 1 to 5 µs.[3, 4] Moreover, the invariant phosphor decay of the image intensifier screen can be used for accurate timing of photon arrival well below the camera exposure time. By taking ratios of the intensity of the photon events in two subsequent frames, decays of ruthenium and iridium-containing compounds with lifetimes of around 1 µs were measured with 18.5 µs frame exposure time (54 kHz camera frame rate), including in living HeLa cells.[5] These approaches bring together advantageous features for time-resolved live cell imaging such as low excitation intensity, single photon sensitivity, ultra-fast camera frame rates and short acquisition times.

We also report on nanosecond fluorescence lifetime imaging (FLIM) microscopy based on a 40 mm diameter crossed delay line anode detector with picosecond time resolution, where the readout is performed by three standard TCSPC boards.[6, 7] We apply this wide-field TCSPC detector to FLIM of cells labelled with membrane dyes imaged with a TIRF microscope. Moreover, we demonstrate FLIM lightsheet microscopy with this detector.

**References**

[1] L. M. Hirvonen, and K. Suhling, "Wide-field TCSPC: methods and applications," Measurement Science and Technology, 28(1), 012003 (2017).

[2] K. Suhling, L. M. Hirvonen, W. Becker, S. Smietana, H. Netz, J. Milnes, T. Conneely, A. L. Marois, O. Jagutzki, F. Festy, Z. Petrášek, and A. Beeby, "Wide-field time-correlated single photon counting-based fluorescence lifetime imaging microscopy," Nuclear Instruments and Methods in Physics Research Section A, 942, 162365 (2019).

[3] L. M. Hirvonen, F. Festy, and K. Suhling, "Wide-field time-correlated single-photon counting (TCSPC) lifetime microscopy with microsecond time resolution," Optics Letters, 39(19), 5602-5605 (2014).

[4] L. M. Hirvonen, M. Fisher-Levine, K. Suhling, and A. Nomerotski, "Photon counting phosphorescence lifetime imaging with TimepixCam," Review of Scientific Instruments, 88(1), 013104 (2017).

[5] L. M. Hirvonen, Z. Petrášek, A. Beeby, and K. Suhling, "Sub-µs time resolution in wide-field time-correlated single photon counting microscopy obtained from the photon event phosphor decay," New Journal of Physics, 17(2), 023032 (2015).

[6] W. Becker, L. M. Hirvonen, J. Milnes, T. Conneely, O. Jagutzki, H. Netz, S. Smietana, and K. Suhling, "A wide-field TCSPC FLIM system based on an MCP PMT with a delay-line anode," Review of Scientific Instruments, 87, 093710 (2016).

[7] L. M. Hirvonen, W. Becker, J. Milnes, T. Conneely, S. Smietana, A. Le Marois, O. Jagutzki, and K. Suhling, "Picosecond wide-field time-correlated single photon counting fluorescence microscopy with a delay line anode detector," Applied Physics Letters, 109, 071101 (2016).

# Entangled two-photon absorption and the quantum advantage in sensing

**D. Tabakaev[1], G. Haack[1], H. Zbinden[1], R. Thew[1]**

[1]*Group of applied physics, University of Geneva, Geneva, Switzerland*

Two-photon absorption is a well-studied process, also well-known for its quadratic dependence of the absorption rate on the input flux, and thus for its inefficiency – typical two-photon absorption cross-section values for different materials are about $10^{-50}$ $cm^4$ s $photon^{-1}$, requiring high power laser pulses to compensate it. It automatically excludes samples with the low damage threshold from consideration.

More recently, the concept of entangled two-photon absorption (ETPA) has been proposed, which predicts a linear dependence of its rate on the pairs flux in the low-power regime [1,2], and provides a tool to overcome this obstacle – linear process is obviously more efficient than quadratic, althought this presents new challenges for collecton and detection of the signal. To show this signature, the ETPA induced fluorescence intensity of Rh6G in an ethanol solution was measured as a function of 1064 nm spontaneous down-converted (SPDC) Type-0 pairs flux and Rh6G concentration (Fig. 1). The corresponding Rh6G ETPA cross-sections for the mentioned wavelength were also determined for Rh6G first time.

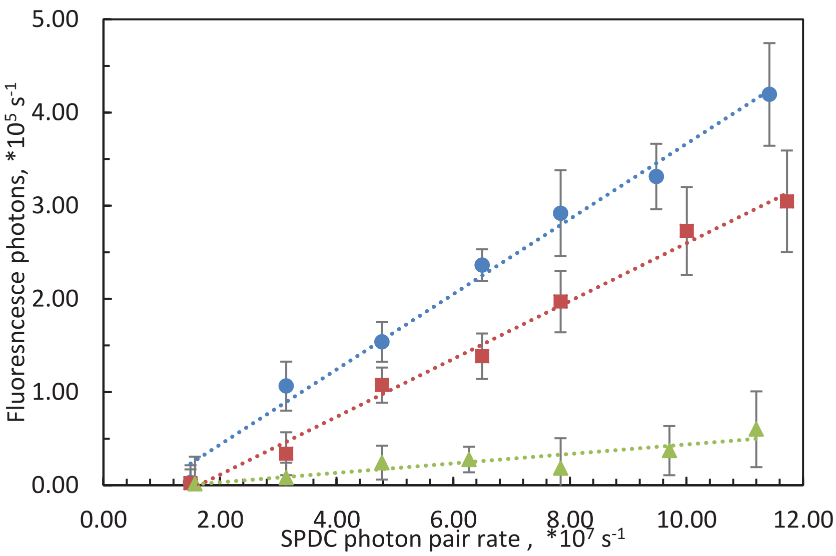


Fig. 1 The dependence of Rhodamine 6G ethanol solution fluorescence on the input flux for different concentrations: 110mM (circles); 4.5 mM (squares); 38 uM (triangles).

To clarify the role of entanglement in ETPA and its possible influence on the applications, we studied the dependence of the fluorescence intensity on a relative time delay and polarization angle of the SPDC pairs. This let us demonstrate, first to our knowledge, reliable data for ETPA in molecular systems and rule out all degrees of freedom, which seem not to contribute to ETPA-induced fluorescence.

The developed methods have possible applications in sensing, spectroscopy, imaging and fluorescence microscopy, especially for biological objects in vivo and in vitro, due to absence of any possible damage for the typical SPDC fluxes and unique combination of sharp temporal response and penetration depth, typical for pulsed two-photon absorption systems and high spectral resolution inherent to continuous-wave systems [3,4].

**References**

[1] H.-B. Fei, B. M. Jost, S. Popescu, B. E. Saleh, and M. C. Teich, Physical review letters 78, 1679 (1997)

[2] F. Schlawin, Journal of Physics B: Atomic, Molecular and Optical Physics, 50(20), 203001 (2017).

[3] B. Dayan, Physical Review A 76, 043813 (2007).

[4] B. Dayan, A. Pe'Er, A. A. Friesem, and Y. Silberberg, Physical review letters 93, 023005 (2004)

# Towards General-Purpose Passive Imaging with Single-Photon Sensors

**Atul Ingle, Andreas Velten*, Mohit Gupta***

*University of Wisconsin-Madison, Madison, WI, USA*

Single-photon avalanche diodes (SPADs) are an emerging sensor technology with a unique ability to detect individual photons with very high timing resolution. Due to these capabilities, SPADs are becoming increasingly popular in low light and active imaging applications such as LiDAR and fluorescence lifetime imaging microscopy. In this work we propose a new imaging modality that uses SPADs in a different way. We operate a SPAD passively, in ambient illumination, without any active light source to capture 2D intensity images. We call this new imaging modality *passive free-running SPAD* (PF-SPAD) [1].

**Dynamic Range of a PF-SPAD:** A PF-SPAD pixel is operated like a conventional sensor pixel where it accumulates a photon count over a fixed exposure time. Unlike a conventional image sensor pixel, the output of a PF-SPAD is a non-linear function of the incident flux and does not suffer from a hard saturation limit. This enables a PF-SPAD to operate at much higher flux levels than previously thought possible. When combined with its ability to operate in extremely low flux levels, a PF-SPAD pixel achieves extremely high dynamic range as shown in Fig. 1 (a). Observe the graceful drop in SNR at high flux levels which extends the PF-SPAD's dynamic range by several orders of magnitude. Figs. 1 (b-d) show experimental results from our single-pixel raster-scanning PF-SPAD hardware prototype with a dead-time of 150 ns. The PF-SPAD captures the extreme dynamic range (>$10^6$:1) of this table-top scene in a single exposure.

**PF-SPAD vs. Quanta Image Sensor (QIS):** A QIS uses photon counting and spatial oversampling with sub-diffraction-limit-sized pixels to obtain a non-linear (logarithmic) response curve [2]. The key distinction is that a QIS has a pre-defined frame rate at which the binary frames of photon counts are read out. A PF-SPAD pixel, on the other hand, is asynchronous by virtue of being photon-driven. This enables a PF-SPAD to *adaptively reject* a fraction of the incident photons, proportional to the incident photon flux, thus providing an even higher over-exposure latitude than a QIS's logarithmic response [3].

**Challenges:** SPAD technology is still in a nascent stage and cannot compete with CMOS and CCD array sensor technology for general-purpose passive imaging. Our work makes a case for developing high-resolution photolithography and 3D stacking techniques to realize high-fill-factor megapixel SPAD arrays with in-pixel timing and counting electronics with fully parallel readout. This will have implications for a wide range of applications including consumer photography, scientific imaging and machine vision that deal with extreme variations in scene brightness.

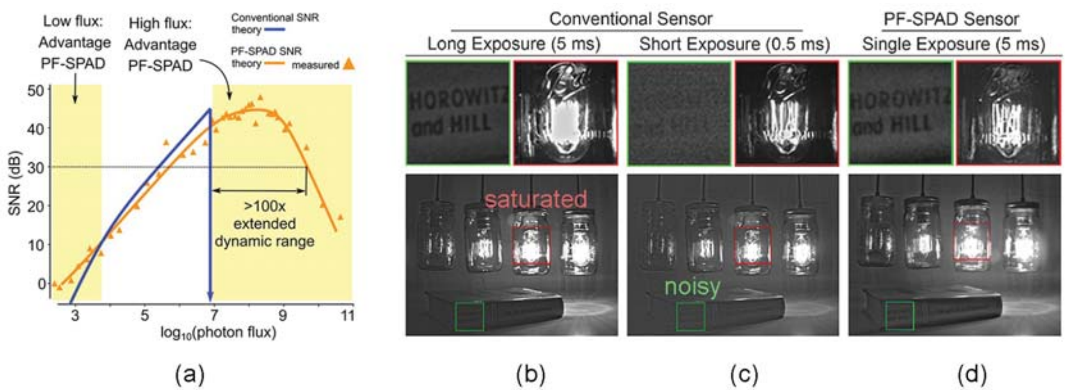


Figure 1 **Experimental Results with our PF-SPAD Hardware Prototype**: (a) SNR comparison with a conventional sensor pixel. (b-c) A conventional camera needs at least two exposures to reliably capture the bright filament and the dark text in this high dynamic range. (d) The PF-SPAD sensor simultaneoulsy captures extremely bright and extremely dark scene points in a single 5 ms exposure.

**References**

[1] Atul Ingle, Andreas Velten, Mohit Gupta, "High-Flux Passive Imaging with Single-Photon Sensors," Proc. CVPR 2019.

[2] Eric Fossum, Jiaju Ma, Saleh Masoodian, Leo Anzagira, Rachel Zizza, "The Quanta Image Sensor: Every Photon Counts," Sensors, vol. 16, no. 8, pp. 1260, 2016.

[3] Ivan Antolovic, Caludio Bruschini, Edoardo Charbon, "Dynamic Range Extension for Photon Counting Arrays," Opt. Ex., vol. 26, no. 17, pp. 22234-22248, 2018.

* Equal contribution. Research supported by ONR, DARPA and Wisconsin Alumni Research Foundation.

# Efficient Confocal Non-Line-of-Sight Imaging

**David B. Lindell[1], Matthew O'Toole[2], and Gordon Wetzstein[1]**
[1]*Department of Electrical Engineering, Stanford University, Stanford, CA 94305, USA*
[2]*Robotics Institute and Department of Computer Science, Carnegie Mellon University, PA, Pennsylvania 15213, USA*

Non-line-of-sight (NLOS) imaging enables new capabilities in a wide range of applications including autonomous vehicle navigation, remote sensing, medical imaging, and 3D scene understanding, among others. Recent approaches to solving this problem use time-resolved photodetectors and ultrafast pulsed lasers to measure the time it takes for a pulse of light to travel to a visible wall, scatter to a hidden object, and scatter back to the wall (*cf.* Fig. 1). Sensitive single-photon detectors are especially useful for this task because they capture the extreme low signal of backscattered photons from the hidden object. By capturing measurements at multiple scanned locations on the wall, the 3D geometry of the hidden object can be recovered.

Capturing and reconstructing NLOS scenes is challenging because the signal of interest from multiply scattered light is incredibly faint. Furthermore, recovering the hidden 3D geometry requires solving a large-scale inverse problem, which usually becomes prohibitive for measurements captured at high resolution or for large scenes. Moreover, NLOS light transport models usually make restrictive assumptions that the hidden objects are Lambertian (diffuse) or retroreflective. As a result, NLOS imaging has mostly been limited to small, simple scenes with limited reflectance properties reconstructed at low resolution.

We introduce efficient methods [1, 2] for NLOS imaging based on a confocal sampling scheme. Here, the laser and detector share an optical path, illuminating and imaging the same points on a visible wall. While non-confocal techniques are commonly employed to prevent saturating the detector with light returning directly from the wall (inhibiting observation of the indirect light), we find that confocal sampling is achievable and enables highly-efficient reconstruction methods. Using confocal NLOS imaging techniques, we demonstrate NLOS imaging of room-sized scenes with complex reflectance properties (shown in Fig. 1), and NLOS imaging at real-time rates and outdoors.

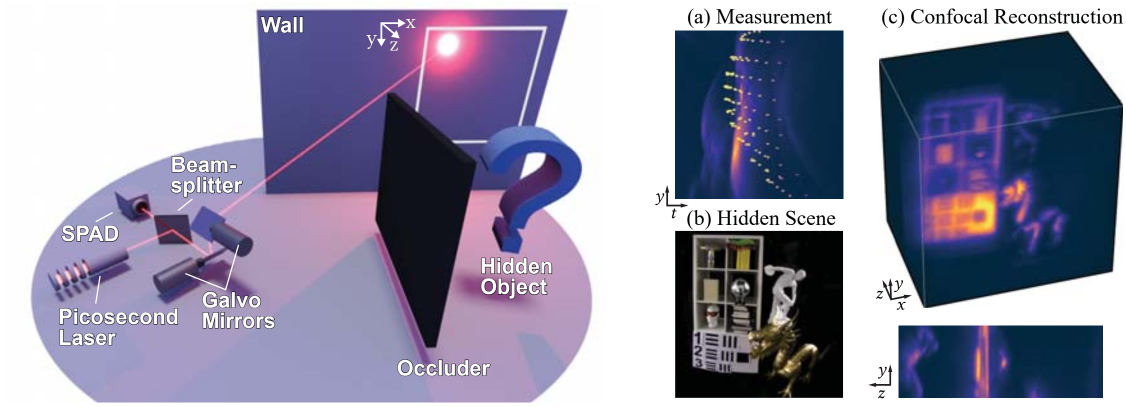


**Fig. 1.** Overview of confocal NLOS imaging. **(Left)** A confocal NLOS imaging system illuminates and images a point on a wall, measuring the time it takes for light to travel to the wall, and scatter to the hidden object and back. **(Right)** Scanning a grid on the wall produces a 3D measurement volume which captures indirect lighting effects and 3D geometry. **(a-b)** A disco ball in the hidden scene results in bright spots in a *y*-*t* slice of the captured time-resolved measurements. **(c)** The reconstruction of the confocal measurements reveals the geometry of the hidden scene.

## References

[1] M. O'Toole, D. Lindell, and G. Wetzstein, "Confocal non-line-of-sight imaging based on the light-cone transform," *Nature*, vol. 555, no. 7696, pp. 338–341, 2018.

[2] D. B. Lindell, G. Wetzstein, and M. O'Toole, "Wave-based non-line-of-sight imaging using fast f–k migration," *ACM Trans. Graph. (SIGGRAPH)*, vol. 38, no. 4, p. 116, 2019.

# Realtime photon-number resolution
# & Imaging via photon counting

**Geoffrey Gillett[1], Leonardo Assis[2,3], Lewis Howard[2,3], Thomas Gerrits[4], Sae Woo Nam[4], Mark Pearce[5], Raphael Abrahao[2,3], Till Weinhold[2,3], Pieter Kok[5], & Andrew G. White[2,3]**

[1]*Quantum Valley Ideas Laboratories, Waterloo, Canada*

[2]*Centre for Engineered Quantum Systems,* [3]*School of Mathematics and Physics, University of Queensland, Brisbane, Australia*

[4]*Faint Photonics Group, National Institute of Standards and Technology, Boulder, United States of America*

[5]*Department of Physics and Astronomy, University of Sheffield, Sheffield, United Kingdom*

*Realtime photon-number resolution.* Transition-edge sensors (TES's) are are extremely sensitive calorimeters able to measure energies of the order of a few electronvolts. They are now well-known in the quantum technology community because of their superb combination of high-efficiency— higher than 95% for photons in the near infrared range [1]—essentially zero dark counts, and photon-number resolution. One of the main challenges when working with TES's is to extract the photon-number information from the continuous output signal of the detectors. The usual procedure is to accumulate signals over some time—typically 100 GB in 20 minutes or so—and then use post-processing techniques to obtain photon-number resolution from the recorded signals [2]

Here we introduce an FPGA circuit that analyses TES signals in real-time—recording only specific characteristics such as signal area, height, and length—allowing near realtime photon-number resolution and reducing the memory requirements by orders-of-magnitude. Using this new capability, we are able to optimise the number-resolution of the detector to the range we are interested in for each new experiment.

In a preliminary study, we calibrated the TES with a weakly-pulsed 820 nm diode laser, and using just the area data from the FPGA were able to distinguish up to 15 photons, correctly assigning photon numbers with certainties higher than 95%. Defining $p_n^f$ to be the probability of assigning photon number *n* to a measurement of Fock state *f*, we measured $p_1^2 = 2 \text{ x } 10^{-7}\%$, $p_2^2 = 99.9999996\%$, & $p_3^2 = 1.5 \text{ x } 10^{-7}\%$; retaining high certainty even at large *n*, e.g. $p_{12}^{12} = 98.5\%$, $p_{13}^{12} = 0.9\%$, $p_{13}^{13} = 98.0\%$, and so on. These certainties were achieved by just using signal area, accuracy can be further improved using the other digitized characteristics, such as signal height and risetime.

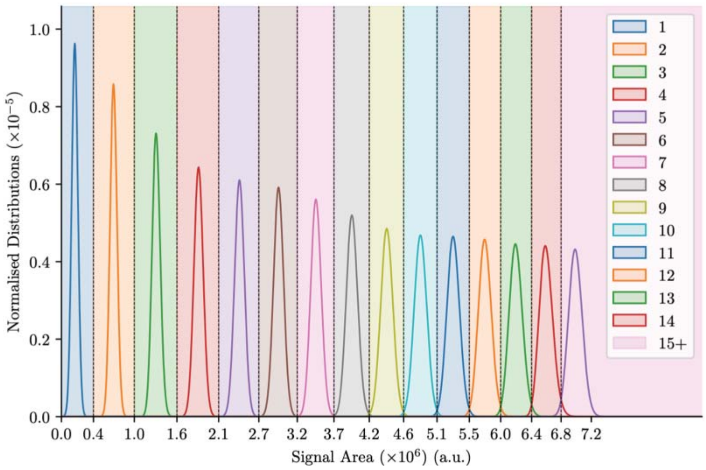


*Imaging via counting.* It is well known that there are physical limits to the precision with which an image can be formed. There are ways in which this limit can be circumvented, for example using super-resolution techniques that exploit the physical structure of the object, or object illumination with entangled states of light. However, in many applications—for example when the object is very far away—we cannot directly interact with the object, or illuminate it with entangled light: the quantum state of the light field is all that is accessible to the observer. Given a finite size imaging system in the far field—i.e., systems with a finite effective numerical aperture—we show the best way to extract the spatial characteristics of the light source.

We implement a general imaging method by measuring the complex degree of coherence using linear optics and photon-number-resolving detectors. In the absence of collective or entanglement-assisted measurements, our method is optimal over a large range of practically relevant values of the complex degree of coherence [3]. We measure the size and position of a small distant source of pseudo-thermal light, and show that our method outperforms the traditional imaging method by an order of magnitude in precision. Additionally, we show that a lack of photon-number resolution in the detectors has only a modest detrimental effect on measurement precision, further highlighting the practicality of this method as a way to gain significant imaging improvements in a wide range of imaging applications.

**References**

[1] A. E. Lita, A. J. Miller, and S. W. Nam, *Optics Express* **16**, 3032 (2008).
[2] G. Brida, et al., *New Journal of Physics* **14**, 085001, (2012).
[3] L. A. Howard, et al., "Optimal imaging of remote bodies using quantum detectors", *arXiv*:1811.02192 (2018).

## Wednesday, October 23, 2019

| | | |
|---|---|---|
| 09:00 | Session 9<br>Applications IV<br><br>Chair: F. Bussieres | **J. Matthews - Integrated Homodyne Detection for Large Scale Silicon Quantum Photonics** |
| 09:30 | | F. Ceccarelli - Low-power reconfigurable photonic integrated circuits fabricated by femtosecond laser micromachining |
| 09:50 | | P. Connolly - Multispectral single-photon imaging using high efficiency plasmonic metasurface filters |
| 10:10 | | S. Olivier - Towards an integrated quantum photonics platform on silicon for secured communications |
| 10:30 | | J. Renema - Imperfect Gaussian Boson Sampling is Classically Simulable |
| 10:50 | Coffee break (offered by ID Quantique) | |
| 11:20 | Session 10<br>Metrology III<br><br>Chair: S. Kueck | **I. Degiovanni - Light sources characterisation and optical modes reconstruction** |
| 11:50 | | Y.-L. Mao - Error-Disturbance Trade-off in Sequential Quantum Measurements |
| 12:10 | | A. Paterova - Infrared metrology with visible light |
| 12:30 | | K. Laiho - Characterizing heralded single photons from a Bragg-reflection waveguide loss-tolerantly via moment generating function |
| 12:50 | Platinum sponsor presentation: PicoQuant | |
| 12:55 | Lunch | |
| 14:10 | Session 11<br>Detectors III<br><br>Chair: A. Tosi | **B. Aull - Large-Format Image Sensors Based on Integration of Custom Geiger-Mode Avalanche Photodiode Arrays with All-Digital CMOS Circuits** |
| 14:40 | | C.-Y. Park - Room temperature operation of InP/InGaAs single photon avalanche diode |
| 15:00 | | G. Buller - Planar Geometry Ge-on-Si Single-Photon Avalanche Diode Detectors for the Short-Wave Infrared |
| 15:20 | | G. Acconcia - Fully integrated electronics for high-performance and high-speed acquisition with Single Photon Avalanche Diodes |
| 15:40 | | M. Salomoni - Future perspective of SiPM technology |
| 16:00 | Coffee break | |
| 16:30 | Session 12<br>Sources II<br><br>Chair: C. Toninelli | C.A. Solanas - Scalable interfacing of quantum photonic platforms: solid-state single-photon sources and reconfigurable photonic circuits |
| 16:50 | | T. Heindel - Single-Photon QKD using Engineered Solid-State Quantum-Light Sources |
| 17:10 | | S.D. Tchernij - Electrical control of Nitrogen – Vacancy centers in diamond |
| 17:30 | | S. Ecker - Overcoming noise in entanglement distribution through high-dimensional encoding |
| 17:50 | Transfer to Castello Sforzesco | |
| 18:30 | Guided tours of Castello Sforzesco | |
| 20:00 | Dinner at Castello Sforzesco | |
| 23:00 | End | |

# Integrated Homodyne Detection for Large Scale Silicon Quantum Photonics

**J Tasker[1], J Frazer[1], G Ferranti[1], J C F Matthews[1]**
[1]*Quantum Engineering Technology Labs, University of Bristol, Bristol, UK*

Silicon quantum photonics is emerging as a sophisticated platform to perform quantum information technology demonstrations and quantum optics experiments [1]. Recent efforts have brought together on-chip generation of correlated photon pairs using four-wave mixing, with the inherent stability of nested interferometers to program electrically the manipulation quantum states to implement large scale quantum optics experiments [2]. For example, one such recent device is a fully programmable two-qubit quantum processor that comprises more than 200 photonic components, and was used to implement 98 different two-qubit unitary operations (with an average quantum process fidelity of 93.2±4.5%), demonstrate a two-qubit quantum approximate optimization algorithm, and simulation of Szegedy directed quantum walks [3].

A requirement of any integrated quantum optics platform is the integration into the monolithic architecture of methods to measure quantum states and characterise quantum processes. To this end, we will discuss efforts to realise homodyne detection integrated with silicon-on-insulator quantum photonics in large-scale photonic circuits. We report measured performance characteristics that are sufficient to perform quantum optics experiments [4]. We will discuss how these performance characteristics can be improved by use of integrated electronics to perform the low noise amplification component of the detector, and we will show how this may perform beyond the state of the art with bulk optics and discrete electronics.

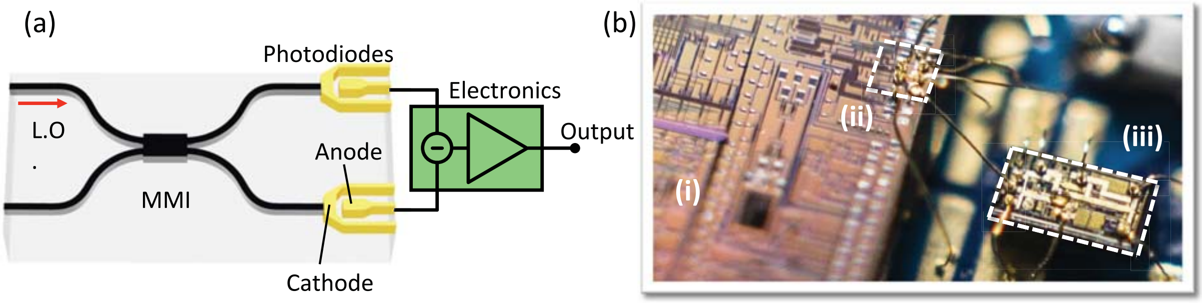


Fig. 1 (a) Cartoon of integrating the photonics for a homodyne detector, taken from [4]. Germanium-Silicon photodiodes are fabricated as part of the monolithic chip. Electronics perform substruction and amplification, for device characterisation and tomography. The device reported in [4] used discrete electronics to implement the transimpedence amplifier and demonstrated a detector bandwidth of ~150MHz, with shot noise clearance of 11dB. (b) A new device that we will report in our presentation. (i) The silicon chip hosts the photonics for a homodyne detector (ii), simular to (a). This chip is wire-bonded to integrated electronics chip (iii) to improve bandwidth to O(GHz).

**References**

[1] J. W. Silverstone, D. Bonneau, J. L. O'Brien and M. G. Thompson, Silicon Quantum Photonics, IEEE Journal of Selected Topics in Quantum Electronics, 22, 390 (2016)

[2] J. Wang et al, Multidimensional quantum entanglement with large scale integrated optics, Science, 360, 285 (2018)

[3] X. Qiang et al Large Scale Silicon Quantum Photonics Implementing Arbitrary two Qubit Processing, Nature Photonics, 12, 534 (2018)

[4] F. Raffaelli et al, A homodyne detector integrated onto a photonic chip for measuring quantum states and generating random numbers, Quantum Science and Technology, 3, 025003 (2018)

# Low-power reconfigurable photonic integrated circuits fabricated by femtosecond laser micromachining

**F. Ceccarelli[1,2], S. Atzeni[1,2], F. Pellegatta[1,2], A. Crespi[1,2], and R. Osellame[1,2]**

[1]*Istituto di Fotonica e Nanotecnologie - Consiglio Nazionale delle Ricerche (IFN-CNR), piazza Leonardo da Vinci 32, 20133 Milano, Italy.*

[2]*Dipartimento di Fisica - Politecnico di Milano, piazza Leonardo da Vinci 32, 20133 Milano, Italy.*

Femtosecond laser micromachining (FLM) [1] is a powerful technique that allows rapid and cost-effective fabrication of photonic integrated circuits, even when a complex 3D waveguide geometry is required. Such circuits are today widely exploited in diverse single-photon applications, ranging from photonic boson sampling [2] to quantum interferometry [3]. Among the features of these devices, it is worth mentioning the possibility to dynamically reconfigure the circuit by thermal phase shifting [4], a technique exploited to extend the capabilities of the device and to allow the implementation of different single-photon experiments [3]. However, integrated microheaters dissipate more than 500 mW to induce a $2\pi$ phase shift in FLM devices operating at telecom wavelength (i.e. 1550 nm) [4]. Such a high value prevents the integration of more than a few microheaters on the same chip, thus strongly limiting the complexity of the circuit.

In order to cope with this problem, we devised a new fabrication process able to reduce the power dissipation for a given phase shift of more than one order of magnitude, with no compromise either on the compactness or on the optical performance of the circuit. Thanks to a water-immersion fabrication setup, we demonstrate high-quality single-mode waveguides (0.29 dB/cm propagation losses and 0.27 dB/facet coupling losses at 1550 nm) in a borosilicate glass (Corning Eagle XG), fabricated along with isolating microstructures that are realized by water-assisted laser ablation of the substrate [5]. More specifically, two different structures are presented: isolation trenches on the sides of the heated photon path and a bridge waveguide (i.e. a structure similar to the former one, but in which the ablation is performed also under the optical path, see Fig. 1, on the left).

Both the strategies are employed for the fabrication of compact reconfigurable Mach-Zehnder interferometers (MZIs) having 127 μm interwaveguide pitch and whose microheaters are fabricated with Cr/Au, following the design guidelines reported in [6]. The experimental characterization shows a power dissipation for a $2\pi$ phase shift never attained before with FLM devices. On the one hand, interferometers featuring isolation trenches show a reconfiguration period down to 57 mW. On the other hand, bridge waveguides result in a further improvement, with a $2\pi$ phase shift that can be induced with an electrical power as low as 37 mW (Fig. 1, on the right). These results will lead to a steep increase of the device complexity attainable with the FLM technology, opening up new scenarios in both quantum information and quantum sensing applications.

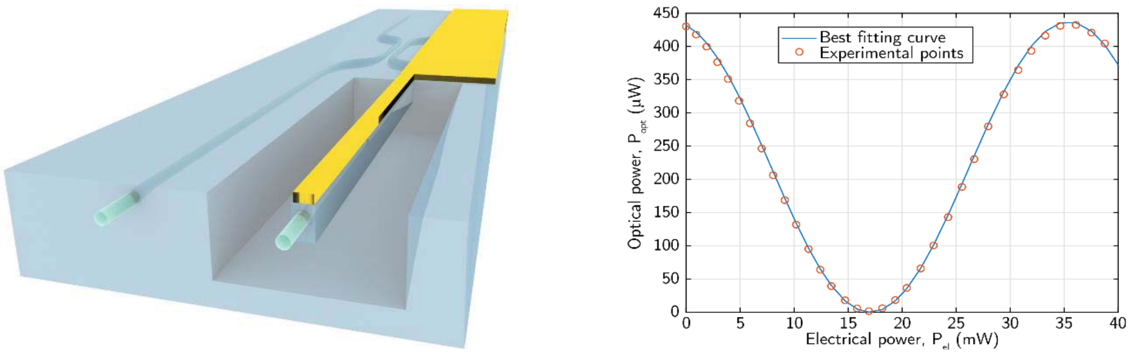


Fig. 1: On the left, 3D section of a MZI featuring a bridge waveguide under a Cr/Au microheater. On the right, optical power transmitted through a reconfigurable MZI featuring a bridge waveguide: a complete shift is achieved for a dissipated power as low as 37 mW.

**References**

[1] R. R. Gattass and E. Mazur, "Femtosecond laser micromachining in transparent materials," *Nature Photonics*, **2**(4), 219–225 (2008).

[2] A. Crespi et al., "Integrated multimode interferometers with arbitrary designs for photonic boson sampling," *Nature Photonics*, **7**(7), 545–549 (2013).

[3] E. Polino et al., "Experimental multiphase estimation on a chip," *Optica*, **6**(3), 288–295 (2019).

[4] F. Flamini et al., "Thermally reconfigurable quantum photonic circuits at telecom wavelength by femtosecond laser micromachining," *Light: Science & Applications*, **4**(11), e354 (2015).

[5] Y. Li et al., "Three-dimensional hole drilling of silica glass from the rear surface with femtosecond laser pulses," *Optics Letters*, **26**(23), 1912–1914 (2001).

[6] F. Ceccarelli et al., "Thermal phase shifters for femtosecond laser written photonic integrated circuits," *Journal of Lightwave Technology*, preprint available online (2019).

# Multispectral single-photon imaging using high efficiency plasmonic metasurface filters

**Peter W. R. Connolly[1], Yash D. Shah[2], Ximing Ren[1], Yoann Altmann[1], James P. Grant[2], Danni Hao[2], Claudio Accarino[2], Mitchell Kenney[2], Valerio Annese[2], Mohammed A. Al-Rahwani[2], Kirsty G. Rew[2], Zoë M. Greener[1], Daniele Faccio[3], Gerald S. Buller[1] and David R. S. Cumming[2]**

[1]*School of Engineering and Physical Sciences, Heriot-Watt University, Edinburgh, UK.*

[2]*School of Engineering, University of Glasgow, Glasgow, UK.*

[3]*School of Physics and Astronomy, University of Glasgow, Glasgow, UK.*

The ability to extract multispectral data from single-photon imaging systems is one which is of great interest in many areas of research including remote depth profiling, fluorescence lifetime imaging and astrophysical spectroscopy. Various approaches have been made to obtain multispectral information from single-pixel single-photon avalanche diode (SPAD) based systems, for applications including target identification [1] and physiological differentiation of arboreal samples [2], often using multi-shot approaches such as filter wheels [3], or requiring incident light to be split into its component wavelengths and directed to different detectors [4]. The development, and increased usage, of large format SPAD arrays, with 32 × 32 formats becoming relatively common, presents the opportunity to dramatically increase the speed with which images can be acquired and allows new methods of multispectral differentiation to be developed. While mosaic filtering is a relatively common approach to colour imaging in CCD cameras, the use of mosaic filters with SPAD arrays is more difficult, due in part to the relatively low transmission of typical filters. The ever shrinking pixel pitch of SPAD arrays makes fabrication of traditional thin-film based filters challenging, and the multi-stage processes required increase the likelihood of fabrication and alignment errors on this small scale.

We present the first realisation of a mosaic filter array integrated with a SPAD array. The mosaic filter array is fabricated in a single-step process utilising an e-beam written plasmonic metasurface which permits high efficiency transmission. A 4-f optical system is used to image colour targets, with a bespoke reconstruction algorithm used to reconstruct full colour images. The filters, once integrated with a SPAD array, achieved a maximum transmission of ~40% at four wavelengths representing red, yellow, blue and NIR. Filters were bonded to two CMOS Si-SPAD arrays, a 32 × 32 and a 64 × 64 array. Our bespoke algorithm was able to reconstruct colour images of a four colour target using single-photon counting.

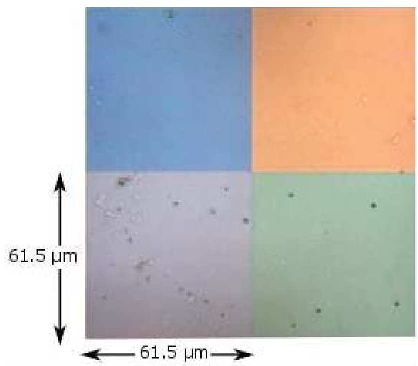


Figure 1: Reflection micrograph of four-colour mosaic filter at x50 magnification

The ability to fabricate high efficiency mosaic filter arrays in a single step, combined with the technology to quickly and accurately bond the filter to a SPAD array, opens up a host of opportunities for full colour, high-speed, single-photon imaging which could revolutionise the sector.

## References

[1] Buller G S et al 2005 Multiple wavelength time-of-flight sensor based on time-correlated single-photon counting Rev. Sci. Instrum. 76 083112

[2] Wallace A M, McCarthy A, Nichol C J, Ren X, Morak S, Martinez-Ramirez D, Woodhouse I H and Buller G S 2014 “Design and evaluation of multispectral lidar for the recovery of arboreal parameters,” IEEE Trans. Geosci. Remote Sens. 52 4942–54

[3] H. U. Keller et. al., "OSIRIS - The scientific camera system onboard Rosetta," Space Sci. Rev. 128(1-4), 433-506 (2007).

[4] G.S. Buller, R.D. Harkins, A. McCarthy, P.A. Hiskett, G.R. MacKinnon, G.R. Smith, R. Sung, A.M. Wallace, R.A. Lamb, K.D. Ridley, J.G. Rarity, "A multiple wavelength time–of–flight sensor based on time–correlated single–photon counting," Rev. Sci. Instrum., 76 (8), 083112 (2005)

# Towards an integrated quantum photonics platform on silicon for secured communications

**S. Olivier[1], C. Sciancalepore[1], H. El Dirani[1], K. Hassan[1], R. Rhazi[1]**
**C. Agnesi[2], G. Vallone[2]**
**D. Bacco[3], Y. Ding[3], K. Rottwitt[3]**
**F. A. Sabattoli[4], M. Galli[4], D. Bajoni[4]**

[1] *Univ. Grenoble-Alpes, CEA-LETI, 17 av. des Martyrs, 38000 Grenoble, France.*
[2] *Dipartemento di Inegneria del'Informatione, Universita degli Studi di Padova, via Gradenigo 6B, 35131, Padova, Italy*
[3] *DTU Fotonik, Department of Photonics Engineering, Technical University of Denmark, Orsteds Plads 340, 2800 Kgs. Lyngby, Denmark*
[4] *Dipartimento di Fisica, Università degli Studi di Pavia, via Bassi 6, 27100 Pavia, Italy*

When a fault-tolerant computer will be available, the classical encryption/decryption methods will no longer be secure. Quantum communications and quantum Key Distribution (QKD) have made large progress over the last 20 years but are still challenged by major barriers. In particular, low-cost and scalable integrated technology will be required to build QKD-secured fiber-based quantum communication networks compatible with the existing fibre infrastructure and the co-existence with classical channels.

Silicon photonics based on CMOS technology is very attractive to build compact, low-cost and scalable quantum photonics integrated circuits addressing the requirements of (Measurement) Device Independent (MDI) QKD protocols. Silicon photonics technology has now reached a high level of maturity for datacom and telecom applications with the development of high-speed and energy efficient optical transceivers. For this purpose, we have developed a full library of components, and associated technology on 200 mm SOI substrates, for efficiently coupling/decoupling light to/from a silicon photonics chip, for multiplexing several wavelength channels, for high-speed modulation and detection at 50 Gb/s and for integrating hybrid III-V/Si laser sources using direct bonding [1]. Recently, ultra-low loss monomode silicon waveguides below 1 dB/cm were achieved thanks to hydrogen annealing after etching to reduce the roughness of the walls [2].

Building further on this platform, we aim at developing a versatile Q-grade platform for fully integrated quantum transmitters and receivers based either on superposition or entanglement approaches and combining both quantum and classical channels [3]. For the superposition approach, we are developping hybrid III-V/Si lasers, high-rejection filters and variable optical attenuators to generate weak coherent pulses (WCPs). As a preliminary result, we show the experimental observation of Hong-Ou-Mandel interference with 46% visibility between WCPs generated by two independent III-V/Si integrated lasers emitting around 1550 nm wavelength. For the entanglement approach, efficient sources of photon pairs based on spontaneous four-wave mixing, possibly integrated with hybrid III-V on Si pump lasers, and high rejection pump filters are required. As a first step, we demonstrate high-Q micro-ring resonators (loaded Q factor around $4.10^5$) generating heralded photon pairs at a rate of 3.1 MHz for 136 µW pump power.

For both approaches, we are also developing high quality NbN superconducting material on our 200 mm platform to build single photon detectors.

These results pave the way for a fully Q-grade silicon photonic platform on 200 mm or 300 mm SOI substrates for future complex integrated quantum transmitter and receiver circuits meeting the requirements of advanced QKD protocols.

**References**

[1] B. Szelag et al., "CMOS compatible 200 mm silicon photonics platform suitable for high bandwidth applications", International Conference on Solid State Devices and Materials (SSDM), August 2017

[2] C. Bellegarde et al., "Improvement of sidewall roughness of submicron SOI waveguides by hydrogen plasma and annealing", IEEE Photon. Technol. Lett.30 (2018)

[3] https://www.era-learn.eu/network-information/networks/quantera/quantera-call-2017/silicon-photonics-for-quantum-fibre-networks

[4] H. El Dirani et al., "Low-loss silicon technology for high-Q bright quantum sources", oral presentation at Group IV Photonics, Singapore, August 2019.

[5] C. Agnesi et al., "Hong-Ou-Mandel interference between independent III-V on silicon waveguide integrated lasers", Opt. Lett 44, 271 (2019)

**Acknowledgments**

The authors acknowledge funding from the IRT-Nanoelect, DOPT 2020 (CEA-Leti) and QuantERA SQUARE projects.

# Imperfect Gaussian Boson Sampling is Classically Simulable

**J. J. Renema[1)]**
[1]*Adaptive Quantum Optics Group, Mesa+ Institute for Nanotechnology, University of Twente, Enschede, the Netherlands*

Demonstrating a quantum advantage is the next major milestone in experimental quantum information processing. In photonics, this takes the form of boson sampling [1], where a set of single photons are sent through a linear unitary network followed by single photon detection. Under reasonable complexity-theoretic assumptions, the problem of sampling from the output distribution of such a device is believed to be hard.

However, pure on-demand single photons are not readily available. This has led to the proposal of variants of boson sampling, where different quantum states are sent to the interferometer. One leading contender is Gaussian boson sampling (GBS), which involves sending two-mode squeezed states to a linear interferometer and performing photon counting at the output. Unlike regular boson sampling, there is no general hardness proof for GBS: all hardness proofs work by reduction to specific (exponentially unlikely) cases.

A further problem is the sensitivity to noise. A quantum advantage demonstration is only meaningful if a realistic implementation cannot be simulated by an algorithm that somehow uses the noise in the system to achieve an classically efficient simulation. The two main sources of noise in a boson sampler are photon distinguishability and optical loss.

In recent work [2 3], we outlined a strategy to simulate boson sampling in the presence of imperfections, including distinguishability and loss. We showed that for any level of imperfections, boson sampling is efficiently classically simulable above some given size of the boson sampler. Using this result, we computed the quality of optical components (sources, detectors, interferometers) required to outperform a supercomputer (and hence demonstrate a quantum advantage) using photonics.

In this presentation, I will review these results, and show their extension to arbitrary input quantum states, including Gaussian states. I will present 3 results: first, I will show that for weak squeezing, Gaussian boson sampling passes our hardness test. Second, I will show that strong squeezing also constitutes an imperfection, due to emission of double photon pairs. I will give an upper bound on the permissible level of squeezing in Gaussian boson sampling. Third, I will show that Gaussian boson sampling is at least as susceptible to noise as regular boson sampling.

These results show that while the hardness of Gaussian boson sampling remains unproven in the general case, there is at least some evidence of hardness using the latest simulation techniques. Furthermore, these results show that while Gaussian boson sampling successfully solves the problem of lack of deterministic single-photon sources, it inherits the strong noise sensitivity of regular boson sampling. I will discuss what these results imply for the amount of experimental resources necessary to demonstrate a quantum advantage using Gaussian states.

**References**

[1] S. Aaronson, A. Arkhipov, Theor. Comput. **9** 143–252 (2013).
[2] J.J. Renema *et al*, Phys. Rev. Lett. **120** (22), 220502 (2018).
[3] J.J. Renema, V. Shchesnovich, R. Garcia-Patron, arXiv: arXiv:1809.01953 (2018).

# Light sources characterisation and optical modes reconstruction

**I. P. Degiovanni[1], P. Traina[1], E. Moreva[1], J. Forneris[2], F. Piacentini[1], S. Ditalia Tchernij[3], E. Bernardi[1], G. Brida[1], I. Burenkov[4], E. A. Goldshmidt[5], S. V. Polyakov[4], P. Olivero[3], M. Genovese[1]**

[1]*INRIM, Strada delle cacce 91, 10135 Torino, Italy*

[2] *Istituto Nazionale di Fisica Nucleare (INFN) Sez. Torino, 10125 Torino, Italy*

[3] *Physics Department and "NIS" inter-departmental Centre–University of Torino, 10125 Torino, Italy*

[4] *National Institute of Standards and Technology, Gaithersburg, MD, USA*

[5] *Army Research Laboratory, Adelphi, MD, USA*

In single-photon metrology [1] the characterization of the emission statistics of the sources in order to quantifying the non-classical properties is of the utmost importance, i. e. the quality of the single photon state produced. This is particularly relevant in quantum cryptography, where uncontrolled fluctuations in the number of photons may open serious security issues. The most used parameter for this characterization is the second order Glauber's correlation function (g(2)) [3], which, despite having the advantage of being independent of the quantum efficiency of the detectors, has also several drawbacks, especially when one aims at the characterization of clusters of emitters or single emitters in noisy background. For these systems, new tools based on parameters that are resilient to noise and exploiting multifold coincidence events are being proven to be effective in specific contexts. In this framework we will report on the first experimental demonstration of a recently proposed criterion (Filip's $\theta$ function) [4] addressed to detect nonclassical behavior in the fluorescence emission of ensembles of single-photon emitters (applied in particular to clusters of Nitrogen-Vacancy centres in diamond) [5]. In a nutshell, the difference between the Glauber's and the Filip's functions is that the former relies on the multi-detection of photons in coincidence, while the latter relies on simultaneous "non-detection" of photons. We will introduce simulation results on the application of a novel technique exploiting higher order Glauber's and Filip's functions ($\theta(n)$ and $g(n)$ with $n > 2$) simultaneously to entirely reconstruct the modes hidden in more complex optical fields such as, e.g., single photon sources in a noise-bath. This mode reconstruction method is based on optimisation algorithms requiring as input data, as said, higher order Glauber's and Filip's functions (that are somehow connected to high order moments of the statistics of the input photons), whose associated uncertainties increase with the order. We show that the use of both $\theta(n)$ and $g(n)$ (rather than using only $g(n)$ as it was done in the past [2]) allows to reduce the functions order necessary to carry on the reconstruction, hence improving its performances.

**References**

[1] C.J. Chunnilall, I.P. Degiovanni, S. Kück, I. Müller, and A. G. Sinclair, Opt. Eng. 53, 081910 (2014)
[2] E.A. Goldschmidt, F. Piacentini, I. Ruo Berchera, S.V. Polyakov, S. Peters, S. Kück, G. Brida, I.P. Degiovanni, A. Migdall, and M. Genovese, Phys. Rev. A 88, 013822 (2013)
[3] P. Grangier, G. Roger, and A. Aspect, Europhys. Lett. 1, 173 (1986)
[4] L. Lachman, I. Slodicka, and R. Filip, Sci. Rep. 6, 19760 (2016)
[5] E. Moreva, P. Traina, J. Forneris, I. P. Degiovanni, S. Ditalia Tchernij, F. Picollo, G. Brida, P. Olivero, and M. Genovese, Phys. Rev. B 96, 195209-1 (2017)

# Error-Disturbance Trade-off in Sequential Quantum Measurements


**Ya-Li Mao[1,2,3,4], Qi-Chao Sun[3,4], Qiang Zhang[3,4], Jingyun Fan[1,2,3,4], and Jian-Wei Pan[3,4]**

[1] *Center for Quantum Computing, Peng Cheng Laboratory, Shenzhen 518055, China*
[2] *Shenzhen Institute for Quantum Science and Engineering and Department of Physics, Southern University of Science and Technology, Shenzhen 518055, China*
[3] *Shanghai Branch, National Laboratory for Physical Sciences at Microscale and Department of Modern Physics, University of Science and Technology of China, Shanghai 201315,China*
[4] *Shanghai Branch, CAS center for Excellence and Synergetic Innovation Center in Quantum Information and Quantum Physics, University of Science and Technology of China, Shanghai 201315, China*


Uncertainty is an essential feature of quantum mechanics, which underlies the quantum measurement and the emerging quantum information science and is best reflected in the joint measurements of a pair of noncommutative observables $\hat{A}$ and $\hat{B}$. For sequential (or joint) measurements which is an important aspect of the quantum uncertainty principle, a simple and intuitive tradeoff between the error $\varepsilon(\hat{A})$ and the disturbance $\eta(\hat{B})$ has remained a long sought goal. Heisenberg's intuition, $\varepsilon(\hat{A})\eta(\hat{B}) \geq \frac{1}{2}|\langle[\hat{A},\hat{B}]\rangle|$ [1], was negated in the experiments. Here, we show that the error and disturbance quantified by the statistical distances of probability distributions in the sequential measurements are naturally constrained by a triangle inequality for statistical distance. This relation satisfies the natural and significant requirements for operational error and disturbance, is free of the shortcomings of Ozawa's relation and state-dependent [2].

Consider a given quantum state $\rho$ and two observables, $\hat{A} = \sum_i a_i\hat{A}_i$ and $\hat{B} = \sum_i b_i\hat{B}_i$, where $\{\hat{A}_i\}$ $\{\hat{B}_i\}$ and $\{a_i\}$ and $\{b_i\}$ are the projective measurements. $p_{ai} = \langle\hat{A}_i\rangle$ ($p_{bi} = \langle\hat{B}_i\rangle$) is the measurement probability with respect to $\{a_i\}$ ($\{b_i\}$). We define the statistical distance, $\zeta_{\hat{A}\hat{B}} := \sum_i |p_{ai} - p_{bi}|$. In the general measurement model, we introduce $\{\hat{M}_i\}$ on the meter state, $\hat{C}_i = \hat{U}^\dagger(\hat{I}\otimes\hat{M}_i)\hat{U}$ and $\hat{D}_i = \hat{U}^\dagger(\hat{B}_i\otimes\hat{I})\hat{U}$ are general measurements associated with $\hat{A}$ and $\hat{B}$, with the probabilities $p_{ci} = \langle\hat{C}_i\rangle$ and $p_{di} = \langle\hat{D}_i\rangle$. We define the error and disturbance as $\varepsilon(\hat{A}) = \zeta_{\hat{A}\hat{C}} = \min\sum_i |p_{a\sigma(i)} - p_{ci}|$ and $\eta(\hat{B}) = \zeta_{\hat{B}\hat{D}} = \min\sum_i |p_{b\sigma(i)} - p_{di}|$. Assume $\varepsilon(\hat{A}) = \sum_i |p_{ai} - p_{ci}| = \sum_i |p_{a\sigma(i)} - p_{c\sigma(i)}|$ (similarly for $\eta(\hat{B})$), we define $\xi_{G,max} = \max\xi_G = \max|\sum_i[|p_{a\sigma(i)} - p_{bi}| - |p_{c\sigma(i)} - p_{di}|]|$, where the minimization (maximization) takes over all index permutations $\sigma(i)$ of $i$. We then reach the following theoretical result:

**Theorem.** The sequential measurements associated with observables $\hat{A}$ and $\hat{B}$ satisfy the following error-disturbance tradeoff,

$$\varepsilon(\hat{A}) + \eta(\hat{B}) \geq \xi_{G,max}. \tag{1}$$

We present an experimental verification of relation (1) with the measurements of a pair of noncommutative

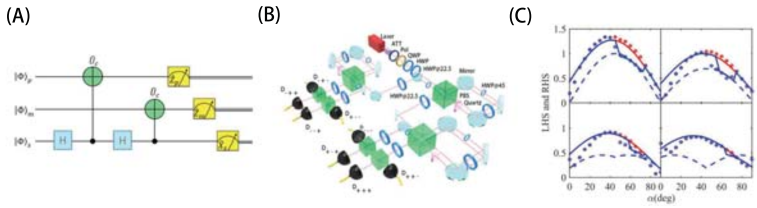


Fig. 1: (A) Quantum circuit model of measuring observable $\hat{X}$ ($\hat{Z}$) with (without) applying Hadamard gates $\hat{H}$. The system qubit $|\Phi\rangle_s = \cos\alpha|0\rangle_s + e^{i\phi}\sin\alpha|1\rangle_s$ is sequentially coupled (via a unitary operation $\hat{U}_C$) to a probe qubit, $|\Phi\rangle_p = \gamma|0\rangle_p + \bar{\gamma}|1\rangle_p$, and a meter qubit, $|\Phi\rangle_m = \cos\theta|0\rangle_m + \sin\theta|1\rangle_m$, with measurement outcomes $z_p$, $z_m$ and $x_s$, respectively. (B) Experimental schematics. we encode the system, probe and meter qubits using the polarization and path degree-of-freedoms of single photons, respectively. The unitary coupling $\hat{U}_C$ is implemented by a Sagnac interferometer. Pol: polarizer, ATT: attenuator, QWP (HWP): quarter (half) wave plates, PBS: polarization beam splitter, Quartz: quartz plate, HWP@45 (22.5): A HWP is set to 45°(22.5°) oriented from the vertical, D: single photon detector. (C) Experimental measurements of the LHS and RHS of relation (1). From (a) to (d), $\theta$ in the measurement strength $\cos 2\theta$ is set to 0°, 9°, 18°, and 27°, respectively. We set $\gamma = 0.766$. LHS: red, RHS: blue. Dashed line: ideal theory, smooth line: theory corrected with the imperfection in PBS, circles and dots: experimental results.The error bars stand for one standard deviation, assuming Poissonian statistics.

Pauli operators $\hat{A} = \hat{Z}$ and $\hat{B} = \hat{X}$ on a photonic qubit system. The quantum circuit and experimental setup are given in Fig. 1(A) and Fig. 1(B), respectively. As shown in Fig. 1(C), for the linearly polarized system qubit, $|\Phi\rangle_s = \cos\alpha|0\rangle_{pol} + \sin\alpha|1\rangle_{pol}$, we vary the linear polarization of system qubit and the measurement strength. we plot the values of the left and right hand side (LHS/RHS) of relation (1). They generally coincide with each other with a few exceptions that the LHS and is greater than RHS. By incorporating the imperfection of PBS, we theoretically reproduce the experimental observations, hence verifying the error-disturbance relation (1) [3].

## References


1. W. Heisenberg, Zeitschrift fur Physik 43, 172 (1927).
2. K. Korzekwa, et al., Phys. Rev. A 89, 052108 (2014) .
3. Y. Mao, et al.,Phys. Rev. Lett. 112, 090404 (2019).

# Infrared metrology with visible light


<u>Anna Paterova</u>[1], Hongzhi Yang[1], Chengwu An[2], Dmitry Kalashnikov[1] and Leonid Krivitsky[1]

[1] *Institute of Materials Research and Engineering, Agency for Science Technology and Research (A*STAR), 138634 Singapore*
[2] *National Metrology Centre, Agency for Science Technology and Research (A*STAR), 118221 Singapore*
e-mail: Paterova_Anna@imre.a-star.edu.sg


The infrared (IR) spectroscopy and imaging are used for many applications, including sensing, bio-imaging. Recently, an approach to the IR metrology was suggested, which is based on using optical instruments for the visible range [1, 2]. The idea is to use the nonlinear interference of spontaneous parametric down conversion (SPDC) radiation from two nonlinear crystals set into a common pump beam. The SPDC photon pairs are generated in non-degenerate regime, where signal and idler SPDC photons have visible and IR range wavelengths, respectively. Both signal and idler SPDC photons propagate thought the gap between crystals, where a medium of interest can be inserted. The interference of the signal SPDC photons in such scheme depends on the phase and amplitude of the idler photons as well. As a result, absorption and refractive index of the sample in the IR-range can be inferred from the interference pattern of visible photons.

In the current work we demonstrate the method of IR metrology using a nonlinear Michelson interferometer, where only one nonlinear crystal in used and SPDC photons can be generated at the forward and backwards paths of the pump beam though the crystal (see Figure 1a). The signal and idler SPDC photons are split into different paths (visible and IR) in the interferometer, and sample under study is placed in the path of idler photons only. Current configuration of the interferometer allows multiple type of measurements, including IR spectroscopy [3], IR optical coherence tomography (OCT) [4], IR imaging and IR polarimetry [5]. Figure 1(b-d) demonstrates results for the IR spectroscopy, IR OCT and IR imaging, respectively. The demonstrated technique of the IR metrology shows good agreement of the measurements with theoretical values, which promotes the possibility of the practical applications of the method.

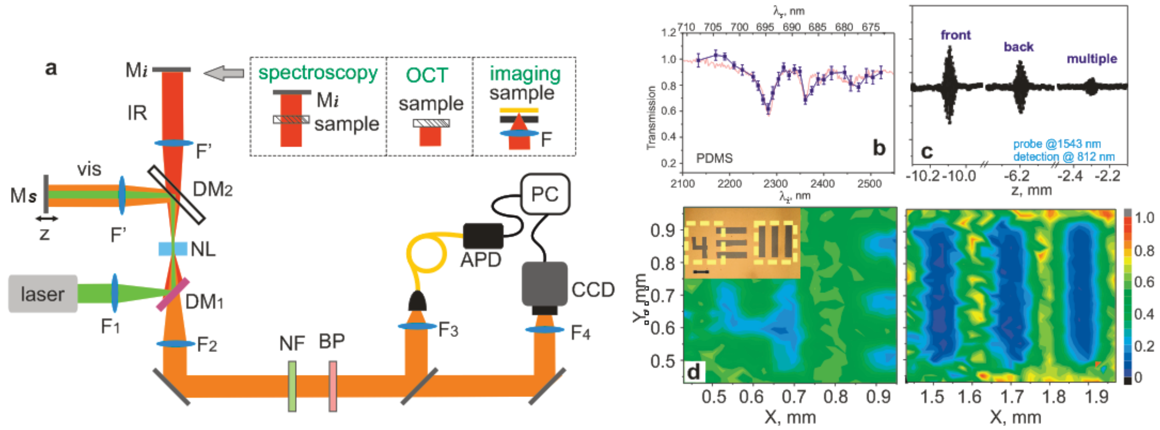


Figure 1: (a) IR spectroscopy of a polydimethylsiloxane (PDMS) sample. Blue points show the data obtained in our measurements, pink curve indicates the data measured by conventional method. Top abscissa indicates the detected wavelengths at the visible range; bottom abscissa shows their conjugate wavelengths at the IR range. (b) IR OCT of the Silicon plate, where interference peaks correspond to the reflecting surfaces of the sample. (c) IR point-by-point imaging of an interface of the sandwiched sample: resolution test target with the Silicon plate in front. Insert shows the image of the resolution test under the standard visible range microscope. The color scale indicates the intensity reflectance.

## References


[1] D. Kalashnikov, A. Paterova, S. Kulik, and L. Krivitsky, Nature Photonics **10**, 98-101 (2016).
[2] A. Paterova, S. Lung, D. Kalashnikov, L. Krivitsky, Scientific reports **7**, 42608 (2017).
[3] A. Paterova, H. Yang, Ch. An, D. Kalashnikov, and L. Krivitsky, New J. Phys. **20** 043015 (2018).
[4] A. Paterova, H. Yang, Ch. An, D. Kalashnikov, and L. Krivitsky, Quantum Sci. Technol. **3** 025008 (2018).
[5] A. Paterova, H. Yang, Ch. An, D. Kalashnikov, and L. Krivitsky, Optics Express **27(3)** 2589 (2019).

# Characterizing heralded single photons from a Bragg-reflection waveguide loss-tolerantly via moment generating function


K. Laiho[1], M. Schmidt[1,2], H. Suchomel[3], M. Kamp[3], S. Höfling[3,4], C. Schneider[3], J. Beyer[2], G. Weihs[5] and S. Reitzenstein[1]

[1]*Technische Universität Berlin, Institut für Festkörperphysik, Hardenbergstr. 36, 10623 Berlin, Germany*
[2]*Physikalisch-Technische Bundesanstalt, Abbestr. 2-12, 10587 Berlin, Germany*
[3]*Technische Physik, Universität Würzburg, Am Hubland, 97074 Würzburg, Germany*
[4]*School of P hysics & Astronomy, University of St Andrews, St Andrews, KY16 9SS, United Kingdom*
[5]*Institut für Experimentalphysik, Universität Innsbruck, Technikerstraße 25, 6020 Innsbruck, Austria*


The non-linear optical process of parametric down-conversion (PDC), which produces twin beams with strict photon-number correlation, is nowadays routinely employed for preparing heralded quantum states of light, like single photons. Often, however, experimental imperfections degrade these states and therefore, accurate methods for predicting and measuring their characteristics are utterly important. Here, we employ the normalized higher-order moments combined with a loss-tolerant measurement of the mean photon-number of the studied state for reconstructing the photon-number parity via *the moment generating function* [1].

For that purpose, we investigate the heralded single-photon state preparation via PDC. We start by theoretically predicting the photon-number parity of the heralded states in terms of the heralding efficiency and the mean photon-number of the PDC emission as shown in Fig. 1(a). To find the most profitable combination of the photon-state preparation and manipulation parameters we also calculate the probability, at which the desired state is heralded as shown in Fig. 1(b). We then produce broadband type-II PDC emission in the telecom C-band from a ridge Bragg-reflection waveguide (BRW) made of layered AlGaAs compounds and record the joint photon statistics of the emitted twin beams with two transition-edge sensors, being true photon-number resolving detectors [2,3]. We then extract the normalized second-order moment of the heralded single photons shown in Fig. 1(c). Due to experimental imperfections, our BRW source is suitable for the heralded state preparation only at low pump powers, where the mean photon-number of the PDC emission is low. Thereafter, we take use of the moment-generating function to access the negative photon-number parity of the heralded single photons in a loss-tolerant fashion as illustrated in Fig. 1(d). We further provide boundaries for the successful state reconstruction region limited by the highest experimentally resolved photon number. Our results show, that a good control of the parameters involved in heralded state's production is needed to suppress the undesired higher photon-number contributions. We believe that our method can be employed to characterize other photon-number states and can also be implemented with bucket detectors.

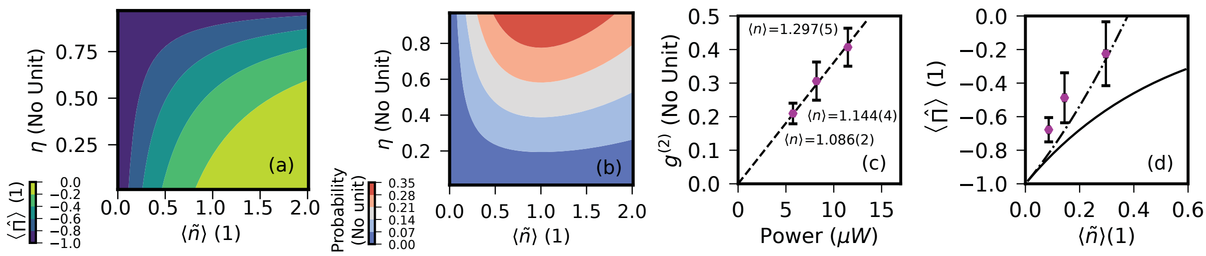


Figure 1: Theoretical prediction of (a) the photon-number parity of heralded single photons and (b) the probability of their successful heralding in terms of the heralding efficiency $\eta$ and the mean photon-number of the multimode PDC emission $\langle\tilde{n}\rangle$ as well as the experimentally measured values (symbols) for the heralded state state characteristics described by (c) the normalized second-order moment $g^{(2)}$ in terms of pump power and (d) the photon-number parity accessed by truncating the moment generating function to $\langle\hat{\Pi}\rangle \approx 1-2\langle n\rangle+2g^{(2)}\langle n\rangle^2$ in terms of $\langle\tilde{n}\rangle$. The loss-corrected mean photon-numbers $\langle n\rangle$ of the heralded states are marked in (c). The dashed line in (c) is a linear fit, while the dash-dotted line in (d) shows the theoretical expectation with the truncation of the moments to the 2nd order and the solid line is expected if moments with much higher orders can be measured.


[1] K. Laiho et al., arXiv:1906.12191 (2019).
[2] M. Schmidt et al., J. Low Temp. Phys. **193**, 1243 (2018).
[3] T. Günthner et al., J. Opt. **17**, 125201 (2015).

# Large-Format Image Sensors Based on Integration of Custom Geiger-Mode Avalanche Photodiode Arrays with All-Digital CMOS Circuits

**Brian Aull, Erik Duerr, Jonathan Frechette, Chris Leitz, Abigail Licht, Alex McIntosh, Kevin Ryu, Daniel Schuette, Vyshnavi Suntharalingam, Richard Younger**

*MIT Lincoln Laboratory, Lexington, Massachusetts, USA*

MIT Lincoln Laboratory develops photon-counting image sensors for lidar, passive imaging, wavefront sensing, and communications. These sensors are based on hybridizing or 3D integrating custom arrays of Geiger-mode avalanche photodiodes (GmAPDs) with all-digital CMOS circuits. This presentation reviews ongoing technology development work at the Laboratory on three fronts: (1) Silicon and InGaAsP/InP GmAPD arrays, (2) Novel readout circuits architectures for lidar and photon-starved passive imaging, and (3) 3D integration and rapid prototyping techniques.

# Room temperature operation of InP/InGaAs single photon avalanche diode

C.Y.Park[1], S.H.Baek[1], J.H.Kim[1], B.R.Jeon[1], S.C.Yang[1], C.W.Park[2], S.B.Cho[2]

[1]*Wooriro Co,. Ltd: 102-22. Pyeongdongsandan 6beon-ro, Gwangsan-gu, Gwangju, 62453, South Korea*

[2]*ID Quantique, 6 Hwangsaeul-ro 258beon-gil, Bundang-gu seongnam-si, Gyeonggi-do, 13595, South Korea*

Room temperature operation of single photon avalanche diode(SPAD) is an important issue in the points of device cost reduction and mass production. The main obstacle to operate SPAD at room temperature is the dark count noise generally known as dark count rate(DCR) or dark count probability(DCP) per gate. To suppress DCR or DCP, a low temperature operation is widely used. This causes, however, the increased device size and cost due to adoption of thermo-electric cooler(TEC) inside package. In this paper, we fabricated an SPAD having small active volume[1] to reduce DCP for room temperature operation.

The device structure having floating guard ring was shown in Fig.1. The backside illumination structure was designed to increase quantum efficiency. In order to reduce DCP, it is important to reduce the volume of InGaAs absorption layer. A relatively thin absorption layer thickness of 1.2um was employed to reduce dark current. An active diameter of 16um was designed to reduce active volume. Double Zn-diffusion technique was employed in order to define pn junction and multiplication layer. The flip-chip bonding was applied on the quartz carrier where the Au/Sn solder bumper was formed. The round-trip of photon is very helpful to increase device quantum efficiency. Even the relatively thin absorption layer, responsivity was measured to exceed 0.9 A/W at 1550nm wavelength. A very low dark current at 0.98VB was measured less than 200pA at room temperature. This chip-on-carrier(CoC) was packaged on TO8 header. A 3-stage TEC and thermistor were employed to control the device temperature. A specially designed aspherical lens cap was resistance-welded in nitrogen atmosphere to satisfy hermetic sealing. Finally, optical fiber pigtail was carried out by laser welding technique.

The Geiger-mode characteristics were measured for fabricated SPAD devices. Attenuated laser pulse having 190ps of FWHM and 1550nm wavelength has been used as a single photon source. Gate frequency and gate width were 10MHz and 2ns, respectively. The photon incident frequency was 100kHz. The averaged photon number of 0.1 was used. Fig. 2 shows DCP versus photon detection efficiency(PDE) for five SPAD devices as functions of device temperature. All five devices showed considerably uniform performances. As PDE increases from 10% to 30%, DCP increases $1\times10^{-7}$ to $2\times10^{-6}$ at -40°C, which is very small. At room temperature, DCP of $5{\sim}6\times10^{-6}$ at 10% of PDE and $3{\sim}4\times10^{-5}$ at 30% PDE were obtained, which means that this device can be applied in QKD system with high PDE. After-pulse probability(APP) decreases as temperature increases. This is because APP is generated carrier capture-emission process at crystal defect center and carrier emission time is faster when temperature increases. At 25% PDE, the total APP was decreased from 2% at -40°C to 1% at 20°C. However, the total APP at 30% PDE decreased from 8% at -40°C to 1.8% at 20°C.

In conclusion, we successfully fabricated and demonstrated room temperature operable SPAD having small active volume. Very low DCP and APP have been obtained.

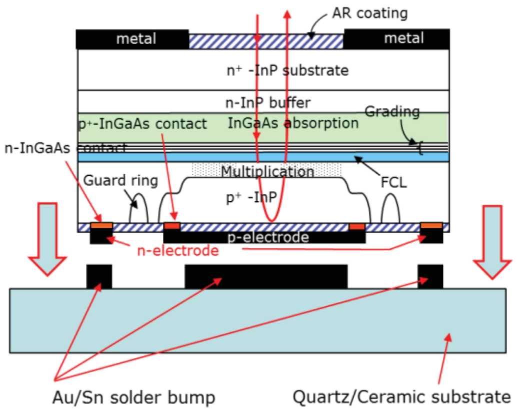


Fig. 1 SPAD chip structure studied in this work

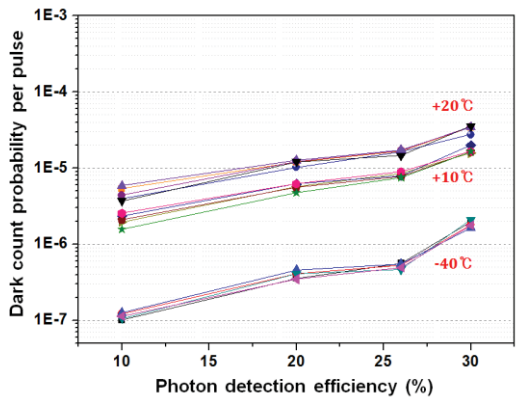


Fig. 2 DCP per gate for 5-devices were shown. The measurement was made by using conventional gating method. (2ns gate width and 10MHz gate frequency)

## References

[1] A. Tosi, A. Dalla Mora, F. Zappa, S. Cova, M.A. Itzler, X. Jiang., "InGaAs/InP Single-photon Avalanche Diodes show low dark counts and require moderate cooling" Proc. Of SPIE Vol. 7222 72221G-1(2009)

# Planar Geometry Ge-on-Si Single-Photon Avalanche Diode Detectors for the Short-Wave Infrared

**Gerald S. Buller[1], Kateryna Kuzmenko[1], Peter Vines[1], Zoë Greener[1], Jarosław Kirdoda[2], Derek C.S. Dumas[2], Muhammad M. Mirza[2], Lourdes Ferre Llin[2], Ross W. Millar[2], Douglas J. Paul[2]**

[1]*Institute of Photonics and Quantum Science, School of Engineering and Physical Sciences, Heriot-Watt University, Edinburgh EH14 4AS, United Kingdom*

[2]*School of Engineering, University of Glasgow, Rankine Building, Oakfield Avenue, Glasgow G12 8LT, United Kingdom*

One approach for SPAD device design capable of operation in the short-wave infrared (SWIR) region is the use of germanium-containing absorbing layers in conjunction with an adjacent silicon avalanche multiplication layer [1,2,3]. We demonstrate a new generation of planar geometry germanium-on-silicon (Ge-on-Si) single-photon avalanche diode (SPAD) detectors for SWIR operation. The use of this planar geometry SPAD has enabled a significant step-change in performance when compared to previous optimised mesa geometry devices [4].

The planar geometry Ge-on-Si SPAD is shown schematically in Figure 1(a). Incident SWIR radiation is absorbed in the Ge layer and the photo-generated electron initiates the impact ionisation process in the Si multiplication layer. In between these regions, the selectively implanted charge sheet controls the electric field so that the field is high enough in the multiplication region to ensure that avalanche breakdown is reached yet sufficiently low to prevent band-to-band and trap-assisted tunnelling. The use of the selectively implanted charge sheet meant that the high electric field is confined to the centre of the SPAD, reducing the possibility of carriers originating at the sidewalls initiating breakdown events.

The devices were fully characterised in terms of single-photon detection efficiency, dark count rate and jitter under a variety of operational temperatures an over-bias levels. Single-photon detection efficiency of 38 % at 125 K at a wavelength of 1310 nm was observed with a jitter of approximately 300ps in a large (100 µm diameter) devices. This corresponded to a fifty-fold improvement in noise equivalent power compared with optimised mesa geometry SPADs, as shown in Fig. 1(b). Significantly, the Ge-on-Si SPADs exhibited considerably less afterpulsing in a direct comparison with an InGaAs/InP SPAD under identical operating conditions.

We present a study of these devices in terms of potential for these devices in single-photon LIDAR applications. The use of the relatively inexpensive Ge-on-Si platform provides a route towards large arrays of efficient Ge-on-Si SPADs for use in eye-safe automotive LIDAR and future quantum technology applications.

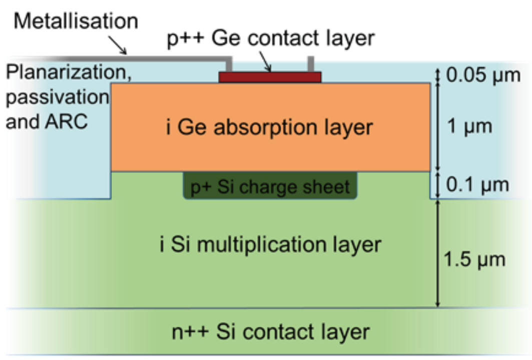


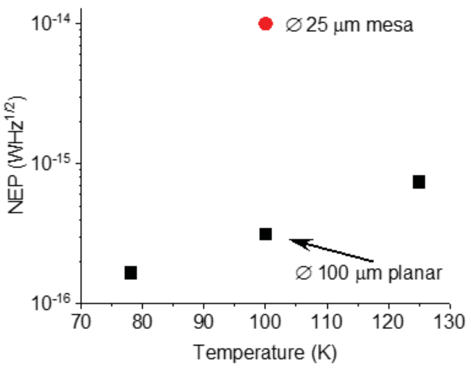


Fig. 1(a) Schematic of device. (b) Noise equivalent power (NEP) as a function of operating temperature, with comparison to mesa geometry.

**References**

[1] Loudon, A. Y. et al. "Enhancement of the infrared detection efficiency of silicon photon-counting avalanche photodiodes by use of silicon germanium absorbing layers", Opt. Lett. 27, 219–221 (2002)

[2] Warburton, R. E. et al. "Ge-on-Si single-photon avalanche diode detectors: design, modeling, fabrication, and characterization at wavelengths 1310 and 1550 nm" IEEE Trans. Electron Dev. 60, 3807–3813 (2013)

[3] Zhiwen Lu et al., "Geiger-mode operation of Ge-on-Si avalanche photodiodes" IEEE J Quantum Electron., 47 (5), (2011)

[4] Vines, P. et al. "High performance planar germanium-on-silicon single-photon avalanche diode detectors", Nature Comms., 10:1086 (2019)

# Fully integrated electronics for high-performance and high-speed acquisition with Single Photon Avalanche Diodes

**Giulia Acconcia[1], Angelo Gulinatti[1], Massimo Ghioni[1], Ivan Rech[1]**

[1]*Politecnico di Milano, Dipartimento di Elettronica, Informazione e Bioingegneria, Milan, Italy*

Nowadays, single photon sensitivity can be achieved with different kind of detectors, as Photomultiplier Tubes (PMTs), Single Photon Avalanche Diodes (SPADs) and Superconducting Nanowire Single-Photon Detectors (SNSPDs). Compared to the others, SPADs offer clear advantages being solid-state devices that can be operated at room temperature or with moderate cooling. Many applications currently benefit from the exploitation of SPADs both in counting and in timing measurements. Nevertheless, operating SPADs at high count rates is still an open challenge. A remarkable research effort has been made in the past few years to increase the speed of SPAD-based acquisition system. High speed, indeed, would open the way to the exploitation of SPADs in even a larger number of applications and advanced measurements as the study of the ocean environment to investigate the effects of climate changes by spaceborne LiDAR [1] or *in vivo* measurements in biosciences. To address speed issues that currently limit SPAD-based systems, we have developed fast and fully-integrated electronics. Our approach is based on the exploitation of custom-technology SPADs, also developed by us at Politecnico di Milano, because they have been proven suitable to achieve excellent results in terms of high photon detection efficiency (also in the red region of the spectrum), along with low noise (both in terms of dark counts and afterpulsing) and timing performance. Custom SPADs require external electronics to be operated at the best of their possibilities. To this aim, we designed a fully integrated Active Quenching Circuit (AQC) able to drive different kinds of external detectors up to a rate as high as 160Mcps as shown in Fig. 1 (Left). To the best of our knowledge, this is the highest count rate achieved so far with an external custom SPAD. The prompt quench of the avalanche current and the high quality of the SPAD fabrication process allow us to limit the afterpulsing probability below few percent even with a dead time as short as 6.2ns. In timing, we demonstrated that, with fast and high-performance electronics designed on purpose, it is possible to push the operating speed of a single channel well beyond the actual limitations (typically 1% or 5% of the excitation rate) while avoiding that pile-up distortion affects the measurement [2]. To demonstrate the practical feasibility of this solution we designed an AQC with a finely tunable dead time to match the excitation period of a 80MHz laser and a fully differential pick-up circuit providing picoseconds timing jitter even at high count rates. The timing signal has then to be fed to a time measurement circuit. Exploiting a Si-Ge 0.35µm technology we developed a Time-to-Amplitude Converter (TAC) able to provide a state-of-art timing precision of less than 4.3ps rms (corresponding to 10ps FWHM). Fig. 1 (Right) shows the rms timing jitter as a function of the measured start-stop interval. The new TAC provides excellent performance both in terms of precision and linearity with a Differential Non Linearity lower than 0.25% of the LSB rms (1.5% peak to peak). Featuring an area occupation of 1mm$^2$ (considering also the integrated DAC to use the dithering technique) and an overall power dissipation as low as 70mV, the designed circuit will be the building block of future multichannel systems.

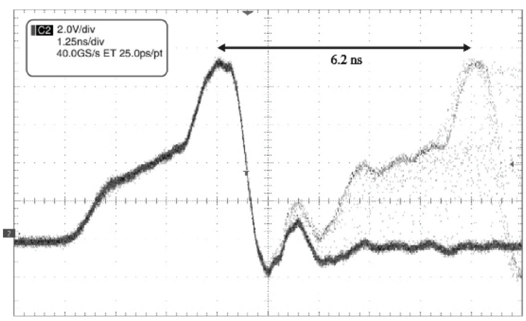


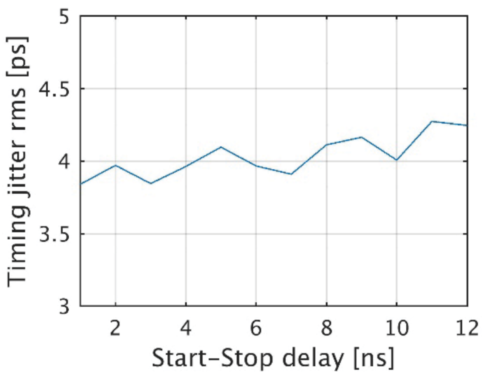


Fig. 1 (Left) Anode waveform of a custom-technology SPAD driven at 160Mcps by an external fully integrated AQC (Right) Timing precision of the TAC: rms jitter is lower than 4.3ps on the whole Full Scale Range

**References**

[1] Hostetler, C. A., Behrenfeld, M. J., Hu, Y., Hair, J. W. and Schulien, J. A., “Spaceborne Lidar in the Study of Marine Systems,” Ann. Rev. Mar. Sci. **10**(1), 121–147 (2017).

[2] Cominelli, A., Acconcia, G., Peronio, P., Ghioni, M. and Rech, I., “High-speed and low-distortion solution for time-correlated single photon counting measurements: A theoretical analysis,” Rev. Sci. Instrum. **88**(12) (2017)

# Future perspective of SiPM technology

**Matteo Salomoni[*†], Etiennette Auffray[†], Stefan Enoch[‡], Alberto Gola[§], Stefan Gundacker[*†], Paul Lecoq[†], Marco Toliman Lucchini[¶], Alberto Mazzi[§] and Marco Paganoni[*]**

[*]*University of Milano-Bicocca. Piazza dell'Ateneo Nuovo, 1, 20126 Milan, Italy*
[†]*European Organization for Nuclear Research (CERN). Geneva, Switzerland*
[‡]*Aix Marseille Univ., CNRS, Centrale Marseille, Institut Fresnel, Marseille, France*
[§]*Fondazione Bruno Kessler. Via Santa Croce, 77, 38122, Trento, Italy*
¶*Princeton University, Princeton, New Jersey, USA*

This work will present the advancement in the development of a new generation of SiPM photodetectors with improved single photon time resolution (SPTR) and photo-detection efficiency (PDE). Two complementary approaches are being explored in the framework of the ATTRACT project PHOTOQUANT:
1. to exploit the high light concentration power of resonant structures to guide the photons to an individual single photon avalanche diode (SPAD) of the SiPM;
2. make use hyperbolic meta-materials (HMMs) to enhance in well-defined regions of the SiPM structure the electromagnetic energy density of the photons.

Regarding the first approach, SiPMs are composed of many separated SPADs, which require some dead border at the edges, for electrical and optical isolation and to prevent edge breakdown. This dead border reduces the fill factor (FF), which has been traditionally the most important aspect limiting the photo-detection efficiency (PDE) of SiPMs, the other one being the quantum efficiency (QE)[1]. This project proposes to use close to omni-directional concentrators to overcome the FF limitations. Indeed, it will be possible to focus light in a very small central spot of the micro-cell, obtaining almost 100% FF for light detection while leaving plenty of space to increase the width of the dead border even in very small cells (≤ 5 μm). These structures will essentially decouple FF, cell size and dead border. With this new design freedom, it will be possible to design SiPMs with: (i) very small cell size, thus reduced gain, primary and correlated noise, dead time and much-increased cell density; (ii) increased dead border with room for better intra-cell optical isolation and separation between active area and cell edge, allowing to further reduce primary and correlated noise.

For what concerns the second approach, SPTR of the SiPM is strongly related to the homogeneity of the electron generation across the SPAD, which is affected by border effect and vertical depth. The use of hyperbolic meta-materials gives the possibility to create strong spot-like photo-conversion region[2] in a well-defined position of the SPAD, making the detection process tunable and the electronic avalanche generation independent from the photon's impinging point and direction.

Simulations and first proof of concept tests will be performed and the results will be presented at the time of the conference.

**References**

[1] F. Acerbi, A. Gola, V. Regazzoni, G. Paternoster, G. Borghi, N. Zorzi, and C. Piemonte, "High efficiency, ultra-high-density silicon photomultipliers," *IEEE Journal of Selected Topics in Quantum Electronics*, vol. 24, pp. 1–8, mar 2018.

[2] A. Poddubny, I. Iorsh, P. Belov, and Y. Kivshar, "Hyperbolic metamaterials," *Nature Photonics*, vol. 7, pp. 948–957, nov 2013.

# Scalable interfacing of quantum photonic platforms: solid-state single-photon sources and reconfigurable photonic circuits

**C. Antón[1], J. C. Loredo[1], G. Coppola[1], N. Viggianello[2], H. Ollivier[1], A. Harouri[1], N. Somaschi[3], A. Crespi[4,5], I. Sagnes[1], A. Lemaître[1], L. Lanco[1,6], R. Osellame[4,5], F. Sciarrino[2], P. Senellart[1]**

[1]*Center of Nanosciences and Nanotechnology - CNRS, Univ. Paris-Saclay, Route de Nozay, 91460, France*

[2]*Dipartimento di Fisica, Sapienza Universitá di Roma, Piazzale Aldo Moro 5, Roma I-00185, Italy*

[3]*Quandela, SAS, 86 Rue de Paris, 91400 Orsay, France*

[4]*Istituto di Fotonica e Nanotecnologie, CNR, P. Leonardo da Vinci, 32, Milano I-20133, Italy*

[5]*Dipartimento di Fisica, Politecnico di Milano, Piazza Leonardo da Vinci, 32, Milano I-20133, Italy*

[6]*Université Paris Diderot - Paris 7, 75205 Paris CEDEX 13, France*

The development of optical quantum technologies relies on the use of many single-photons to solve milestone problems spanning from secure quantum communication, quantum simulation and distributed quantum computing. This requires efficient sources producing highly indistinguishable single-photons as well as photonic circuits showing high reconfigurability, phase stability and low losses.

Integrated photonics circuits on glass are an excellent platform to tackle a vast variety of complex quantum protocols such as Boson Sampling [1], quantum Fourier transforms [2], and quantum random walks [3,4]. So far, these photonic chips have been operated with heralded single-photon sources that show limited efficiency: these sources are typically operated with a brightness (i.e. probability to generate a photon-pair per pulse) around 1%, since the probability of generating more than one heralded photon scales as the source brightness.

Alternatively, electrically-controlled semiconductor quantum dots (QDs) coupled to microcavities have been shown recently to be near-optimal single-photon sources. They deliver true single- photon pulses with indistinguishability above 90% and brightness around 15% [5].

In this work we combine for the first time these two promising platforms, QD-based single- photon sources and an integrated photonic circuit, in order to demonstrate the potential of such interface for scaling up optical quantum protocols. The chosen case study in this experiment is quantum interference of three indistinguishable single-photons [6-8].

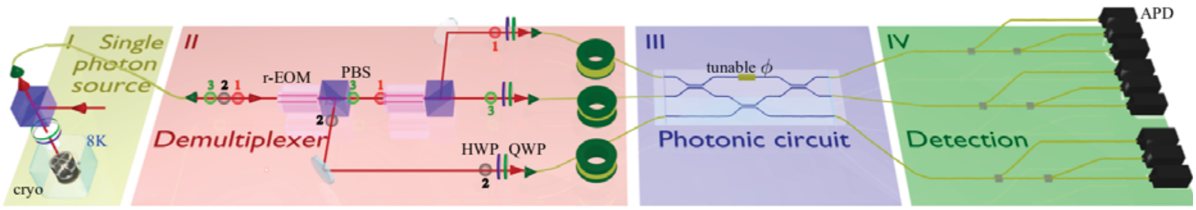


Fig. 1. **Experimental scheme of the three photon coalescence**. (I) Generation of single-photons from a QD-micropillar device under resonant fluorescence excitation. (II) Preparation of the three photons simultaneously arriving to the tritter input via active demultiplexing. (III) Photonic circuit of the tritter to perform the three photon coalescence. (IV) Detection of the quantum state of light at the tritter output.

The QD-cavity device is resonantly excited under pulsed excitation (at a high repetition rate of 324 MHz) to generate a stream of single-photons with $g^{(2)}(0)<5\%$ and indistinguishability >85% (between 80 ns delayed photons), see Fig. 1-I. We have developed a fast active demultiplexer to distribute three temporally distant single-photons into three spatial fiber modes, Fig. 1-II. The active photon-routing renders a three-single-photon generation rate of 3.9 kHz, three orders of magnitude higher than the same experiment performed with heralded single-photon sources [6].

The three photons are injected in the reconfigurable photonic tritter (see a sketch of the circuit in Fig. 1-III). The output quantum state of light is collected in three fibers, where pseudo-photon number resolving detection is implemented with nine standard Silicon avalanche photodiodes (see sketch in Fig. 1-IV). The combined detection of three photon coincidences in the detectors (at a rate of threefold coincidences of 0.25 Hz) allows the final reconstruction and characterization of the multi-photon coalescence state.

**References**

[1] N. Spagnolo, et al., Nature Photon. 8, 615 (2014).
[2] A Crespi, et al., Nature Commun. 7, 10469 (2016).
[3] L. Sansoni, et al., Phys. Rev. Lett. 108, 010502 (2012).
[4] A. Crespi, et al., Nature Photon. 7, 322 (2013).
[5] N. Somaschi, et al., Nature Photon. 10, 340 (2016).
[6] N. Spagnolo, et al., Nature Commun. 4, 1606 (2013).
[7] J. B. Spring, et al., Optica 4, 90 (2017).
[8] M. Zukowski, et al., Phys. Rev. A 55, 2564 (1997).

# Single-Photon QKD using Engineered Solid-State Quantum-Light Sources


**Timm Kupko[1], Lucas Rickert[1], Martin v. Helversen[1], Alexander Schlehahn[1], Sven Rodt[1], Christian Schneider[2], Sven Höfling[2,3], Markus Rau[4], Harald Weinfurter[4], Stephan Reitzenstein[1], and Tobias Heindel[1]**

[1]*Institut für Festkörperphysik, Technische Universität Berlin, 10623 Berlin, Germany*

[2]*Technische Physik, Universität Würzburg, 97074 Würzburg, Germany*

[3]*SUPA, School of Physics and Astronomy, University of St Andrews, St Andrews, United Kingdom*

[4]*Fakultät für Physik, Ludwig-Maximilians-Universität, 80799 München, Germany*


Tremendous progress has been achieved in the engineering of solid-state-based non-classical light sources during the last two decades [1]. In this context, quantum-light sources based on semiconductor quantum dots (QDs) are of particular interest. Allowing for the generation of close-to-ideal flying qubits these devices are predestinated for implementations of quantum communication scenarios.

In this contribution, we review our progress in this field, striving towards the ultimate goal of a global secure communication. We will revisit proof-of-concept quantum key distribution (QKD) experiments using electrically-pumped QD single-photon sources (SPSs) [2,3] (cf. Fig. 1(a)) and discuss the development of state-of-the-art components for QKD, such as plug-and-play SPSs and receiver modules. Practical SPSs are presented comprising

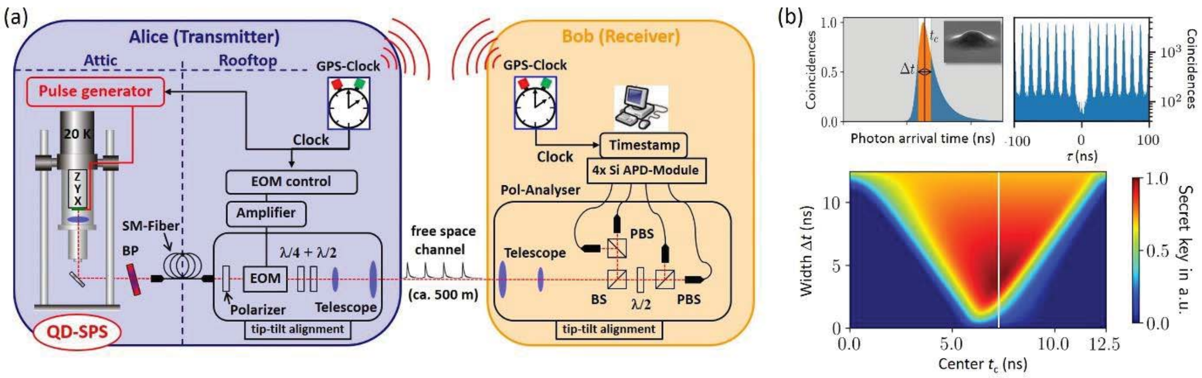


Fig. 1 (a) Setup for QKD field experiments using electrically pumped single-photon sources in a 500 m free-space optical link in downtown Munich [3]. (b) Performance optimization of single-photon QKD exploiting temporal filtering of the triggered single-photon pulses emitted by a quantum dot embedded in a deterministically fabricated photonic microlens [6].

QD-based devices integrated in a compact Stirling cryocooler for user-friendly operation [4]. We address the direct, robust, and efficient coupling of quantum light sources to optical single-mode fibers [5], representing one crucial next step towards applications. Furthermore, we developed a portable receiver module designed for polarization-encoded QKD and analyze its performance using deterministically fabricated and optically triggered SPSs based on QD-microlenses (see Fig. 1(b), inset). In this framework, we exploit temporal filtering of single-photon pulses to optimize the performance for QKD systems implemented with realistic quantum-light sources. For this purpose, we analyze the sifted key fraction, the quantum bit error ratio, and $g^{(2)}(0)$ expected in full implementations of the BB84 protocol under variation of the acceptance time-window (see Fig. 1(b)). This routine enables us to choose optimal filter settings depending on the losses of the quantum channel. Moreover, we demonstrate real-time security monitoring with sub-poissonian light sources by using our receiver-module for evaluating $g^{(2)}(0)$ inside the quantum channel [6].

The results presented in this work are an important contribution towards the development of functional multi-user quantum-secured communication networks based on quantum-light sources – a challenge which we tackle in our recently founded *Quantum Communication Systems* group at Technische Universität Berlin [7].

**References**


[1] S. Rodt, S. Reitzenstein, and T. Heindel, Topical Review Article, *under review* (2019)
[2] T. Heindel et al., *New Journal of Physics* **14**, 083001 (2012)
[3] M. Rau, T. Heindel et al., *New Journal of Physics* **16**, 03003 (2014)
[4] A. Schlehahn et al., *Scientific Reports* **8**, 1340 (2018)
[5] L. Rickert et al., Design Study for Telecom-Wavelength Quantum Light-Sources Based on Hybrid Circular Bragg-Gratings, *arXiv:1908.08408* (2019)
[6] T. Kupko et al., Performance Optimization and Real-Time Security Monitoring for Single-Photon Quantum Key Distribution, *arXiv:1908.02672* (2019)
[7] Website: *Quantum Communication Systems* Group at TU Berlin

# Electrical control of Nitrogen – Vacancy centers in diamond

S. Ditalia Tchernij[1,2], J. Forneris[2,1], N. Skukan[3], M. Jakšić[3]; G. Amato[4], L. Boarino[4], I.P. Degiovanni[4], E. Enrico[4], E. Moreva[4], P. Traina[4], M. Genovese[4], P. Olivero[1,2]

*1 Physics Department and "NIS" Inter-departmental Centre - University of Torino, Torino, Italy*
*2 Istituto Nazionale di Fisica Nucleare (INFN), Sez. Torino, Torino, Italy*
*3 Ruđer Bošković Institute, Zagreb, Croatia*
*4 Istituto Nazionale di Ricerca Metrologica (INRiM), Torino, Italy*

Color centers in diamond are promising systems for the development of appealing quantum technologies. As several ground-breaking works in this research field were conducted by means of the optical stimulation of NV centers, an efficient electrical control of their photo-physical properties would enable a further degree in integration in opto-electronic quantum devices. The fabrication of integrated graphitic micro-channels allows to define arbitrary electrode geometries in the diamond bulk (i.e. up to several micrometers below the sample surface) by exploiting the radiation-induced graphitization of the material occurring at the end of the MeV ion penetration range [1], and could therefore represent a useful strategy to achieve such integration.

In this work, we present results obtained on devices consisting of pairs of sub-superficial (i.e. ~3 µm deep) graphitic micro-electrodes with ~10 µm spacing, fabricated into single-crystal diamond substrates with a 6 MeV $C^{3+}$ microbeam. The current-voltage characteristics of the graphite-diamond-graphite junctions displays an ohmic behavior, associated with a moderate current injection ("low-current regime") at bias voltages below a threshold value $V_c$. At $V > V_c$, the device exhibits an abrupt transition to a high-current regime dominated by a Poole-Frenkel conduction mechanism and providing stimulation of electroluminescence emission from NV centers and interstitial-related defects in the inter-electrode gap [2].

The electroluminescence spectral analysis evidenced a bright emission from native neutrally-charged nitrogen-vacancy centers ($NV^0$). Moreover, the graphitic micro-electrodes were exploited to stimulate single-photon emission from isolated $NV^0$ centers in an "electronic grade" diamond sample through the injection of a stable and non-destructive pump current in the inter-electrode gap.

Ensemble photoluminescence (PL) spectra (532 nm laser excitation) acquired under electrical bias in low-current regime exhibited a linear increase with the injected current in the $NV^-$ population at the expense of the $NV^0$ charge state [3].

This result indicates the effectiveness of graphite-diamond-graphite junctions to stabilize the negative charge state of the NV centers for spin manipulation protocols. Finally, the distribution of the electric field in the active region of the junction was investigated by spatially mapping the Stark-shifted optically-detected magnetic resonances (ODMR) from NV centers in the active region of the device [4].

These results provide promising perspectives on the utilization of integrated electrical structures for the stimulation and control of deep color centers in diamond located at micrometric distances from the diamond surface, for which longer spin coherence times are expected [5].

[1] F. Picollo et al., New J. Phys. 14 (2012).
[2] J. Forneris et al., Sci. Rep. 5:15901 (2015).
[3] J. Forneris et al., Carbon 113 (2017).
[4] J. Forneris et al., Phys. Rev. Appl. 10, 1 (2018)
[5] T. Staudacher et al., APL 101 (2012) 212401.

# Overcoming noise in entanglement distribution through high-dimensional encoding


**Sebastian Ecker[1,2], Frédéric Bouchard[3], Lukas Bulla[1,2], Florian Brandt[1,2], Oskar Kohout[1,2], Fabian Steinlechner[1,2,4], Robert Fickler[1,2,5], Mehul Malik[1,2,6], Yelena Guryanova[1,2], Rupert Ursin[1,2], Marcus Huber[1,2]**

[1]*Institute for Quantum Optics and Quantum Information (IQOQI), Austrian Academy of Sciences, Boltzmanngasse 3, 1090 Vienna*

[2]*Vienna Center for Quantum Science and Technology (VCQ), Faculty of Physics, University of Vienna, Boltzmanngasse 5, A-1090 Vienna*

[3]*Department of physics, University of Ottawa, Advanced Research Complex, 25 Templeton, Ottawa ON Canada, K1N 6N5*

[4]*Fraunhofer Institute for Applied Optics and Precision Engineering IOF, Albert-Einstein-Strasse 7, 07745 Jena, Germany*

[5]*Photonics Laboratory, Physics Unit, Tampere University, Tampere, FI-33720, Finland*

[6]*Institute of Photonic and Quantum Sciences (IPaQS), Heriot-Watt University, Edinburgh, Scotland, UK EH14 4AS*


Quantum entanglement is a key resource in Quantum information processing and an indispensable ingredient in most Quantum communication protocols. However, distributing entangled photon pairs between communicating parties separated by long distances is currently the main obstacle in practical Quantum communication, where both the detection of background photons and the loss of photons across the link limit the channel distance and capacity. While high-dimensional entanglement has the potential to overcome noise levels which wouldn't allow for the distribution of qubit-entanglement, this hasn't been demonstrated in an experimentally meaningful fashion.

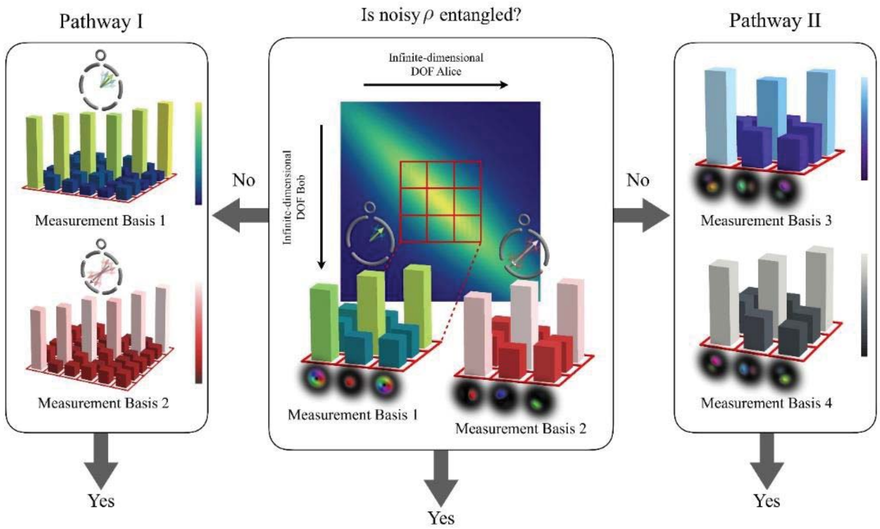


Fig. 1 Pathways to Noise Resilience

We identified two pathways to noise resilience (Fig. 1) and showcase an actual advantage by increasing the state space dimensions of spatiotemporal properties of entangled photon pairs in two separate experiments [1]. Pathway I is based on further discretizing a continuous degree of freedom, thereby 'diluting' the noise in the resulting high-dimensional state space. Our experimental demonstration is performed with energy-time entangled photon pairs which are measured in the time of arrival basis and a superposition basis realized by a Franson interferometer [2]. With an appropriate entanglement witness we observed entanglement in a noisy environment up to a noise fraction of 92% in a 80-dimensional state space. Pathway II relies on the availability of further mutually unbiased measurement bases in higher dimensions, which provide additional information about the coherence of the entangled state. This pathway is experimentally demonstrated using photon pairs entangled in their orbital angular momentum. With a novel technique known as intensity flattening [3] we were able to project on mutually unbiased bases with spatial light modulators and mode filters, resulting in the presence of entanglement up to a noise fraction of 63% in a 7-dimensional state space.

Despite the fact that resolving larger state spaces necessarily leads to additional noise channels, we revealed entanglement in both experiments which was otherwise obscured by noise. This increased robustness against noise can be utilized for distributing entanglement over long-distance fiber links, which are limited by detector dark counts, or satellite-ground free-space links in the presence of high levels of sky noise. Further theoretical work has to be conducted in order to extract a secure key in quantum key distribution or perform other quantum communication protocols in noisy environments where no qubit communication is possible.

**References**


[1] **arXiv: 1904.01552** [2] Franson, J. D. (1989). Physical Review Letters, 62(19), 2205–2208

[3] Bouchard, F. et al. Optics Express 26, 31925 (2018)

# Thursday, October 24, 2019

| | | |
|---|---|---|
| 09:00 | Session 13<br>Sources III<br><br>Chair: T. Gerrits | **C. Toninelli - Single-molecule based single photon sources** |
| 09:30 | | R. Schofield - Nanophotonic waveguide coupling to organic molecules in micro-capillaries |
| 09:50 | | H. Abudayyeh - Quantum light manipulation: A path towards efficient pure room-temperature single photon sources |
| 10:10 | | H. Wang - Single photons for quantum technologies |
| 10:30 | | G. Solomon - Filter-free single-photon emission in an integrated cavity-waveguide device |
| 10:50 | Coffee break (offered by attocube / Quandela) | |
| 11:20 | Session 14<br>Applications V<br><br>Chair: S. W. Nam | **K. Srinivasan - Quantum source and frequency conversion technologies based on integrated nanophotonics** |
| 11:50 | | J. Adcock - Programmable mutliphoton graph states on a silicon chip |
| 12:10 | | G. Kavuri - Towards a loophole-free Bell experiment on a tabletop |
| 12:30 | | Z.-H. Xiang - Network Integration of Quantum Dot Device and Entanglement in Cambridge Fiber Network |
| 12:50 | Platinum sponsor presentation: Excelitas | |
| 12:55 | Lunch | |
| 14:10 | Session 15<br>Detectors IV<br><br>Chair: I. Rech | **S. W. Nam - From dark matter detection to artificial intelligence: applications of superconducting nanowire single photon detectors** |
| 14:40 | | M. Perrenoud - High detection rate and high efficiency with parallel SNSPDs |
| 15:00 | | S. Buckley - Progress in superconducting optoelectronic networks for neuromorphic computing |
| 15:20 | | T. Takumi - Time-resolved measurement of a single-photon wave packet with an optical Kerr effect |
| 15:40 | | E. Fossum - Quanta Image Sensor Progress Review |
| 16:00 | Coffee break | |
| 16:30 | Session 16<br>Applications VI<br><br>Chair: F. Zappa | **S. Verghese - Self-driving cars and lidar** |
| 17:00 | | G. Musarra - Single-photon, single-pixel intelligent Lidar |
| 17:20 | | A. Maccarone - Three dimensional imaging of dynamic underwater scenes using single photon detection |
| 17:40 | | R. Tobin - Depth imaging through obscurants using single photon detection in the short-wave infrared |
| 18:00 | | M. Laurenzis - Computational imaging with SPADs at SWIR wavelengths |
| 18:20 | Poster session II | |
| 19:40 | End | |

# Single-molecule based single photon sources

**P. Lombardi[1], M. Colautti[1], M. Lopez[2], S. Kück[2], C. Toninelli[1]**

[1]*CNR-INO and LENS, Istituto Nazionale di Ottica, Via Carrara 1, 50019 Sesto F.no, Italy*
[2]*Physikalisch-Technische Bundesanstalt (PTB), Bundesallee 100, 38116 Braunschweig, Germany*

In this contribution we discuss the state of the art of single-molecule based single photon sources developed in Florence. In particular we will present our latest results concerning the integration of organic molecules into different photonic architectures, from optical planar antennas [1], to silicon nitride waveguide [2] and polymeric structures [3][4].

Finally we will elaborate on the applications of such single photon sources for quantum metrology. The science and technology of measuring accurately light at the few photon level is one of the fields where non-classical light states might be more beneficial than classical sources. Intrinsic intensity squeezing in the emission from single quantum object will guarantee a precise definition and measurement of photon fluxes in the fW range.

We will hence present a molecule-based single photon source that, operated at 3 K, delivers a constant stream of photons with beyond 1-Mcps flux at the detector, a spectrometer-limited bandwidth of 0.2 nm and single photon high purity. This source is used to calibrate a silicon avalanche photodiode directly against an analog photodetector, previously referred to the primary standard [5].

**References**

[1] S. Checcucci et al., “Beaming light from a quantum emitter with a planar optical antenna”, Light: Science and Applications, (2017) 6, e16245
[2] P. Lombardi et al., “Photostable molecules on chip: integrated single photon sources for quantum technologies”, ACS Photonics 5, 1, 126-132 (2017)
[3] S. Pazzagli et al., “Photostable single-photon emission from self-assembled nanocrystals of polycyclic aromatic hydrocarbons”, ACS Nano 12, 4295−4303 (2018)
[4] K. Schädler et al., “Electrical Control of Lifetime-Limited Quantum Emitters Using 2D Materials”, Nanoletters (2019), DOI: 10.1021/acs.nanolett.9b00916
[5] P. Lombardi et al., “A Molecule-Based Single-Photon Source Applied in Quantum Radiometry”, submitted

# Nanophotonic waveguide coupling to organic molecules in micro-capillaries

**Ross C. Schofield[1], Sebastien Boissier[1], Lin Jin[2], Anna Ovvyan[2], Salahuddin Nur[1], Kyle D. Major[1], Frank Koppens[3], Costanza Toninelli[4], Wolfram Pernice[2], E. A. Hinds[1], and Alex S. Clark[1,*]**

*[1]Centre for Cold Matter, Imperial College London, UK*
*[2]Westfälische Wilhelms-Universität Münster, Germany*
*[3]ICFO, Barcelona, Spain*
*[4]LENS, Florence, Italy*
*[*]contact: alex.clark@imperial.ac.uk*

Over the past decade, integrated optical devices for quantum applications have received a lot of attention. Planar nanophotonic platforms have been used for quantum algorithms [1], boson sampling [2], and quantum simulation [3], but in all of those cases the photon source used was probabilistic and based on a spontaneous nonlinear process. Single molecules make excellent on-demand quantum emitters as they have been shown to have unity quantum yield, they can be efficiently put in an excited state [4], and at cryogenic temperature they decay giving narrowband, lifetime-limited photons [5]. A challenge comes in coupling them to a well-known guided optical mode. Here we present our recent work in coupling single dibenzoterrylene (DBT) molecules to nanophotonic silicon nitride waveguides by filling a gap in the waveguide via an on-chip micro-capillary.

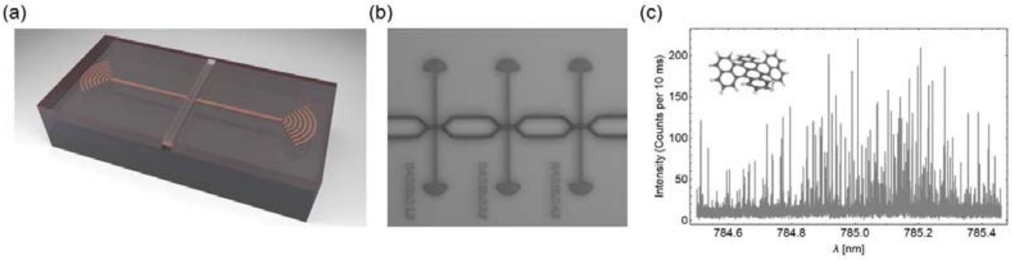


Figure 1: (a) Schematic of the micro-capillary and nanophotonic waveguide, with grating couplers. (b) White light microscope image of the final fabricated device, showing three waveguides and tapering micro-capillaries. (c) Photoluminescence excitation spectrum of many molecules in anthracene inside a tapered micro-capillary. The structure of DBT is inset.

A schematic of the waveguide and capillary is shown in Fig. 1(a). The silicon nitride waveguides sit on a silica-on-silicon substrate and were fabricated using electron beam lithography and reactive ion etching. We then added polymer channels again using electron beam lithography which run perpendicular to the chip and traverse gaps at the centre of waveguides. We then added a silica layer on top, and baked the device at 400°C, which removes the polymer and leaves open micro-capillaries, shown in Fig. 1(b). These are then filled with molten DBT-doped anthracene, which crystallises in the capillaries. By illuminating the capillaries at cryogenic temperature and tuning the laser wavelength we see many resonances from DBT molecules (Fig. 1(c)).

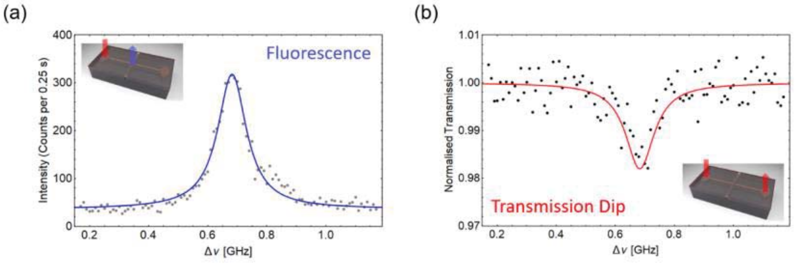


Figure 2: (a) Fluorescence from a molecule pumped through the waveguide. (b) Transmission of the same laser through the waveguide. The dip arises through interference between the resonantly scattered light from a molecule and the laser.

Sending the laser through an input grating coupler we observe both fluorescence out of the plane of the device and extinction of the laser in transmission, shown in Fig. 2(a) and (b), from which we can calculate a coupling efficiency to the waveguide of 7%. We are now working to add nanophotonic cavities to these waveguides to further enhance the coupling and build an array of unidirectional and indistinguishable photon sources.

**References**
[1] J. C. F. Matthews et al., Science **325**, 1221 (2009).
[2] J. B. Spring et al., Science **339**, 798-801 (2013).
[3] C. Sparrow et al., Nature **557**, 660–667 (2018).
[4] R. C. Schofield et al., J. Phys. Commun. **2**, 115027 (2018).
[5] S. Grandi et al., Phys. Rev. A **94**, 063839 (2016).

# Quantum light manipulation: A path towards efficient pure room-temperature single photon sources

**H. Abudayyeh [1], B. Lubotzky [1], S Majumder [2], N. Nikolay [3], J. Hollingsworth [2], O. Benson[3], and R. Rapaport [1]**

[1]*Racah Institute for Physics and the Center for Nanoscience and Nanotechnology, The Hebrew University of Jerusalem, Jerusalem 9190401, Israel*

[2] *Materials Physics and Applications Division: Center for Integrated Nanotechnologies, Los Alamos National Laboratory, Los Alamos, New Mexico 87545, United States*

[3] *AG Nanooptik, Humboldt Universität zu Berlin, Newtonstraße 15, D-12489 Berlin, Germany*

In the past few decades there has been continuous efforts to harness quantum mechanics to develop new technologies such as quantum computation, encryption, simulations, communications, etc. Quantum light and in particular single photons have become essential resources for a growing number of such applications in which solid-state atom-like systems such as semiconductor quantum dots and color defects in crystals excel. A particular interest has been developed in nanocrystal quantum dots and color centers in diamond as potential compact room-temperature emitters. There are however several challenges that inhibit the use of such sources in current technologies including low photon extraction efficiency, low emission rates and relatively low single photon purities. In this talk I will review our efforts in overcoming these technical difficulties using several complementary methods including designing several nanoantenna devices that enhance the directionality and emission rate of the nanoemitter approaching record high collection efficiencies of over 80% [1][2][3] and Purcell factors of over 100 thus achieving an enhancement factor of over 1000 in the single photon brightness [2]. In addition, we developed several temporal heralding techniques to increase the single photon purity of nanocrystal quantum dots from <90% to over 99.5% [4]. These combined techniques show great promise for producing highly pure, bright and efficient single photon sources on-chip.

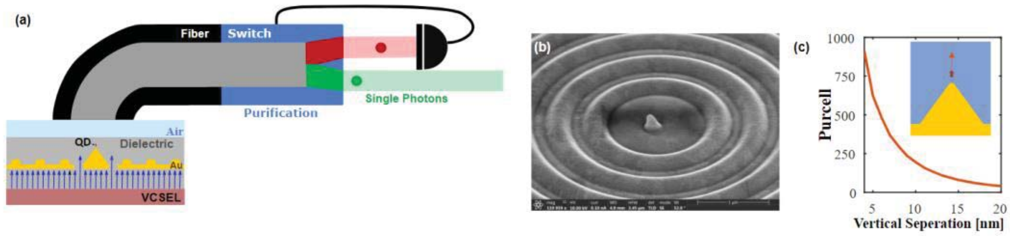


Fig. 1 : Schematic of proposed system for high brightness – high purity single photon source, (b) SEM image of nanocone bullseye antenna, and (c) Purcell factor resulting from such an antenna as a function of vertical separation between emitter and nanocone.

## References

[1] Livneh, N., et al. "Highly directional room-temperature single photon device." Nano letters 16.4 (2016): 2527-2532.

[2] Abudayyeh, H. et al. "Quantum emitters coupled to circular nanoantennas for high-brightness quantum light sources." Quantum Science and Technology 2.3 (2017): 034004.

[3] Nikolay, N., et al. "Accurate placement of single nanoparticles on opaque conductive structures." Applied Physics Letters 113.11 (2018): 113107.

[4] Abudayyeh, H., et al. "Purification of single photons by temporal heralding of quantum dot sources." ACS Photonics 6.2 (2019): 446-452.

# Single photons for quantum technologies

**Hui Wang, Chao-Yang Lu and Jian-Wei Pan**
*University of Science and Technology of China, Hefei, P.R. China*
*whui@mail.ustc.edu.cn*

**Abstract:** We develop single- and entangled-photon sources that simultaneously combines high purity, efficiency, and indistinguishability. We demonstrate entanglement among 12 single photons. We construct high-performance multi-photon boson sampling machines to race against classical computers.

Quantum computers can in principle solve certain problems faster than classical computers. Despite substantial progress in the past decades, building quantum machines that can actually outperform classical computers for some specific tasks—a milestone termed as "quantum supremacy"—remained challenging. Boson sampling has been considered as a strong candidate to demonstrate the "quantum supremacy" [1]. The challenge for realizing a large-scale boson sampling mainly lies in the lack of perfect quantum light sources.

To this end, using single semiconductor quantum dot coupled to micropillars, we produced polarized single photons with near-unity purity, indistinguishability for >1000 photons, and high extraction efficiency—all combined in a single device compatibly and simultaneously [2,3]. The quality of the single photons are sufficient high to be interfered with sunlight with a raw visibility of 80% [4]. We have also developed phase-locked two-color excitation and polarized microcavities to deterministically generate single polarized single photons [5,6]. We built boson sampling machines with increasingly large number of photons to race against classical computers [7,8,9]. Our latest boson sampling involved 12 photons fed into a 60*60 modes.

We also developed SPDC entangled two-photon source with simultaneously a collection efficiency of 97% and an indistinguishability of 96% between independent photons [10]. The probabilistic nature of SPDC could be overcome using cascaded transition of a single quantum dot embedded in a broadband microcavity [11]. These platform will provide enabling technologies for teleportation of multiple properties of photons [12] and high-dimensional quantum teleportation [13], and efficient scattershot boson sampling [14].

References:

[1] A. W. Harrow and A. Montanaro. Quantum computational supremacy, Nature 549, 203 (2018).

[2] H. Wang et al. Near transform-limited single photons from an efficient solid-state quantum emitter, Phys. Rev. Lett. 116, 213601 (2016).

[3] X. Ding et al. On-demand single photons with high extraction efficiency and near-unity indistinguishability from a resonantly driven quantum dot in a micropillar, Phys. Rev. Lett. 116, 020401 (2016).

[4] Y.-H. Deng et al. Quantum interference between light sources separated by 150 million kilometers. arXiv: 1905.02868 (2019).

[5] Y.-M. He et al. Coherently driving a single quantum two-level system with dichromatic laser pulses, accepted by Nature Physics (2019), see also arXiv: 1905.00275 (2019).

[6] H. Wang et al. Towards optimal single-photon sources with polarized cavities, accepted by Nature Photonics (2019)

[7] H. Wang et al. High-efficiency multiphoton boson sampling, Nature Photonics 11, 361 (2017)

[8] Y. He, et al. Time-bin-encoded boson sampling with a single-photon device, Phys. Rev. Lett. 118, 190501 (2017)

[9] H. Wang et al. Toward scalable boson sampling with photon loss, Phys. Rev. Lett. 120, 230502 (2018).

[10] H.-S. Zhong et al. 12-photon entanglement and scalable scattershot boson sampling with optimal entangled-photon pairs from parametric down-conversion, Phys. Rev. Lett. 121, 250505 (2018).

[11] H. Wang et al. On-demand semiconductor source of entangled photons which simultaneously has high fidelity, efficiency and indistinguishability, Phys. Rev. Lett. 122, 113602 (2019).

[12] X.-L. Wang et al. Quantum teleportation of multiple degrees of freedom of a single photon, Nature 518, 516 (2015).

[13] Y.-H. Luo et al. Quantum teleportation in high dimensions, arXiv: 1906.09697 (2019).

# Filter-free single-photon emission in an integrated cavity-waveguide device

**G. S. Solomon[1,2], T. Huber[1,3], M. Müller[1], Y. Shuai[1], and M. Davanco[2]**

[1] *Joint Quantum Institute, National Institute of Standards and Technology, & University of Maryland, College Park, MD, USA*
[2] *National Institute of Standards and Technology, Gaithersburg, MD, USA*
[3] *Currently: Technische Physik, University of Würzburg, Würzburg, Germany*

Semiconductor quantum dots (QD) embedded in micro-cavities are excellent sources of single-photon light, especially under resonant excitation [1]. Besides excellent single-photon properties, the underlying materials are similar to those used in well-established integrated photonics, motivating research on chip-scale photonic integration of these light sources. Indeed, some fundamental integration has begun in various laboratories.

Here, we discuss our recent progress in efficient chip-scale integration of quantum light sources. We have fabricated and tested a source based on the coupling of micro-pillar cavities containing QDs that are connected to ridge waveguides; see Fig. 1. This geometry allows us to resonantly excite single quantum-dot states in the plane of the chip *via* the waveguide while the quantum light is directed orthogonally in the vertical, off-chip collection axis. Our approach has several benefits. Often, in these sources the same spatial mode is used to resonantly excite the QD and to collect the emitted single photons, requiring cross-polarization to reduce the uncoupled scattered laser light. This inherently reduces the source brightness to 50 %, and could be critical for applications where the total efficiency—from generation to detection—must to be greater than 50 %. In addition, our measurements are completely filter-free: QD light is directly collected from the sample and (broadband) fiber-coupled into our detection scheme.

The device consists of a distributed Bragg reflector (DBR) cavity of GaAs and AlAs with a 4λ cavity (1.05 µm) of GaAs with a dilute layer of InAs QDs in the cavity center (Fig 1a). The planar structure is dry etched to form pillar cavities connected through ridge waveguides as shown in Fig. 1b-c. The pillar diameters are intentionally varied around 2.5 µm and the waveguide diameters are varied around 0.95 µm. Critical to suppressing scattered laser light is a polymer planarization of the device, on top of which gold is deposited with opening in the cavity regions. The waveguide regions are flared at the ends for free-space light-beam coupling, although we have used glued fiber coupling in the past [2].

The pillar cavity quality factors (Q's) are approximately 4000. The single QD emission lifetime is modified from 1000 ps (in the waveguide region) to 400 ps – the Purcel factor is about 2.5. Some applications require degenerate cavity modes while others require polarization. Here we show both cases. Second-order autocorrelation measurement results provide a suppression of multi-photon states [$g^{(2)}(0)$] of ~ zero (error: + 4.3 – 0 %) with no filtering at a Rabi frequency of 1 GHz – see Fig. 1d. At 6 GHz the source produces 20 Mcts/s when accounting for the detector efficiency and deadtime. We will discuss chip-scale integration schemes, including on-chip, real-time metrology [3].

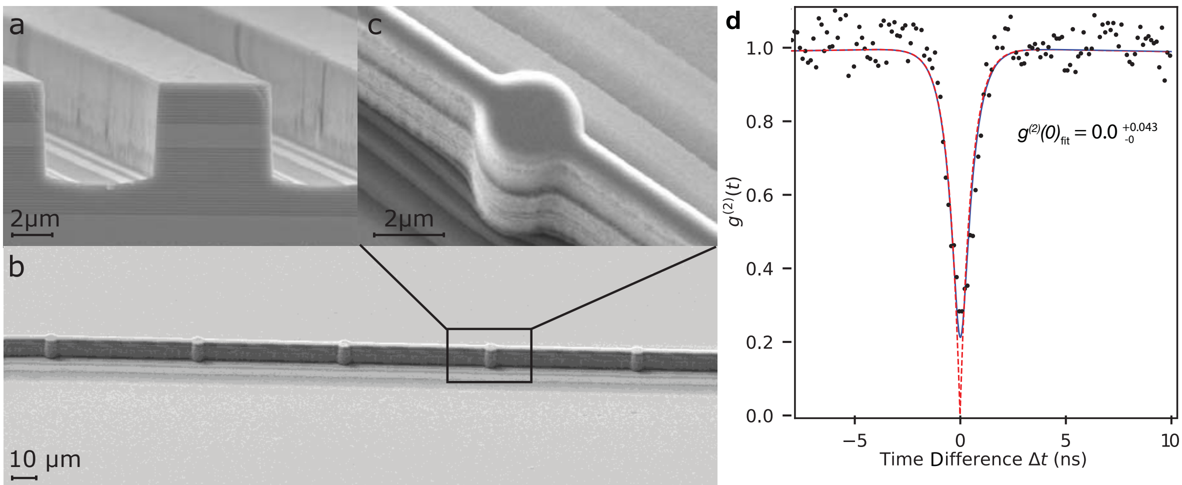


Figure 1. (a-c) Scanning-electron microscopy images. (a) Cleaved edge, showing cavity and DBR pairs—here, 5.5 µm wide for coupling. (b) The waveguide connecting micro-pillar cavities—5 shown here. (c) Single micro-pillar cavity, 2.8 µm in diameter, where the waveguide is 1.25 µm wide. (d) Second-order autocorrelations with no filtering showing multi-photon suppression to approximately zero.

**References**

[1] P. Senellart, G. S. Solomon, and A. White, Nat. Nanotech. **12**, 1026 (2017).
[2] E. B. Flagg, S. V. Polyakov, T. Thomay and G. S. Solomon, Phys. Rev. Lett. **109**, 163601 (2012).
[3] T. Thomay, *et al.*, Phys. Rev. X **7**, 041036 (2017).

# Quantum source and frequency conversion technologies based on integrated nanophotonics

**Kartik Srinivasan**[1,2]

[1] *Microsystems and Nanotechnology Division, NIST, Gaithersburg, MD, USA*

[2] *Joint Quantum Institute, NIST/University of Maryland, College Park, MD, USA*

Chip-integrated technologies based on scalable nanofabrication processes can help enable many applications in quantum communication, simulation, and metrology. In this talk, I will focus on our developments in building quantum source and frequency conversion technologies based on integrated photonic chips. The core physical resources that we rely on are on-demand emission of quantum light using single epitaxial quantum dots embedded in GaAs photonic structures [1], nonlinear-wave mixing in silicon nitride nanophotonics [2], and heterogeneous integration of dissimilar material platforms [3]. These resources have been used in collaboration with many colleagues in the US, Europe, and Asia to build a number of different quantum photonic device technologies, leading to demonstrations of: high-performance single-photon generation [4] and polarization-entangled photon pair generation [5] based on single quantum dots in circular grating microcavities, visible-telecom entangled photon pair generation based on four-wave mixing in silicon nitride microrings [6], quantum frequency conversion of a quantum dot single-photon source using four-wave mixing Bragg scattering in a silicon nitride microring resonator[7], tunable quantum interference of single photons using a microcavity quantum frequency converter[8], and heterogeneous integration of quantum dot single-photon sources with silicon nitride phtotonic circuits [9-10]. I will discuss our latest efforts in improving the performance of these devices and discuss some of the challenges we need to overcome moving forward.

Acknowledgements: I acknowledge the many students, postdocs, and collaborators that have been the key contributors to this work, including Vikas Anant, Antonio Badolato, Marcelo Davanço, Sven Hofling, John Lawall, Qing Li, Jin Liu, Xiyuan Lu, Richard Mirin, Gregory Moille, Sae Woo Nam, Armando Rastelli, Stephan Reitzenstein, Luca Sapienza, Peter Schnauber, Christian Schneider, Anshuman Singh, Jin Dong Song, Rongbin Su, Varun Verma, Xuehua Wang, and Daron Westly.

**References:**

[1] P. Senellart, G. Solomon, and A. White, "High-performance semiconductor quantum-dot single-photon sources," Nature Nanotechnology, vol. 12, no. 11, pp. 1026–1039, Nov. 2017.

[2] D. J. Moss, R. Morandotti, A. L. Gaeta, and M. Lipson, "New CMOS-compatible platforms based on silicon nitride and Hydex for nonlinear optics," Nature Photonics, vol. 7, no. 8, pp. 597–607, Jul. 2013.

[3] T. Komljenovic et al., "Heterogeneous Silicon Photonic Integrated Circuits," J. Lightwave Technol., vol. 34, no. 1, pp. 20–35, Jan. 2016.

[4] L. Sapienza, M. Davanço, A. Badolato, and K. Srinivasan, "Nanoscale optical positioning of single quantum dots for bright and pure single-photon emission," Nature Communications, vol. 6, no. 1, Dec. 2015.

[5] J. Liu et al., "A solid-state source of strongly entangled photon pairs with high brightness and indistinguishability," Nat. Nanotechnol., vol. 14, no. 6, pp. 586–593, Jun. 2019.

[6] X. Lu et al., "Chip-integrated visible–telecom entangled photon pair source for quantum communication," Nature Physics, vol. 15, no. 4, pp. 373–381, Apr. 2019.

[7] A. Singh et al., "Quantum frequency conversion of a quantum dot single-photon source on a nanophotonic chip," Optica, vol. 6, no. 5, p. 563, May 2019.

[8] Q. Li et al., "Tunable quantum beat of single photons enabled by nonlinear nanophotonics," arXiv:1905.01698 [physics, physics:quant-ph], May 2019.

[9] M. Davanco et al., "Heterogeneous integration for on-chip quantum photonic circuits with single quantum dot devices," Nature Communications, vol. 8, no. 1, Dec. 2017.

[10] P. Schnauber et al., "Indistinguishable Photons from Deterministically Integrated Single Quantum Dots in Heterogeneous GaAs/Si 3 N 4 Quantum Photonic Circuits," Nano Lett., p. acs.nanolett.9b02758, Sep. 2019.

# Programmable mutliphoton graph states on a silicon chip

**Jeremy C. Adcock, Caterina Vigliar, Sam Morley-Short, Raffaele Santagati, Joshua W. Silverstone and Mark G. Thompson**

*Quantum Engineering Technology (QET) Labs, H. H. Wills Physics Laboratory & School of Computer, Electronic Engineering & Engineering Mathematics, University of Bristol, Merchant Venturers Building, Woodland Road, Bristol BS8 1UB, UK*

Quantum computers promise a paradigm shift in humanity's ability to process information, but require precise control over large arrays of quantum systems—a formidable challenge. Meanwhile, silicon photonics offers a scalable, high-performance and ultimately reconfigurable platform to control single photons, with large-scale devices [1], and multiphoton capability already demonstrated [2].

Graph states are the predominant language of entanglement between qubits, and are central to the prevailing model of quantum information processing—measurement-based quantum computing [3]. A graph state's vertices are qubits and its edges are entanglement between them. Modern quantum error correction—a crucial component of large-scale quantum computation—relies centrally on graph state entanglement [3]. Different graphs enable different computational tasks, and so the generation of *arbitrary* graph states is powerful.

So far, the creation of optical graph states has been limited to just a few species, realised with bespoke, static apparatus in bulk-optics. Here, we explore the programmable generation of arbitrary photonic graph states using a single device, aided by the reconfigurable postselected entangling gate (R-PEG) (see Fig. 1) [5]. We develop rules for the successful postselection of graph states, and probe which states are *inaccessible*. Further, we identify optimal photonic circuits capable of generating *accessible* graph states up to 8 qubits This provides an endgame strategy for the final era of postselected experiments, before heralded devices become a necessity.

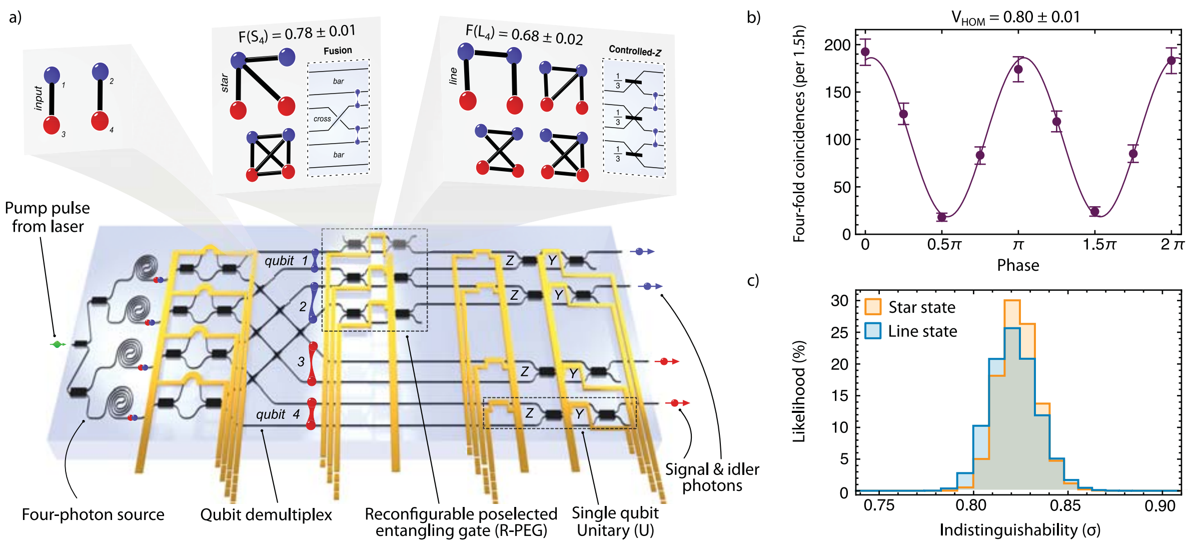


**Fig. 1** Generating optical graph states. a) Our four-photon device creates the star and line graph states, which represent both types of four-qubit graph state entanglement. b) A proposed 6-photon graph state generator can produce 63 of the 101 six-photon graph states, occupying 6 different entanglement classes. A representative member of each accessible class is shown.

We demonstrate the simplest of these schemes, implementing a four-photon, four-qubit graph state generator in silicon photonics. We successfully create representatives of both types of four-qubit graph state entanglement—the 'star' and 'line' graph states—for the first time in optics, achieving fidelities $0.78 \pm 0.01$ and $0.68 \pm 0.02$ respectively (see Fig. 1). Furthermore, we use the device to obtain record on-chip Hong-Ou-Mandel interference of $0.82 \pm 0.02$, and perform a basic measurement based protocol, generating two- and three-qubit states with fidelities above 0.77.

These results leverage silicon photonics' powerful reconfigurability for the generation of entangled resource states, illuminating the the path to increased multi-photon capability and expediting progress towards measurement-based quantum computing with photons.

## References

[1] Jianwei Wang, et al. "Multidimensional quantum entanglement with large-scale integrated optics." Science (2018): eaar7053.
[2] Imad I. Faruque et al. "On-chip quantum interference with heralded photons from two independent micro-ring resonator sources in silicon photonics." Optics express **26**.16 (2018): 20379-20395.
[3] Robert Raussendorf. "Measurement-based quantum computation with cluster states." International Journal of Quantum Information **7**.06 (2009): 1053-1203.
[4] Jeremy C. Adcock et al. "Hard limits on the postselectability of optical graph states." Quantum science and technology, **4**.1 (2018).

# Towards a loophole-free Bell experiment on a tabletop

**G. A. Kavuri[1,3], M. J. Stevens[1], P. G. Kwiat[2], S. W. Nam[1], L. K. Shalm[1,3]**
[1]*National Institute of Standards and Technology (NIST), 325 Broadway, Boulder, Colorado 80305, USA*
[2]*Department of Physics, University of Illinois, 1110 W Green St., Urbana, IL, USA*
[3]*Department of Physics, University of Colorado, Boulder, CO 80309*

The only way to generate certified random bits is by the use of a loophole-free Bell test. In 2018, we demonstrated device-independant random number generation, producing 1024 bits certified to have less than a $10^{-12}$ bias from a uniform distribution [1]. However, simultaneously closing all loopholes required our measurement stations to be separated by more than 185 m. We are currently developing a next-generation loophole-free Bell setup that would be able fit on a tabletop (5m). This will enable us to improve our random number generation rates by about 3 orders of magnitude, paving the way for simpler and more practical device-independant technologies.

The primary difficulty in shrinking our setup while still closing the locality loophole is the fast measurements that Alice and Bob must make, as illustrated in Fig 1. About 10 ns are available in which to finish setting up the polarizations to successfully close the locality loophole. In order to do this, we require the measurements to take place at GHz bandwidths. However, there are no known switches that can achieve this while also having low loss (less than 5%), which is vital for closing the detection loophole. We will present a scheme for an all-optical switch that can meet these challenging requirements simultaneously.

The switch is based on coherently upconverting signal photons with the use of a strong, fast modulated pump. Similar switch designs have already been demonstrated to be able to reach a 99.4% upconversion efficiency [2], albeit at lower rates than are desired. In order to be able to coherently upconvert polarization states of a photon, we propose an interferometric scheme that involves separating the two orthogonal polarization states of the incoming photon and copropagating an intense, fast-modulated pump through an upconversion crystal. The upconverted photons are then rotated back to their original polarizations and interferometrically recombined. This results in an upconverted photon whose orthogonal polarizations have the same relative phase as the copropagating pump. The pump can be modulated in a lossy way via conventional means such as a fast lithium niobate waveguide.

This tabletop apparatus would serve as a stepping stone to an on-chip loophole-free Bell experiment, which would open up new fundamental tests such as a loophole-free chained-Bell experiment and be useful for both public sources of randomness such as beacons and private randomness for cryptographic purposes.

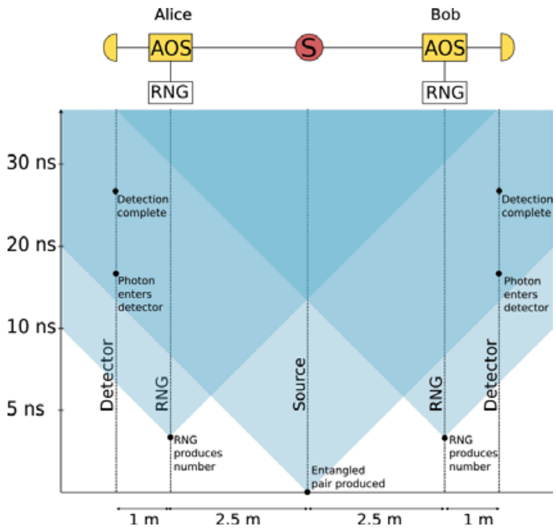


Figure 1: Space-time diagram for a Bell experiment on a tabletop. Light-cones are shaded in blue. To close the locality loophole, Alice (Bob) must complete the measurement before information about Bob's (Alice's) measurement setting from the random number generator (RNG) has time to reach them. The all optical switch (AOS) must be switched within the time window between the RNG stopping and the photon entering the detector (about 10ns).

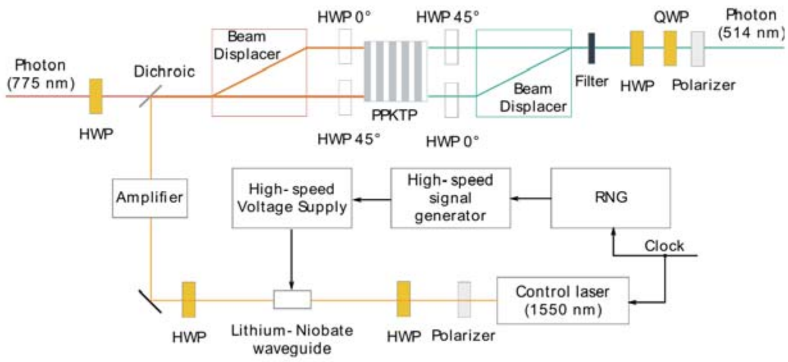


Figure 2: Schematic of the all optical polarization switch. The random number generator seeds the lithium niobate waveguide modulator which modulates the polarization of the pump. That phase information is then imprinted coherently on the upconverted photon which leaves us with a polarization modulated, upconverted signal.

## References

[1] P. Bierhorst, E. Knill, S. Glancy, Y. Zhang, A. Mink, S. Jordan, A. Rommal, Y.-K. Liu, B. Christensen, S. W. Nam, M. J. Stevens, and L. K. Shalm, "Experimentally generated randomness certified by the impossibility of superluminal signals," *Nature*, vol. 556, pp. 223–226, Apr. 2018.

[2] A. P. Vandevender and P. G. Kwiat, "High efficiency single photon detection via frequency up-conversion," *Journal of Modern Optics*, vol. 51, pp. 1433–1445, June 2004.

# Network Integration of Quantum Dot Device and Entanglement in Cambridge Fiber Network


**Z-H. Xiang[1,2], J. Huwer[1], R. M. Stevenson[1], J. Skiba Szymanska[1], M. B. Ward[1], I. Farrer[2, †], D. A. Ritchie[2], A. J. Shields[1]**

*1 Toshiba Research Europe Limited, Cambridge Research Laboratory, 208 Science Park, Milton Road, Cambridge, CB4 0GZ, UK.*
*2 Cavendish Laboratory, JJ Thomson Ave, Cambridge, CB3 0HD, UK.*
*† Present Address: Department of Electronic & Electrical Engineering, University of Sheffield, Sheffield S1 3JD, UK.*
*Author e-mail address: zx238@cam.ac.uk*


Entanglement provides means to transfer quantum information between distant nodes of a network and serves as the key resource for scalable quantum networks. Its practical use requires the integration of robust entangled photon sources, making the semiconductor-based QD light sources a promising candidate system. In this work [1], we have integrated an entangled QD device with the Cambridge Fiber Network. Such installed fiber typically suffers the variation of fiber birefringence over time, putting a negative impact on the transmission of entanglement. To compensate for these drifts, we have introduced a polarization maintaining sub-system, enabling stable long-term transmission of entangled photon pairs over 18km of installed fiber from a sub-Poissonian entangled photon pair source.

A transmission system consisting of a photon emission and detection sub-system and a polarization maintenance sub-system have been built for enabling the field-based qubit transmission, as is shown in Figure 1. The quantum dot photon source is located in a cryostat and optically excited with a laser at 1064nm. The emitted biexciton (XX) and exciton (X) photons are separated using a spectral filter. One of the entangled photons is sent over an installed loop-back fiber in the Cambridge Fiber Network before being measured.

To stabilize the polarization states of the transmitted photons, a time-multiplexed reference laser light at the same wavelength (1320nm) as the transmitted photons is split into two modes and the outputs of both arms are aligned to have orthogonal directions on the Poincaré sphere before being sent over the same fiber. The polarization state after the transmission is detected using two power meters after a polarizing beam splitter and a polarization controller. By stabilizing both references using an electronic polarization controller (EPC 5) and a fiber wave plate (FWP), we effectively lock arbitrary polarization rotation to a minimum on the Poincaré sphere.

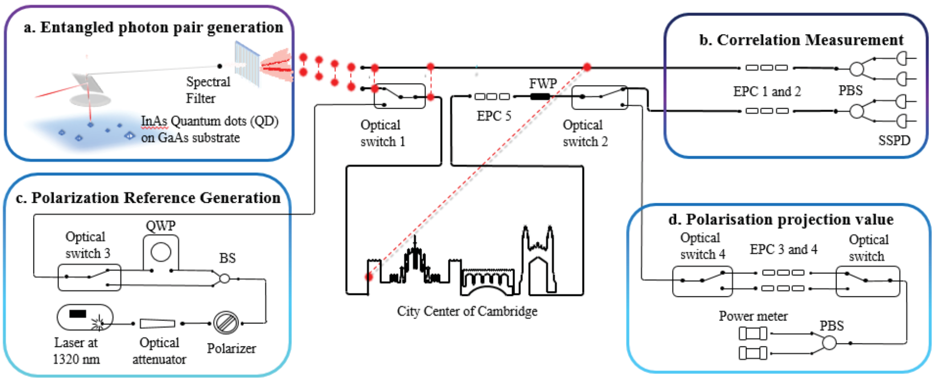


**Figure 1** Experimental setup for entangled photon transmission over installed fiber: The whole setup consists of 4 parts, entangled photon generation, correlation measurement, classical polarization reference generation and polarization reference measurement. The entangled photons are generated from an optically excited quantum dot in (a), whose entanglement fidelity is evaluated by correlation measurements in (b). Two classical polarization references are created using a 1320nm laser in (c), whose polarization state is detected in (d). Optical switches 1 and 2 are used for time-multiplexing the quantum and reference signal. EPC 5 and FWP are used for compensating the polarization drift of the field fiber that is installed across the Cambridge city center.

The entanglement is evaluated by measuring correlations $c_{PQ}$ between X and XX photons for co- and cross-polarized states P and Q in three detection bases HV, DA and RL and by using the following equation [2]:

$$F = (1 + C_{HV} + C_{DA} - C_{RL})/4$$

In which $C_{MN}$ denotes the correlation contrast. We have recorded correlation data for 7 days and observe a stable transmission of entanglement with a high fidelity of 91.3%. This corresponds to a drop by 3.4% compared to the measurements taken without photon transmission over the field fiber. The polarisation maintenance system has a low loss of 3.49dB and operates with a high duty cycle of 98%, enabling a high transmission efficiency of the photons. These results indicate a great potential for the practical use of QD entangled photon pair sources over existing telecommunication networks.


[1] Xiang, Zi-Heng, et al. "Long-term transmission of entangled photons from a single quantum dot over deployed fiber." Scientific reports 9.1 (2019): 4111.

[2] Ward, M. B., et al. "Coherent dynamics of a telecom-wavelength entangled photon source." Nature communications 5 (2014): 3316.

# From dark matter detection to artificial intelligence: applications of superconducting nanowire single photon detectors

**Sae Woo Nam**[1]

[1]*National Institute of Standards and Technology, Boulder, CO, USA*

Single-photon detectors are an essential tool for a wide range of applications in physics, chemistry, biology, communications, computing, imaging, medicine, and remote sensing. Ideally, a single photon detector generates a measurable signal only when a single photon is absorbed. Furthermore, the ideal detector would have 100% detection efficiency, no false positive (dark counts), and transform-limited timing resolution. Since the first reported detection of a single photon using a superconducting nanowire in 2001[1], steady progress has been made in the development and application of superconducting nanowire single photon detectors (SNSPD or SSPD) with ideal properties. I will briefly describe progress in detector developments, use of these detectors in new applications, and opportunities for future work.

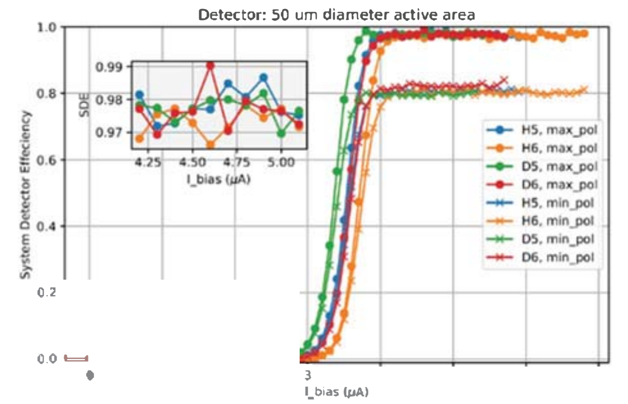


Figure 1 : Preliminary data from multiple pixels with high system detection efficiency at 1550nm with a SNSPD.

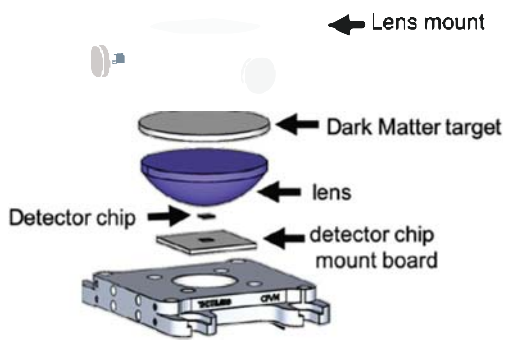


Figure 2 : Schematic of dark matter detection using SNSPDs.

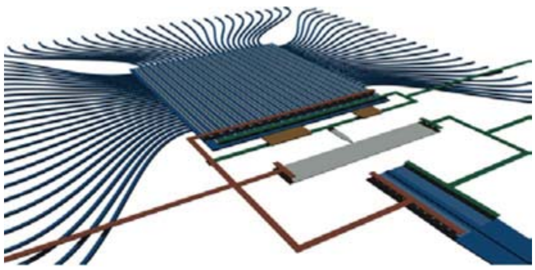

Figure 3 : Sketch of an artificial neuron using a single photon detector (SNSPD) and a weak light source (few photons).

**References**

[1] Gol'tsman, G. N., O. Okunev, G. Chulkova, A. Lipatov, A. Semenov, K. Smirnov, B. Voronov, A. Dzardanov, C. Williams, and Roman Sobolewski. "Picosecond Superconducting Single-Photon Optical Detector." *Applied Physics Letters* 79, no. 6 (August 1, 2001): 705–7. https://doi.org/10.1063/1.1388868.

# High detection rate and high efficiency with parallel SNSPDs

**Matthieu Perrenoud[1], Misael Caloz[1], Claire Autebert[1], Christian Schönenberger Hugo Zbinden[1], Félix Bussières[1,2]**

[1] *Group of Applied Physics – Quantum Technologies, University of Geneva, Geneva, Switzerland*

[2] *ID Quantique SA, Carouge, Switzerland*

Achieving ultra-high detection rate with high efficiency is crucial for many applications requiring fast single photon detection, such as Quantum Key Distribution. SNSPDs have the potential to reach very large counting rates, but the ubiquitous SNSPD design based on a single meander exhibits a limited detection rate due to its recovery time, the latter being essentially limited by the device's kinetic inductance and latching effects. One potential approach to increase the counting rate of SNSPD consists in splitting the SNSPD meander in several sections connected in parallel [1,2]. This allows for a reduced kinetic inductance per section and to virtually no dead-time (the efficiency is never equal to zero after a single detection), with the advantage of requiring a single coaxial line readout instead of one per pixel, as it is necessary for multi-pixel SNSPDs [3]. In practice, such a design is however subjected to electrical cross-talk between the parallelly-connected sections, which leads to current pile-up in other sections as the counting rate increases. This can ultimately cause all nanowires to become resistive simultaneously through a cascading effect (even though only a few might have clicked at first), which can lead to latching. Overall, the potential for high-count rates of parallel SNSPDs is seriously hindered by these effects.

Here we report on a new approach to mitigate the effects of cross-talk and the latching it can cause in parallel SNSPDs. Specifically, we developed parallelly-connected SNSPDs with additional unexposed sections acting as a current redistribution means [4]; see Fig. 1a. By carefully choosing the number of current redistribution means, their geometries (length, cross section) and series resistances, we can reduce cross-talk and completely eliminate latching at high count rates. Using this method, we will report on MoSi-based SNSPDs with high efficiency (~77%) at 1550 nm and detection rates as high as 200 MHz. The mean efficiency per photon as a function of the detection rate with an illumination by a continuous wave laser is shown on Fig. 1b. The efficiency is reduced to 40% with a 80 MHz detection rate, and to ~10% with a 200 MHz detection rate. This kind of design can also be used for photon number resolution, which we measured for up to 6 photons. Its use for high-speed quantum key distribution will be discussed. We will further discuss the potential improvements and application of SNSPD based on this design.

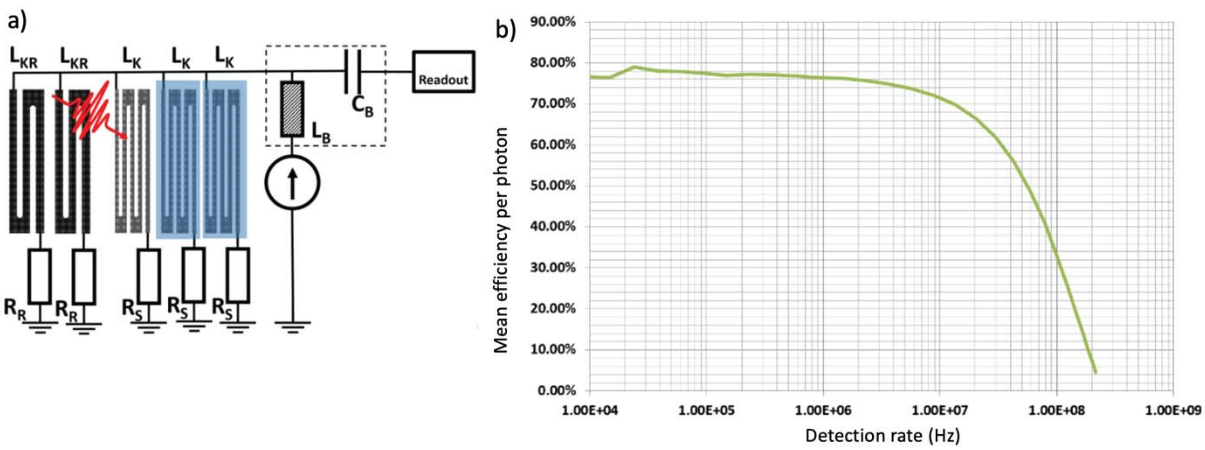


Fig. 1 **a**) Schematics of the electrical structure. Only the active meander sections (light grey) are exposed to light. When a photon is absorbed in one of the section, electrical crosstalk is seen in the other remaining sections (blue rectangles). The additional unexposed paths (dark grey) reduce the crosstalk amplitude and prevent unwanted cascading effects.
**b)** Efficiency of the detector as a function of the detection rate when illuminated by a CW laser. The 3dB-efficiency drop rate is situated around 80 MHz, and detection rates as high as 200 MHz are still achievable with an efficiency close to 10%.

## References
[1] Ejrnaes M. et al, "A cascade switching superconducting single photon detector", *Appl. Phys. Lett*, ***91** 262509* (2007)
[2] Tarkhov M. et al, "Ultrafast reset time of superconducting single photon detectors", *Appl. Phys. Lett*, ***92** 241112* (2007)
[3] Rosenberg D. et al, "High-speed and high efficiency superconducting nanowire single photon detector array", *Optics Express, Vol 21, no2* (2013)
[4] Patent pending

# Progress in superconducting optoelectronic networks for neuromorphic computing

**S. M. Buckley, J. T. Chiles, A. N. McCaughan, A. N. Tait, R. P. Mirin, S. W. Nam, J. M. Shainline**

*National Institute of Standards and Technology, NIST, Boulder CO 80301*

We have previously proposed a superconducting opto-electronic platform for neuromorphic computing which utilizes semiconductor LED light sources coupled to integrated waveguides for communication, and superconducting single photon detectors and superconducting electronics for computation. In this talk we will review the progress in realizing this platform.

The basic principle, shown in Fig. 1 (a), is that computation is performed by integrate and fire neurons, which use a semiconductor LED as the "fire", sending light down a series of on-chip waveguides. Downstream neurons will detect this firing event on "synapses", which consist of superconducting nanowire single photon detectors (SPDs), whose weights can be controlled either directly for simple demonstrations [1], or via superconducting circuits [2]. The main elements of this platform are therefore 1) Waveguide coupled silicon LEDs 2) Waveguide coupled SPDs 3) Superconducting amplifiers 4) Waveguide networks for communication and 5) Superconducting circuits based on josephson junctions and mutual inductors. Strong experimental progress in each of these elements has been made in the past year, which we will detail in this talk. Spiking neural networks with a high degree of physical connectivity and operating at speeds thousands of times faster than that of the brain can be realized with these components.

The LED light sources are based on W centers in Si. We have previously demonstrated waveguide coupled Si W center LEDs integrated with waveguide coupled SPDs [3]. In the past year we have been designing improvements for the next generation of LEDs, which should show efficiencies improved by several orders of magnitude. Furthermore, a high degree of scalability is required for this hardware platform, and therefore reproducible waveguide coupled SPDs with saturated internal quantum efficiencies are required. We have recently optimized a high-Si content WSi recipe that shows saturating internal quantum efficiency at 1550 nm for wire widths in excess of 1 um wide. An optical microscope image of a high dynamic range detector array incorporating 15 such saturating waveguide integrated SPDs on in a single photonic device is shown in Fig. 1(b). Finally, in order to interface the superconducting nanowire detectors with the semiconductor LED, a voltage amplifier is required. This is due to the fundamental bandgap mismatch between superconductors and semiconductors. We have demonstrated a h-Tron voltage amplifier which can provide the voltage and current needed to power the waveguide LED (Fig 1 (c)).

Using evolutionary optimization, we have run simulations to design spiking neural networks to demonstrate that we can perform simple classification and control tasks with just these components, at very low on-chip energy densities [1]. While the aforementioned elements (1-4) provide the core necessary functionality for such simple demonstrations, the real strength of this platform lies in the ability to emulate, in hardware, many of the important features of the brain that lead to cognition, at high speed and large scale [2]. For this computational complexity, further superconducting circuits are required [2] (Fig. 1 (d)). We have designed and simulated superconducting circuits, based on Josephson's junctions and mutual inductors, to implement biological functionality including spike timing dependent plasticity, synaptic plasticity, dendridic compartments and more.

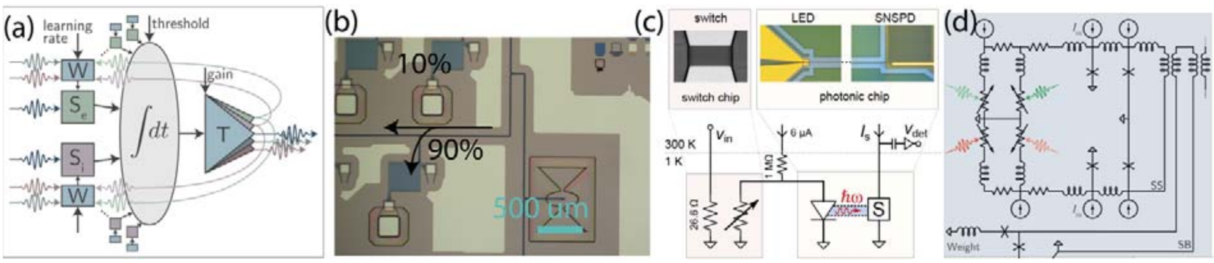


Fig. 1 The basic elements of the superconducting opto-electronic neuromorphic hardware platform.

## References

[1] Buckley et al., 2018 IEEE International Conference on Rebooting Computing
[2] Shainline et al., J. Appl. Physics 124 (2018)]
[3] Buckley et al., Appl. Phys. Lett. 111, 141101 (2017)
[4] McCaughan et al., ArXiv: 1903.10461v1 (2019)

# Time-resolved measurement of a single-photon wave packet with an optical Kerr effect

**Takahiro Takumi[1], Fumihiro China[2], Masahiro Yabuno[2], Shigehito Miki[2], Hirotaka Terai[2], Ryosuke Shimizu[1]**
*[1]Univ. of Electro-Comm., Tokyo, Japan, [2]NICT, Tokyo, Japan*

Single-photon detection with precise arrival timing information is of vital importance for many applications in the field of quantum information and quantum optical technologies. Recent technological developments of single-photon detectors allow us to observe photons with temporal resolution down to ~20 ps [1]. However, it is still a challenging task to achieve sub-picosecond temporal resolution. In this range, optical gating with an ultrashort laser pulse provides an effective way to observe photons. Up to now, the optical gating utilizing a frequency up-conversion has been reported and achieved sub-picosecond temporal resolutions. Using this technique, we have verified time-frequency duality of biphotons [2]. However, the frequency up-conversion process requires a phase-matching condition, resulting in the limitation of observed wavelength or bandwidth. On the other hand, an optical Kerr gate technique has been well-developed in the field of an ultrafast spectroscopy. The optical Kerr effect is expected to offer a higher temporal resolution than the frequency up-conversion technique because of no requirement in the phase-matching condition. Nevertheless, there is no report using optical Kerr gate for a single-photon detection. Here we present the first experimental demonstration of a single-photon detection using the optical Kerr effect.

Schematic diagram of our experiment is depicted in Fig. 1. In our method, we utilized cross-phase modulation induced in a photonic crystal fiber (PCF), placed in a Sagnac interferometer, with the length of 28cm. In the measurement of a single-photon wave packet, we prepared heralded single photons from a PPKTP crystal. The gate pulses were co-propagated with the single photon in the counter-clockwise direction, and the clockwise propagating photons in the Sagnac interferometer were used as the reference. We measured coincidence counting rates by scanning the relative delay between the gate pulse and the single-photon wave packet. Observed data is shown in Fig. 2. From this experiment, we can clearly see the single photon wave packet with the temporal width of ~4 ps, which is a good agreement with the theoretically expected one. The temporal resolution of our system is estimated to be ~400 fs from the rising time of the observed wave packet.

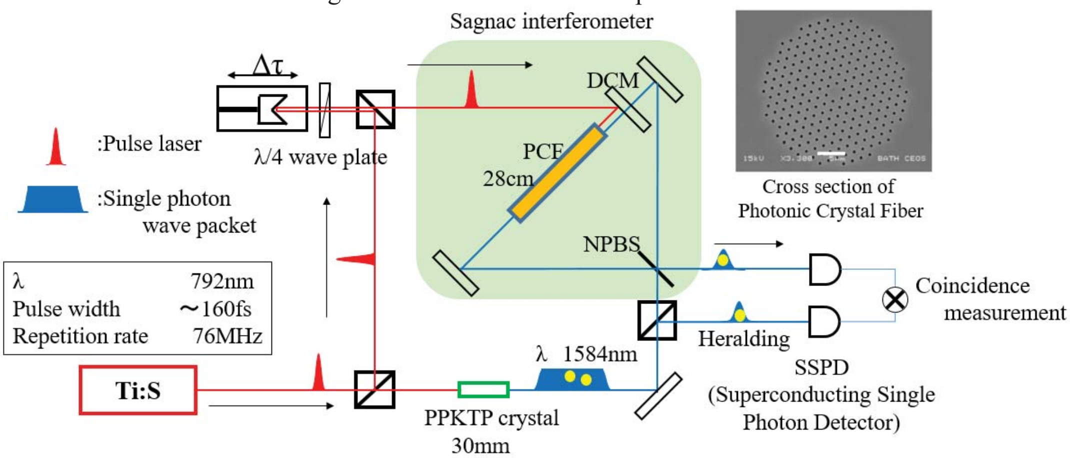


Fig. 1 Schematic diagram of our experimental set up.

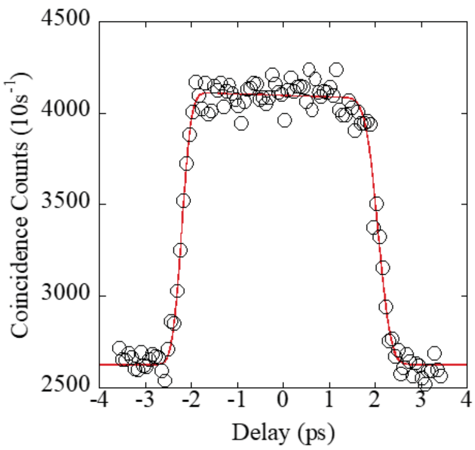


Fig. 2 Observed single photon wave packet.

**References**
[1] J. Wu, *et al.,* Appl. Opt., 56, 2195 (2017)
[2] R. B. Jin, *et al.,* Phys. Rev. Appl., 10, 034011 (2018)

# Quanta Image Sensor Progress

**Jiaju Ma**[1], **Stanley Chan**[2], **and Eric R. Fossum**[3]

[1]*Gigajot Technology Corporation, Pasadena, CA USA*

[2]*Electrical and Computer Engineering Department, Purdue University, W. Lafayette, IN USA*

[3]*speaker, Thayer School of Engineering at Dartmouth, Hanover, NH 03894 USA* eric.r.fossum@dartmouth.edu

The Dartmouth Quanta Image Sensor (QIS) was presented at SPW2017 in Boulder. This is a CMOS room-temperature, megapixel resolution, small pixel pitch, photon-number-resolving image sensor [1]. The purpose of this paper is to update the single photon detector community of progress made since SPW2017. There are a number of contributors to this progress and the final author list may be adjusted accordingly. For now we list the principals.

Progress has been made on several fronts. A Dartmouth spin-off startup company, Gigajot Technology, has produced a user-friendly scientific-type camera based on the technology and this camera has been evaluated by a number of groups, confirming the performance of the QIS device. (e.g., an independent paper from RIT will also be submitted) Gigajot has continued to develop the technology and a brief summary of their progress will be reported.

Additional computation imaging work by Purdue on denoising low-photon-count images will be included. (Gigajot and Purdue propose to report color results in a separate submitted paper).

At Dartmouth, further lower temperature (down to -70C) measurements have been made on device characteristics such as conversion gain and read noise. Read noise is dominated by 1/f noise, typically modelled as McWhorter interface trap effects [1]. However, as we peel the read-noise onion, we believe the mobility-fluctuation scattering model of Hooge [2], as later suggested as a component in the "unified" Berkeley 1/f noise model [3], needs to be resuscitated to explain the experimental results. Reasonable agreement is achieved between measurement and the new model (see graphs below). The model may help explain unexpected persistent 1/f noise in our JFET devices.

Additional progress, such as on efficient calibration of arrays, will also be reported as time allows.

References:

[1] J. Ma, S. Masoodian, D. Starkey, E.R. Fossum, Photon-number-resolving megapixel image sensor at room temperature without avalanche gain, OSA Optica, vol. 4, no. 12, pp.1474-1481, December 2017. https://doi.org/10.1364/OPTICA.4.001474

[2] A.L. McWhorter, "1/f noise and related surface effects in germanium," Ph.D. dissertation, MIT, Cambridge, MA, 1955.

[3] F.N. Hooge. "1/*f* noise is no surface effect," Phys. Lett A 29.3 (1969): 139-140.

[4] K.K. Hung, P. K. Ko, C. Hu, and Y. C. Cheng, "A unified model for the flicker noise in metal-oxide-semiconductor field-effect transistors," IEEE Trans. Electron Devices, vol. 37, no. 3, pp. 654–665, 1990.

Noise modelling results from Dartmouth PhD student Wei Deng shown below, as an example.

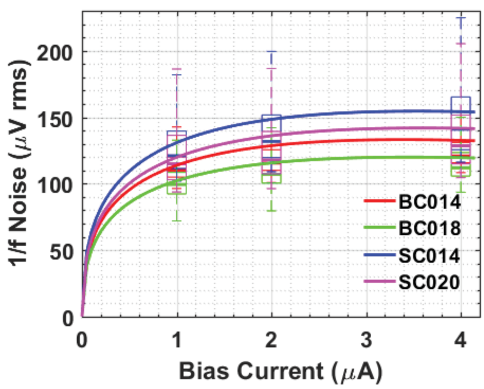


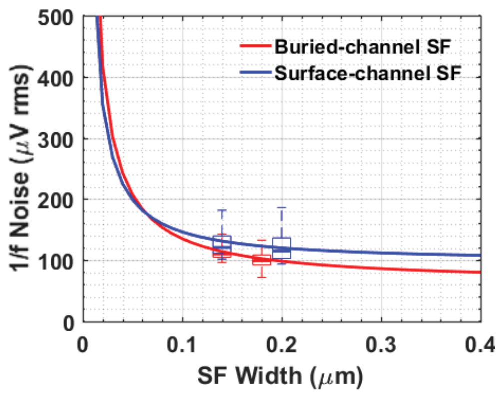


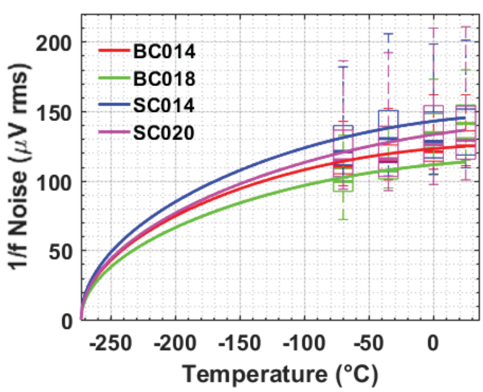

# Self-driving cars and LIDAR: Opportunities for Single Photon Detectors

**S. Verghese, C. Onal, J. Dunphy**
*Waymo, Mountain View, CA, USA*

Waymo's self-driving car fleet has been using custom LIDAR sensors for several years. In their latest revision, the LIDARs are designed to meet the challenging requirements we established through autonomously driving over 10 million highly-telemetered miles on public roads. Our goal for our sensors is to approach price points required for wide-scale deployment while meeting the performance needed for Level 4 fully autonomous self-driving. This talk will review some history of the project and describe a few use-cases for LIDARs on Waymo cars. Out of that will emerge key differences between single photon sensors for self-driving and traditional applications (biochemistry, astrophysics, mapping lidar) which could provide opportunities for optimizing single photon sensitive detectors for automotive LIDAR receiver implementations. We will discuss some of the unique requirements and challenges of using such detectors in high-dynamic-range environments, keeping in mind the scalability and durability constraints for long term deployment in a self driving fleet.

# Single-photon, single-pixel intelligent Lidar

**Gabriella Musarra[1], Alex Turpin[1,2], Ilya Starshynov[1], Ashley Lyons[1], Enrico Conca[3], Federica Villa[3], Daniele Faccio[1]**

*[1]School of Physics and Astronomy, University of Glasgow, Glasgow G12 8QQ, United Kingdom*

*[2]Leibniz Institute of Photonic Technology, Jena 07745, Germany*

*[3]Dipartimento di Elettronica, Informazione e Biongegneria, Politecnico di Milano, 20133 Milan, Italy*

The 3D imaging of direct line of sight scenes is a crucial task with applications in self-driving vehicles, robotics and face-recognition. Recent LiDAR systems demonstrated the 3D imaging of a scene by structure illuminating the scene and collecting the return signal by using time-resolved, single-photon sensitive detectors and inferring the depth information by the time required to the light to travel back to the sensor [1-2]. However current 3D imaging systems can be bulky devices with relatively low frame rate requiring scanning parts or many pixels sensors. Here we demonstrate a 3D imaging approach for intelligent-LiDAR, iLiDAR, in which laser pulses flood (flash) illuminate the scene and the return light is focused and collected with a time-resolving, single pixel detector, in this case a single pixel Single Photon Avalanche Diode (SPAD) detector. The SPAD sensor records only the arrival times of the return photons from the whole scene in a temporal histogram via Time-Correlated Single-Photon Counting (TSCPC), whilst the 3D information is recovered through previous Artificial Neural Network (ANN) training of the system using a commercial Time-of-Flight (ToF) camera.

The experimental approach is shown in Fig.1(a): the scene, in this case a person freely moving in a room, is flood illuminated with a pulsed light source and the back-scattered light is collected by single-point, time-resolving detector and recorded in a temporal histogram. We then use a pre-trained machine learning algorithm to reconstruct the full 3D image of scene by a fully-connected layer, feed-forward ANN. In our case, the input layer corresponds to the temporal histograms, while the output layer is an image with intensity-encoded depth. We train the ANN using a ToF camera to record 8000 pairs of 3D scenes (people and targets moving in random positions within a 2x2 $m^2$ area up to 4 m distance) together with their corresponding SPAD histograms.

As can be seen in Fig. 1(b), the single-point LiDAR is able to distinguish the general features of the scene and its distance from the sensor. In the first column we present experimentally recorded temporal histograms. The trained artificial neural network then retrieves a 3D image of the scene (second column). The corresponding, ground-truth, 3D images acquired by the ToF camera are shown in the third column for comparison. Our results demonstrate the possibility of achieving a scanless, compact, genuine single-pixel LiDAR system, providing a new approach for real-time 3D imaging and pattern recognition.

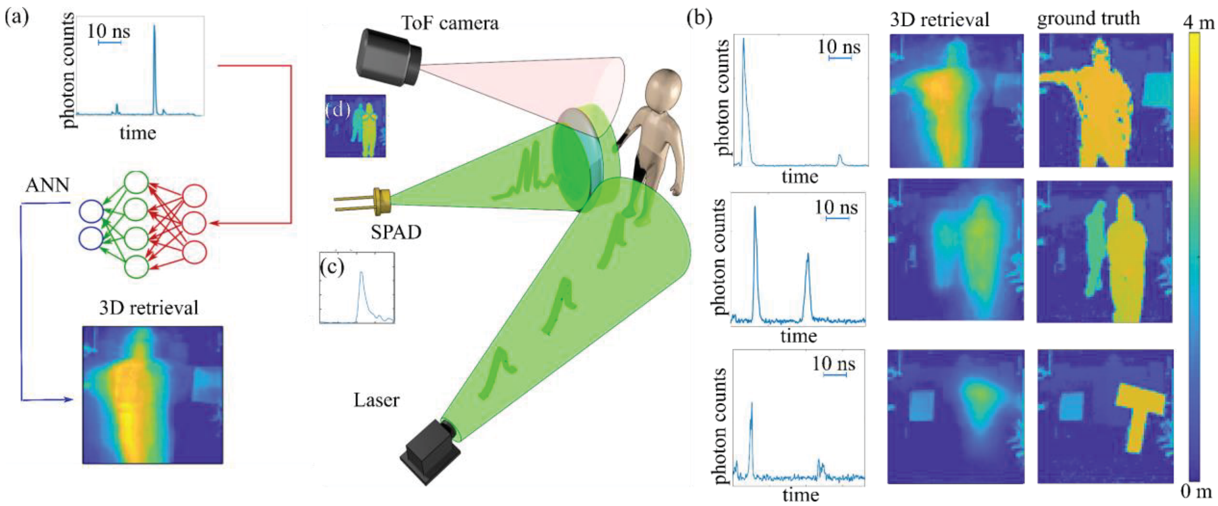


Fig.1. (a): A supercontinuum fiber pulsed laser (NKT SuperK Extreme, 20 ps pulse width, 19 MHz pulse repetition rate,) with a narrow filter at 550±50 nm is flash illuminating the scene and a single-pixel, time-resolving SPAD sensor [3] is collecting the return photons from the whole scene in a temporal histogram [inset (c)]. A ToF camera (PMD CardBoard Pico Flexx) is used to retrieve the 3D information of the scene, which is used for the training of the ANN [inset (d)]. 3D images of the scene are then obtained in a single-frame from the single-pixel temporal histograms after the ANN training. (b) Experimental results for a person, two people and a “T” target in the first, second and third row respectively. The first column represents the temporal histogram of the return photons collected by the SPAD sensor never used during the training of the ANN. The second column shows the 64x64 pixels 3D retrieved image from each histogram, while the third column shows the corresponding ground truth image.

**References**

[1] B. Schwarz, “Lidar: mapping the world in 3D,” Nat. Photon. 4, 429–430 (2010).
[2] P. Dong and Q. Chen, “LiDAR Remote Sensing and Applications”, (CRC Press, 2017).
[3] M. Sanzaro et all, “Single-Photon Avalanche Diodes in a 0.16μm BCD Technology With Sharp Timing Response and Red-Enhanced Sensitivity”, IEEE J. Sel. Top. Quantum Electron. 24, 2, 1-9 (2018).

# Three-dimensional imaging of dynamic underwater scenes using single-photon detection

**Aurora Maccarone[1], Aongus McCarthy[1], Julián Tachella[1], Francesco Mattioli Della Rocca[2], Yoann Altmann[1], Stephen McLaughlin[1], Robert Henderson[2], Gerald S. Buller[1]**

[1]*School of Engineering and Physical Sciences, Heriot-Watt University, Edinburgh, EH14 4AS, United Kingdom*
[2]*School of Engineering, University of Edinburgh, Edinburgh EH9 3FF, United Kingdom*

Time-correlated single photon counting (TCSPC) has emerged as a key detection technology for lidar and depth profiling in a number of application areas due to its high optical sensitivity and excellent surface-to-surface resolution. We have applied this technique to measure three-dimensional scenes of stationary and moving targets at 1.7 metres in several underwater environments using two different optical transceivers: (1) a single-pixel optical scanner system with an individual single-photon avalanche diode (SPAD) detector; and (2) a non-scanning camera based on a CMOS single-photon detector array. The first system used a monostatic transceiver scanning unit fibre-coupled to a silicon SPAD to raster scan the target and collect the single-photon returns [1]. The illumination was provided by a supercontinuum pulsed laser source with a wavelength tunable acousto-optic filter (AOTF), which allowed the selection of an individual operational wavelength based on the level of scattering of the environment. The laser source operated at a repetition rate of 19.5 MHz and average optical power of less than 3 mW. Several experiments were performed in dark laboratory conditions, demonstrating depth and intensity profiles of targets up to nine attenuation lengths between transceiver and target (i.e. 18 attenuation lengths round-trip) [2, 3]. The second system comprised a 192 × 128 pixel format CMOS SPAD detector array with picosecond timing electronics integrated in each pixel [4]. The transceiver system used for this SPAD detector array was configured in a bi-static layout and used a pulsed laser diode emitting at a wavelength of 670 nm with a repetition rate of 40 MHz. Experiments in a number of scattering environments demonstrated depth and intensity profiles of stationary targets achievable at up to 7.2 attenuation lengths and detection of moving targets at up to 6.7 attenuation lengths. We will show how this parallel data acquisition was exploited to adapt the camera system to show real-time three-dimensional video with low latency.

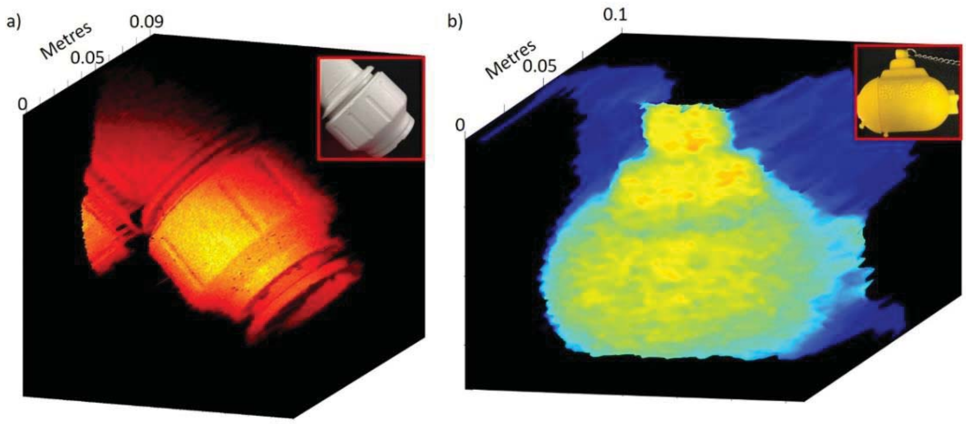


Fig. 1 a) Depth and intensity profiles of a plastic pipe connection target obtained with the single-pixel scanning system. The profile was measured at 8 attenuation lengths between system and target (i.e. 16 attenuation lengths round-trip), using a pixel format of 240 × 240, a per pixel acquisition time of 30 ms, and average optical power of 2.6 mW. The area scanned was 48 mm × 48 mm at a distance of approximately 1.70 meters. b) Depth and intensity profiles of a silicon submarine target obtained with the SPAD detector array system. The profile was measured at 1.2 attenuation lengths between system and target, aggregating 100 binary frames (of 1 ms acquisition time per frame), and using an average optical power of 2.5 mW. The area scanned was 48 mm × 60 mm at a distance of approximately 1.70 meters.

## References

[1] A. Maccarone, A. McCarthy, X. Ren, R. E. Warburton, A. M. Wallace, J. Moffat, Y. Petillot, and G. S. Buller, Underwater depth imaging using time-correlated single-photon counting. Opt. Express, 23(26), 33911-33926 (2015).
[2] A. Maccarone, A. McCarthy, A. Halimi, R. Tobin, A. M. Wallace, Y. Petillot, and G. S. Buller, Depth imaging in highly scattering underwater environments using time correlated single photon counting. Proc. SPIE 9992, Emerging Imaging and Sensing Technologies, 99920R (October 2016).
[3] A. Halimi, A. Maccarone, A. McCarthy, S. McLaughlin, and G. S. Buller, Object depth profile and reflectivity restoration from sparse single-photon data acquired in underwater environments. IEEE Trans. Comput. Imaging, 3(3), 472 - 484 (2017).
[4] R. K. Henderson, N. Johnston, F. Mattioli Della Rocca, H. Chen, D. Day-Uei Li, G. Hungerford, R. Hirsch, D. McLoskey, P. Yip, and D. J. S. Birch, A 192 × 128 Time Correlated SPAD Image Sensor in 40-nm CMOS Technology. IEEE J. Solid-St. Circ., 54(7), 1907-1916 (2019).

# Depth imaging through obscurants using single-photon detection in the short-wave infrared

**R. Tobin[1], A. McCarthy[1], A. Halimi[1], J. Tachella[1], Y. Altmann[1], M. Laurenzis[2], F. Christnacher[2], P. Soan[3], K. J. McEwan[3], S. McLaughlin[1], and G. S. Buller[1]**

[1] *School of Engineering and Physical Sciences, Heriot-Watt University, Edinburgh, EH14 4AS, United Kingdom*

[2] *French-German Research Institute of Saint-Louis, 5 Rue du Général Cassagnou, Saint-Louis, 68301, France*

[3] *Defence Science and Technology Laboratory, Porton Down, Salisbury, United Kingdom, SP4 0LQ*

In recent years, the time-correlated single-photon counting technique has emerged as a candidate algorithm for the depth and intensity profiling of targets in a wide range of LiDAR applications, such as long-range imaging [1,2], imaging in turbid underwater environments [3], multispectral imaging [4,5], and imaging in highly scattering environments [6]. The picosecond timing resolution and excellent surface-to-surface resolution of the technique allows high-resolution, three-dimensional imaging of long-range targets in extremely challenging environments, with very low visibilities.

We present two depth-imaging systems for free-space imaging in highly attenuating environments, such as in smoke and water-based fog. The first system is comprised of a custom-built, monostatic scanning transceiver unit fibre-coupled to a single-pixel, Peltier cooled InGaAs/InP single-photon avalanche diode (SPAD) detector. The second is a bistatic system using a 32 × 32 pixel array based on InGaAs/InP Geiger-mode avalanche photodiode (GmAPD) detector technology. Both of these systems use a pulsed laser source at an operating wavelength of 1550 nm with milliwatt average optical power levels, resulting in eye-safe imaging. These systems were used to obtain three-dimensional depth profiles of targets in high levels of obscurants, as shown in Fig. 1. The obtained results demonstrate the benefits of short-wave infrared (SWIR) wavelengths for imaging through highly scattering media, when compared to visible band sensors.

We also present a bespoke image processing algorithm, which was designed to exploit spatial correlations in sparse single-photon data to provide real-time reconstruction [7]. These algorithms can be applied to scenarios that result in many 'missing' pixels in the image where there was insufficient photon returns to provide a depth estimate, such as targets behind camouflage netting. The use of such algorithms can allow for successful target reconstruction in highly attenuating environments, even when using shorter acquisition times, high frame-rates, and low levels of optical power, even in the sparse photon regime.

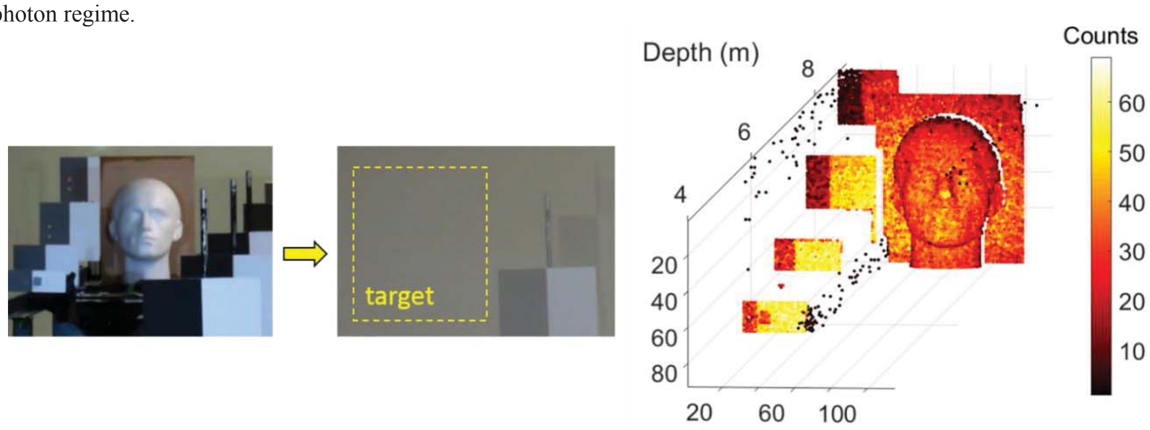


**Fig. 1:** High resolution depth profiling of a target through 24 metres of a scattering media obtained using the time-correlated single-photon counting technique and the time-of-flight approach reconstructed using a simple pixel-wise cross-correlation algorithm. These results were obtained using an illumination wavelength of 1550 nm and milliwatt average optical power levels.

## References

1. A. McCarthy et al., "Kilometer-range depth imaging at 1550 nm wavelength using an InGaAs/InP single-photon avalanche diode detector," Opt. Express, OE **21**(19), 22098–22113 (2013).
2. A. M. Pawlikowska et al., "Single-photon three-dimensional imaging at up to 10 kilometers range," Opt. Express, OE **25**(10), 11919–11931 (2017).
3. A. Maccarone et al., "Underwater depth imaging using time-correlated single-photon counting," Opt. Express, OE **23**(26), 33911–33926 (2015).
4. A. M. Wallace et al., "Design and Evaluation of Multispectral LiDAR for the Recovery of Arboreal Parameters," IEEE Transactions on Geoscience and Remote Sensing **52**(8), 4942–4954 (2014).
5. R. Tobin et al., "Comparative study of sampling strategies for sparse photon multispectral lidar imaging: towards mosaic filter arrays," J. Opt. **19**(9), 094006 (2017).
6. R. Tobin et al, "Three-dimensional single-photon imaging through obscurants," Optics Express **27**(4), 4590 (2019).
7. J. Tachella et al., "Real-time 3D reconstruction of complex scenes using single-photon lidar: when image processing meets computer graphics," in arXiv:1905.06700 [physics] (2019).

# Computational imaging with SPADs at SWIR wavelengths

**Martin Laurenzis, Stéphane Schertzer, Emmanuel Bacher, Frank Christnacher**
*French-German Research Institute of Saint-Louis, Saint-Louis, France*

Single Photon Counting Avalanche Diode (SPAD) sensors can be driven with reverse bias voltages beyond the breakdown point to count single photon events by triggering an avalanche effect. The event time can be read out with sub-nanosecond to a few 10 picosecond precision. Thus, SPAD sensors have the potential to revolutionize optical sensing by combining high sensitivity and high timing precision, and they can be used for computational imaging. In our experiments we used InGaAs SPAD devices as gated single diodes as well as 32x32 array detectors to perform active imaging at a laser wavelength of 1.5 µm.
As illustrated in Figure 1, due to high sensitivity, it is possible to observe light pulse in flight only slightly scattered by air. We investigated the propagation of light pulses with arbitrary flight path and developed an analysis method to determine both, the flight path and the position of the laser source, from few scattered photons [1,2]. From our results, we propose the application of SPAD array detectors for Laser Warning Devices which can detect and analyze laser irradiation without direct illumination. Further, we performed 3D imaging of static scene and rapidly moving targets to measure motion vectors and rotation velocities. Finally, we used both sensors (array and single diode) to measure the round trip times of photons with the aim to localize objects outside the line of sight. In our approach, we try to expand our field of regard or perception range not only to objects around a corner in a so-called 3-bounce scenario but also to object which are hidden deeper in the phase space (e.g. 5-bounce scenario and higher). As a resume of out work, we summarize our results and give predictions for future SPAD sensor development needs.

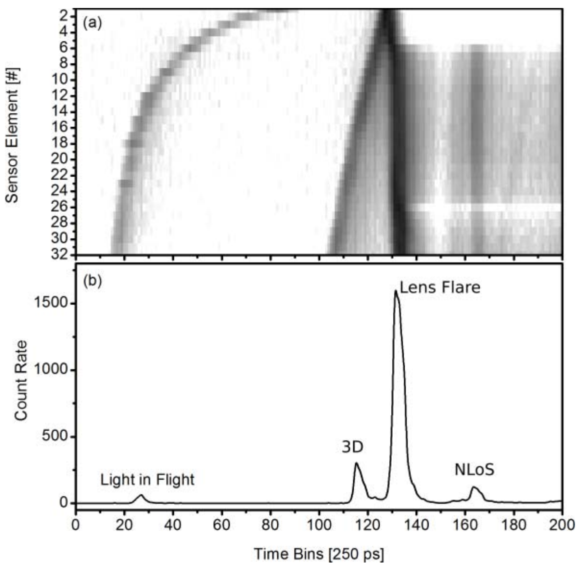


Fig. 1 Example of a multi-return SPAD signal for computational imaging containing returns from light-in-flight, 3D imaging, lens flare and non-line-of-sight targets [1].

**References**

[1] Laurenzis, M., Klein, J., Bacher, E., & Metzger, N. (2015). *Multiple-return single-photon counting of light in flight and sensing of non-line-of-sight objects at shortwave infrared wavelengths*. Optics Letters, 40(20), 4815-4818.

[2] Laurenzis, M., Klein, J., & Bacher, E. (2016). *Relativistic effects in imaging of light in flight with arbitrary paths*. Optics Letters, 41(9), 2001-2004.

[3] Laurenzis, M., La Manna, M., Buttafava, M., Tosi, A., Nam, J. H., Gupta, M., & Velten, A. (2018). *Advanced active imaging with single photon avalanche diodes*. Proceedings of SPIE, *Emerging Imaging and Sensing Technologies for Security and Defence III; and Unmanned Sensors, Systems, and Countermeasures*, 10799, 1079903

# Friday, October 25, 2019

| | | |
|---|---|---|
| 09:00 | Session 17<br>Detectors V<br><br>Chair: F. Villa | **J. Rothman - Reaching for GHz single photon detection rates with HgCdTe APD detectors** |
| 09:30 | | L. Gasparini - CMOS-SPAD arrays for Quantum Imaging Applications |
| 09:50 | | M. Zarghami - A Novel Approach to High Dynamic Range Imaging with CMOS-SPADs |
| 10:10 | | G. Jegannathan - Current-assisted single photon avalanche diode(CASPAD) in 350 nm CMOS |
| 10:30 | | G. Tortarolo - Towards Single-Photon Microscopy: Exploiting Extra Spatio-Temporal Information Provided by SPAD Array Detectors in Laser Scanning Microscopy |
| 10:50 | Coffee break (offered by MPD /OEC) | |
| 11:20 | Session 18<br>Sources IV<br><br>Chair: F. Piacentini | **P. Michler - Quantum dots at telecom wavelengths for single- and entangled photon sources** |
| 11:50 | | S. Francesconi - Engineering two-photon wavefunction and exchange statistics in a semiconductor chip |
| 12:10 | | C. P. Lualdi - High-Efficiency Time-Multiplexed Single-Photon Source |
| 12:30 | | C. Marvinney - Toward control of the quantum state of hBN single-photon emitters |
| 12:50 | | J. Grim - Three-Quantum-Dot Superradiance in a Photonic Crystal Waveguide Enabled by Scalable Strain Tuning |
| 13:10 | Lunch | |
| 14:15 | Session 19<br>Applications VII<br><br>Chair: I. Degiovanni | **Q. Zhang - Single photon technology in Long Distance Quantum Communication** |
| 14:45 | | F. Xu - Experimental quantum repeater without quantum memory |
| 15:05 | | A. Scriminich - Hong-Ou-Mandel interference of polarization qubits stored in independent room-temperature quantum memories |
| 15:25 | | S. Grandi - Towards long distance entanglement between a photon and a solid-state quantum memory |
| 15:45 | | M. F. Askarani - Entanglement and non-locality between disparate solid-state quantum memories mediated by photons |
| 16:05 | Concluding remarks | |
| 16:15 | Farewell coffee | |
| 16:45 | End | |

# Reaching for GHz single photon detection rates with HgCdTe APD detectors

**Johan Rothman[1], Salvatore Pes[1], Pierre Bluet[1], Julie Abergel[1], Sylvain Gout[1], Philippe Ballet[1] Jean-Louis Santailler[1], Jean-Alain Nicolas[1], Jean-Pierre Rostaing[1], Sebastien Renet[1], Lydie Mathieu[1], Jérôme Le Perchec[1]**

[1]*CEA-Leti, Grenoble, France*

The high gain and low excess noise factor in HgCdTe APDs enables down to single photon detection with a detection efficiency that are expected to exceed 90%. As the detection is done in linear mode these detectors conserve a high dynamic range that enables to detect multi-photon states on a single detector and do not exhibit a dead-time after the detection of one or a number of photons. The latter means that the detection rate is only limited by the bandwidth of the APD and the pre-amplifier, which is why rates in excess of 1 GHz can be achieved in such detectors[1], surpassing other single photon detection technologies by a factor 10 to 1000. Such high count-rates makes HgCdTe APDs and interesting candidate both for classical free space optical communications and for quantum optics application such as quantum cryptography and quantum computing.
The GHz single photon rate landmark has been approached at CEA/Leti by the development of a detection module for deep space FSO in collaboration of ESA. The detection module is a four quadrant HgCdTe APDs, designed to minimize the collection time of the carriers and hybridized to a dedicated CMOS circuit with resistive trans-impedance amplifier (RTIA). The bandwidth and count rate of each channel is limited to 400 MHz by the low noise RTIA. Single photon detection has been demonstrated up to count rates of 500 MHz with such module, implying a cumulated detection rate of 2 GHz if the signal is dispatched over all four quadrants. Fig. 1 compares the dark signal at the output of the detector with a pulsed signal at 500 MHz with about one photon per pulse. The aim of this communication is to discuss the expected optimal performance of HgCdTe APDs at GHz count rates in perspective of the most recent results, such as detection efficiency jitter, dark-count rate and maximum count-rate, which have been measured on present detector modules.

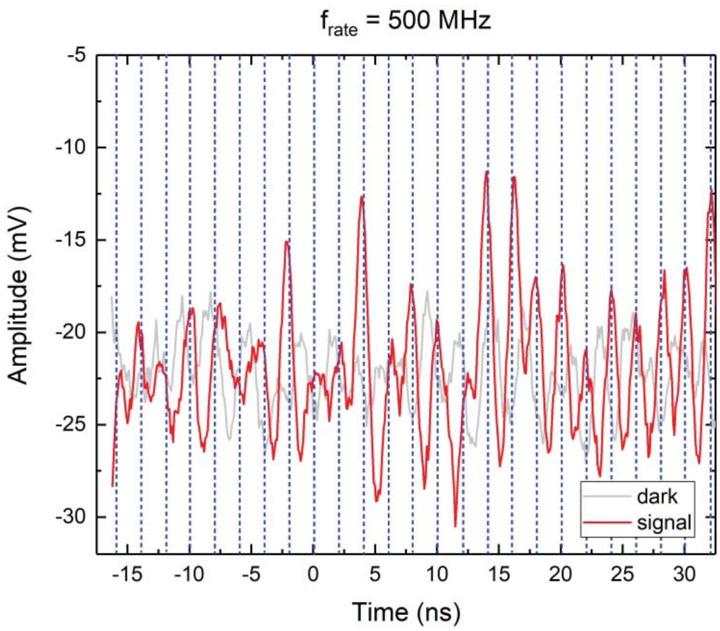


Fig. 1 Single photon level signal with a pulse repetition rate of f=500 MHz detected using a free space coupled HgCdTe APD detector (red trace). The blue dashed lines indicates the instant of arrival of the photons. The signal is compared with a typical dark measurement (without laser light on the detector), plotted with a gray trace.

**References**

[1] Johan Rothman, Pierre Bleuet, Luc André, Quentin Abadie, Geoffroy Bordot, Sylvette Bisotto, Guillaume Audoit, Jean-Alain Nicolas, Bertrand Dupont, Jean Pierre Rostaing, Gilles Lasfargues, "HgCdTe APDs for free space optical communications", Proceedings of SPIE Vol. 10524, 1052411 (2018)

# CMOS-SPAD arrays for Quantum Imaging Applications

**L. Gasparini[1], M. Zarghami[1], M. Perenzoni[1], L. Parmesan[1], M. M. Garcia[1], V. Mitev[2], L. Balet[2], N. Torcheboeuf[2], D. Boiko[2], M. Unternährer[3], B. Bessire[3], A. Stefanov[3]**

[1]*Fondazione Bruno Kessler, Trento, Italy*

[2]*CSEM, Neuchâtel, Switzerland*

[3]*Institute of Applied Physics, University of Bern, Bern, Switzerland*

SUPERTWIN is a H2020 European FET-OPEN project that aims at building an all-solid-state super-resolution quantum microscope. The basic idea consists in exploiting the non-classical correlations existing among entangled N-photon states to overcome the diffraction limit by a factor of N. The project poses significant challenges on the detector in terms of efficiency. The parameters of interest include photon detection efficiency (PDE), timing resolution, spatial resolution and duty cycle.

Superconducting Nanowire Single Photon Detectors represent the state of the art in terms of PDE and timing resolution, but array implementations are limited to few channels. Correlated imaging is therefore achieved through N-dimensional scanning, which becomes unfeasible for large values of N. Scanning can be avoided using image sensor-based technologies, such as intensified cameras. In this case, the main limitation is given by the poor duty cycle, in the order of $10^{-6}$.

Recently, arrays of single photon avalanche diodes (SPADs) in CMOS technology have been proposed for this application. For example, [1] consists of a 32×32 array of photon-timestamping pixels, each including a SPAD and an 8-bit, 205-ps Time-to-Digital Converter. The sensor, fabricated in a fully standard 150-nm CMOS technology, achieves a state-of-the-art pixel fill-factor of 19.48% on a 44.64 µm pitch. Fig. 1 shows the details of the pixel. By means of smart readout mechanisms implemented on chip, the sensor achieves a duty cycle which is 4 orders of magnitude larger than intensified cameras.

The sensor has been successfully employed in a number of quantum optics experiments, including imaging of a Spontaneous Parametric Down-Conversion (SPDC) source of entangled photons, shown in Fig. 2, super-resolution quantum imaging at the Heisenberg limit using SPDC photons [2], the investigation of diffraction patterns of bi-photon states [3].

At the time of the workshop, we will summarize the results achieved by the SUPERTWIN project from the detector perspective, highlighting advantages and limitations of CMOS SPAD technology in quantum optics applications.

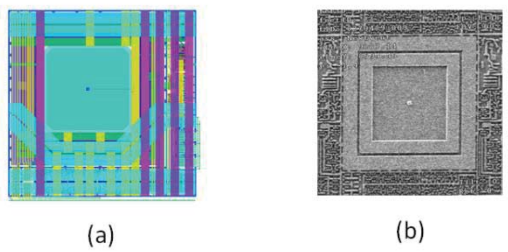


Fig. 1 (a) Layout and (b) picture after poly deposition of the pixel. The large square rings around the SPAD correspond to dead area needed to avoid punch-through between the SPAD well, which operates at >20 V, and the 1.8 V logic.

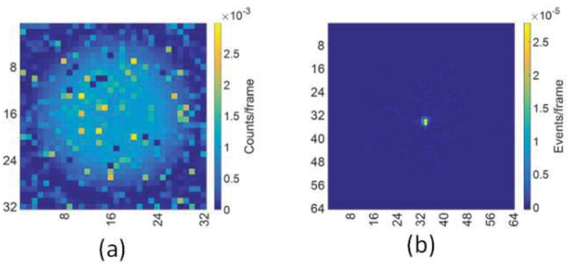


Fig. 2 (a) Far-field image of the 810-nm photon flux generated by an SPDC source and (b) 2D histogram of the barycenter of detected bi-photons, demonstrating that the biphotons are anti-correlated in their direction of emission.

**Acknowledgements**

We thankfully acknowledge the support of the European Commission through the SUPERTWIN project, id. 686731.

**References**

[1] L. Gasparini *et al.*, "A 32×32-pixel time-resolved single-photon image sensor with 44.64µm pitch and 19.48% fill-factor with on-chip row/frame skipping features reaching 800kHz observation rate for quantum physics applications," *2018 IEEE Int. Solid-State Circuits Conference (ISSCC)*, San Francisco, CA, 2018, pp. 98-100.

[2] M. Unternährer *et al.*, "Super-resolution quantum imaging at the Heisenberg limit," *Optica* 5, 1150-1154 (2018)

[3] V. Mitev *et al.*, "Validation of échelle-based quantum-classical discriminator with novelty SPAD array sensor," *Proc. SPIE 10934, Optical, Opto-Atomic, and Entanglement-Enhanced Precision Metrology, 109341V* (1 March 2019);

# A Novel Approach to High Dynamic Range Imaging with CMOS-SPADs

**Majid Zarghami[1,2], Leonardo Gasparini[1], Matteo Perenzoni[1], and Lucio Pancheri[1,2]**

[1]*Fondazione Bruno Kessler (FBK), Center for Material and Microsystems (CMM), Trento, Italy*

[2]*Department of Industrial Engineering, University of Trento, Trento, Italy*

High Dynamic Range (HDR) operation is required for applications such as automotive to cover a large variation of illumination intensity[1]. The capability to count single photons up to 100's Mphotons/s enabled Single Photon Avalanche Diodes (SPADs) to achieve a HDR [1]. This work exploits the excellent timing resolution of SPADs to extend the dynamic range beyond the saturation level by extracting the intensity of light from the photon inter-arrival times, reaching 138.7-dB dynamic range within 30-ms integration time [2]. The SuperEllen chip [3] was employed to experimentally validate the proposed method. The sensor features 32×32 pixels with 44.64-μm pitch, 19.48% fill-factor, each containing one SPAD and an 8-bit Time-to-Digital Converter (TDC). For this experiment, the TDC timing resolution was set to ~300-ps. Several ($N_{obs}$) observations were taken to populate a histogram of inter-arrival times, accumulating an effective integration time of 30-ms. Every histogram contains two pieces of information: the number of detected photons ($N_{ph}$) and their Average Arrival Time (AAT). At low photon flux densities, the intensity of light can be estimated from the number of photons detected ($N_{ph}/N_{obs}$), as done in a standard photon counting pixel (Fig. 1(a)). When the flux is higher as shown in Fig. 1(b) and (c) , the counter saturates ($N_{ph}/N_{obs}=1$), so we can estimate the flux from the AAT. Fig. 1(c) displays a sample condition with very high flux density having an AAT much lower than the SPAD dead time. This is possible thanks to a quenching mechanism that turns on the SPAD synchronously with the opening of the observation window. Fig. 1(d) shows that the proposed method extends the dynamic range by 42.8-dB with respect to the standard mode based on the photon counting. Fig. 2 contains a sample HDR image. Fig. 2(a) shows the observed scene. Fig. 2(b), (c) display the captured image when estimating the photon flux from $N_{ph}$ and AAT, respectively. Each mode represents either low flux or high flux part in detail, not both. Fig. 2(d) merges the two images into a single HDR image, demonstrating the effectivity of the proposed method by identifying different intensities at all flux levels.

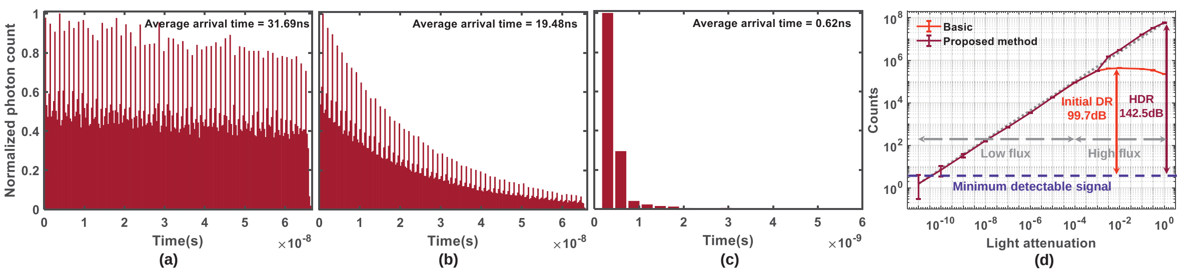


Fig. 1. (a), (b), and (c) histograms of photon arrival times at low, medium, and high light intensity in a pixel, (d) estimated optical signal together with noise represented as error bar at different illumination levels by using the basic photon-counting and the proposed method. The plot shows that the achieved dynamic range is 142.5dB by exploiting the AAT.

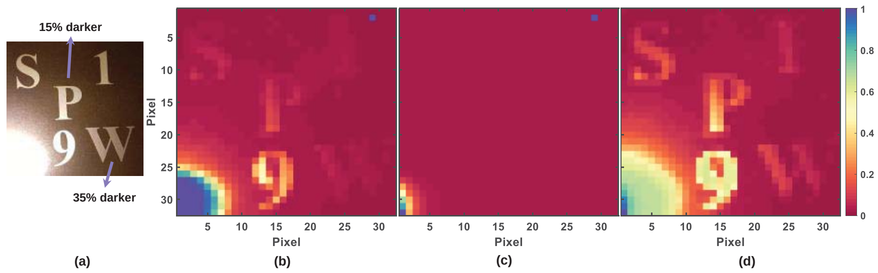


Fig. 2. (a) photograph of the captured scene, acquired with a conventional camera in an indoor environment with black walls and lights off, (b) photon counting-based image, acquired by SuperEllen chip, (c) image based on average photon arrival time, (d) reconstructed HDR image by the proposed method.

## References

[1] R. Henderson, et al., "A 256×256 40nm/90nm CMOS 3D-Stacked 120dB Dynamic-Range Reconfigurable Time-Resolved SPAD Imager," *2019 IEEE International Solid - State Circuits Conference - (ISSCC)*, San Francisco, CA, 2019, pp. 106-108.

[2] M. Zarghami, et al., "High dynamic range imaging with TDC-based CMOS SPAD arrays," *Instruments*, vol. 3, no. 3: 38(12) Aug. 2019.

[3] L. Gasparini, et al., "A 32×32-pixel time-resolved single-photon image sensor with 44.64-μm pitch and 19.48% fill-factor with on-chip row/frame skipping features reaching 800-kHz observation rate for quantum physics applications," *2018 IEEE International Solid - State Circuits Conference - (ISSCC)*, San Francisco, CA, 2018, pp. 98-100.

Acknowledgement

We thankfully acknowledge the support of the European Commission through the SUPERTWIN project, id. 686731.

# Current-assisted single photon avalanche diode (CASPAD) in 350 nm CMOS

**Gobinath Jegannathan, Hans Ingelberts, Maarten Kuijk**

*LAMI, Department of electronics and informatics (ETRO), Vrije Universiteit Brussel (VUB), 1050 Elsene, Belgium*

A novel type of SPAD is presented consisting of a small 1-fF avalanche diode in its center and surrounded by a large collection volume for photo-generated minority carriers. A current-assisted drift field [1] guides each photo-generated electron in the volume towards the center diode for the purpose of triggering a diode breakdown. The pn-junction consists of an $n^+$-diffusion embedded in an n-well and surrounded by a $p^+$-diffusion in a high resistivity $p^-$-EPI layer (~1000 Ohm.cm). Using the n-well makes the avalanche multiplication to happen before unwanted band-to-band tunneling at increasing reverse bias voltage.
An additional $p^+$-diffusion at the edge of the volume delineates the photo-sensitive area (*ring* seen in Fig 1a) and is used to guide the photocarriers quickly towards the middle by application of a negative bias, thereby generating an electric drift field in the underlying neutral volume together with a majority-carrier hole-current linked by ohms law. The hole current starts in the $p^+$-anode and ends in the $p^+$-ring and comes at the cost of some power dissipation, therefore preference is given to a high-ohmic resistive EPI-layer. Further, by choosing a thick EPI-layer, deeply-generated NIR photoelectrons get detected too, provided that the backside is applied with the same bias as the ring, thereby modifying the drift field to also direct these electrons towards the center pn-junction. The holes in the volume can't generate a breakdown event because they are present at the anode side instead of at the cathode side and drifting away from the avalanche junction to the ring.
As this CASPAD has a completely different topology and operates at much smaller breakdown currents compared to traditional SPADs, it has different merits, disadvantages and trade-offs. This first version of its kind is not yet optimized because it is merely based on 350-nm CMOS technology options for making MOS transistors. The present detector is characterized for both its performance in the linear mode (as an avalanche photodiode) and in Geiger mode (as a SPAD). Performance parameters such as timing jitter, dark count rate (DCR), after-pulsing, photon detection efficiency (PDE) for CASPAD will be presented.

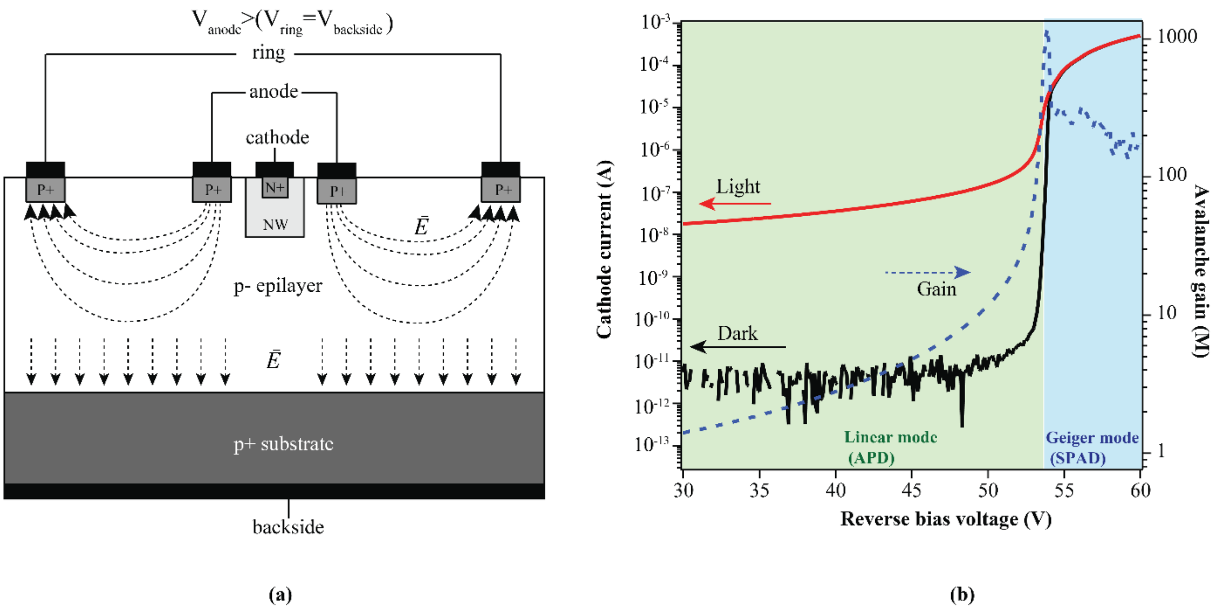


Fig. 1 (a) Cross section of the CASPAD with the avalanching pn junction in the middle and current assisting "ring", and (b) Measured IV characteristics of the CASPAD with calculated gain from the photocurrent on the right Y-axis.

**References**

[1] D. Van Nieuwenhove, W. Tempel and M. Kuijk, "Novel standard CMOS detector using majority current for guiding photo-generated electrons towards detecting junctions," in Proceedings Symposium IEEE/LEOS Benelux, 2005.

**Acknowledgement**

Sponsored by Sony Depthsensing Solutions NV and by the Vrije Universiteit Brussel (SRP 19).

# Towards Single-Photon Microscopy: Exploiting Extra Spatio-Temporal Information Provided by SPAD Array Detector in Laser Scanning Microscopy

**Giorgio Tortarolo[1,2], Marco Castello[1], Mauro Buttafava[3], Sami Koho[1], Eli Slenders[1], Alessandro Rossetta[1,2,4], Paolo Bianchini[4], Federica Villa[3], Alberto Diaspro[4,5], Alberto Tosi[3], Giuseppe Vicidomini[1]**

*[1]Molecular Microscopy and Spectroscopy, Istituto Italiano di Tecnologia, Genoa, Italy, [2]DIBRIS, University of Genoa, Genoa, Italy, [3]DEIB, Politecnico di Milano, Milan, Italy, [4]Optical Nanoscopy & NIC@IIT, Istituto Italiano di Tecnologia, Genoa, Italy, [5]DIFI, University of Genoa, Genoa, Italy*

Laser scanning microscopy is one of the most common architecture in fluorescence microscopy, e.g., confocal, two-photon excitation (TPE), and stimulated emission depletion (STED) microscopy. In a nutshell: (i) the objective lens focuses the laser beam(s) to the sample and generates an effective excitation spot which is raster scanned across the sample; (ii) for each position/pixel the fluorescent image of the spot is projected into a single-element detector, which – typically – spatially and temporally integrates the fluorescent light over the detector sensitive area and during the pixel dwell-time, thus providing a single-intensity value per pixel; (iii) all pixel intensity values are registered to build up a digital image. It is clear that the spatio-temporal integration performed by the single-element detector hinders any additional information potentially encoded in the dynamic and image of the fluorescent spot.

To address this limitation, we recently upgraded [1] the detection unit of a laser scanning microscope, replacing the traditional single-element detector with a novel SPAD (single photon avalanche diode) array detector (Fig. 1 A).

First, we have shown that the additional spatial information provided by such a detector allows to overcome the tradeoff between resolution and signal-to-noise ratio (SNR) proper of confocal microscopy (Fig 1 B): indeed, this architecture represents the natural implementation of image scanning microscopy (ISM). The same spatial information is explored in a STED microscope [2] to mitigate the usually non-negligible chance of photo-damaging the sample with the high-intensity STED beam, and in a TPE microscope to compensate distortions/aberrations occurring for deep-imaging.

We then exploited the temporal information, in particular the single-photon timing ability of the SPAD array – all detector elements are fully parallel with < 200 ps timing jitter and 40 MHz maximum count-rate – to combine intensity and fluorescence lifetime (FL) imaging: the results show higher spatial resolution and better accuracy of the lifetime estimate with respect to the confocal counterpart (Fig 1 B).

Lastly, we discuss how the proposed SPAD-based laser scanning microscope can be used in the context of single-molecule experiments, such as imaging, tracking, and spectroscopy. We envisage that this implementation will trigger a transition from single-molecule microscopy to single-photon microscopy.

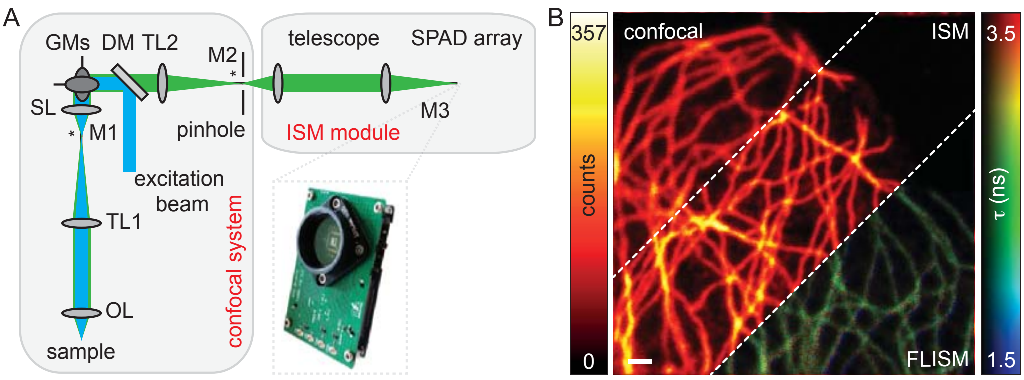


Fig. 1. (A) Scheme of the SPAD-based laser scanning microscope. (B) Example of imaging with the SPAD-based system. The image compares confocal microscopy, image scanning microscopy (ISM), and fluorescence lifetime ISM.

**References**

[1] Castello, M. et al. A robust and versatile platform for image scanning microscopy enabling super-resolution FLIM. Nat. Methods 16, 175–178 (2019)

[2] Vicidomini, G., Bianchini, P. & Diaspro, A. STED super-resolved microscopy. Nat. Methods 15, 173–182 (2018)

# Quantum dots at telecom wavelengths for single- and entangled photon sources

**Peter Michler**[1]

[1]*Universtiy of Stuttgart, Institute for Semiconductor Optics and Functional Interfaces, Center for Integrated Quantum Science and Technology (IQST) and SCoPE, Stuttgart, Germany*

The emission of semiconductor quantum dots (QDs) has been shown to exhibit excellent properties in terms of single photon purity, photon indistinguishability and entanglement fidelity, i.e. essential prerequisites for quantum communication. Emission in the telecom O- or C-band will boost the range of communication schemes due to the favourable absorption and dispersion properties of silica fibers employed in the existing global fiber network.

By metal-organic vapor-phase epitaxy, we have fabricated InAs quantum dots on InGaAs/GaAs metamorphic buffer layers on a GaAs substrate with area densities that allow addressing single quantum dots. The photoluminescence emission from the quantum dots is shifted to the telecom C-band at 1.55 µm with a high yield due to the reduced stress in the quantum dots. Single- and polarization-entangled photon emission is demonstrated [1,2]. Furthermore, the coherence properties of photons emitted by InAs/InGaAs QDs emitting directly in the telecom C-band, are examined under above-band excitation and in resonance fluorescence [3]. The average linewidth is reduced from 9.74 GHz in above-band excitation to 3.5 GHz in resonance fluorescence. Two-photon excitation of the biexciton is investigated as a resonant pumping scheme. A deconvoluted single-photon purity value of $g^{(2)}(0) = 0.07$ and a postselected degree of indistinguishability of $V_{HOM} = 0.89$ are determined for the biexciton transitions (see Fig.1).

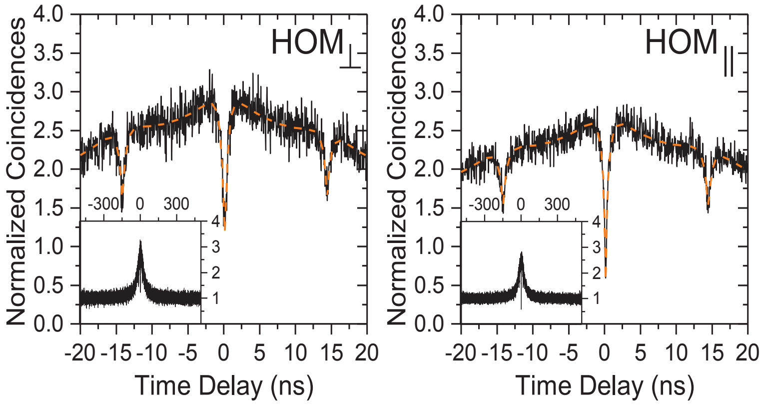


Fig. 1 Two-photon interference of distinguishable and indistinguishable photons after two-photon excitation of the quantum dot with the respective fit functions (orange). The insets show the same data with a correlation window of ± 500 ns.

Finally, to boost the extraction efficiency, the applicability of an approach combining a nano-membrane containing QDs, with a GaP hemispherical lens is presented for a sample emitting in the telecom O-band.

**References**

[1] M. Paul, F. Olbrich, J. Höschele, S. Schreier, J. Kettler, S. L. Portalupi, M. Jetter, and P. Michler, Single-photon emission at 1.55 µm from MOVPE-grown InAs quantum dots on InGaAs/GaAs metamorphic buffers, Appl. Phys. Lett. **111**, 033102 (2017).

[2] F. Olbrich, J. Höschele, M. Müller, J. Kettler, S. L. Portalupi, M. Paul, M. Jetter and P. Michler, Polarization-entangled photons from an InGaAs-based quantum dot emitting in the telecom C-band, Appl. Phys. Lett. **111**, 133106 (2017).

[3] C. Nawrath, F. Olbrich, M. Paul, S. L. Portalupi, M. Jetter and P. Michler, Coherence and indistinguishability of highly pure single photons from non-resonantly and resonantly excited telecom C-band quantum dots, Appl. Phys. Lett. **115**, 023103 (2019).

# Engineering two-photon wavefunction and exchange statistics in a semiconductor chip

**S. Francesconi[1], F. Baboux[1], A. Raymond[1], N. Fabre[1], A. Lemaître[2], P. Milman[1], M. Amanti[1] and S. Ducci[1]**

[1] *Laboratoire MPQ, USPC, Université de Paris - CNRS UMR 7162 Paris, France*

[2] *C2N, CNRS/Université Paris Sud, UMR 9001, 91460 Marcoussis, France*

Nonclassical states of light are key resources for quantum information technologies thanks to their easy transmission, robustness to decoherence and variety of degrees of freedom to encode information. In recent years, great efforts have been directed towards entanglement into high-dimensional degrees of freedom of photons (e.g. orbital angular momentum, path, frequency) as a mean to strengthen the violation of Bell inequalities, increase the density and security of quantum communication and enhance flexibility in quantum computing. Among the investigated degrees of freedom frequency is particular attractive thanks to its robustness to propagation in optical fibers and its capability to convey large scale of quantum information into a single spatial mode. Reaching a high versatility and a precise control over this degree of freedom is therefore desirable in order to employ the same source of quantum states of light for a wide range of applications [1]. In this framework, the technological maturity and optoelectronic capabilities of III-V materials make them an ideal platform to develop efficient and scalable devices to generate and manipulate frequency-encoded quantum states [2].

In this work, we exploit the high flexibility offered by Spontaneous Parametric Down Conversion in a semiconductor AlGaAs microcavity under a transverse pump geometry [3] (see Fig. 1a). We demonstrate that tailoring the spatial profile (intensity and phase) of the pump beam enables the control of the spectral correlations and wavefunction symmetry of the photon pairs directly at the generation stage, without any post-selection. In particular, tuning the pump beam waist allows to produce correlated, anti-correlated and separable frequency states, while modifying the spatial phase profile allows to switch between symmetric and antisymmetric spectral wavefunctions and modify the exchange statistics of the photons.

As shown in Fig. 1a, using a spatial light modulator we can control the phase shift between the two halves of the pump beam impinging of the AlGaAs ridge cavity. The first row of the right part of the figure reports the results for a flat phase ($\varphi'=0$) pump beam: the emitted two-photon state has an almost Gaussian joint spectrum (Fig 1b) and in a Hong-Ou-Mandel interferometer it shows a bunching behavior (Fig 1c,d), typical of bosonic statistics. On the other hand, if we apply a $\pi$ phase shift ($\varphi'=\pi$), as shown in the second row, the joint spectrum splits into two lobes (Fig 1e) and the coincidence probability features a clear change to an anti-bunching behavior (Fig 1f,e), typical of fermionic statistics [4].

These results, obtained with an integrated chip, at room temperature and telecom wavelength, could be harnessed to study the effect of exchange statistics in various quantum simulation problems, and to implement communication and computation protocols exploiting antisymmetric high-dimensional quantum states [5]. Moreover, undergoing studies have shown that other exotic nonclassical states, like Schrodinger's cat in the frequency-time domain, can be generated with the same device, broadening the range of its possible applications for quantum technologies.

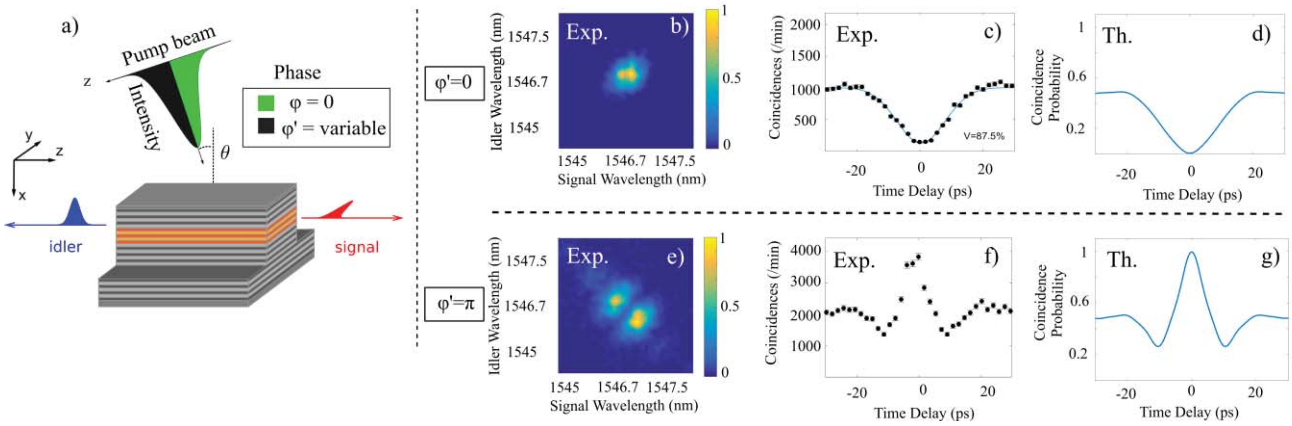


Figure 1: a) Sketch of the AlGaAs ridge microcavity emitting photon pairs by SPDC in a transverse pump geometry. b-d) Joint spectrum measured with a fiber spectrograph for a flat phase pump beam ($\varphi'=0$), and corresponding measured and calculated HOM interferograms. e-g) Joint spectrum and HOM interferograms for a pump beam with a $\pi$ phase step ($\varphi'=\pi$).

## References

[1] M. Kues et al., Nature Photonics 13, 170 (2019)

[2] A. Orieux et al., Rep. Prog. Phys. 80, 076001 (2017)

[3] A. Orieux et al., Phys. Rev. Lett. 110, 160502 (2013)

[4] S. Francesconi et al., in preparation.

[5] A. Crespi et al., Phys. Rev. Lett. 114, 090201 (2015)

# High-Efficiency Time-Multiplexed Single-Photon Source

**Colin P. Lualdi[1], Fumihiro Kaneda[1, 2], Joseph C. Chapman[1], Paul G. Kwiat[1]**

[1]*Department of Physics, University of Illinois at Urbana-Champaign, Urbana, Illinois, USA*

[2]*Frontier Research Institute for Interdisciplinary Sciences, Tohoku University, Sendai, Japan*

A single-photon source capable of on-demand or periodic generation of indistinguishable single- and multi-photon states is a key requirement for optical quantum information processing (QIP) applications. While heralded single-photon sources (HSPSs) via spontaneous parametric down-conversion (SPDC) have long served as single-photon sources, their probabilistic nature and low generation rates make them unsuitable for large-scale optical QIP applications.

To overcome this limitation and to realize a periodic single-photon source, we utilize time-multiplexing techniques [1,2] by pairing an ultra-low loss, adjustable delay line with our high-efficiency HSPS generating highly indistinguishable photons. An optical-pulse train from a laser pumps an SPDC crystal to generate pairs of signal and idler photons in one or more time slots; the detection of a signal photon heralds which time slot contains the corresponding idler photon. The idler photon is then switched into a variable-length storage cavity where it is delayed such that any of the time slots containing a heralded photon is multiplexed onto a single output time window at the end of each multiplexing cycle (Fig. 1a). This increases the single-photon probability at a periodic pre-determined time as a function of the number of pump pulses (time slots) used for one multiplexing cycle.

We report our most current results using this technique [3]. Figure 1b shows how by multiplexing 40 time bins, we have observed up to a 66.7±2.4% presence probability of single photons collected into a single-mode optical fiber per cycle, a ten-fold enhancement over the non-multiplexed case. We also confirmed that the spectral and temporal indistinguishability of our photons are unaffected by pump power or time-multiplexing, by directly observing Hong-Ou-Mandel (HOM) interference between photons generated by our time-multiplexed source and a conventional HSPS using the same SPDC source, with background-corrected HOM visibilities above 90%.

In the regime of a 66.7% single-photon probability per cycle we measured a second-order correlation function $g^{(2)}(t = 0)$ of 0.269. This is a consequence of relatively inefficient heralding detectors which require our SPDC source to be driven at high powers to have at least one heralded photon for each time-multiplexing cycle, increasing the probability of multiple-pair down-conversion events. Therefore, we also discuss ongoing work to suppress the $g^{(2)}$ by improving the detection efficiency and photon-number resolution of our heralding system.

Despite a relatively low repetition rate of 500 kHz, the high efficiency of our source already allows it to generate multiple individual photons at rates much higher than less-efficient single-photon source technologies, including state-of-the-art conventional HSPS and quantum dot sources [4]. For instance, our source can be used to generate thousands of 12-photon states per second and ~1 30-photon state per second. Moreover, modifying our time-multiplexing methods can enable exponentially more efficient creation of more exotic multi-photon states, such as *N*00*N* states and deterministic photon-subtracted states [5]. We believe that these methods will enable a plethora of new photonic quantum information applications.

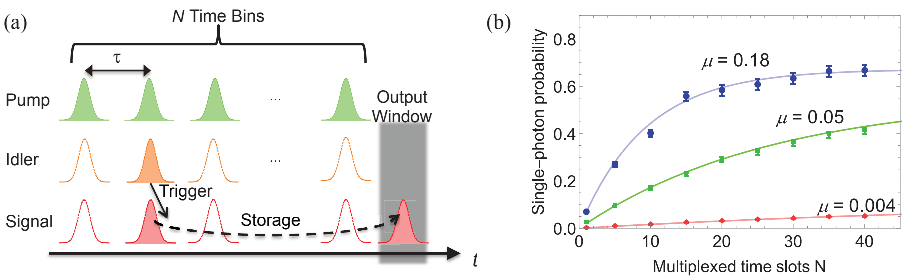


Fig. 1 (a) Visualization of multiplexing process. (b) Single-photon probability as a function of multiplexed time bins (N) for three SPDC pumping powers corresponding to mean photon numbers per pump pulse of μ = 0.004, 0.05, and 0.18 [3].

## References

[1] E. Jeffrey, N. A. Peters and P. G. Kwiat. "Towards a periodic deterministic source of arbitrary single-photon states," New J. Phys. **6**, 100 (2004)

[2] T. Pittman, B. Jacobs, and J. Franson. "Single photons on pseudodemand from stored parametric down-conversion," Phys. Rev. A **66**, 042303 (2002)

[3] F. Kaneda and P. G. Kwiat. "High-efficiency single-photon generation via large-scale active time multiplexing," Science Advances, to appear, arXiv:1803.04803v1 (2018)

[4] N. Somaschi et al. "Near-optimal single-photon sources in the solid state," Nat. Photonics **10**, 340–345 (2016)

[5] K. T. McCusker and P. G. Kwiat. "Efficient Optical Quantum State Engineering," Phys. Rev. Lett. **103**, 163602 (2009)

# Toward control of the quantum state of hBN single-photon emitters

**Claire E. Marvinney,[1,*] Matthew A. Feldman,[1, 2,*] Nathan Rosenmann,[3] Tristan Carlson,[4] Yu-Chuan Lin,[5] Yiyi Gu,[3] Kai Xiao,[5] James H. Edgar,[6] Ivan I. Kravchenko,[5] Alexander A. Puretzky[5] Richard F. Haglund,[2] and Benjamin J. Lawrie[1]**

[1]*Quantum Information Science Group, Oak Ridge National Laboratory, Oak Ridge, TN 37831, USA*
[2]*Department of Physics and Astronomy, Vanderbilt University, Nashville, TN 37235, USA*
[3]*Department of Physics, University of Illinois, Chicago, Chicago, IL 60607, USA*
[4]*Department of Physics and Astronomy, University of the South, Sewanee, TN 37383, USA*
[5]*Center for Nanophase Materials Sciences, Oak Ridge National Laboratory, Oak Ridge, TN 37831, USA*
[6]*Department of Chemical Engineering, Kansas State University, Manhattan, Kansas 66506, USA*
*These authors contributed equally

The study of two-dimensional (2D) materials is of growing interest for a range of integrated quantum technology applications. Hexagonal boron nitride (hBN) is a 2D material of interest for quantum photonic and phononic applications because its defect-based single photon emitters (SPEs) are bright, have narrow linewidths, and are stable at room temperature [1], and because, for isotopically pure samples, the phonon interactions can have ultra-low losses [2]. To date, discovering the atomistic origins of SPEs in hBN has proven challenging. Recent results have shown that spectrally resolved, two-color Hanbury Brown-Twiss (HBT) interferometry can be used to characterize electron-phonon interactions in hBN [1]. To create a description of the combined photonic and phononic quantum state in hBN of varying isotopic concentration, measurements of spectrally resolved correlation functions as in [1] are employed to study the electron-phonon and electron-electron interactions in isotopically enriched and naturally abundant hBN samples.

Here, our initial results are on naturally abundant hBN, where we explore both the autocorrelation and two-color correlation functions for spectrally distinct electronic transitions. While some of the features in Fig. 1a can be attributed to phonon replicas, at least two features appear to be zero-phonon lines (ZPLs). Fig. 1b illustrates strong photon antibunching dynamics in the two-color correlation function for the ZPLs near 540 nm and 575 nm, which can be explained by attributing the transitions to either different excited states of the same defect or to two strongly interacting defects. To definitively determine which case is correct, further experiments are being employed, such as spectrally tunable optical excitation of these states with improved spectral resolution at liquid helium temperatures, where resonantly pumping one transition while collecting on another becomes possible. Additional experiments exploring the variation in electron-electron and electron-phonon interactions with changing boron isotope within the hBN are currently underway, where samples (Fig 1e-f) with $B^{10}$:$B^{11}$ ratios of 100:0, 50:50, 20:80, and 0:100 are being studied with these same techniques.

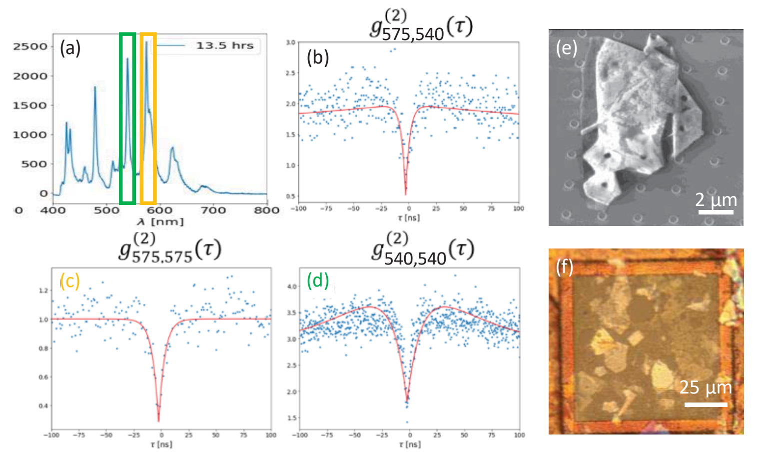


Fig. 1: (a) Localized defect microphotoluminescence spectra for a few-layer hBN flake irradiated with a 40 µW, 405-nm wavelength, 1µm$^2$ spot size CW laser after 13.5 hrs irradiation. (b) – (d) Spectrally resolved Hanbury Brown-Twiss interferometry of defect photoluminescence at 575 nm (c) and 540 nm (d), with two-color antibunching measurements demonstrating strong anticorrelations between the emitters at these two wavelengths (b). (e) SEM image of an hBN flake with isotope ratio of 50:50 $B^{10}$:$B^{11}$ deposited on an array of $SiO_2$ nanopillars (d = 450 nm, h = 130 nm), where the pillars can create strain localized defect emitters [3]. (f) Optical image of 50:50 $B^{10}$:$B^{11}$ hBN flakes on a TEM grid for characterization of suspended flakes.

This research was sponsored by the Laboratory Directed Research and Development Program of ORNL, managed by UT-Battelle, LLC, for the U. S. DOE, by the IC Postdoctoral Fellowship, and by the NDSEG Graduate Fellowship. The nanofabrication and some of the optical and electron spectroscopies were performed at the Center for Nanophase Materials Sciences, which is a DOE Office of Science User Facility.

[1] Feldman, Matthew A., et al. *Physical Review B* **2019**, 99(2), 020101.
[2] Giles, Alexander J., et al. *Nature materials* **2018**, 17(2), 134.
[3] Proscia, Nicholas V., et al. *Optica* **2018**, 5(9), 1128-1134.

This manuscript has been authored by UT-Battelle, LLC, under Contract No. DE-AC05-00OR22725 with the U.S. Department of Energy. The United States Government retains and the publisher, by accepting the article for publication, acknowledges that the United States Government retains anon-exclusive, paid-up, irrevocable, worldwide license to publish or reproduce the published form of this manuscript, or allow others to do so, for United States Government purposes. The Department of Energy will provide public access to these results of federally sponsored research in accordance with the DOE Public Access Plan (http://energy.gov/downloads/doe-public-access-plan).

# Three-Quantum-Dot Superradiance in a Photonic Crystal Waveguide Enabled by Scalable Strain Tuning


**Joel Q. Grim[1*], Allan S. Bracker[1], Maxim Zalalutdinov[1], Samuel G. Carter[1], Alexander C. Kozen[2], Mijin Kim[3], Chul Soo Kim[1], Jerome T. Mlack[4], Michael Yakes[1], Bumsu Lee[4], Daniel Gammon[1]**

[1] U.S. Naval Research Laboratory, Washington D.C.

[2] *ASEE postdoctoral research fellow at the U.S. Naval Research Lab*

[3] *KeyW corporation*

[4] *NRC research associate at the U.S. Naval Research Lab*

* *joel.grim@nrl.navy.mil*


The prospect of an integrated quantum optics platform consisting of networks of stationary qubits interfaced with photons has motivated solid-state quantum research for decades. Substantial progress has been made with semiconductor quantum dots (QDs) toward this goal with advanced demonstrations as indistinguishable photon sources, single photon switches, quantum transistors, and spin-photon and spin-spin entanglement. However, these efforts have been limited to one, and at most, two QDs. A roadblock for further scaling is the wide distribution of QD emission energies, spanning 10s of meV, compared to the few μeV for a single QD linewidth. The probability of finding QDs with the same emission energy is negligible, a challenge shared by all solid-state emitters. We have developed a technique that addresses this challenge by locally tuning individual QDs via laser-crystallization of a thin $HfO_2$ film deposited on the surface of photonic structures[1]. With this approach individual QDs can be tuned across the inhomogeneous distribution, with a step size down to the homogeneous linewidth, and sub-micron spatial resolution. We leverage these capabilities to tune multiple QDs into resonance within the same nanophotonic waveguide, as shown in Fig. 1b for three QDs.

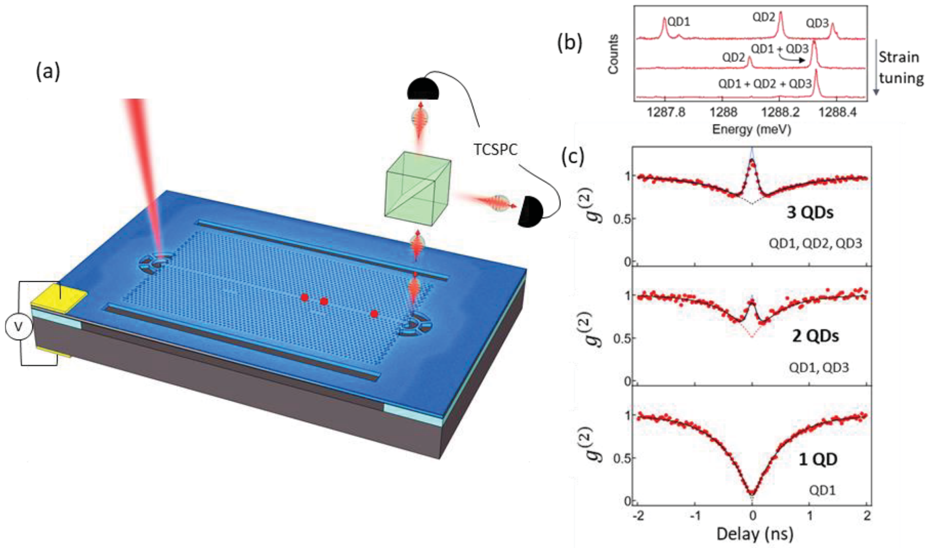


**Fig. 1** (a) Photonic crystal waveguide with grating output couplers as well as a schematic of second-order photon correlation measurements. The positions of three QDs are indicated with red circles. (b) Spectra of three QDs prior to tuning (top), and after tuning two (middle) and three (bottom) QDs into resonance. (c) Second-order correlation measurements for one, two, and three QDs.

We show the prospect of this approach for scalable integrated quantum optics with photon-mediated interactions – in the form of superradiance – for up to three QDs. Second-order photon correlation measurements on a single QD shows antibunching down to zero, as expected for a single-photon emitter. When two QDs are resonant, a $g^{(2)}$ *bunching* peak around zero delay emerges, which is a clear signature of superradiance. With three QDs resonant, this bunching peak approaches the theoretical limit of $g^{(2)}_{N=3}(0) = 4/3$, limited by the ~100 ps time resolution of the detection system.


[1] J. Q. Grim, A. S. Bracker, M. Zalalutdinov, S. G. Carter, A. C. Kozen, M. Kim, C. S. Kim, J. T. Mlack, M. Yakes, B. Lee & D. Gammon , “Scalable *in operando* strain tuning in nanophotonic waveguides enabling three-quantum-dot superradiance,” *Nature Materials* (2019) https://www.nature.com/articles/s41563-019-0418-0

# Single photon technology in Long Distance Quantum Communication

**Qiang Zhang**[1,2]
[1]*University of Science and Technology of China, Shanghai 201315, P. R. China*
[2]*Jinan Institute of Quantum Technology, Jinan, Shandong 250101, P. R. China*

Quantum communication can provide unconditional security based on the basic law of quantum mechanics. One of the main goal of the field is to extend the transmission distance to large scale, like 1000 km. Here in this talk, I shall review the single photon transmission, interference, frequency conversion technology developed in our group and their applications in long distance quantum communication, including MDI-QKD, quantum repeater and free space quantum communication.

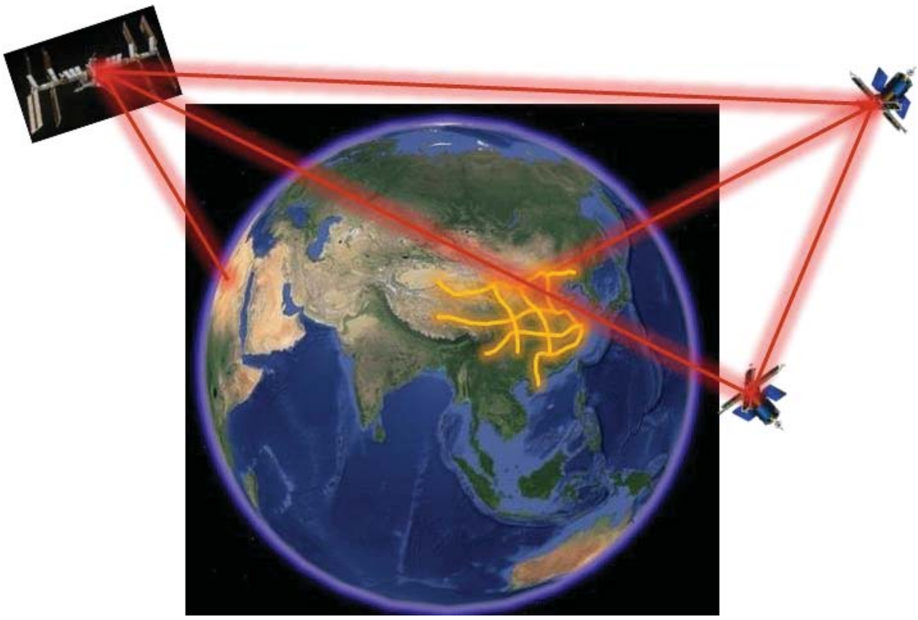

Fig. 1 The future perspective of quantum communication

# Experimental quantum repeater without quantum memory

**Zheng-Da Li[1,2,] Rui Zhang[1,2], Xu-Fei Yin[1,2], Li-Zheng Liu[1,2], Yi Hu[1,2], Yu-Qiang Fang[1,2], Yue-Yang Fei[1,2], Xiao Jiang[1,2], Jun Zhang[1,2], Feihu Xu[1,2,*], Yu-Ao Chen[1, 2, *] & Jian-Wei Pan[1, 2]**

[1] *Shanghai Branch, National Laboratory for Physical Sciences at Microscale and Department of Modern Physics, University of Science and Technology of China, Shanghai 201315, China*

[2] *CAS Center for Excellence and Synergetic Innovation Center in Quantum Information and Quantum Physics, University of Science and Technology of China, Shanghai 201315, China*

[*] *Email: feihuxu@ustc.edu.cn; yuaochen@ustc.edu.cn*

Quantum repeater [1] – an important ingredient of the global quantum internet – enables the distribution of entanglement over long distances. The standard paradigm for a quantum repeater relies on a necessary demanding requirement of quantum memory [2]. Despite significant progress [2], its limited performance makes practical quantum repeaters still a great challenge. Notably, the proposal of all-photonic quantum repeater [3] completely avoids quantum memories. Different from the conventional repeaters, the all-photonic scheme introduces an explicit construction of a repeater graph state (RGS) consisting of a complete subgraph of $K$ core photons each connected to an additional photon forming $K$ external arms. All-photonic quantum repeater presents the resilience against photon loss, whereas it avoids the coherence time limitations of quantum memories and the requirement of long-distance heralding. These features attract much attention to all-photonic quantum repeater recently.

Experimentally, we simplify the original scheme by replacing the RGS with a GHZ-state. Further, to implement arbitrary connections of different channels, we design a passive-choice measurement (PCM) which can realize Bell state measurement and projection measurement simultaneously via post-selection. As a proof-of-principle demonstration, we experimentally build the $2 \times 2$ parallel all-photonic quantum repeater with twelve manipulated photons [4]. A schematic drawing of the set-up is shown in Fig. A. In experiment, to verify its ability of manipulating 12 photons, we measure the photon distribution in Z basis, and obtain a signal-to-noise ratio as 1420:1. For the $2 \times 2$ parallel structured all-photonic quantum repeater, we register the eightfold coincidence events with downconversion probability $p = 0.0344$ for a duration of 39 h. In comparison, we also register the eightfold coincidence events for the upper (lower) channel of the parallel entanglement swapping by removing the $PCM_1$ and $PCM_4$ ($PCM_2$ and $PCM_3$) with the same $p$ and duration. The counting ratio is $r = 1.89 \pm 0.10$. In addition, we increase the power of pump laser and perform the same evaluation with $p = 0.0483$ for a duration of 22 h. The ratio is $r = 1.74 \pm 0.07$. These results are shown in Fig.B. The average fidelities for four entangled state with different down-conversion probabilities is evaluated as $0.606 \pm 0.010$ and $0.546 \pm 0.006$. It obviously indicate genuine entanglement of the final state. Thus we experimentally demonstrate a $2 \times 2$ parallel all-photonic quantum repeater. Our experiment suggests that the all-photonic scheme represents an alternative path—parallel to matter-memory-based schemes—towards realizing practical quantum repeaters. **Further details of our work can be seen in Ref. [4].**

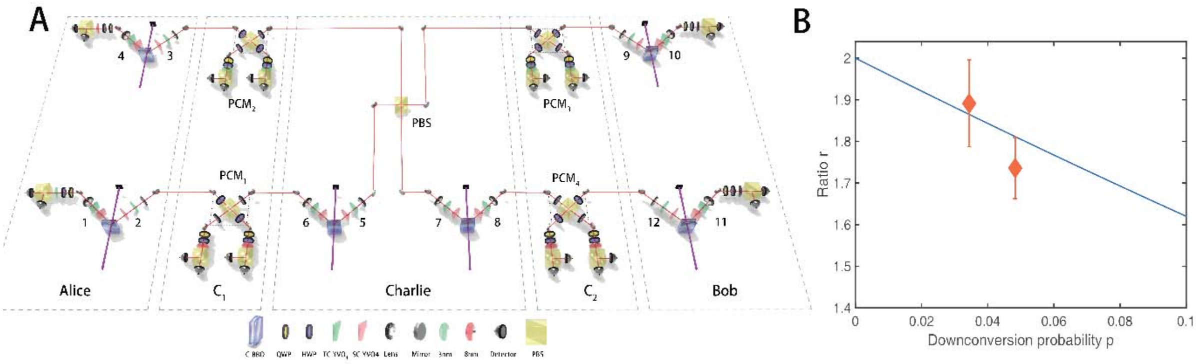


**Fig. A :** The experimental set-up of all-photonic quantum repeater.The Circular polarisation beam splitter in PCM is implemented by a PBS centered among four HWP with 22.5°. SC-YVO4 and TC-YVO4 represent for spatial compensation (SC) and temporal compensation (TC) YVO4 crystals. **Fig. B :** The ratio of $2 \times 2$ parallel quantum repeater to the parallel entanglement swapping with different down-conversion probabilities. The blue line denotes the ratio in ideal cases. The diamonds denote experiment result.

**References**

[1] H.-J. Briegel et al., Phys. Rev. Lett. 81, 5932–5935 (1998).
[2] N. Sangouard et al., Rev. Mod. Phys. 83, 33–80 (2011).
[3] K. Azuma et al., Nat. Commun. 6, 6787 (2015).
[4] Z.-D. Li et al., “Experimental quantum repeater without quantum memory,” Nat. Photon. DOI: http://doi.org/10.1038/s41566-019-0468-5 (2019).

# Hong-Ou-Mandel interference of polarization qubits stored in independent room-temperature quantum memories

**A. Scriminich**[1*], **M. Flament**[2*], **S. Gera**[2*], **Y. Kim**[2*], **M. Namazi**[2*], **S. Sagona-Stophel**[2], **G. Vallone**[1], **P. Villoresi**[1], **and E. Figueroa**[2]

[1] *Department of Information Engineering, University of Padova, via Gradenigo 6b, 35131 Padova, Italy.*

[2] *Department of Physics and Astronomy, Stony Brook University, Stony Brook, NY 11794, USA.*

**equally contributing authors*

An optical Quantum Memory (QM) is a device capable of performing coherent storage and on-demand retrieval of a quantum state via a controlled light-matter interaction. The possibility offered by QMs to coherently manipulate quantum information has important applications in the field of Quantum Communication. QMs are an essential building block for future large photonic quantum networks based on Memory-Assisted Measurement-Device Independent Quantum Key Distribution (MA-MDI-QKD), and for Quantum Repeaters, which may enable the distribution of entanglement beyond the limits imposed by the quantum channel [1]. A significant challenge in creating MA-MDI-QKD networks and Quantum Repeaters consists in demonstrating high-visibility Hong-Ou-Mandel (HOM) interference between two quantum states stored in two QMs.

The QMs employed in this experiment are based on Electromagnetically-Induced Transparency (EIT) realized in a vapor of $^{87}$Rb atoms heated at 60°C. Under EIT, the absorption, storage and retrieval of a weak probe pulse is mediated by a strong control pulse. Specifically, the QM exploits the Λ-level hyperfine structure of the $^{87}$Rb D1 line at 795nm. EIT can be used to slow the group velocity of light in the medium, and ultimately to store light in a collective atomic excitation by dynamic adjustment of the control pulse intensity. Storage of an arbitrary polarization state is achieved by means of a dual-rail configuration. We previously demonstrated ultra-low noise storage of single-photon-level polarization qubits with a fidelity above 90% and storage time up to 40μs [2, 3].

We present an elementary quantum network consisting of two qubit sources generating phase-randomized polarization-encoded attenuated coherent pulses with a FWHM of 400ns and a repetition rate of 25kHz, two independent room-temperature QMs and a measurement node. We investigate the indistinguishability of the qubits after retrieval from the QMs via HOM interference, by exploiting both the temporal and the polarization degrees of freedom.

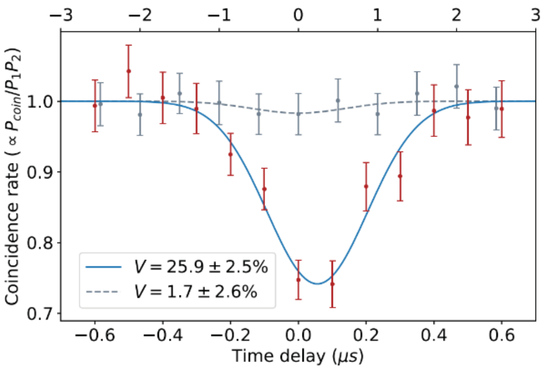


We first benchmark the performance of the network excluding the QM, obtaining a qubit interference visibility of V = (42.4 ± 0.6) %, compared to the maximum observable of 50% in the case of weak coherent states. We observed HOM interference of the qubits retrieved from the QM after a storage time of 1μs with different mean photon number at the input of the QMs. In the case of few-photon-level inputs, we observed V = (41.9 ± 2.0) %, while in the case of single-photon-level inputs we observed V = (25.9 ± 2.5) %, with a background visibility of V = (1.7 ± 2.6) %.

The result obtained for the HOM visibility after storage and retrieval in two QMs opens the way to the implementation of our system in a cryptographic network, exploiting protocols such as MA-MDI-QKD. Although our single-photon level result is below the minimum visibility of 37% that ensures a positive secret key-generation rate in the MDI-QKD protocol, we find that the primary parameter affecting HOM visibility in our experiment is the low signal-to-background ratio (SBR). By implementing the noise-cancelling protocol proposed in [2], we expect to achieve a single-photon-level input visibility of above 41%. Moreover, the room-temperature operation of our system significantly decreases the technological overhead required to realize a scalable quantum network containing many portable quantum memories.

**References**

[1] N. Lo Piparo, N. Sinclair, and M. Razavi, *"Memory-assisted quantum key distribution resilient against multiple- excitation effects,"* Quantum Sci. Tech. 3, 014009 (2018).

[2] M. Namazi, C. Kupchak, B. Jordaan, R. Shahrokhshahi, and E. Figueroa. *"Ultralow-Noise Room-Temperature Quantum Memory for Polarization Qubits,"* Phys. Rev. Appl. 8, 034023 (2017).

[3] M. Namazi, G. Vallone, B. Jordaan, C. Goham, R. Shahrokhshahi, P. Villoresi, and E. Figueroa. *"Free space quantum communication with a portable quantum memory,"* Phys. Rev. Appl. 8, 64013 (2017).

[4] A. Scriminich, M. Flament, M. Namazi, S. Gera, S. Sagona-Stophel, G. Vallone, P. Villoresi, and E. Figueroa. *"A multi-node room-temperature quantum network,"* arXiv: 1808.07015 (2018).

# Towards long distance entanglement between a photon and a solid-state quantum memory

**S. Grandi, J. Rakonjac, D. Lago-Rivera, A. Seri and H. de Riedmatten**
*ICFO-Institut de Ciencies Fotoniques, The Barcelona Institute of Science and Technology, 08860 Castelldefels (Barcelona), Spain*

As the reach of quantum technologies extends ever further in communication and information science, a reliable way of transferring quantum information between distant locations becomes ever more crucial. While photons are widely accepted as excellent carriers due to their speed and low decoherence, losses of transmission (in free space or fibre) and the impossibility of cloning quantum information still pose a great challenge. The quantum repeater architecture was suggested as a solution to both problems [1]. In a quantum repeater the information encoded in an input state is transferred to a new one through entanglement swapping, that is then sent on along the channel.
In this work we present our advances towards the realisation of a quantum repeater. Our system of choice combines a solid-state quantum memory with a source of photon pairs**.** The memory is based on a Rare-Earth Doped crystal, where quantum information can be stored in $Pr^{3+}$ ions as a collective excitation using the Atomic Frequency Comb technique. On demand retrieval of the information is realised by transferring the excitation to a long-lived spin state. Record values of storage times and retrieval efficiencies have been demonstrated in this system [2]. Pair of single photons are generated by parametric down conversion in a periodically poled crystal placed inside a bow-tie cavity. This allows us to generate narrow band photons pairs, where the signal is spectrally matched to the memory (606nm), while the idler is in the telecom band [3]. Such a configuration allows us to benefit from the high performance of the memory, while at the same time overcoming the high optical losses of 606nm photons by pair generation of a telecom photon.

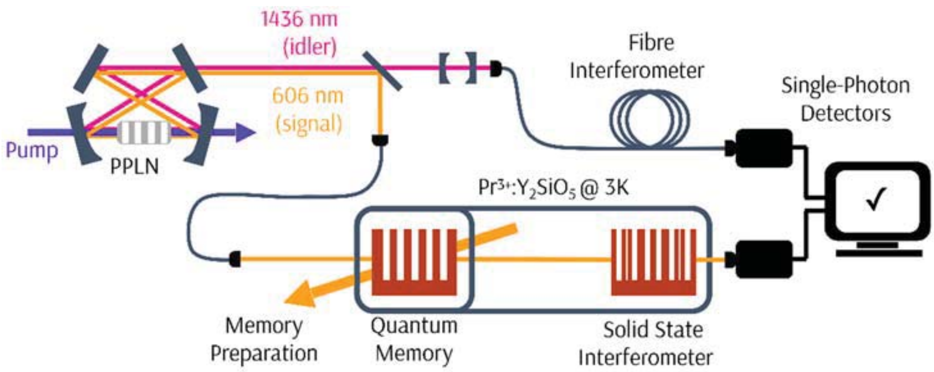


Fig. 1: schematics of the experimental setup for spin wave storage of energy-time entanglement

The first stepping stone, progress towards which is presented in this work, is the successful demonstration of energy-time entanglement between the telecom idler photon and the signal photon, stored as spin-wave excitation. The entanglement analysis will be made through time-bin qubits analysers made of a fibre-based Mach-Zehnder interferometer, for the former, and a solid-state equivalent based on two AFC with different storage times, for the latter [4]. In this direction we have already doubled the efficiency of the storage protocols, that will be beneficial to count rates and signal-to-noise ratio. We improved the purity of the entanglement by reducing the linewidth of the pump laser, as well as increased the spectral-matching between the source and the memory [5]. Demonstration of the successful transfer of quantum information between the signal photon and the long-lived solid-state excitation will open the way to the demonstration of long-distance entanglement between individual nodes in a quantum network.

**References**
[1] C. Simon, H. de Riedmatten, M. Afzelius, N. Sangouard, H. Zbinden and N. Gisin, Phys. Rev. Lett. **98** 190503 (2007)
[2] A. Seri, A. Lenhard, D. Rielander, M. Gundogan, P. Ledingham, M. Mazzera and H. de Riedmatten, Phys. Rev. X **7** 021028 (2017)
[3] D. Rielander, A. Lenhard, M. Mazzera and H. de Riedmatten, New J. of Phys. **18** 123013 (2016)
[4] C. Clausen, I. Usmani, F. Bussieres, N. Sangouard, M. Afzelius, H. de Riedmatten and N. Gisin, Nature **469** 508 (2011)
[5] A. Seri, D. Lago-Rivera, A. Lenhard, G. Corrielli, R. Osellame, M. Mazzera and H. de Riedmatten, arXiv 1902.06657

# Entanglement and non-locality between disparate solid-state quantum memories mediated by photons

**Marcel.li Grimau Puigibert,[1, 2] Mohsen Falamarzi Askarani,[1, 3] Jacob H. Davidson[1, 3] Varun B. Verma,[4] Matthew D. Shaw,[5] Sae Woo Nam,[4] Thomas Lutz,[1, 6] Gustavo C. Amaral,[1, 3] Daniel Oblak,[1] and Wolfgang Tittel[1, 3]**

[1]*Institute for Quantum Science and Technology, and Department of Physics & Astronomy, University of Calgary, 2500 University Drive NW, Calgary, Alberta, T2N 1N4, Canada*

[2]*University of Basel, Klingelbergstrasse 82, CH-4056 Basel, Switzerland*

[3]*QuTech and Kavli Institute of Nanoscience, Delft University of Technology, 2600 GA Delft, The Netherlands* [4]*National Institute of Standards and Technology, 325 Broadway, Boulder, Colorado 80305, USA*

[5]*Jet Propulsion Laboratory, California Institute of Technology, 4800 Oak Grove Drive, Pasadena, California 91109, USA*

[6]*ETH Z¨urich, Otto-Stern-Weg 1, 8093 Z¨urich, Switzerland*

Entangling quantum systems with different characteristics through the exchange of photons is a prerequisite for building future quantum networks. Proving the presence of entanglement between quantum memories for light working at different wavelengths furthers this goal. Here, we report on a series of experiments with a thulium-doped crystal, serving as a quantum memory for 794 nm photons, an erbium-doped fibre, serving as a quantum memory for telecommunication wavelength photons at 1535 nm, and a source of photon pairs created via spontaneous parametric down-conversion, as shown in Fig.1. Characterizing the photons after re-emission from the two memories, we find nonclassical correlations with a cross-correlation coefficient of $g^{(2)}_{12} = 53 \pm 8$; entanglement preserving storage with input-output fidelity of $F_{IO} \approx 93 \pm 2\%$; and non-locality featuring a violation of the Clauser-Horne-Shimony-Holt Bell-inequality with $S = 2.6 \pm 0.2$. Our proof-of-principle experiment shows that entanglement persists while propagating through different solid-state quantum memories operating at different wavelengths.

## Poster Abstracts (online only)

| | | |
|---|---|---|
| **Section I:** | **Tuesday, October 22, 2019** | **at 18:10** |
| **Section II:** | **Thursday, October 24, 2019** | **at 18:20** |

The poster sections will be held in the room adjacent to the workshop room (Building BL28, Via Lambruschini 4, 20156 Milano (MI), Italy).
The posters of Section I will be exposed from Tuesday morning to Wednesday evening and the posters of Section II from Thursday morning to Friday evening.

All the posters abstracts are available in the online version of "Book of Abstracts" on SPW website (https://spw2019.polimi.it).

# Abstracts of

# Poster session I

# Structures for integrated photonics quantum random number generators

**Fabio Acerbi[1], Nicolo Leone[2], Alberto Gola[1], Nicola Zorzi[1], Stefano Azzini[2], Giorgio Fontana[2], Lorenzo Pavesi[2]**

*1. Fondazione Bruno Kessler (FBK), via Sommarive 18, Trento, Italy*

*2. Department of Physics, University of Trento, Via Sommarive 14, Povo (Trento), Italy*

Nowadays different electronic devices (Internet of Things, IoT) require the development of low cost, robust and secure communication to protect the links and the data. Mass manufacturable, integrated, robust and cheap hardware security modules (HSM) are needed. At the heart of any HSM there is a random number generator (RNG) system which provides the seed for the digital key generation. Silicon technologies can provide both the required high volume as well as the low cost and the small size. This opens the possibility to produce very compact RNG that are essential for the implementation in portable electronic devices.

In this work we focused on the development of a solid-state, fully-integrated, low power, very compact photonic quantum random number generators (PQRNGs), which exploit the unpredictability of quantum mechanics in order to ensure the maximum level of security. In particular, we implemented a compact structure with photon-emitter very close to the single-photon detectors. The emitter and the detector are both based on p-n junctions, being either SPADs or mini silicon photomultiplier (SiPM), and they are actually realized with the same fabrication process steps. The emitter can be forward or reverse biased.

Starting from the first implementation, based on NUV technology [1], designed and produced in FBK (Trento, Italy), which has been successfully used for the generation of up to 100kbit/s random bits, certified by NIST and other different tests [1], we analyzed what are the main limiting issues and we developed new chips. These are produced with the new NIR-HD (NIR sensitive technology), developed in FBK, thus giving the single-photon detector higher efficiency. Moreover, thanks to the deep-trench isolation which is present in the NIR-HD technology, we were able to electrically isolate the emitter and the detector, improving the possible operating conditions and obtaining better performance. With the first NUV QRNG structure, we successfully used a recently developed robust quantum-random number extraction method described in [2]: here the random symbols are generated based on the photon arrival position inside discretized time bins, inside a periodic time window. The afterpulsing of the detector is counteracted by adding a no-bit time period at the beginning of the window. This method proved to be robust against moderate fluctuation of the emitter intensity and the fluctuation of SPAD bias.

As a last development, the first NUV QRNG structure has been also used to test the feasibility with an integrated emitter-detector approach of the novel “Semi-Device-Independent” method proposed in [3]. In the latter, no assumptions about the measurement device (and its performance) are needed. The front end-electronics (described in [1]) has been modified to be able to drive the emitter with arbitrary pulses. The setup include an arbitrary waveform generator, driving a RF amplifier with an external DC-bias regulation, thus modulating the emitter bias below the breakdown voltage or above.

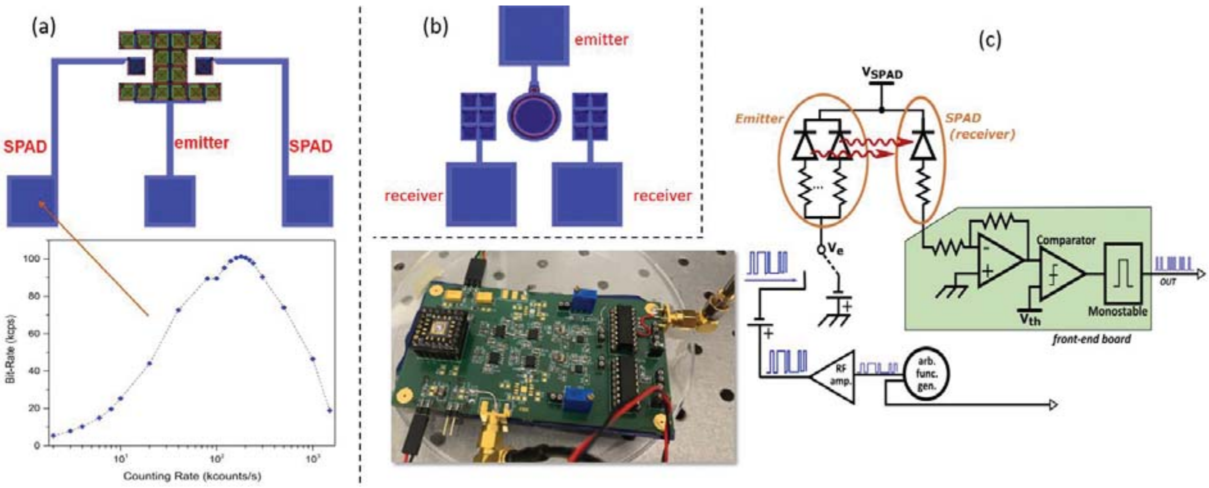


Fig. 1 Layout and extracted bit rate vs. emitter rate of the first NUV QRNG, with mini-SiPM as the emitter and SPADs as receivers (a), layout of one of the new NIR-HD QRNG structures, with big circular SPAD as the emitter and mini-SiPMs as the receivers (b) and schematic of the emitter/detector with front-end board and emitter driving scheme (c).

## References

[1] F. Acerbi et. al., IEEE journal of selected topics in quantum electronics, vol. 24, no. 6, p. 6101107 (2018)
[2] Z. Bisadi, et. al., Journal of Lightwave Technology, vol. 35, no. 9 (2017) DOI 10.1109/JLT.2017.2656866
[3] J. B. Brask, A. Martin, W. Esposito, R. Houlmann, J. Bowles, H. Zbinden and N. Brunner, Physical Review Applied, vol. 7, 054018 (2017), DOI: 10.1103/PhysRevApplied.7.054018

# Quantum Random Number Generator based on Quantum Jitter of Single Photon Avalanche Photodiode (SPAD)

**Mano Rahul K Pakalapati[1], Susan K Earles[1], Ersoy Subasi[1], Mano Varun K Pakalapati[1]**

[1]*Florida Institute of Technology, Melbourne, Florida, USA*

Quantum jitter based random number generator which produces $a^n$ random combinations of numbers is presented in this paper where, a is the radix of the generated random string of length $n$. The proposed Quantum Random Number Generator (QRNG) uses detection windows and SPAD quantum jitters such as dark counts and or photon arrival times as seeds to generate high-quality random numbers. The detection window implementation in the proposed QRNG reduces the effect of noise sources within SPAD that cause periodicity in the generated random numbers. Generated random numbers are subjected to NIST Statistical Test Suite and Dieharder test Suite and the results are reported.

Producing true random numbers on a deterministic system requires a disordered random seed [1-5]. The probabilistic quantum phenomenon is a source of true randomness in nature. In the experimental setup shown in fig.1(b), dark counts of SPAD are used as source of quantum jitter. The time of arrival between detection windows and a SPAD avalanche is measured using Time to Digital Converter (TDC). The measured time intervals are concatenated into a binary string of length $n$ using a shift register, which gives $2^n$combinations of random binary values. The entire concatenated string is then type-casted as one $n$-bit binary number so that any periodic information between measurements is lost, generating true random numbers. Tables 1 and 2 show the Dieharder and NIST STS test results of the generated random data of 35 unsigned numbers of length 3000.

| *Test* | *P-Values* |
|---|---|
| diehard_birthdays | 0.9565 |
| diehard_operm5 | 0.8590 |
| diehard_rank_32x32 | 0.4025 |
| diehard_rank_6x8 | 0.3103 |
| diehard_bitstream | 0.5028 |
| diehard_opso | 0.6633 |
| diehard_oqso | 0.7624 |
| diehard_dna | 0.6413 |
| diehard_count_1s_str | 0.4405 |
| diehard_count_1s_byt | 0.9377 |
| diehard_parking_lot | 0.6164 |
| diehard_2dsphere | 0.6937 |
| diehard_3dsphere | 0.4771 |
| diehard_squeeze | 0.8112 |
| diehard_sums | 0.2803 |
| diehard_runs | 0.9112 |
| diehard_craps | 0.8550 |
| marsaglia_tsang_gcd | 0.7345 |
| sts_monobit | 0.5728 |
| sts_runs | 0.9969 |
| sts_serial | 0.4796 |
| rgb_bitdist | 0.4253 |
| rgb_minimum_distance | 0.4284 |
| rgb_permutations | 0.6003 |
| rgb_lagged_sum | 0.5727 |
| rgb_kstest_test | 0.6760 |
| dab_bytedistrib | 0.9019 |
| dab_dct | 0.3428 |
| dab_filltree | 0.3366 |
| dab_filltree2 | 0.7672 |
| dab_monobit2 | 0.3151 |

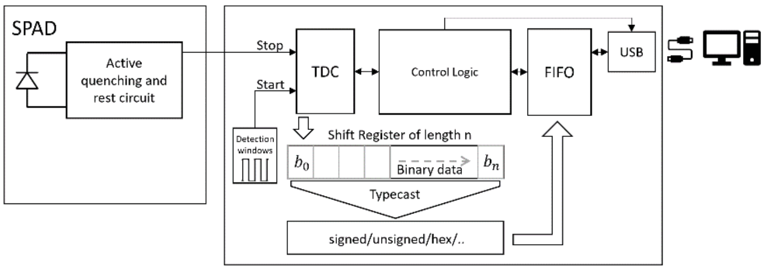


(b)

| *Test* | *P-Values* | *Proportion* |
|---|---|---|
| Frequency | 0.66549 | 0.99091 |
| BlockFrequency | 0.82631 | 1.00000 |
| CumulativeSums | 0.96058 | 0.99091 |
| CumulativeSums | 0.12894 | 0.97273 |
| Runs | 0.20325 | 1.00000 |
| LongestRun | 0.38072 | 0.97273 |
| Rank | 0.13586 | 1.00000 |
| FFT | 0.57117 | 0.97273 |
| NonOverlappingTemplate | 0.50886 | 0.98790 |
| OverlappingTemplate | 0.64658 | 0.97273 |
| Universal | 0 | 0 |
| ApproximateEntropy | 0.23459 | 0.99091 |
| RandomExcursions | 0.26206 | 1.00000 |
| RandomExcursionsVariant | 0.20629 | 0.98413 |
| Serial | 0.69578 | 1.00000 |
| LinearComplexity | 0.26953 | 0.98182 |

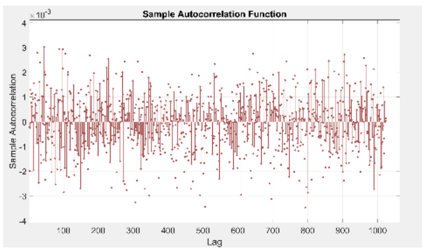


(a) (c) (d)

Fig. 1 (a) Table 1: Dieharder Test Suite results of the generated random data. (b) Table 2: NIST Statistical Test Suite (STS) results of the generated random data (b) Autocorrelation coefficients evaluated for a generated sequence sample of 1024 bits.

**References**

[1] Oded Goldreich, Shafi Goldwasser, Silvio Micali, How to construct random functions, Journal of the ACM (JACM), Oct. 1986.

[2] S. Tisa, F. Villa, A. Giudice, G. Simmerle and F. Zappa, "High-Speed Quantum Random Number Generation Using CMOS Photon Counting Detectors," IEEE Journal of Selected Topics in Quantum Electronics, 2015.

[3] M. Nicola, L. Gasparini, A. Meneghetti and A. Tomasi, "A SPAD-Based Random Number Generator Pixel Based on the Arrival Time of Photons," 2017 New Generation of CAS (NGCAS), 2017.

[4] H. Xu, D. Perenzoni, A. Tomasi and N. Massari, "A16x16 Pixel Post-Processing Free Quantum Random Number Generator Based on SPADs," IEEE Trans. on Circuits and Systems II: Express Briefs, 2018.

[5] A. Khanmohammadi, R. Enne, M. Hofbauer and H. Zimmermanna, "A Monolithic Silicon Quantum Random Number Generator Based on Measurement of Photon Detection Time," in IEEE Photonics Journal, vol. 7, no. 5, pp. 1-13, Oct. 2015.

# Quantum signals: shaping temporal correlations and photon statistics

**Ivo Straka, Miroslav Ježek**

*Department of Optics, Faculty of Science, Palacký University, Olomouc, Czechia*

In this work, we present stochastic approaches to modulating classical light intensity to tailor the intensity cross-correlation ($g^{(2)}(t)$). Two of these approaches address both generation of a pre-set $g^{(2)}(t)$ shape and generation of a pre-set classical photon-number distribution (in a set time window) [1].

We propose three methods:

1. The first method is capable of generating any shape of ($g^{(2)}(t)$-1) that is a cross-correlation of a non-negative function, or any superposition thereof. Examples include Gaussian, Cauchy-Lorentz, or hyperbolic secant shapes. The vertical scaling is also arbitrary with any value of $g^{(2)}(0) \geq 1$ possible. Examples are shown in Fig. 1.
2. The second method generates simultaneously an arbitrary classical photon statistics [1] along with an arbitrary convex $g^{(2)}(t)$, meaning that $d^2g^{(2)}(t)/dt^2 > 0$ needs to be satisfied.
3. The third method is numerical and therefore approximate, but allows generation of both arbitrary classical photon statistics and arbitrary $g^{(2)}(t)$ without the convexity constraint.

Methods 1 and 2 are formulated analytically and can be algebraically shown to be accurate solutions of the respective problems. Method 1 relies on a random stream of superimposed pulses, which can be experimentally implemented by a digital controller driving the modulation, or – approximately for a highly bunched light – by a signal generator triggered at random times.

Method 2 generates the specified photon statistics by random switching between discrete intensity levels, because this approach was experimentally shown to produce accurate results even for photon statistics that theoretically arise from continuous intensity distributions [1]. The $g^{(2)}(t)$ shape is then achieved by stochastic changes to the modulation period. The discreetness, however, poses some restrictions on available methods of shaping the $g^{(2)}(t)$. We have been able to prove that a solution of such a problem exists for a convex $g^{(2)}(t)$ shape.

Method 3 employs a random mixture of various "comb" intensity profiles of alternating mutual correlations that numerically approximate the desired $g^{(2)}(t)$ shape, while preserving the intensity/photon-number distribution. The solution is obtained as a least-squares fit in a rather extensive parameter space and it seems to converge point-wise with increasing number of free parameters.

The proposed methods are a fundamental result that addresses the problem of arbitrary quantum optical signal generation. Experimental implementations can be used for probing or simulating complex systems that exhibit memory and nonlinear behaviour; for example generating time-correlated noise, or complex non-Markovian metrology of quantum detectors [2].

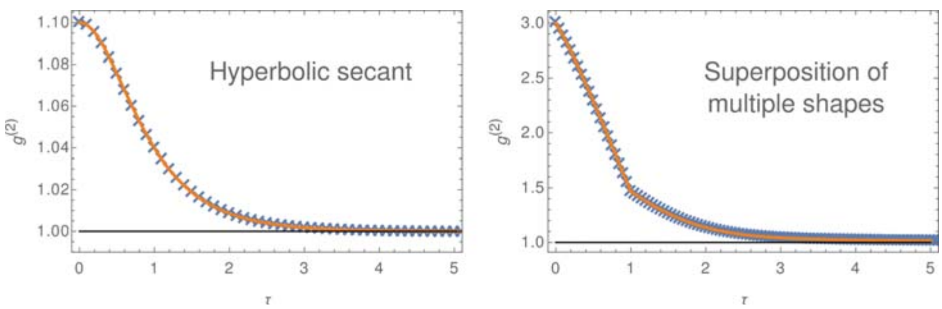


Fig. 1: Intensity cross-correlations of simulated stochastic signals (Method 1). Orange line is the desired shape and blue crosses are the cross-correlation samples computed from the simulation.

**References**

[1] I. Straka, J. Mika, and M. Ježek, Opt. Express **26**, 8998-9010 (2018).
[2] F.-X. Wang et al., J. Lightwave Technol. **34**, 3610-3615 (2016).

# Hong-Ou-Mandel interference at a metasurface

**Jakub Szlachetka[1], Karolina Słowik[1], Piotr Kolenderski[1]**
[1] Institute of Physics, Nicolaus Copernicus University in Toruń

Photons produced in the Spontaneous Parametric Down-Conversion (SPDC) process typically propagate through optical elements such as waveguides, lenses and beam splitters . We aim to exploit unconventional optical elements, whose fabrication has recently become possible due to the rapid development of nanotechnologies [1]. Such miniaturized devices are typically integrated on microchips that may later become parts of larger quantum circuits. An example is provided by metamaterials, which are periodic arrays of metallic nanoparticles. These nanoparticles support surface plasmon polaritons - hybrid excitations that combine electromagnetic fields with coherent oscillations of valence-electron plasma [3, 4]. Here we experimentally characterize a nanostructural beam splitter, which was designed to feature 25 % of reflection and transmission, and 50 % of absorption [5]. Furthermore we used photons in weak coherent state to observe Hong-Ou-Mandel effect on metamaterial beamsplitter .

**References**

[1] J. Li, A. Salandrino, and N. Engheta , Shaping light beams in the nanometer scale: A Yagi-Uda nanoantenna n the optical domain, Phys. Rev. B **76**, 245403 (2007).
[2] J. S. Fakonas, A. Mitskovets and H. A. Atwater , Path entanglement of surface plasmons , New J. Phys. **17**, 023002 (2015)
[3] G. Fujii, D. Fukuda, and S. Inoue , Direct observation of bosonic quantum interference of surface plasmon polaritons using photon-number-resolving detectors , Phys. Rev. B **90**, 085430 (2014).
[4] G. Di Martino, Y. Sonnefraud, M. S. Tame, S. K´ena-Cohen, F. Dieleman, S ̧. K.̈Ozdemir, M. S. Kim, and S. A. Maier , Observation of Quantum Interference in the Plasmonic Hong-Ou-Mandel Effect , Phys. Rev. A. **1**, 034004 (2014).
[5] S. M. Barnett, J. Jeffers, A. Gatti, R. Loudon , Quantum optics of lossy beam splitters , Phys. Rev. A. **3**, 57 (1998)

# Generation of hybrid maximally entangled states in a one-dimensional quantum walk

Aikaterini Gratsea,[1] Maciej Lewenstein,[1,2] and Alexandre Dauphin[1]

[1] *ICFO-Institut de Ciències Fotòniques, The Barcelona Institute of Science and Technology, Av. Carl Friedrich Gauss 3, 08860 Barcelona, Spain*
[2]*ICREA-Institució Catalana de Recerca i Estudis Avançats, Lluis Companys 23, 08010 Barcelona, Spain*

We study the generation of hybrid entanglement in a one-dimensional quantum walk. In particular, we explore the preparation of maximally entangled states between position and spin degrees of freedom. We address it as an optimization problem, where the cost function is the Schmidt norm. We then benchmark the algorithm and compare the generation of entanglement between the Hadamard quantum walk, the random quantum walk and the optimal quantum walk. Finally, we discuss an experimental scheme with a photonic quantum walk in the orbital angular momentum of light along with the scheme for the experimental measurement.

---

[1] R. Horodecki, P. Horodecki, M. Horodecki, and K. Horodecki, Rev. Mod. Phys. **81**, 865 (2009).
[2] S. Pirandola, J. Eisert, C. Weedbrook, A. Furusawa, and S. Braunstein, Nat. Photonics **9**, 641 (2015).
[3] V. Scarani, H. Bechmann-Pasquinucci, N. J. Cerf, M. Dušek, N. Lütkenhaus, and M. Peev, Rev. Mod. Phys. **81**, 1301 (2009).
[4] D. Rosset, J.-D. Bancal, and N. Gisin, J Phys A-Math Theor **47**, 424022 (2014).
[5] N. Brunner, O. Gühne, and M. Huber, J Phys A-Math Theor **47**, 420301 (2014).
[6] N. Brunner, D. Cavalcanti, S. Pironio, V. Scarani, and S. Wehner, Rev. Mod. Phys. **86**, 419 (2014).
[7] M. Krenn, M. Malik, M. Erhard, and A. Zeilinger, Philos. Trans. Royal Soc. A **375** (2016).
[8] M. A. Can, A. Klyachko, and A. Shumovsky, J. Opt B Quantum Semiclassical Opt. **7**, L1 (2005).
[9] E. Karimi, J. Leach, S. Slussarenko, B. Piccirillo, L. Marrucci, L. Chen, W. She, S. Franke-Arnold, M. J. Padgett, and E. Santamato, Phys. Rev. A **82**, 022115 (2010).
[10] F. Flamini, N. Spagnolo, and F. Sciarrino, Rep. Prog. Phys. **82**, 016001 (2018).
[11] X.-Y. Lü, G.-L. Zhu, L.-L. Zheng, and Y. Wu, Phys. Rev. A **97**, 033807 (2018).
[12] X.-L. Wang, X.-D. Cai, Z.-E. Su, M.-c. Chen, D. Wu, L. Li, N.-L. Liu, C.-Y. Lu, and J.-W. Pan, Nature **518**, 516 (2015).
[13] C. Vitelli, N. Spagnolo, L. Aparo, F. Sciarrino, E. Santamato, and L. Marrucci, Nat. Photonics **7**, 521 (2013).
[14] R. Vieira, E. P. M. Amorim, and G. Rigolin, Phys. Rev. A **89**, 042307 (2014).
[15] M. Zeng and E. H. Yong, Sci. Rep. **7**, 12024 (2017).
[16] M. Erhard, R. Fickler, M. Krenn, and A. Zeilinger, Light Sci Appl. **7**, 17146 (2017).
[17] L.-P. Deng, H. Wang, and K. Wang, J. Opt. Soc. Am. B **24**, 2517 (2007).
[18] J. Lopes, W. Soares, B. Bernardo, D. Caetano, and A. Canabarro, , arXiv:1811.04001 (2018), 1811.04001.
[19] M. A. Nielsen and I. L. Chuang, *Quantum Computation and Quantum Information: 10th Anniversary Edition*, 10th ed. (Cambridge University Press, New York, NY, USA, 2011).
[20] D. Cozzolino, D. Bacco, B. Da Lio, K. Ingerslev, Y. Ding, K. Dalgaard, P. Kristensen, M. Galili, K. Rottwitt, S. Ramachandran, and L. K. Oxenløwe, Phys. Rev. Applied **11**, 064058 (2019).
[21] D. Cozzolino, E. Polino, M. Valeri, G. Carvacho, D. Bacco, N. Spagnolo, L. K. Oxenlwe, and F. Sciarrino, arXiv e-prints , arXiv:1903.03452 (2019),1903.03452.
[22] K. Manouchehri and J. Wang, *Physical Implementation of Quantum Walks* (Springer Publishing Company, Incorporated, 2013).
[23] M. Karski, L. Förster, J.-M. Choi, A. Steffen, W. Alt, D. Meschede, and A. Widera, Science **325**, 174 (2009).
[24] F. Zähringer, G. Kirchmair, R. Gerritsma, E. Solano, R. Blatt, and C. F. Roos, Phys. Rev. Lett. **104**, 100503 (2010).
[25] H. Schmitz, R. Matjeschk, C. Schneider, J. Glueckert, M. Enderlein, T. Huber, and T. Schaetz, Phys. Rev. Lett. **103**, 090504 (2009).
[26] F. Meinert, M. J. Mark, E. Kirilov, K. Lauber, P. Weinmann, M. Gröbner, A. J. Daley, and H.-C. Nägerl, Science **344**, 1259 (2014).
[27] M. A. Broome, A. Fedrizzi, B. P. Lanyon, I. Kassal, A. Aspuru-Guzik, and A. G. White, Phys. Rev. Lett. **104**, 153602 (2010).
[28] A. Schreiber, K. N. Cassemiro, V. Potoček, A. Gábris, P. J. Mosley, E. Andersson, I. Jex, and C. Silberhorn, Phys. Rev. Lett. **104**, 050502 (2010).
[29] S. Barz, I. Kassal, M. Ringbauer, Y. Ole Lipp, B. Dakić, A. Aspuru-Guzik, and P. Walther, Sci Rep. **4**, 6115 (2014).
[30] P. Walther, K. J Resch, T. Rudolph, E. Schenck, H. Weinfurter, V. Vedral, M. Aspelmeyer, and A. Zeilinger, Nature **434**, 169 (2005).
[31] F. Cardano, F. Massa, H. Qassim, E. Karimi, S. Slussarenko, D. Paparo, C. de Lisio, F. Sciarrino, E. Santamato, R. W. Boyd, and L. Marrucci, Sci Adv. **1**, e1500087 (2015).
[32] F. Cardano, A. D'Errico, A. Dauphin, M. Maffei, B. Piccirillo, C. de Lisio, G. De Filippis, V. Cataudella, E. Santamato, L. Marrucci, M. Lewenstein, and P. Massignan, Nat. Commun. **8**, 15516 (2017).
[33] R. Vieira, E. P. M. Amorim, and G. Rigolin, Phys. Rev. Lett. **111**, 180503 (2013).
[34] T. Giordani, E. Polino, S. Emiliani, A. Suprano, L. Innocenti, H. Majury, L. Marrucci, M. Paternostro, A. Ferraro, N. Spagnolo, and F. Sciarrino, Phys. Rev. Lett. **122**, 020503 (2019).
[35] G. Abal, R. Siri, A. Romanelli, and R. Donangelo, Phys. Rev. A **73**, 042302 (2006).
[36] A. C. Orthey and E. P. M. Amorim, Quantum Inf. Process. **16**, 224 (2017).
[37] M. Cande, *Entangled photons in disordered media : from two-photon speckle patterns to Schmidt decomposition*, Ph.D. thesis, Université de Grenoble (2014).
[38] Q.-Q. Wang, X.-Y. Xu, W.-W. Pan, K. Sun, J.-S. Xu, G. Chen, Y.-J. Han, C.-F. Li, and G.-C. Guo, Optica **5**, 1136 (2018).
[39] C. M. Chandrashekar, R. Srikanth, and R. Laflamme, Phys. Rev. A **77**, 032326 (2008).
[40] R. Reuvers, Proc. Royal Soc. Lond. A **474**, 20180023 (2017).
[41] D. J. Wales and J. P. K. Doye, J Phys Chem A **101**, 5111 (1997).
[42] F. Cardano, M. Maffei, F. Massa, B. Piccirillo, C. de Lisio, G. De Filippis, V. Cataudella, E. Santamato, and L. Marrucci, Nat. Comm. **7**, 11439 (2016).
[43] A. D'Errico, F. Cardano, M. Maffei, A. Dauphin, R. Barboza, C. Esposito, B. Piccirillo, M. Lewenstein, P. Massignan, and L. Marrucci, arXiv e-prints , arXiv:1811.04001 (2018), 1811.04001.
[44] J. Dressel, M. Malik, F. M. Miatto, A. N. Jordan, and R. W. Boyd, Rev. Mod. Phys. **86**, 307 (2014).
[45] J. Torres and L. Torner, *Twisted Photons: Applications of Light with Orbital Angular Momentum* (Wiley-VCH, 2011) p. 243.

# Quantum memory in anti-relaxation coated gas cell

**Lijun Ma, Xiao Tang and Oliver Slattery**

*National Institute of Standards and Technology, Gaithersburg, MD 20899, USA*

Quantum memories based on alkali atomic vapors have attracted plenty of attention, since this is a relatively easy approach and can be implemented at room temperature. So far, electromagnetically induced transparency (EIT), Raman memory, and gradient echo memory (GEM) have been demonstrated in alkali atomic vapors, e.g. Cs or Rb atoms[1].

One of main challenges for the vapor-based memories is the decoherence caused by collisions between atoms and the vapor cell wall. Such decoherence limits the storage time of the quantum memories and leads to additional noise. One approach to achieve longer coherence times is with the use of an anti-relaxation coating on the inner wall of the vapor cell. Paraffin has been the most common anti-relaxation coating used for this purpose. Recently, a new anti-relaxation coating, alkene, has been reported to show longer spin relaxation times in alkali atomic vapor cells[2].

To investigate the new coating performance for quantum memory in an atomic vapor cell, we have implemented a quartz Cesium (Cs) cell that is coated with alkene. The cell was experimentally studied in a quantum memory experiment based on EIT. The energy structure of the EIT is shown in Fig.1 (a), and the control and the signal fields are resonant with the $6^2S_{1/2}$ F=3 $\rightarrow$ $6^2P_{1/2}$ F'=4 and $6^2S_{1/2}$ F=4 $\rightarrow$ $6^2P_{1/2}$ F'=4 transitions of Cs respectively and are detuned by 100 MHz. Fig. 1 (b) shows the experimental configuration: the control and signal beams are combined with a polarizing beam splitter (PBS) and sent into the alkene coated Cs cell. After the cell, a Glan-Thompson polarizer and three Etalon filters remove the control beam. The signal photons are then detected by a single photon counting module (SPCM).

The linewidth of the EIT resonance corresponds to the decoherence rate and a narrower linewidth will result in higher retrieval efficiency. As shown in Fig. 1 (c), the full width half maximum (FWHM) linewidth of spectra of the EIT using alkene is in the kHz range, which is much narrower than EIT using paraffin in the same experimental set-up. Fig. 1(d) shows the storage and retrieval of a 2-μs second photon pulse. In the experiment, the control beam diameter (1.5 mm) is much smaller than the diameter of cell (19 mm). During the retrieval process, only when the stored atoms without decoherence move into the control beam area, photons can be retrieved. In that case, the longer the decoherence time, the longer the tail of the retrieval pulse will become. The experimental results show a much longer retrieval tail. From these experimental results, the alkene coating cell can provide long coherence time, and thus can provide higher storage efficiency and longer storage time.

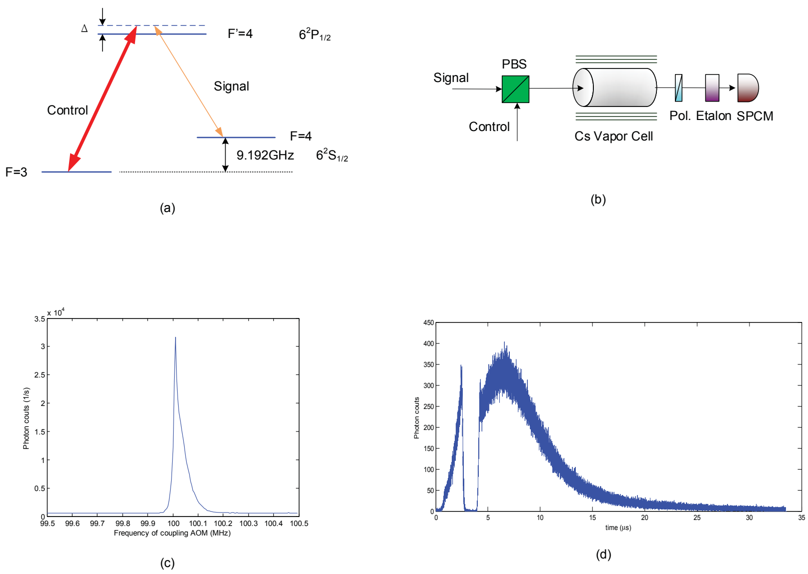


Fig. 1 experimental setup and results. (a) energy structure for EIT memory, (b) experimental setup, (c) EIT transparent window, (d) photon pulse storage and retrieval.

## References

[1] C. Simon, *et al.*, "Quantum memories," *The European Physical Journal D,* vol. 58, pp. 1-22, 2010.

[2] M. Balabas, *et al.* , "Polarized alkali-metal vapor with minute-long transverse spin-relaxation time," *Physical review letters,* vol. 105, p. 070801, 2010.

# Maximisation of Quantum Correlations under Local Filtering Operations

Sabine Wollmann[1], Andrés F. Ducuara[1], Xiaogang Qiang[2,3], Joel F. Tasker[1], Xiaoqi Zhou[4], Jianwei Wang[5], Callum M. Wilkes[1], Thomas Loke[6], Sean O'Gara[1], Laurent Kling[1], Graham D. Marshall[1], Raffaele Santagati[1], Timothy C. Ralph[7], Jingbo B. Wang[6], Jeremy L. O'Brien[1], Mark G. Thompson[1], Paul Skrzypczyk[1], and Jonathan C. F. Matthews[1]

[1] *Quantum Engineering Technology Labs, University of Bristol, Bristol BS8 1FD, UK.*

[2] *Institute for Quantum Information&State Key Laboratory of High Performance Computing, College of Computer, National University of Defense Technology, Changsha, China.*

[3] *National Innovation Institute of Defense Technology, AMS, Beijing, China.*

[4] *State Key Laboratory of Optoelectronic Materials and Technologies and School of Physics, Sun Yat-sen University, Guangzhou, China.*
[5] *State Key Laboratory for Mesoscopic Physics and Collaborative Innovation Centre of Quantum Matter, Peking University, Beijing, China.*
[6] *School of Physics, The University of Western Australia, Crawley, Western Australia, Australia.*
[7] *Centre for Quantum Computation and Communication Technology, School of Mathematics and Physics, University of Queensland, Brisbane, Queensland, Australia.*

Nonclassical correlations are a key resource to explore foundational quantum information tasks and for applications in device-independent protocols. Quantum steering was recently formalized [1] and describes the effect of a local measurement on one system and affecting the measurement results on the other system.
This can be visualized for two-qubit states using quantum steering ellipsoids (QSE), which is the set of Bloch vectors that Alice can collapse Bob's state to. They are theoretically well studied [2-5] and have been recently experimentally demonstrated [6].

Here, we experimentally demonstrate QSEs using a fully reconfigurable silicon quantum photonic device able to implement universal two-qubit unitary quantum operations. It is adopting an optical linear-combination protocol that utilizes only two-photon-entanglement and extended spatial freedom of photons (Fig.1) [7]. We generate arbitrary two-qubit states and Alice measures her part of the shared state with randomly distributed projective measurements along the Bloch sphere. We tomographically reconstruct Bob's state and show the distribution over the theoretically expected steering ellipsoid.
Further, we use the QSE to study the role that filters with regards to the QSE. In particular, we identify and demonstrate the optimal local filters on two-qubit states that lead to the biggest increase in the volume of the QSE which is related to properties like Bell nonlocality, steerability, and entanglement [5, 8, 9].

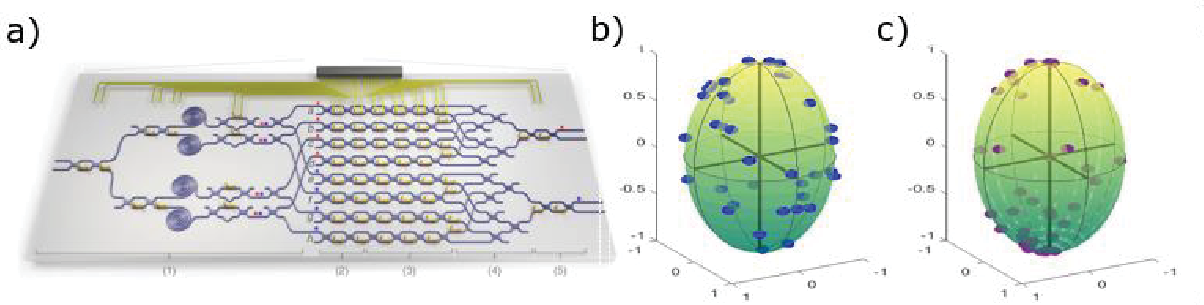


Fig. 1 (a) We generate a maximally entangled state with a high fidelity (F=93.78%) on an integrated photonics platform [8]. Alice's measurement settings (b) are randomly distributed across the Bloch sphere. Bob's steered state (c) is tomographically reconstructed and plotted along the theoretically expected surface of the QSE.

**References**
[1] H. M. Wiseman et al., Phys. Rev. Lett. **98**, 140402 (2007).
[2] F. Verstraete, Ph.D. thesis, Katholieke Universiteit Leuven (2002).
[3] M. Shi et al., New J. Phys. **13**, 073016 (2011).
[4] M. Shi et al., J. Phys. A: Math. and Theor. **44**, 415304 (2011).
[5] S. Jevtic et al., Phys.Rev. Lett. **113**, 020402 (2014).
[6] Z. Chao et al., arXiv:1809.08011 (2018).
[7] X. Qiang et al., Nat. Phot. **12**, 534 (2018).
[8] A. Milne et al., New J. Phys. **16**, 083017 (2014).
[9] A. Milne et al., Phys. Rev. A **90**, 024302 (2014).

# Experimental realization of device-independent quantum randomness expansion

**Ming-Han Li[1, 2], Xingjian Zhang[3], Wen-Zhao Liu[1, 2], Si-Ran Zhao[1, 2], Bing Bai[1, 2], Yang Liu[1, 2], Qi Zhao[1, 2], Jun Zhang[1, 2], Xiongfeng Ma[3], Qiang Zhang[1, 2], Jingyun Fan[1, 2], and Jian-Wei Pan[1, 2]**

[1] *Shanghai Branch, National Laboratory for Physical Sciences at Microscale and Department of Modern Physics,University of Science and Technology of China, Shanghai 201315, P. R. China*

[2] *Shanghai Branch, CAS Center for Excellence and Synergetic Innovation Center in Quantum Information and Quantum Physics, University of Science and Technology of China, Shanghai 201315, P. R. China*

[3] *Center for Quantum Information, Institute for Interdisciplinary Information Sciences, Tsinghua University, Beijing 100084, P. R. China*

Randomness is not only a vital resource for nowadays information processing tasks, but also related to fundamental questions in science and philosophy. In general, random number generators can be classified into two categories: classical and quantum mechanical. The classical random number generation is completely predictable given the full knowledge of the random number generator. On the contrary, inherent randomness in quantum theory enables unpredictable quantum random number generation. However, the securities of many quantum random number generators are based on the full characterization of devices, which poses significant challenge even to the most skillful experimentalist. Loophole free violation of Bell inequality provides us an alternative way to generate genuine randomness without characterizing the inner working of the untrusted devices [1], which is referred as device-independent quantum random number generator (DIQRNG). The security of DIQRNG against both classical and quantum adversaries was proven [2-4], which led to a number of remarkable experimental exhibitions [2, 5] and the recent loophole free realizations [6-7]. This success directly inspires the device-independent quantum randomness expansion (DIQRE) [3], which takes a short random sequence as input and outputs a long sequence of random bits in a device-independent manner. The scientific merit of DIQRE is bi-fold, aside from being a unique quantum phenomenon that helps to understand the fundamentals about randomness and quantum theory, it is of practical usage in that DIQRE is resource-efficient in the generation of intrinsically unpredictable random numbers which are desired by a number of applications demanding high levels of security and randomness uniformity.

Realization of DIQRE presents a significant challenge to the experimental physics. While experimental realization of loophole free violation of Bell inequality is already a formidable task, experimentally efficient DIQRNG requests a larger violation of Bell inequality, and DIQRE raises the bar even higher. On one hand, entangled atomic systems [8] promise large violation of Bell inequality, these systems are currently constrained by low event rates, which makes it hard to accumulate enough statistics for analysis within a reasonable amount of time. On the other hand, entangled photonic systems [9-10] exhibit relatively small violation of Bell inequality but can be operated at high repetition rate, providing an opportunity. We present here a concrete realization of DIQRE based on loophole free violation of Bell inequality with entangled photons taking advantage of two recent advancements. One is the development of cutting-edge single-photon detection with near unity efficiency, which significantly improves the violation and output entropy in loophole free Bell test experiments, enabling the realization of DIQRE. The other is the development of randomness analysis techniques in DIQRNG protocols which generate random numbers efficiently. We note that two theoretical DIQRNG protocols caused recent attention. One is based on the Entropy Accumulation Theorem (EAT) [4] and was employed in arecent photonic realization of DIQRNG against quantum adversaries [6]. A more recent developments [11] based on EAT can be used to implement DIQRE on such systems at the expense of a large number of experimental experiments, but with good asymptotic performance. The other is the quantum probability estimation framework, which is safe for quantum opponents and is more efficient for small entropy violations of Bell inequalities [12]. We adopt the spot-checking protocol [3] for DIQRE experimental implementions using two theoretical DIQRNG protocols respectively.

**References**

[1] R. Colbeck, Ph.D. thesis, Trinity College, University of Cambridge (2006).
[2] S. Pironio, *et al.*, Nature **464**, 1021 (2010)
[3] C. A. Miller and Y. Shi, in *Proceedings of the 46th Annual ACM Symposium on Theory of Computing,* STOC ’14 (ACM, New York, NY, USA, 2014) pp. 417-426.
[4] R. Arnon-Friedman, F. Dupuis, O. Fawzi, R. Renner, and T. Vidick, Nat. Commun. **9**, 459 (2018).
[5] P. Bierhorst, *et al.*, Nature **556**, 223 (2018)
[6] Y. Liu, *et al.*, Nature **562**, 548 (2018).
[7] Y. Zhang, *et al.*, arXiv:1812.07786 (2018).
[8] B. Hensen, *et al.*, Nature **526**, 682 (2015).
[9] L. K. Shalm, *et al.*, Phys. Rev. Lett. **115**, 250402 (2015).
[10] M. Giustina, *et al.*, Phys. Rev. Lett. **115**, 250401 (2015).
[11] P. J. Brown, S. Ragy, and R. Colbeck, arXiv:1810.13346 (2018).
[12] E. Knill, Y. Zhang, and H. Fu, arXiv:1806.04553 (2018).

# Super-resolution phase imaging by detecting entangled photons with a SPAD-array camera


**Robin Camphausen[1], Alvaro Cuevas[1], Roland Terborg[1], Luc Duempelmann[1], Fabian Steinlechner[2], Valerio Pruneri[1,3]**

[1]*ICFO—Institut de Ciencies Fotoniques, Mediterranean Technology Park, 08860 Castelldefels (Barcelona), Spain,*

[2]*Fraunhofer Institute for Applied Optics and Precision Engineering IOF, Albert-Einstein-Strasse 7, 07745, Jena, Germany,*

[3]*ICREA—Institució Catalana de Recerca i Estudis Avançats, Pg. Lluís Companys 23, 08010 Barcelona, Spain.*


Phase imaging techniques such as interference contrast microscopy are commonly used for analysing transparent samples, for example cells in liquids or defects in materials. This relies on the interference between two beams of light, where one measures an intensity dependent on the sample inducing an optical path difference – a phase. Notably, it is well known that entanglement can be used to enhance interference-based sensing [1]. In particular, interfering an entangled state of the form $(|N, 0\rangle + |0,N\rangle)/\sqrt{2}$, a so-called NOON state, results in an N-fold multiplication of the phase induced by the sample. In this case, in order to obtain the quantum multiplication effect, rather than measuring the intensity of light, it is necessary to count photon coincidences.

NOON state phase super-resolution has been previously demonstrated, also in quantum imaging. However, it has only been achieved in a confocal microscope configuration requiring point-by-point scanning of the sample [2,3]. Here instead, we demonstrate entanglement-enhanced phase detection in a widefield imaging configuration. We utilise a novel large field-of-view lensless interferometric microscope [4], where it is possible to illuminate with a two-photon NOON state entangled in polarisation, and detect the transmitted photon pairs (Fig. 1a). As the generated entangled photons possess a non-classical spatial distribution we collect spatially-resolved coincidences with a SPAD-array camera (Fig. 1b). In our proposal the sample phase information can be retrieved using an evolution of the technique from [5]. However in our case it is possible to extract the super-resolved phase from all spatially separated 2-photon coincidences, making the SPAD-array camera work as a number-resolving photon detector.

Here we show the predicted two-fold enhanced phase contrast of a test scan compared to the classical measurement, thereby confirming the potential of SPAD-array cameras in entanglement-enhanced quantum imaging.

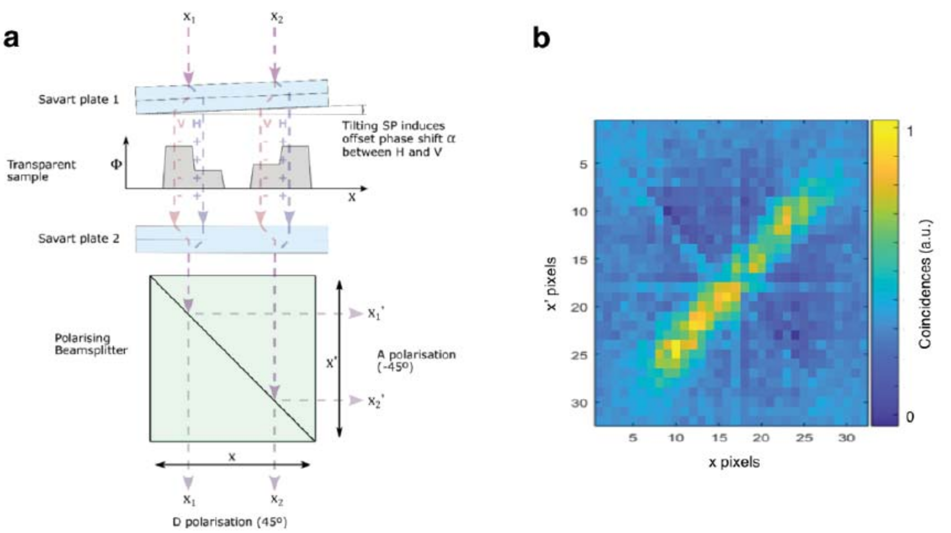


Fig. 1a : Spatially separated, polarisation-entangled photon pair propagating through novel lensless interferometric microscope. Fig. 1b : Spatially resolved coincidences from photon pairs. Note the clear spatial correlation between the two photons generated in an SPDC process.


**References**

[1] Dowling, J.P., 2008. Quantum optical metrology–the lowdown on high-N00N states. *Contemporary physics*, 49(2), pp.125-143.

[2] Ono, T., Okamoto, R. and Takeuchi, S., 2013. An entanglement-enhanced microscope. *Nature communications*, *4*, p.2426.

[3] Israel, Y., Rosen, S. and Silberberg, Y., 2014. Supersensitive polarization microscopy using NOON states of light. *Physical review letters*, *112*(10), p.103604.

[4] Terborg, R.A., Pello, J., Mannelli, I., Torres, J.P. and Pruneri, V., 2016. Ultrasensitive interferometric on-chip microscopy of transparent objects. *Science advances*, *2*(6), p.e1600077.

[5] Chrapkiewicz, R., Jachura, M., Banaszek, K. and Wasilewski, W., 2016. Hologram of a single photon. *Nature Photonics*, *10*(9), p.576.

# Optimizing quantum enhanced imaging in realistic conditions

**Alice Meda [1] , Elena Losero[1,2] , Ivano Ruo-Berchera[1], Alessio Avella[1] and Marco Genovese[1,3]**

[1]*INRIM, Strada delle Cacce 91, 10135 Torino, Italy*

[2]*Politecnico di Torino, Corso Duca degli Abruzzi 24, 10129 Torino, Italy*

[3]*INFN, Via P. Giuria 1, 10125 Torino, Italy*

Quantum correlations represent a fundamental tool for overcoming classical limits on precision of measurement. However, preserving these advantages in practical systems, where experimental imperfections are unavoidable, is a challenge of the utmost importance.
Here we report our recent efforts in the measurement of the absorption coefficient of a faint object, analyzing the application of different measurement strategies and estimators by optimizing them in presence of optical losses and noise. We report, in a wide field sub-shot noise imaging experiment , the best sensitivity ever achieved in loss estimation without any kind of post selection [1].

By extending such optimization procedure to the measurement of the absorption pattern of a faint object we show a sensitivity improvement up to a factor 2 with respect to the simple protocol used in previous demonstrations [2]. In wide field sub-shot noise imaging there is a trade-off between the resolution and the sensitivity, due to the fact that pixels smaller than the characteristic size of the correlated spatial modes reduces the collection efficiency, deteriorating quantum correlations. Thus, in another way, the optimized protocol allows to significantly improve the resolution without giving up quantum advantage in the sensitivity.

**References**

[1] E. Losero et al. Unbiased estimation of an optical loss at the ultimate quantum limit with twin-beams. *Scient. Rep.* **8**(1), 7431 (2018).

[2] N. Samantaray , I. Ruo-Berchera, A. Meda, M. Genovese. Realization of the first sub-shot-noise wide field microscope. *Light: Science & Applications* **6**, e17005 (2017).

# Detection efficiency calibration of InGaAs/InP single-photon detectors

**A. Meda[1], I. Ruo berchera[1], M. Gramegna[1], G. Brida[1], M. Genovese[1], M. López[2],**

**G. Porrovecchio[3], R. Kirkwood[4] , S. Kück[2] , M. Šmid[3], C. Chunnilall[4], and I. P. Degiovanni[1]**

*[1] Istituto Nazionale di Ricerca Metrologica (INRIM), Strada delle cacce 91, 10135 Torino, Italy*

*[2] Physikalisch-Technische Bundesanstalt (PTB), Bundesallee 100, D-38116, Braunschweig, Germany*

*[3] Cesky Metrologicky Institut (CMI), Okruzni 31, Brno 63800, Czech Republic*

*[4] National Physical Laboratory (NPL), Hampton road, Teddington, TW11 0LW, United Kingdom*

Single-photon avalanche diodes (SPAD) based on InGaAs/InP semiconductor materials are the most exploited detectors in many quantum technologies, such as quantum communication and Quantum Key Distribution [1, 2]. The successful development of such new technologies and products requires the solution to a number of metrological challenges; for this reason a metrological characterization in terms of detection efficiency, dead time, afterpulsing and dark counts of single photon detectors is mandatory.

We present the current results achieved on the calibration of the detection efficiency of a free-running InGaAs/InP SPAD detector and the results of a pilot study to compare different detection efficiency measurement strategies at the wavelength of 1550 nm performed by four European National Metrology Institutes: CMI, INRIM, NPL and PTB. The device under test was a commercial free-running fibre-coupled InGaAs/InP single-photon detector. The setup and the reference standard used as well as a detailed estimation of the measurement uncertainty of the detection efficiency is presented. A mathematical model including the effects of dead time, dark counts and afterpulsing of the detectors was developed and applied in the reported results.

**References**

[1] R. H. Hadfield, Nature Photonics 3, 696–705 (2009)

[2] D. Stucki, et al., Journal of Modern Optics, 48, Issue 13, 1967-1981 (2001)

# Fibre photon-pair sources for quantum imaging and spectroscopy

**Emma L. Pearce[1], Rupert F. Oulton[1], and Alex S. Clark[1]**

[1]*Blackett Laboratory, Department of Physics, Imperial College London, London, England*

Correlations between photon pairs generated by nonlinear optical processes offer advantages in many aspects of quantum imaging. In particular there have been a number of demonstrations of the improved precision of sub-shot noise absorption measurements [1] and using induced coherence to image an object at one wavelength while detecting light at a different wavelength [2], where one can probe a sample using IR light (e.g. a gas or a biological sample) but use more efficient, visible-range detectors. Implementations so far have relied on spontaneous parametric down-conversion (SPDC) in nonlinear crystals as a source of correlated photon pairs. We instead use spontaneous four-wave mixing (SFWM) in optical fibre, which has several benefits. Phase matching of the process is ensured by the birefringence of the fibre [3] which allows a wide separation in wavelength between the shorter wavelength signal and longer wavelength idler photons generated. Such a source can provide an idler photon in the IR while the signal photon is in the visible wavelength range. Suitable fibres are both affordable and readily available. Single mode propagation in the fibre makes alignment of such setups much easier, particularly with respect to overlapping idler photons from two distinct sources in an induced coherence experiment.

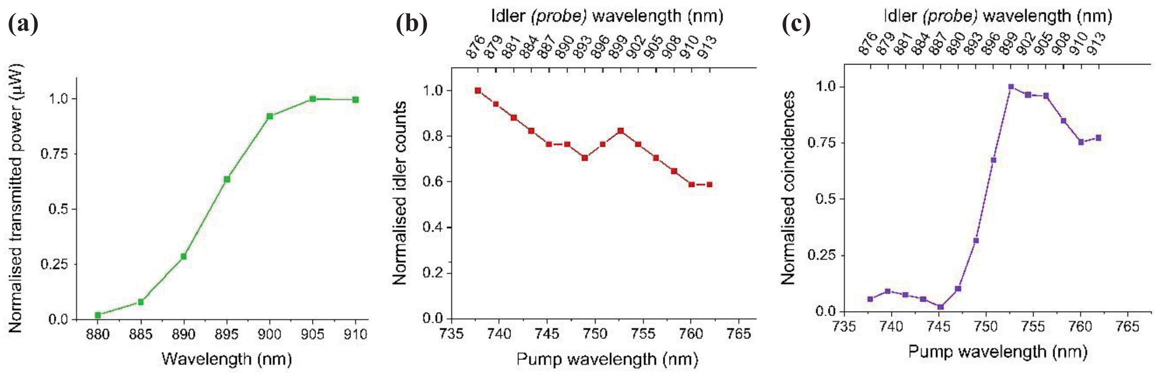


**Fig. 1 | Absorption measurement with a fibre photon-pair source. (a)** Classical absorption measurement of a GaAs sample using a tuneable laser shows an absorption edge feature as expected. **(b)** Idler photons generated by spontaneous four-wave mixing in a fibre pass through the GaAs sample and are detected by an APD. A strong Raman component in the idler beam means no absorption feature can be seen, as it is hidden in the thermal background. **(c)** When the idler photons passing through the sample are detected in coincidence with the signal photons, we can reject the uncorrelated Raman contribution and the absorption edge is revealed again.

Here we use a wavelength-tuneable fibre photon-pair source to measure the absorption at the band edge of a gallium arsenide (GaAs) sample. The fibre used is a polarisation-maintaining fibre with a nominal birefringence of $3.5 \times 10^{-4}$, providing a broad phase matching bandwidth for SFWM. Calculations show that a pump wavelength of 950 nm would generate signal photons at 786 nm and idler photons at 1200 nm. A tuneable pulsed Ti:Sapphire laser is filtered to ~2 nm and used to pump the fibre to generate signal and idler photons, whose wavelength is dependent on the pump wavelength. By tuning the pump between 735 nm and 765 nm we are able to generate signal and idler photons from 640 nm to 659 nm and 876 nm to 913 nm respectively. These signal and idler photons are then separated by a dichroic mirror, spectrally filtered, coupled to single mode fibres and sent to two separate silicon avalanche photodiodes (APDs). The GaAs sample is then added to the idler arm, which allows us to probe the GaAs absorption across the idler wavelength range, while also detecting the coincident correlated photons in the signal arm. When only counts on the idler detector are considered (Fig. 1b), a strong Raman component at this wavelength means any absorption feature is masked by the thermal background. By detecting signal and idler counts in coincidence (Fig. 1c), we can eliminate the uncorrelated Raman contribution and recover the absorption edge expected from a classical transmitted power measurement (Fig. 1a). We now intend to use this setup to perform sub-shot noise absorption of organic molecules, use high-numerical aperture objectives to use these photons for imaging, and use fibre photon-pair sources in nonlinear interferometers to perform imaging experiments with induced coherence at large signal and idler wavelength separations. Fibres with greater birefringence or photonic crystal fibres would open up further wavelength ranges to be used for such experiments.

### References

[1] P. Moreau et al., *Scientific Reports* **7**, 6256, (2017).
[2] G. Lemos, V. Borish, G. Cole, S. Ramelow, R. Lapkiewicz and A. Zeilinger, *Nature* **512**, 409-412, (2014).
[3] R. Stolen, M. Bösch and C. Lin, *Optics Letters* **6**, 213 (1981).

# BCD SPAD arrays for quantum optics applications

**Fabio Severini, Francesca Madonini, Alfonso Incoronato, Federica Villa, Franco Zappa**
*Dipartimento di Elettronica, Informazione e Bioingegneria, Politecnico di Milano, via Golgi 40, Milano, Italy*

Quantum optics is a field that profits by the granular nature of light to process information. It branches into various applications, particularly quantum imaging and quantum communication.
In this work we present two different SPAD imagers, a 96 × 96 array for quantum enhanced microscopy (Fig. 1 left) and a 32 × 1 array to be primarily employed in the Quantum Random Generator block within a quantum key distribution system (Fig. 1 right).
The first imager has been designed to accomplish the requirements of the European Project Q-MIC (Quantum-enhanced on-chip interference MICroscopy), which aims at developing a miniaturized on-chip interferometric microscope without lenses and illuminated by short wavelength entangled photon pairs. This solution allows to reach unprecedented sensitivity in the imaging of ultrathin transparent materials, such as photosensitive cells, single protein layers and biomarkers. From the detection standpoint, Q-MIC needs a SPAD image sensor array able to detect short wavelength single photon coincidences, within a coincidence time window as short as possible. With such a large number of pixels, each consisting of 10 µm SPAD and 50 µm pitch, resolution is boosted. However, the major breakthrough is the ability to detect photon coincidences spread over the entire array directly on chip and to provide the addresses of the triggered pixels only when a coincidence is detected, thanks to a novel event-driven logic. The coincidence detection is performed in an analog way based on 12 × 12 sub-arrays bringing to coincidence windows of about 2 ns, while the way each triggered pixel communicates its address is similar to an I2C architecture. The readout lasts 330 ns, whereas state-of-art 96 × 96 arrays require tens of microseconds.
A second European project, UNIQORN (Affordable Quantum Communication for Everyone: Revolutionizing the Ecosystem from Fabrication to Application) proposes to conceive a full Quantum System on Chip (QSoC) for telecom application for QKD (Quantum Key Distribution). For this purpose, a source of random keys needs to be introduced, leading to the design of the aforementioned 32 × 1 SPAD array. The chip has three operation modes. First one is Single-Hit Mode, needed to reveal the position of the pixel triggered by a single photon in a time window synchronous with the laser emission. The 5-bit address of the pixel position is provided, representing a pseudo- random number. Multi-Hit Mode is used to identify a coincidence of a certain number of photons, detected within a specified time window, for applications such as background rejection in Light Detection and Ranging. This operation mode employs a logic able to detect the presence of more than a user-selectable number of photons impinging on the array, namely one, two, three or four. At last, Simple Detector Mode provides an output pulse for each of the 32 pixels, synchronous with the photon detection on the array.
The linear array architecture consists of 32 pixels, each made by 4 SPADs with different diameter (5 µm, 10 µm, 20 µm, 50 µm) and their own quenching circuit. A coincidence logic circuit based on a selectable multi-threshold current comparator implements both single-hit and multi-hit modes. At last, an output block deals with signals readout, operating either in serial or parallel mode. The design has been performed in 0.16 µm BCD technology.

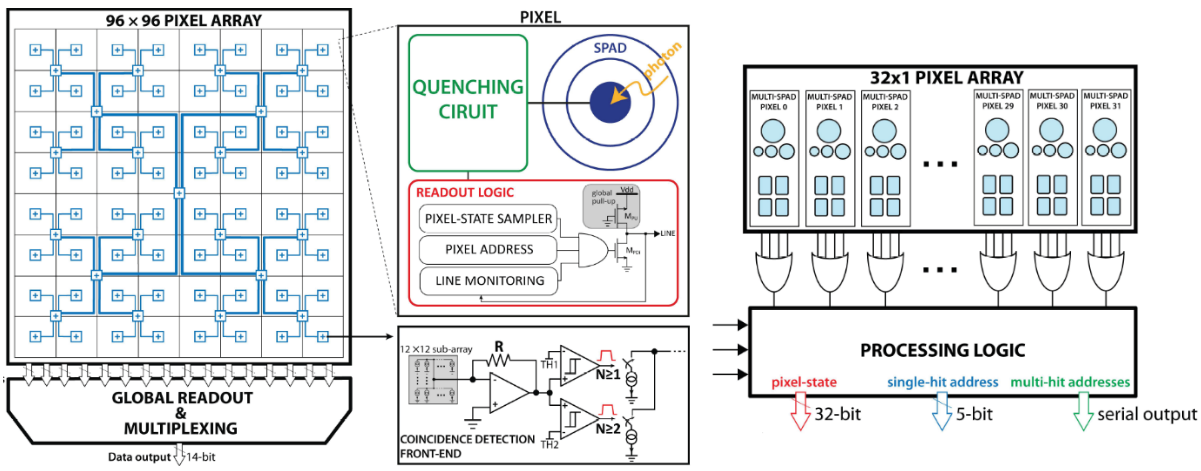


Fig. 1 Architectures of the Q-MIC 96 × 96 event-driven detector (left) and the UNIQORN linear array for coincidence detection (right).

**Acknowledges**
This project has received funding from the European Union’s Horizon 2020 research and innovation programme under grant agreement No 801060 and No 820474.

# Large area SiPM and high-throughput timing electronics: how to boost performances of time-domain diffuse optical instruments

L. Di Sieno[1], A. Behera[1], E Ferocino[1], D. Contini, A. Torricelli[1,2], S. Rohilla[3,4], B. Krämer[3] F. Koberling[3], F. Acerbi[5], A. Gola[5], A. Pifferi[1,2] and A. Dalla Mora[1]

[1] *Politecnico di Milano - Dipartimento di Fisica, Piazza Leonardo da Vinci 32, 20133, Milano, Italy.*

[2] *Consiglio Nazionale delle Ricerche - Istituto di Fotonica e Nanotecnologie, Piazza Leonardo da Vinci 32, 20133, Milano, Italy*

[3] *PicoQuant GmbH, Rudower Chaussee 29 (IGZ), 12489 Berlin, Germany.*

[4] *Charité – Universitätsmedizin Berlin, corporate member of Freie Universität Berlin, Humboldt-Universität zu Berlin, and Berlin Institute of Health, Department of Internal Medicine/Infectious Diseases and Respiratory Medicine, Charitéplatz 1, 10117 Berlin, Germany.*

[5] *Fondazione Bruno Kessler (FBK), Center for material and microsystems (CMM), Via Sommarive 18, 38123 Trento, Italy.*

Time-domain (TD) diffuse optical spectroscopy relies on the injection of short optical pulses in a diffusive medium (such as biological tissues) and on the collection, through a single-photon detector, of the time-of-flight distribution of the re-emitted photons. The use of the TD approach in reflectance geometry, among other advantages (e.g. determination of tissue optical properties, namely absorption and reduced scattering coefficients), allows to discriminate the depth reached by photons on the basis on their re-emission time (the later they are re-emitted, the deeper the region they probed). However, to reach deep structures/organs to non-invasively analyze their functionality we need to collect the very few late photons. Thus, a large area (i.e. high light harvesting) detector is needed to collect even the faint late signal while keeping a good temporal resolution. To this extent, we used a 3x3 $mm^2$ SiPM (S13360-3050CS, Hamamatsu Photonics) equipped with a custom-made front-end electronics. This solution permits to increase the light harvesting capability 9-fold. In order to fully exploit this high photon rate, a high throughput timing electronics is needed. For this reason, we used a MultiHarp 150 (PicoQuant GmbH, Germany) which can sustain a nominal count-rate up to 160 Mcps due to its low dead-time of 650 ps. To further increase the number of detected photons, we operated the system much beyond the single-photon statistics up to a count rate of approximately 30 Mcps with a pulsed diode laser at 40 MHz. Hence, a suitable post processing correction [1] has been applied to in order to reduce the effect of the pile-up and other distortions due to the dead-time of the detector.

We tested the depth sensitivity of the system using as figures of merit the contrast (i.e. relative perturbation produced by an inhomogeneity into a diffusive medium) and contrast-to-noise ratio –CNR– (i.e. an index of the signal robustness), whose definition is given in Ref [2]. We repeated the measurements with the large area SiPM at 3 different count-rates (1 Mcps, 15 Mcps and 30 Mcps) and then we compared the results obtained with those achieved using the same system coupled to a 1 mm SiPM detector working at 1 Mcps (i.e. state of the art). Fig. 1 clearly show that, as expected, the contrast for a late gate is nearly the same notwithstanding the high count-rate used while the improvement can be clearly appreciated in the CNR which increases of more than 200%. Finally, we challenged our system with *in-vivo* brain activation measurements, showing an improvement in signal-to-noise ratio as compared to the acquisition done with 1 mm SiPM working at 1 Mcps (data not shown).

In conclusion, large area SiPM coupled to high-throughput electronics allows to improve the performances of time-domain diffuse optical instruments, thereby opening new scenarios for non-invasive optical imaging. Moreover, to push the technique to its ultimate limits, in the SP-LADOS project we are now developing a new SiPM with 1x1 $cm^2$ area featuring low noise (dark count rate < 2 Mcps in 1 $cm^2$) and good timing resolution (FWHM < 500ps).

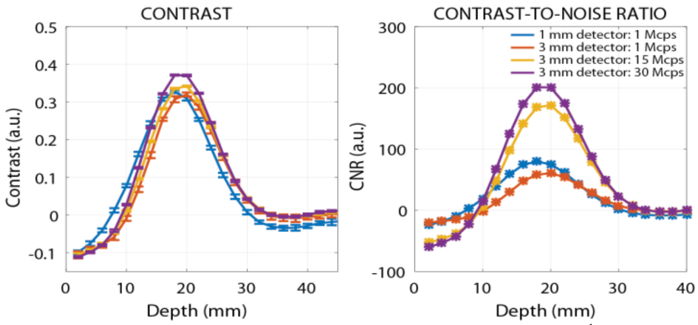


Fig. 1 Contrast (left) and CNR (right) computed for an inclusion featuring a $\Delta\mu_a = 0.17\ cm^{-1}$ using a state of the art detector (1 mm SiPM at 1 Mcps) and the proposed system at both standard (1 Mcps) and high count rates (15 and 30 Mcps).

**Acknowledgements**

This project has received funding from the ATTRACT project funded by EU under grant agreement no 777222 and from the European Union's Horizon 2020 research and innovation program under grant agreement no 675332 (BitMap)

**References**

[1] P. B. Coates, *J. Phys. E.*, vol. 1, no. 8, p. 878, 1968.

[2] H. Wabnitz *et al.*, *J. Biomed. Opt.*, vol. 19, no. 8, p. 86012, 2014.

# A multimodal imaging system hosting an innovative photonic module to improve breast cancer diagnosis: the SOLUS project

**L. Di Sieno[1], A. Dalla Mora[1], E. Ferocino[1], A. Pifferi[1], A. Tosi[2], E. Conca[2], V. Sesta[2], A. Giudice[3], A. Ruggeri[3], S. Tisa[3], A Flocke[4], B. Rosinski[5], J.-M. Dinten[6], M. Perriollat[6], D. Savery[7], H. Sportouche[7] S. Arridge[8], A. Farina[9], P. Panizza[10], E. Venturini[10], P. Gordebeke[11], P. Zolda[11], P. Taroni[1]**

*[1]Politecnico di Milano - Dipartimento di Fisica, Milano (Italy); [2]Politecnico di Milano - Dipartimento di Elettronica, Informazione e Bioingegneria, Milano (Italy); [3]Micro Photon Devices Srl, Bolzano (Italy); [4]iC-Haus, Bodenheim (Germany); [5]Vermon SA, Tours (France); [6]CEA-LETI, Grenoble, France; [7]Supersonic Imagine, S.A., Aix en Provence (France); [8]University College London, Department of Computer Science, London (UK); [9]Consiglio Nazionale delle Ricerche, Istituto di Fotonica e Nanotecnologie, Milano (Italy); [10]Scientific Institute (IRCCS) Ospedale S. Raffaele-Breast Imaging Unit, Milano (Italy); [11]European Institute for Biomedical Imaging Research, Vienna (Austria)*

Breast cancer is the most common cancer in women and early diagnosis is fundamental to maximize survival rate and patient's quality life. For this reason, the availability of cost-effective and non-invasive diagnostics tools with high sensitivity and specificity is a real clinical need. The SOLUS project [1] aims to develop an innovative multimodal tomographic breast imaging system making use of 3 different non-invasive diagnostic techniques to improve the specificity of breast cancer diagnosis. Specifically, the SOLUS system will combine: i) ultrasound imaging (US) to assess the presence of lesions and provide *a-priori* information for the optical tomographic reconstruction; ii) shear wave elastography (SWE) which provides a quantitative measurement of the tissue stiffness; iii) time domain (TD) diffuse optical tomography that, through the measurements of the optical properties of tissue (i.e. absorption and reduced scattering), improves the discrimination of cancerous lesions (often characterized by high blood, water and collagen content, and a relatively low quantity of lipids [2]).

The multimodal tomographic system relies on combining a commercial instrument for US and SWE (Aixplorer by SuperSonic Imagine S.A.) with state-of-the-art TD diffuse optics, so that a single probe can perform imaging in the three modalities. To this extent, a new photonic module is being developed. It exploits the so-called "small source-detector approach" coupled to high-dynamic range (HDR) range fast-gated (FG) acquisition [3] to significantly improve light harvesting and spatial resolution. Each photonic module (see Figure 1) hosts: i) 8 pulsed lasers in the range between 635 and 1064 nm (to sample the different constituents of the breast tissue); ii) a large-area single-photon FG digital SiPM to enable HDR acquisition of the photons that probed deeper within tissue; iii) the acquisition electronics to record the time-of-flight distribution of re-emitted photons. Eight of those photonic modules (divided in 2 groups of 4 modules each) are arranged around the US transducer of the SOLUS probe, thus allowing multiple view acquisition and tomographic reconstruction. The module is also a stand-alone device for multiple wavelength TD diffuse optical imaging/spectroscopy with a wide range of potential applications (from medical imaging, to athlete training monitoring to non-destructive assessment of fruit quality). In the first 18 months of the project, all the main components of the photonic module were conceived, developed and validated in laboratory settings. Currently, the realization and characterization of the single photonic module is ongoing together with the development of the final probe, that aims at providing high multi-modal imaging performance and be ergonomic and easy-to-use for the radiologist. The development and testing of a highly automated software for image processing and optical tomographic reconstruction is in progress, also exploiting the anatomical information obtained by US. Multi-parametric analysis of data provided by the three techniques is being developed. Once the final multimodal system is ready, the clinical validation will start to test the system usability and investigate whether the SOLUS system is capable of providing high specificity and to improve the non-invasive *in-depth* characterization of breast lesions.

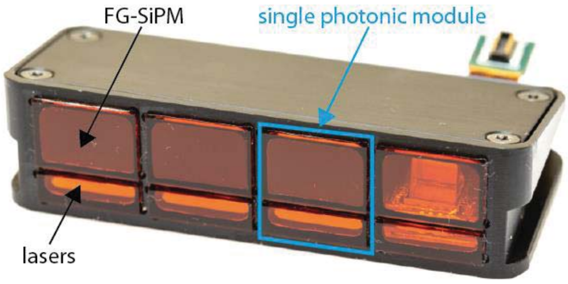


Figure 1. Photo of a set of 4 photonic modules, each one composed of a FG-SiPM (with timing electronics) and 8 lasers.

**Acknowledgment**

This work was supported by the European Union's Horizon 2020 research and innovation programme under G.A. 731877 (SOLUS). SOLUS is an initiative of the Photonics Public Private Partnership.

**Reference**

1. "SOLUS project," http://www.solus-project.eu/.
2. G. Quarto et al, Biomed. Opt. Express **5**, 3684–98 (2014).
3. A. Dalla Mora et al, IEEE Sel. Top. Quantum Electron. **16**, 1023–1030 (2010).

# Time- and frequency-resolved fluorescence with a single TCSPC detector via a Fourier-transform approach

**A. Perri[1,2], J. H. Gaida[3], A. Farina[1], F. Preda[1,2], C. D'Andrea[1], G. Cerullo[1,2], and D. Polli[1,2]**

[1] *IFN-CNR, Dipartimento di Fisica, Politecnico di Milano, Piazza Leonardo da Vinci 32, 20133, Milano, Italy*

[2] *NIREOS S.R.L., Via G. Durando 39, 20158 Milano (Italy)* www.nireos.com

[3] *4th Physical Institute – Solids and Nanostructures, University of Göttingen, Göttingen, Germany*

Fluorescence spectroscopy, by analyzing the different frequencies of the emitted light, along with their relative intensities, can elucidate the structure of the different electronic and vibrational levels of a sample after excitation. In particular, time-resolved emission spectroscopy (TRES), adding the temporal resolution to the spectral information, opens up a completely new paradigm in chemical, biological and medical research as well as materials science. The outcome is a 3-D surface that can be "sliced" to allow the temporal evolution of the fluorescence to be monitored, as well as the resolution of spectrally overlapping species. This can be used to provide information concerning e.g. fluorophore mixtures and solvent relaxation.

Here, we will present an elegant and compact system for mapping a sample's fluorescence as a function of emission wavelength and decay time with both high temporal and spectral resolution [1,2]. The setup is based on a high-throughput common-path interferometer [3] coupled with a single-photon avalanche photodiode and time-correlated single photon-counting unit. It features unprecedented broadband spectral coverage (UV to SWIR), high sensitivity, variable spectral resolution (without affecting throughput), exceptional stability and insensitivity to vibrations, in a compact, lightweight and turn-key system. A measurement example of Rhodamine B in acetone solution is provided in Fig. 1. The recorded two-dimensional fluorescence map as a function of emission time and position x of the interferometer is plotted in Fig. 1(a). Figure 1(b) reports the fluorescence interferogram as a function of x, obtained by integrating the map in (a) along the temporal axis. Computing the Fourier-transform of (a) we obtain the two-dimensional emitted fluorescence map as a function of detection wavelength and emission time. Marginals of (c), obtained by integrating the map along the horizontal and vertical directions, are plotted in Fig. 1(d) and 1(e), respectively, showing the overall fluorescence spectrum and decay dynamics.

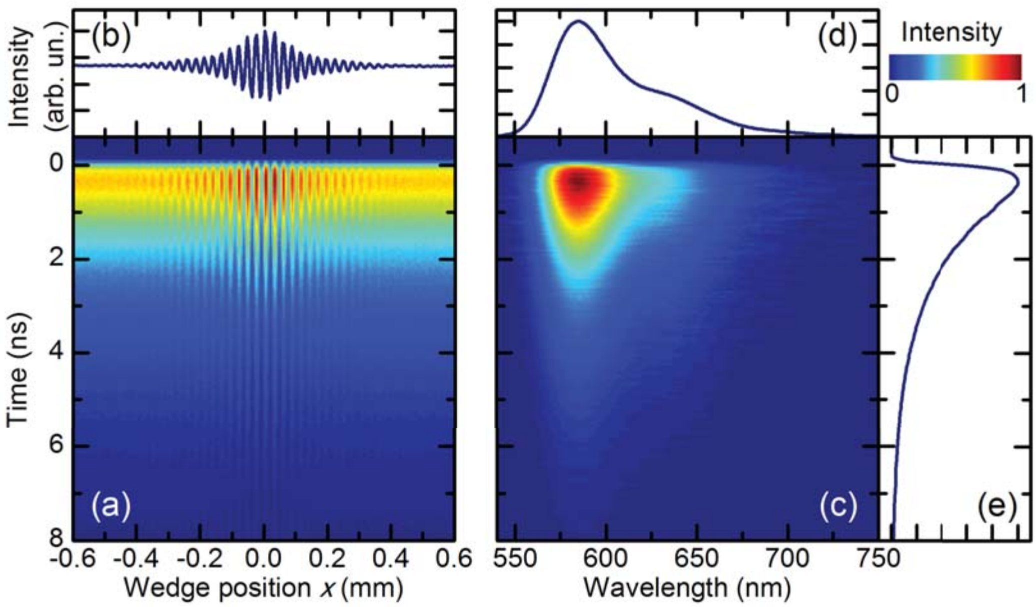


Fig. 1 Time- and wavelength-resolved fluorescence signal of Rhodamine B dye in acetone solution.

**References**

[1] A. Perri *et al.*, "Time- and frequency-resolved fluorescence with a single TCSPC detector via a Fourier-transform approach", Optics Express **26**, pp. 2270-2279 (2018) https://doi.org/10.1364/OE.26.002270

[2] A. Perri *et al.*, "Excitation-emission Fourier-transform spectroscopy based on a birefringent interferometer", Opt. Expr. **25**, A483-A490 (2017) http://dx.doi.org/10.1364/OE.25.00A483

[3] F. Preda *et al.*, "Linear and nonlinear spectroscopy by a common-path birefringent interferometer", IEEE J. Sel. Topics Quantum Electron. **23**, pp. 1-9 (2017) http://dx.doi.org/10.1109/JSTQE.2016.2630840

# An Optical Interference Suppression Scheme for TCSPC Flash LiDAR Imagers

**Lucio Carrara[1], Adrian Fiergolski[1]**

[1]*Fastree3D SA, Chemin de la Dent d'Oche 1, CH-1024 Ecublens, Switzerland*

This paper describes an optical interference suppression scheme that allows flash light detection and ranging (LiDAR) imagers to run safely and reliably in uncontrolled environments where multiple LiDARs are expected to operate concurrently. The issue of optical interference is a potential show-stopper for the adoption of flash LiDAR as a technology of choice in multi-user application fields such as automotive sensing and autonomous vehicle navigation. The relatively large emission angle and field of view of flash LiDAR imagers make them especially vulnerable to optical interference. This work illustrates how a time-correlated single-photon counting LiDAR can control the timing of its laser emission to reduce its statistical correlation to other modulated or pulsed light sources. This method is based on a variable random delay applied to the laser pulse generated by LiDAR and to the internal circuitry measuring the time-of-flight. The statistical properties of the pseudorandom sequence of delays determines the effectiveness of LiDAR resilience against unintentional and intentional optical interference. For basic multi-camera operation, a linear feedback shift register (LFSR) was used as a random delay generator, and the performance of the interference suppression was evaluated as a function of sequence length and integration time. Direct interference from an identical LiDAR emitter pointed at the same object was reduced up to 50 dB. Changing integration time between 10 ms and 100 ms showed a marginal impact on the performance of the suppression (less than 3 dB deviation). LiDAR signal integrity was characterized during suppression, obtaining a maximum relative deviation of the measured time-of-flight of 0.1%, and a maximum deviation of measurements spread (full-width half-maximum) of 3%. The LiDAR signal presented an expected worst-case reduction in intensity of 25%.

**References**

[1] See previous SPW installments.
[2] List of all the topics is available on SPW 2019 website.
[3] LiDARs For Automotive And Industrial Applications 2018; Yole Développement: Lyon, France, May 2018.
[4] Wu, T.; Tsai, C.; Guo, J. LiDAR/camera sensor fusion technology for pedestrian detection. In Proceedings of the APSIPA Annual Summit and Conference, Kuala Lumpur, Malaysia, 12–15 December 2017.
[5] Lindner, P.; Wanielik, G. Multi level fusion for an automotive pre-crash safety system. In Proceedings of the IEEE International Conference on Multisensor Fusion and Integration for Intelligent Systems, Seoul, Korea, 20–22 August 2008.
[6] Kwon, S.K.; Hyun, E.; Lee, J.H.; Lee, J.; Son, S.H. A low-complexity scheme for partially occluded pedestrian detection using LiDAR-radar sensor fusion. In Proceedings of the IEEE 22nd International Conference on Embedded and Real-Time Computing Systems and Applications, Daegu, Korea, 17–19 August 2016.
[7] Kocić, J.; Jovičić, N.; Drndarević, V. Sensors and sensor fusion in autonomous vehicles. In Proceedings of the 26th Telecommunications forum TELFOR, Belgrade, Serbia, 20–21 November 2018.
[8] Kohlbrecher, S.; Von Stryk, O.; Meyer, J.; Klingauf, U. A flexible and scalable SLAM system with full 3D motion estimation. In Proceedings of the IEEE International Symposium on Safety, Security, and Rescue Robotics, Kyoto, Japan, 1–5 November 2011.
[9] Deng, Y.; Shan, Y.; Gong, Z.; Chen, L. Large-Scale Navigation Method for Autonomous Mobile Robot Based on Fusion of GPS and Lidar SLAM. In Proceedings of the Chinese Automation Congress (CAC), Xi'an, China, 30 Novemner–2 December 2018.
[10] Polyakov, V.M.; Vitkin, V.V.; Lychagin, D.I.; Krylov, A.A.; Buchenkov, V.A.; Kashcheev, S.V. Compact Q-switched high repetition rate Nd:YLF laser with 100mJ pulse energy for airborne lidars. In Proceedings of the International Conference on Laser Optics, St. Petersburg, Russia, 30 June–4 July 2014.
[11] Iga, K. Surface-emitting laser—Its birth and generation of new optoelectronics field. IEEE J. Sel. Top. Quantum Electron. 2000, 6, 1201–1215.
[12] Niclass, C.; Rochas, A.; Besse, P.A.; Popovic, R.S.; Charbon, E. CMOS imager based on Single-Photon Avalanche Diodes. In Proceedings of the 13th International Conference on Solid-state Sensors, Actuators and Microsystems, Seoul, Korea, 5–9 June 2005.
[13] Parmesan, L.; Dutton, N.A.; Calder, N.J.; Holmes, A.J.; Grant, L.A.; Henderson, R.K. A 9.8 µm sample and hold time to amplitude converter CMOS SPAD pixel. In Proceedings of the 44th European Solid State Device Research Conference (ESSDERC), Venice, Italy, 22–26 September 2014.

# Whispering-Gallery-Mode optical resonator with embedded NV-color centers

**Sungwan Cho[1], Muhammed Kaan Yildiz[2], In Hwan Do[2], Dong-In Jung[2], Jung Hyun Shim[3], Ki Seok Hong[3], Hee Jin Lim[3], Jae Hoon Lee[3], Hyun Gyu Hong[3], Jung Bae Yoon[4], Dong Hun Lee[4], Hansuek Lee[2]**

[1]*Electronics and Telecommunications Research Institute, Daejeon, Republic of Korea*

[2]*Korea Advanced Institute of Science and Technology, Daejeon, Republic of Korea*

[3]*Korea Research Institute of Standards and Science, Daejeon, Republic of Korea*

[4]*Korea University, Seoul, Republic of Korea*

Development of reliable optical devices with stable photon source is crucial for applications in quantum technology, as well as fundamental experiment and metrology. Due to their high photo-stability, optically active defect centers in solid, especially NV(Nitrogen-vacancy) color center in diamond, are among the promising candidate for photon source. Although coupling of color centers with an high-Q optical cavity has potential in manipulating their photon-emission properties, fabricating optical cavities embedding color centers have been challenging tasks with recent initial demonstrations.

Here, we present a novel approach to fabricate hybrid UHQ (ultra-high-Q) optical WGM (Whispering-Gallery-Mode) resonator comprising NV-color center (Fig.1). Starting from disk resonator[1] coated with nanodiamond particles, we fabricate microtoroid optical resonator with CO2 laser reflow process.[2] Fabricated microtoroid resonator with NV-center has Q-factor above $10^7$ at telecom wavelength, which is close to the value of microtoroid resonators made from silica. A scanning photoluminescence spectrum also confirms stable photoemission of NV-color center inside the microtoroid resonators. With further development of this hybrid UHQ resonator, we expect the realization of robust single photon platform for cavity QED and quantum metrology.

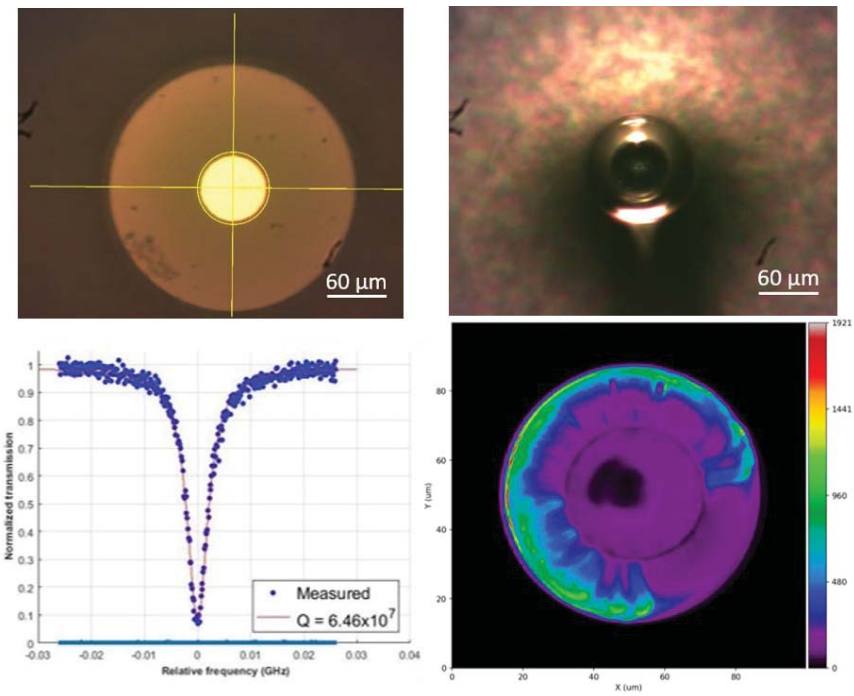


Fig. 1 Wedge-resonator coated with nanodiamond (top left), Microtoroid resonator after CO2 reflow (top right), Measured Q factor (bottom left), Scanned image of PL(Photo-Luminescence) from microtoroid resonator (bottom right).

**References**

[1] Hansuek Lee, et al., Chemically etched ultrahigh-Q wedge-resonator on a silicon chip, Nature Photonics 6, 369-373 (2012).

[2] D. K. Armani, et al., Ultra-High-Q toroid microcavity on a chip, Nature 421, 925-928 (2003).

# Bio-Sensing with NV centers in diamonds

**E. Bernardi[1], E. Moreva[1], P. Traina[1], A. Sosso[1], J. Forneris[3], S. Ditalia Tchernij[2,3], I. P. Degiovanni[1], V. Carabelli[2], P. Olivero[2,3,1], M. Genovese[1]**

[1]*Istituto Nazionale di Ricerca Metrologica, Torino (To), Italy*

[2] *Universita' degli studi di Torino, Dipartimento di Fisica, Via Giuria 1, Torino (To), Italy*

[3] *Istituto Nazionale di Fisica Nucleare, Torino (To), Italy*

Local detection and measurement of environment properties as temperature, magnetic and electric fields is possible using Nitrogen-vacancy centers in diamonds. This leads to applications not only in quantum metrology but also in bio-sensing[1].

This detection capacity is based on the measurement of the frequency shift of the resonance of a single NV center or of an an ensemble of NV centers. The frequency of this resonance is related to the energy difference between the triplet ground states of the NV center. The energy of this states is influenced by environment properties.

The resonance is usually detected monitoring the NV photoluminescence(PL). For single center, PL is detected using single photon avalanche detector (SPAD). Instead photodiodes are commonly used when dealing with large ensemble. Photodiodes are usually used in combination with lock-in techniques in order to increase the signal to noise ratio.

Here we present the most recent results obtained in sensing with NVs by a collaboration among the Italian National Metrology Institutes (INRiM), the University of Turin and the Italian National Institutes of Nuclear Physics (INFN). We will illustrate how applying a magnetic field orthogonal to NV axis causes an enhancement of the resonance contrast and an improvement in temperature sensitivity. We will also investigate the use of single photon avalanche detector in combination with lock-in techniques.

**References**

1. Barry, J. F., M. J. Turner, J. M. Schloss, D. R. Glenn, Y. Song, M. D. Lukin, H. Park, and R. L. Walsworth (2016), Proc. Natl. Acad. Sci. 113 (49), 14133.

# Absorption of a heralded single photon by a nitrogen-vacancy center in diamond

**Maria Gieysztor[1], Marta Misiaszek[1], Joscelyn van der Veen[1,2], and Piotr Kolenderski[1]**

[1]*Faculty of Physics, Astronomy and Informatics, Nicolaus Copernicus University, Torun, Poland*

[2]*Department of Physics and Astronomy, University of Waterloo, Waterloo, Canada*

Nitrogen-vacancy (NV) center emerges as an important system exhibiting promising properties for applications in quantum technologies, including quantum information processing, quantum metrology as well as single photon sources. In our work a simple, room temperature, cavity- and vacuum-free interface for photon-matter interaction is implemented. Here we report an experiment in which a heralded single photon is absorbed by a single atom-like system, which is an NV center in diamond. The NV center emits then another photon, which arrival time is measured. The heralded single photon source is based on spectrally non-degenerate spontaneous parametric down conversion (SPDC) process, where a detection of an infrared photon is used as a herald for the visible photon. The heralded single photon source used in the experiment is tunable in the range of 452-575 nm [1]. The single photon at 532 nm was chosen but other pumping scenarios were tested as well. In Fig. 1 the obtained NV fluorescence decay pumped with heralded single photons is shown.

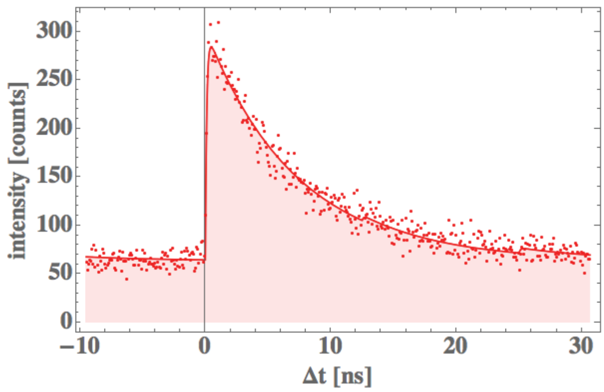


Fig. 1 Fluorescence decay from NV- pumped with 532 nm quantum light. The fluorescence was filtered with 700 nm longpass filter.

## References

[1] A. Divochiy, M. Misiaszek, Y. Vakhtomin, P. Morozov, K. Smirnov, P. Zolotov, and P. Kolenderski, Opt. Lett. 43, 6085 (2018).

# Pseudo-density operator reconstruction: the open time-like curve case


**Enrico Rebufello[1,2], Chiara Marletto[3,4,5], Vlatko Vedral[3,4,5,6], Salvatore Virzì[2,7], Alessio Avella[2], Fabrizio Piacentini[2], Marco Gramegna[2], Ivo Pietro Degiovanni[2], Marco Genovese[2,8]**

[1]*Politecnico di Torino, Corso Duca degli Abruzzi 24, Torino 10129, Italy;*
[2]*Istituto Nazionale di Ricerca Metrologica, Strada delle Cacce 91, Torino 10135, Italy;*
[3]*Claredon Laboratory, University of Oxford, Parks Road, Oxford OX1 3PU, United Kingdom;*
[4]*Fondazione ISI, via Chisola 5, Torino 10126, Italy;*
[5]*Center for Quantum Technologies, National University of Singapore, 3 Science Drive 2, Singapore 117543, Singapore;*
[6]*Department of Physics, National University of Singapore, 2 Science Drive 3, Singapore 117542, Singapore;*
[7]*Università degli Studi di Torino, via Pietro Giuria 1, Torino 10125, Italy;*
[8]*INFN – Sezione di Torino, via Pietro Giuria 1, Torino 10125, Italy*


Quantum Mechanics and general relativity each provide well-verified predictions in their respective domains, even though a theory unifying them is still far. In particular, there are predictions connected to space-time correlations that seem to be in contrast with the standard properties of quantum theory, namely linearity [1]. In order to preserve linearity, a novel approach to the description of the quantum states has been proposed: the pseudo-density operator (PDO) formalism [2], which is an extension of the density operator [3]. PDOs can describe both spatial and temporal correlations of involved particles, whereas the density operator can only describe spatial correlations. In contrast to the density operator, instead, PDO is non-positive definite.

Here we present the first reconstruction [4] (not achievable with standard tomographic techniques) of a PDO describing a two-photon entangled state in presence of an open time-like curve, i.e. a scenario in which one of the photons travels back in time without causally affecting itself. This scenario can be described as a three-photon (Q1, Q2, Q3) state, where Q2 and Q3 represent, respectively, the copies of the same photon entering and appearing from the open time-like curve. Both in distant past and distant future, the photons form a maximally-entangled bipartite state. However, in the chronology-violating region the state is described by a three-photon PDO $R_{123}$, in which Q1 is maximally entangled both with Q3 and Q2, therefore violating the entanglement monogamy [5], which states that if two particles are maximally-entangled, they cannot have any other correlation with a third particle.

We implemented a quantum optical setup able to simulate the open time-like curve scenario, generating a two-photon entangled state in which one photon (A) that can be measured at two different times ($t_1$ and $t_2$), while the other one (B) can only be measured once at time $t_1$.
To perform the $R_{123}$ reconstruction, we exploited different measurement sets to collect the three-point and the two-point correlations on the two photons. The three-point and two-point measurement sets were properly chosen in order to form a minimal set for a full tomographic reconstruction of $R_{123}$.

Uhlmann's fidelities of the reduced density matrices $R_{12}$ ($F_{12} = 0.964$) and $R_{13}$ ($F_{13} = 0.963$) certify that our experimental results are in good agreement with the theoretical predictions.

Furthermore, we quantified the entanglement within the three-photon state under exam, obtaining a 160 standard deviations violation (predicted by the PDO formalism) of the entanglement monogamy bound.
This shows that PDO formalism provides a faithful description of the open time-like curve, while maintaining the linear-operator approach of Quantum Mechanics.

We hope that this innovative technique, which allows to reconstruct the PDO and, at the same, to time verify its predictions, will contribute to the widespread use of this new quantum-mechanical tool.

**References**


[1] D. Deutsch, Quantum mechanics near closed timelike lines, *Phys. Rev. D* **44** (10): 3197–3217 (1991)
[2] J. F. Fitzsimons, J. A. Jones, V. Vedral, Quantum correlations which imply causation. *Sci. Rep.* **5**, 18281 (2015)
[3] J. von Neumann, Wahrscheinlichkeitstheoretischer Aufbau der Quantenmechanik, *Göttinger Nachrichten* ***1*** 245–272 (1927)
[4] C. Marletto, V. Vedral, S. Virzì, E. Rebufello, A. Avella, M. Gramegna, I. P. Degiovanni, M. Genovese, Theoretical description and experimental simulation of quantum entanglement near open time-like curves via pseudo-density operators, *Nat. Commun.* **10**, 182 (2019)
[5] V. Coffman, J. Kundu, W. K. Wootters, Distributed entanglement, *Phys. Rev. A* **61**, 052306 (2000)

# Generalised Photon Subtraction for Heating or Cooling Thermal Light

**Gioan Tatsi, Luca Mazzarella and John Jeffers**

*Department of Physics, University of Strathclyde, John Anderson Building, 107 Rottenrow, Glasgow G4 0NG, U.K.*

Photon subtraction[1] is a process by which photons are removed from a mode of the electromagnetic field. It has been shown that this non-unitary operation, realisable probabilistically using a beam splitter, a vacuum auxiliary state and a photodetector, can lead to counterintuitive results such as preservation of the mean photon number of coherent states and increase of the mean photon number of thermal states[2,3]. It is used in many applications ranging from amplification of the amplitude of quantum states[4] to generation of Schrödinger cat states[1].

Thermal states have played an important role in experiments such as that of Hanbury-Brown and Twiss[5]. The application of photon subtraction to thermal states has shown phenomena such as the "quantum vampire" effect[6] and the possibility to realise an all photonic Maxwell demon[7].

In this work we investigate the effect on thermal states of a process that we dub displaced photon subtraction, in which we displace a thermal state and then perform a photon subtraction whose auxiliary state is an anti-displacing coherent state. We show that displaced photon subtraction can lead to a "cooling" effect on input thermal states and that this can be harnessed to realise a linear optical photonic Maxwell demon.

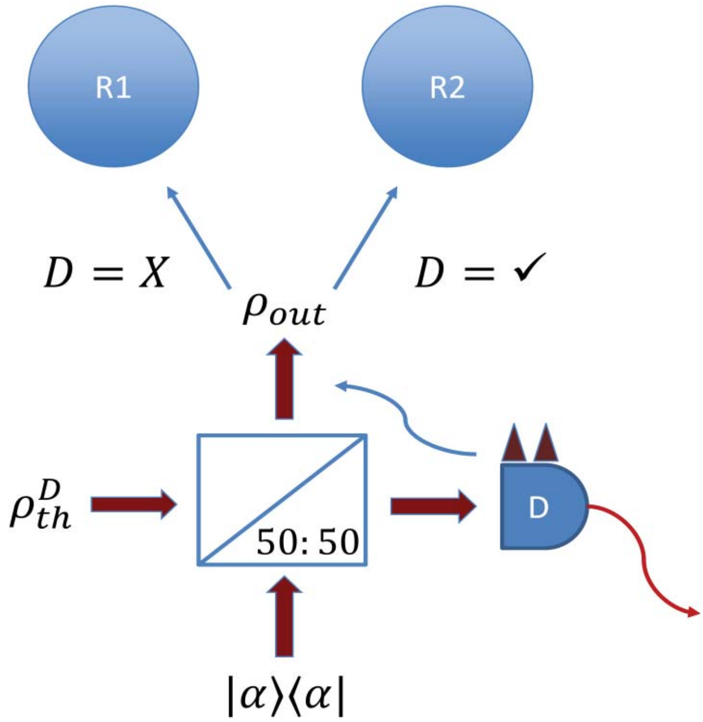


Fig. 1 "A realisation of a Photonic Maxwell Demon based on displaced photon subtraction and the result of photodetection ."

**References**

[1] A. Ourjoumtsev *et. al*,Science **312**,83(2006)
[2] A. Zavatta *et. al*,New J. Phys. **10**,123006(2008)
[3] Y.I. Bogdanov *et.al*,Phys. Rev. A **96**,063803(2017)
[4] P. Marek, R. Filip,Phys. Rev. A **81**,022302(2010)
[5] R. Hanbury-Brown,R. Q. Twiss, Nature **177**, 27(1956)
[6] I.A. Fedorov *et.al*,Optica **2**,112-115 (2015)
[7] M.D. Vidrighin *et.al*,Phys.Rev.Lett. **116**,050401(2016)

# Parity Swap Cat-State Comparison Amplifier

**Gioan Tatsi, Luca Mazzarella and John Jeffers**

*Department of Physics, University of Strathclyde, John Anderson Building, 107 Rottenrow, Glasgow G4 0NG, U.K.*

Optical Schrödinger cat states, are superpositions of coherent states and have been widely studied for the significant role they could play in quantum information, computation and in fundamental tests as resource states. For such applications cat states with high coherent amplitude ($\alpha \geq 1.2$) and high fidelity are desirable, but difficult to produce. This gives rise to the need for amplification.

Most suggestions rely on cat state *breeding*; a process whereby small amplitude *kittens* are mixed coherently at a beam splitter and a postselection measurement projects one of the two outputs in an amplified state based on the constructive interference of the two input modes. Such a process relies upon non-Gaussian (experimentally expensive) resource cat states that must be bred to generate the larger output cat state.

Here we introduce an amplifier for optical Schrödinger cat states that is based on the state comparison amplifier [1-3] and relies only on Gaussian resources, beamsplitters and on/off detectors. It offers reasonable gain at high fidelity for the range of input cat sizes of interest, and produces cat states of the required output amplitude range.

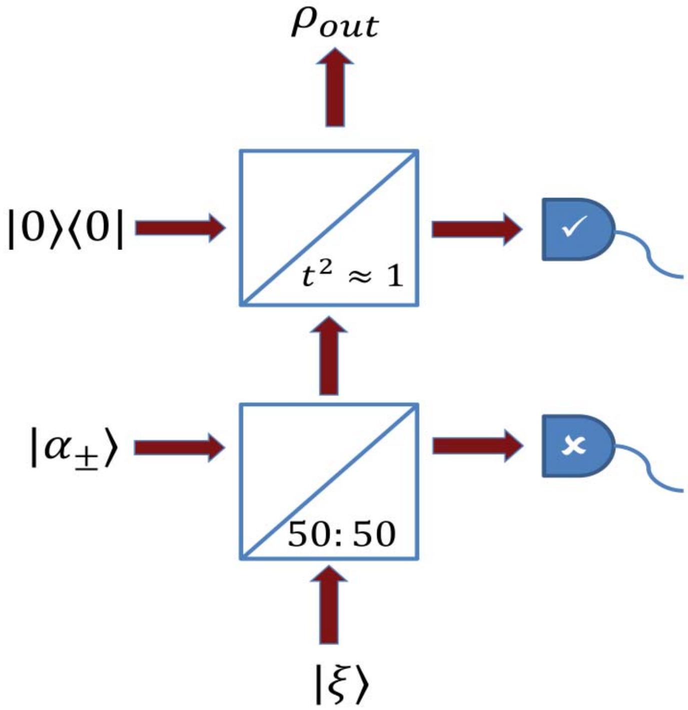


Fig. 1 "Amplification scheme for Schrödinger cat states based on the state comparison amplifier and a squeezed vacuum resource state ."

**References**

[1] E. Eleftheriadou et al., Physical review letters 111, 213601 (2013).
[2] RJ Donaldson et al., Physical review letters 114, 120505 (2015).
[3] RJ Donaldson et al., Communications Physics 1, 54 (2018).

# Optimal estimation of entanglement and discord in two-qubit states


**S. Virzì[1,2], E. Rebufello[2,3], A. Avella[2], F. Piacentini[2], M. Gramegna[2],**
**I. Ruo Berchera[2], I.P. Degiovanni[2], M. Genovese[2,4]**

[1] *Università degli Studi di Torino, Dipartimento di Fisica, Via Giuria 1, 10125, Torino, Italy*
[2] *INRIM, Strada delle Cacce 91, 10135, Torino, Italy*
[3] *Politecnico di Torino, Corso Duca degli Abruzzi 24, I-10129, Torino, Italy*
[4] *INFN, Via P. Giuria 1, I-10125 Torino, Italy*


Recently, the fast development of quantum technologies led to the need for tools allowing the characterization of quantum resources. In particular, the ability to estimate non-classical aspects, e.g. entanglement and quantum discord, in two-qubit systems, is relevant to optimize the performance of quantum information processes. Among the most relevant and exploited quantum resources, a crucial role is played by entanglement and discord, whose estimation is of the utmost relevance for present and upcoming quantum technologies. Usually, it is necessary to know the density operator in order to extrapolate the amount of quantum correlation in a quantum state. The experimental reconstruction of a density operator is allowed by the quantum state tomography[1] technique. However, quantum state tomography is a demanding procedure in terms of quantum resources due the high number of measurements required on identical copies of the system[2]. Moreover, reconstructions are based on optimization algorithms applied to likelihood functions, therefore, a tomography does not allow to perform an easy estimation of the uncertainty associated to the reconstructed density matrix.

In my talk, I'm going to present an experiment in which the amount of entanglement and discord of two-photon states are estimated by exploiting different parameters[3]. A quantitative measure of entanglement corresponds to a non-linear function of the density operator, and it is not possible to identify a quantum observable directly associated to it. For estimating the amount of entanglement we consider negativity[4], concurrence[5] and log-negativity[4]. Quantum discord, instead, is a figure of merit that can be used to quantify non-classicality of correlations within a physical system. Separability of the density matrix describing a multi-partite state does not guarantee vanishing of the discord, demonstrating that absence of entanglement does not imply classicality. Quantum discord has been proposed as the key resource needed for certain quantum communication tasks and quantum computational models not entirely relying on entanglement. Due to the high interest on quantum discord, both for foundational aspects of quantum mechanics and for applications, techniques allowing to estimate this quantity are demanded. Unfortunately, in general, quantum discord doesn't present an analytical expression. Therefore, we take in account a geometrical approximation for our estimation task: the quantum geometric discord[6]. In this work are introduced estimators for each parameter. Among them, some will prove to be optimal, i.e., able to reach the ultimate precision bound allowed by quantum Cramér-Rao bound[7]. These estimation techniques have been tested with a specific family of states ranging from nearly pure Bell states to completely mixed states. By evaluating the statistical uncertainties as the standard deviations on repeated measurements, we achieve a good agreement between the theoretical predictions and the experimental results. In particular, we demonstrate that optimal estimators reach the ultimate theoretical precision limit represented by the quantum Cramér-Rao bound. The agreement between uncertainty bars and theoretical uncertainty curves, also for what concerns non-optimal estimators, represents a further check on the consistency between our experimental data and the theory. These results pave the way to the diffuse use of these estimators in quantifying resources for quantum technologies.

**References**


[1] M.G.A. Paris, J. Rehacek, *J. Lecture Notes Physics*, vol. **649** (Springer, Berlin, 2004).
[2] G.M. D'Ariano, C. Macchiavello, M.G.A. Paris, *Phys. Lett. A* **195**, 31 (1994).
[3] S.Virzì, E. Rebufello, A. Avella, F. Piacentini, M. Gramegna, I. Ruo Berchera, I.P. Degiovanni, M. Genovese, *Scientific Reports* **9**, 3030 (2019).
[4] G. Vidal, R.F. Werner, *Phys. Rev. A* **65**, 032314 (2002).
[5] S. Hill, W.K. Wootters, *Phys. Rev. Lett.* **78**, 5022 (1997).
[6] B. Darkic, V. Vedral, C. Brukner, *Phys. Rev. Lett.* **105**, 190502 (2010).
[7] M.G.A. Paris, *Int. J. Quant. Inf.* **7**, 125 (2009).

# The EURAMET European Metrology Network for Quantum Technologies

**I. Degiovanni[1], M. Gramegna[1*], S. Bize[2], H. Scherer[3], C. Chunnilall[4], S. Kück[3], F. Pereira Dos Santos[2], T. Lindstrom[4], F. Schopfer[5], M. Lassen[6]**

[1] *INRIM, Strada delle Cacce 91, 10135 Torino, Italy*
[2] *LNE-SYRTE, Observatoire de Paris, Université PSL, CNRS, Sorbonne Université, 61 avenue de l'Observatoire, 75014 Paris, France*
[3] *PTB, Bundesallee 100, 38116 Braunschweig, Germany*
[4] *NPL, Hampton Road, Teddington TW11 0LW, United Kingdom*
[5] *LNE, 1 rue Gaston Boissier 75724 Paris Cedex 15, France*
[6] *DFM A/S, Kogle Allé 5, DK-2970 Hørsholm, Denmark*

*EMN-Q email contact: quantum@euramet.org

EURAMET is the European association of national metrology institutes (NMIs) and the regional metrology organisation (RMO) of Europe. EURAMET recently created European Metrology Networks (EMNs) [1]. They will analyse the European and global metrology needs and address these needs in a co-ordinated manner. EMN members will formulate common metrology strategies addressing aspects such as research, infrastructure, knowledge transfer and services.

Quantum technologies were selected as one of the relevant areas, leading to the creating of a European Metrology Network on Quantum Technologies (EMN-Q) [2]. EMN-Q is divided in three sections: quantum clocks & atomic sensors, quantum electronics, and quantum photonics.

We will present the EMN-Q and its background, scope and goals. Anticipated future activities comprise surveying capabilities of European NMIs, contacting industrial and academic stakeholders and collecting their needs, engaging with Quantum Flagship project co-ordinators, developing a strategic agenda to address these needs, anticipating the need for standards and standardisation. This will serve as a starting point for EMN-Q members to collect suggestions, advice and requirements from SPW2019 participants.

Forthcoming events organised by EMN-Q will be advertised. For example, immediately after the end of IQuMS 2019 [3], the "International conference on quantum Metrology and Sensing", a meeting devoted to collecting stakeholder needs will take place on Friday December 13th afternoon at SYRTE - Observatoire de Paris.

Industry, governmental agencies, academic sectors or any other type of potential stakeholder are welcome to contact the EMN-Q and to express their metrology needs. These can relate not only to quantum characteristics of quantum devices, but also metrology of key enabling technologies, metrology that can improve the supply chain of industrial quantum devices or other industrial needs connected quantum technologies.

Another initiative of EMN-Q is to edit a special issue on Quantum Metrology & Quantum Enhanced Measurement of the European Physical Journal on Quantum Technology [4]. Participants are welcome to submit articles for peer-reviewed publication in this special issue.

**References**

1. https://www.euramet.org/european-metrology-networks/
2. https://www.euramet.org/european-metrology-networks/quantum-technologies/
3. https://iqums.sciencesconf.org/
4. https://www.springeropen.com/collections/qmqem

# Using photon statistics to characterize two-photon absorption

**Michael D. Mazurek[1,2], Alexander Mikhaylov[2], Kristen M. Parzuchowski[2], Daniel J. Lum[3], L. K. Shalm[1], Christian Drago[4], J. E. Sipe[4], Sae Woo Nam[1], Marcus T. Cicerone[3], Charles H. Camp Jr.[3], Ralph Jimenez[2], T. Gerrits[1], Martin J. Stevens[1]**

*[1]National Institute of Standards and Technology, Boulder, CO, USA, [2]JILA, University of Colorado, Boulder, CO, USA, [3]National Institute of Standards and Technology, Gaithersburg, MD, USA, [4]Department of Physics, University of Toronto, Ontario, Canada*

Two-photon excitation microscopy is the most widely used technique for optically imaging deep within biological tissues. Because two-photon absorption (TPA) in fluorescent molecules is such a weak effect—scaling quadratically with input photon flux—the technique requires high-power lasers that can damage or disrupt biological function. It has been reported [1,2] that if fluorescent molecules are excited with correlated photon pairs produced via spontaneous parametric downconversion (SPDC), the resulting absorption signal will scale *linearly* with input flux, allowing for excitation with far lower power. However, it can be difficult to confirm whether a change in transmission through such a system was caused by TPA, or by single-photon loss due to scattering, absorption, or misalignment: all these processes scale linearly with flux. Here, we propose a way to distinguish between TPA and single-photon loss by measuring changes in the photon statistics of a beam transmitted through a two-photon-absorbing medium.

The second-order correlation function, $g^{(2)}$, contains information about photon statistics and can be readily measured with a Hanbury Brown-Twiss interferometer (Fig. 1a). Any single-photon loss process (such as scattering) *does not* affect a state's $g^{(2)}$, but a two-photon loss process (such as TPA) *does*. It should be possible to distinguish between these two effects by measuring how $g^{(2)}$ is affected by interaction with a medium.

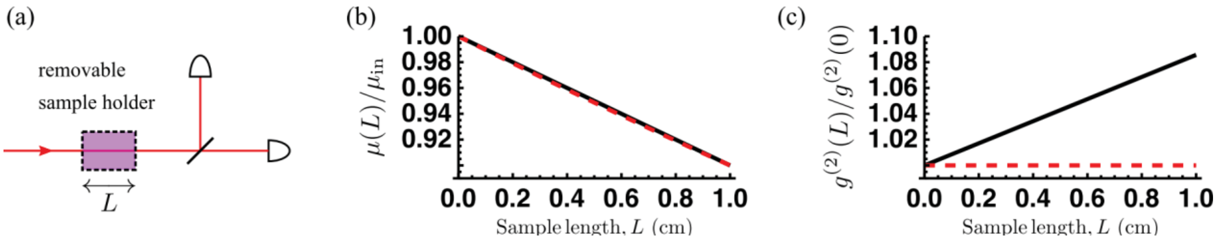


Fig. 1 (a) Hanbury Brown-Twiss interferometer for $g^{(2)}$ measurement. Theoretical dependence of (b) flux and (c) $g^{(2)}$ of single-mode squeezed vacuum on sample length for two-photon absorbing sample (solid black lines) and sample with only single-photon loss (dashed red lines). Parameters were chosen so 10% of the input light is lost after traveling through a 1 cm length of each sample.

Following a procedure outlined in [3], we can compute the effect of TPA on $g^{(2)}$ for a single-mode squeezed vacuum state, as generated via SPDC. After interaction with a two-photon absorber with length $L$, the resulting mean photon number is

$$\mu(L) \approx \mu_{\text{in}} - \kappa L(2\mu_{\text{in}} + 6\mu_{\text{in}}^2),$$

where $\mu_{\text{in}}$ is the initial mean photon number and $\kappa$ describes the strength of the TPA interaction. For small values of $\mu_{\text{in}}$, the linear term will dominate absorption. In samples with only single-photon loss mechanisms, the amount of light transmitted by the sample also scales linearly with $\mu_{\text{in}}$. If only the flux transmitted by the sample is measured, it is not possible to differentiate single-photon loss from TPA (see Fig. 1(b)).

In contrast, after passage through a two-photon-absorbing medium,

$$g^{(2)}(L) \approx 3 + \frac{1}{\mu_{\text{in}}} + \kappa L\left(\frac{2}{\mu_{\text{in}}} - 18 - 24\mu_{\text{in}}\right).$$

For an SPDC source with a small mean photon number, $g^{(2)}(L)$ scales roughly linearly with the strength of the interaction, $\kappa L$ (see Fig. 1(c)), and in this limit we expect $g^{(2)}$ to increase under TPA. For a bright squeezed vacuum ($\mu_{\text{in}} >> 1$), $g^{(2)}$ should *decrease* with TPA. In contrast, samples with only single-photon loss do not affect $g^{(2)}$. Thus, when the input beam is a squeezed vacuum, a change in $g^{(2)}$ is the definitive signature that distinguishes TPA from single-photon loss. The resulting change can then be related to the strength of the two-photon interaction.

**References**

[1] L. Upton *et al.*, J. Phys. Chem. Lett. **4**, 2046 (2013).
[2] J.P. Villabona-Monsalve *et al.*, J. Phys. Chem. A **121**, 7869 (2017).
[3] L. Gilles and P.L. Knight, Phys. Rev. A **48**, 1582 (1993).

# Searching for Enhanced Two Photon Absorption of Entangled Photon Pairs


**Kristen M. Parzuchowski[1,2], Alexander Mikhaylov[1], Michael D. Mazurek[2,3], Daniel J. Lum[4], Martin J. Stevens[3], Thomas Gerrits[3], Charles H. Camp Jr.[4], Ralph Jimenez[1,3,5]**

*[1]JILA, University of Colorado, Boulder, CO, USA, [2]Department of Physics, University of Colorado, Boulder, CO, USA, [3]National Institute of Standards and Technology, Boulder, CO, USA, [4]National Institute of Standards and Technology, Gaithersburg, MD, USA, [5]Department of Chemistry, University of Colorado, Boulder, CO, USA*


Two-photon absorption (TPA) of classical laser light is an inherently weak process due in part to its quadratic photon flux dependence. If the TPA excitation source is replaced with an entangled photon pair source, the entangled two-photon absorption (eTPA) signal should scale linearly with photon flux [1]. Some experimental groups [2,3] have set out to measure eTPA and found orders-of-magnitude signal enhancement. The inferred absorption rates were obtained by comparing the rate of transmission of entangled photon pairs through a cuvette before and after a two-photon absorbing sample is added. A major difficulty with these types of experiments lies in distinguishing TPA from linear, single-photon loss mechanisms (such as scattering) caused by placing the sample in the beam path.

We built an apparatus to characterize eTPA through transmittance measurements. Initially we implemented a transmittance measurement technique similar to that of previous groups to measure the eTPA cross section of Zinc tetraphenylporphyrin (ZnTPP) at 810 nm (Fig.1). We assign an eTPA cross section of $10^{-17}$cm$^2$, in agreement with published literature [2,3]. However, further characterization of our setup showed that linear loss was increased by adding the sample, and that there was no clear eTPA signal.

We have developed two methods to help distinguish eTPA from linear losses: second order correlation function, $g^{(2)}(0)$, and time delay transmittance measurements. The value of $g^{(2)}(0)$ is insensitive to linear losses, such as beam misalignment or scattering, but *is* sensitive to nonlinear loss caused by eTPA. First, we measure the $g^{(2)}(0)$ of our light as its transmitted through the solvent toluene. Next, we repeat the measurement through ZnTPP dissolved in toluene. A change in $g^{(2)}(0)$ between the two measurements is indicative of eTPA. An additional tool in our apparatus is an interferometer to control the time delay between photons in a pair, and to measure this delay with Hong-Ou-Mandel interference. Controlling the time delay lets us vary the amount of eTPA that can occur.

We find that our $g^{(2)}(0)$ and time delay transmittance measurements place an upper limit on the eTPA cross section of ZnTPP at 810nm. Our work improves on the sensitivity of previous techniques and demonstrates the importance of distinguishing eTPA from linear losses. We will discuss how to further improve the sensitivity of eTPA transmittance measurements and present our progress on measuring entangled two-photon excited fluorescence.

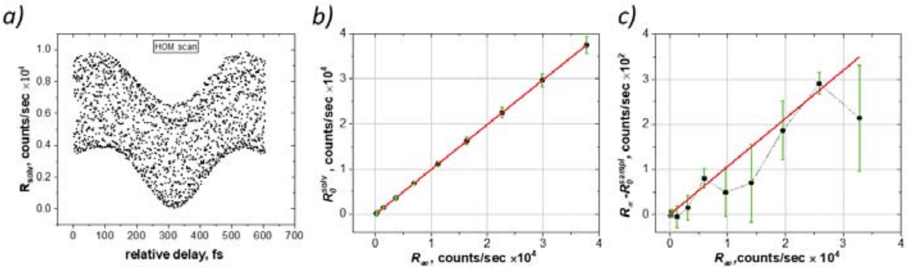


Fig.1 Results of transmittance measurements. a. Hong-Ou-Mandel interference scan b. $R_0^{solv}$ vs. $R_\infty$ c. $R_\infty$ - $R_0^{sampl}$ vs. $R_\infty$ (Rate of coincidences through sample and solvent at zero and long time delay = $R_0^{sampl}$, $R_\infty$. Rate of coincidences through solvent at zero time delay and as a function of time delay = $R_0^{solv}$, $R_{solv}$)

## References


[1] J. Javanainen and P. L. Gould, Phys. Rev. A 41, 5088 (1990).
[2] L. Upton *et al.*, J. Phys. Chem. Lett. 4, 2046 (2013).
[3] J.P. Villabona-Monsalve *et al.*, J. Phys. Chem. A 121, 7869 (2017).

# Characterization of solid-state single-photon sources for metrological applications

**Philip R Dolan[1], Alex Browning[1], Cristina E Giusca[1], Christopher J Chunnilall[1], Sarah Fischbach[2], Stephan Reitzenstein[2], Alastair G Sinclair[1]**

[1]*The National Physical Laboratory (NPL), Hampton Road, Teddington, TW11 0LW, U.K.*

[2]*Institut für Festkörperphysik, Technische Universität Berlin, Hardenbergstraße 36, D-10623 Berlin, Germany*

Solid-state single-photon sources (SPSs) are based on quantized emission from an isolated electronic system. They are of interest as they have the capacity to deterministically emit single photons with high purity. This contrasts with attenuated lasers and spontaneous parametric down conversion, which are restricted to emitting coherent states or cannot produce photons on demand. In recent years single-photon emission has been identified in a plethora of new host materials[1–4]. To establish the relevance of these new emitters for sensing and metrological applications, and their potential for development into commercially viable technology, it is important to accurately characterize their properties. In this paper we compare three types of emitters: the negatively charged nitrogen vacancy center in nanodiamond (NV)[5] and InGaAs/GaAs quantum dots (QDs)[6], which have been widely studied over the last two decades, and the recently identified emitters in the two-dimensional hexagonal allotrope of boron nitride (hBN). Emission spectra from all three sources are plotted in figure 1.

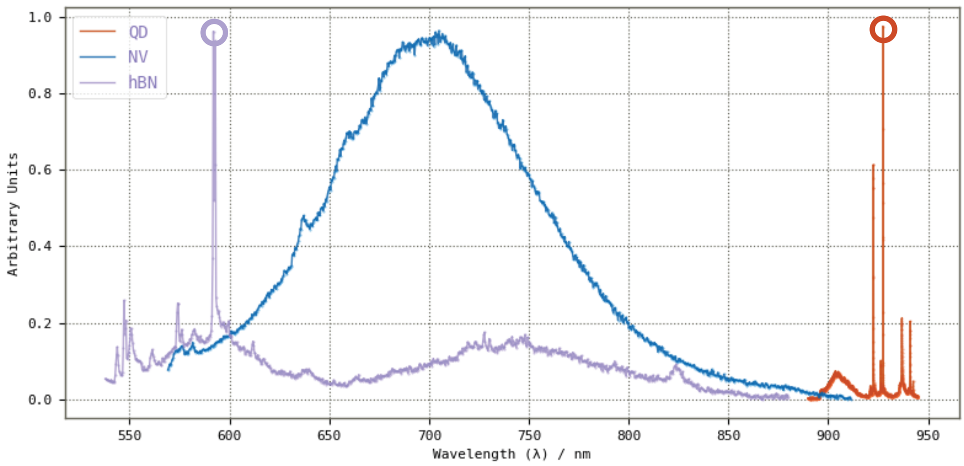


Fig. 1 Normalised emission spectra of QDs taken at 10 K, NVs taken at 293 K and hBN taken at 83 K. Peaks giving single-photon emission for the QDs and hBN have been marked with circles.

In addition to spectral and brightness considerations the singularity, or purity, of the single photons emitted is also a crucial figure of merit for a single-photon source. To determine the purity for the single-photon sources shown above, continuous wave Hanbury Brown Twiss interferometry is used, and results for several emitters will be presented. The range of sources investigated highlights several applications. QDs have shown some of the highest collection efficiencies and are one of the closest to achieving 'true' single-photon emission. The NV's single-photon emission is coupled to a ground state spin, and therefore has potential in various sensing schemes. hBN exhibits bright, spectrally narrow room temperature emission which may facilitate development of lower cost, commercially relevant devices. Extensions to this work and the role of traceable single photon measurements will also be discussed.

The work reported in this paper is funded by the project EMPIR 17FUN06 SIQUST. This project received funding from the EMPIR programme co-financed by the Participating States and from the European Union Horizon 2020 research and innovation programme.

1. Tran, T. T., Bray, K., Ford, M. J., Toth, M. & Aharonovich, I. Quantum Emission From Hexagonal Boron Nitride Monolayers. *Nat. Nanotechnol.* **11**, 1–12 (2015).
2. Castelletto, S. *et al.* A silicon carbide room-temperature single-photon source. *Nat. Mater.* **13**, 151–156 (2014).
3. Ma, X., Hartmann, N. F., Baldwin, J. K. S., Doorn, S. K. & Htoon, H. Room-temperature single-photon generation from solitary dopants of carbon nanotubes. *Nat. Nanotechnol.* **10**, 671–675 (2015).
4. He, Y. M. *et al.* Single quantum emitters in monolayer semiconductors. *Nat. Nanotechnol.* **10**, 497–502 (2015).
5. Dolan, P. R. *et al.* Robust, tunable, and high purity triggered single photon source at room temperature using a nitrogen-vacancy defect in diamond in an open microcavity. *Opt. Express* **26**, 7056 (2018).
6. Fischbach, S. *et al.* Efficient single-photon source based on a deterministically fabricated single quantum dot - Microstructure with backside gold mirror. *Appl. Phys. Lett.* **111**, (2017).

# Metrological characterization of single-photon sources for radiometric application

**Beatrice Rodiek[1], Andreas W Schell[1,2], Justus Christinck[1], Hristina Georgieva[1], Helmuth Hofer[1], Marco A López[1], Stefan Kück[1]**

[1]*Physikalisch Technische Bundesanstalt (PTB), Braunschweig, Germany*

[2]*Institut für Festkörperphysik, Leibniz Universität Hannover, Hannover, Germany*

Single-photon sources become more and more important in several fields e.g. in quantum key distribution, quantum computing, and quantum-enhanced optical measurements [1] and furthermore in metrology and radiometry. An ideal single-photon source can be used for the efficiency calibration of single-photon detectors as a new single-photon standard in radiometry [2]. Such source is also needed to close the gap between classical and quantum radiometry, which is necessary for the comparison of single-photon detectors and analogue detectors [3].

In order to achieve that goal, we already characterized a single-photon source based on a nitrogen-vacancy (NV-) center in nanodiamond by an unbroken traceability chain back to the primary standards in terms of its absolute spectral photon flux per wavelength and absolute spectral radiant flux per wavelength at room temperature [4] including the measurement uncertainty budget [5]. However, the NV-center is not a perfect emitter (e.g. broad spectral bandwidth) with respect to the application in radiometry, which leads to the next step of characterizing other emitters, for instance Hexagonal Boron Nitride (hBN).

Quantum emitters in hBN were recently discovered and possess properties making them potential candidates as a source of single photons in metrology: they are bright and photostable emitter that can be used at room-temperature [6]. Nevertheless, the properties of these emitters, such as quantum efficiency and energy level scheme [7] are not fully understood yet, making it important to benchmark these emitters in a comparison with the long time known and well researched NV-center in diamond.

At the conference, we will present the current results of the emitter comparison.

**Acknowledgement:**

The work reported on this paper was funded by project EMPIR 17FUN06 SIQUST. This project received funding from the EMPIR program co-financed by the Participating States and from the European Union Horizon 2020 research and innovation program.

**References**

[1] M. D. Eisaman, J. Fan, A. Migdall, and S. V. Polyakov, “Single-photon sources and detectors,” *Rev. Sci. Instrum. 82*, 071101 (2011).

[2] W. Schmunk, M Gramegna, G. Brida, I. P. Degiovanni, M. Genovese, H. Hofer, S. Kück, L. Lolli, M. G. A. Paris, S. Peters, M. Rajteri, A. M. Racu, A. Ruschhaupt, E. Taralli and P. Traina, “Photon number statistics of NV centre emission”, *Metrologia 49*, 156-160 (2012).

[3] J. Y. Cheung, C. J. Chunnilall, G. Porrovecchio, M. Šmid, E. Theocharous, “Low optical power reference detector implemented in the validation of two independent techniques for calibrating photon-counting detectors”, *Optics Express 19*, 20347 (2011).

[4] B. Rodiek et al., Experimental realization of an absolute single-photon source based on a single nitrogen vacancy center in a nanodiamond, *Optica 4* (1), 71-76 (2017).

[5] B. Rodiek et al., The absolutely characterized nitrogen vacancy center - based single-photon source - measurement uncertainty of photon flux and angular emission properties, *Journal of Physics: Conf. Series 972*, 012008 (2018).

[6] T. T. Tran, et al. "Quantum emission from hexagonal boron nitride monolayers." *Nature nanotechnology* 11 (1), 37 (2016).

[7] A. W. Schell, M. Svedendahl, and R. Quidant, Quantum emitters in hexagonal boron nitride have spectrally tunable quantum efficiency. *Advanced Materials*, *30*(14), 1704237, (2018).

# Sub-Doppler single photon spectroscopy of rubidium

**Kyle D. Major[1], Paul Burdekin[1], Rielly Newbold[1], Samuele Grandi[1,2], E. A. Hinds[1], and Alex S. Clark[1]**

[1]*Centre for Cold Matter, Imperial College London, UK*
[2]*ICFO, Casteldefels, Barcelona, Spain*

The ability to interface photons from the solid state with long-lived atomic quantum memories will enable a vast array of quantum technologies to become viable, including quantum computation protocols and advanced quantum simulators. Single dibenzoterrylene (DBT) molecules embedded in crystals of anthracene show emission from 780 nm to 795 nm, and exhibit lifetime-limited linewidths of ~40 MHz when cooled to cryogenic temperature [1], meaning they are compatible with the D1 and D2 transitions in rubidium [2].

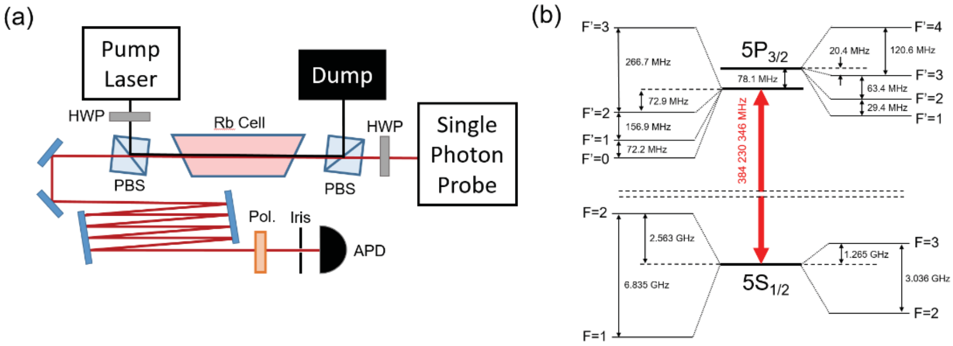


Figure 1: (a) Pump-probe sub-Doppler spectroscopy setup. (b) Energy level structure of $^{87}$Rb (left) and $^{85}$Rb (right).

To show the feasibility of measuring sub-Doppler features using a single-photon source, we have built a pump-probe spectroscopy setup, shown in Fig. 1(a). The pump is an intense laser propagating left to right through a rubidium cell, while the probe laser is attenuated to the single photon level (~0.1 photons per detector gate) propagating from right to left through the cell. Both can be frequency tuned independently across the D2 absorption spectrum of rubidium, whose level structure is shown in Fig. 1(b). To isolate the probe from the pump they are orthogonally polarized, and to remove spontaneous emission from the probe detector we allow the probe to propagate over 1 m from the cell before collection to optical fibre.

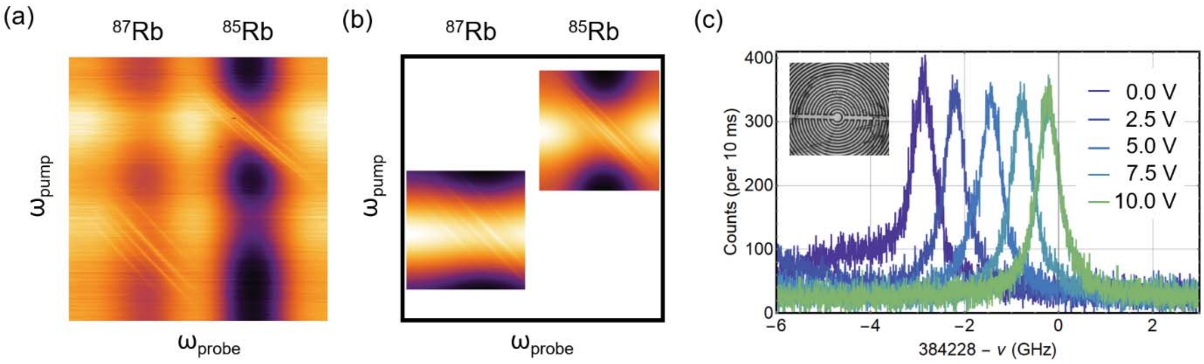


Figure 2: (a) Experimental spectrum of rubidium. (b) Calculated theoretical spectrum. (c) Resonant laser scans of the zero-phonon line of a single DBT molecule in an anthracene crystal, taken for varying bias voltages on local circular interdigitated electrodes.

The experimental spectrum is shown in Fig. 2(a). The sub-Doppler features appear as anti-diagonal stripes in the spectrum, as the Doppler shift is cancelled for many red-blue detuned frequency combinations. The spectrum agrees with our theoretical prediction, shown in Fig. 2(b), calculated using rate equations for all the hyperfine levels and setting the power and optical depth. We are now working to replace the probe laser with a Stark-tunable DBT molecule [3]. In Fig. 2(c) we show the Stark tuning of a single DBT molecule across Rb transitions by varying the static electric field using circular interdigitated electrodes. Using this we will show that DBT emission can be interfaced with rubidium, with a future aim to construct a quantum memory in Rb to store such photons.

**References**

[1] S. Grandi et al., Phys. Rev. A **94**, 063839 (2016).
[2] P. Siyushev et al., Nature **509**, 66-70 (2014).
[3] K. G. Schädler et al., Nano Lett. **19**, 3789–3795 (2019).

# Predictable Quantum Efficient Detector based on n-type silicon induced junction photodiodes as a primary standard for low photon flux

**T. Dönsberg[1], S. Porrasmaa[2], F. Manoocheri[2], E. Ikonen[1,2]**
[1]*National Metrology Institute VTT MIKES, VTT Technical Research Centre of Finland Ltd, Espoo, Finland*
[2]*Metrology Research Institute, Aalto University, Espoo, Finland*

The Predictable Quantum Efficient Detector (PQED) [1-2] is a semiconductor based primary standard of optical power that can be operated at room temperature [3]. It consists of two induced-junction photodiodes, where a $SiO_2$ layer is thermally grown on top of very lightly doped p-type silicon substrate. This structure inherently contains trapped positive surface charge close to the Si-$SiO_2$ boundary, which generates an n-type inversion layer in the p-type silicon and produces a depletion region required for photocurrent generation [1]. The photodiodes area mounted in a wedged trap configuration for the control of specular reflectance losses. Using one-dimensional modelling, the near-zero internal quantum deficiency (IQD) of the custom photodiodes has been predicted with an estimated standard uncertainty of 70 ppm in the visible wavelength range [4]. The modelled results have been experimentally confirmed with measurements against cryogenic radiometers [2].
The semiconductor based primary standard has the benefit of high dynamic range. Even at room temperature, it allows for linear radiant power measurements over seven orders of magnitude. Thus, it can be used directly in various low flux applications [5-6], which greatly simplifies the traceability chain.
Recently, a new type of PQED photodiodes were introduced [7] that utilize induced junction, which is manufactured using n-type silicon substrate. The underlying structure of the new photodiode, shown in Fig. 1(a), is similar to the previous design, but the n-type substrate requires negative charge to be trapped in the passivation layer in order to form the depletion region. This was achieved by fabricating an $Al_2O_3$ layer on top of the substrate using atomic layer deposition (ALD), which provides a controlled method to produce uniform oxide layers to an atomically specified thickness.

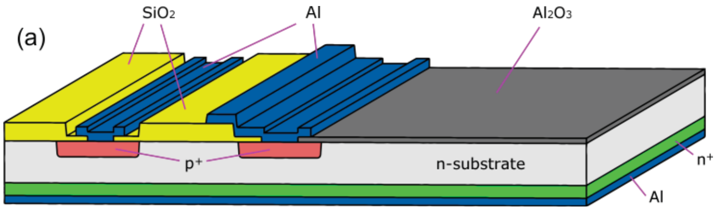


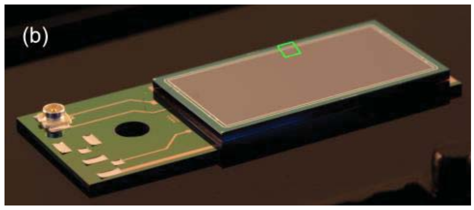


Fig. 1 (a) Cross section of the n-type PQED photodiode (not to scale). Only one of the 16 guard rings (the outermost $p^+$ implantation) is drawn. (b) A PQED photodiode having the size of 11 mm x 22 mm attached to the photodiode carrier. The added green square indicates the area of (a).

Due to smaller doping concentration and additional guard rings in the photodiode layout, the n-type PQED photodiodes have significantly smaller dark currents than p-type photodiodes – around 1 nA at room temperature when biased with a 10 V voltage. When the photodiode is cooled in a cryostat [8], the dark current decreases exponentially; approximately a decade for every decrease of 15 °C in temperature. Therefore, the cooled n-type PQEDis a primary standard suitable for single or few photon applications [9].
In terms of spatial uniformity of responsivity and absolute responsivity, the n-type PQED is compatible to the p-type device, meaning that the manufacturing of PQEDs is no longer dependent on the availability of a particular silicon process. Moreover, due to the improved dark current properties, this primary standard can be utilized in applications ranging from single photon applications to milliwatt levels of optical power.

**References**

[1] M. Sildoja et al, *Metrologia* **50**, 385–394 (2013).
[2] I. Müller et al, *Metrologia* **50**, 395–401 (2013).
[3] T. Dönsberg et al, *Metrologia* **51**, 197-202 (2014).
[4] J. Gran et al, *Metrologia* **49**, S130-S134 (2012).
[5] T. Dönsberg et al, *Metrologia* **51**, S276-S281 (2014).
[6] T. Pulli et al, *Light Sci. Appl.* **4**, e332 (2015).
[7] T. Dönsberg et al, *Metrologia* **54**, 821-836 (2017).
[8] F. Manoocheri et al, *J. Phys. Conf. Ser.* **972**, 012021 (2018).
[9] A. Vaigu et al, *Metrologia* **54**, 218-223 (2017).s

This work was funded by EMPIR-projects 17FUN06 'SIQUST' and 13SIB57 'NewStar'. The EMPIR initiative is co-funded by the European Union's Horizon 2020 research and innovation programme and the EMPIR Participating States.

# Accuracy Issues in Measurement of Detection Efficiency of Single Photon Avalanche Photodiodes by Direct Comparison with a Photodiode

**D.-H. Lee[1], I.-H. Bae[1], S. Park[1], K.-S. Hong[1], H. S. Park[1], J. S. Borbely[2]**

[1]*Korea Research Institute of Standards and Science, Daejeon, Korea*

[2]*Measurement Standards Laboratory, Lower Hutt, New Zealand*

We recently developed a system for measuring the detection efficiency (DE) of a single photon avalanche photodiodes (SPAD) by directly comparing it with a photodiode whose spectral responsivity is calibrated. By using a focused monochromatic beam, we can measure the DE of a free-space-coupled Si SPAD in a wide wavelength range from 250 nm to 1000 nm with a typical uncertainty of less than 1 % as a relative standard uncertainty ($k$ = 1). Figure 1 shows the schematic setup of the system. Details of the system is described in [1].

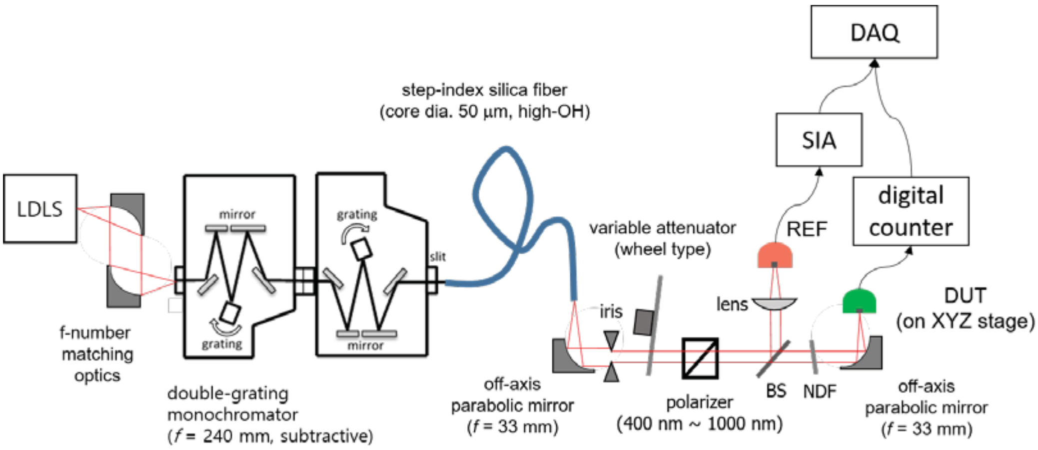


Fig. 1 Schematic setup for the detection efficiency measurement of a free-space-coupled SPAD by direct comparison with a photodiode at KRISS [1].

In this work, we would like to discuss the accuracy issues, which should be carefully considered in the DE measurement of a Si SPAD. First, we show how we realized the spatial alignment of the focused beam on the detector's active area. As the size of the beam at the focus was not much smaller than the size of the active area of the SPAD, a careful verification of the spatial matching was required.

Furthermore, we discuss the non-linearity issue of the Si SPAD under test. As a SPAD is an ON-OFF detector of single photons, its DE generally depends on the mean photon number of the input monochromatic beam under Poissonian photon statistics. We applied a linear correction model for considering the effects of the hold-off time and afterpulsing probability in the measurement equation of the DE. The validity range of the applied correction model had to be carefully tested for each SPAD under test and matched to the linearity range of the measurement system.

We present our experimental procedures to evaluate the two major accuracy issues, spatial alignment and non-linearity, at an example of a Si SPAD and also their influences on the DE results.

**References**

[1] In-Ho Bae *et al.*, Detection efficiency measurement of single photon avalanche photodiodes by using a focused monochromatic beam tunable from 250 nm to 1000 nm, *Metrologia*, 56, 035003 (2019).

# Calibration of free-space and fiber-coupled single-photon detectors

**Thomas Gerrits[1], Alan Migdall[2], Joshua C. Bienfang[2], John Lehman[1], Sae Woo Nam[1], Jolene Splett[1], Igor Vayshenker[1], Jack Wang[1]**

[1]*National Institute of Standards and Technology, Boulder, CO, 80305 (USA)*

[2] *Joint Quantum Institute, University of Maryland, National Institute of Standards and Technology, Gaithersburg, MD, 20899 (USA)*

We report on our progress towards implementing a calibration service for single-photon detectors. This calibration is made using transfer standard optical fiber power meters. We also describe a superconducting nanowire single-photon detector system developed and built for use as an in-house reference for single photon detection efficiency measurements. This system can also be packed and shipped from NIST to other NMIs for comparative measurements.

Our measurement of single-photon detector efficiencies is based on a beamsplitter method (Fig.1(a)), where an attenuator is used to attenuate from higher light levels that allow high-accuracy absolute-power measurements to lower levels compatible with photon-counting detectors[1]. First, the transmittance of the beamsplitter is measured at optical powers that allow both its input and output powers to be accurately measured with optical power meters, then its input power is reduced such that the output is in the range compatible with the device under test (DUT). Using this measured transmittance and the measured input power, the low-level optical power on the DUT can be determined, thus allowing the calibration of a transfer standard optical power meter (in our setup a Si trap detector) to be transferred to the DUT. We have implemented both, fiber-coupled and free-space measurement systems.

For use as in-house reference and comparisons between NIST and other NMIs, we have built a superconducting nanowire single-photon detector (SNSPD) system. The system is based on a 1K cryostat design, capable of operating our WSi SNSPDs[2]. Currently, the system hosts two SNSPDs, optimized for 1550 nm. The compact and robust detector packaging[3] allows shipping of the SNSPDs inside the cryostat without measurable degradation of the SNSPD performance over many temperature cycles. The system is fully automated and turn-key and as such, the operator does not need extensive cryogenic experience or knowledge.

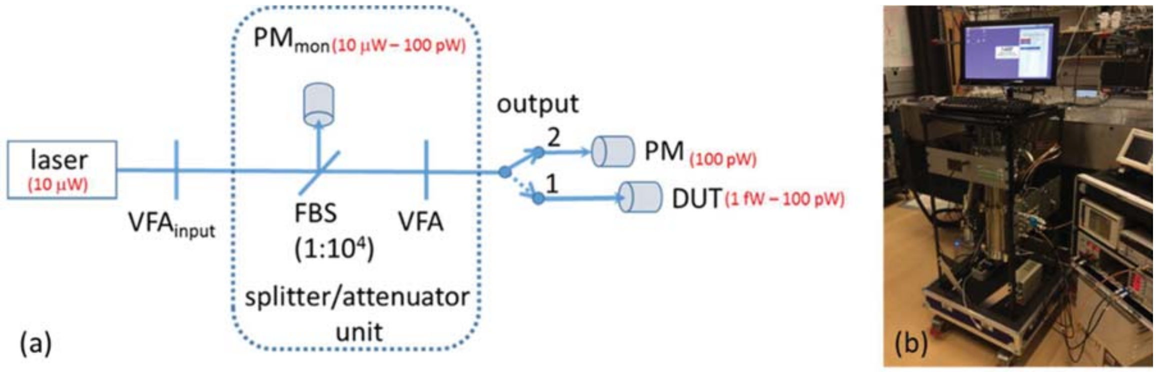


Fig 1. (a) Schematic of the setup. A fiber-coupled laser is coupled to a variable fiber attenuator (VFA$_{input}$) followed by a beam splitter/attenuator unit consisting of a monitor power meter (PM$_{mon}$), a fiber beam splitter (FBS) with a 1:10$^4$ split ratio, and another variable fiber attenuator (VFA). Switching the output controls whether the light goes to the calibrated power meter (PM) or the detector under test (DUT). (b) 1K SNSPD system used as in-house reference.

**References**

[1] Gerrits, T., et al, *Calibration of free-space and fiber-coupled single-photon detectors*", arXiv:1906.02258 (2019).
[2] Marsili, F., et al., *Detecting single infrared photons with 93% system efficiency.* Nat Photon, 2013. 7: p. 210.
[3] Miller, A.J., et al., *Compact cryogenic self-aligning fiber-to-detector coupling with losses below one percent.* Opt. Express, 2011. 19(10): p. 9102-9110

# Photonic Holography of Subatomic Space

**Eugene Machusky**[1]

[1] *Kyiv Polytechnic Institute, Ukraine*

Absolute values of fundamental quantum units of standard physical model are defined analytically by means of inverse functional analysis. Computed values of quantum constants and variables fully coordinate special and general relativity within the framework of harmonic vector field theory.

The standard physical model is based on the metric SI units, three of which are now defined as conditionally exact after careful measurements and calculations of the optical spectra of primary chemical elements: The speed of light in free space C = 299792458 m/s (by the radiation frequency of caesium-133). The triple point of water TPW = 100*K - 1/100 = 273.15 degree Celsius (oxygen-16 and two hydrogen-1). The relative molar mass RMM = 12/1000 = 0.012 (by carbon-12). For a more accurate estimate of quantum units in a unified system of positional calculations, we can use only two simple expressions connecting the transcendental numbers pi and e with the progressive (N+1) and inverted 1/(N+1) natural sets. These are recently discovered exact expressions for the stroboscopic speed C of a three-dimensional circular motion and the stroboscopic speed K for a one-dimensional radial motion [1-3]:

C = [(R/10^8 + 4*pi*C/10^18)^64]*(10^7) = [299792457.86759134] – upper speed unit of Maxwell.
K = e + AS + BS = [2.7315999984590452] – upper background temperature unit of Kelvin.
R = Integer{10^8*(C/10^7)^(1/64)} = 105456978 – reference integer of Dirac.
A = Lim[1/Sum{729927/10^(8*N)}] = 137 – reference integer of Sommerfeld.
AS = Lim[1/100/Sum{[A + (A - 100)*N]/[10^(3*N + 2)]}] = [0.00729] – Sommerfeld's integral.
B = 602214183 – reference integer of Avogadro.
BS = Lim[Sum{B/10^(3*N + 8)}] = [0.00602817] – Avogadro's integral.

[Ri] = 1+2/100*(e+[Ai]*(1+Sqrt(2*pi*e)/10))) – normalized field of inverse radius – matrix of Dirac.
[Pi] = 2*pi*[Ri] – normalized field of inverse perimeter – matrix of Planck.
[Ci] = ([Ri]^64)/10 – normalized field of speed of waves – temporal matrix of Maxwell-Kelvin.
[Gi] = [Pi]*(1+[Ai]) – normalized field of density of wave fronts – gravity matrix of Newton-Wien.
[Ni] = 100*(Sqrt(8*pi*e/(8*pi*e+A^2))/(1+2*[Ai]/1000) - 5/(10^8)) – entropy matrix of Avogadro.
[Mi] = 12 - [Ai]/10 – normalized field of relative amplitudes – molar mass matrix of Amagat.
[Ki] = Cos[Mi] - Sin[Mi] – normalized field of relative phases – polarization matrix of Boltzmann.

| | AVOGADRO-[Ni] | DALTON-10/[Ni] |
|---|---|---|
| A4 = 4/A-3*A0 | 6.0221410025819227 | 1.6605390002845527 |
| AH = 1/16/pi/e | 6.0221410053902884 | 1.6605389995101768 |
| NB = B/(1+4*pi/10^8)/10^8 | 6.0221410732354338 | 1.6605389808026261 |
| AL = 1/(1+59*Ln(10)) | 6.0221411450151730 | 1.6605389610101549 |

| | PLANCK-[Pi] | DIRAC-[PI]/(2*pi) |
|---|---|---|
| A1 = 1/A | 6.6260710055755005 | 1.0545719538152265 |
| AF = 1/(A+36/1000) | 6.6260706650236630 | 1.0545718996147182 |
| A0 = (pi*e/100)^2 | 6.6260698398254579 | 1.0545717682803448 |
| AS = 1/100/(10/(10-1))^3 | 6.6260693592370495 | 1.0545716917923240 |

| | MAXWELL-[Ci] | BOLTZMANN-[Ki] |
|---|---|---|
| RC = (R+4*pi*C/10^10)/10^8 | 299792457.86759134 | 1.3806484502840000 |
| RE = (R+1/e)/10^8 | 299792456.25727419 | 1.3806484501880000 |
| RA = (R+1/(e+AS))/10^8 | 299792456.07825451 | 1.3806484501770000 |
| RK = (R+1/K)/10^8 | 299792455.93094320 | 1.3806484501680000 |

## References

[1] E. Machusky "Quantum metric of classic physics" IOP Conf. Series: Materials Science and Engineering 239 (2017) 011002 doi:10.1088/1757-899X/239/1/011002
[2] E. Machusky "Complex geometry of wave motion" International Journal of Engineering and Technology vol.10, no.2 pp.184-188, (2018).
[3] E.Machusky "Natural qubit matrix of primary elements of matter" MATEC Web of Conferences 186, 01005 (2018)

# Traceable standard detector for calibration of single photon detectors and sources at telecom wavelengths

**Geiland Porrovecchio[1], Marek Smid[1], Robert Kirkwood[2], Christopher Chunnilall[2]**

[1]*Cesky Metrologicky Institut (CMI), V Botanice 4, 15072 Praha 5, Czech Republic*

[2]*National Physical Laboratory (NPL), Hampton Road, Teddington, TW11 0LW, U.K.*

We present a low photon flux fibre-coupled standard detector for the infrared spectral wavelengths (LOFIR) that can be used to calibrate single-photon detectors and sources with an uninterrupted traceability chain to the primary standard of optical power.

The LOFIR comprises a dual-stage thermally-cooled Hamamatsu G6805-23 InGaAs photodiode in conjunction with high-sensitivity, low-noise, switched integrator (SIA) custom-made electronics [1]. The G6805-23 photodiode with its circular sensitive area of 3 mm diameter was selected based upon the optimal trade-off between noise, typically proportional to the size of detector, and its minimum sensitive area required to achieve underfilled configuration for both free-space and fibre-coupled incident radiation.

The photodiode includes a dual-stage Peltier cooling device that can be stabilized between -20° C and +30° C. The LOFIR is equipped with a fibre coupler designed to keep the tip of the fibre at a minimum distance from the photodiode housing window that is 6 mm from the photodiode's sensitive surface. Considering the numerical aperture of the single-mode fibre, the distance of its end from the sensitive area and the photodiode's sensitive area geometry, the optical radiation underfills the photodiode. All the parts of the fibre coupler facing the photodiode have been painted in black to minimize inter-reflections. Two O-rings placed between the photodiode housing and the coupler minimize the amount of undesired external light impinging the photodiode. The photodiode current is converted to voltage by a switched integrator with a 1pF mica capacitor. The integration time can be set from 0.001s to 1s that translates to an I/V conversion factor from $10^9$ to $10^{12}$. The value of the integration capacitor is calibrated using the method described in [2] and it is traceable to quantum Hall and Josephson primary standards with a relative standard uncertainty of 0.2%.

The LOFIR's photodiode spectral responsivity has been measured using a free-space beam double monochromator-based facility. The LOFIR photodiode's photocurrent was compared against the photocurrent of a InGaAS reference detector traceable to the primary standard of optical radiation: the cryogenic radiometer. Both detectors have been underfilled with incident quasi-monochromatic radiation with a power level of few nW. The LOFIR photodiode's responsivity has been calibrated in the spectral range from 1200 nm to 1650 nm with a relative standard uncertainty of about 0.4%.

During a measurement campaign performed in INRIM to calibrate the detection efficiency of fibre-coupled single photon detectors [3] the LOFIR measured down to 88 fW of optical power with a relative noise of 1.2% and a total relative standard uncertainty of 2%. LOFIR will be a valuable tool for low photon flux calibrations, such as required for calibrating quantum key distribution hardware.

*The work reported on this paper was funded by project EMPIR 14IND05 MIQC2. This project received funding from the EMPIR programme co-financed by the Participating States and from the European Union Horizon 2020 research and innovation programme.*

**References**

[1] J. Mountford, G. Porrovecchio, M. Smid and R. Smid, "Development of a switched integrator amplifier for high- accuracy optical measurement," *Applied Optics,* vol. 47, no. 31, pp. 5821-5828, 2008.

[2] G. Porrovecchio, M. Smid, M. Lopez, B. Rodiek, S. Koeck and H. Hofer, "Comparison at the sub-100 fW optical power level of calibrating a single-photon detector using a high-sensitive, low-noise silicon photodiode and the double attenuator technique," *Metrologia,* no. 53, pp. 1115-1122, 2016.

[3] M. Lopez, A. Meda, G. Porrovecchio, R. Kirkwood, M. Genovese, G. Brida, M. Smid, C. Chunnilall, I. Degiovanni and S. Kueck, "Pilot study on the detection efficiency measurement of InGaAs/InP single-photon detectors," *In preparation.*

# Compact all-fiber polarization-independent up-conversion single-photon detector

**Longyue Liang[1], Junsheng Liang[2], Mingyang Zheng[1], Xiuping Xiu[1], Qiang Zhang[1,3,*]**

[1]*Jinan Institute of Quantum Technology, Jinan, China*

[2]*Shandong Institute of Quantum Science and Technology Co., Ltd., Jinan, China*

[3]*University of Science and Technology of China, National Laboratory for Physical Sciences at Microscale and Department of Modern Physics, Hefei, China*

Telecom band single-photon detectors (SPDs) play a critical role in optical quantum communication, and the SPD performance directly limits the transmission distance and key rate of fiber-based quantum key distribution (QKD). Compared with InGaAs/InP avalanche photodiodes (APDs) and superconducting SPDs, the performance of up-conversion SPD satisfies the need of long-distance QKD and is suitable for field implementation, where the detection spectral range of silicon APDs is extended into the 1.55-μm telecom band using sum-frequency generation (SFG) with periodically poled lithium niobate (PPLN) waveguides [1].
However, as a low-noise and high-efficiency wavelength conversion device, proton exchanged PPLN waveguide guides only the light wave polarized along the c-axis of the z-cut crystal [2], and all the interacting waves are of the same polarization for type-0 SFG, making use of the highest nonlinear coefficient $d_{33}$. Up-conversion SPD based on a single waveguide is therefore polarization dependent and extra caution should be taken when up-conversion SPD is used in polarization-independent systems.
We demonstrate a compact all-fiber polarization-independent up-conversion detector (Fig. 1) for single photon counting at 1.55 μm based on the polarization diversity configuration. An integrated dual-channel reverse proton exchanged (RPE) PPLN waveguide device with two adjacent waveguides of the same design parameters is used. After being separated with a fiber-coupled polarization beam splitter (PBS), the horizontal and vertical polarized components of the randomly polarized signal pass two orthogonally polarized polarization maintaining (PM) fibers, combine with the pump waves and enter the waveguide device. Optical filtering for the outputs is achieved by combining multi-mode fiber filter with multi-mode fiber combiner (MMFC). Such an all-fiber configuration makes the system compact and stable. Based on this detector, the polarization-independent single-photon counting at 1.55 μm is achieved with a system detection efficiency of 29.3%, a dark count rate of 1600 counts per second, and a polarization dependent loss of 0.1dB. The detection efficiency remains stable when the polarization of the signal is changed, and this detector can be used in practical QKD systems for complex environmental applications [3].

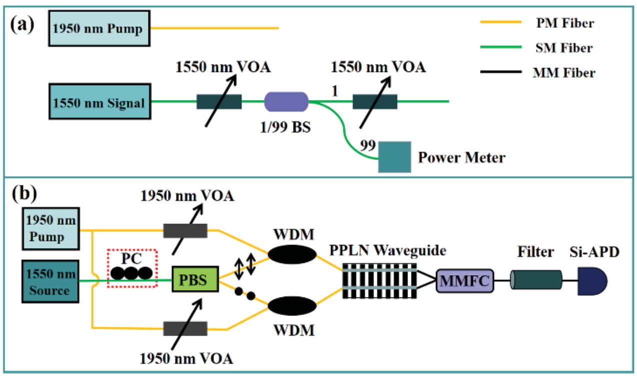


Fig. 1 (a) Preparation of the pump and signal sources. (b) Schematic diagram of the polarization-independent up-conversion SPD. VOA: variable optical attenuator, BS: beam splitter, PM: polarization maintaining, SM: single-mode, MM: multi-mode, PC: polarization controller, PBS: polarization beam splitter, WDM: wavelength division multiplexer, PPLN: periodically poled lithium niobate, MMFC: multi-mode fiber combiner, Si-APD: silicon avalanche photodiode.

**References**

[1] A. P. Vandevender, P. G. Kwiat, High efficiency single photon detection via frequency up-conversion, J. Mod. Opt. 51 (2004) 1433-1445.
[2] F. Lenzini, S. Kasture, B. Haylock, M. Lobino, Anisotropic model for the fabrication of annealed and reverse proton exchanged waveguides in congruent lithium niobate, Opt. Express 23 (2015) 1748-1756.
[3] L. Y. Liang, J. S. Liang, Q. Yao, M. Y. Zheng, X. P. Xie, H. Liu, Q. Zhang, J. W. Pan, Compact all-fiber polarization-independent up-conversion single-photon detector, Opt. Commun. 441 (2019) 185-189.

# A multi-channel up-conversion single-photon detector at telecom band

**Ming-Yang Zheng[1], Quan Yao[1], Bing Wang[2], Xiuping Xie[1], and Qiang Zhang[1, 2]**

[1]*Jinan Institute of Quantum Technology, Jinan 250101, China*

[2]*National Laboratory for Physical Sciences at Microscale and Department of Modern Physics, University of Science and Technology of China, Hefei 230026, China.*

A multi-channel telecom-band up-conversion single-photon detector (SPD) based on a multi-channel reverse-proton-exchange periodically poled lithium niobate (PPLN) waveguide has been demonstrated. Pumped by a 1950-nm single frequency laser module before the waveguide chip and spectrally filtered by an optical fiber filtering system after nonlinear frequency mixing, sum-frequency generation signals are detected by a silicon avalanche photodiode (APD) module. As proof of principle, we show an eight-channel up-conversion single-photon detector based on an eight-channel waveguides. An average detection efficiency (DE) of 25.1% and noise count rate (NCR) of 1500 counts per second (cps) are achieved, with a standard deviation of 0.94% and 273cps between different channels, which is excellent for its extensive application in high-rate quantum key distribution, single-photon imaging, quantum lidar and so on.

Single photon detection technology at telecom band has extremely important applications in quantum communication, quantum lidar, single-photon imaging, deep space detection, etc. Single-photon detectors at telecom band based on superconducting materials, InGaAs-APD and up-conversion process have been achieved [1-3]. Further realizing the spatial resolution capability of single photon detector by the multi-pixel array can expand the application scenario greatly. The implementation of array single photon detectors based on the above three technologies has its own advantages and disadvantages. Due to the large volume of cryogenic device, superconducting detectors are not conducive to achieving a large number of pixels, and the cost would be very high. InGaAs-APD is the only technical way that has been realized for an array detector at telecom band so far. The Lincoln laboratory of the Massachusetts Institute of Technology has been developing this technology since the early 2000s, and in 2007 reported the first 32×32 array single photon detector based on InGaAs-APD. However, some parameters are poor (NCR is about 20 kHz, dead time is 6 us, time resolution is about 300-400 ps), and there are serious crosstalk between pixels [4]. With continuously optimization and improvement, the number of pixels reaches 128×32 with NCR of 5 kHz, time resolution of 300 ps and crosstalk of 8%. The working frame rate can reach 100 kHz [5]. However, there still be a certain crosstalk between adjacent pixels.

By using a multi-channel up-conversion single photon detector, we can compensate for some of the inadequacies of the InGaAs-APD array detector. Single-photon detection based on reverse-proton-exchange PPLN waveguides can achieve a typical dark count of about 1 kHz, and channel isolation more than 30 dB due to the independence between different waveguide channels. The use of Si APD for photon detection can provide high time resolution no less than the state-of-art InGaAs-APD array, even reaching dozens of picoseconds. In addition, by using a block readout method, the frame rate limitation brought by the data transmission can be broken, and the working frame rate of the order of megahertz could be realized.

Here, an eight-channel up-conversion single-photon detector has been implemented based on an eight-channel PPLN waveguide chip. At quasi-phase matching condition, an efficient frequency conversion of eight-channel 1550-nm band signals have been realized. An average DE of 25.1% and NCR of 1500 Hz have been achieved.

**References**

[1] F. Marsili, V. B. Verma, J. A. Stern, et al. "Detecting single infrared photons with 93% system efficiency," Nat. Photonics 7(3), 210-214 (2013).

[2] J. Zhang, M. A. Itzler, H. Zbinden, et al. "Advances in InGaAs/InP single-photon detector systems for quantum communication," Light Sci. Appl. 4(5), 286-286 (2015).

[3] L. Ma, O. Slattery, and X. Tang, "Single photon frequency up-conversion and its applications," Phys. Rep. 521(2), 69-94 (2012).

[4] S. Verghese, J. P. Donnelly, E. K. Duerr, et al. “Arrays of InP-based Avalanche Photodiodes for Photon Counting,” IEEE Journal of Selected Topics in Quantum Electronics, 13(4), 870-886 (2007).

[5] M. A. Itzler, M. Entwistle, X. Jiang, et al. “Geiger-mode APD single-photon cameras for 3D laser radar imaging,” IEEE Aerospace Conference, 1-12 (2014).

# A NIR-enhanced silicon BSI SPAD with low sensitivity to process fluctuations and 15 µm pitch

**Edward Van Sieleghem[1,2], Andreas Süss[2,3], Pierre Boulenc[2], Maarten Rosmeulen[2], Chris Van Hoof[1,2]**

[1]*KU Leuven, ESAT, Kasteelpark Arenberg 10, B-3001 Leuven, Belgium*

[2]*Imec, Kapeldreef 75, B-3001 Leuven, Belgium*

[3]*now at OmniVision Technologies, Santa Clara CA 95054, USA*

Single-photon avalanche diodes (SPADs) are known for their time resolving capabilities of individual photons. Various recent publications focus on system integration of silicon SPADs for time-resolved imaging [1,2,3]. These works demonstrate the need for uniform SPAD arrays with a small pitch. In practical applications such as automotive LIDAR, high sensitivity to near-infrared (NIR) radiation is beneficial. For backside-illuminated (BSI) silicon SPADs, a deep depletion region extending to the back of the device can enhance the NIR sensitivity while maintaining efficient carrier transport.

This work presents a CMOS compatible NIR-enhanced silicon BSI SPAD with low sensitivity to process fluctuations, 15 µm pitch and an estimated PDE above 15% at 905 nm. Fig. 1 shows the cross-section of the doping profile. The device is rotationally symmetric and has a breakdown voltage around 51 V. The doping profile consists of multiple narrow n-type implants and ring-shaped p-type implants for the formation of the cathode and anode respectively. The cathode and anode are separated by a lowly doped fully depleted volume which extends approximately 10 µm deep. The backside is biased at the same voltage as the anode. A dedicated implant for creating the multiplication field is absent. Consequently, the device relies on geometry for the formation of a field peak near the cathode. The crowding of the electric field lines is demonstrated in Fig. 1. The field peak is radially uniform and spaced away from the oxide interface. The overall field distribution results in fast transport and a large multiplication probability of electrons generated throughout the lowly doped volume.

A TCAD study is conducted on the design and optimization of the detector for uniform and fast detection of photogenerated charges. Furthermore, the uniformity, dark count rate (DCR) and photon detection efficiency (PDE) are characterized on fabricated 200 mm BSI wafers and packaged frontside-illuminated (FSI) samples through a monolithically integrated digital counter circuit. The FSI samples include a highly doped p-type substrate below the depletion region. The variability of the breakdown voltage across a BSI wafer is measured to be less than 0.6%. This is more than an order of magnitude lower than the measured variability for a NIR-enhanced reference SPAD on the same wafer. The reference SPAD resembles the device presented by Takai et al. [4] but includes a 10 µm epi and a depleted bulk. Based on FSI measurements, the BSI PDE is estimated to be above 15% at 905 nm. The measured DCR of FSI samples is in the order of 10 kHz per SPAD at an excess bias of 3.3 V and room temperature. The DCR on a BSI wafer is measured to be in the order of 100 kHz per SPAD under the same conditions. The BSI PDE and excessive BSI DCR are under investigation at the time of writing. Overall, this work demonstrates the viability of a uniform NIR-sensitive BSI SPAD based on a geometry-constrained electric field and with near-unity fill factor. Dark noise, sensitivity and crosstalk will be addressed in future developments.

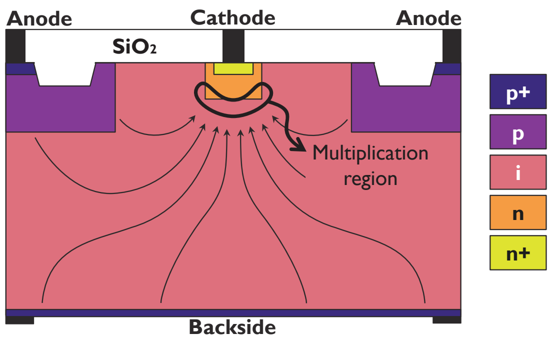


Fig. 1: Cross-section of the doping profile of a rotationally symmetric NIR-enhanced SPAD. Field lines (black solid arrows) and the multiplication region (black enclosure) are indicated.

**References**

[1] R. K. Henderson *et al.*, *2019 IEEE ISSCC*, (2019).

[2] A. R. Ximenes *et al.*, *2018 IEEE ISSCC*, (2018).

[3] C. Zhang *et al.*, *IEEE JSSC*, vol. 54, no. 4, p. 1137-1151, (2018).

[4] I. Takai *et al.*, *Sensors*, vol. 16, p. 459, (2016).

# Thick CMOS Single-Photon Avalanche Diode Optimized for Near Infrared with Integrated Active Quenching Circuit

**Michael Hofbauer[1], Bernhard Steindl[1], Kerstin Schneider-Hornstein[1], Horst Zimmermann[1]**

[1]*Institute of Electrodynamics, Microwave and Circuit Engineering, TU Wien, Vienna, Austria*

In recent years, more and more applications, such as quantum key distribution, quantum random number generation, and LIDAR (i.e. light detection and ranging) have been utilizing highly sensitive single-photon avalanche diodes (SPADs). For many of these applications a high degree of integration and a high photon detection probability (PDP) in the near infrared range are crucial. In this paper, we present a thick SPAD integrated in a high-voltage 0.35µm CMOS process with an active quenching circuit utilizing cascoding for doubling the maximum possible excess bias. The active quenching circuit is similar to the one presented in [1]. Contrary to the SPAD presented in [1] and [2], the SPAD presented in this paper includes an anti-reflective coating (ARC) preventing interference effects in the oxide stack. Consequently, the spectral PDP is much smoother.

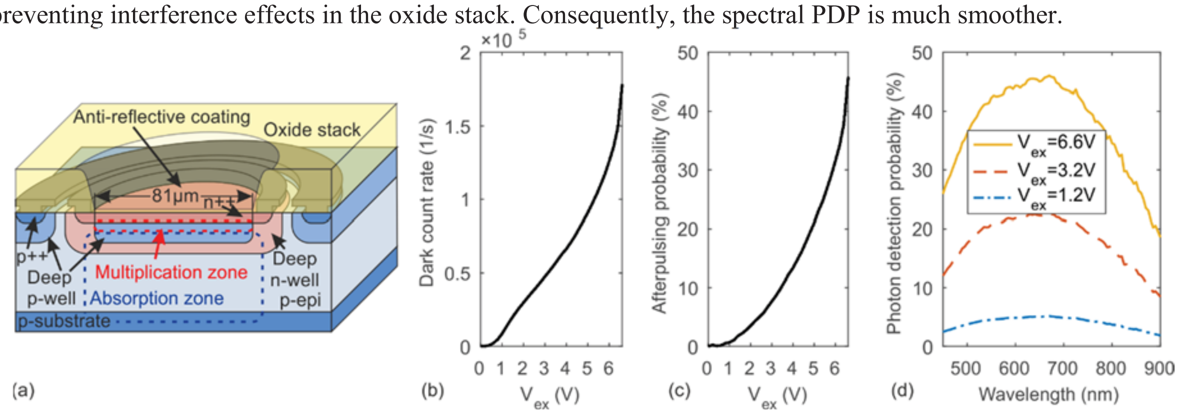


Fig. 1 Cross section of the SPAD (a), dark count rate (b), afterpulsing probability (c) and photon detection probability (d), all measured at room temperature (25°C) for a dead time of 9ns.

Figure 1 (a) depicts a cross section of the SPAD. The active diameter is 81µm. The multiplication zone is formed by the region around the junction between n++ cathode and the p-well. The deep n-well reduces the effective deep p-well doping to allow a reach-through of the depletion region down to the p-epi layer. This low-doped p-epi layer is approximately 10µm thick and is fully depleted at the operating bias. The thick depleted region helps to increase the PDP for longer wavelengths. The breakdown voltage $V_{br}$ is approximately 68 V.

The active quenching circuit (AQC) has an adjustable dead time between 6 ns and 33 ns. The dark count rate (DCR) and the afterpulsing probability (APP) characterized at a dead time of 9 ns are shown in Fig. 1 (b) and (c), respectively. All measurements were done at room temperature (25°C). Since the AQC's dead time is adjustable, the trade-off between dead-time and afterpulsing probability can be adjusted to the specific application's need. For a dead time of 33 ns APP decreases drastically to 2.2% and 9.2% for excess biases of $V_{ex}$=3.2 V, and $V_{ex}$=6.6 V, respectively.

Fig. 1 (d) shows the spectral PDP for three different excess biases of $V_{ex}$=1.2 V, $V_{ex}$=3.2 V, and $V_{ex}$=6.6 V for the wavelength range from 450 nm to 900 nm. Dark-counts and afterpulses are already subtracted for the shown PDP. Due to the ARC, the spectral PDP is relatively smooth. The relatively high PDP for longer wavelengths is achieved due to the thick absorption zone. At 800 nm a PDP of ~35% is reached at $V_{ex}$=6.6V. In comparison, the SPAD integrated in a 130 nm CMOS process in [3] reaches a PDP of ~20% at 800nm for a comparable excess bias. The DCR and the APP in [3] are much lower, because of a considerably smaller SPAD diameter (~8 µm) and a considerably longer dead time (>30 ns, extracted from Fig. 2 in [3]). Our presented PDP at 800 nm competes even with most of the SPADs using specialized processes, which are compared in [3].

By increasing the excess bias, we plan to further increase the PDP in future. Decreasing the DCR is easily possible by cooling the device, by implementing SPADs with a smaller active diameter, or by pre-selecting the SPADs with the lowest DCR. A smaller active diameter would also reduce the APP.

**References**

[1] R. Enne, B. Steindl, M. Hofbauer, H. Zimmermann, "Fast Cascoded Quenching Circuit for Decreasing Afterpulsing Effects in 0.35µm CMOS," *IEEE Solid-States Circuits Letters*, vol. 1, no. 3, pp. 62-65, 2018.

[2] H. Zimmermann, B. Steindl, M. Hofbauer, R. Enne, "Integrated Fiber Optical Receiver Reducing the Gap to the Quantum Limit," *Scientific Reports*, vol. 7, article no: 2652, 2017.

[3] E.A.G. Webster, L.A. Grant, and R.K. Henderson, "A High-Performance Single-Photon Avalanche Diode in 130-nm CMOS Imaging Technology," *IEEE Electron Device Letters*, vol. 33, no. 11, pp. 1589-1591, 2012.

# Behavior and models for quench efficiency in Single-Photon Detection

**Y.OUSSAITI [1,2], D.RIDEAU [1], J.R.MANOUVRIER[1], B.MAMDY[1], H.WEHBE-ALAUSE[1], M.PALA[2]**

[1] *STMicroelectronics – 38920 Crolles, France.*

[2] *Centre de Nanosciences et de Nanotechnologies – 91120 Palaiseau, France.*

**Abstract – We present results of numerical simulations for quench efficiency in Single-Photon Avalanche Diodes (SPADs), using both *TCAD* and *SPICE* tools. We discuss the impact of the device internal properties as well as external readout electronics on the quench behavior. Then, we assess the role of a new proposed circuitry in estimating afterpulses and detection efficiency. The results show a good agreement with experiments: we conclude that these models can predict the electrical response in such photodetectors.**

**Introduction -** SPADs are reverse-biased *pn* junctions operating at a voltage $V_A$ initially below the breakdown voltage $V_B$. When the device reaches the latter value, the electric field in active area is strong enough that an injected carrier may trigger an avalanche through impact ionization mechanisms [1]. Consequently, the current increases promptly and it has to be quenched using an external circuit so that the device can restore its initial conditions. Nowadays, SPADs are used in many fields taking advantages mainly of their high quantum efficiency [2], high field properties [3]. Through this study, we investigate Silicon-SPAD internal capacitance and well-resistance from one side, and the external quenching circuits on the device dynamics (recharge, power consumption..etc), on the other. For our study, we used *Synopsys* [4] Drift-Diffusion and SPICE Verilog-A models to simulate the device response. By fitting results with experimental data, we point out the circuitry contribution in detecting afterpulses, and in estimating the quench efficiency in a range of Si-SPAD representative structures.

**Results**

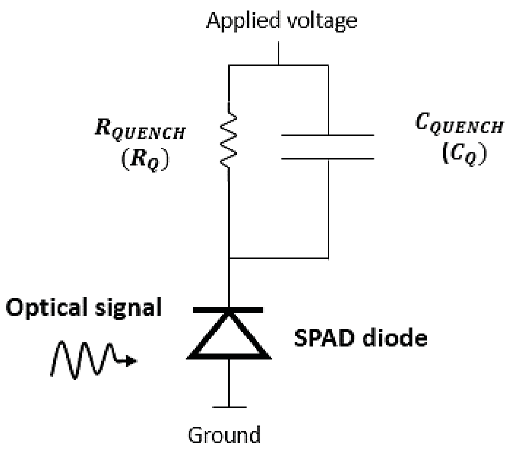


(a)

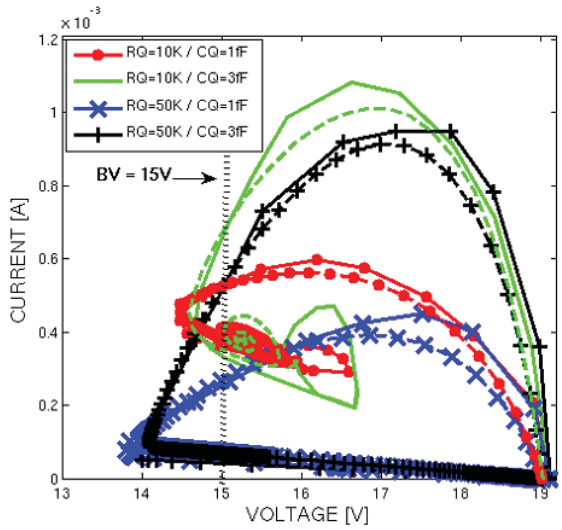


(b)

Fig. 1 : (a) SPAD diode connected to Passive-Quenching Circuit (PQC) from the cathode node (b) SPAD I-V characteristic: solid lines refer to SPICE Verilog-A model, dashed ones to TCAD Drift-Diffusion soft. The impact of both quenching resistance and capacitance is evidenced. Typically, a low resistance induces a non-quench behavior; the current is not completely attenuated. As a consequence, the device starts second avalanches (spirals) which strongly impact the SPAD dead-time. Throughout this study, the excess bias is fixed at 4 volts for all simulations.

**Conclusion**

We have developed models to simulate and predict SPAD's electrical response. Among series of simulations coupled with experiments, we prospect the device quench behavior, efficiency and fit its internal parameters to reach the performance target. These models provide a significant support for SPAD design and characterization.

**References**

[1] A. Spinelli and A.L. Lacaita, "Physics and numerical simulation of Single Photon Avalanche Diodes," IEEE transactions on electron devices, vol. 44, No. 11, november 1997

[2] X. Y. Zou, L. J. Wang, and L. Mandel, "Induced coherence and Indistinguishability in optical interference," Phys. Rev. Lett., vol. 67, pp. 318–321, 1991.

[3] A. Lacaita, F. Zappa, S. Bigliardi, and M. Manfredi, "On the bremsstrahlung origin of hot-carrier-induced photons in silicon devices," IEEE Trans. Electron Devices, vol. 40, pp. 577–582, 1993.

[4] Synopsys, Inc. Version O-2018.06, June 2018.

# High-speed gated thick reach-through silicon SPAD approaches 100 × $10^6$ counts per second

**Michael A. Wayne[1], Alan L. Migdall[1], and Joshua C. Bienfang[1]**

[1]*Joint Quantum Institute: University of Maryland and the National Institute of Standards and Technology, 100 Bureau Drive, Gaithersburg MD, USA*

High-speed gating is an effective method to improve the performance of single-photon avalanche diodes (SPADs), albeit at the expense of detection duty cycle [1]. This technique has been applied mainly to InGaAs/InP SPADs, where the prompt termination of the avalanche current achieved by short (sub-nanosecond) high-repetition-rate (gigahertz) bias gates has enabled performance metrics that surpass those achieved by traditional methods [2], particularly in count rate and efficiency. In this work we show that high-speed gating can also have a significant impact on the performance of a commercially available, high-efficiency (thick) reach-through silicon SPAD. In these devices, which have breakdown voltages of 270 V or more, we show that the charge per avalanche can be suppressed by more than two orders of magnitude below that of its original actively quenched system. While there is an attendant reduction in afterpulsing, the primary benefit for thick Si SPADs is the reduction in the power dissipated per avalanche, which allows count rates significantly higher than previously achieved [3]. In preliminary measurements we observe count rates up to 75 × $10^6$ $s^{-1}$ with no degradation in efficiency, and we have operated the device at count rates above 100 × $10^6$ $s^{-1}$, though our initial instrumentation inhibited making an efficiency measurement at these rates. These count rates are an order of magnitude higher than previously demonstrated with devices of this class.

Thick reach-through devices are generally not well suited to high-speed gating due to their higher junction capacitance, higher operating voltages, and significant packaging inductance; previous work [3,4] has explored gating up to 152 MHz. We use the interferometric readout scheme presented in [2] and illustrated in Fig. 1(a) to push to higher gating frequencies. We gate the SPAD with a 44 V peak-to-peak sine wave at the cathode and suppress the lowest three harmonics of the gate at the anode with destructive interference, allowing for sensitive discrimination of avalanche signals in the millivolt range (when appropriately tuned). Higher-order harmonics are low-pass filtered (LPF). Figure 1(b) shows analog avalanche signals when every $4^{th}$ gate is stimulated by a 65(5) ps optical pulse with a mean photon number of 0.3(1) and the count rate is ≈ 30 × $10^6$ $s^{-1}$. Figure 1(c) shows the afterpulse probability versus time after an illuminated gate as measured in each bias gate after an illuminated gate, at 20 $^{o}$C. Based on the observed performance with this preliminary system, we anticipate that higher gate rates can be applied and higher count rates can be achieved. We have designed a second system for a 1 GHz gate, and we will discuss the performance of these systems and characterize their efficiency and noise properties at high count rates.

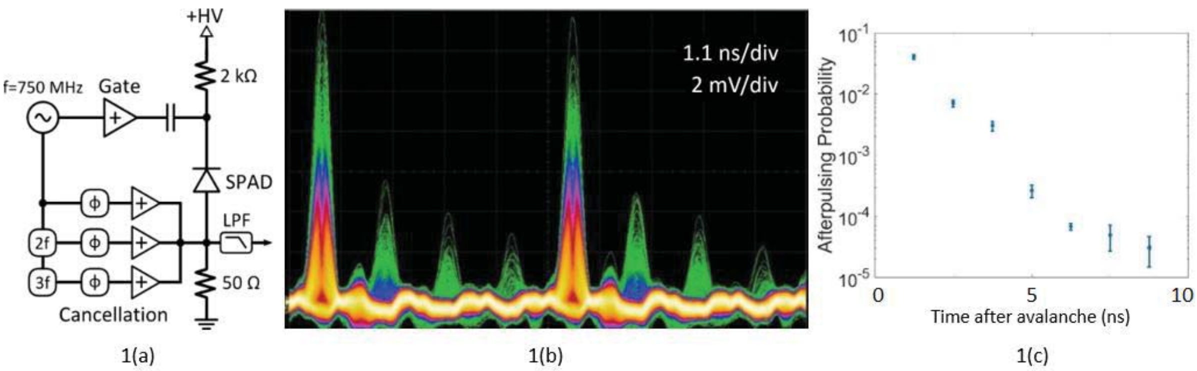


**Figure 1.** (a) Schematic of the multi-harmonic interferometric bias and readout system. (b) Signals at the anode when the SPAD is gated by a 750 MHz, 44 V peak-to-peak sine wave. The SPAD is illuminated with an attenuated laser pulse in every $4^{th}$ gate and is counting at an average rate of ≈ 30 × $10^6$ $s^{-1}$. (c) The conditional afterpulse probability versus time, as measured in each of 7 gates following an illuminated gate.

## References

[1] A. L. Migdall, S. V. Polyakov, J. Fan, and J. C. Bienfang. *Exp. Methods in the Phys. Sci.* **45** (2013).
[2] A. Restelli, J. C. Bienfang, and A. L. Migdall. *Appl. Phys. Lett.* **102**, 141104 (2013).
[3] N. Zhou, W-H Jiang, L-K Chen, Y-Q Fang, Z-D Li, H. Liang, Y-A Chen, J. Zhang, and J-W Pan. *Rev. of Sci. Instr.* **88**, 083102 (2017).
[4] S. Suzuki, N Namekata, K. Tsujino, and S. Inoue. *Appl. Phys. Lett.* **104**, 041105 (2014).

# A Monolithic QRNG based on an array of SPADs

**Nicola Massari[1], Hesong Xu[2]**

[1]*Fondazione Bruno Kessler: via Sommarive 18, Povo (TN), Italia*

[2]*AMS AG Tobelbader Strasse 30 8141 Premstaetten, Austria*

Quantum Random Number Generator (QRNG) based on photonics have shown to be a competitive alternative to true RNGs [1]. Nevertheless, the main bottleneck of this technology is represented by the cost. A possible way to reduce the cost is through the integration of the source of photons in silicon [2-3]. In this work an implementation of a QRNG based on a monolithic approach is proposed. The present chip consists of an array of 16x8 elements (see Fig.1 left). Each element consists of a p+/nwell junction, used as a source and placed around the detector, and a p+/nwell SPAD placed in the centre (see Fig.1 right). Specifically, the p+/nwell junction is biased in forward mode and the current flowing in it is regulated by a pMOS transistor (see in Fig2 left). Photons generated by the source are detected by the SPAD then random bits are extracted from the measurement of the arrival time. An embedded time to amplitude converter samples two consecutive events that are compared, at the end of the sampling, in order to extract a random bit. First experimental results in Fig.2 (right) shows that the increment of activity due to the emitter is physically demonstrated. Further results, aimed at characterizing the random sequence, will be performed soon to check the output quality.

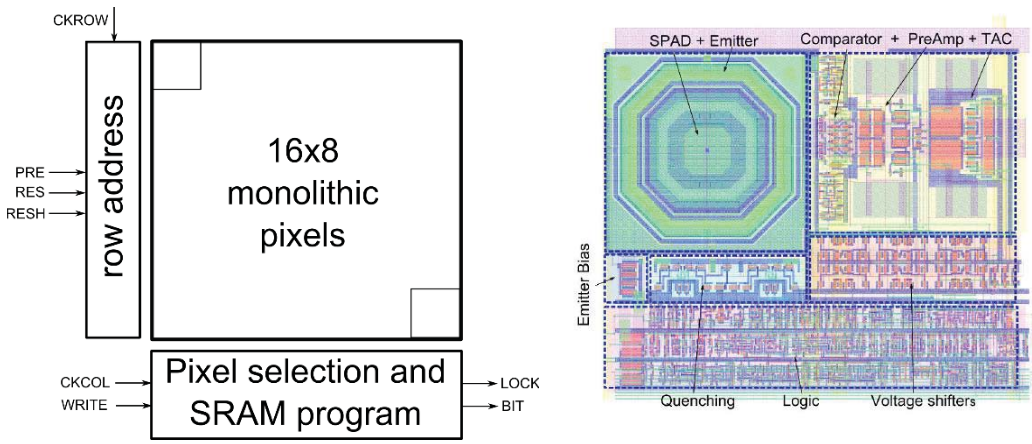


Fig. 1 Main building blocks of the array of 16x8 monolithic pixels (left) and the layout of each element (right)

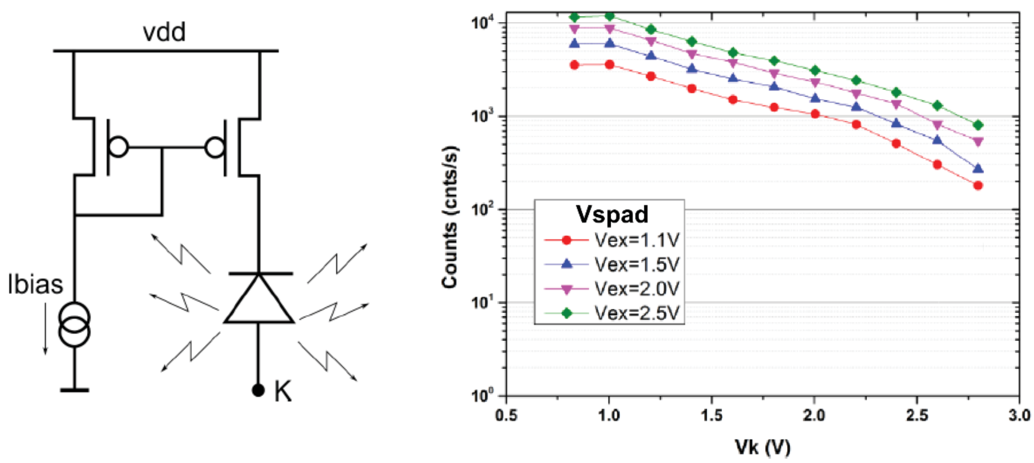


Fig. 2: Bias circuit for the reference emitter (the pMOS is used to control the current) (left) and the change of activity of the SPAD as the voltage applied to the emitter changes (right)

**References**

[1] https://www.idquantique.com/random-number-generation/products/quantis-random-number-generator/
[2] A.Khanmohammadi et al., IEEE Photonics Journal, Volume 7, Number 5, October 2015.
[3] F. Acerbi et al., IEEE Journal of Selected Topics in Quantum Electronics, vol. 24, no. 6, pp. 1-7, 2018.

# Hybrid intensified single photon camera with adaptive gating

**Jerzy Szuniewicz, Konstantin Rusakov, Radek Lapkiewicz**
*Institute of Experimental Physics, Faculty of Physics, University of Warsaw, Poland*

Single photon sensitive cameras have found numerous applications in a wide range of fields including quantum metrology and imaging, 3D time-of-flight measurements, and fluorescence lifetime imaging. Technological platforms of spatially-resolved photon counting include SPAD arrays [2, 3], EMCCD cameras and intensified cameras, with each platform offering different advantages. Intensified cameras allow nanosecond gating, enabling high temporal resolution measurements at megapixel spatial resolution. Moreover single photon events can be easily distinguished from camera readout noise which results in a high SNR. As a result, spatially resolved coincidence photon detection can be performed and used to observe quantum optical effects [1].

Due to the use of either CMOS or CCD sensors, the time between consecutive frame rates obtained by intensified cameras is typically 6 orders of magnitude longer than the minimum gating time of such a system. For instance an I-sCMOS camera Andor iStar can obtain a framerate of 50Hz at a full spatial resolution with the gate length of 2 ns. This results in a very low duty cycle and is therefore inefficient for observation of random processes. For instance, if one wants to observe a photon pair created in Spontaneous Parametric Down Conversion (SPDC) of light from a continuous wave laser, the only way is to gate the intensifier once per camera frame. In this case the length of the intensifier gate constitutes the coincidence window. In order to reduce the rate of accidental photon coincidence detection, the average photon flux should be kept lower than one photon per coincidence window. As a result, most of the frames are empty (no detected photons) and the measurement times are long [1].

We propose and experimentally demonstrate a setup in which the number of photons detected within each frame can be controlled. We achieve this by gating the image intensifier adaptively depending on the number of detected events. Our hybrid intensified camera is built from of-the-shelf components which incorporates an Image Intensifier and two detectors: one with high spatial resolution (sCMOS Camera) and one with high temporal resolution (photomultiplier tube, PMT). Single photon detection at the gated photocathode of the Image Intensifier (II) results in generation of a short pulse of light at the output of the II. Light from such pulses is imaged with a system of lenses and a beamsplitter on two detectors (an sCMOS Camera and a PMT). The signal of the detected photons is registered by the PMT and converted into TTL pulses by a discriminator. A custom FPGA registers the signal of detected photons and a signal of the camera acquisition and controls the gate of the II. With such a feedback loop we can control the gating time and ensure that each frame will contain a chosen number of detected photons. This allows for much more versatility for planning the measurement and allows to drastically reduce the experiment time.

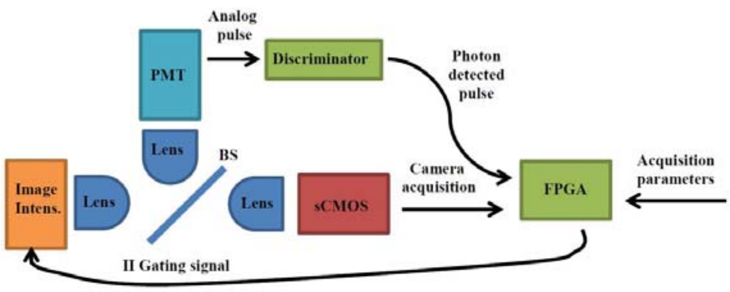


Fig. 1 Schematic of the experimental setup which allows for adaptive gating of the Image Intensifier without interrupting the measurement. FPGA registers signals from the setup and controls the Image Intensifier gate.

With our system, the gating time of the image intensifier is adjusted to the rate of event detection in real time. On-the-fly data analysis is performed with a custom FPGA. We show the use of adaptive gating with photon pairs from the SPDC process and analyze the average duration of the gated frames for different photon fluxes. The use of our system can increase the data acquisition rate and therefore enable photon counting experiments which were not feasible using standard intensified cameras.

**References**

[1] Chrapkiewicz, R., Jachura, et al. (2016). Hologram of a single photon. Nature Photonics, 10(9), 576.

[2] Bronzi, D., et al. (2014). 100 000 frames/s 64× 32 single-photon detector array for 2-D imaging and 3-D ranging. IEEE journal of selected topics in quantum electronics, 20(6), 354-363.

[3] Niclass, C., et al. (2005). Design and characterization of a CMOS 3-D image sensor based on single photon avalanche diodes. IEEE Journal of Solid-State Circuits, 40(9), 1847-1854.

# Research toward realization of NbTiN SSPD imaging array system

**Shigehito Miki[1,2], Masahiro Yabuno[2], Shigeyuki Miyajima[1] and Hirotaka Terai[1]**

[1]*Advanced ICT Research Institute, National Institute of Information and Communications Technology, Kobe, Japan*

[2]*Graduate School of Engineering Faculty of Engineering, Kobe University, Kobe, Japan*

Superconducting nanowire single-photon detector (SSPD or SNSPD [1]) has high detection efficiency in a wide spectral range, low dark count rate, small timing jitter, and high maximum counting rate without after-pulsing. Accordingly, if SSPD array system with large number of pixels is realized, it would be a novel single photon imager with those attractive features of SSPD. A critical issue in development of practical SSPD imaging array with a large number of pixels is how to reduce the number of readout lines resulting in significant heat inflow from room temperature to cryogenic environment. To overcome this, we have proposed and been developing multipixel SSPD array system with cryogenic signal processor based on superconducting single flux quantum (SFQ) circuits, which can operate at same cryogenic enviroment as SSPD with very low power consumption and hence can drastically reduce the numbrer of readout cables from room temperature enviroment. In this work, we report the development of NbTiN SSPD array system with event-driven SFQ encoder circuit which can encode the address information from SSPD pixels to serial digital codes without degrading temporal resolution. First, we successfully developed and demonstrated the 64 pixel NbTiN SSPD array with 64 input channels SFQ encoder circuit installed in a 0.1 W GM-cryocooler system [2]. We were able to obtain an address and high resolved temporal information for the photon detection in the SSPD even through the SFQ encoder. The overall observed FWHM jitter was 56.5 ps. In addition, we are trying to increase the number of SSPD pixels by adopting a row-column readout architecture [3] in our SSPD array system. Since this architecture allows to read out an N×N pixel SSPD array using 2×N readout lines, our system can increase the number of pixels to 1024 (32×32) pixel by utilizing 64 input channels SFQ encoder. As a feasibility study, we have developed 16 (4×4) pixel NbTiN SSPD array with row-column architecture and 8 input channels SFQ encoder circuit , and have successfully confirmed the correct operation.

**References**

[1] G. N. Gol'tsman, O. Okunev, G. Chulkova, A. Lipatov, A. Semenov, K. Smirnov, B. Voronov, A. Dzardanov, C. Williams, and R. Sobolewski, “Picosecond superconducting single-photon optical detector,” Appl. Phys. Lett., 79, 705–707, 2001.

[2] S. Miyajima, M. Yabuno, S. Miki, T. Yamashita, and H. Terai, “High-time-resolved 64-channel single-flux quantum-based address encoder integrated with a multi-pixel superconducting nanowire single-photon detector,” Opt. Exp., 26, 29045-29054, 2018.

[3] V. B. Verma, R. Horansky, F. Marsili, J. A. Stern, M. D. Shaw, A. E. Lita, R. P. Mirin, and S. W. Nam, "A four-pixel single-photon pulse-position array fabricated from WSi superconducting nanowire single-photon detectors," Appl. Phys. Lett., 104, 051115-1-4, 2014.

# Improvement of NbTiN and NbN thin films for superconducting nanowire single photon detectors in vertical and guided architectures on Silicon

**Raouia Rhazi[1, 2], Houssaine Machhadani[1], Julien Zichi[3], Catherine Bougerol[4], Stéphane Lequien[5], Jean-Luc Thomassin[1], Nicolas Mollard[5], Val Zwiller[3], Guillaume Rodriguez[6], Richard Souil[6] Eva Monroy[1], Ségolène Olivier[2] and Jean-Michel Gérard[1]**

[1] *Univ. Grenoble-Alpes, CEA-IRIG, PHELIQS, 17 av. des Martyrs, 38000 Grenoble, France.*
[2] *Univ. Grenoble-Alpes, CEA-LETI, 17 av. des Martyrs, 38000 Grenoble, France.*
[3] *KTH Stockholm, Department of Applied Physics, SE-114, 128 Stockholm, Sweden.*
[4] *Univ. Grenoble-Alpes, CNRS-Institut Néel, 25 av. des Martyrs, 38000 Grenoble, France.*
[5] *Univ. Grenoble-Alpes, CEA-INAC, MEM, 17 av. des Martyrs, 38000 Grenoble, France.*
[6] *Univ. Grenoble-Alpes, CEA-LETI, DPFT, 17 av. des Martyrs, 38000 Grenoble, France.*

There is an increasing demand of highly efficient detectors of single photons for many emerging fields such as quantum key distribution, time-of-flight depth ranging applications, and singlet oxygen detection for medical screening. Today, thin films such as NbN and NbTiN are widely used materials for superconducting single photon detection technology thanks to their good superconducting properties and high degree of stability after several thermal cycles.

The use of III-nitride semiconductors as a buffer layer for Nb(Ti)N presents interesting advantages, since GaN and AlN are almost lattice matched with Nb(Ti)N, and they are transparent to visible and near-IR radiation.

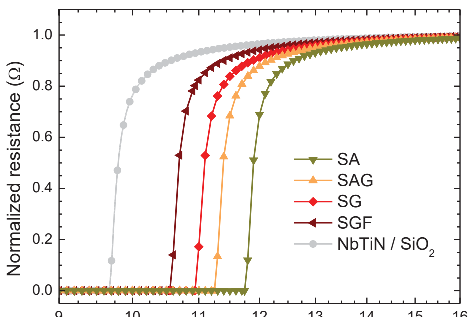


*Figure 1: Critical temperature of NbTiN grown on different subsrates*

For this work, we started first by studying the impact of a crystalline III-nitride (GaN or AlN) buffer layer on the properties of ultrathin films of NbTiN (11nm) deposited by reactive magnetron sputtering [1]. Best results were obtained using AlN, which leads to NbTiN with a superconducting critical temperature $T_c$ = 11.8 K, and sharp superconducting transition ($\Delta T$ = 0.83 K) as shown in figure 1. This is a major improvement in comparison with NbTiN deposited on $SiO_2$ on Si ($T_c$ = 9.8±0.3 K with $\Delta T \approx$ 0.87). The first SNSPD in vertical cavity on AlN have been demonstrated[1].

Now we are developing high-quality NbN material with ultra-thin AlN buffer layer on 8" SOI wafers in order to build integrated detectors with silicon waveguides. A thin AlN layer of 10 nm was developed, leading to improved crystallinity of the NbN material and thus to a higher critical temperature of 9K with a sharp superconducting transition. The good performances of the material for single photon detection were validated in a vertical cavity architecture (figure3). Integrated SSPDs on silicon waveguides (figure 2) is a key component for future large-scale quantum photonic integrated circuits to generate manipulate and detect a large number of photonic qubits for secure communications and quantum computing applications.

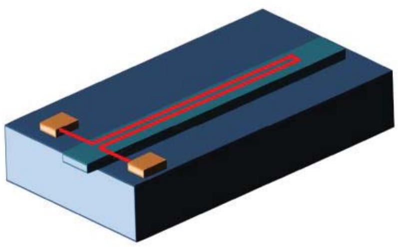

*Figure 2: : SSPDs in waveguide geometry*

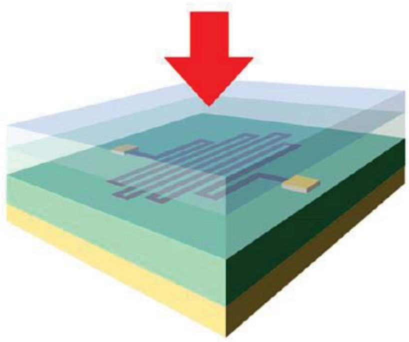

*Figure 3: SSPDs in vertical geometry*

[1] Machhadani et al., SST 32 035008 (2019).

# Direct measurement of the recovery time of SNSPDs

**C. Autebert[1,2], G. Gras[1,2], E. Amri[1,2], M. Perrenoud[1], M. Caloz[1], H. Zbinden[1], F. Bussières[1,2]**

[1]*Group of Applied Physics, University of Geneva, CH-1211 Geneva 4, Switzerland*

[2] *ID Quantique, CH-1227 Carouge, Switzerland*

Superconducting nanowire single-photon detectors (SNSPDs) are a key technology for optical quantum information processing [1]. Their low dark count rate, fast response time, small jitter, and high system detection efficiency (SDE) favours their use in various demanding quantum optics applications such as high-speed or long-distance quantum key distribution, quantum networking, device-independent quantum information processing and deep-space optical communication.

Determining the recovery time of a single-photon detector efficiency after a first detection allows to obtain the most complete information about the detector's time dynamics as well as making general predictions about its performances in applications such as quantum communication. But this is a non-trivial problem, as the current value in the detector after a detection depends on the electro-thermal feedback and high photon count rates can influence the dynamics in a non-trivial manner. Here we will report on a simple and highly sensitive method of characterizing SNSPDs in terms of recovery time for different kind of MoSi SNSPDs structures [2], especially in the limit of the high-count rate regime. The method used is based on an auto-correlation measurement between successive detection, where the first detection is triggered with a pulsed laser and the second one with a CW laser. It allows a fast and direct observation of the recovery of the efficiency, as well as to investigate in a fast way afterpulsing effect and tiny reflections in the setup (see figure). This technique is also applicable to any wavelength and any single-photon detector (Fig. 1). Furthermore, its results are directly usable for other experiments requiring a precise knowledge of the recovery time of the efficiency, such as ultra-fast quantum key distribution protocols [3] or ultra-fast single-photon sources [4] and we believe that it could become a benchmark measurement of detectors for this kind of applications. We use this technique to study the recovery time dependency on the bias current in the detector and the detector's kinety inductance.

Finally, we will describe several applications such as long-distance quantum key distribution [5] and characterization of novel integrated photon pairs source [6].

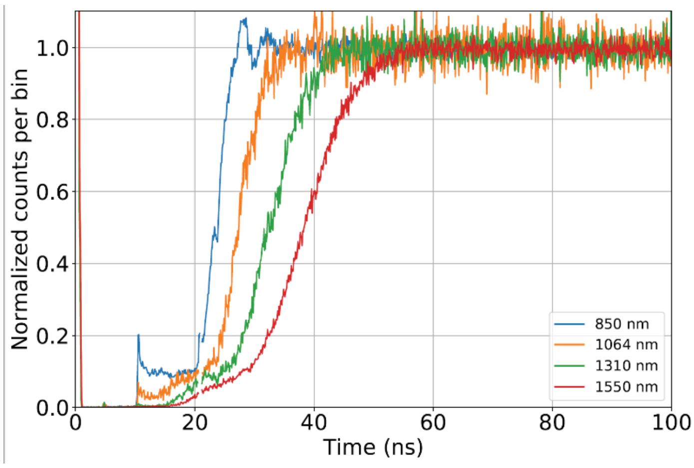


Fig. 1: Normalized efficiency as a function of time after a first detection at different wavelengths.

**References**

[1] G. N. Gol'tsman *et al.*, App. Phys. Lett **79**, 705 (2001)
[2] M. Caloz *et al.*, APL **112**, 6 (2018)
[3] A. Tanaka *et al.*, Opt. Exp. **16**, 15 (2008)
[4] L. A. Ngah *et al.*, Laser & Phot. Rev. **9**, 2 (2015)
[5] A. Boaron *et al.*, Phys. Rev. Lett. **121**, 190502 (2018)
[6] F. Samara *et al.*, Opt. Exp. **27**, 14 (2019)

# High-yield waveguide-integrated superconducting nanowire detectors with saturating internal quantum efficiency

**S. M. Buckley, J. T. Chiles, A. N. McCaughan, A. N. Tait, R. P. Mirin, S. W. Nam, J. M. Shainline**

*National Institute of Standards and Technology, NIST, Boulder CO 80301*

Waveguide-integrated superconducting nanowire single photon detectors have broad range of applications both for classical and quantum technologies. To realize larger and more complex integrated photonic circuits, these must have a high yield with a high on-chip detection efficiency. In this study, we use a high Si content, reduced thickness $W_xSi_{1-x}$ material to demonstrate Si integrated circuits of up to 15 detectors each, showing 100% detector yield with saturating internal quantum efficiency and fabricated with UV I-line stepper photolithography. We optimize the detector geometry and measure the ratio of background scattered to the waveguide coupled light, an important metric for on-chip nonlinear quantum light sources.

The nanowires were fabricated by depositing 2.2 nm of WSi onto a silicon wafer with a silicon nitride insulating spacer layer on the surface, then patterning with UV I-line photolithography and plasma etching. The standard nanowire width was 475 nm. They were fabricated in an out-and-back geometry using an on-chip meandered inductor to protect from latching. Si waveguides were then patterned with electron beam lithography and etched with an $SiO_2$ hardmask and a pseudo bosch etch chemistry. A 50 um SU8 layer was used for packaging the fibers to the chip, as described in [1]. Two types of devices were fabricated. The first were high dynamic range detector arrays (HiDRA), shown in schematic in Fig. 1 (a). There are three HiDRA connected by one grating in the figure. Each HiDRA is a waveguide with a series of five beam taps, each designed to have a splitting ratio of either 90/10, 99/1 or 999/1. For example in a 90/10 HiDRA, the first detector receives 90% of the light, the second detector 9% of the light, and so on (fabricated devices deviate from these designed values). An optical microscope image of a fabricated device illustrating this is shown in Fig. 1 (b). We first tested the uniformity of these detectors by flood illuminating with light at 1.55 µm. Fig. 1 (c) shows the response of ten detectors illuminated in this way. The difference in switching current and dark counts between the detectors is likely a result of imperfections in the photolithography mask, as electron beam lithography in the same material gives more uniform results. However, a large region of saturated internal quantum efficiency is seen for every detector, and there is a single bias current at which every detector exhibits saturated internal quantum efficiency, as illustrated by the blue shaded region in Fig. 1 (d). We next couple light through an on chip grating. A single input grating is used to split the light to three different HiDRAs, such that 15 detectors are coupled to the same input (see Fig. 1 (a)). Fig. 1 (d) shows the counts versus bias curve when the same HiDRA is waveguide coupled. Finally, to further verify that the light is waveguide coupled, we fabricated several devices with an intentionally broken waveguide connected to the detectors. We then scan the laser power and measure counts on all devices. We can see that the broken waveguide devices are 40 dB suppressed when compared with the highest coupled detector. This demonstrates that for our chips, the scattered light level is 40 dB below the coupled light.

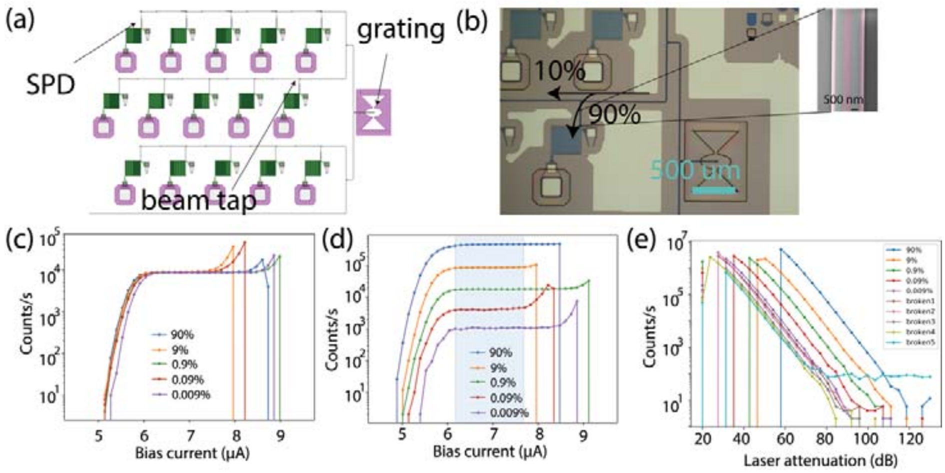


Fig. 1 The HiDRA device (see text).

The second type of device are trees of 50/50 beamsplitters which split the light to seven detectors and one reference grating. These devices are still under test at this time.

## References

[1] Shainline et al., Optics Express Vol. 25, Issue 9, pp. 10322-1033 (2017)

# Superconducting nanowire single photon detectors with high efficiency and low dark count rate


**Lixing YOU[1,2,3,*], Weijun ZHANG[1,2], Hao LI[1,2], Xiaoyan YANG[1,2], Zhen WANG[1,2], Xiaoming XIE[1,2]**

*[1] State Key Laboratory of Functional Materials for Informatics, Shanghai Institute of Microsystem and Information Technology (SIMIT), Chinese Academy of Sciences, 865 Changning Rd., Shanghai 200050, China*

*[2] CAS Center for Excellence in Superconducting Electronics (CENSE), Shanghai 200050, China*

*[3] Shanghai Photon Technology Co Ltd, Shanghai 200050, China*

** Email: lxyou@mail.sim.ac.cn*


As a novel single photon detector(SPD), superconducting nanowire single photon detector (SNSPD) surpasses the semiconducting SPDs with many merits, such as high detection efficiency, low dark count rate, low timing jitter, higher counting rate etc. SNSPDs have advanced various QIP experiments in the past decade. Now you may buy the commercial SNSPD systems including the cryogenics from several start-up companies. In this talk, we will present the latest results of SNSPDs developed by SIMIT. We will show how to improve the detection efficiency of NbN SNSPDs with optimized optical design, with ion implantation. We will also show the methods and results on suppressing the dark count rate of SNSPD, with on-chip filter, with filter integrated on the tip of pigtail, and with low temperature filter bench. The SNSPDs with high efficiency and low dark count rate have been applied in various applications such as QKD, optical quantum simulation, LIDAR, quantum random number generation etc.
.

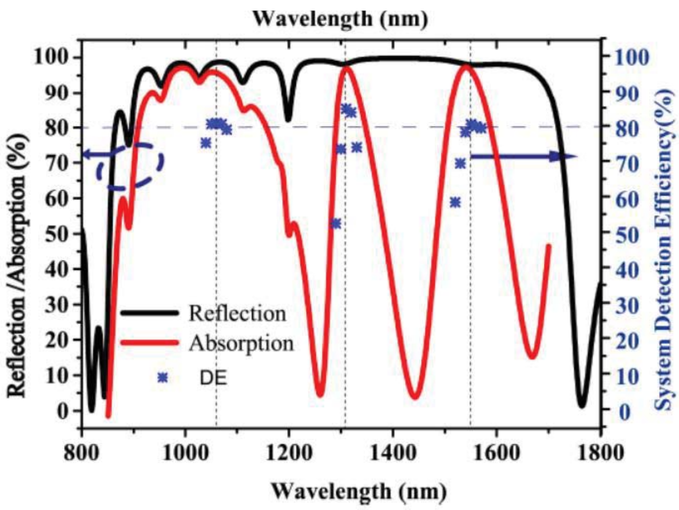


Fig. 1: Multispectral SNSPD with high efficiency over 80% at three distinct wavelengths[OE 27: 4727 (2019)] .

**References**


[1] W. Zhang et al. NbN superconducting nanowire single photon detector with efficiency over 90% at 1550 nm wavelength operational at compact cryocooler temperature. Science China Physics, Mechanics & Astronomy 60(12): 120314. (2017)

[2] H. Li et al. Multispectral superconducting nanowire single photon detector. Optics Express 27(4): 4727-4733. (2019)

[3] W. J. Zhang et al. Fiber-coupled superconducting nanowire single-photon detectors integrated with a bandpass filter on the fiber end-face. Superconductor Science and Technology 31(3): 035012. (2018)

[4] L. You et al, Superconducting nanowire single photon detection system for space applications. Optics Express 26(3): 2965-2971. (2018)

[5] H.-L. Yin et al, Measurement-Device-Independent Quantum Key Distribution Over a 404 km Optical Fiber. Physical Review Letters 117(19): 190501. (2016)

[6] H.-S. Zhong, et al, 12-Photon Entanglement and Scalable Scattershot Boson Sampling with Optimal Entangled-Photon Pairs from Parametric Down-Conversion. Physical Review Letters 121(25): 250505. (2018)

[7] Y. Liu et al. Device-independent quantum random-number generation. Nature 562(7728): 548-551. (2018)

# Direct calibration of SNSPDs

**Johannes Tiedau, Evan Meyer-Scott, Tim J. Bartley, and Christine Silberhorn**
*Integrated Quantum Optics Group, Applied Physics, University of Paderborn, 33098 Paderborn, Germany*

Accurate calibration of single photon detectors is a demanding task. Typically calibrated attenuators are used to bridge the gap between reference power meters (>100pW) on the one hand and click detectors (<100fW) on the other (for example in Ref. [1]). Here we show a new approach enabling direct light detection over a large dynamic range of 123dB from $10^{-7}$ photons per pulse to over $2 \cdot 10^5$ photons per pulse. This allows direct calibration of SNSPDs without the need for calibrated attenuators [2]. In addition our setup is robust and easy to use enabling fast calibration.
The new calibration approach is based on a simple setup using a single beam splitter and a fiber delay loop (Fig. 1a). Pulsed light is sent to this setup and some fraction is coupled into the loop. Depending on the beam splitter reflectivity and loop loss, a specific ratio is coupled out of the loop each round trip, resulting in an exponentially decreasing pulse train. We investigate the click probability for this outgoing pulse train in the time domain (time bins, Fig. 1b). This time multiplexing setup was introduced by [3] and investigated in the few photon regime in the past. Here we explore the response behavior for high light intensities where saturation of the first bins is inherent (area I Fig. 1b). Saturation effects are typically treated as a limiting factor for multiplexing. However, in case of decreasing light intensities as given by this setup, far from the saturated region, the click detector responds linearly to the incident light intensity. Higher light intensities will shift this region to higher bin numbers. By exploiting this fact, and that the saturation of the early bins does not change the response of the detector at later bins, we can extract the incident light levels with high accuracy over a large dynamic range. To do so, we can show that, perhaps surprisingly, SNSPDs have a higher latching threshold if a large number of photons arrive in a single pulse compared to an equivalent CW power level. In our experiment over 200000 photon/s per pulse with a laser repetition rate of 50kHz can be send to SNSPDs without any latching. This corresponds to an average optical power value above 1nW. We also present a calibration routine converts the measured click probabilities to a mean photon number enabling direct calibration of SNSPDs without the need for calibrated attenuators.

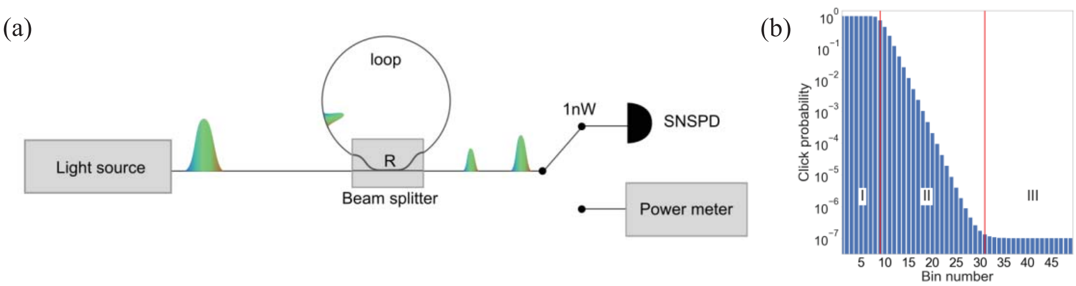


Fig. 1 (a) Schematic picture of the calibration setup. An incoming pulse is send to a beam splitter connected to a fiber loop. Each roundtrip some proportion of the light is coupled out of the loop resulting in an exponential decaying pulse train. Up to 1nW optical power can either send to a SNSPD detector without latching or to a calibrated power meter. (b) Typical click probability of the SNSPD detector per time bin. Three different areas can be identified: (I) saturation region with near deterministic click probability, (II) exponential decay region with a linear slope in the logarithmic click probability plot and (III) noise level resulting from dark counts.

**References**

[1] Gerrits, Thomas, et al. "Calibration of free-space and fiber-coupled single-photon detectors." *arXiv preprint arXiv:1906.02258* (2019)
[2] Tiedau, Johannes, et al. "A high dynamic range optical detector for measuring single photons and bright light." *Optics express* 27.1 (2019): 1-15, Patent
[3] Banaszek, Konrad, and Ian A. Walmsley. "Photon counting with a loop detector." *Optics letters* 28.1 (2003): 52-54.

# Prospects of single-photon detection in micron-wide superconducting strips for practical applications

**Yu. Korneeva[1], N. Manova[1], M. Polyakova[1,2], E. Smirnov[1], D. Vodolazov[1,3], A. Korneev[1,2]**

[1]*Moscow State Pedagogical University, Moscow, Russia*

[2]*National Research University Higher School of Economics, Moscow, Russia*

[4]*Institute for Physics for Microstructures, Russian Academy of Sciences, Nizhny Novgorod, Russia*

In many applications of quantum optics there is a strong need of optical coupling from free space or from a multi-mode optical fibres. On the other hand, a superconducting nanowire single-photon detector (SNSPD) [1] has become a device of choice in study of single-photon sources, single-molecule fluorescence, quantum computing and quantum cryptography. Most of the realizations of SNSPDs (including commercially available) exploit meander-shape design of the superconducting strip with the width of about 100 nm and covering maximum area of 15 µm x 15 µm or a 10 -- 15 µm in diameter circle; thus, significantly hampering free-space and multimode fibre coupling. There are reports on SNSPD coupling to multi-mode fibres. A straightforward solution, i.e. long meandering strip covering e.g. 30 µm x 30 µm area results in ~200 ns response time and 74 ps timing jitter [2] due to large kinetic inductance of the strip (and even larger response time and jitter for 100- µm-in-diameter SNSPD [3]). More elaborated designs require either a complicated micro-lens optics focusing light from the multimode fibre to the small area of SNSPD, or a multiplexed connection of several small-area meanders [4].

We shall present an alternative approach to the large-area SNSPD design based on our recent discovery of single-photon response in micron-wide superconducting strips [5]. The solution of the time-dependent Ginzburg-Landau equations predicts that if the superconducting strip is biased sufficiently close to the depairing current (e.g. above 70%) and the bias current is distributed uniformly over the strip cross-section, the single-photon response is expected even in infinitely wide strip [6]. Here we present the SNSPD made as a 20 to 50-µm-diameter spiral with the 1-µm-wide strip. The device characterization results will be presented.

The work is supported by the Russian Science Foundation (RSF) Project No.17-72-30036.

**References**

[1] C. M. Natarajan, M. G. Tanner, and R. H. Hadfield, Supercond. Sci. Technol. 25, 063001 (2012).
[2] Min, G. et al., Chin. Phys. B, 24(6), (2015)
[3] Lv, C. L. et al. (2017), Supercond. Sci. Technol, 30(11), p. 115018.
[4] Murphy, R. P. et al. (2015), SPIE Sensing Technology + Applications, 9492, p. 94920E.
[5] Yu.P. Korneeva et. al. Phys. Rev. Appl. 9, 064037 (2018)
[6] D. Y. Vodolazov, Phys. Rev. Appl. 7, 034014 (2017)

# Physics of single-photon detection in micron-wide superconducting strips

**Yu. Korneeva[1], N. Manova[1], M. Polyakova[1,2], E. Smirnov[1], D. Vodolazov[1,3], A. Korneev[1,2]**

[1]*Moscow State Pedagogical University, Moscow, Russia*

[2]*National Research University Higher School of Economics, Moscow, Russia*

[3]*Institute for Physics for Microstructures, Russian Academy of Sciences, Nizhny Novgorod, Russia*

Superconducting nanowire single-photon detector (SNSPD) [1] is a novel and rapidly evolving type of the detector which was successfully used in many applications ranging from quantum cryptography to deep space optical communication. Meanwhile, the physics of SNSPD operation is not quite clear yet.

Until recently the SNSPD was described by the "geometric hot-spot model" first presented in Ref. [2] and improved further in subsequent works (a good review of SNSPD detection mechanisms is given in Ref. [3]). In the framework of the "geometric model" it is assumed that the single photon detection occurs only in a superconducting strip with a width comparable to the size of the hot spot, being in the range of 50 to 150 nm. It has led to devices consisting of fairly narrow and very long strips arranged in such a way that they fill a much larger area for good optical coupling. A more thorough theoretical approach is applied to the problem of photon-detection in a superconductor in Ref [4]. It is based on the theory of non-equilibrium superconductivity capable of treating processes depending on space and time. It predicts that in samples with a supercurrent above ~0.7 of the depairing current, and uniform over the cross-section of the strip, the detection efficiency is not dependent on the width of the strip. Recently we have experimentally demonstrated single-photon detection in up-to 5-micron-wide constriction-type bridges made of polycrystalline NbN, using photons of wavelength ranging from 408 nm to 1550 nm [5].

Here we present the study of the single-photon detection in straight NbN strips with the width ranging from 0.5 to 5 μm. In these samples, we clearly observe a step-like dependence of the detection efficiency on the bias current in wavelength range below 1.3 μm prompting 100% internal detection efficiency (IDE), i.e. each absorbed photon produces a 'click' of the detector. The check of the model is performed by the study of photon count rate dependence on the magnitude of the magnetic field perpendicular to the sample.

The work is supported by the Russian Science Foundation (RSF) Project No.17-72-30036.

**References**

[1] C. M. Natarajan, M. G. Tanner, and R. H. Hadfield, Supercond. Sci. Technol. 25, 063001 (2012).
[2] A. Semenov, G. Goltsman and A. Korneev, Physica C, 351, 349-356 (2001)
[3] A. Engel, J J Renema, K Il’in and A. Semenov Supercond. Sci. and Technol., 28, 114003 (2015)
[4] D. Y. Vodolazov, Phys. Rev. Appl. 7, 034014 (2017).
[5] Yu.P. Korneeva et. al. Phys. Rev. Appl. 9, 064037 (2018)

# Superconducting single photon detectors on 3C silicon carbide

**F. Martini, A. Gaggero, F. Mattioli and R. Leoni**
*Istituto di Fotonica e Nanotecnologie - CNR, Via Cineto Romano 42, 00156 Roma, Italy*

We implemented superconducting nanowire single photon detectors (SNSPDs) on top of 3C silicon carbide (SiC). This material is among the most promising candidates for the development of a photonic platform for large-scale quantum-optics experiments, due to the coexistence of both quantum emitters and a non-centrosymmetric crystal structure. The atom-like behavior of SiC divacancies, together with the possibility of a fast optical modulation, are essential for photonic quantum technologies. As both SiC linear photonics and solid-state emitters are undergoing a fast development [1] [2], the fabrication of SNSPDs atop this material constitutes the last fundamental building block towards a monolithic platform for quantum technologies. Nevertheless, the fabrication of SNSPDs on SiC was hampered from a generally poor surface quality and from the difficulties in its micromachining. Here we employed a chemical mechanical polished SiC layer with a RMS roughness < 1nm and a novel technique for the alignment of multiple SNSPDs with standard fibers for their electro-optical characterization at the telecom frequency range (Fig.1a). The alignment is obtained thanks to both a 6 channel fiber array controlled by a 6-axis stage and two alignment mirrors, where the light coming from a CW laser is reflected from the substrate surface and collected from the same fiber. We obtained a maximum of the reflected light when the fiber is placed on top of the Au mirror. Once both the first and the sixth fiber were aligned on the corresponding mirrors, the FA is glued to the sample using a cyanoacrylate adhesive and cooled down for electro-optical characterization. The measured system detection efficiency indicates an internal efficiency of the superconducting nanowire close to unity (Fig.1b), where the system detection efficiency (SDE) reaches the value of ~5.5% that corresponds to the maximum value expected from numerical simulations. These results show that high detection-efficiency SNSPDs can be integrated in SiC photonic platforms, boosting the range of applications allowed by this platform.

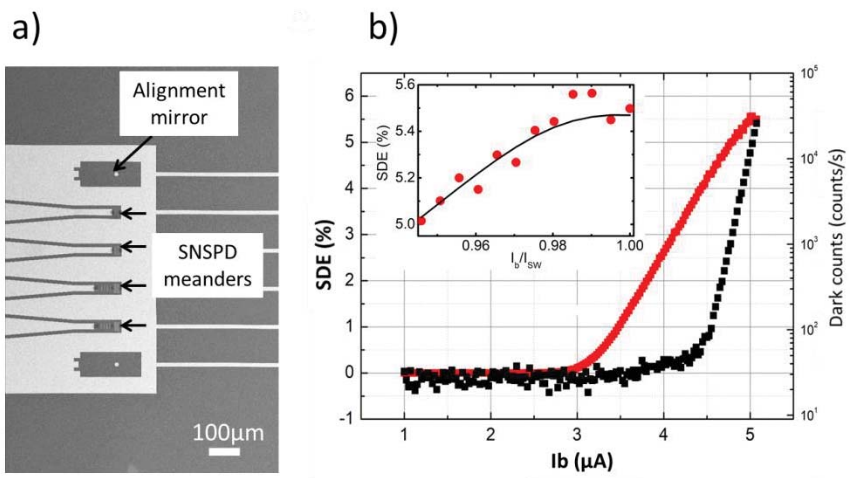


Fig. 1 a) Device layout with four SNSPDs fabricated on top of 3C SiC together with two alignment mirrors. b) Detection efficiency of the 60nm-wide 3x3µm$^2$ meander with a saturated SDE for $I_b \approx I_c$ (inset).

**References**

1. W. F. Koehl, B. B. Buckley, F. J. Heremans, G. Calusine, and D. D. Awschalom, "Room temperature coherent control of defect spin qubits in silicon carbide.," Nature **479**, 84–87 (2011).
2. F. Martini and A. Politi, "Linear integrated optics in 3C silicon carbide," Opt. Express **25**, 10735–10742 (2017).

# Accurate detection of arbitrary photon statistics

**J. Hloušek[1], M. Dudka[1], I. Straka[1], and M. Ježek[1]**

[1] *Department of Optics, Palacký University, 17. listopadu 1192/12, 771 46 Olomouc, Czech Republic*

The probability distribution of the number of photons in an optical mode carries a great deal of information about physical processes that generate or transform the optical signal. Precise characterization of photon statistics is a crucial requirement for many applications in the field of photonic quantum technology such as quantum metrology [1,2], non-classical light preparation and quantification [3,4,5], quantum secure communication [6], and photonic quantum simulations [7,8,9]. Measurement of statistical properties and non-classical features of light also represents enabling technology for many emerging biomedical imaging and particle-tracking techniques [10,11].

We present a fully reconfigurable near-ideal photon-number-resolving detection scheme with custom electronic processing and a novel photon statistics retrieval method using expectation-maximization iterative algorithm weakly regularized by the maximum-entropy principle [12]. We achieve unprecedentedly accurate measurement of various photon-number distributions of chaotic, classical, non-classical, non-Gaussian, and negative-Wigner-function light. Despite uncorrected systematic errors and significant variability of the input signal, our approach shows superior fidelity across the board with typical values exceeding 99,8% for mean photon numbers up to 20 and the $g^{(2)}$ parameter reaching down to a fraction of a percent. Our results open new paths for optical technologies by providing full access to the photon-number information without the necessity of detector tomography.

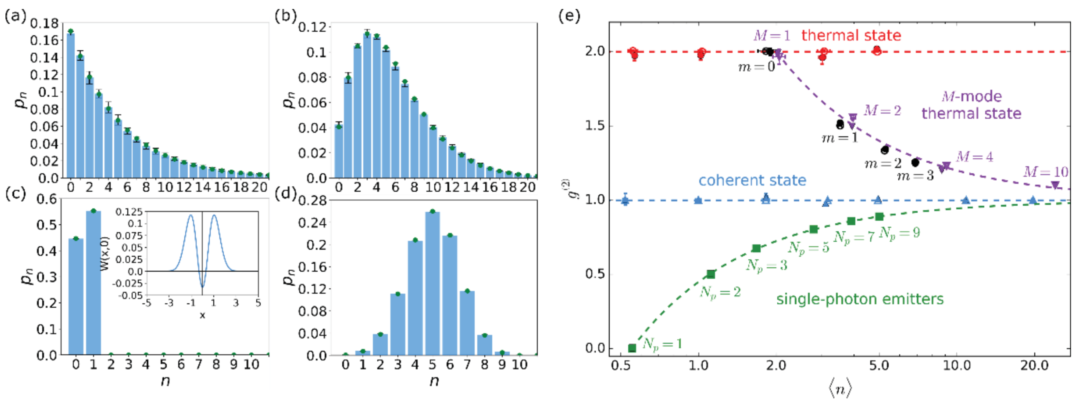


Fig. 1: Measured (blue bar) and the corresponding theoretical photon statistics (green dot) for (a) Thermal state with < n>=5, (b) 2-photon subtracted thermal state, (c) single-photon and (d) 9-photon states emulating emission from clusters of single-photon emitters. Inset: Wigner function evaluated from the measured statistics. (e) The normalized second-order intensity correlation $g^{(2)}$ evaluated from the measured photon statistics of various optical signals with mean photon number < *n*>.

## References

[1] J. C. F. Matthews, et al., Towards practical quantum metrology with photon counting, npj Quantum Information 2, 16023 (2016).
[2] S. Slussarenko, et al., Unconditional violation of the shot-noise limit in photonic quantum metrology, Nat.Photonics 11, 700-703 (2017).
[3] G. Harder, et al., Single-mode parametric-down-conversion states with 50 photons as a source for mesoscopic quantum optics, Phys. Rev. Lett. 116 (2016).
[4] I. Straka et al., Quantum non-Gaussian multiphoton light, npj Quant. Inf. 4, 4 (2018).
[5] H. E. Kondakci, et al., Sub-thermal to super-thermal light statistics from a disordered lattice via deterministic control of excitation symmetry, Optica 3, 477 (2016).
[6] J. F. Dynes, Testing the photon-number statistics of a quantum key distribution light source, Optics Express 26, 22733 (2018).
[7] M. D. Vidrighin, et al., Photonic Maxwell's demon, Phys. Rev. Lett. 116 (2016).
[8] N. Cottet, et al., Observing a quantum Maxwell demon at work, Proc. Natl. Acad. Sci. U.S.A. 114, 7561-7564 (2017).
[9] J. Hloušek, et al., Sci. Rep. 7, 13046, (2017).
[10] H. Ta, et al., Mapping molecules in scanning far-field fluorescence nanoscopy, Nat. Commun. 6, 7977 (2015).
[11] S. J. Sahl, et al., Fluorescence nanoscopy in cell biology, Nat. Rev. Mol. Cell Biol. 18, 685--701 (2017).
[12] J. Hloušek, et al., Accurate detection of arbitrary photon statistics, arXiv:1812.02262.

# Two Billion Photons Per Second, One Photon at a Time

**Timothy Rambo, Amy Conover, Aaron Miller**
*Quantum Opus LLC, Novi, Michigan, USA*

The wildly successful commercialization of superconducting nanowire single-photon detector (SNSPD) technology has fulfilled a long-time need of the quantum optics community for high efficiency, low-noise, low-jitter detection technology[1]. Now that the technology is infused into the community, researchers are looking ahead with new goals[2] and asking for "more": more channels, more counts per second, more optical bandwidth, and even more efficiency. As part of an industry-wide push to meet these demands, we report construction of a 32-channel SNSPD system in a 3U cryostat enclosure with two 16-channel 1U electronics modules.

The system is optimized for operation at 900 nm with mean *system* detection efficiency of 91.3% (including front panel connector loss) with estimated ±2% systematic calibration error, ≤1 dark-counts per second per channel, and 14.5 ns reset-time to full efficiency. Across all channels, the system can count 2.2 Billion photons per second at full efficiency with ≤32 dark counts per second. To achieve the high (69 MHz per channel) count-rate, we employed a novel cryogenic DC coupling circuit[3] that provides bias input to, and DC-coupled RF output from, each detector with a single coaxial connection at room temperature. Compared to conventional DC coupling techniques this is a two-fold reduction in wiring and the associated heat-load, volume, and feedthrough space requirements. The SNSPDs were fabricated by Quantum Opus using our standard commercial process.

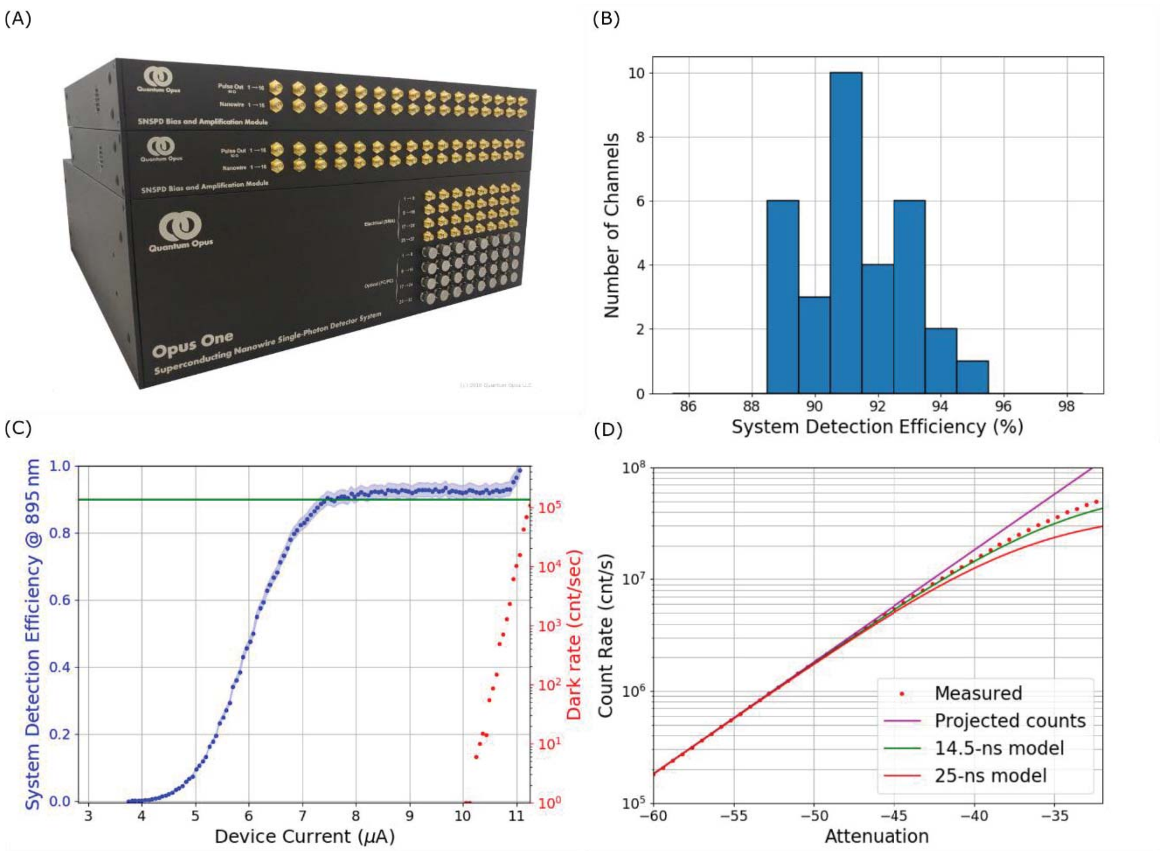


Fig. 1(A) A photo of the 32-channel SNSPD system in 3U enclosure with two 16-channel 1U electronics modules, external compressor not shown (B) Histogram of system detection efficiencies (C) Efficiency and dark counts as a function of device bias for a representative device, the green line is at 90%, shading indicates estimated ±2% systematic calibration uncertainty. (D) Poisson pile-up data with models for representative device under CW illumination.

## References

[1] F. Marsili et al. Nature Photonics volume B, pages 210–214 (2013)
[2] H. Wang et al. Nature Photonics volume 11, pages 361–365 (2017)
[3] Patent Pending (application number 16/399,207)

# Calibration of free-space single-photon detectors using 10-element transmittance traps

**Christopher Chunnilall[1*], Geiland Porrovecchio[2†], Robert Starkwood (Kirkwood)[1], Marek Smid[2]**

[1]*National Physical Laboratory (NPL), Hampton Road, Teddington, TW11 0LW, U.K.*

[2]*Cesky Metrologicky Institut (CMI), V Botanice 4, 15072 Praha 5, Czech Republic*

* christopher.chunnilall@npl.co.uk , † geiland.porrovecchio@cmi.cz

The measurement of light at the single-photon level underpins a rapidly-developing range of applications. These range from applications transitioning into the single-photon regime in order to provide improved sensitivity and/or energy efficiency, as well as new applications that operate solely in this regime, such as quantum key distribution and certain types of quantum random number generators.

NPL and CMI have developed facilities for calibrating free-space coupled single-photon detectors in the silicon spectral region which use a ten-element trap (10ET) with transmittance of the order of $10^{-5}$ as the attenuating element [1]. The 10ET provides a fixed attenuation and a measure of the optical power incident at its entrance. The NPL facility uses its 10ET as a linear, but not absolute, attenuator while at CMI their 10ET is used as a monitor detector and attenuator.

At NPL, the power transmitted by its 10ET is measured by a three-element silicon photodiode trap detector (3ET) at a high incident power on the 10ET (< 0.1 mW). The photocurrent ratio from the traps is also measured. The 3ET carries the SI reference. The transmittance and responsivity of the 10ET are taken to be independent of the incident optical power (< 0.1 mW), once the alignment and polarisation of the beam through the 10ET remain constant. The power incident on the 10ET can then be reduced, and the 10ET photocurrent used to infer the photon flux incident at the 3ET. The 3ET and the device under test (DUT) are both mounted on a motorised linear translation stage, and the DUT can be positioned where the 3ET was located, and its detection efficiency measured. At the DUT, the beam waist diameter is ~ 25 μm (FWHM), photon fluxes can be less than 1000 photons $s^{-1}$, and detection efficiency can be measured with an uncertainty of less than 1% ($k$=2) for detectors with good spatial uniformity of response.

At CMI, their 10ET is used as an attenuator and as a detector to monitor the temporal stability of the incident laser radiation. The photocurrent induced by the input beam at the first two photodiodes of the 10ET is measured using a calibrated switched integrator amplifier (SIA) [2]. The SIA uses a 100 pF integration capacitor, and the I/V conversion factor can be varied from $1 \times 10^7$ to $1 \times 10^{10}$. The DUT and a calibrated reference detector, the Low Photon Flux standard detector (LOFD) [3], are then mounted on a motorised linear translation stage. The DUT and LOFD are sequentially illuminated by the focussed attenuated beam. The noise equivalent power of the LOFD can be as low as 1 fW $Hz^{-½}$, enabling provision of SI traceability down to the photon-counting regime; photon fluxes of the order of $1 \times 10^5$ photons $s^{-1}$ have been measured with a noise to signal ratio below 3% for a measurement time of 80 s.

A detailed description of the facilities, and the uncertainty budgets for measurement at 633 nm and 850 nm, will be presented.

**References**

[1] T. Kubarsepp and M. White, *Applied Optics,* **49**, 3774-3779, (2010).
[2] J. Mountford, G. Porrovecchio and M. Smid, *Applied Optics,* **30**, 5821-5828, (2008)
[3] G. Porrovecchio, M. Smid, M. Lopez, B. Rodiek, S. Koeck and H. Hofer, *Metrologia,* **53**, 1115-1122, (2016)

*This work was funded by project EMPIR 14IND05 MIQC2 (NPL and CMI) and Innovate UK ISCF Pioneer Project 104616 (NPL). Project EMPIR 14IND05 MIQC2 received funding from the EMPIR programme co-financed by the Participating States and from the European Union Horizon 2020 research and innovation programme.*

# Talbot Effect of OAM lattices with single photons

**S. Schwarz[1, 2], C. Kapahi[1, 2], R. Xu[1, 3], A.R. Cameron[1, 2], D. Sarenac[1, 2], J.P.W. MacLean[1, 2], K.B. Kuntz[1, 2], D.G. Cory[1, 4, 5, 6], T. Jennewein[1, 2], K.J. Resch[1, 2], D.A. Pushin[1, 2],**

[1] *Institute for Quantum Computing, University of Waterloo, Waterloo, ON, Canada, N2L 3G1*

[2] *Department of Physics & Astronomy, University of Waterloo, Waterloo, ON, Canada, N2L 3G1*

[3] *Department of Electronic & Computer Engineering, University of Waterloo, Waterloo, ON, Canada, N2L 3G1*

[4] *Department of Chemistry, University of Waterloo, Waterloo, ON, Canada, N2L 3G1*

[5] *Perimeter Institute for Theoretical Physics, Waterloo, ON, Canada, N2L 2Y5*

[6] *Canadian Institute for Advanced Research, Toronto, ON, Canada, M5G 1Z8*

The self-imaging, or Talbot Effect, that occurs with the propagation of periodically structured waves has enabled several unique applications in optical metrology, image processing, data transmission, and matter-wave interferometry [1]. In this work, we report on the first demonstration of a Talbot Effect with single photons prepared in a lattice of orbital angular momentum (OAM) states. The lattice is prepared by pairs of birefringent linear gradients whose optical axes are perpendicular to each other. Such linear gradients are implemented via "Lattice of Optical Vorticies" (LOV) prism pairs [2]. We observe that upon propagation, wavefronts of the single photons manifest a Talbot Effect whereby the OAM lattice intensity profile is recovered. Furthermore, we show that the intensity at the fractional Talbot distances is indicative of a periodic helical phase structure corresponding to a lattice of OAM states. This phenomenon provides a powerful addition to the toolbox of orbital angular momentum and spin-orbit techniques that have already enabled many recent developments in quantum optics. Such structured beams might present a novel spatial mode to transmit time- and mode-multiplexed information. Moreover, our technique offers a new prospective resource in quantum communication protocols and free-space communication links based on OAM and spin-orbit states.

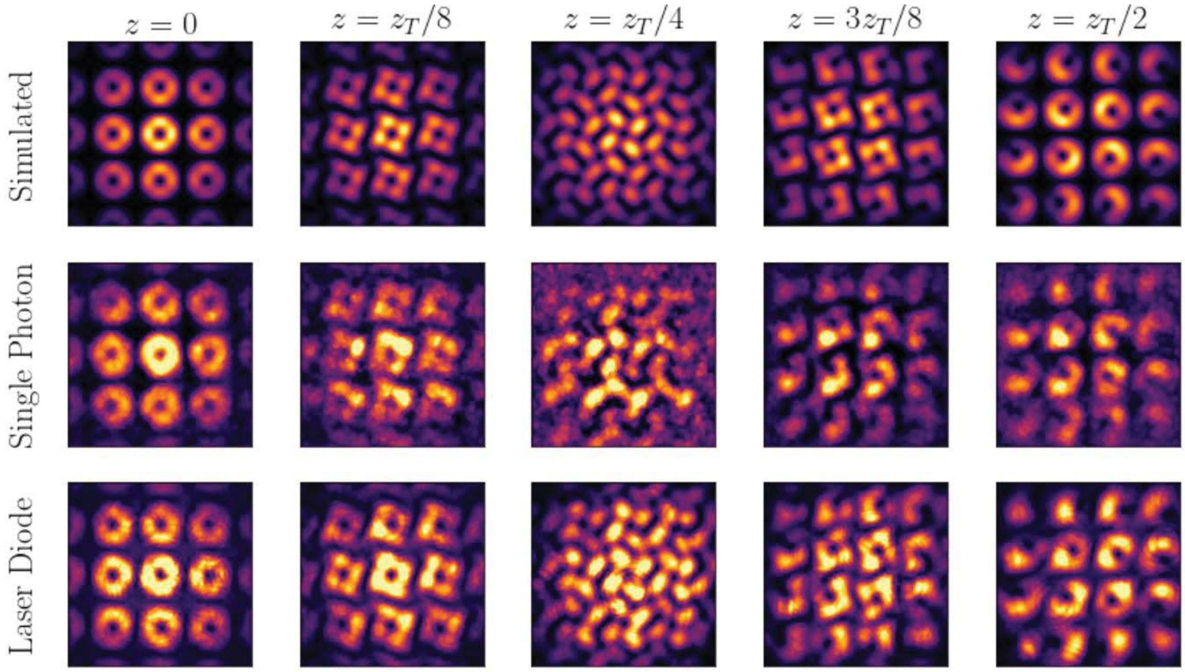


Fig. 1 Simulated and observed self-images at different fractional Talbot lengths. We measure the two-dimensional intensity profile. In the simulation, we multiply a Gaussian beam envelope with the beam waist measured in the experiment to account for features occurring due to finite beam sizes when propagating along the z-axis. Good qualitative agreement is found between the simulated and observed profiles.

**References**

[1] J. Wen, Y. Zhang, and M. Xiao, "The Talbot effect: recent advances in classical optics, nonlinear optics, and quantum optics," Advances in Optics and Photonics **5**, 83–130 (2013).

[2] D. Sarenac, D.G. Cory, J. Nsofini, I. Hincks, P. Miguel, M. Arif, C.W. Clark, M.G. Huber, and D.A. Pushin, "Generation of a lattice of spin-orbit beams via coherent averaging," Physical Review Letters **121**, 183602 (2018).

# Photon counting instrumentation optimized for laser time transfer applications

**Josef Blazej** [1], **Ivan Prochazka** [1], **Jan Kodet** [1,2]

[1] *Czech Technical University in Prague, Brehova 7, Prague, Czech Republic*
[2] *Geodätisches Observatorium Wettzell, Technische Universität München, München, Germany*

We are presenting the development and achievements of photon counting instrumentation for laser time transfer applications. In presented experiments the single photon counting approach was verified to provide ultimate precision and accuracy. Satellite Laser Ranging (SLR) is a technique in which a network of observing stations measures the round-trip time of flight of ultrashort laser pulses to satellites equipped with retroreflectors. It is the most accurate technique to determine the distances in space scale with sub-millimeter precision and few millimeters accuracy. Laser time transfer enables to compare time scales on ground and in space by means of an extension of SLR type measurements.

For laser time transfer applications new photon counting detectors and epoch timing systems were developed. They do provide ultimate timing resolution and extreme detection delay stability. The ground segment is based on a single pixel solid state photon counting detectors on silicon having an active area diameter of 0.2 mm are providing timing resolution better than 20 ps. The space segment is based on a similar detector with active area diameter 0.1 mm and controlled by a circuit providing passive detection delay temperature compensation. The epoch timing systems provide sub-picosecond timing resolution, linearity and stability. An entire photon counting measurement chain exhibits unique long-term detection delay stability of the order of hundreds of femtoseconds over several hours, as it is illustrated in figure 1. Even though single shot precision is about 20 ps, the floating average of detection relative delay over 600 s remain in 1 ps window. The space segment SPADs were qualified for space missions. Recently nine units are operational in space for laser time transfer three new missions are under preparation.

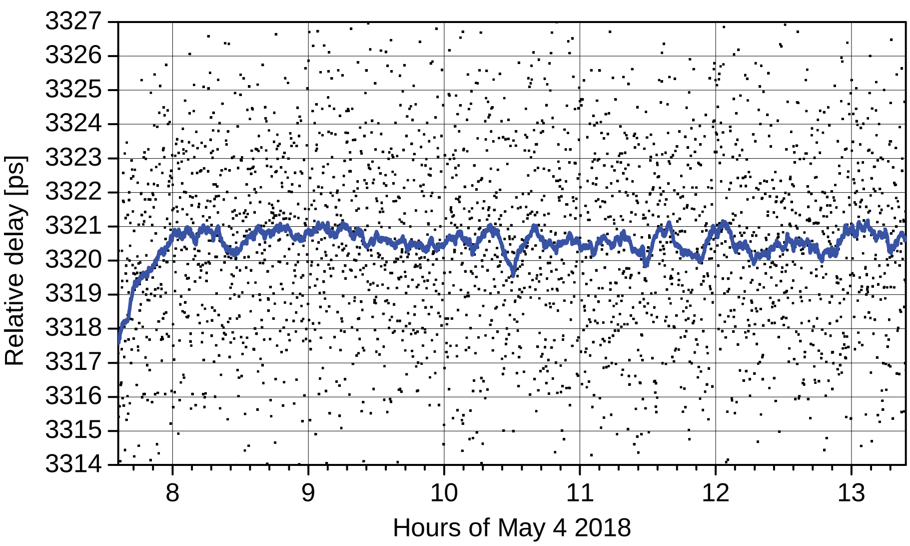


Fig. 1 The long-term stability of entire time-correlated single photon counting experiment, individual points represent the mean values of 256 single detections, the solid line is a moving average over 600 s.

**References**

[1] I. Prochazka, J. Blazej, T. Flekova, J. Kodet, "Silicon Based Photon Counting Detector Providing Femtosecond Detection Delay Stability," submitted to IEEE JSTQE, 2019.

[2] I. Prochazka, J. Blazej, J. Kodet, "Space qualified solid state photon counting detector with reduced detection delay temperature drift," Review of Scientific Instruments 89(5), art. 056106, 2018.

[3] P. Panek, J. Kodet, I. Prochazka, "Event timing device providing subpicosecond precision," In: 2013 Joint European Frequency and Time Forum & International Frequency Control Symposium (EFTF/IFC), pp. 167-170, IEEE, 2013.

# A European effort for the development of single-photon sources as new quantum standards – the SIQUST-project

**S. Kück[1], H. Georgieva[1], M. López[1], B. Rodiek[1], F. Manoocheri[2], G. Porrovecchio[3], M. Smid[3], G. Brida[4], P. Traina[4], T. Kübarsepp[5], C. Giusca[6], P. Dolan[6], L. Hao[6], C. J. Chunnilall[6], T. Dönsberg[7], P. Lombardi[8], C. Toninelli[8], B. Alén[9], S. Götzinger[10], J. Forneris[11], S. Rodt[12], S. Reitzenstein[12], P. Fuchs[13] C. Becher[13], P. Olivero[14], M. Jetter[15], P.Michler[15], S. L. Portalupi[15]**

*[1]Physikalisch-Technische Bundesanstalt (PTB), Bundesallee 100, 38116 Braunschweig, Germany*

*[2]Aalto-korkeakoulusäätiö sr (Aalto), Otakaari 1, 02150 Espoo, Finland*

*[3]Ceský Metrologický Institut (CMI), Okruzni 31, 63800 Brno, Czech Republic*

*[4]Istituto Nazionale di Ricerca Metrologica (INRIM), Strada delle Cacce 91, 10135 Torino, Italy*

*[5]AS Metrosert (Metrosert), Teaduspargi 8, EE-12618, Tallinn, Estonia*

*[6]National Physical Laboratory (NPL), Hampton Road, Teddington, TW11 0LW, U.K.*

*[7]Teknologian tutkimuskeskus VTT Oy (VTT), Tekniikantie 1, 02150 Espoo, Finland*

*[8]Istituto Nazionale di Ottica (CNR-INO), via N. Carrara 1, Sesto F.no (FI) 50019, Italy*

*[9]Instituto de Micro y Nanotecnología, IMN-CNM, CSIC (CEI UAM+CSIC), Isaac Newton, 8, E-28760, Tres Cantos, Madrid, Spain*

*[10]Friedrich-Alexander-Universität Erlangen – Nürnberg (FAU), Günther-Scharowsky-Str.1/Geb. 24, 91058 Erlangen, Germany*

*[11]Istituto Nazionale di Fisica Nucleare (INFN) - Sez. Torino, 10125, Torino, Italy*

*[12]Technische Universität Berlin (TUB), Hardenbergstraße 36, Berlin, Germany*

*[13]Universität des Saarlandes (UdS), Fachrichtung 7.2, Campus E2.6, 66123 Saarbrücken, Germany*

*[14]Physics Department, University of Torino (UNITO), via Pietro Giuria 1, 10125 Torino, Italy*

*[15]Institut für Halbleiteroptik und Funktionelle Grenzflächen, Center for Integrated Quantum Science and Technology (IQST) and SCoPE, University of Stuttgart (USTUTT), Allmandring 3, 70569 Stuttgart, Germany*

In this presentation, the EURAMET joint research project "Single-photon sources as new quantum standards" (SIQUST) [1], funded within the European Union Horizon 2020 research and innovation programme, will be presented.

The aim of this project is to carry out the fundamental work needed to develop new quantum standards, assessing and establishing new materials and designs for single-photon sources and thus to develop new absolute standard radiation sources, which exploit the discrete and quantum nature of photons. These sources will be based on single-photon emitters with a calculable photon emission rate and high purity, i.e. with a very low multiple photon emission probability. Such sources hold promise as new quantum standards which will have a large number of applications, e.g. for use in the calibration of single-photon detectors, for the realization of the SI base unit candela, for quantum random-number generation, for quantum key distribution, for sub-shot noise metrology, for quantum-enhanced metrology, and for photon-based quantum computation. Furthermore, the essential elements of supporting measurement and metrology infrastructure, such as amplifiers and detectors will be developed and characterized. The specific objectives are to develop single-photon sources as new quantum standards in the visible, near-infrared and telecom wavelength range, based on optically and electrically-driven impurity centres in nano- and bulk diamonds, quantum dots in semiconductor structures and molecules having, simultaneously, photon rates > $1 \times 10^6$ photons per second, emission bandwidths < 2 nm and high purity emission indicated by $g^{(2)}(t = 0)$ values < 0.05; to assess new materials and concepts for single-photon sources, such as 2D materials (e.g. hexagonal boron nitride and thin transition-metal dichalcogenides) and coupling designs to optimise the collection efficiency (e.g. micro-resonators, waveguides, optical antennas) and to assess the impact of excitation schemes on the quantum optical properties of single-photon sources; to establish sources of indistinguishable and entangled photons based on near infrared (< 1 µm) quantum dot single-photon sources with photon indistinguishability > 90 % and novel sensing and measurement techniques based on these sources; to develop metrology infrastructure for traceable single-photon source characterisation, i.e. detectors, amplifiers, single-photon spectroradiometers and to promote the results, to trigger commercialisation of products, and to deliver input to standardisation organisations. In addition to the presentation of the project, first results of the project will be reported at the conference.

The work reported on this paper is funded by project EMPIR 17FUN06 SIQUST. This project received funding from the EMPIR programme co-financed by the Participating States and from the European Union Horizon 2020 research and innovation programme.

**References**

[1] https://www.siqust.eu

# Characterising phonon interactions in single molecules for non-classical light sources

**Chloe Clear[1], Ross Schofield[2], Kyle Major[2], Jake Ils-Smith[3], Alex Clark[2] and Dara McCutcheon[1],**

*[1] Quantum Engineering Technology Labs, H. H. Wills Physics Laboratory and Department of Electrical and Electronic Engineering, University of Bristol, Bristol BS8 1FD, UK.*

*[2]Centre for Cold Matter, Blackett Laboratory, Imperial College London, Prince Consort Road, London SW7 2AZ, UK.*

*[3]Department of Physics and Astronomy, University of Sheffield, Sheffield S3 7RH, UK.*

Single organic molecules have recently gained attention as novel non-classical light sources with Quantum information applications. Dibenzoterrylene (DBT) encased in a nano-crystal of anthracene is an example of such a deterministic single photon emitter which has generated research interest due to its high photostability and tunability [1]. With all solid-state photon emitters, it is crucial that the dephasing processes are well understood to allow for their prevention. Here we present a theoretical model which simulates the temperature dependent emission spectra for an organic molecule single photon emitter. These simulations are directly compared against raw experimental data taken from collaborators[2], see figure 1.

The theoretical model utilises a polaron transformation to derive a master equation in the formalism of open quantum systems theory which describes the dynamics and optical properties of the system [3]. The DBT molecule is modelled as a two-level electronic system (TLS) with a singlet ground and excited state. The model reproduces the zero-phonon line (ZPL) which is in the near-infrared range (784nm) and three local vibrational modes of the DBT molecule. The local vibrational modes which appear in the spectrum have been concluded to come from the local libration of the molecule and are treated as harmonic oscillators [4]. The spectrum is broadened by the photonic environment and thermal phonon residual baths which couple separately to the TLS and the local vibrational modes. These phonon baths originate from the anthracene crystal environment. The TLS-bath interaction is taken to second order to capture the temperature dependent homogenous broadening of the ZPL. Finally, a broad sideband on all spectral peaks can be seen, this due to the non-Markovian nature of the TLS-bath that is captured by moving into the polaron frame. This work enables the complete modelling of the dynamics from this organic molecule single photon emitter, characterising the phonon coupling influence on the optical properties.

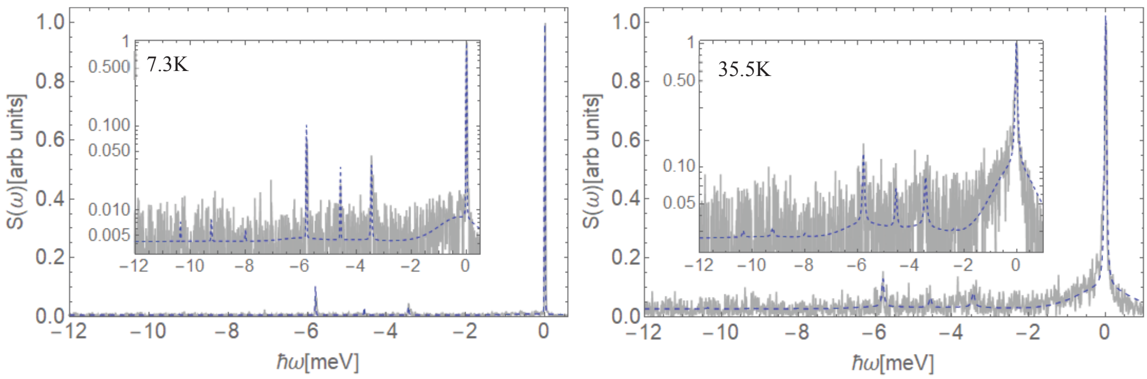


*Fig. 1: Emission spectrum of a single DBT molecule encased in an anthracene crystal at 7.3K (left) and 35.5K (right). Experimental data shown in Grey and the Blue dashed line shows the theoretical model. The ZPL is centred on 0meV which corresponds to emission at 784nm. Inset displays the spectra with an intensity log scale highlighting the sideband. Resolution of the spectrometer captured in the theoretical model via convolution with a gaussian kernel.*

**References**

[1] Nicolet, A. A., Bordat, P. , Hofmann, C. , Kol'chenko, M. A., Kozankiewicz, B. , Brown, R. and Orrit, M. (2007), Single Dibenzoterrylene Molecules in an Anthracene Crystal: Main Insertion Sites. ChemPhysChem, 8: 1929-1936. doi:10.1002/cphc.200700340

[2] Ross C Schofield *et al* 2018 *J. Phys. Commun.* **2** 115027

[3] Jake Iles-Smith et al. “Phonon scattering inhibits simulta-neous near-unity efficiency and indistinguishability in semi-conductor single-photon sources”. In:Nature Photonics11.8(2017), pp. 521–526.

[4] Philippus de Bree and Douwe A. Wiersma. “Application ofRedfield theory to optical dephasing and line shape of elec-tronic transitions in molecular mixed crystals”. In:The Jour-nal of Chemical Physics70.2 (1979), pp. 790–801.

# Generating non-classical light in photon-number superpositions

**J. C. Loredo,[1,*] C. Antón,[1,*] B. Reznychenko,[2] P. Hilaire,[1,4] A. Harouri,[1] C. Millet,[1] H. Ollivier,[1] N. Somaschi,[3] L. De Santis,[1] A. Lemaitre,[1] I. Sagnes,[1] L. Lanco,[1,4] A. Auffeves,[2] O. Krebs,[1] and P. Senellart[1]**

*[1] CNRS Centre for Nanoscience and Nanotechnology, Université Paris-Sud, Université Paris-Saclay, 91120 Palaiseau, France*

*2 Univ. Grenoble Alpes, CNRS, Grenoble INP, Institut Néel, 38000 Grenoble, France*

*3 Quandela SAS, 86 rue de Paris, 91400 Orsay, France*

*4Université Paris Diderot, Paris 7, 75205 Paris CEDEX 13, France*

Resonant excitation of quantum emitters has thus far focused on developing optimal single-photon sources. However, the finding of more general quantum states of light remains scarce. Here, we demonstrate the on-demand generation of photon Fock-state coherent superpositions from solid-state emitters. We show that resonantly exciting a semiconductor quantum dot produces non-classical light in superpositions of photon-numbers along the Rabi cycles. The coherent driving of the atomic system, up to full atomic inversion, results in quantum superpositions of ground and excited atomic states, which via spontaneous emission leads to superpositions of vacuum and a single-photon, with their relative populations controlled by the driving laser intensity. Moreover, we show that driving the system with stronger pulses beyond full-inversion results in a coherent superposition of vacuum, one, and two photons, where the two-photon term exceeds the single-photon component; a state incidentally resembling a small Schrödinger-cat state. New paths for optical quantum technologies with access to the photon-number degree-of-freedom may now be accessible.

∗Equally contributing authors.

# Evanescent coupling of quantum dot nanowires with integrated photonic circuits

**David Northeast[1], Dan Dalacu[1], Khaled Mnaymneh[1], Joe McKee[1], Philip J. Poole[1], Jean Lapointe[1], Alex Koujelev[2], Eric Gloutnay[2], Andrew Gibson[2], Stephane Gendron[2], and Robin L. Williams[1]**

[1] *National Research Council of Canada, Ottawa, Canada*

[2] *Canadian Space Agency, Montreal, Canada*

Future quantum technologies such as quantum computing and encryption will benefit from efficient and on-demand sources of quantum light. Semiconductor quantum dots have proven to be excellent sources of both high-purity single photons [1] and high-fidelity entangled pair quantum states [2,3]. Practical use of such sources will benefit from on-chip integration with existing photonic circuit technologies. This approach can eliminate the requirement of active alignment for exciting the dot and collecting its emission, thereby increasing the source stability.

In this work, we show the controlled incorporation (Fig. 1(a)) of previously characterised quantum dots into integrated photonic circuits [4], providing bright light sources for experiments in optical quantum computing and metrology. InAsP quantum dots in InP nanowires—emitting between 900 nm and 1000 nm—are transferred from the growth substrate and evanescently coupled to SiN ridge waveguides. Photoluminescence (Fig. 1(b)) and second order correlation measurements (Fig. 1(c)) are made before and after integration to assess the effects of transferring using a nano-manipulator probe system. We report progress investigating source photon purity and indistinguishability.

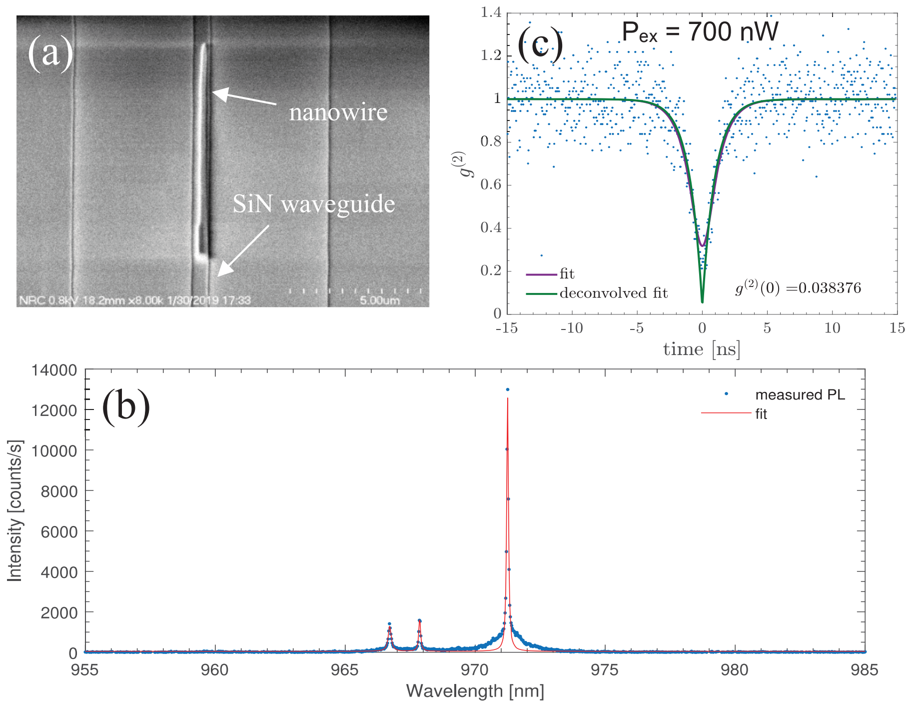


Figure 1: A scanning electron microscope image (a) shows an InP nanowire (with InAsP quantum dot) on top of a SiN ridge waveguide. Photoluminescence spectroscopy (b) shows bright emission, and a $g^{(2)}$ measurement (c) demonstrates the quantum dot is a high-quality single photon source.

## References

[1] Dalacu et al., Nano Lett., 2012, DOI: 10.1021/nl303327h
[2] Versteegh et al., Nat. Commun, 2014, DOI: 10.1038/ncomms6298
[3] Huber et al., Nano Lett., 2014, DOI: 10.1021/nl503581d
[4] Mnaymneh et al., Advanced Quantum Technologies, 2019, DOI: https://doi.org/10.1002/qute.201900021

# Single atom silicon devices for quantum technologies: from nanoelectronics to optics

**Enrico Prati[1], Takahiro Shinada[2], Takashi Tanii[3]**

[1]*Istituto di Fotonica e Nanotecnologie – Consiglio Nazionale delle Ricerche, Milano, Italy*

[2]*CIES Tohoku University, Sendai, Japan*

[3]*Waseda University, Tokyo, Japan*

Single atom devices enable spin physics in silicon single electron/single hole quantum dots at cryogenic temperature, but alternative from conventional microelectronic dopants can be implanted to access optical states up to room temperature. We review photon-related single atom effects including P, As, Ge-V complex and Er-Ox complex in silicon, by addressing their behaviour and exploitation in single photon emission and detection. Single ion implantation enables to control doping by implanting atoms one by one, thus creating intentional geometrically controlled quantum dots. In particular, single implanted P and As [1,2] are considered for their capability of raising photon assisted tunneling, microwave controlled Kondo effect, electrically controlled single photon counting at cryogenic temperature. Single implanted Ge-V [3] in silicon shows bound electrons up to room temperature because of its deep donor states, whose spectrum potentially opens relevant optical transitions. Finally, single ion Er coimplanted with oxygen is discussed. Experiments involving few Er atoms [4,5] down to single atom for both emitting and capturing telecom frequency single photons are discussed.

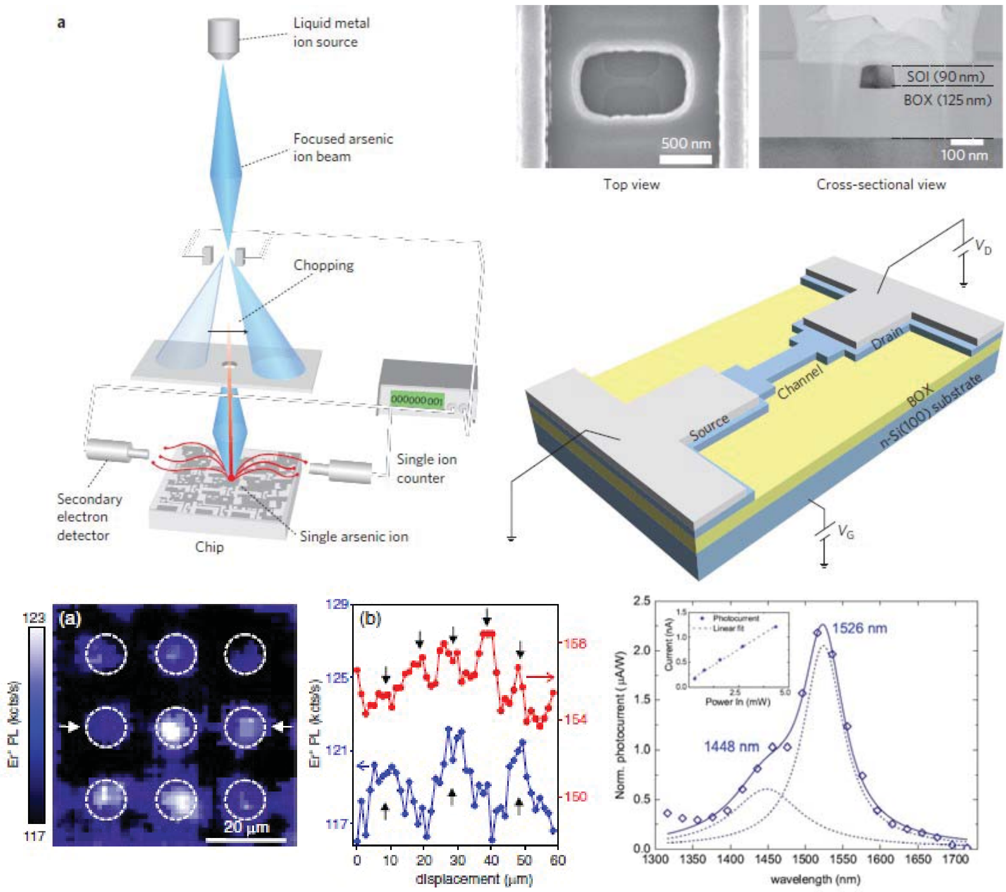


Fig. 1 Top: the single ion implantation method, based on a modified FIB [1]. Bottom left (a,b): photoluminescence of dots constituted by few hundred of Er atoms implanted in silicon at room temperature [4] Bottom right: photocurrent of a transistor doped with few thousands of Er atoms at room temperature [5].

**References**

[1] E. Prati et al. Nature Nanotechnology 2012

[2] E. Prati et al. Nature Scientific Reports 2016

[3] S. Achilli et al. Nature Scientific Reports 2018

[4] M. Celebrano et al. Optics Letters 2017

[5] M. Celebrano et al. Nanomaterials 2019

# Generation of strongly correlated photons using atoms weakly coupled to an optical mode

**Adarsh Prasad[1], Jakob Hinney[1], Klemens Hammerer[2], Sahand Mahmoodian[2], Samuel Rind[1], Philipp Schneeweiss[1,3], Anders S. Sørensen[4], Jürgen Volz[1,3], and Arno Rauschenbeutel[1,3]**

[1]*Vienna Center for Quantum Science and Technology, TU Wien-Atominstitut, Stadionallee 2, 1020 Vienna, Austria*

[2]*Institute for Theoretical Physics, Institute for Gravitational Physics (Albert Einstein Institute), Leibniz University Hannover, Appelstraße 2, 30167 Hannover, Germany*

[3]*Department of Physics, Humboldt-Universität zu Berlin, 10099 Berlin, Germany*

[4]*Center for Hybrid Quantum Networks (Hy-Q), Niels Bohr Institute, University of Copenhagen, Blegdamsvej 17, DK-2100 Copenhagen, Denmark*

The realization of complex quantum many-body physics of photons is an outstanding challenge of modern quantum optics as it arises from interactions in out-of-equilibrium systems. Typical schemes for generating correlated states of light require a highly nonlinear medium strongly coupled to an optical mode. Such approaches are often strongly impaired by unavoidable dissipative processes which reduce the nonlinearity and cause photon loss.

Here, we experimentally demonstrate the opposite approach where a highly dissipative, weakly coupled medium can be harnessed to generate and study strongly correlated states of light [1]. Specifically, we measure the second-order correlation function of light transmitted through an ensemble of atoms that weakly couple to the optical mode of an optical nanofiber. Dissipation removes uncorrelated photons while preferentially transmitting highly correlated photons created through nonlinear interactions. As a result, the transmitted light constitutes a highly correlated many-body state of light which reveals itself in the second order correlation function that exhibits antibunched or bunched photon statistics depending on the optical depth of the atomic ensemble.

## References

[1] S. Mahmoodian et al., Phys. Rev. Lett. 121, 143601 (2018)

# Optimization of Si emitters for cryogenic light sources

**S. M. Buckley[1], A. Tait[1], J. T. Chiles[1], A. N. McCaughan[1], S. Olson[2], J. Hermann[2], S. Papa Rao[2], R. P. Mirin[1], S. W. Nam[1], J. M. Shainline[1]**

*1. National Institute of Standards and Technology, NIST, Boulder CO 80301*

*2. SUNY Poytechnic Institute, 257 Fuller Rd., Albany NY 12203*

An on-chip, silicon-compatible light source has long been pursued for classical optical telecommunications without significant success. However, for applications where cryogenic operation is already required, for example, in quantum optics or neuromorphic or superconducting computing, point defects in Si may provide a suitable light source. We have previously demonstrated [1] an electrically injected waveguide-coupled Si LED based on this technology. Here we show that we can obtain an order of magnitude improvement in brightness than this previous demonstration, due to the depth dependence of the emission.

W-centers are defect centers in Si composed of Si interstitials. They are generated by bombardment with Si ions [2]. With photoresist masking, W-center regions can be selectively defined (e.g. in the i-region of a p-i-n diode). They emit sub-bandgap light at 1.22 µm wavelength (Fig. 1 (a)). The temperature and power dependence of the W center are shown in Fig. 1 (b) and (c). To generate waveguide coupled light, the W-centers were implanted in a ridge waveguide in 220 nm thick Si on buried oxide insulator (SOI). To optimize the implant conditions, we have implanted Si ions in SOI wafers with different ion energies and fluences, and performed photoluminescence on the samples. The data was taken with a 632 nm laser and with the sample cooled to 30 K in a closed cycle cryostat. We have found that in SOI, there is a much stronger dependence of the photoluminescence intensity on the implant energy and fluence than in bulk Si.

In our previous demonstration, the implant energy was simulated to stop the majority of the silicon ions at the center of the Si device layer. However, by implanting in 220 nm Si on 3 um insulator (SOI B, 72 mm wafer) and 220 nm Si on 170 nm insulator (SOI A, 300 mm wafer), we have found that the W centers are actually much deeper than the initial stopping range of the Si ions [3], likely due to the importance of higher order collisions in generating the W centers. By moving from this implant energy to a lower implant energy, one to two orders of magnitude improvement can be obtained. This is shown in Fig 1 (d). Fig 1 (e) shows that for higher energy implants, the W centers are actually implanted through the buried oxide for SOI A, further demonstrating that the W centers are generated deeper than expected. We have also optimized the fluence and anneal temperature of the W centers implanted in SOI for another factor of 4 improvement. We have also demonstrated that these implants can be done at the 300 mm scale and measured the cross wafer uniformity to be better than the uncertainty in our setup.

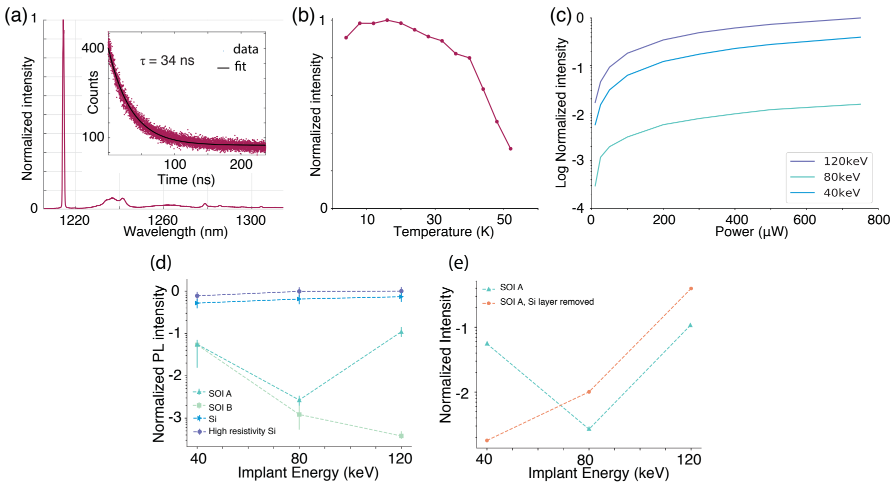


Fig. 1 The HiDRA device (see text).

## References

[1] Buckley et al., Appl. Phys. Lett. 111, 141101 (2017)

[2] J. Bao et al., Opt. Express 15, 6727-6733 (2007)

# Realization of single photon sources based on various single emitters

**Kee Suk Hong [1], Hee-Jin Lim[1], Dong Hoon LEE [1], Seongchong Park[1], Hee Su Park[1], Kwang-Yong Jeong[2].**

*[1]Korea Reasearch Institute of Standards and Science (KRISS), Daejeon 34113,*

*[2]Department of Physics, Korea University, Seoul 02841, South Korea*

Single photon sources based on solid state single emitters such as quantum dots and impurities in a diamond are of great interest for many application fields such as quantum computer, quantum communication, and quantum sensing [1, 2]. In photometry and radiometry, a single-photon source, which can emit only one photon in a well-defined time and frequency domain, is the promising candidate to realize a photon number-based primary standard for quantum radiometry [3]. At KRISS, we realized single photon sources based on various single emitters at room temperature. The experimental setup and the preliminary various single photon results are presented in this conference.

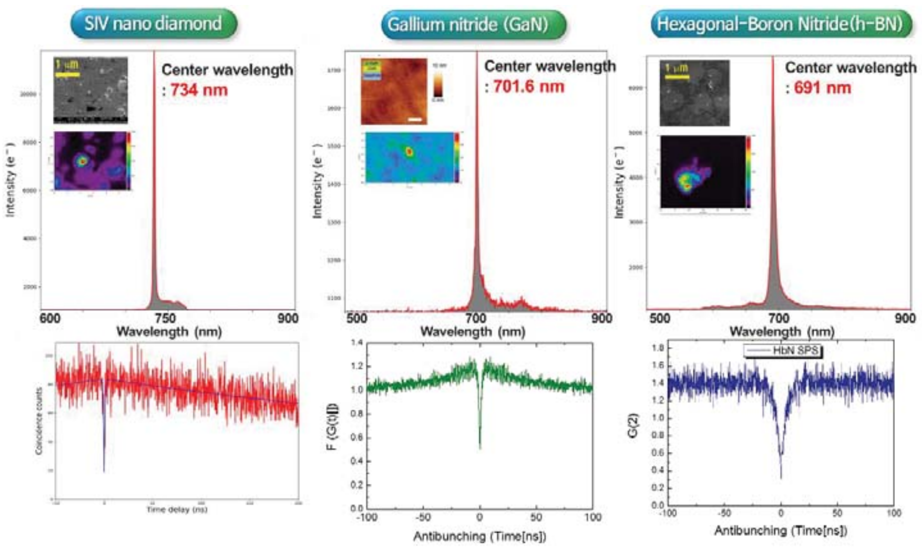


Fig. 1 The spectrum and purity factor g(2) of a single photon sources are shown with various nanomaterials (Silicon Vacancy nano-diamond, Gallium nitride, Hexagonal-Boron Nitride).

Realization of single photon generation for quantum radiometry, KRISS evaluated single photon characteristics using various materials such as silicon vacancy nano-diamond, gallium nitride and hexagonal-boron nitride. The distribution of nano-size emitters were identified using SEM images and mounted on a piezo-controlled XYZ-stage and scanned until an isolated single center is found. When pump light is injected to single emitter, single photon is generated. The pump light is removed purity through a several of optical filters, and the pure single photon can be characterized through a number of automated switch-type channels. Three channels are configured to measure the purity of factor (g(2)), the spectrum and photon flux of single photon source which partially shown in Figure 1. The spectrum of the fluorescence is measured by using a photon-level spectrometer. The Wavelength of the ZPL(zero phonon line) is 691,701.6 and 734 and that the FWHM is less than 4nm. A Hanbury-Brown-Twiss interferometer is used to measure the second-order correlation function $g(2)(\tau)$, which characterizes the single photon purity. The purity of g(2) is less than or equal to 0.5 in CW pumping, all of which are measured in Time Tag mode. And positional motor stage was placed so that switched integration amplifier (SIA) could determine the photon flux to single photon avalanche photodiodes (SPAD). The measured wavelengths are 640 to 780 nm and the single photon source excited about 50000 ~ 500000 photons. The photon flux of each single photon source is measured by using a Si SPAD whose detection efficiency is calibrated as a function of wavelength [4].

**References**

[1] B. Lounis and W. Moerner, Single photons on demand from a single molecule at room temperature", Nature. 407 491~493 (2000)

[2] E. Waks, K. Inoue, C. Santori et al, "Secure communication: Quantum cryptography with a photon turnstile", Nature 420 762 (2002)

[3] A. Vaigu, G. Porrovecchio, et al, Experimental demonstration of a predictable single photon source with variable photon flux, Metrologia 54, 218 (2017).

[4] In-Ho Bae, Seongchong Park, et al, " Detection efficiency measurement of single photon avalanche photodiodes by using a focused monochromatic beam tunable from 250 nm to 1000 nm ," Metrologia . 56, 035003 (2019)

# A bubble-induced ultrastable and robust single-photon emitter in hexagonal boron nitride


**Yi-Tao Wang[1,2], Wei Liu[1,2], Zhi-Peng Li[1,2], Shang Yu[1,2], Zhi-Jin Ke[1,2], Yu Meng[1,2], Jian-Shun Tang (tjs@ustc.edu.cn)[1,2], Chuan-Feng Li[1,2], and Guang-Can Guo[1,2]**

[1]*CAS Key Laboratory of Quantum Information, University of Science and Technology of China, Hefei, Anhui 230026, China.*

[2]*CAS Center For Excellence in Quantum Information and Quantum Physics, University of Science and Technology of China, Hefei, Anhui 230026, China.*



Quantum emitters in van der Waals (vdW) materials have attracted lots of attentions in recent years, and shown great potentials to be fabricated as quantum photonic nanodevices. Especially, the single photon emitter (SPE) in hexagonal boron nitride (hBN) emerges with the outstanding room-temperature quantum performances, whereas the ubiquitous blinking and bleaching restrict its practical applications and investigations critically. The bubble in vdW materials exhibits the stable structure and can modify the local bandgap by strains on nanoscale, which is supposed to have the ability to fix this photostability problem. Here we report a bubble-induced high-purity SPE in hBN under ambient conditions showing stable quantum-emitting performances, and no evidence of blinking and bleaching for at least one year. Remarkably, we observe the nontrivial successive activating and quenching dynamical process of the fluorescent defects at the SPE region under low pressures for the first time, and the robust recoverability of the SPE after turning back to the atmospheric pressure. The pressure-tuned performance indicates the SPE origins from the lattice defect isolated and activated by the local strain induced from the bubble, and sheds lights on the future high-performance quantum sources based on hBN.


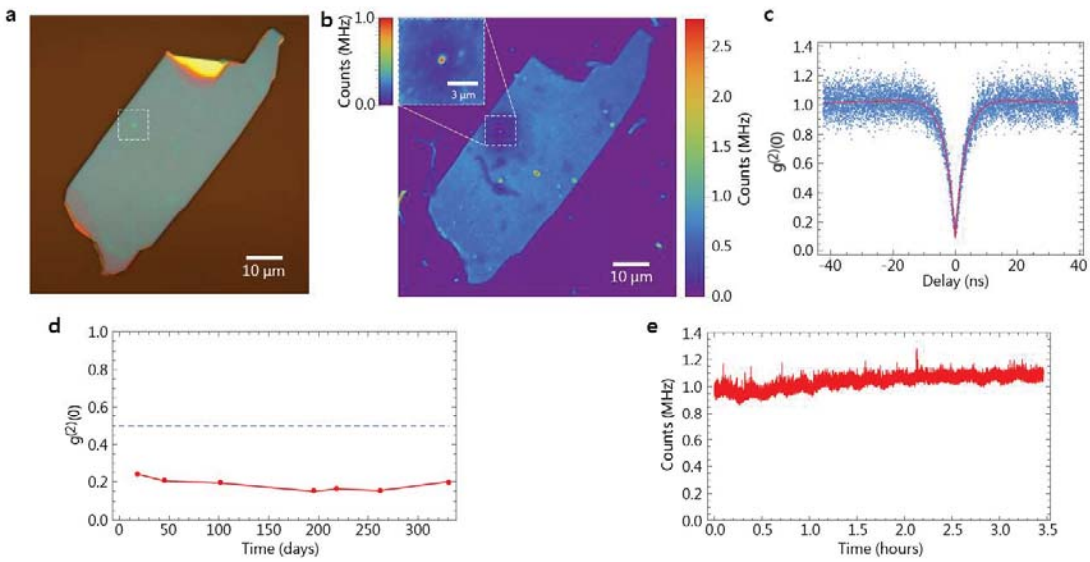


FIG. 1: **The bubble-induced blinking-free, bleaching-free and high-purity single-photon emitter (SPE) in the hexagonal boron nitride (hBN) flake.** (a) the optical microscope image of the hBN flake. (b) the confocal fluorescence image of the same hBN flake. The SPE is located at the center of the white dashed box marked in (a) and (b), enlarged by the top-left inset. (c) The antibunching second-order time correlation $g^{(2)}(\tau)$ of the SPE under 0.3-mW excitation with an additional long-pass filter (see Methods). The blue dots are the experimental data and the red curve shows the corresponding fitting result using three-level model. The lifetimes of the excited and metastable states are 3.38 ns and 24.95 ns, respectively. $g^{(2)}(0) = 0.089 \pm 0.006$ indicates the SPE possesses the high single-photon purity. (d) The quantum-emitting performance of the SPE evaluated by $g^{(2)}(0)$ during more than eleven months. The blue dashed line indicates the quantum-emitting boundary of $g^{(2)}(0) = 0.5$. (e) The photon counts of the SPE measured for continuing 3.5 hours, with the 100-ms time resolution. Both (d) and (e) illustrate the perfect photostability of the blinking-free and bleaching-free SPE.

# Room temperature near infra-red quantum emitters in gallium nitride

**Anthony J. Bennett[1], Sam Bishop[1], John P Hadden[2] Diana Huffaker[1,2]**

[1]*School of Engineering, Cardiff University, Queen's Buildings, The Parade, Cardiff, UK, CF24 3AA*

[2.] *School of Physics and Astronomy, Cardiff University, Queen's Building, The Parade, Cardiff, UK, CF24 3AA*

Gallium Nitride (GaN) is a wide-bandgap semiconductor widely used in solid state lighting, high power transistors and blue lasers. GaN also provides an ideal platform for integrated quantum optics with no 2-photon or inter-band absorption in the near infra-red, but with well -established industrial processes for growth on Silicon and Sapphire substrates. However, there exists a large built in electric field in c-plane GaN which limits efficient quantum well emission to wavelengths below ~500nm.

In the last two years quantum emission from point-like emitters has been reported in off-the-shelf gallium nitride (GaN)[1]. This new discovery shows GaN can host emitters from the ultra-violet out to the telecommunication C-band. As a result of the large GaN bandgap this emission persists up to room temperature. The origin of the emitters has been attributed to structural crystal imperfections, but a recent study has indicated a more complex relationship between different types of stacking fault and the emission[2].

We will report on spectral, time-resolved and autocorrelation measurements of quantum emitters in GaN samples synthesized under different conditions. We have observed that, unlike other wideband gap semiconductors such as diamond and silicon carbide, there is a continuous range of emission energies for different emitters in the same sample suggesting they are not due to a simple, single-site defect. Figure 1 shows an example of one localized emitter in semi-polar GaN with a single optical transition at 816nm at room temperature. An auto-correlation histogram reveals anti-bunching from the single state with a lifetime of ~1ns, plus a pronounced bunching effect with a timescale of 30ns. Detailed analyses of the phonon-broadened spectral line as function of temperature and excitation energy will be presented, showing a surprising decrease in intensity at lower temperatures. Finally, we will discuss our development of a suspended GaN photonic crystal waveguide, and the prospects for GaN integrated quantum photonics based on these emitters.

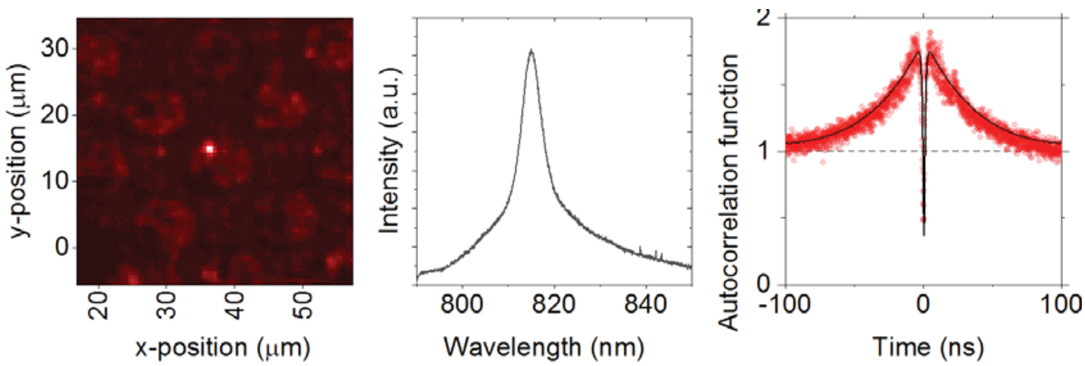


Fig. 1 (a) Room temperature scan of GaN wafer, displaying a bright localised emitter (b) spectrum under 532nm laser excitation and (c) auto-correlation function showing anti-bunching with a lifetime of 1.0ns.

**References**

1. Berhane, A. M. *et al.* Bright Room-Temperature Single-Photon Emission from Defects in Gallium Nitride. *Adv. Mater.* **29**, 1–13 (2017).
2. Nguyen, M. *et al.* Effects of microstructure and growth conditions on quantum emitters in Gallium Nitride. *APL Materials.* 7–9 (2018).

# Simulation of Photon Echoes in Pr:YSO (Yttrium Orthosilicate)

**Zachary H. Levine**[1]

[1] *National Institute of Standards and Technology, Gaithersburg, Maryland, 20988-8441, USA*

The prospects for single-photon storage both in bulk crystal and in waveguides of praseodymium-doped yttrium orthosilicate (Pr:YSO) are considered using numerical simulation, in support of an experimental effort [1,2] to generate photon echoes in a solid medium. The experiment makes use of two electronic levels of Pr, each split into three hyperfine levels. The inhomogeneous broadening of the Pr impurities' optical transition energies in the crystal is required to create a broad bandwidth frequency comb. [3] *In the first step* of the experiment, a spectral hole is burned in the crystal using a periodically chirped (i.e., serrodyne modulated) laser of relatively high power. In contrast to previous efforts, there is no repopulation of the hole. Modeling of the spectral hole burning was performed using the rate equations, and, separately, the density matrix, based on the 6-state Hamiltonian developed by Lovric et al. [4] as well as a simplified 3-state model that has the same oscillator strengths in the non-magnetic case. The purpose of the periodically chirped laser is to create a frequency comb. The comb itself may be modelled with the rate equation, but the density matrix can predict the widths of the teeth of the frequency comb. Suggestions for creating high quality combs include ensuring periodicity of the phase of the chirp and an optimized FM pulse. *In the second step,* relaxation to the hyperfine ground states is modeled. *In the third step,* an optical pulse enters the crystal and is partially absorbed and partially transmitted. *In the fourth step,* individual oscillators in the material respond with a phase and amplitude given by the filtered input pulse. Subsequent pulses are possible at a small integer multiple of this time, limited by the comb width. The quality of the comb has a great influence on the photon echoes.

Work performed in collaboration with Eli Weisler, Harvey Mudd College and NIST.

Classification: Optical quantum-state generation and photon manipulation

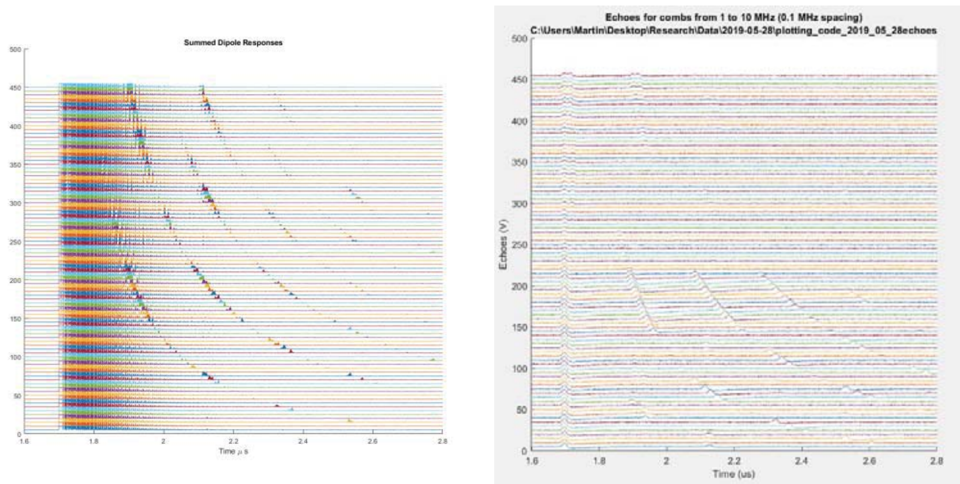


Fig. 1 Photon echoes (left) as predicted from an observed optical comb. Dipoles at a given frequency are given a strength based on the transmission times an overall Gaussian to describe the incident pulse, phased according to the time delay, and summed ; (right) as observed experimentally.

## References

[1] E. A. Goldschmidt, S. E. Beavan, S. V. Polyakov, A. L. Migdall, and M. J. Sellers. "Storage and retrieval of collective excitations on a long-lived spin transition in a rare-earth ion-doped crystal," *Optics Express* **21,** 183321 (2013).

[2] H. Q. Fan, H. K. Kagalwala, S. V. Polyakov, A. L. Migdall. E. A. Goldschmidt, "Electromagnetically induced transparency in inhomogeneously broadened solid media," *Phys. Rev. A* **99,** 053821 (2019).

[3] M. Afzelius, C. Simon, H. de Riedmatten, and N. Gisin, "Multimode quantum memory based on an atomic frequency comb," *Phys. Rev. A* **79,** 052329 (2009).

[4] M. Lovric, P. Glasenapp, and D. Suter, "Spin Hamiltonian characterization and refinement for $Pr^{3+}$:$YAlO_3$ and $Pr^{3+}$: $Y_2SiO_3$" *Phys. Rev. B* **85,** 014429 (2012).

# Abstracts of

# Poster session II

# POGNAC: an all-fiber self-compensating polarization modulator for QKD

**Costantino Agnesi, Marco Avesani, Andrea Stanco, Paolo Villoresi, Giuseppe Vallone**

*Dip. di Ingegneria dell'Informazione, Università degli Studi di Padova, Via Gradenigo 6B - Padova, Italy*

Quantum key distribution (QKD) allows distant parties to exchange cryptographic keys with unconditional security by encoding information on the degrees of freedom of photons. Polarization encoding has been extensively used for QKD along free-space, optical fiber, and satellite links. However, the polarization encoders used in such implementations are unstable, expensive, complex and can even exhibit side channels that undermine the security of the protocol [1]. To address these criticalities, we propose and test a new polarization encoder: the POGNAC (for POlarization SaGNAC [2].

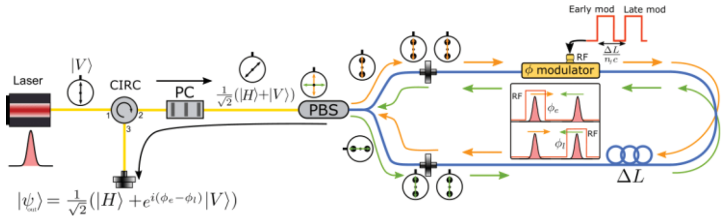


Fig. 1 Schematic representation of the POGNAC. Single Mode fibers are indicated in yellow while Polarization Maintaining fibers in blue. Figure from [2].

Our proposed polarization modulator can be seen in Fig. 1. The photons emerge from the POGNAC with a polarization state given by

$$\left|\psi_{\text{out}}^{\phi_e,\phi_\ell}\right\rangle = \frac{1}{\sqrt{2}}\left(|H\rangle + e^{i(\phi_e-\phi_\ell)}\,|V\rangle\right),$$

where the phases $\phi_e$ and $\phi_l$ can be set by carefully timing the applied voltage on a Lithium Niobate phase modulator. This can be achieved with a System on a Chip (SoC). If no voltages are applied by the SOC, the polarization is given by

$$\left|\psi_{\text{out}}^{0,0}\right\rangle = |+\rangle = \frac{1}{\sqrt{2}}\left(|H\rangle + |V\rangle\right).$$

Instead, if $\phi_e$ is set to $\frac{\pi}{2}$ while $\phi_l$ remains zero, the output state becomes

$$\left|\psi_{\text{out}}^{\frac{\pi}{2},0}\right\rangle = |L\rangle = \frac{1}{\sqrt{2}}\left(|H\rangle + i\,|V\rangle\right).$$

Alternatively, if $\phi_e$ remains zero while $\phi_l$ is set to $\frac{\pi}{2}$, the output state becomes

$$\left|\psi_{\text{out}}^{0,\frac{\pi}{2}}\right\rangle = |R\rangle = \frac{1}{\sqrt{2}}\left(|H\rangle - i\,|V\rangle\right).$$

The POGNAC combines a simple design and high stability reaching a low intrinsic quantum bit error rate as reported in Fig. 2. The self-compensating Sagnac-loop design greatly improves long-term stability over inline implementation, making it insensible to temperature fluctuations and DC drifts. Since realization is possible from the 800 to the 1550 nm band using commercial off-the-shelf devices, our polarization modulator is a promising solution for free-space, fiber, and satellite-based QKD.

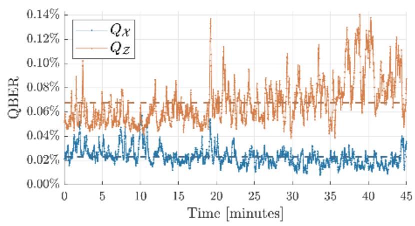


Fig. 2 Intrinsic Stability of the POGNAC. The average QBER measured for the key-generation basis was 0.07 $\pm$ 0.02% while an average 0.02 $\pm$ 0.01% was measured for the control basis.

**References**

[1] Lee, M. S. *et al.* Quantum hacking on a free-space quantum key distribution system without measuring quantum signals. *J. Opt. Soc. Am. B* **36**, B77–B82 (2019).

[2] Agnesi, C., Avesani, M., Stanco, A., Villoresi, P. & Vallone, G. All-fiber self-compensating polarization encoder for quantum key distribution. *Opt. Lett.* **44**, 2398 (2019).

# Photon-Level Simulation of Quantum Key Distribution with Picosecond Accuracy


**Xiaoliang Wu[1,2], Joaquin Chung[1], Alexander Kolar[1,3], Eugene Wang[1], Tian Zhong[4], Rajkumar Kettimuthu[1], Martin Suchara[1]**

*[1]Argonne National Laboratory, Lemont, IL, USA, [2]Illinois Institute of Technology, Chicago, IL, USA, [3]Northwestern University, Evanston, IL, USA, [4]University of Chicago, Chicago, IL, USA*


Recent experimental advances make quantum communication networks a reality. Experimentalists around the world are building quantum network testbeds with ever increasing complexity. These efforts include a 30-mile optical fiber link connecting Argonne and Fermilab to test long distance communication, and FQNET, an onsite teleportation and entanglement experiment at Fermilab. Our work complements these experimental efforts by building a Simulator of QUantum Network Communication (SeQUeNCe) that models quantum hardware, network protocols, and simulates transmission of individual photon pulses and control messages with picosecond accuracy. SeQUeNCe is capable of comparing alternative experiment design choices in highly complex systems with many possible designs of quantum repeaters, network topologies, quantum memories, and transduction systems.

Here we report on our use of SeQUeNCe to simulate quantum key distribution with the BB84 protocol [1], key reconciliation with Cascade [2], and detection of photon splitting attacks with a decoy-state protocol [3]. Fig. 1 depicts quantum and classical communication of the BB84 and Cascade protocols implemented in the simulator.

Our hardware model used an attenuated photon source with 80 MHz frequency and mean photon number 0.1. The detector had 80% efficiency, dark count rate 10 /sec, time resolution 10 ps, and maximum count rate 50,000,000 /sec. The quantum channel parameters were polarization fidelity of 97% and attenuation of 0.2 dB/km. The classical communication channel used by control messages had a round-trip-time of 2 ms in addition to propagation delay to accommodate message processing, TCP/IP packet formation, and buffering. The ratio among the signal pulses, decoy pulses, and vacuum pulses used by the decoy protocol were 8:1:1.

Fig. 2 shows the achieved key bit throughput (left axis) and the latency contributions of the BB84 and Cascade protocols (right axis) as a function of the optical fiber length. As expected, the key throughput (blue color) decreases exponentially with distance. Latency contribution of the BB84 protocol (red color) when transmitting a key was increasing with the fiber length due to decreasing throughput. The latency of Cascade (green color) was relatively constant at 1.8 sec to 2.4 sec. With 1.4% bit error rate, Cascade needed to correct approximately 140 error bits in each 10,240-bit frame, leading to 1,100 ~ 1,500 communication rounds.

In the past, quantum network simulations were used to study individual protocols in isolation or focused on applications [4]. Recently developed simulators, such as SeQUeNCe and NetSquid [5], allow comprehensive modeling of quantum hardware, quantum network protocols, and their interaction. We plan to use SeQUeNCe in the future to understand the effects of physical processes such as fiber dilation, perform hardware and software parameter tuning, as well as aid with experiment planning and design.

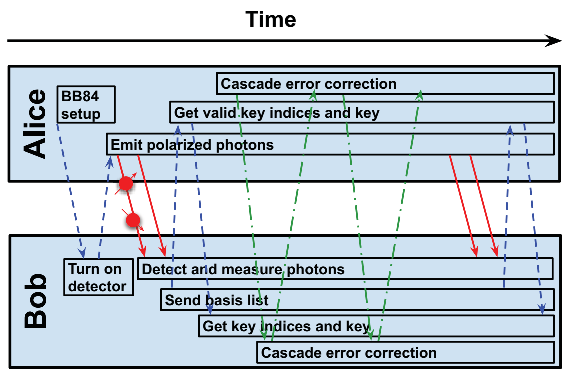


Fig. 1 Simulated photon pulses (red color), classical messages transmitted by BB84 (blue color), and Cascade (green color).

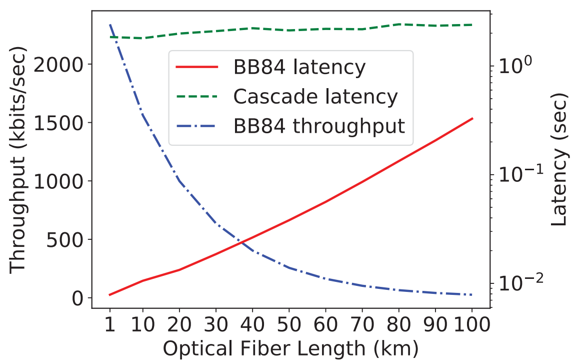


Fig. 2 Simulated key throughput and contributions of BB84 and Cascade protocols to latency.

## References


[1] C. Bennett and G. Brassard, Proc. IEEE Int. Conf. on Computers, Systems and Signal Processing, p.175, 1984
[2] G. Brassard and L. Salvail, Advances in Cryptology - EUROCRYPT '93, p.410, 1993
[3] W. Hwang, Physical Review Letters, 91, p. 057901, 2003
[4] A. Dahlberg and S. Wehner, Quantum Science and Technology, 4, p. 015001, 2014
[5] NetSquid: Network Simulator for Quantum Information Using Discrete Events, https://netsquid.org/

This material is based upon work supported by Laboratory Directed Research and Development (LDRD) funding from Argonne National Laboratory, provided by the Director, Office of Science, of the U.S. Department of Energy under contract DE-AC02-06CH11357.

The submitted manuscript has been created by UChicago Argonne, LLC, Operator of Argonne National Laboratory ("Argonne"). Argonne, a U.S. Department of Energy Office of Science laboratory, is operated under Contract No. DE-AC02-06CH11357. The U.S. Government retains for itself, and others acting on its behalf, a paid-up nonexclusive, irrevocable worldwide license in said article to reproduce, prepare derivative works, distribute copies to the public, and perform publicly and display publicly, by or on behalf of the Government. The Department of Energy will provide public access to these results of federally sponsored research in accordance with the DOE Public Access Plan (http://energy.gov/downloads/doe-public-access-plan).

# Integration of a Cost-Effective QKD Implementation in WDM Optical Networks

**P. Martelli, M. Brunero, P. Parolari, F. Rossi, A. Tosi, and M. Martinelli**

*Politecnico di Milano, Dipartimento di Elettronica Informazione e Bioingegneria, Via G. Ponzio 34/5, 20133 Milano, Italy*

Nowadays encryption is exploited for protecting information exchange in several applications. Nevertheless the security of commonly used encryption algorithms is based on the extremely high computational costs required for message decryption. On the other hand, quantum key distribution (QKD) allows the key exchange between two users (Alice and Bob) in a way which has been proved as unconditionally secure, thanks to the fundamental principles of quantum physics [1,2]. However to make the QKD a reliable and effective widespread solution, it is essential to reduce the cost and enhance the scalability.

In the present work we experimentally demonstrate the integration of a cost-effective QKD implementation in a typical WDM optical network. The considered QKD system is based on a modified version [3] of the polarization-encoded BB84 protocol [1], where Bob uses a Faraday rotator (FR) variable over four states and only one single-photon avalanche detector (SPAD), as shown in Fig. 1(a). Alice transmits to Bob a stream of polarized single photons, obtained by a strongly attenuated laser followed by a polarization controller. The polarization of each photon is set by Alice in one state of polarization among four possible states (horizontal, vertical, diagonal, anti-diagonal). A key bit is exchanged in a secure way through the quantum channel when Alice and Bob choose the same basis (either "rectilinear" or "diagonal") and a photon is detected by the SPAD after a polarizer set in a fixed state (e.g., vertical). Bob chooses the FR rotation angle among four possible values (0°, 45°, 90°, 135°), making two binary choices. The first one (i.e., a rotation of either 0° or 45°) represents the choice of the measurement basis and is communicated to Alice through the public channel, while the second one (i.e., an additional rotation of either 0° or 90°) is maintained secret and allows Bob for determining the key bit.

The integration of the proposed scheme of QKD in a WDM optical network has been tested according to the scheme depicted in Fig. 1(b). The QKD channel is in L band at the wavelength of 1583 nm, while the classical WDM channels, used for carrying the conventional data traffic, are in C band in the wavelength range from 1528 to 1559 nm. In our experimentation the classical WDM channels are emulated by filtering the amplified spontaneous emission (ASE) of an Erbium-doped fiber amplifier (EDFA) through a programmable optical filter, in order to reproduce the same optical spectrum of a typical WDM signal consisting of 80 channels with 50-GHz spacing and 28-GBaud symbol rate. The QKD channel is multiplexed/demultiplexed in the WDM network by exploiting commercially available L/C WDM couplers. The detection of the single photons is carried out through an InGaAs/InP SPAD, as described in [4]. The experimental results confirm the feasibility of the proposed cost-effective QKD implementation in WDM optical networks, achieving a quantum bit-error rate (QBER) below the accepted limit (11%) for secure QKD [2], in typical operating conditions.

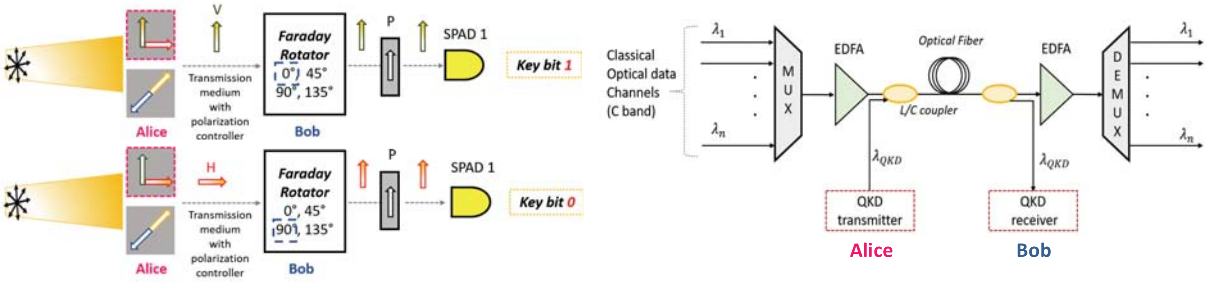


Fig. 1 Scheme of the single-SPAD implementation of BB84 (a); integration of QKD in WDM optical network (b).

## References

[1] C.H. Bennett and G. Brassard, "Quantum cryptography: public key distribution and coin tossing," in Proc. IEEE Internat. Conf. on Computers, Systems and Signal Processing 1984, Bangalore, 175.

[2] P.W. Shor and J. Preskill, "Simple proof of the security of the BB84 quantum key distribution protocol," Phys. Rev. Lett. **85**, 441 (2000).

[3] P. Martelli et al., "Single-SPAD implementation of quantum key distribution," in Proc. ICTON 2019, We.C5.1.

[4] A. Tosi et al., "Fully programmable single-photon detection module for InGaAs/InP single-photon avalanche diodes with clean and sub-nanosecond gating transitions," Rev. Sci. Instrum. **83**, 013104 (2012).

# Spectral Domain in Quantum Optical Coherence Tomography

**Sylwia M. Kolenderska[1,2†], Piotr Kolenderski[3†], Frédérique Vanholsbeeck[1,2]**
[1]*The Dodd-Walls Centre for Photonic and Quantum Technologies, New Zealand;*
[2]*The Department of Physics, The University of Auckland, Auckland 1010, New Zealand;*
[3]*Faculty of Physics, Astronomy and Informatics, Nicolaus Copernicus University, Grudziądzka 5, 87-100 Toruń, Poland;*
[†]*These authors contributed equally to this work.*

Optical Coherence Tomography (OCT) is a high-resolution 3D imaging technique based on white-light interferometry that is non-destructive and non-invasive[1]. However, OCT images are degraded by chromatic dispersion, what makes it unsuitable for imaging of bulk dispersive objects, such as a whole human eye. Quantum OCT (Q-OCT) [2] is free of this problem and additionally offers an enhanced axial resolution. In Q-OCT, the classical light is replaced by a source of frequency-entangled photon pairs and the traditional interferometer – by the Hong-Ou-Mandel (HOM) interferometer (Fig. 1a). Due to the indistinguishability of the entangled photons, the coincidence signal – and thus the depth profile – is not affected by dispersion. However, Q-OCT in its current form has many shortcomings. It is very slow due to the need for mechanical scanning and its detection scheme induces image-scrambling artifacts. Also, for the dispersion cancellation additional technical conditions have to be met: the pump light should be very narrowband to produce photons with the proper spectral correlation [3].

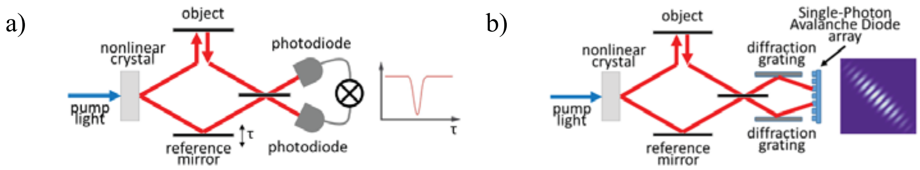


Fig. 1 In Q-OCT, a monochromatic pump generates entangled photon pairs. One photon propagates through the object in one arm, and the other one is reflected from the reference mirror in the other arm. They both overlap at a beamsplitter. (a) In Q-OCT, a Hong-Ou-Mandel dip is formed in the signal when the interferometer's arms' lengths are the same. (b) In JS-Q-OCT, joint spectrum is measured.

We propose a novel Q-OCT method based on joint spectrum detection (JS-Q-OCT) (Fig. 1b). It offers artefact-free images and dispersion cancellation without any restrictions on the photon pair source. The main diagonal of the joint spectrum (Fig. 2b), when Fourier transformed, gives a depth profile with a perfect dispersion cancellation (Fig. 2c). The previous "time-domain" implementation of Q-OCT doesn't have access to spectral information, therefore the source must produce photon pairs whose joint spectrum is as narrow along the main diagonal as possible. In JS-Q-OCT the dispersion-cancelled signal is extracted during post-processing. We also found that in JS-Q-OCT there are always two artefacts for every two interfaces (compared to one artefact for every two interfaces in "time-domain" Q-OCT), but the information present in the joint spectrum can be used to remove them. Fourier transformation of the off-diagonals positioned parallel to the main diagonal produces depth profiles with varying height of artefacts. A certain off-diagonal exists (Fig. 2d) for which the height of the artefacts drops to zero (Fig. 2e). This is a basis for an artefact removal algorithm for multi-layered objects.

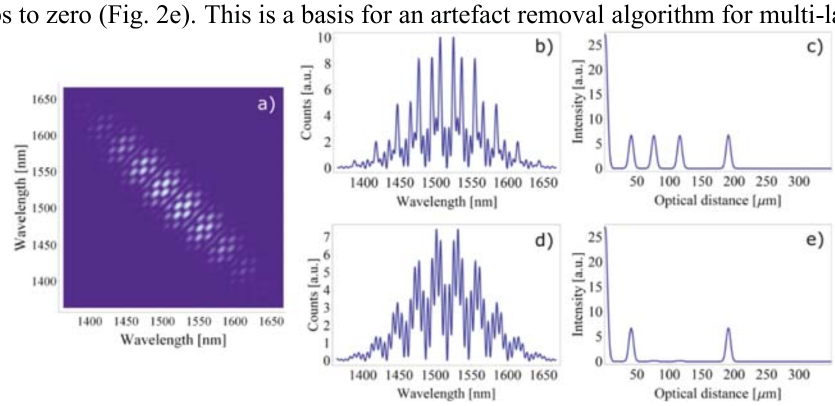


Fig. 2 The joint spectrum corresponding to a 100-μm thick layer positioned 40 μm away from zero delay point. (b) Main-diagona spectrum (c) Its Fourier transform, which incorporates artefact peaks (d) An off-diagonal spectrum can be chosen so that (e) its Fourier transform depicts only the structure.

**References**

[1] Drexler & Fujimoto, *Optical coherence tomography: technology and applications* (Springer, 2015).
[2] Abouraddy et. al. Phys. Rev. A, **65**, 053817 (2002)
[3] Okano et al.,. *Phys. Rev. A,* **88**, 043845 (2013)

# Bounding the Survival-Depth of Time-Energy Entanglement Through Absorptive & Scattering Media for Entangled Two-Photon Absorption

**Daniel J. Lum[1], Michael D. Mazurek[2,3], Alexander Mikhaylov[3], Kristen Parzuchowski[3], Sae Woo Nam[2], Marcus T. Cicerone[1], Ralph Jimenez[3], T. Gerrits[2], Martin J. Stevens[2], Charles H. Camp Jr.[1]**

[1]*National Institute of Standards and Technology, Gaithersburg, MD, USA,* [2]*National Institute of Standards and Technology, Boulder, CO, USA,* [3]*JILA, University of Colorado, Boulder, CO, USA*

In this work, we present the development of a Franson interferometer to assess the maintenance of time-energy entanglement through biological samples as function of sample thickness. The purpose of the unique interferometer design and entangled source is to assess the power of entangled photons to enhance the sensitivity and depth-penetration of two-photon microscopy for deep biological microscopy.

Two-photon microscopy is an imaging modality in which the combined energy of two photons excites fluorescent probes. The use of near-infrared or infrared sources enables deep penetration (≈1 mm), owing to low linear absorption and scatter. The method relies on two-photon absorption (TPA), a second-order nonlinear optical mechanism, which is intrinsically weak and scales quadratically with incident laser intensity. As this mechanism requires two photons to co-localize spatially and temporally, a highly-correlated pump source (e.g., *entangled)* should increase the efficiency of TPA. Indeed, theory shows the entangled-TPA (eTPA) signal will scale linearly with pump power for low-photon flux [1]. Additionally, experimental demonstrations of eTPA suggest orders-of-magnitude enhancement over classical TPA [2,3]. Our task is to evaluate the operational depth over which time-energy entangled photons retain their correlations through tissue.

To achieve unprecedented depth penetration in bioimaging using TPA/eTPA microscopy, requires understanding the correlation range. Ideally, we need to characterize the time-energy correlations as a function of media depth with well-defined scattering and absorption coefficients. However, measuring these correlations is challenging. Instead, we verify the presence of nonlocal correlations by using a Franson interferometer to violate a Bell inequality [4]. By "nonlocal", we mean the correlations appear linked in a way that exceeds faster-than-light communication. While violating a Bell inequality is a stringent method to witness nonlocal correlations, it is easier than performing quantum-state tomography. Figure 1 (a) presents the experimental setup with a type of folded polarization-based Franson interferometer. By measuring the sample thickness at which point the fringe contrast in coincidence counts drops below 70.7 %, we will learn at what depth the photons lose their nonlocal correlations. Correlations not strong enough to violate a Bell inequality may still exist deeper in the sample, but eTPA will need to be measured directly while a Bell inequality will provide a useful lower operational bound that is easier to measure. As a baseline (without a tissue sample), Fig. 1 (b) shows that our interferometer obtains a fringe contrast of at least 97 % and demonstrates that our photons exhibit nonlocal correlations.

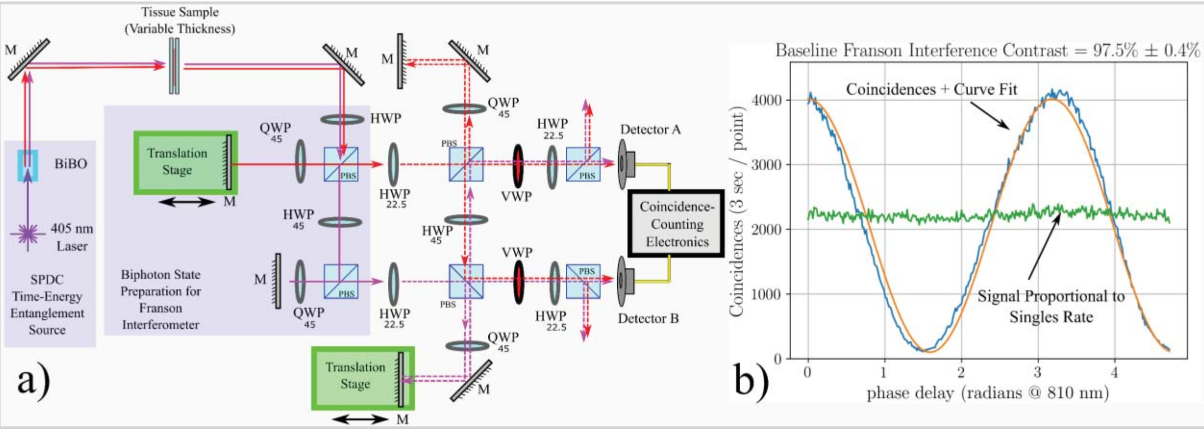


Fig. 1 (a) Folded polarization-based Franson interferometer for verifying the survival of time-energy entanglement through tissues. SPDC: spontaneous parametric down-conversion, BiBO: Bismuth Borate nonlinear crystal, M: Mirror, PBS: polarized beamsplitter, QWP: quarter-wave plate, HWP: half-wave plate, VWP: variable-wave plate. (b) Franson interference observed in the absence of a tissue sample.

**References**

[1] Dayan, Barak. *Physical Review A* 76.4, 043813 (2007)
[2] Dayan, Barak, et al. *Physical Review Letters* 94.4, 043602 (2005)
[3] Upton, L., et al. *The Journal of Physical Chemistry Letters* 4.12, 2046 (2013)
[4] Franson, James D. *Physical Review Letters* 62.19, 2205 (1989)

# Homodyne-like Tomographic reconstruction of Quantum States with Photon-Number-Resolving Detectors

**A. Allevi[1], S. Olivares[2], M. G. A. Paris[2], M. Bondani[3]**

[1]*University of Insubria, Department of Science and High Technology, Como, Italy*

[2]*University of Milan, Department of Physics, Milan, Italy*

[2]*CNR, Institute for Photonics and Nanotechnologies, Como, Italy*

Quantum optical states are usually reconstructed by means of optical homodyne tomography [1] based on homodyne detection. In standard homodyne detection, the optical signal interferes at a balanced beam splitter with a high-intensity coherent state, the local oscillator (LO). The two outputs of the beam splitter are detected by two p-i-n photodiodes, whose difference photocurrent is amplified, divided by the value of the LO amplitude and recorded as a function of the LO phase. This procedure is a measure of the signal-field quadrature and can be used to retrieve the complete information on the state through the implementation of a tomographic reconstruction of the Wigner function or of the density matrix of the optical state.
As an alternative, we implement a homodyne-like (HL) detection scheme, in which a low-energy LO and two photon-number-resolving detectors (HPD, Hamamatsu) are used. Such a hybrid configuration provides direct access to the number of photons measured by each detector separately. The measured numbers can then be used to obtain different kinds of information about the state to be analyzed. First of all, the photon number distributions of the states at the outputs of the beam splitter can be retrieved [2]. Second, from the measurement of the mean number of photons values, an estimation of the phase difference between signal and LO can be obtained [3]. Third, from the shot-by-shot difference of detected numbers the quadrature operator of the signal can be sampled at different phase differences and from them the tomographic reconstruction of the states can be implemented [4].
The potentiality of the HL detection scheme has been successfully exploited for a state-discrimination protocol with coherent states [5,6] and suggested to outperform standard homodyne detection in quantum key distribution with continuous variables [7].
Here we demonstrate the tomographic reconstruction of continuous-variable optical states using the HL detection scheme [4]. In particular, we reconstructed the density matrix of single-mode quantum states, and we computed the expectation values of the first moments of the quadrature operator.

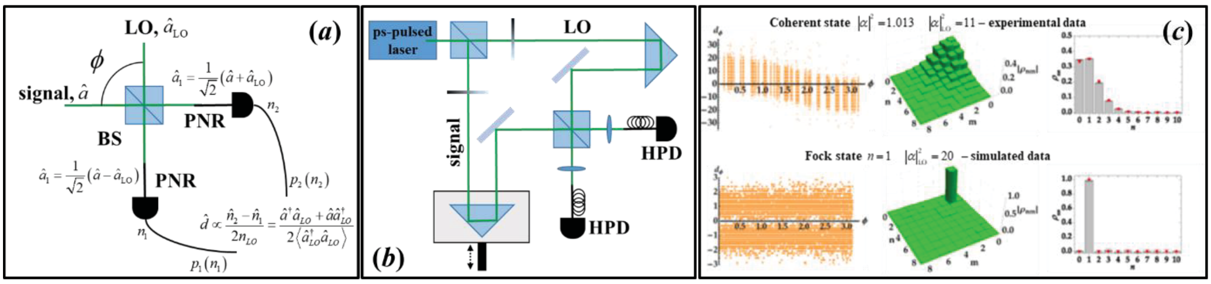


Fig. 1 (*a*) Scheme of HL detection; (*b*) Experimental setup; (*c*) Tomographic reconstruction of optical states: results for a set of experimental data (coherent state) and for a set of simulated data (Fock state $n = 1$).

We have tested the HL scheme on a number of quantum states, using experimental data (coherent and phase-averaged coherent states) and simulated data (Fock states and odd and even cat states). Our results demonstrate that a highly intense LO is not necessary to perform homodyne detection: even a modest imbalance between signal and LO is sufficient to successfully perform quantum-state tomography.

## References

[1] A. I. Lvovsky et al., Rev. Mod. Phys. 81, 299 (2009)
[2] M. Bondani et al., Adv. Sci. Lett., 2 463 (2009).
[3] M. Bondani et al., J. Opt. Soc. Am. B, 27 333 (2010).
[4] S. Olivares et al., arXiv:1809.00818.00818v1
[5] M. Bina et al., Opt. Express 25, 10685 (2017).
[6] A. Allevi et al., Int. J. Quantum Inf. 15, 1740016 (2017).
[7] M. Cattaneo et al., Phys. Rev. A 98, 012333 (2018).

# Temporal Mode Manipulation using a Raman Quantum Memory

**S. E. Thomas[1,2], J. H. D. Munns[1,2], M. Hynes[1], T. M. Hird[1,3], P. M. Ledingham[1], D. J. Saunders[1], J. Nunn[4], B. Brecht[1,5], and I. A. Walmsley[1,2]**

[1]*Clarendon Laboratory, University of Oxford, Parks Road, Oxford, OX1 3PU, UK*
[2]*Blackett Laboratory, Imperial College London, London SW7 2BW, UK*
[3]*Department of Physics and Astronomy, University College London, London WC1E 6BT, UK*
[4]*Centre for Photonics and Photonic Materials, University of Bath, North Road, Bath, BA2 7AY, UK*
[5]*Integrated Quantum Optics, Applied Physics, Paderborn University, 33098 Paderborn, Germany*

There are many architectures for quantum information processing, each with their own distinct advantages and drawbacks, and the route towards scalable quantum technologies is likely to involve combining these unique advantages in a hybrid system. Photons are a promising platform for quantum communication and for interfacing different nodes of a quantum network. However, to optimally couple different devices and components of a quantum network we require the capability to engineer and manipulate the spectral-temporal wavepacket of pulsed photons, the so-called temporal mode (TM) [1]. The ability to coherently manipulate TMs, for example by adjusting the bandwidth, is therefore a key capability of future quantum technologies.

We demonstrate TM manipulation of weak coherent pulses in a Raman quantum memory in warm atomic caesium vapour [2]. The Raman interaction can be described as a time non-stationary light-matter beam splitter that acts on a single temporal mode [3]; the stored and retrieved TMs are determined by the temporal amplitudes of the strong control pulses used to drive the memory. This enables storage, delay and re-shaping of a user-defined TM in one single device.

The Raman memory operates on pulses in the MHz and GHz regime, and can therefore interface narrowband atomic systems with fast, GHz-bandwidth communication networks. We demonstrate coherent bandwidth conversion of ns-duration Gaussian pulses by increasing and decreasing the bandwidth by a factor of 25, as shown in Figure 1(a). We compare the efficiency of this process to that of using a passive intensity filter, and find that the memory can outperform a filter at large compression factors.

Furthermore, TMs of light have been highlighted as an appealing basis for quantum information processing [1]. They enable compact, high-dimensional encodings, whilst remaining compatible with single-mode optical fibres and waveguide devices. As an example we demonstrate mode conversion using Hermite-Gaussian (HG) polynomials as a qudit basis for photons. We demonstrate coherent conversion between different Hermite-Gaussian modes, and Figure 1(b) shows that we can perform arbitrary conversions on this five-dimensional alphabet with a constant high efficiency of 35%.

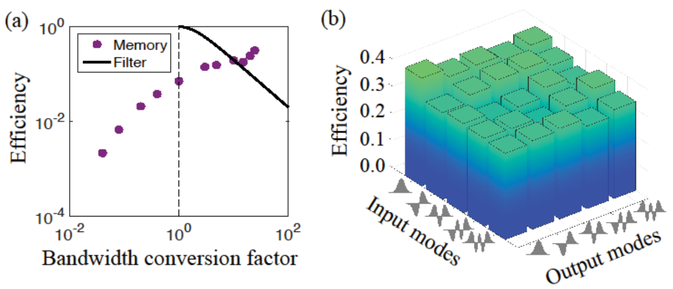


Fig. 1 (a) Efficiency of bandwidth conversion using the Raman memory. The solid line shows the equivalent efficiency for a bandwidth filter. (b) The efficiency of conversion between different Hermite-Gaussian temporal modes.

We have shown that the Raman memory is a versatile device for coherent temporal mode manipulation. Its applications include interfacing different solid state systems such as atoms and quantum dots, where you require not only bandwidth conversion but also re-shaping (temporal inversion) of the temporal wavepacket. It also will enable quantum key distribution using temporal modes as a high dimensional encoding alphabet to realise fibre-compatible qudits. Finally, it can be used as a coherent buffer to optimally filter photons from solid-state single photon sources [4], thus circumventing the challenges of indistinguishability and source reproducibility. This highlights its potential as a key device in future quantum networks.

**References**

[1] B. Brecht *et al.*, Phys. Rev. X, **5** 041017 (2015)
[2] K. F. Reim *et al.*, Phys. Rev. Lett., **107** 053603 (2011)
[3] J. Nunn *et al.*, Phys. Rev. A, **75** 011401 (2007)
[4] S. Gao *et al.*, arXiv 1902.07720 [quant-ph] (2019)

# Quantum Seeing in the Dark: Testing the Limits of Human Vision

**Paul G. Kwiat[1], Rebecca Holmes[2], Julia Spina[1], Michelle Victora[1], and Ranxiao Frances Wang[3]**

[1] Department of Physics, University of Illinois at Urbana-Champaign, IL USA 61801
[2] Los Alamos National Laboratory, Los Alamos, NM 87545 USA
[3] Department of Psychology, University of Illinois at Urbana-Champaign, IL USA 61801

One of the earliest low-light human vision experiments was conducted by Hecht, Shlaer and Pirenne in 1942 [1]. The accuracy of their results, as well as those of similar early experiments, was severely limited by the randomness of classical light sources, which can never produce single photons without a sizable likelihood of producing more two or more. Since then, the ability to create efficient and tunable single-photon sources has greatly improved, enabling proper investigations of the true limits of human vision [2,3] and potentially allowing the eventual study of quantum phenomena using the visual system (e.g., entanglement and superposition). We report the latest results from our experiment using heralded single photons from SPDC to test a trained subject's ability to recognize single-photon stimuli. Our SPDC pair source produces single photons with a heralding efficiency of 37% at a wavelength of 505 nm, near the maximal sensitive wavelength of the rod photoreceptor cells (low-light receptors in the retina). The heralded $g^{(2)}(0)$ was also measured to be 0.0023±.001, indicative of a suitably low probability of multi-photon events. Single photons from this source travel to a viewing station through one of two optical fibers, chosen at random for each event; the output of each fiber is aligned to one of two spots on the peripheral (area of the eye densest with rod cells) of the dominant eye of the fully dark-adapted observer. Upon receiving the stimulus, the observer indicates *which* fiber they believe emitted the stimulus, as well as their corresponding level of confidence in their response. With this 'forced-choice' protocol, if the subject's recognition accuracy is statistically above 50%, we can definitely conclude they had interpreted the stimulus and consciously recognized a single photon.

With this source we previously set new limits on the low-light temporal integration time of the human visual system, observing times exceeding 500 ms [4]. We also previously observed that stimuli consisting of an average of 3 photons on the retina could be observed, at least by some subjects, with success rates up to 60%. After several system upgrades, we are now completing our single-photon trials. Based on previous results, we estimate a success rate >50.5% in all trials, and > 55% in our high-confidence trials. With these estimated success rates, we are conducting ~2500 trials split between several different trained observers, which will allow us to draw a conclusion with enough statistical power to make definite statements about the limits of human vision. While our preliminary overall recognition accuracy does not yet provide definitive evidence that our subjects can perceive single photons, our high confidence accuracy shows active recognition of single photons within a confidence interval of ~83%.

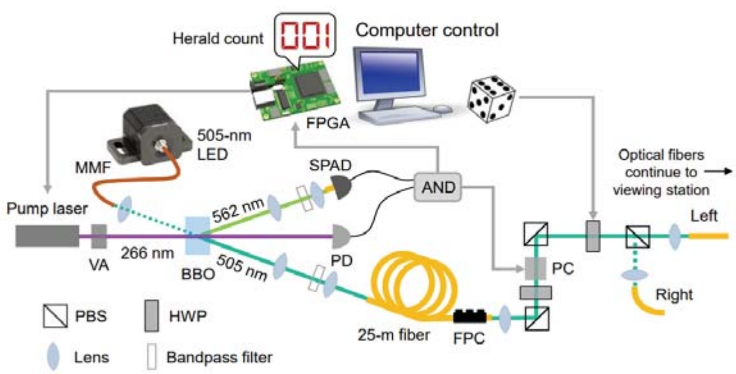


Fig. 1. Vision-optimized single-photon source [3]. A UV pump laser produces 505- and 562-nm photon pairs inside a BBO crystal. The 562-nm herald photons are detected by a single-photon avalanche photodiode (SPAD) in coincidence with a photodiode (PD) – in order to eliminate background noise – and recorded by an FPGA. The 505-nm photons are delayed by a 25-m optical fiber before passing through a polarizing beam splitter (PBS) and half wave plate (HWP). The Pockels cell (PC) works with the FPGA to deliver a single 505-nm signal photon, which is subsequently directed to either the "Left" or "Right" viewing station fiber.

## References

[1] S. Hecht, "Energy, Quanta, and Vision", The Journal of General Physiology **25**, 819-840 (1942).
[2] J. Tinsley et al., "Direct detection of a single photon by humans", Nature Comm. **7**, 12172 (2016).
[3] R. M. Holmes, et al, "Testing the limits of human vision with quantum states of light: past, present, and future experiments," Proc. SPIE **10659**, Advanced Photon Counting Techniques XII, 1065903 (2018).
[4] R. Holmes, R., M. Victora, R. F. Wang, and P. G. Kwiat, "Measuring temporal summation in visual detection with a single-photon source," Vision Research **140**, 33 (2017).

# Designing linear-optical interferometers for quantum gate implementation

**I. V. Dyakonov[1], M. Yu. Saygin[1], I. V. Kondratyev[1], S. A. Mironov[2,3,4], S. S. Straupe[1] and S. P. Kulik[1]**

[1]Quantum Technologies Center, Faculty of Physics, Lomonosov Moscow State University, Leninskie Gory 1, building 35, 119991, Moscow, Russia.
[2]Institute for Nuclear Research of the Russian Academy of Sciences, 60th October Anniversary Prospect, 7a, 117312 Moscow, Russia
[3]Institute for Theoretical and Experimental Physics, Bolshaya Cheriomyshkinskaya, 25, 117218 Moscow, Russia
[4]Moscow Institute of Physics and Technology, Institutski pereulok, 9, 141701, Dolgoprudny, Russia

Experimental implementation of a quantum computing algorithm strongly relies on the ability to construct required unitary transformations applied to the input quantum states. In particular, near-term linear optical computing requires universal programmable interferometers, capable of implementing an arbitrary transformation of input optical modes. So far, these devices were composed as a circuit with well-defined building blocks, such as balanced beamsplitters [1]. This approach is vulnerable to manufacturing imperfections inevitable in any realistic experimental implementation, and the larger the circuit size grows, the stricter the tolerances become. In this work we demonstrate a new methodology for the design of the high-dimensional mode transformations, which overcomes this problem, and carefully investigate its features. The circuit in our architecture is composed of interchanging mode mixing layers, which may be almost arbitrary, and layers of variable phaseshifters, allowing to program the device to approximate any desired unitary transformation.

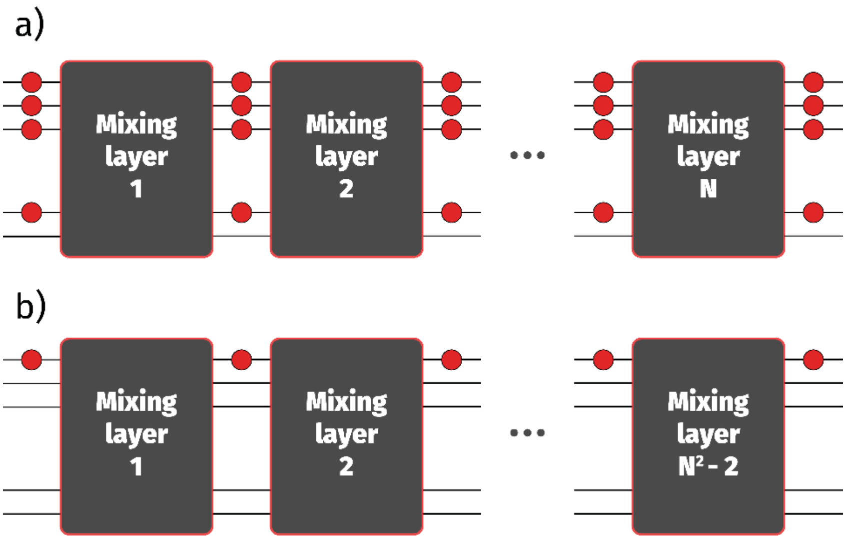


Fig. 1. The illustration of the general layout of the proposed circuit. The picture a) depicts the he layout with N-1 phases per layer. The picture b) demonstrates the possible modification of the first scheme.

We propose an optical circuit architecture which is extremely robust even to quite large fabrication errors. Furthermore, the mode mixing elements comprised in the proposed circuit should not be created according to the predefined template such as the balanced 50:50 beamsplitters forming the Mach-Zehnder interferometer but may be quite arbitrary mode-coupling elements. Our numerical experiments show strong evidence, that this architecture is capable of realizing large-scale arbitrary unitary transformations with high fidelity.

We also present a numerical package designed for efficient computation of the fock state transformations implemented by the interferometer with the given unitary matrix. The development of this software tool is motivated due to necessity of the quantum gate with optimized success probability since the linear optical multi-qubit gates are intrinsically non-deterministic. The computationally heavy code is implemented in C++ and exposed to the Python interface making it really easy to use.

The preprint of the work is published on arXiv [2].

References:
1. W. R. Clements, et al. Optica 3, 12, 1460-1465 (2016)
2. M. Saygin, et al. arXiv e-prints, arXiv:1906.06748 (2019)

# Quantum Teleportation between Multiple Senders and Receivers


**Sang Min Lee[1], Seung-Woo Lee[2], Hyunseok Jeong[3], Hee Su Park[1]**

[1]*Korea Research Institute of Standards and Science, Daejeon 34113, South Korea*

[2]*Quantum Universe Center, Korea Institute for Advanced Study, Seoul 02455, South Korea*

[3]*Department of Physics and Astronomy, Seoul National University, Seoul 08826, South Korea*


Quantum teleportation is a key protocol for realizing quantum networks. Teleportation of quantum information shared by multiple parties can help to build versatile quantum networks that incorporate distributed quantum communications and computations. We propose a protocol to teleport an arbitrary logical secret qubit (encoded in GHZ-like state) shared by $m$ senders to $n$ receivers through a $(m + n)$-qubit GHZ state and distributed Bell measurements [1, 2], and experimentally demonstrate the case of $m = n = 2$. Figure 1(a) illustrates the teleportation protocol (for $m = 3$, $n = 4$) and Fig. 1(b) shows the schematic of the experimental setup ($m = n = 2$).

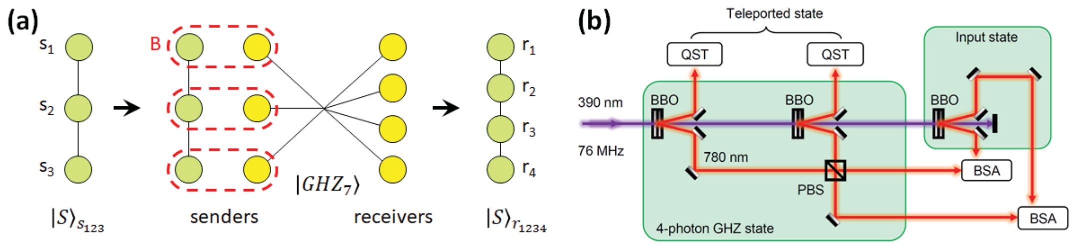


Fig. 1 Teleportation of shared logical qubits. (a) Protocol to transfer a logical secret qubit state $|S\rangle$ between three senders and four receivers; circle: qubit, line: GHZ-type entanglement, B: Bell-state measurement. (b) Experimental scheme to demonstrate the $m = n = 2$ case; BBO: beta barium borate crystal, PBS: polarizing beam splitter, QST: quantum state tomography, BSA: Bell-state analyzer.

The logical secret qubit is defined with $N$ photons as $\alpha|H\rangle^{\otimes N} + \beta|V\rangle^{\otimes N}$ in terms of horizontal $|H\rangle$ and vertical $|V\rangle$ polarizations of a single photon. Within this encoding, projection measurements to logical Bell states are composed of $N$ times of single-photon-qubit Bell state measurement, and can reach near-unity success probability $1 - 2^{-N}$ for large $N$ using linear optics [1]. This advantage, however, cannot be straightforwardly realized in experiments using conventional Bell-state analyzers with one non-polarizing beam splitter and two polarizing beam splitters [3] because the failure event in which two photons reside in one output mode must be distinguished from photon loss. Therefore, a unit Bell state analyzer (BSA) of this experiment includes additional four non-polarized beam splitters to the end and total eight photon detectors in contrast to four-photon detectors in the original design. The Bell state analyzers and the quantum state tomography setup utilize birefringence-compensated optical fiber devices to reduce the occupied space and improve the overall stability.

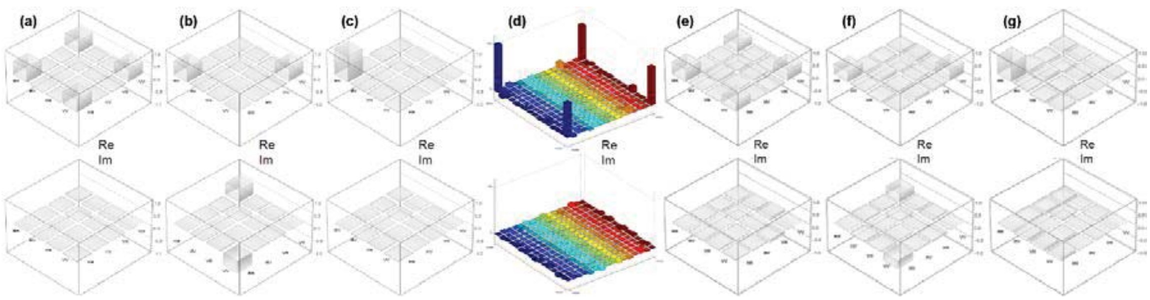


Fig. 2 Reconstructed quantum states of (a-c) three inputs, (d) $GHZ_4$, and (e-g) three outputs of $|HH\rangle + |VV\rangle$, $|HH\rangle + i|VV\rangle$, and $|HH\rangle$.

Three input/output states and a four-photon GHZ state were initially generated and reconstructed as shown in Fig. 2. The fidelities of the input states and the GHZ state with the ideal states were 0.967(1) ~ 0.992(1) and 0.73(1), respectively. The reconstructed teleported output states had fidelities of 0.84(4), 0.78(6), and 0.75(5) with the three input states, respectively, and beat the classical bound (2/3) by 1.7 ~ 4.3 standard deviations. The proposed protocol does not require a trusted node to connect the participants. It can be further extended to be fault-tolerant if error correction encodings are employed [2].


**References**

[1] S.-W. Lee *et al.* PRL **114**, 113603 (2015).

[2] S. M. Lee *et al.* arXiv:1812.00565 (2018).

[3] K. Mattle *et al.* PRL **76**, 4656 (1996).

# Broadband Nonlocal Dispersion Compensation In Buried Telecommunications Fiber

**James A. Grieve[1], Yicheng Shi[1], Ho Shun Poh[1] Christian Kurtsiefer[1], Alexander Ling[1]**

[1]*Centre for Quantum Technologies, 3 Science Drive 2, National University of Singapore, 117543 Singapore*

[2]*Department of Physics, National University of Singapore, Blk S12, 2 Science Drive 3, 117551 Singapore*

Correlated photon pairs created via spontaneous parametric downconversion (SPDC) in a nonlinear crystal are a core component in many entanglement-based quantum communication tasks such as quantum key distribution (QKD) [1] and clock synchronization [2]. While photons produced by this mechanism share a high degree of temporal correlation, they are in general broadband. When transmitted through optical fibers, chromatic dispersion may obscure timing correlations, complicating the task of identifying pairwise events. For this reason, photon pair sources deployed over fiber are often filtered spectrally [3] or make use of less efficient narrow-band phasematching processes both of which reduce the throughput of the system.

Photon pairs produced by SPDC share time-energy entanglement, and are tightly anticorrelated in frequency. When two time-energy entangled photons experience equal and opposite dispersion, the effects may cancel. Known as nonlocal dispersion compensation [4], this phenomenon has been studied in a laboratory context, typically making use of specialized optical elements to achieve negative dispersion [5]. For practical use, single mode optical fibers contain both positive and negative dispersion within the spectral window surrounding the zero dispersion wavelength (ZDW). In telecom fibers, this lies in the O-band around 1310nm. Photon pairs degenerate around this wavelength will experience nonlocal dispersion compensation without the use of any additional optical elements. All-fiber dispersion compensation was utilized in a QKD field test in 1998 [6].

In this contribution, we explore the use of this mechanism in scenarios where the precise location of the ZDW varies, for example due to the multi-segment nature of most deployed fiber. By using a broadband photon pair source spanning 100 nm in the telecommunications O-band, we observe nonlocal dispersion compensation over up to 80 km lab-based fiber. Timing correlations are also preserved after transmission over a pair of 10 km deployed fibers comprising multiple segments with differing ZDW. The effect is remarkably robust, with compensation achieved without active tuning of the photon pair source. We believe this will be of interest to those working to leverage photon pair technologies in real-world applications.

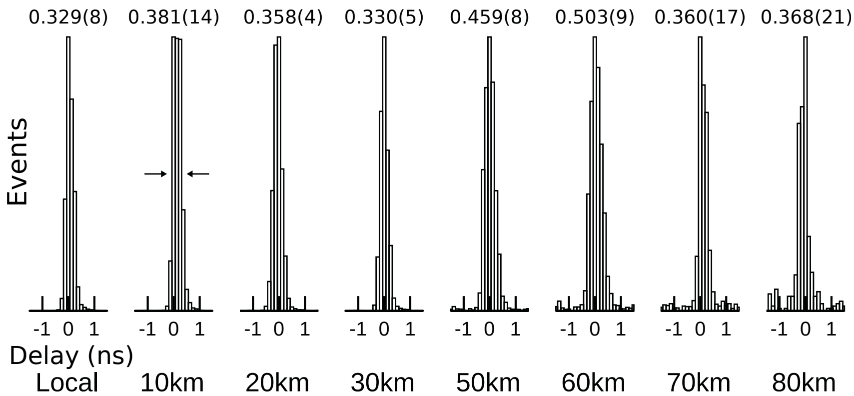


Fig. 1 Histograms of coincident events after transmission through a series of lab-based fiber spools, with varying zero dispersion wavelength. Three spools were used with 10 km, 20 km and 50 km lengths, other distances were achieved by combination of these spans. In all cases dispersion compensation preserved timing correlations to within 0.5 ns.

## References

[1] M. P. Peloso, I. Gerhardt, C. Ho, A. Lamas-Linares, & C. Kurtsiefer, New J Physics, 11 (2009).
[2] C. Ho, A. Lamas-Linares, & C. Kurtsiefer, New J Physics, 11, 114 (2009).
[3] S. Fasel, N. Gisin, G. Ribordy, & H. Zbinden, Eur Phys J D, 30, 143–148 (2004).
[4] J. D. Franson, Phys Rev A, 45(5) 3126–3132 (1992)
[5] K. A. O'Donnell, Phys Rev Lett, 106(6), 1–4 (2011).
[6] W. Tittel, J. Brendel, H. Zbinden, & N. Gisin, Phys. Rev. Lett. 2, 69 (1998)

# Characterization of a Multi-core Optical Fiber as a Carrier of Spatial Qudits of Single Photons

**Hee Su Park[1], Hee Jung Lee[1,2], Jae Hyeong Youn[3], and Kwang Yong Song[3]**

[1]*Korea Research Institute of Standards and Science, Daejeon, South Korea*

[2]*currently at Agency for Defense Development, Daejeon, South Korea*

[3]*Chung-Ang University, Seoul, South Korea*

Spatial modes of single photons are a useful quantum information carrier that has infinite intrinsic dimensionality and provides relative ease of arbitrary unitary operations compared to temporal modes. Fiber transport of such spatial *qudits* has been demonstrated through superposition states of multiple cores inside a single multi-core optical fiber (MCF) [1], where generation, transmission, and measurement of arbitrary four-dimensional entanglement between two distinct fibers were realized. This work introduces experimental methods to characterize an MCF to test its achievable transmission distance and phase stability.

Decoherence between the core modes is mainly caused by the inter-core differential group delay. When the group delay between core $i$ and core $j$ becomes greater than the coherence length of photons, a superposition state over the two core modes $a|i\rangle + b|j\rangle$ evolves to a mixed state $|a|^2|i\rangle\langle i| + |b|^2|j\rangle\langle j|$, removing the superposition and entanglement incorporating the two components. The inter-core group delay can be quantified by a wavelength-domain interferometry as shown in Fig. 1(a) [2]. The period of interference fringes in the output spectrum of the Mach-Zehnder interferometer reveals the difference of group indices between the interfering cores. The interfering beams are split and combined by a spatial light modulator and single-mode-fiber coupling.

The difference of phase indices induces phase instability owing to ambient temperature change or vibrations, and is characterized by the *beat length* between different core modes. We fabricate an acousto-optic long-period fiber grating along an MCF to couple a core mode to an anti-symmetric cladding mode as shown in Fig. 1(b). By comparing the frequencies that couples different core modes to a common cladding mode, the beat length between the core modes, averaged along the grating length, is measured. The results show the phase or group index differences ranging from $10^{-5}$ to $10^{-4}$, which limits the practical transmission distance to a few meters for a moderate photonic wavelength bandwidth (~1 nm) and without an active phase stabilization.

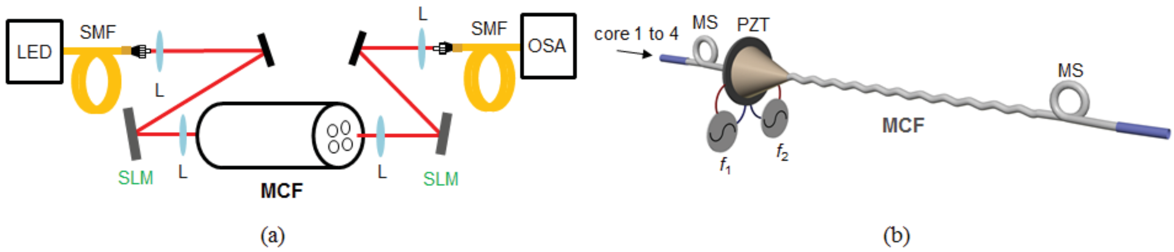


Fig. 1. Experimental setup. (a) Wavelength-domain interferometry. (b) Acousto-optic long-period fiber grating. MCF: multi-core fiber, SMF: single-mode fiber, L: lens, MS: mode stripper.

**References**

[1] H. J. Lee and H. S. Park, Photonics Res. **7**, 19-27 (2019).

[2] H. J. Lee, H. S. Moon, S.-K. Choi, and H. S. Park, Opt. Express **23**, 12555-12561 (2015).

# Improved Light-Matter Interaction in a Thulium Cavity Memory for Qubit Storage

Jacob H. Davidson,[1,2] Pascal Lefebvre,[1] Jun Zhang,[1] Varun B. Verma,[3] Sae Woo Nam,[3] Daniel Oblak,[1] and Wolfgang Tittel[2]

[1] *Institute for Quantum Science and Technology, and Department of Physics & Astronomy, University of Calgary, 2500 University Drive NW, Calgary, Alberta, T2N 1N4, Canada*

[2] *QuTech and Kavli Institute of Nanoscience, Delft University of Technology, 2600 GA Delft, The Netherlands*

[3] *National Institute of Standards and Technology, 325 Broadway, Boulder, Colorado 80305, USA*

We design and implement an atomic frequency comb quantum memory using thulium ions in an impedance matched optical cavity to create absorption of more than 90% of input signal, resulting in a memory efficiency of $\eta = 27\%$. Our low finesse optical cavity enables efficient storage over the large frequency bandwidths ($\geq 500$ MHz) often present for single photons and high communication rates. We store one member of a spontaneous parametric down-conversion pair and, by measuring a value of $g^{(2)} = 9.3 \pm 1.2 > 2$ for the cross-correlation function of the photons, verify that the non-classical nature of the light persists after storage in the cavity memory. Using time-bit qubits encoded into weak coherent pulses and heralded single photons we characterize the fidelity of this high-bandwidth quantum memory to be $\mathcal{F}_{WC} = 95\%$ and $\mathcal{F}_{SP} = 75\%$ confirming non-classical storage. These results demonstrate progress toward efficient, faithful, and high bandwidth storage of single photon qubits for quantum networking.

# Qudit processing implemented in temporal modes of single photons

**Karolina Sędziak-Kacprowicz[1] and Piotr Kolenderski[2]**

[1]*Faculty of Physics, Astronomy and Informatics, Nicolaus Copernicus University, Grudziądzka 5, 87-100 Torun, Poland*

Quantum communication protocols can be significantly enhanced by careful preparation of photon wavepackets. Unfortunately, most realistic sources produce photons, which are spectrally broadband. As a consequence of this, signal is affected by temporal broadening during its propagation through dispersive media. This effect can considerably limit the efficiency of temporal filtering in long-distance applications. In [1,2] we proposed a method to reduce temporal broadening. Recently, we have shown how careful preparation of spectral entanglement and time-resolved heralding can substantially narrow the wavepacket of the propagated photons, as compared to the classical case [3]. Next step of utilizing spectrally-entangled photon pairs is application to encoding information in the temporal mode of a single photon wavepacket [4]. We performed the theoretical analysis and compared the distribution of measurement points on the Bloch sphere in ideal and realistic scenario, when detection system suffers from timing jitter (Fig. 1). Also, we extend our analysis of optimal parameters problem by length of telecom fiber with constraint, which allowed us to fully reconstruct the wave function. Then we apply the experimental technique and the proper control of the pump spectral mode in order to generate and measure entangled qudit pairs encoded in temporal modes of photon pair. Our method and a technique of entangled photon pairs production can be extended in order to generate correlated states of multilevel systems.

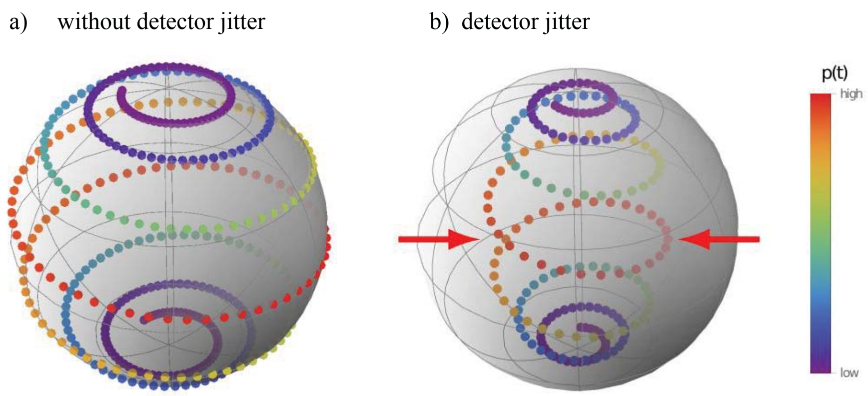


Fig. 1 Distribution of measurement points on the Bloch sphere in for ideal detectors (a) and including the detector jitter (b). Colour of dots represents the probability density distribution that measurement will occur. Red arrows show how measurement points collapsed on the Bloch sphere by the detector jitter.

**References**

[1] 1. K. Sedziak, M.Lasota and P. Kolenderski, Optica 4, 84 (2017).
[2] 2. M.Lasota and P. Kolenderski, Phys. Rev. A 98, 062310 (2018).
[3] 3. K. Sedziak-Kacprowicz, M.Lasota and P. Kolenderski, Sci. Rep. 9, 3111 (2019).
[4] 4. K. Sędziak-Kacprowicz and P. Kolenderski, Encoding quantum information in the temporal mode of a single photon, in preparation (2019).

# Portable system for Time-Resolved Near-Infrared Spectroscopy

**Mauro Buttafava[1], Michele Lacerenza[2], Marco Renna[1], Davide Contini[2], Alessandro Torricelli[2,3], Alberto Dalla Mora[2], Franco Zappa[1], Antonio Pifferi[2,3], Alberto Tosi[1]**

[1]*Dipartimento di Elettronica, Informazione e Bioingegneria, Politecnico di Milano, Italy*
[2]*Dipartimento di Fisica, Politecnico di Milano, Italy*
[3]*Consiglio Nazionale delle Ricerche, Istituto di Fotonica e Nanotecnologie, Italy*

*mauro.buttafava@polimi.it*

The interest in non-invasive optical monitoring techniques is growing in several fields (e.g. biomedical, pharmaceutical, agricultural and chemical industries). Diffuse optics investigates photon propagation phenomena in highly scattering media, recovering information about their optical properties [1]. In Time-Resolved Near-Infrared Spectroscopy (TR-NIRS), picosecond light pulses are injected into the sample and diffused photons are collected (at a certain distance from the injection point) by means of time-resolved single-photon detectors, measuring their arrival times. TR-NIRS is able to retrieve more accurate information from deeper sample layers compared to other approaches (e.g. Continuous Wave) and has the capability of measuring absolute optical parameters, also exhibiting lower artifacts sensibility [1]. This is achieved thanks to the natural disentanglement between absorption and scattering phenomena and the strong relationship between sample penetration depth and photon arrival times. In the biomedical field, the demand for monitoring and imaging instrumentation based on TR-NIRS is constantly increasing in applications like functional brain imaging, muscle oximetry, optical mammography. Up to now, most of TR-NIRS instruments are custom-made prototypes based on commercial components [2], thus intrinsically exhibiting scalability problems, high complexity and high cost.
Trying to answer to this demand, we present a portable full-custom TR-NIRS instrument, developed starting from years of research activity on diffuse optics and dedicated hardware at Politecnico di Milano. Fig. 1 shows the simplified block diagram of the system, which includes all the fundamental building blocks of a complete TR-NIRS setup, with extremely compact dimensions (200×160×50 $mm^3$) and weight (~ 2.5 kg) [3]. It includes: i) two compact pulsed laser sources (at 830 and 670 nm wavelengths) based on gain-switched laser diodes, able to deliver optical pulses having duration shorter than 250 ps with up to 3 mW of average optical power (at 50 MHz repetition rate); ii) a photo-detection module, based on a 1.3×1.3 $mm^2$ area Silicon Photomultiplier (SiPM), custom designed to optimize its single-photon timing performance; iii) a system control board, also integrating the time-measurement electronics based on a custom Time-to-Digital Converter (TDC) having 10 ps temporal resolution and 40 ps single-shot precision. The instrument is able to directly acquire the Distributions of Time-of-Flights (DTOFs) of photons emitted from the tissue under test. Data is transferred in real-time to the embedded computer via a USB link for data analysis and recording. The system can be battery operated and remotely controlled, ensuring several hours of operation. Characterization on solid phantoms and results obtained from in-vivo measurement campaigns (especially on-field, like the oximetry measurement in Fig. 2, acquired during a bicycle exercise), have shown the excellent performance of the instrument [4] which, thanks to its portability and ease of operation, can pave the way towards the diffusion of time-resolved NIR spectroscopy.

*This work was supported in part by the European Union's Horizon 2020 research and innovation programme under Grant agreement 688303 (LUCA). The LUCA project is an initiative of the Photonics Public Private Partnership.*

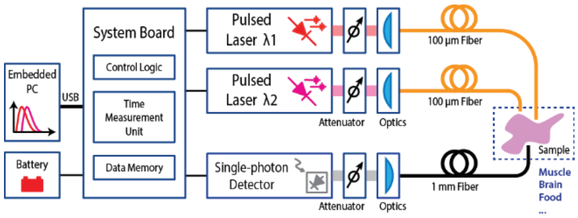


Fig. 1 : Simplified block diagram of the instrument, composed by two pulsed laser sources and a time-resolved single-photon detection channel, based on SiPM and 10-ps resolution TDC. Battery operation ensures several hours of on-field measurements.

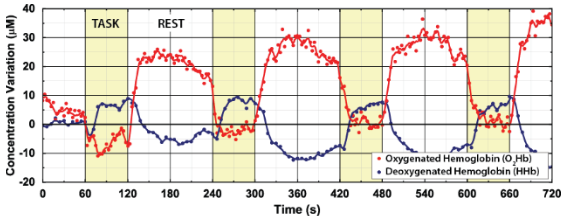


Fig. 2 : Oximetry measurement on the right-leg vastus lateralis during a bicycle riding exercise (4 repetitions). The instrument is worn by the subject as a backpack. Variations are calculated respect to values measured before starting the exercise.

## References

[1] A. Pifferi *et Al.*, "New frontiers in time-domain diffuse optics, a review," J. Biomed. Opt. 21(9), 2016.
[2] D. Contini *et Al.*, "A multichannel time-domain brain oximeter for clinical studies," Proc. SPIE 7369, Diffuse Optical Imaging II, 2009.
[3] M. Buttafava *et Al.*, "A compact two-wavelengths Time-Domain NIRS system based on SiPM and Pulsed Diode Lasers", IEEE Photonics Journal 9 (1), 2017.
[4] M. Lacerenza *et Al.*, "A wearable time domain near-infrared spectroscopy system," Proc. SPIE 11074, Diffuse Optical Spectroscopy and Imaging VII, 2019.

# Quantum interference of photon pairs from biexciton toward Fourie transform spectroscopy

**Hiroya Seki[1], Yuta Uchihori[2], Satoru Efumi[2],**
**Jun Ishihara[2], Kensuke Miyajima[2], Ryosuke Shimizu[1]**
[1]*Univ. of Electro-Comm., Tokyo, Japan*
[2]*Tokyo Univ. of Sci, Tokyo, Japan*

Two-photon quantum interference described by the second-order correlation function has been extensively studied in the quantum optics field, and utilized in demonstration of quantum information protocols, quantum imaging, and quantum sensing. Recently, we found that Fourier transform of the two-photon quantum interference patterns give an intensity spectrum of photon pairs with the sum- or difference-frequency, and demonstrated with photon pairs from spontaneous parametric down-conversion [1]. This method with the second-order correlation function could offer a new approach to Fourier transform spectroscopy with a quantum manner, while the conventional Fourier transform spectroscopy is governed by the first-order correlation function. In order to show a practical application of the quantum Fourier transform spectroscopy (QFT), we present a quantum interference experiment with photon pairs generated via biexciton in a semiconductor crystal. The final goal of our study is to observe the biexciton spectrum by QFT, which could be obtained by the sum-frequency quantum interference pattern, but we have to carry out the difference-frequency quantum interference, generally known as Hong-Ou-Mandel (HOM) interference, in advance.

In our experiment, photon pairs are generated via biexciton in CuCl single crystal. The wavelengths of the photons are at around 389nm, pumped by a frequency-doubled Ti:sapphire laser, and emitted into a noncollinear direction. It has been already reported photon pairs from CuCl form an entangled state in polarization degree of freedom [2] but expected to also be entangled in frequency degree of freedom. This implies the HOM patterns with the beating frequency of the constituent photons could be observed. Figure 1. (a) shows the experimental result of HOM interference with the fitting. We can clearly see a fringe pattern with the beating oscillation. As far as we know, this is the first experimental observation of the HOM with photon pairs via biexciton. Making a Fourier transform of the fitting curve, we obtained the intensity spectrum with the difference-frequency of the photon pairs. Figure 1. (b) is the comparison of spectra taken by QFT to that by a grating spectrometer. Here it should be noted that we did not use any spectral filers in our measurement because this is the demonstration in terms of spectroscopy. This result shows the oscillation period of the HOM is a good agreement with the frequency-difference of the constituent photons. The narrower spectral width of the QFT spectrum may result in better spectral resolution than the grating spectrometer.

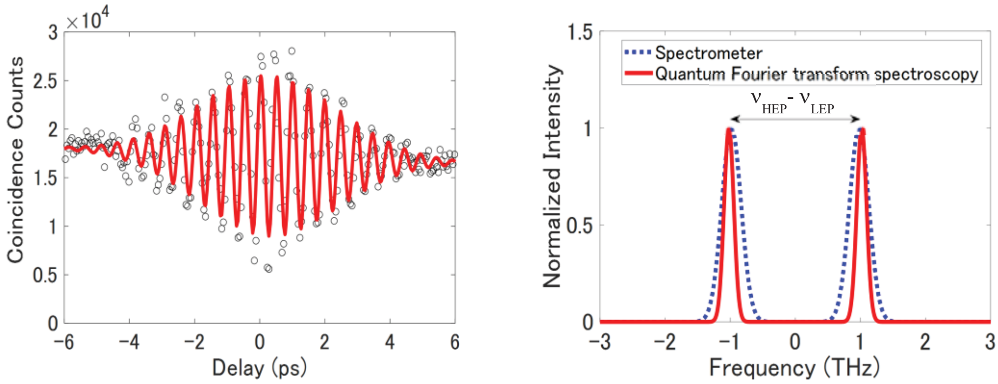


(a) (b)

Figure 1. (a) HOM beating pattern. (b) Spectrum estimated by quantum interference (red curve) and measured by a grating spectrometer (blue dotted curve).

**References**
[1] R. B. Jin and R. Shimizu, Optica **5**, 93 (2018).
[2] K. Edamatdu, G. Ohata, R. Shimizu, T. Itoh, Nature, **431**, 167 (2004).

# TCSPC-based light-sheet fluorescence lifetime microscopy for biological imaging

Jakub Nedbal[1], Liisa Hirvonen[2], Norah Almutairi[3], Stephen Sturzenbaum[3], Klaus Suhling[1]
[1]*Department of Physics, NMS, King's College London, Strand, London, WC2R 2LS, UK*
[2]*Randall Centre for Cell and Molecular Biophysics, FoLSM, King's College London, Guy's Campus, London, SE1 1UL, UK*
[3]*School of Population Health & Environmental Sciences, FoLSM, King's College London, 150 Stamford Street, London, SE1 9NH, UK*

We present the development and applications of a light-sheet microscope equipped with a time- and spatially-resolved single-photon sensitive light detector. This microscope allows three-dimensional (3D) imaging of fluorescence lifetime contrast in thick biological specimens. Compared with past implementations, it offers the highest photon-utilization efficiency and accuracy of fluorescence lifetime estimation, thanks to employing time-correlated signal photon counting (TCSPC). This high efficiency limits photobleaching and phototoxicity, allowing imaging of live biological samples.

**Introduction**

Light-sheet microscopy revolutionized biological imaging, especially in developmental and neurological research [1]. Compared to conventional microscopy techniques, it allows 3D imaging of thick specimens with minimum photo-toxicity, essential for studies of live cell behavior in complex in-vivo environment. Fluorescence lifetime imaging microscopy (FLIM) provides image contrast based on fluorescence lifetime. This quantity is largely independent of the fluorophore concentration and offers a readout of the molecular environment surrounding the fluorophore (e.g. refractive index, pH, ion-strength, redox potential, other nearby fluorophores). Several light-sheet FLIM microscopes have been described in the past. They mostly rely on photon-hungry methods for fluorescence lifetime estimation. Here, we present an implementation of photon-efficient TCSPC FLIM lightsheet microscope and its applications.

**Results**

We built a TCSPC lightsheet microscope [2] using a picosecond pulsed laser for excitation and a MCP-based delay line detector for imaging. We have imaged three types of specimens, including artificial fluorescent microparticles, fixed fluorescently-labelled spheroids and living organisms expressing inducible green fluorescent protein. A mixture of agarose-embedded 10 µm diameter microparticles with similar emission spectra shows different lifetimes (2.5 ns and 4.0 ns), as seen in one slice of a 3D image stack (Fig 1a). Human breast cancer cell-derived spheroids expressing Lifeact-GFP were surface-stained with spectrally similar Alexa488 anti-TOMM20 antibody. Strong fluorescence lifetime contrast is visible between the GFP-only core of the spheroid and its GFP and Alexa488 co-stained outer shell (Fig 1b). Imaging the gut of living nematode worms (*C. elegans*) expressing P*mtl-1*::GFP after induction with $Cd^{2+}$ allows study of how heavy metals effect metalloproteins, such as metallothoneins, in living animals (Fig 1c).

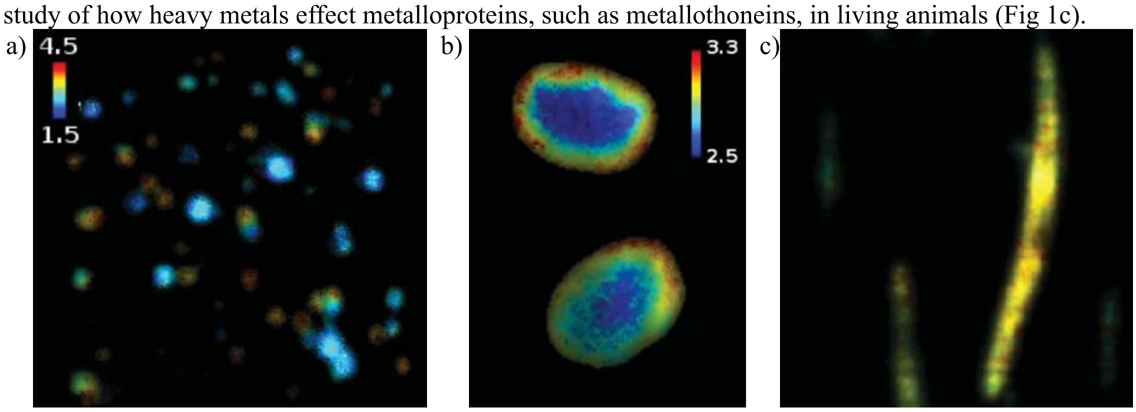


*Fig 1. Single sections from image stacks of: (a) Mixed fluorescent microparticle suspension. (b) Spheroids expressing Lifeact-GFP and surface labeled with Alexa488 anti-Tomm20 antibody. (c) C. elegans worms expressing Pmtl-1::GFP.*

**Conclusion and Discussion**

A summary of experimental results obtained with the TCSPC FLIM light-sheet microscope is presented. This microscope offers unprecedented sensitivity and accuracy by reliably operating with low photon budget thanks to employing TCSPC. The microscope will enable research on living samples, including whole organisms, by providing sectioned fluorescence lifetime imaging in 3D. The limitations compared to past FLIM lightsheet microscopes include lower pixel resolution and lower frame rate. The main advantages are the low phototoxicity enabling live-organism imaging and high accuracy of fluorescence lifetime determination, including multiexponential decay analysis.

**References**

[1] Corsetti et al., J Neurosci Methods (2019) 319:16-27
[2] Pitrone et al., Nat Methods (2013) 10:598-9
[3] Jagutzki et al., Nucl Instrum Meth A (2002) 477:256-61
[4] Barber et al., J R Soc Interface (2009) 6:S93-105
[5] Kelm et al., Biotechnol Bioeng (2003) 83:173-80

**Methods**

The lightsheet microscope is derived from the OpenSPIM design [2] modified to use a picosecond pulsed excitation laser (479 nm, DD-485L, Horiba) for excitation and a custom detector (Photek) for detection. The detector consists of a multichanel plate (Photek) and a pair of perpendicular meandering delay line read-out anodes (DLD40, Roentdek, Germany) [3]. The readout is done by three TCSPC modules (SPC-150, Becker&Hickl). The data is reconstructed using a custom Matlab script and fluorescence lifetime analysis is performed in TRI2 [4]. The specimens consisted of fluorescent microparticles (94050, Sigma-Aldrich & G1000, Thermo Fisher). The spheroids were prepared according to [26] from MCF-7 cells virally infected to express Lifeact-GFP. The spheroids were fixed in 4% PFA and their surface was labeled with Alexa488-conjugated anti-Tomm20 antibody (sc-17764- AF488, Santa Cruz Biotechnology). The C. elegans worms containing an integrated P*mtl-1*::GFP construct were chronically exposed to 60 µM $Cd^{2+}$ during their development. They were immobilized with 5 mM $NaN_3$ for the imaging.

# Coupling of Emission from SiV at $Si_3N_4$ Photonic Platform

**Dmitry A. Kalashnikov[1], Victor Leong[1], Jibo Dai[1], Gandhi Alagappan[2], Ting Hu[3], Valery A. Davydov[4], Viatcheslav N. Agafonov[5], Leonid A. Krivitskiy[1]**

1. *Institute of Materials Research and Engineering, Agency for Science, Technology and Research (A*STAR), 13834 Singapore*
2. *Institute of High Performance Computing, Agency for Science, Technology and Research (A*STAR), 13832 Singapore*
3. *Institute of Microelectronics, Agency for Science, Technology and Research (A*STAR), 13834 Singapore*
4. *L.F. Vereshchagin Institute for High Pressure Physics, The Russian Academy of Sciences, Troitsk, Moscow, 142190 Russia*
5. *GREMAN, UMR CNRS-7347, Université F. Rabelais, 37200, Tours, France*

Developing of quantum networks using integrated photonic technologies is one of the key challenges for realising practical quantum applications. Atomic defects in diamond, or color centers, such as silicon-vacancy (SiV) centers, can be used as building block for quantum networks. They possess bright emission line at 737 nm, high Debye-Waller factor (~0.7), and their stable single-photon emission is insusceptible to electric field fluctuations. The feasible way to realize quantum networks based on diamond nodes is to integrate them with on-chip optical structures and devices. Photonic diamond nanostructures with artificially implanted color centers have been demonstrated recently, but their fabrication is challenging and requires sophisticated technique [1,2].

Here, we present an alternative approach by coupling SiV centers in nanodiamonds (NDs) to a photonic circuit based on silicon nitride ($Si_3N_4$) structures (waveguides and ring resonators) deposited on silicon dioxide. The fabrication of our photonic devices is relatively straightforward as silicon nitride is a well-known dielectric material, which is transparent in VIS-NIR and beyond, compatible with CMOS-based and photolithography processes, and possesses relatively high refractive index (n~2). NDs are distributed in isopropanol solvent and spin-coated onto the device, resulting in some probability of NDs landing on or next to the ring cavities. We identify NDs containing SiVs using a confocal microscope with a 532nm pump and spectrometer, and then bring them into contact with a ring cavity using an atomic force microscope (AFM) tip. Successful positioning is confirmed with both scanning electron microscope (SEM) and confocal scan images (Fig 1a).

Under optical excitation, the SiV fluorescence that matches the cavity resonances is evanescently coupled to the ring cavity and to a straight bus waveguide, which is then collected with an external objective lens. Fig. 1b compares the spectra collected at room temperature by the confocal microscope and through the waveguide. The confocal SiV spectrum shows a broad peak (~10nm) due to multiple SiV centers in the nanodiamond [3], while the spectra collected through the waveguide is modulated by the cavity resonances, demonstrating the SiV-cavity interaction. In order to match the resonance of a cavity with the emission lines of single SiV at cryogenic temperatures we developed the tuning technique based on deposition on nanometer scale layer of silicon dioxide for coarse tuning within several nanometers and heating by auxiliary laser for fine tuning within several pm.

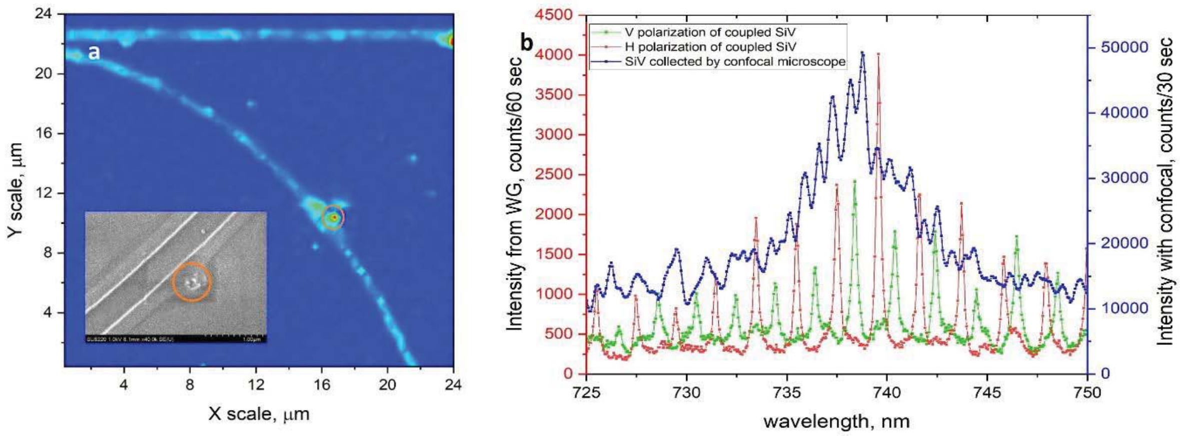


Fig. 1 (a): Confocal scan image and scanning electron microscope (SEM) of a nanodiamond (yellow circled) positioned next to the ring cavity (b): Spectra of the SiV fluorescence collected via the confocal microscope and through the waveguide (WG).

Our efforts will further focus on isolating single SiV centers via resonant excitation at 4K, and studying their coupling to the ring resonators. Placing NDs into small holes etched into the ring could also position the SiVs at the field maximum of the resonator mode, significantly improving the ND-cavity coupling strength [4].

**References**

[1] J. Riedrich-Moller *et al*. Nature Nanotech. **7**, 69 (2012).
[2] M.J. Burek *et al.* Phys. Rev. Appl. **8**, 024026 (2017).
[3] S. Choi *et al.* Sci. Rep. **8**, 3792 (2018).
[4] G. Alagappan *et al.* ACS Omega **3**, 4733 (2018).

# State-dependent enhancement of cavity-cavity coupling rate via a 3-level atomic ensemble

**Jae I. Park**

*National Institute of Standards and Technology, Boulder, Colorado 80305, USA*

We derive an effective theory that describes two cavities coupled to differing transitions of a common 3-level atomic ensemble. We determine the inter-cavity coupling rate conditioned on the state of the atomic ensemble and as a function of experimentally controllable detunings (Fig. 1). We verify that our results are consistent with previous predictions [1] in the limit of large detunings between cavity, corresponding atomic transition, and driving field frequencies. Our result provides a means to suppress or enhance the inter-cavity coupling rate in real-time.

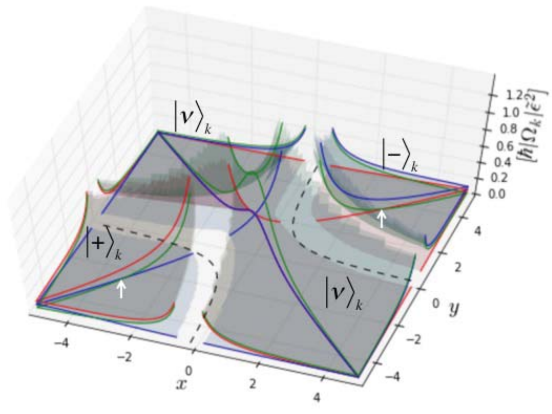


Fig. 1 The magnitude of the inter-cavity coupling rate as a function of dimensionless detunings. The red, blue, and green surfaces (and respective line-cuts) correspond to different eigenstates of the atomic ensemble.

## References

[1] Lewis A Williamson, Yu-Hui Chen, and Jevon J Longdell. Magneto-optic modulator with unit quantum efficiency. Physical review letters, 113(20):203601, 2014.

# Single-photon computational 3D imaging at 45 km

**Zheng-Ping Li [1,2], Xin Huang[1,2], Yuan Cao[1,2], Bin Wang[1,2], Yu-Huai Li[1,2], Weijie Jin[1,2],Chao Yu[1,2], Jun Zhang[1,2], Qiang Zhang[1,2], Cheng-Zhi Peng[1,2], Feihu Xu[1,2*], Jian-Wei Pan[1,2]**

[1] *Shanghai Branch, National Laboratory for Physical Sciences at Microscale and Department of Modern Physics, University of Science and Technology of China, Shanghai 201315, China*

[2] *CAS Center for Excellence and Synergetic Innovation Center in Quantum Information and Quantum Physics, University of Science and Technology of China, Shanghai 201315, China*

[*] *Email: feihuxu@ustc.edu.cn*

Single-photon LiDAR (light detection and ranging) offers single-photon sensitivity and picosecond timing resolution, which is desirable for high-precision three-dimensional (3D) imaging over long distances. Tremendous efforts have been devoted to the development of single-photon LiDAR for long-range 3D imaging. Single-photon 3D imaging up to a distance of 10 km has been reported [1]. Moreover, recent developments in active imaging have become increasingly dependent on computational power. Computational algorithms have the potential to greatly improve the imaging range [2]. Despite important progress, further extending the imaging range presents enormous challenges because only weak echo photons return and are mixed with strong noise.

We tackled these challenges by developing an advanced technique based on *both* hardware and software implementations, which are particularly designed for adapting the long-range application [3]. On the hardware side, we designed a high-efficiency coaxial-scanning system (see Fig. A(a)) to efficiently collect the weak echo photons and suppress system background noise. On the software side, we developed a computational algorithm to handle the data of low photon counts mixed with high background noise, with high photon efficiency and super-resolution capability in the transverse domain. With these improvements, we are able to demonstrate super-resolution single-photon 3D imaging over a *record-breaking* distance of 45 km with a low return-signal level of ~1 photon per pixel and high background noise (SNR ~1/30) [3]. We also compare the performance with the previous state-of-the-art computational algorithms (see Fig. B). By comparison, we can see our algorithm recovers the fine features of the building, allowing the scenes with multilayer distribution to be accurately identified (see Fig. B(e)). The other algorithms, however, fail in this regard.

The 3D images, generated at the single-photon-per-pixel level, allow for target recognition and identification at low light levels. The proposed high-efficiency single-photon LiDAR system, noise-suppression method, and advanced computational algorithm open new opportunities for rapid and low-power LiDAR. By refining the setup, our system is feasible for a few hundreds of kilometers. Overall, our results open a new venue for high-resolution, fast, low-power 3D optical imaging over ultralong ranges. **Further details of our work can be seen in Ref. [3].**

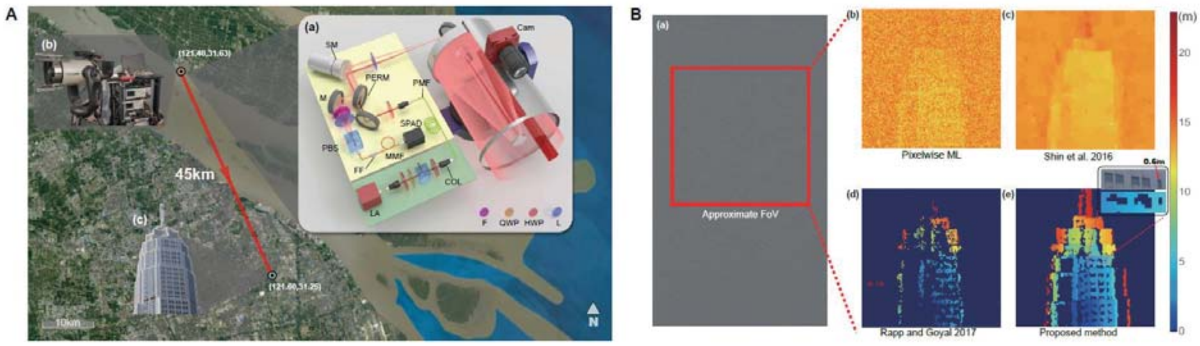


**Fig. A :** Illustration of long-range active single-photon LiDAR. Satellite image of the experiment layout in the urban area of Shanghai City, with the single-photon LiDAR positioned on Chongming Island. (a) Schematic diagram of experimental setup. (b) Photograph of experimental setup, including the optical system (left) and the electronic control system (right). (c) Close-up photograph of the target, the Pudong Civil Aviation Building, The building is 45 km from the single-photon LiDAR setup. **Fig. B :** Long range 3D imaging results over 45 km. (a) Real visible-band image (tailored) of the target taken with a standard astronomical camera. This photograph is substantially blurred in the urban environment. The red rectangle indicates the approximate LiDAR FoV. (b)-(e), The reconstruction results obtained by using the pixelwise maximum likelihood (ML) method, the photon-efficient algorithm by Shin, the unmixing algorithm by Rapp and Goyal, and the proposed algorithm, respectively. The data was an average ~2.59 photon per pixel, and the SNR was ~0.03. Our algorithm in (e) performs much better than the other state-of-art photon-efficient computational algorithms and provides super-resolution capability to clearly resolve the 0.6-m-wide windows (see expanded view in inset of panel (e)).

**References**

[1] A. M. Pawlikowska et al., Opt. express 25, 11919 (2017).
[2] A. Kirmani et al., Science 343, 58 (2014).
[3] Z.-P. Li et al., "Single-photon computational 3D imaging at 45 km." arXiv:1904.10341 (2019).

# CSPAD-based 3D flash LiDAR

**Jan Henning Drewes, Jennifer Ruskowski, Werner Brockherde**
*Fraunhofer Institute for Microelectronic Circuits and Systems IMS, Duisburg, Germany*

For accurate scene recognition, LiDAR systems require photon detectors with highest sensitivity and both high spatial and temporal resolution. Still, most LiDAR systems rely on mechanically scanning mirrors to capture a wide field of view, reducing the margin for a reduction in cost and form factor. Therefore, several approaches towards a reliable, accurate and cost efficient LiDAR are being pursued in parallel including MEMS Scanners, optical phased arrays and completely motion-free flash LiDAR based on avalanche photo diodes or single-photon avalanche diodes (SPADs).

The combination of low-noise CMOS SPADs (CSPADs) and the corresponding read-out electronics (ROIC) on the same chip is pioneering for a range of - especially cost-effective and robust - LiDAR applications. In this manner, the Fraunhofer IMS CSPAD detectors, fabricated in an automotive CMOS process, provide single-photon sensitivity with a low dark count rate (~10 cps) and a high dynamic range (134 dB). With current CSPAD detectors, the modular Flash LiDAR camera Owl developed by Fraunhofer IMS can achieve a range of 40 m with a distance resolution of 5 cm and a framerate of 25 fps.

To achieve high maximum distances and high frames rates for any weather condition, a flexible change of measurement mode is crucial for LiDAR applications. With the implemented ROIC on chip, current CSPADs allow for recording 4D-datasets, i.e. distance information and intensity (background light photon statistics) values simultaneously in every pixel. This is possible by using two modes: In *timing mode,* a time stamp of the first detected photon is generated. In *counting mode,* the number of photons in a pre-defined time window is registered. Moreover, an important feature of our CSPADs is the powerful sunlight suppression mechanism for outdoor applications which is achieved through an adaptive coincidence mechanism implemented on the chip for every pixel [1].

The large number of tasks the ROIC has to perform, e.g. active quenching, time-to-digital conversion and coincidence detection, leads on to an increased floor space and limits the pixel fill factor or even in the amount of pixels. This is particularly true for LiDAR systems, where every pixel should provide a time stamp for each incoming photon in order to not waste light information or measurement time.

Our novel wafer-to-wafer bonding process with a backside illuminated CSPAD wafer and a ROIC wafer allows 2-dimensional pixel arrangements without sacrificing the pixel number or fill factor. Currently, a 64 x 48 pixel SPAD array detector (CSPAD3000, both wafers in 0.35 µm CMOS) is in fabrication. In the future, this bonding technology will also allow for the combination of an optimized SPAD process in Fraunhofer IMS with a more advanced CMOS technology for the read-out part of the detector. As a result, both higher temporal and spatial resolution can be realized, rendering CSPAD detectors even more attractive for LiDAR applications.

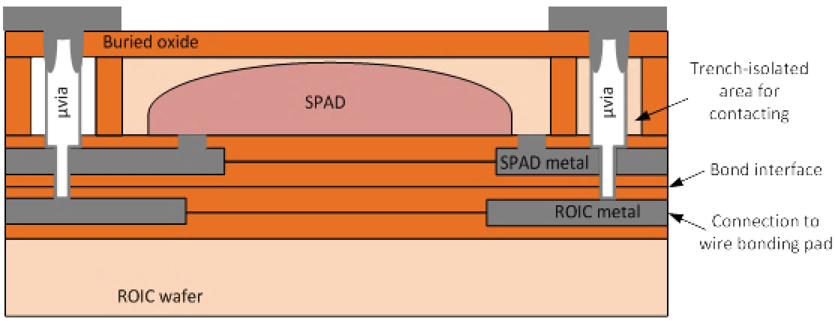


Figure 1: Schematic drawing representing the wafer-to-wafer bond process

## References

[1] Beer, Maik et al. “Background Light Rejection in SPAD-Based LiDAR Sensors by Adaptive Photon Coincidence Detection.” *Sensors (Basel, Switzerland)* vol. 18,12 4338. 8 Dec. 2018, doi:10.3390/s18124338

# Single-Photon LiDAR in High Ambient Light

**Anant Gupta, Atul Ingle, Andreas Velten, Mohit Gupta**
*University of Wisconsin-Madison, Madison, WI, USA*

Time-resolved single-photon detectors such as single-photon avalanche diodes (SPADs) are a promising new optical sensor technology for high-resolution long-range 3D imaging due to their high sensitivity and timing resolution. A single-photon LiDAR system uses a pulsed light source (e.g. a picosecond laser) in synchronization with a SPAD. The laser transmits a periodic train of pulses towards a fixed scene point. For each laser pulse, the SPAD records the time-of-arrival of the first returning photon with picosecond precision. Typically, these measurements are repeated over many laser pulses and a histogram of photon arrival times is constructed. Ideally, in case of negligible ambient light, the temporal location of the peak of this histogram corresponds to the round-trip time delay. With the knowledge of the speed of light in the imaging medium, the distance of the scene point can be estimated.

**Problem of High Ambient Light:** A LiDAR system in the real world must deal with high ambient light scenarios (e.g. sunlight) where the laser power is negligible compared to the total ambient light energy incident on the sensor. In these scenarios, the ambient light photons overwhelm the SPAD – after each laser pulse, the SPAD detects an early-arriving ambient light photon with very high probability. This prevents the detection of true signal (laser) photons that would have arrived later, causing a non-linear distortion of the histogram data called *pile-up*.

**Optimal Photon Flux Criterion:** Conventional wisdom suggests that the total photon flux incident on the SPAD sensor must be attenuated to <5% of the pulse repetition frequency of the laser source [1]. In recent work [2] we showed that this rule-of-thumb is too conservative, and in fact, the optimal fraction of light that should be allowed to impinge the SPAD is much higher. Our photon flux criterion states that, for minimum mean squared depth reconstruction error, when operating in high ambient light, the total photon flux incident on the SPAD should be reduced such that on average 1 photon is incident on the SPAD per laser cycle. Photon flux incident on the SPAD can be controlled adaptively for each scene point using a variety of optical techniques. We use neutral density filtering as shown in Fig. 1 (a). If no attenuation is used, the photon histogram data is corrupted by pile-up and leads to distorted depth maps, as shown in Fig. 1 (b). If the conventional 5% rule-of-thumb (extreme attenuation) is used, the reconstructions suffer from shot noise, as shown in Fig. 1 (c). Our optimal attenuation method achieves a balance between pile-up distortion and shot noise and provides reliable depth estimates even under high ambient illumination, as shown in Fig. 1 (d).

**Towards Long-Range Low-Power Single-Photon LiDAR:** Development of high resolution and low dead time SPAD detector technology, with precise in-pixel timing electronics and multi-photon capture capabilities will play a pivotal role in future single-photon LiDAR systems. When combined with modern computational data-driven techniques that harness scene priors [3], single-photon LiDARs have the potential to provide low power long range 3D imaging with unprecedented depth resolution.

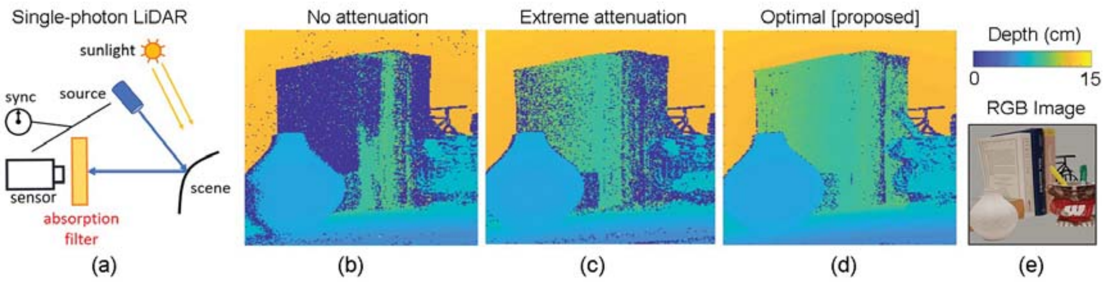


Figure 1 **Experimental Results with our hardware prototype**: Observe that the proposed method provides high quality depth maps that do not suffer from pile-up distortion or shot noise. The ambient illumination was >20,000 lux. We used a 405 nm pulsed laser with an average power of 3 mW, 10 MHz repetition frequency, and 100 ps pulse width.

**References**

[1] Wolfgang Becker. Advanced Time-Correlated Single Photon Counting Applications, Volume 111. Springer, 2015.
[2] Anant Gupta, Atul Ingle, Andreas Velten, Mohit Gupta, “Photon-Flooded Single-Photon 3D Imaging,” Proc. CVPR 2019.
[3] David Lindell, Matthew O’Toole, Gordon Wetzstein, “Single-Photon 3D Imaging with Deep Sensor Fusion,” ACM Trans. Graph. (SIGGRAPH), vol. 37, no. 4, 2018.

* Research supported by ONR, DARPA and Wisconsin Alumni Research Foundation.

# Single photon LIDAR at 2.3µm with SNSPDs

**Gregor G Taylor[1], Dmitry Morozov[1], Kleanthis Erotokritou[1], Nathan Gemmell[2], Robert H Hadfield[1]**

[1]*University of Glasgow, Glasgow, UK*

[2]*University of Sussex, Brighton, UK*

Superconducting nanowire single photon detectors (SNSPDs) offer unrivalled performance advantages in the mid infrared when compared to other single photon counting technologies[1]. Almost negligible dark count rates[2], timing jitter as low as 3ps FWHM[3] and wavelength sensitivity extending up to 10µm[4] allow them to be deployed in a wide variety of applications where these properties can be exploited. In single photon light detection and ranging (LIDAR) the fast timing jitter and low dark count rate allows an excellent depth resolution in photon sparse returns. In this work, we extend the operating wavelength of our LIDAR system to 2.3µm which is advantageous for free space applications due to the lower background solar photon flux, a factor of three reduction from operating at 1550nm, and less atmospheric absorption than at shorter wavelengths[5]. We deliver photons at this wavelength using an optical parametric oscillator (OPO) as a spectrally narrow fast source. We have designed, fabricated and characterised a NbTiN SNSPD optimised for mid IR operation for this work. A schematic of the experimental setup is shown in Fig 1 and Fig 2 shows results from scanning a small model of Big Ben.

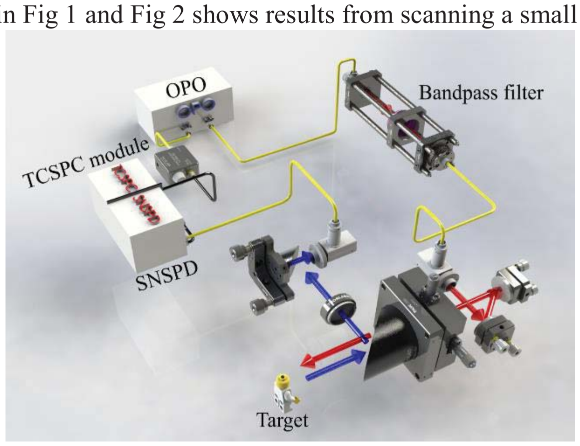


Fig. 1: Experimental setup for 2.3µm LIDAR. The target is scanned to build up an image.

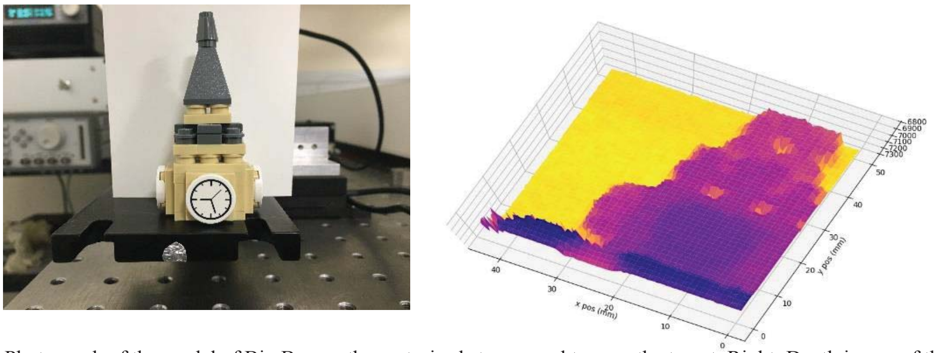

Fig. 2: Left: Photograph of the model of Big Ben on the motorised stages used to scan the target. Right: Depth image of the model after scanning complete. A 1s integration time per pixel and <10uW of emitted optical power was used for this scan. Key features can be picked out including the raised clock face (~3mm depth) and holes in the model.

## References

[1] Natarajan, Chandra M., Michael G. Tanner, and Robert H. Hadfield. "Superconducting nanowire single-photon detectors: physics and applications." *Superconductor science and technology* 25.6 (2012): 063001.

[2] Yang, Xiaoyan, et al. "Superconducting nanowire single photon detector with on-chip bandpass filter." *Optics express* 22.13 (2014): 16267-16272.

[3] Korzh, B. A., et al. "Demonstrating sub-3 ps temporal resolution in a superconducting nanowire single-photon detector." *arXiv preprint arXiv:1804.06839* (2018).

[4] Verma, V. B., et al. "Towards single-photon spectroscopy in the mid-infrared using superconducting nanowire single-photon detectors." *Advanced Photon Counting Techniques XIII*. Vol. 10978. International Society for Optics and Photonics, 2019.

[5] American Society for Testing and Materials. Committee G03 on Weathering and Durability. *Standard tables for reference solar spectral irradiances: direct normal and hemispherical on 37° tilted surface*. ASTM International, 2003.

# Using a superconducting detector in the to measure 229Th nuclear clock transition

**Ricky Elwell[1], Justin Jeet[1], Galen O'Neil[2], Dileep Reddy[2], Christian Schneider[1], Varun Verma[2], Eric Hudson[1], Sae Woo Nam[2]**

[1]*University of California, Los Angeles, CA, USA*

[2]*National Institute of Standards and Technology, Boulder, CO, USA*

The very low energy $^{229}$Th isomer has long been known to exist from gamma-ray spectroscopy, but it has resisted accurate measurement for 40 years. The only proven method to produce $^{229}$Th in the excited isomeric state is alpha decay of $^{233}$U, a man-made nuclear material. The $^{229}$Th isomer energy was recently observed and measured with a room temperature microchannel plate, but poor energy resolution of that detector limits the precision of the result to be between 6.3 eV and 18.3 eV [1]. Many attempts [2,3] to measure the $^{229}$Th nuclear transition directly with more precisition have been made, but are not consistent with each other. Although the anomalously low energy nuclear transition is interesting by itself, there is tremendous interest in the transition because of its extremely narrow linewidth/long lifetime when the $^{229}$Th atom is ionized (reported to be several thousand seconds)[4]. The ratio of radiative width to transition energy is presently estimated at $10^{-19}$ (compared to $10^{-17}$ for Strontium – one of the best atomic clock species). Given the narrow linewidth, the isolation of the nucleus from external perturbations, and the possibility of embedding $10^{14}$ charged Thorium ions in a glass matrix, there is the possibility of ultra-stable "nuclear" lasers and "nuclear" clocks that could rival what is being done now.

To date, measurements have yet to measure the transition energy precisely enough to enable laser spectroscopy of a nucleus. We will describe our progress towards measuring the transition energy using a superconducting nanowire single photon detector. By comparing the count rate from isomeric decay of the Thorium nucleus as a function of detector bias current with careful calibration of the superconducting nanowire single photon detector efficiency as a function of current bias for different energy photons (see Fig 1), we should be able to estimate the energy of the Thorium isomeric transition with an uncertainty less than 1 eV. The basic scheme for measuring the nuclear isomer decay is pictorially decribed in Figure 2. Unfortunately, the isomeric decay of the Thorium nucleus is not the only source of counts in the detector from the $^{233}$U source. We also see detection events from high energy alpha, beta, and gamma radiation. Because any click in the detector from an isomeric decay must be preceded by a click in the detector from a Thorium ion embedding in the detector, we can discriminate between background clicks and isomer energy clicks by looking for events that are preceded by a click ~10 µs in beforehand.

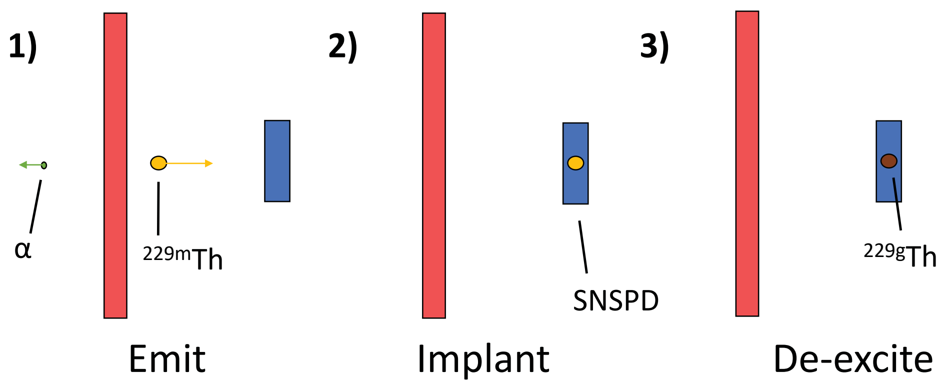


Fig. 1 : Basic scheme to detect the isomeric decay of the $^{229}$Th. The red bar represents a $^{233}$U source. Step 1: $^{233}$U decays via alpha particle emission. 2% of these decays result with a Thorium nucleus in the excited state. Step 2: The Thorium ion implants in an SNSPD detector causing a click. Step 3: The Thorium nucleus decays to the ground state within 10 µs causing a second click.

**References:**

**[1] http://www.nature.com/doifinder/10.1038/nature17669**
**[2] arXiv:1905.06308 (2019)**
**[3] https://e-reports-ext.llnl.gov/pdf/375773.pdf**
**[4] https://link.springer.com/article/10.1007/s11018-018-1337-1**

# Nonlocal Coherent Perfect Absorption

**John Jeffers**

*Department of Physics, University of Strathclyde, John Anderson Building, 107 Rottenrow, Glasgow G4 0NG, U.K.*

Loss in optics is normally thought of as a purely local absorption of light energy, although there have been nonlocal quantum effects based on absorption coefficients [1]. Coherent absorption is a form of optical loss which, at its purest, allows a 50% lossy optical medium to cycle between complete transparency and full absorption [2-4]. Excitations of one particular phased superposition of the input modes pass completely and excitations of the orthogonal one are absorbed. The effects are typically seen in sub-wavelength films for both classical [5] and quantum [6,7] input light.

Here I describe a different form of coherent absorption that occurs jointly at two (or more) spatially separated, macroscopic lossy beam splitters. A superposition mode of any phase can be *chosen* as fully-absorbed or transparent. For two-photon NOON-state input a single photon can survive the pair of beam splitters with certainty, implying nonlocal absorption of one photon and entanglement between two separated beam splitters. This can be detected via the interference in the two-photon survival probability. The consequences for lossy quantum-optical networks are explored.

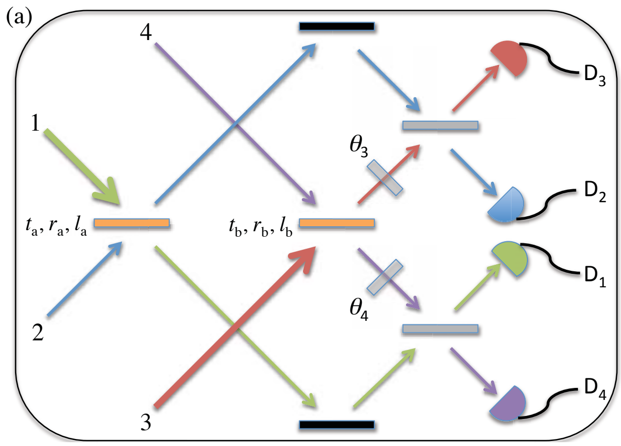


Fig. 1 A simple set-up for nonlocal coherent absorption. The input is in a superposition of modes 1 and 3.

**References**

[1] J. Jeffers and S.M. Barnett, Phys. Rev. A 47, 3291 (1993).
[2] J. Jeffers, J. Mod. Opt. 47, 1819 (2000).
[3] Y. Chong et al., Phys. Rev. Lett. 105, 053901 (2010).
[4] W. Wan et al., Science 331, 889 (2011).
[5] J. Zhang et al., Light: Science & Applications 1, e18 (2012).
[6] T. Roger et al., Nat. Commun. 6, 7031 (2015).
[7] T. Roger et al., Phys. Rev. Lett. 117, 023601 (2016).

# Multiphoton quantum metrology without pre- and post-selected measurements


**C. You[1], P. Bierhorst[3], A. Lita[2], S. Glancy[2], N. Bhusal[1], S. Kolthammer[4], J. P. Dowling[1], E. Knill[2,5], S. W. Nam[2], R. P. Mirin[2], O. S. Magana-Loaiza[1], T. Gerrits[2]**

[1]*Department of Physics and Astronomy, Louisiana State University, Baton Rouge, Louisiana 70803, USA*
[2]*National Institute of Standards and Technology, 325 Broadway, Boulder Colorado 80305, USA*
[3]*Mathematics Department, University of New Orleans, New Orleans, Louisiana 70148, USA*
[4]*QOLS, Blackett Laboratory, Imperial College London, London SW7 2AZ, United Kingdom*
[5]*Center for Theory of Quantum Matter, University of Colorado, Boulder, Colorado 80309, USA*



We demonstrate a protocol for quantum-enhanced phase estimation without pre- and post-selected measurements. Our experiment, with an overall efficiency of 80 %, utilizes two-mode squeezed vacuum states and photon-number-resolving detection to surpass the standard quantum limit.


The possibility of using quantum properties of light to measure small physical parameters with unprecedented precision represents one of the most import goals of quantum photonic technologies [1–4]. Here, we demonstrate a novel scheme that utilizes all the detected photons from two-mode squeezed vacuum states to perform unconditional quantum-enhanced phase estimation with an overall system efficiency of 80 %. Our technique makes use of photon-number-resolving detection with transition edge sensors (TESs).

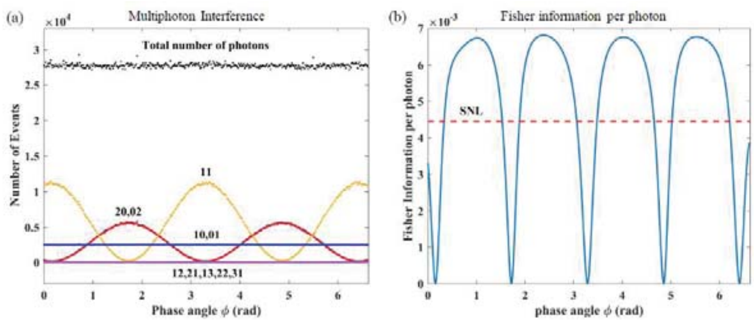


Fig 1: Experimental multiphoton interference and the corresponding Fisher information per photon detected. The multiple detection events produced by multiphoton interference are shown in (a). The blue line in (b) represents the estimated Fisher information per photon as obtained by a fit to the data, the red dashed line represents the standard quantum limit (SQL).

We use a common path interferometer to estimate the phase between the two photon paths [5]. The Hong-Ou-Mandel visibility is approximately 98.5 %. All the multiphoton events shown in Fig. 1(a) convey phase information that is quantified through classical Fisher information, this is given by $F = \sum_i (\partial \ln p_i / \partial \phi)^2$, where the probability $p_i$ includes all the detected events. The multiphoton interference events used to perform phase estimation are plotted in Fig. 1(a). The black dotted line in this plot shows that the total number of photons is conserved during the realization of the experiment. In contrast to the recent protocol in Ref. [5], the photon-number resolving capability of our scheme enables the efficient discrimination among one- and multi-photon events, this possibility leads to a higher Fisher information over a wider range of phases, see Fig. 1(b). In contrast to previous protocols for quantum-enhanced estimation of phases [3–5], the more broadly peaked Fisher information in our experiment enables the efficient use of the quantum properties of light to measure almost 85% of the phase space with unprecedented sensitivities, even in the presence of losses.

## References


[1] C. M. Caves, “Quantum-mechanical noise in an interferometer”, Phys. Rev. D 23, 1693–1708 (1981).

[2] M. Xiao, L. Wu and J. H. Kimble, “Precision measurement beyond the shot-noise limit”, Phys. Rev. Lett. 59, 278–281 (1987).

[3] T. Nagata, R. Okamoto, J. L. O’Brien, K. Sasaki, and S. Takeuchi, “Beating the Standard Quantum Limit with Four-Entangled Photons”, Science 316, 726–729 (2007).

[4] I. Afek, O. Ambar and Y. Silberberg, “High-NOON States by Mixing Quantum and Classical Light”, Science 328, 879–881 (2010).

[5] S. Slussarenko, M. M. Weston, H. M. Chrzanowski, L. K. Shalm, V. B. Verma, S. W. Nam and G. J. Pryde, “Unconditional violation of the shot-noise limit in photonic quantum metrology”, Nat. Photon. 11, 700–703 (2017).

# Metrology of chip-scale QKD devices

**Robert Starkwood (Kirkwood)[1*], Ke Guo[2,1], Christopher Chunnilall[1], Alastair Sinclair[1]**
**Taofiq Paraiso[3], Thomas Roger[3], Mirko Sanzaro[3], Innocenzo De Marco[3], Zhiliang Yuan[3], Andrew Shields[3]**

[1] *National Physical Laboratory, Hampton Road, Teddington, TW11 0LW, UK*

[2]*University of York, Heslington, York, YO10 5DD, UK*

[3]*Toshiba Research Europe Limited, 208 Cambridge Science Park, Cambridge CB4 0GZ, UK*

**robert.starkwood@npl.co.uk*

Several quantum technologies are approaching maturity and commercialisation through recent advances in research and product engineering. Quantum key distribution (QKD) is a prime example of this, bringing together cutting-edge photonics, fast electronics, and single-photon detection, to create products with an ever-growing user base. QKD hardware is developing rapidly and is transitioning to photonic integrated architectures to provide improvements in bit rate, affordability, power consumption, and form factor.

The UK's National Physical Laboratory (NPL) is expanding its measurement capability for characterising the quantum layer of QKD hardware in collaboration with Toshiba Research Europe Ltd (TREL), who are developing chip-scale devices for GHz clock-rate phase-seeded QKD compatible with standard optical telecoms infrastructure [1,2].

We present SI-traceable measurements of various physical parameters of the QKD components, accurate knowledge of which is essential to security assurance of any system. Reference laser light was used to interrogate on-chip interferometers, quantifying their response over a range of wavelengths and temperatures. The output of on-chip lasers which provide phase seeding and phase randomisation of the encoding states was characterised to verify the pulse-to-pulse dictation of optical coherence or phase randomisation.

These results represent a step forward in NPL's measurement capability, concurrent with the evolving state of the art in QKD technology. This measurement capability will contribute to establishing an assurance process for quantum communications in the UK.

**References**

[1] T K Paraiso et al., *Proc. SPIE*, **10921**, 109210U, (2019)
[2] T K Paraiso et al., *npj Quantum Information*, **5,** 42, (2019)

*This work has been funded by Innovate UK projects EQUIP (Project No: 103869) and AquaSeC (Project No: 104615), as part of the UK National Quantum Technologies Programme.*

# Error tolerant design of universal multiport interferometers

**M.Yu. Saygin, S.A. Fldjan, I.V. Dyakonov, S.S. Straupe, A.A. Kalinkin, S.P. Kulik**

*Quantum Technologies Center & Faculty of Physics, M.V. Lomonosov Moscow State University, Moscow, Russia*

Optical interferometers are indispensable experimental tool in both classical and quantum areas. Multiport interferometers are a necessary part of the promising quantum computing platform that leverages linear-optical circuits and non-classical properties of photons to realize quantum algorithms. Recent works have demonstrated the versatility of linear-optical quantum systems and their ability to solve several quantum computing tasks ranging from the well-known algorithms to the more specific ones, such as boson sampling and variational algorithms.

Today, several decomposition methods exist that enable construction of universal interferometers of arbitrary size, in which the actual devices come in the form of network of tunable two-port Mach-Zehnder interferometers (MZIs). However, these schemes are sensitive to errors that usually occur at fabrication, making the interferometer device universal only to a certain degree. This fact limits the scalability of the multiport transformation that can be realized in practice, thus, limiting the complexity of the quantum algorithm that can be implemented with the interferometers.

In this work, we present a novel design of universal multiport interferometers that turns out to be much more resilient to errors, compared to those used today. The advantage of the interferometers constructed with our design is that they do not require redundant static elements of beam-splitters and phase-shifters. Therefore, the interferometer schemes have the same depth and number of elements as in the case of the known optimal design [1].

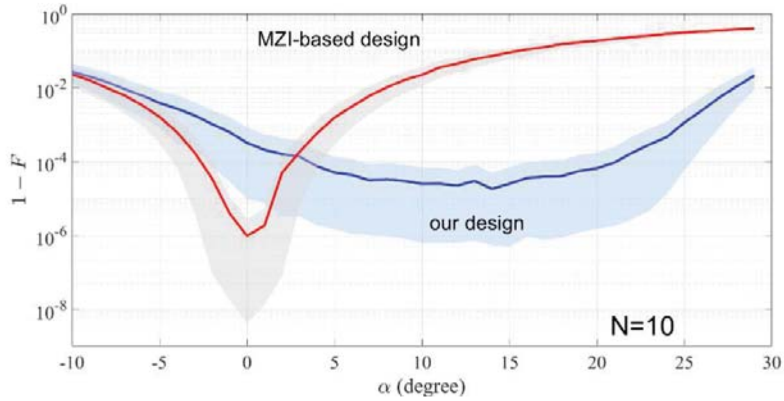


**Fig. 1** Infidelity $1-F$ as a function of error parameter $\alpha$ that quantify the imbalance of static beam-splitters that constituent the interferometer schemes, constructed with the MZI-based design [1] and our design at $N=10$. Each point at fixed $\alpha$ was obtained by a numerical optimization algorithm over a set of 300 randomly generated target matrices $U_0$ from a uniform Haar distribution.

We study the quality of the multiport interferometers by calculating fidelity, defined as

$$F = \frac{1}{N^2}\left|Tr\left(U_0^* U\right)\right|^2$$

which compares a target unitary matrix $U_0$ and an actual transfer matrix realized by the interferometer $U$, where $N$ is the size of the matrices. As a most representative type of errors, we consider the case when all the static beam-splitter that constituent the interferometer are biased by equal angle $\alpha$, which is a typical situation for lithography. Fig. 1 compares the transformation quality of the interferometers constructed with the known design, suggested in [1], and our design. Fig. 1 shows the infidelity of multiport transformation as a function of the error parameter $\alpha$, having the meaning of the angle that quantify the imbalance of the static beam-splitters constituent the interferometer schemes; the ideal case corresponds to balanced beam-splitters with $\alpha = 0$. As can be seen from the figure, the interferometer of our design remains universal at much higher values of $\alpha$, proving its superiority over the known designs.

**References**

[1] W.R. Clements et al. “Optimal design for universal multiport interferometers”, Optica, v. 3, No 12, 1460 (2016).

# Traceable single-photon source based on an InGaAs quantum dot

**H. Georgieva[1], M. López[1], H. Hofer[1], B. Rodiek[1], J. Christinck[1], P. Schnauber[2], A. Kaganskiy[2], T. Heindel[2], S. Rodt[2], S. Reitzenstein[2], S. Kück[1]**

[1]*Physikalisch-Technische Bundesanstalt, Bundesallee 100, 38116 Braunschweig, Germany*

[2]*Institut für Festkörperphysik, Technische Universität Berlin, Hardenbergstraße 36, 10623 Berlin, Germany*

Semiconductor quantum dots are promising candidates in many fields of quantum information processing [1]. The narrow bandwidth of the single-photon emission is favorable for the calibration of non-photon number resolving detectors at a specific well-defined wavelength. For this application, one aims for a high photon flux reaching the detector area with a high single-photon purity. A high photon flux can be achieved by an efficient quantum emitter combined with a low-loss optical setup. The extraction efficiency of the investigated InGaAs quantum dot is enhanced by embedding it into a monolithic microlens, coated with an anti-reflection layer [2]. Furthermore, the overall setup transmission is increased by utilizing two bandpass filters for the spectral filtering, each of them having a transmission of about 90 %.

The complete quantum dot characterization includes measurements of the photon flux and its temporal stability as well as the spectral characteristics and second-order correlation function under non resonant pulsed excitation. The optical power was then determined by using a calibrated spectrometer for the measurement of the quantum dot emission wavelength and a silicon single-photon avalanche detector (Si-SPAD) with a calibrated detection efficiency, traceable via an unbroken calibration chain to the primary standards for spectral radiant flux [3]. Finally, the characterized single-photon source was directly implemented for the calibration of a second Si-SPAD.

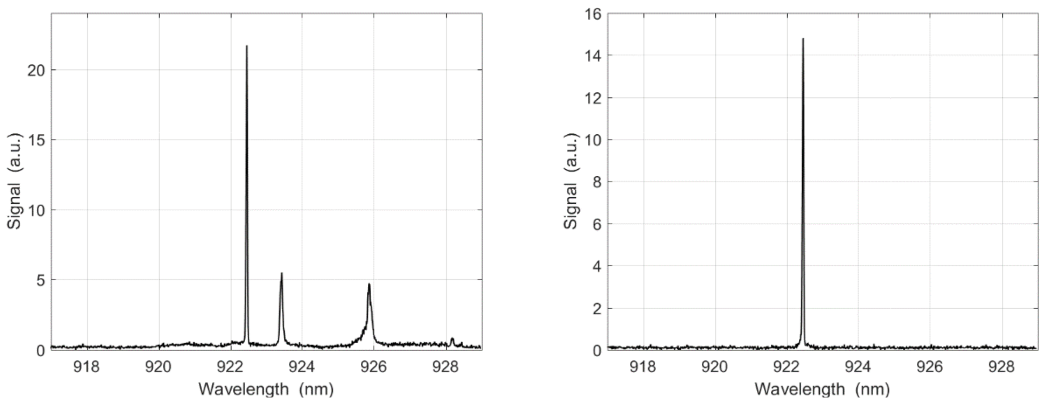


Fig. 1: Left: Micro-photoluminescence spectrum of the InGaAs quantum dot emission. Right: The emission peak with the highest intensity line at about 922.5 nm is filtered out by two bandpass filters with a full width of half maximum of 0.5 nm.

**Acknowledgement**

This work was funded by the project Single-Photon Sources as New Quantum Standards (SIQUST) of the European Metrology Programme for Innovation and Research (EMPIR). The EMPIR is jointly funded by the EMPIR participating countries within EURAMET and the European Union. We gratefully acknowledge the support of the Braunschweig International Graduate School of Metrology B-IGSM and the DFG Research Training Group 1952 Metrology for Complex Nanosystems.

**References**

[1] A. Kiraz et al., A. Quantum-dot single photon sources: Prospects for applications in linear quantum-information processing. Phys. Rev. A 2004, 69, 032305.

[2] P. Schnauber et. al., Bright Single-Photon Sources Based on Anti-Reflection Coated Deterministic Quantum Dot Microlenses, Technologies 2016, 4, 1; doi:10.3390/technologies401000, (2016).

[3] M. López et.al., “Detection efficiency calibration of single-photon silicon avalanche photodiodes traceable using double attenuator technique”, J. Mod. Opt., DOI: 10.1080/09500340.2015.1021724, (2015).

# Quantum Metrology of Solid-State Single-Photon Sources using Photon-Number-Resolving Detectors

**Martin v. Helversen[1], Jonas Böhm[1], Marco Schmidt[1,2], Manuel Gschrey[1], Jan-Hindrik Schulze[1], André Strittmatter[1,3], Sven Rodt[1], Jörn Beyer[2], Tobias Heindel[1], and Stephan Reitzenstein[1]**

[1] *Institut für Festkörperphysik, Technische Universität Berlin, 10623 Berlin, Germany*
[2] *Physikalisch Technische Bundesanstalt, Abbestraße 2-12, 10587 Berlin, Germany*
[3] *Present address: Institut für Experimentelle Physik, Otto-von-Guericke Universität Magdeburg, PF4120, Magdeburg, Germany*

Semiconductor quantum dots (QDs) are promising candidates for applications in quantum photonics and quantum communication, as high levels of single photon purity as well as indistinguishability have been reported [1,2,3]. These properties are usually assessed via time-correlated measurements using standard 'click' detectors in either Hanbury-Brown and Twiss (HBT-) or Hong-Ou-Mandel (HOM-) type configurations. Yet more complex schemes, such as photonic boson sampling [4], will involve multi-photon fock-states and it seems natural to employ true photon-number-resolving detection systems for their characterization. In this work, a two-channel detection system (cf. Fig. 1(a)) based on superconducting transition-edge sensors (TESs) is used to directly access the photon-number distribution of deterministically fabricated solid-state single-photon sources. The obtained results reveal excellent quantitative agreement (cf. Fig. 1 (b) and (c)) of the degree of indistinguishability obtained with PNR (90 ± 7 %) and standard detectors (90 ± 5 %) [5]. This demonstrates the perfect suitability of TES-based detection systems for the quantum metrology of non-classical light sources.

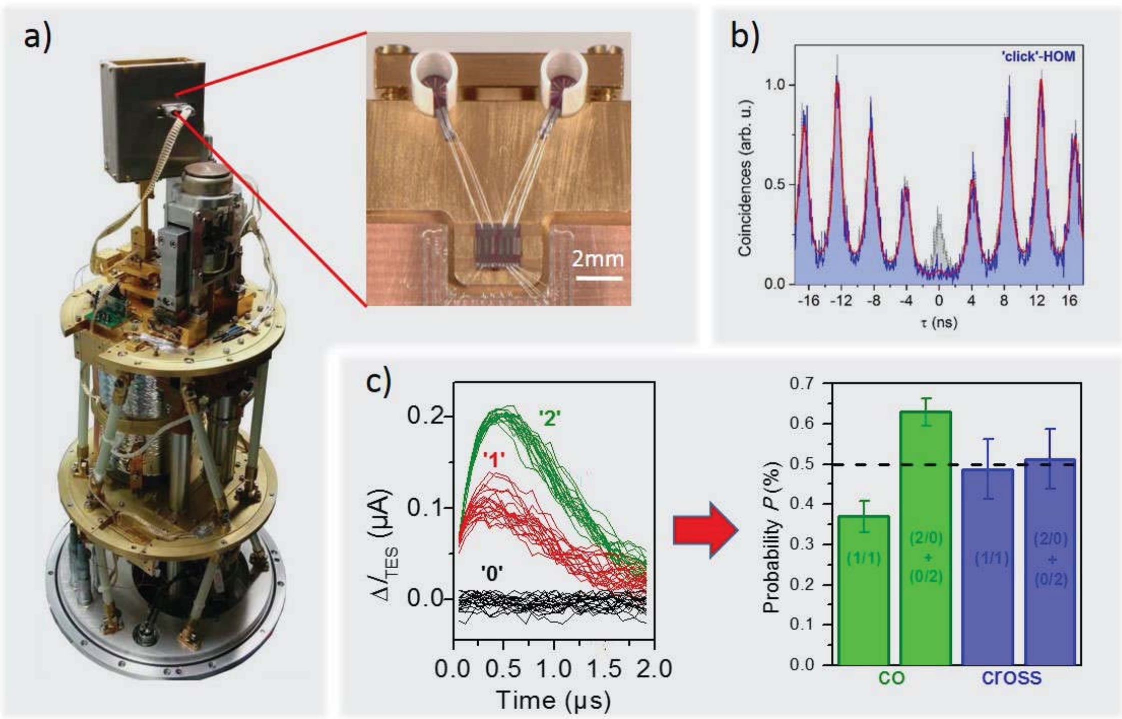


Fig. 1: (a) The fibre-coupled TES-sensors are installed on the experimental platform of an adiabatic demagnetization refrigerator and are operated at 100 mK. (b) Two-photon interference HOM-measurement with SPCM click detectors. (c) Exemplary traces for 0,1,2 photons measured by a TES detector and the extracted probability distribution for the HOM-type measurement.

[1] L. Schweickert et al., *Appl. Phys. Lett*. **112**, 093106 (2018)
[2] Y.-J. Wei et al., *Nano Lett.* **14**, 6515-6519 (2014)
[3] X. Ding et al., *Phys. Rev. Lett.* **116**, 020401 (2016)
[4] H. Wang et al., *Nat. Photonics* **11**, 361–365 (2017)
[5] M. von Helversen et al., *New J. Phys*. **21**, 035007 (2019)

# Progress in Few-Photon Metrology at NRC Canada

**Angela Gamouras[1], Jeongwan Jin[1], Thomas Gerrits[2], Varun Verma[2], Dileep Reddy[2], Sae Woo Nam[2], Dan Dalacu[1], and Robin Williams[1]**

[1]*National Research Council Canada, Ottawa, ON, K1A 0R6, Canada*

[2]*National Institute of Standards and Technology, Boulder, CO, 80305, USA*

The National Research Council (NRC) of Canada is establishing a quantum metrology capability for optical radiometry. Work has been ongoing in both single-photon detector and single-photon source characterization methodologies and measurement techniques. A free-space single-photon detector calibration system for silicon single-photon avalanche diode efficiency measurements, with traceability to the NRC absolute cryogenic radiometer, has been established. In collaboration with the National Institute of Standards and Technology (NIST), a NIST-designed portable optical fibre-coupled superconducting nanowire single-photon detector (SNSPD) system [1] was assembled and tested at NIST Boulder by both NRC and NIST researchers and has been transported back to NRC. The high efficiency SNSPDs in this system operate at wavelengths of 800 nm, 1064 nm, and 1550 nm, and will be used as standard fibre-coupled single-photon detectors as well as for other measurements. Presently, NRC-developed solid-state on-demand single-photon sources based on III-V semiconductor quantum dots [2] are being implemented in metrology applications including investigating the possibility of using these sources as absolute standard single-photon sources and in the development and standardization of single-photon source performance metrics *(i.e.* source efficiency, single-photon purity, etc.) and measurement procedures.

**References**

[1] T. Gerrits, Single-photon quantum metrology, Proc. SPIE 10934, 109341K (2019).

[2] D. Dalacu, *et. al.*, Nanowire-based sources of non-classical light, Nanotechnology 30 (23), 23200 (2019).

# Noise-to-signal as a method to characterize a single-photon detector's maximum useful count rate

**A. Restelli[1], J. C. Bienfang[1] and A. L. Migdall[1]**

[1]*Joint Quantum Institute: University of Maryland and the National Institute of Standards and Technology, 100 Bureau Drive, Gaithersburg MD, USA*

The maximum count rate of a single-photon detector (SPD) is a parameter of interest for applications such as detector calibration, quantum communications, and LIDAR. One common method used to demonstrate a detector's maximum count rate is to measure its linearity/non-linearity versus incident photon flux over multiple orders of magnitude. These measurements are taken up to saturation, a limit usually imposed by the detector's recovery time (c.f. [1]). Spanning multiple orders of magnitude, such measurements are often presented in a log-log format that can obscure subtle but well-known effects in SPDs. For example, afterpulsing noise in avalanche diodes can increase by many orders of magnitude as the mean time between detection events is reduced, and yet still remain in the few-percent range that may not be evident on a log scale. Similarly, the transition from apparent linearity to a state of saturation, where some SPDs essentially become oscillators, is not usefully quantified on a log-log plot. Simple count-rate demonstrations are not well suited to show degradations in the signal-to-noise ratio that can occur as an SPD's count rate increases.

We demonstrate that directly measuring the noise-to-signal ratio as the count rate increases provides a more detailed picture of how the effects like afterpulsing, dark counts, and recovery time impact SPD performance, and at what count rate these various effects are relevant. For applications that impose specific bounds on allowable noise, such as quantum key distribution [2], this measurement can provide a useful means to determine the maximum operable limit of an SPD. Although it was developed for characterizing a high-speed gated InGaAs SPD, this technique is agnostic to detector type and can be applied to gated and free-running detection systems.

To measure noise at high count rates, we illuminate the SPD with attenuated regularly-spaced laser pulses at a rate that exceeds its estimated maximum count rate, allowing the SPD to be driven into the high count-rate regime while keeping the mean photon number per pulse low. To measure noise in the SPD under these conditions, a pulse is occasionally skipped, creating a 'dark' time bin in which there is no light incident on the detector. Post-selective logic circuits are used to count any noise events that occur in these occasional dark time bins. The post-selection system is also used to count detection events that occur in one of the illuminated time bins, and the noise-to-signal is simply the ratio of the count rate in the dark time bin to that of one of the illuminated time bins. This method provides a means to characterize the detector's ability to count at high rates in response to incident photons (ie. linearity), and the noise in the detector under high-count-rate conditions.

An example measurement was made on an InGaAs single-photon avalanche diode gated at 1.25 GHz [3]. Here the laser pulse rate was 625 MHz, with 1/32$^{nd}$ of the pulses being omitted to create dark time bins. Figure 1 shows the ratio of the count rate in the dark time bin (CR(dark)) to the count rate in an illuminated time bin (CR(light)), versus the total count rate in all bins. At low count rates the ratio is dominated by the native dark counts of the detector (operated at -10 °C). For count rates between $50 \times 10^6$ s$^{-1}$ and $150 \times 10^6$ s$^{-1}$ the noise-to-signal ratio remains essentially constant due to the combination of dark counts and the "long-term" afterpulse probability. At rates above $150 \times 10^6$ s$^{-1}$, where the mean time since the last prior avalanche drops below ≈ 7 ns, the noise-to-signal ratio starts to rise due to the increased contribution from afterpulsing at short time scales after an avalanche (short-term afterpulsing). In this particular measurement, the counter in use had a maximum rate of ≈ $200 \times 10^6$ s$^{-1}$, which limited our data range. We will present similar characterizations of an SNSPD, and other commonly used detectors.

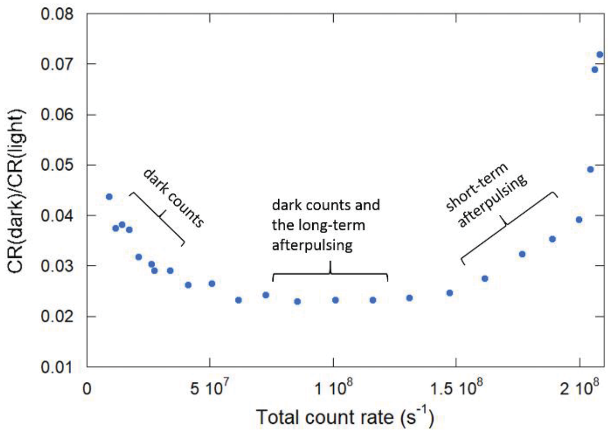


**Figure 1**. Noise-to-signal measurements versus count rate for a gated InGaAs single-photon avalanche diode reveal three regimes: at low count rates dark counts dominate noise, a middle range where dark counts and the long-term afterpulsing dominate, and high count rates where the short-term afterpulse probability dominates noise.

**References**

[1] K.A. Patel, J.F. Dynes, A.W. Sharpe, Z.L. Yuan, R.V. Penty, A.J. Shields, "Gigacount/second photon detection with InGaAs avalanche photodiodes," *Electron. Lett.* **48**, 111 (2012).

[2] Gisin, N., et al., "Quantum Cryptography" *Rev. Mod. Phys.* **74**, 145 (2002).

[3] A. Restelli, J. C. Bienfang, and A. L. Migdall. "Single-photon detection efficiency up to 50% at 1310 nm with an InGaAs/InP avalanche diode gated at 1.25 GHz," *Appl. Phys. Lett.* **102**, 141104 (2013).

# Establishment of a free-space single-photon detection efficiency calibration system at the National Research Council Canada

**Jeongwan Jin[1], Thomas Gerrits[2], and Angela Gamouras[1]**

[1]*National Research Council Canada, Ottawa, ON, K1A 0R6, Canada*

[2]*National Institute of Standards and Technology, Boulder, CO, 80305, USA*

In support of the few-photon metrology capability at National Research Council (NRC) Canada, a detection efficiency calibration system for free-space single-photon detectors has been constructed. This measurement apparatus implements an 850 nm fiber-coupled laser source and utilizes a double-attenuation calibration technique [1]. The calibration of silicon single-photon avalanche photodiodes (SPADs) is SI traceable through a substitution configuration with a silicon transfer standard radiometer, calibrated directly using the NRC cryogenic radiometer. To validate this new single-photon detector efficiency calibration system, SPAD detection efficiencies were measured at NRC with the new calibration system and at the National Institute of Standards and Technology (NIST) in the USA, using a calibration set-up described in Ref. [2]. The results of these measurements and the uncertainty budget for the NRC single-photon detection efficiency calibration system will be presented.

**References**

[1] M. López *et al*., Detection efficiency calibration of single-photon silicon avalanche photodiodes traceable using double attenuator technique, J. Mod. Opt **62**, S21 (2015).

[2] T. Gerrits *et. al*., Calibration of free-space and fiber-coupled single-photon detectors, arXiv:1906.02258 (2019).

# Counting Statistics of Single-Photon Detectors

**Ivo Straka, Jan Grygar, Josef Hloušek, Miroslav Ježek**

*Department of Optics, Faculty of Science, Palacký University, Olomouc, Czechia*

This work presents a model of detection statistics of single-photon detectors exhibiting dead time and afterpulsing under continuous illumination. The basis of the model is a self-exciting point process that can be tailored to cover all the aftereffects of a particular detection technology. We formulate the model for common single-photon avalanche diodes (SPADs), which means covering the effects of recovery time, the probability and temporal distribution of afterpulses, and twilight pulsing. Detector efficiency and dark counts are included implicitly. The full model is shown to be computable numerically using an experimentally measured afterpulse temporal distribution, but we also present explicit algebraic formulas for the detection statistics along with appropriate factor corrections approximating the effect of afterpulsing distribution. Additionally, we derive a detection rate correction factor that allows the inference of real photon incident rate from the number of detected events.

The proposed approach offers an accurate solution to counting statistics and treats afterpulsing behaviour in full detail. It is therefore faithful to experimental data, because the point process is derived from real operational phenomena taking place in the detector (dead/recovery time, transition time and tardiness of twilight pulses, afterpulsing with a temporal distribution) [1][2].

We verified the precision of the model using commercially available thick-junction silicon SPADs. Preliminary results show that the differences in probabilities between data and model are $<10^{-4}$ (measured with a module of 29 ns recovery time, 0.21% afterpulsing probability and 2.8 ns effective reset time). At this level of precision of $\sim10^{-5}$, systematic fluctuations of photon detection efficiency due to thermal stability of the electronics become the limiting factor. In principle, these fluctuations can be factored in by convoluting the whole model over the expected intensity/efficiency noise distribution.

In the coming weeks, we intend to further test our observations and measure more SPADs, especially those exhibiting a higher afterpulsing probability.

The proposed counting model has multiple uses in metrological applications. It provides a better rate correction factor and thus improves photon rate estimation based on a measured number of events in a finite period. As a result, it increases the precision of photometric measurements and also provides more accurate insight into the nonlinearity of single-photon detectors. Counting statistics could also allow observation of certain cumulative or non-Markovian phenomena that cannot be recognized in interarrival histograms alone. The point-process model can be readily modified to accommodate a different detection technology, for example cryogenic detectors that also experience afterpulsing [3][4]. Finally, the simulation approach was already successfully employed in accurate verification of arbitrary statistics generation [5].

An early version of this work can be found in Section 2.3 in reference [6].

**References**

[1] A. Migdall, S. V. Polyakov, J. Fan, and J. C. Bienfang, *Single-photon generation and detection*, Academic Press, 2013.
[2] S. Cova, M. Ghioni, A. Lacaita, C. Samori, and F. Zappa, Applied Optics **35**, 1956-1976 (1996).
[3] V. Burenko, H. Xu, B. Qi, R. H. Hadfield, and H.-K. Lo, J. Appl. Phys., **13**, 213102 (2013).
[4] F. Marsili, F. Najafi, E. Dauler, R. J. Molnar, and K. K. Berggren, Appl. Phys. Lett. **100**, 112601 (2012).
[5] I. Straka, J. Mika, and M. Ježek, Opt. Express **26**, 8998-9010 (2018).
[6] I. Straka, *Generation, Detection and Characterization of Photonic Quantum States*, Ph.D. thesis, Palacký University, 2019. Available online: https://theses.cz/id/6sc3bn/?lang=en

# An optimal multi-detector configuration for photon-number resolving measurements

**Joël Bleuse***, **Bruno Gayral, Jean-Michel Gérard**

*Commissariat à l'Énergie Atomique et aux Énergies Alternatives, IRIG, DEPHY, PHELIQS*
*CEA-CNRS joint team "NanoPhysique & SemiConducteurs", Univ. Grenoble-Alpes, Grenoble, France*

With the advent of quantum information technology and, in particular, the use of an ever-decreasing number of photons to transport bits — or qubits — of information, a huge effort has been devoted to improving the performance of single-photon detectors in metrics such as timing jitter, dark counts, detection rate, and efficiency.

In nearly all of these metrics, the most successful type of detector to date is the so-called superconducting nanowire single-photon detector (SNSPD)[1, 2]. Nevertheless, SNSPD lack photon-number resolution (PNR), as they function as threshold, "on/off" detectors. Attempts to provide PNR with SNSPDs are still not satisfying, as these consist mostly in fanning out photons on many end detectors, each with an efficiency smaller than 1, leading to vanishing fidelity when the number of photons grows larger than 1.

Following previous work[3], we rather considered a detection scheme constituted of many detectors, laid over a waveguide, and probing *in succession* the evanescent part of the guided mode[4]. In addition, we searched for an optimum, if any, by letting the detector efficiencies $\eta_i$ be adjustable.

As a proper metric, we consider the "fidelity", *i.e.* the probability $P(p|p)$ of outputting $p$ detection events when a number state $|\,p\,\rangle$ — made of exactly $p$ photons — enters the detection system. For the above-mentioned systems, for which the photons are fanned out *in parallel* over $N$ space — or time — slots where the photons are detected by end detectors, all of efficiency $\eta$, the fidelity is[5, 6]:

$$P_{\text{parallel}}(N,\{\eta\};p|p) = \frac{N!}{N^p(N-p)!}\eta^p \tag{1}$$

It follows from (1) that getting $\eta$ as close to 1 as possible is mandatory for these parallel detection schemes.

For our favored, serialized waveguide detection scheme, we find that there exists an optimum — *independent on the number p of incoming photons* — in the set of efficiency $N$-uples, which maximizes the fidelity:

$$P_{\text{series}}(N,\{\eta_1,\eta_i=1/i\}_{1<i\leq N};p|p) = \frac{N!}{N^p(N-p)!}\left(1-p\frac{1-\eta_1}{N}\right) \tag{2}$$

In (2), the detectors are numbered from $N$ at the entrance of the waveguide down to 1 at the end of it, their efficiencies being $\eta_i = 1/i$. Although the maximum fidelity comes when $\eta_1 = 1$, we singled out that last detector to show that, in sharp contrast with the parallel scheme, the unavailability of unit efficiency detectors is of small concern.

This result is obtained assuming that: i) the detectors are all of the "on/off" type; ii) they all possess unit internal efficiency: if they absorb one photon or more, it will be a detection event with probability 1; iii) their dark count is negligible; iv) their detection efficiency $\eta$ can be set in the range $]0;1[$, either at the fabrication stage[7] or by adjusting an external parameter. Equation (1) is obtained using the same first three assumptions .

We will discuss the robustness of this multi-detector configuration with regard to inaccuracies in efficiencies, and to relaxation of assumptions ii) and iii), which are very nearly fulfilled by SNSPDs. Moreover, in order to completely benefit from the precise assessment of the fidelity given by (2), we will argue for the necessity of separate readout electronics for each SNSPD, making this multi-detector fully digital.

* corresponding author: joel.bleuse@cea.fr

## References

[1] Gregory N. Gol'tsman *et al.*, Applied Physics Letters **79**, 705 (2001).

[2] *Superconducting Devices in Quantum Optics*. Springer, Cham (2016). Faraz Najafi *et al.*, Ch. 1, and references therein.

[3] *id.* Döndü Sahin *et al.*, Ch. 3, p. 75.

[4] Thomas Gerrits *et al.*, Physical Review A, **84**, 060301 (2011).

[5] M. J. Fitch *et al.*, Physical Review A, **68**, 043814 (2003).

[6] Leaf A. Jiang, Eric A. Dauler, and Joshua T. Chang. Physical Review A, **75**, 062325 (2007).

[7] Luca Redaelli *et al.*, Superconductor Science & Technology, **29**, 065016 (2016).

# Characterization of a Room Temperature Photon Number Resolving Detector for Quantum Information Science and Astrophysics

Donald F. Figer[1], Gregory Howland[1], Justin Gallagher[1], Valerie Fleischauer[1], Gabrielle Picher[1]

[1]*Center for Detectors, Rochester Institute of Technology, Rochester, NY, 14623 USA*

We report characterization results for a room temperature photon number resolving detector. Dartmouth designed and initially characterized the detector, and Gigajot Technology, Inc. made the camera [1, 2]. It is configured as an imaging array detector with one million pixels. Unlike other single photon sensing detector arrays, such as those based on avalanche photodiodes, its pixels have high fill factor and can distinguish photon number. It also operates at room temperature, unlike superconducting single photon sensing detectors. We present measurements of read noise, dark current, persistence, and quantum efficiency. We compare the results to requirements of astrophysics and quantum information science experiments.

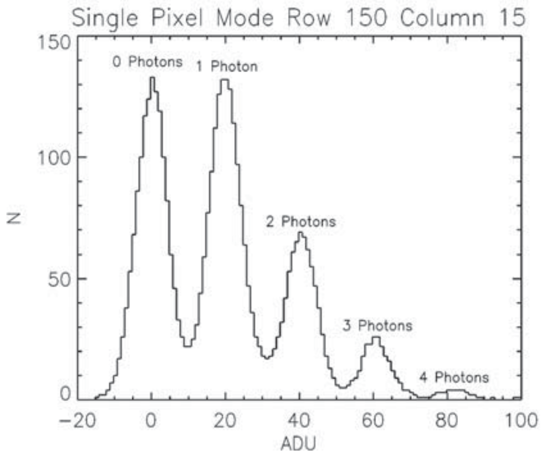


Fig. 1 The picture on the left shows twenty packaged Gigajot Quanta Image Sensor detectors in the RIT Center for Detectors, and the plot on the right shows a histogram of 4,000 values for a single pixel under constant illumination. The deep valleys between the peaks demonstrate single photon sensing and photon number resolution.

**References**

[1] https://www.gigajot.tech/

[2] Ma, J., Masoodian, S., Starkey, D.A., and Fossum, E.R. 2017, “Photon-Number-Resolving Megapixel Image Sensor at Room Temperature without Avalanche Gain,” Optica, Vol. 4, Issue 12, pp. 1474-1481

# MCP-PMT detectors with GHz Single-Photon Counting Capability

**D. A. Orlov[1], R. Glazenborg[1], E. Kernen[1]**

[1]*Photonis Netherlands BV, Dwazziewegen 2, 9301 ZR Roden, The Netherlands*

MCP-PMTs are vacuum tubes, typically consisting of a photocathode, two MCPs and an anode. Photoelectrons generated in the photocathode are emitted into vacuum and accelerated towards the MCPs where they are multiplied to reach a gain of 1E5 to 1E6 for a dual-MCP device. The anode can be single or pixelated and will collect the incoming bunch of electrons.

In terms of spectral range, the Hi-QE photocathodes cover UV to visible spectrum and are tuned to peak at relevant wavelengths (for example laser line of 355 nm and 532 nm), depending on the type of photocathode : Hi-QE UV, Blue, Aqua or Green, as shown on Fig.1. At low rate signal, the Hi-QE photocathodes [1] with a maximum QE above 30 % and extremely low dark rates below 50 Hz/cm2 are providing the ultimate detection capability.
The newly developed Hi-CE MCPs [2] ensure detection quantum efficiency close to 100 % of QE without loss of photoelectron events at the MCP stage. At high photon flux levels the fast timing properties, as shown in the Fig.1 insert, allow to extend the counting detection range up to GHz photon flux rates. Indeed the pulse waveform demonstrate $\tau < 200$ ns and FWHM < 350 ns and the transfer time spread has been measured down to about 20 ps The development of High Linearity MCPs extends the average detection rate, ensuring detection ability without saturation even at high average photon rate of several 100s of MHz [3]. Those unique properties, combined with option for gating and an improved life time, make our new range of MCP-PMTs attractive for demanding single photon counting applications.

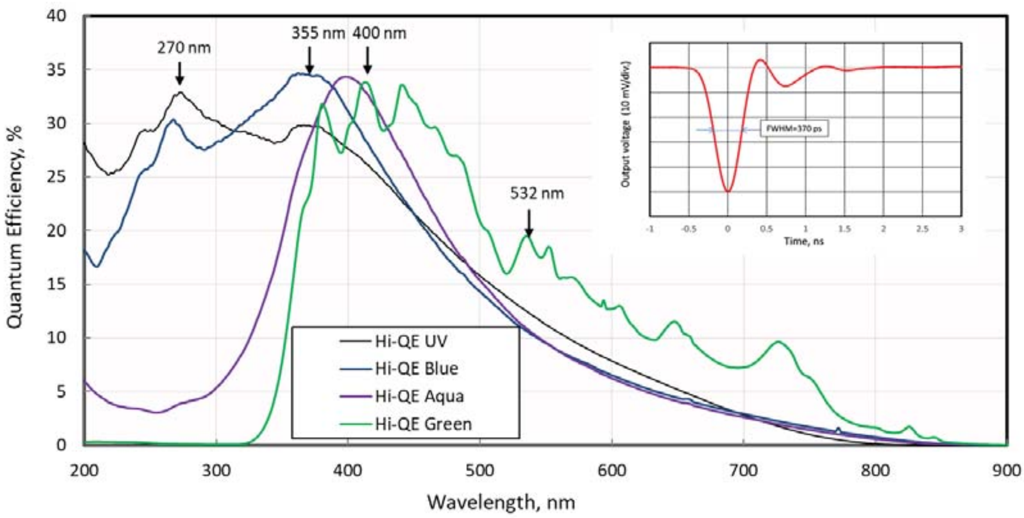


Fig. 1 Quantum efficiency spectra for Photonis Hi-QE S-20 photocathodes: Hi-QE UV (black), Hi-QE Blue (blue), Hi-QE Aqua (purple) and Hi-QE Green (green). The insertion shows the time response waveform of Photonis fast MCP-PMT measured with a 2 GHz 40 dB preamplifier and a 2.5 GHz oscilloscope

## References

[1] D.A. Orlov, J. DeFazio, S. Duarte Pinto, R. Glazenborg, E. Kernen, *"High quantum efficiency S-20 photocathodes in photon counting detectors"*, J. Instrum. 11, C04015 (2016)

[2] D.A. Orlov, T.Ruardij, S. Duarte Pinto, R. Glazenborg, E. Kernen, *"High collection efficiency MCPs for photon counting detectors. J. Instrum."* 13, C01047 (2018)

[3] D. A. Orlov, R. Glazenborg. R. Ortega, E. Kernen, *"UV/visible high-sensitivity MCP-PMT single-photon GHz counting detector for long-range lidar instrumentations"*, CEAS Space Journal https://doi.org/10.1007/s12567-019-00260-0 (2019)

# SiPM technologies for Large Volume Manufacturing

**Alberto Gola[1], Paolo Organtini[2], Giovanni Paternoster[1], Fabio Acerbi[1], Alberto Mazzi[1], Giovanni Margutti[2], Roberto Bez[2]**

[1]*Fondazione Bruno Kessler, Trento, Italy,* [2]*LFoundry, Avezzano, Italy*

Silicon photomultiplier (SiPM), an array of many single-photon avalanche diodes (SPADs), has become a reference technology for many applications that need to detect and count the number of incident photons in both, spatial and temporal domains. Many possible architectures have been proposed [1] in order to optimize the characteristic performance of the SiPM. Among them, there are the ones with optimized response in the near UV (NUV) or in the near IR region (NIR) [2-3] developed by FBK using its 6" line, dedicated to research and development with small and medium volume production capacity. These SiPMs, whose basic architecture is reported in Fig.1, have unique characteristics in terms of Photon Detection Efficiency (PDE), Dark Count Rate (DCR), Direct Cross Talk (DiCT), timing jitter, as reported in Tab.1. These performances in the NUV and NIR spectrum have attracted great interest from both research institutes for large scientific experiments (like "Darkside" [4]) and electronic industries for large applications (especially in the medical and automotive fields) requiring a larger manufacturing capacity available in the 8" production line of LFoundry. The technology transfer has required the optimization of several process steps with the risk of degrading the performances of the SiPM. As a matter of fact, the key parameters have been confirmed, demonstrating the intrinsic robustness of this SiPM structure. Moreover, some aspects have also been improved thanks to the integration into a fab already dedicated to a large volume production of optical sensors. Fig.2 shows the distribution of the breakdown voltage, peaked at about 26.5V for NUV-HD SiPMs, with a maximum variation of 250 mV, due to an advanced process control. Fig.3 shows the comparison of the leakage current as obtained at 6" and 8". Production yield is increased while the level of primary noise (primary DCR) is comparable to FBK, but with increased uniformity at wafer level.

The process engineering capability at 8" will allow further optimization and development of SIPMs with the introduction of dedicated modules to further improve performance, for example to reduce the DiCT compared to what is shown in Fig.4, using optically isolating structures, or to enlarge the range of sensitivity to the electromagnetic spectrum.

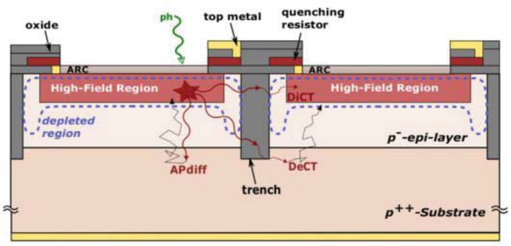


Figure 1 : schematic cross section of a FBK SiPM with deep trench isolation [2]

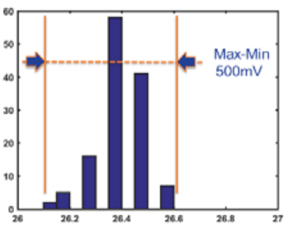


Figure 2: Breakdown Voltage Uniformity over 2000 SiPM

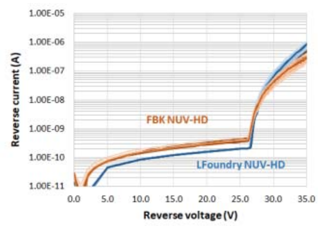


Figure 3: leakage current comparison for SiPM produced at 6" and 8"

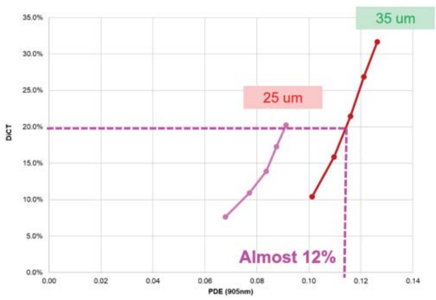


Figure 4: DiCT vs PDE (@905nm) for two different cell size

| Parameter@25°C | NUV-HD | NIR-HD |
|---|---|---|
| Cell Size | 15 - 40 µm | 25 - 35 µm |
| Fill Factor | 55% - 85% | 75% – 85 % |
| Breakdown Voltage | 26.5 V | 27.8 V |
| BV Temp Coefficient | 28 mV/ºC | 28mV/ºC |
| PDE (420nm, 5 Vex) | > 54% | |
| PDE (850nm, 5Vex) | | 13-18% |
| PDE (905nm, 5Vex) | | 8-12% |
| Gain | > $10^6$ | > $10^6$ |
| Peak PDE λ | 410 nm | 545 nm |
| DCR (20°C, 5Vex) | < 150 kHz/mm2 | < 800 kHz/mm2 |
| DiCT | 20% | 14% - 22% |
| DeCT + AP | 2% | 12% - 18% |
| Timing Jitter (FWHM) | ~ 20ps (single cell) | ~ 60ps (single cell) |

Table 1**:** Comparison of main parameters, measured at room temperature, for the NUV and NIR SiPM version

**References**

[1] Sul et. Al., IEEE Electron Device Letters. (2013), 34. 336-338
[2] F.Acerbi et al., Nuclear Inst. And Methods in Physics Research, A, 912 (2018) 309-314
[3] A.Gola et al., Sensors (2019), 19, 308
[4] DarkSide Collaboration, Physical Review D, 98 (2018)

# Using Silicon photomultipliers to test nonclassicality of mesoscopic twin-beam states

**G. Chesi[1], A. Allevi[1], M. Bondani[2]**
[1]*University of Insubria, Department of Science and High Technology, Como, Italy*
[2]*CNR, Institute for Photonics and Nanotechnologies, Como, Italy*

In the last two decades, many efforts have been devoted to the development and testing of different classes of photon-number-resolving (PNR) detectors, required to characterize quantum states of light containing more than single photons. Among PNR detectors, the Silicon photomultipliers (SiPMs) display relevant features, such as an unprecedented photon-number resolution at room temperature. SiPMs are commercial PNR detectors consisting of avalanche diodes arranged in a matrix with a common output. Every diode is reverse-biased and works in Geiger-Muller regime [1]. Even if SiPMs have been massively employed in particle-physics experiments and for positron-emission tomography, they have been marginally used in the field of Quantum Optics, due to a limited quantum efficiency (below 60%) and to the presence of cross-talk effect [2, 3]. Nevertheless, by properly modeling the response of the detectors and minimizing their non-idealities, the reconstruction of light statistics and the measurement of intensity correlations can be achieved [4, 5].

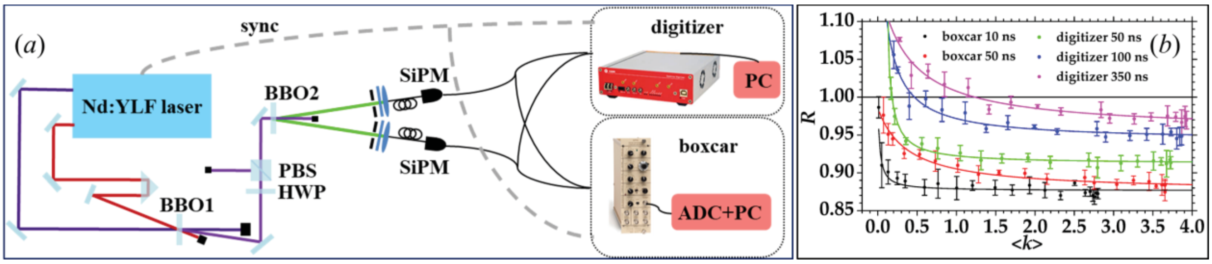


Fig. 1 (*a*) Experimental setup for the generation and detection of twin-beam states via parametric downconversion.
(*b*) Values of *R* for different choices of the integration gate.

Here we show that, by suitably operating on the parameters and properly modeling their outputs [4, 6, 7, 8], the new generation of Hamamatsu SiPMs can be used to observe sub-shot-noise correlations between the two parties of a mesoscopic twin-beam state generated by parametric downconversion. The measurement consists in the determination of the noise reduction factor $R = \sigma^2(k_s - k_i)/\langle k_s + k_i \rangle$, evaluated from the shot-by-shot measurements of the number of photons $k_{s,i}$ in the two parties of the twin beam. If $R < 1$, the state is entangled. For perfect twin beams, $R = 0$, but the detectors imperfections limit the minimum achievable value of $R$.
We show that the measured value of $R$ strongly depend s on the size of the gate over which the detector output is integrated and also on the kind of acquisition system in use. In fact, since for large gate widths detector spurious effects like dark-counts, cross-talks and afterpulses are much more relevant than for short ones, the smaller the gate, the better the characterization of nonclassicality [8].

**Reference**

[1] A. V. Akindinov et al., Nucl. Instrum. Methods Phys. Res. A 387, 231-234 (1997).
[2] I. Afek et al., Phys. Rev. A 79, 043830 (2009).
[3] D. A. Kalashnikov et al., Opt. Lett. 37, 2829–2831 (2012).
[4] M. Ramilli et al., J. Opt. Soc. Am. B 27, 852-862 (2010).
[5] A. Allevi et al., Opt. Lett. 35, 1707-1709 (2010).
[6] M. Bondani et al. J. Mod. Opt. 56, 226–231 (2009).
[7] G. Chesi et al., Sci. Rep. 9, 7533 (2019).
[8] G. Chesi et al., Opt. Lett. 44, 1371-1374 (2019).

# Status of the SIMP project: Towards the Single Microwave Photon Detection

**Paolo Falferi[1,2] on behalf of the Simp collaboration**

[1]*Istituto di Fotonica e Nanotecnologie, CNR Fondazione Bruno Kessler, I-38123 Povo, Trento, Italy*

[2]*INFN, TIFPA, Povo, Trento, Italy*

The low-mass frontier of Dark Matter, the measurement of the neutrino mass, the search for new light bosons in laboratory experiments, all require detectors sensitive to excitations of meV or smaller. Faint and rare signals, such as those produced by vacuum photoemission or by an Axion in a magnetic field, could be efficiently detected only by a new class of sensors.

The Italian Institute of Nuclear Physics (INFN) has financed the three-year SIMP project (2019-2021) in order to strengthen its skills and technologies in this field with the ultimate aim of developing a single microwave photon detector.

This goal will be pursued by improving the sensitivity and the dark count rate of two types of photodetectors: current biased Josephson Junction (JJ) for the frequency range 10-50 GHz and Transition Edge Sensor (TES) for the frequency range 30-100 GHz.

Superconducting circuits based on JJ have been used in the last decades for the realization of artificial atoms with level spacing of few to several GHz sensitive to single microwave photons. In particular, in current biased JJ, the absorption of a photon induces a resonant transition from the superconducting to the resistive state, producing a measurable voltage signal.

The TES calorimeter sensitivity is limited by the magnitude of the thermal energy fluctuations, due to the energy exchange between the sensor and the phonon bath. To obtain an energy resolution lower than 0.1 meV the proximity effect between a superconducting material (Ti or Al) and a normal metal (Au or Cu) will be exploited in order to fabricate a device with a volume of $10^6$ $nm^3$ and a transition temperature of 40 mK or lower. Preliminary results on materials and devices characterization will be presented.

# 40 × 10 SPAD Array for Laser Rangefinders with Region-Of-Interest Selection and Smart TDC Routing

**Renato Federico[1], Vincenzo Sesta[1], Fabio Severini[1], Rudi Lussana[1], Federica Villa[1], Franco Zappa[1], Yuki Matsui[2], Ken Nakamuro[2]**

[1]*Dipartimento di Elettronica, Informazione e Bioingegneria, Politecnico di Milano, Via Golgi 40, Milano, Italy*
[2]*Technology and Intellectual Property H.Q., OMRON Corporation*

In this work we present a new 40 × 10 SPAD array designed for direct Time-Of-Flight single-point distance measurement to be exploited in automated industrial lines. The aim of this project is the design of a reliable detector with good performances when the SPADs are operating in low photon rate regime, and able to reach one centimeter resolution with a minimum range of 1 m even with 3 klux background illumination (corresponding to a halogen lamp impinging directly on the sensing area) and a 3 ns FWHM laser pulse-width and 100 mW peak power. In order to improve the precision, Time-Correlated Single-Photon Counting (TCSPC) histograms must be built and the centroid of the resulting distribution is computed by an external processor [1].

The strong mechanical vibrations typical in industrial environments force the choice of a non-confocal optical setup, which does not require precise alignments, but results in a 1D displacement of the backscattered light on the detector, which depends on the target distance. For this reason, the sensing area has a rectangular shape (40 × 10 SPADs with 24 μm pitch, i.e. 0.96 × 0.24 mm$^2$), with the short side that fits the 150 μm spot diameter and the long one determined by the optical setup specifications and the maximum target distance. As can be seen in Figure 1(a), only about 37 SPADs out of 400 are illuminated by the laser signal, whereas all pixels are exposed to background illumination. Thus a new architecture that implements a Region-Of-Interest (ROI) selection and a smart sharing of the timing electronics (Time-to-Digital Converters, TDCs) has been proposed to connect to the TDCs only those SPADs that have been actually illuminated by the laser spot. As exemplified in Figure 1(b) this implementation is expected to improve the Signal-to-Noise Ratio (SNR) of the TCSPC histogram, by removing the spurious contributions due to the non-illuminated pixels.

The ROI selection is performed by repeatedly subtracting, in each pixel, the number of events detected in a first time slot that includes the laser expected return time, to the number of background events detected in a second time interval without laser. The result of this operation is expected to be different for pixels within the laser spot and the ones exposed to background only, as can be seen in Figure 1(c), allowing to discriminate the pixels which contain useful signal from the others. Only 80 TDCs are shared among the 400 SPADs, with a self-reconfigurable routing which dynamically connects the SPADs within the ROI to the available TDCs. The implemented TDCs are based on a multiphase clock architecture, with 75 ps Least Significant Bit (LSB) and 19.2 ns Full-Scale Range (FSR), ensuring up to 2 m measurements.

The array has been fabricated in 160 nm BCD technology, that allows to achieve State-of-Art SPAD performance [2], and also to integrate SPAD front-end and fast timing electronics [3]. The chip layout is shown in Figure 1(d).

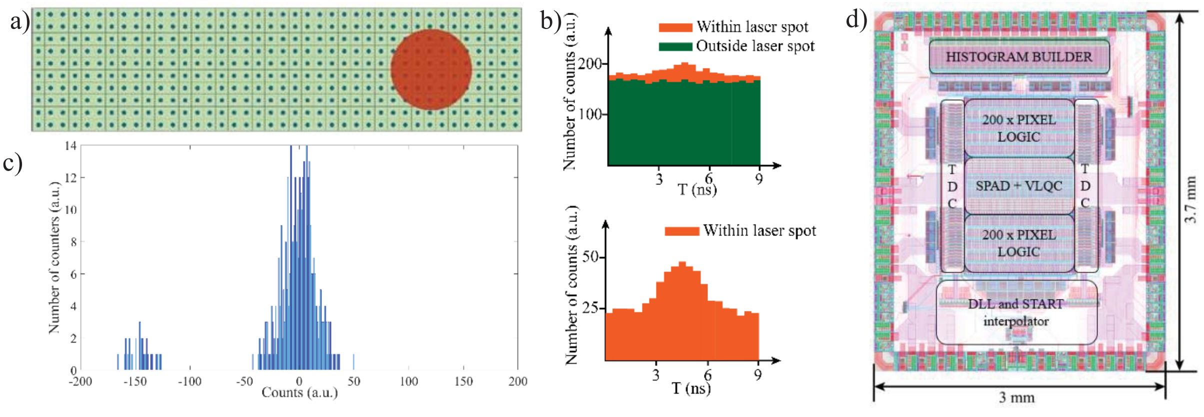


Figure 1. a) Representation of the array where the SPADs exposed to the laser pulse are colored in orange, while those exposed to background only are green. b) Schematic representation of the histograms that can be obtained with the conversions from all SPADs (on the top) or considering only the SPADs exposed (on the bottom). c) Matlab simulation of the possible distribution of counts of the pixel counters in the ROI selection after 500 samples. d) Chip layout.

## References

[1] J. S. Massa, et al., «Laser depth measurement based on time-correlated single-photon counting» OPTICS LETTERS, vol. 22, no. 8, pp. 543-545, 1997.

[2] M. Sanzaro, et al., «Single-Photon Avalanche Diodes in a 0.16 μm BCD Technology With Sharp Timing Response and Red-Enhanced Sensitivity» IEEE J. Sel. Top. Quantum Electron., 24 (2), pp. 1-9, 2018.

[3] D. Portaluppi, et al., «32 × 32 CMOS SPAD Imager for Gated Imaging, Photon Timing, and Photon Coincidence» IEEE J. Sel. Top. Quantum Electron., vol. 24, n. 2, pp. 1-6, 2018.

# Strained SiGe- and Ge- based SPAD Performances Assessment: a Modeling Study.

**D. Rideau, A. Zimmer, D. Golanski, B. Mamdy, and H. Wehbe-Alause**

*STMicroelectronics, 850 rue Jean Monnet, 38920* Crolles

Single Photon Avalanche Diodes (SPAD) are key optoelectronic detectors for medical imaging, camera ranging and automotive LiDAR applications. Today, most of SPADs in the market are composed of a micrometric Silicon PN junction associated to a proximity CMOS electronics biasing the system above the breakdown voltage. Silicon SPADs present low noise and relatively high quantum efficiency, but their sensitivity is limited to photon wavelengths lower than 1000 nm, while class 1 eye-safety devices would requires wavelengths larger than 1300 nm. Moreover, shifting the operation wavelength from 940 nm to e.g. 1310 nm would also result in an improved depth accuracy in LIDAR systems, since higher laser powers can be used in compliance with eye-safety specifications. Infra-Red (IR) InGaAs-based SPADs, typically targeted to operate at 1550nm, are already available, but their relatively high cost and lack of silicon integrated SPADs limit the applications (in particular for high density SPAD arrays working on long wavelengths). Renewal of interest in Ge-based SPAD technology operating at 1310nm appears as a more promising solution for integration on conventional Silicon CMOS technologies. Recent experimental evidences tend to confirm that the Noise Equivalent Power (NEP) in Ge-Si based SPAD at 1310 nm [1] (7 e-16 W/Hz$^{1/2}$ measured at 125K) can compare favorably with InGaAs-InP based devices ones at 1550nm [2] (8e-17 W/Hz$^{1/2}$ measured at 125K), but a clear theoretical benchmark of Ge-based devices performances against III-V-based device is still missing.

We assess Strained SiGe and Ge based SPAD devices performances by means of a multi scale simulation approach, combining rigorous full band Monte Carlo simulations [4] for PDP calculation, optical absorption [5] accounting for strained and temperature dependent band structure effects [6,7], and multiphonon Shockley-Read-Hall (SRH) models [8]. Several template device architectures operating at 1310nm are compared to a reference Si-based one operating at 940nm. Comparisons are also provided with InGaAs-InP devices operating at 1550nm. Fig. 1 shows the NEP for a Ge-Based device featuring a 1 um depleted Ge absorption layer separated from the Si-based avalanche region. The comparison with the Si-based device simulations (well calibrated on measurements) clearly points out the expected and large enhancement of the diffusion current in the Ge-based architecture. The contribution of SRH is also enhanced mainly due to the interface states at the Ge/Si interface, but its impact on the device performance will largely depend on the local electrostatics (interface within a depletion region or not) and its passivation.

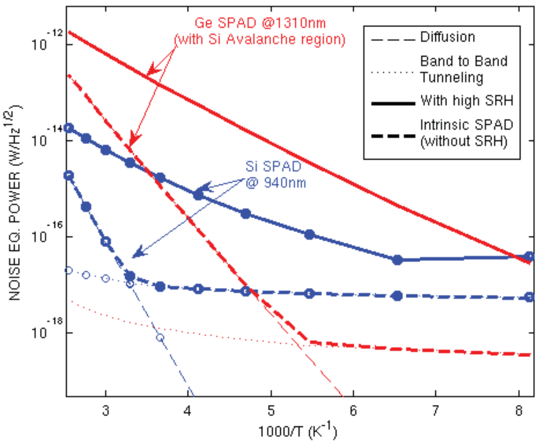


Fig. 1 Noise Equivalent Power for two different SPAD architectures operating at 940nm and 1310nm respectively. In the Si-based one the PN junction is in the Silicon region for photon collection and carrier multiplication. In the Ge-based device (inspired from Ref [1]), the depleted Ge collection region of 1 um is well separated from the Silicon avalanche region.

## References

[1] P. Vines, *et al.*, Nature Communications, Vol **10**, 1086 (2019)
[2] S. Pellegrini, *et al.*, IEEE Journal of Quantum Electronics, Vol **42**, 397 (2006)
[3] D. Bronzi, *et al.*, IEEE Sensors Journal, Vol. **16**, p 3 ( 2016 )
[4] M. Michaillat, *et al.* Journal of Physics: Conference Series **193,** 012037 (2009)
[5] R. Braunstein, *et al,* Phys. Rev. **109**, 695 ( 1958)
[6] Y.M. Niquet, *et al,* Phys. Rev. B, Vol. **79,** p. 245201 (2009)
[7] D. Rideau, *et al,* Proc. Int. Conference on Simulation of Semiconductor Processes and Devices, (2018)
[8] D. Goguenheim and M. Lannoo, J. Appl. Phys. 66, 1059 (1990).

# SPAD ACTIVE QUENCHING AND PROTECTION CIRCUIT

**Alex Komjati[2], Dragan Grubisic[1]**

[1]*Laser Components DG, Inc, Tempe, Arizona, US;* [2]*Consultant, Orlando, Florida, US*

An innovative active quenching architecture shown in Figure 1 applies quenching voltage on the SPAD's cathode when a photon triggers an avalanche [1]. In a few nanoseconds the avalanche is terminated by the applied quenching voltage. The application of this quenching voltage brings the SPAD below its breakdown voltage, thus returning it to its equilibrium state. While the active quenching is taking place, the SPAD's anode current is monitored to protect from overload conditions. Another important part of the design is the custom designed High Voltage DC/DC power supply with excellent transient response to high dynamic load condition thereby further protecting the SPAD.

While Figure 1 only reflects conceptual simplicity, implementing the real circuitry is more involved. One of the goals is to minimize the dead time. This is the time when the SPAD's bias voltage has been restored, but the circuits is not ready to respond to photon detection. This requires very fast quenching and reset pulses. The SPAD is typically biased 8V above its breakdown voltage requiring more than 8V to quench it. A typical quenching voltage may be 12V to provide an additional 4V below the breakdown voltage. Due to circuit parasitic capacitances, large currents are required for the voltage swings. S2 is typically implemented with a DMOS component having nanosecond switching capability [2]. Using only the bias recovery current can create a hang-up due to a stray photon avalanche before the reset is completed. To speed up recovery time and to eliminate the hang-up condition, a recovery current, much larger than the bias current is switched in for this short period of time via S3 and R5. The sense resistor used for the avalanche current detection in this example is 200Ω that feeds one side of the high speed comparator. A temperature compensated reference voltage is generated and applied to the other side of the high speed comparator. When the SPAD avalanches, and it is sensed by the comparator, a digital logic produces a 10nS quenching pulse. This is level shifted and applied to S2 bringing the SPAD cathode voltage below its breakdown voltage and thereby quenching it. When the quenching pulse is completed, the reset pulse is generated to complete the recovery cycle. The reset pulse is terminated when the comparator has sensed the SPAD's cathode voltage returning to its biased level. The reset pulse is level shifted for counter interfacing. At that point, count pulse has been generated as an output and the SPAD is ready to detect the next incoming photon.

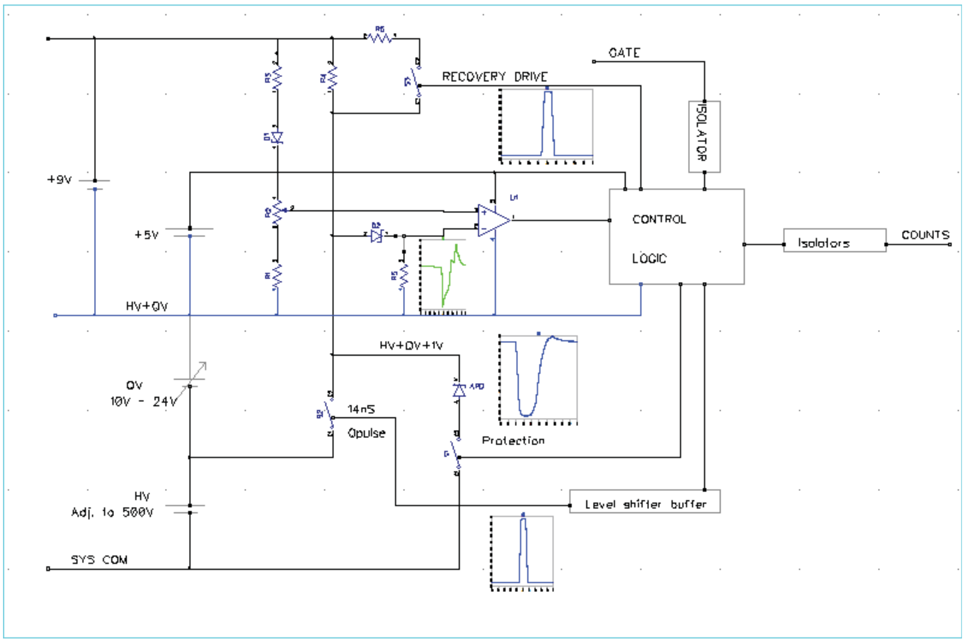


Figure 1. Proposed Active Quenching Arhitecture

## References:

[1] M. Ghioni, S. Cova, F. Zappa, and C. Samori, Compact active quenching circuit for fast photon counting with avalanche photodiodes, Rev. Sci. Instrum. 67 (10), October 1996, pp. 3440 – 3448.

[2] Encyclopedia of Optical Engineering (2003), pp. 128-130.

# Calibration of fiber-coupled, gated InGaAs/InP single-photon detectors

**R. Eßling[1,2], H. Hofer[1], S. M. F. Raupach[1], H. Georgieva[1], B. Rodiek[1], J. Christinck[1], S. Kück[1] and M. López[1]**

[1] *Physikalisch-Technische Bundesanstalt (PTB), Bundesallee 100, D-38116, Braunschweig, Germany*

[2] *Institute for Semiconductor Technology, Braunschweig University of Technology, Hans-Sommer-Straße 66, D-38106 Braunschweig, Germany*

InGaAs/InP-single-photon detectors (SPDs) operated in gate modus are currently the most commonly used detectors in quantum communication and quantum key distribution (QKD) [1-3]. The precise characterization of relevant parameters such as, among others, detection efficiency, dead time, after-pulse probability, temporal photon detection probability profile and dark count probability, is mandatory for their meaningful use in quantum-sensitive detection systems, e.g. in the context of quantum-key distribution [4]. Moreover, validated measurement methods and measurement procedures are a prerequisite for a reliable characterization. Therefore, several National Metrology Institutes (NMIs), such as PTB, and standardisation organisations such as the European Telecommunications Standards Institute (ETSI) are currently putting great efforts in developing and standardizing measurement methods and procedures, which will allow the traceable characterisation of all relevant parameters [4-6].

In this conference, we will present our latest results from the calibration of the detection efficiency of fiber-coupled, gated InGaAs/InP single-photon detectors at the wavelength of 1550 nm. These include the detailed characterization of the most relevant parameters affecting the detection efficiency calibration, such as dead time, after-pulse probability, dark count probability, and the gate window temporal response. Moreover, the setup and the traceability of the reference standard used for the calibration as well as a detailed estimation of the measurement uncertainty will be presented.

**Acknowledgement:**

The work reported on this paper was funded by project EMPIR 17FUN06 SIQUST. This project received funding from the EMPIR program co-financed by the Participating States and from the European Union Horizon 2020 research and innovation program.

## References

[1] Akihisa Tomita, et al., "High speed quantum key distribution system", Optical Fiber Technology, 16, Issue 1, 55-62 (2010).
[2] Damien Stucki, et al., "Photon counting for quantum key distribution with peltier cooled InGaAs/InP APDs", Journal of Modern Optics, 48, Issue 13, 1967-1981 (2001).
[3] M. López, et al, "Detection efficiency calibration of single-photon silicon avalanche photodiodes traceable using double attenuator technique", Journal of Modern Optics 62, S21 – S27, 2015.
[4] "Quantum Key Distribution (QKD); Components and Internal Interfaces", ETSI GR QKD 003 V2.1.1 (2018-03)
[5] G. Porrovecchio, et al., "Comparison at the sub-100 fW optical power level of calibrating a single-photon detector using a high-sensitive, low-noise silicon photodiode and the double attenuator technique", Metrologia 53, 1115-1122 (2016).
[6] "Quantum Key Distribution (QKD); Component characterization: characterizing optical components for QKD systems", ETSI GS QKD 0011 V1.1.1 (2016-05).

# High-speed phonton-number-resolving detction with InGaAs/InP APD

**Yan Liang[1], Qilai Fei[1], Kun Huang[1,2] and Heping zeng[1,2]**

[1] *Shanghai Key Laboratory of Modern Optical System, Engineering Research Center of Optical Instrument and System, Ministry of Education, School of Optical-Electrical and Computer Engineering, University of Shanghai for Science and Technology, Shanghai 200093, China*

[2]*State Key Laboratory of Precision Spectroscopy, East China Normal University, Shanghai 200062, China*

Nowadays, with the development of the quantum information, single-photon detectors (SPDs) capable of photon-number resolution are in urgent need. In the near infrared, InGaAs/InP APD based SPDs are widely used for their compact construction and low cost [1]. The self-differencing technique has been employed to realize photon-number-resolving (PNR) detection with a single InGaAs/InP APD at the repetition frequencies of hundreds of MHz. The gain of the APD was set to be sub-saturated, and the number of the incoming photons determined the amplitude of the avalanche signal. However, while the repetition rate of the gates increases to GHz, the PNR performance of the APD deteriorates dramatically, for the reason that the APD's gain has to be set relatively high to extract the photon-induced avalanche signal from the spike noise.

Here, a GHz InGaAs/InP SPD with the ability to distinguish photon numbers is demonstrated. We use the combining technique that consists of the capacitance-balancing and low-pass filtering to acquire the valid avalanche signals. The spike noise is first subtracted from the output of a mimic capacitance, and then filtered by a low-pass filter, causing the suppression ratio of the spike noise exceed 40 dB. Furthermore, ultrashort gates are employed to improve the performance of the SPD, reducing the error counts and making the PNR performance better. We perform the PNR detection with this InGaAs/InP SPD by measuring the avalanche voltage output and analyzing the peak output voltage probabilistic distribution under different avalanche multiplication of the InGaAs/InP APD. Figure 1 exhibits the distribution of the peak output signal of the APD with different detection efficiencies at 1 GHz. The averaged detected photon number is set to be ~1.35 per pulse. It could be found out that the spike noise is suppressed down to extremely low and the PNR performance is getting better with the increase of the detection efficiency. Finally, the GHz SPD could resolve up to 3 photons with the detection efficiency of 40%, offering a practical solution for high-speed PNR detection.

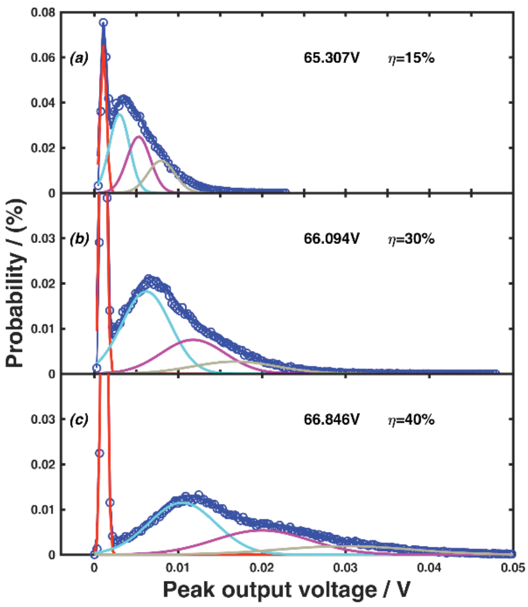


Fig. 1 Distribution of the peak output signal of the APD with different detection efficiencies at 1 GHz.

**References**

[1] Yan Liang, Qilai Fei, Zhihe Liu, Kun Huang, and Heping Zeng, "Low-noise InGaAs/InP single-photon detector with widely tunable repetition rates" *Photonics Research*, **7**(3) A1-A6 (2019).

# High performance of InP/InGaAs APD detectors

Yanli Shi[1,2], Jun Zhang[1,2], Hongxia Zhu[1,2], Xueyan Yang[1,2], Hui Zeng[1,2], Chunhua Hao[1,2], Chen Liu[1,2], Jian Wang[1,2]

*1 School of phyisics and astronomy, Yunnan Yuniversity, 650091*

*2 Key Lab of Quantum Information of Yunnan Province, Yunnan University, Kunming, China*

High performance InP/InGaAs APD is an important APD detectors which can response 0.87-1.7micron infrared irradiation, made it the excellent candidate for laser detecting and application. Besides, it utilizes InGaAs as absorption layer, and InP as multiplication layer, high hole ionization coefficient of InP has obtained and low noise of APD detectors were obtained. InP/InGaAs APD detectors were widely used in quantum communication, laser ladar, and weak signal measurement.

SAGCM APD detectors were designed and prepared, the parameters of charge layer and multiplication layer were calculated and optimized, it were disclosed that punch voltage and breakdown voltage increased with the multiplication layer thickness, and punch-through voltage will increase with increasing doping density of charge layer, on the contrary, breakdown voltage will decrease with it. According to the above theoretical results, InP/InGaAs APDs layer structure were designed and grown by the MOCVD system. Zn diffusion and guard ring was fulfilled by the diffusion stove. APD was prepared and measured with the 1550nm laser as optical source. Both dark current and light current was gained by the semiconductor parameter instrument. From the measurement results the dark current density was $3.55\times10^{-5}$A/cm$^2$ at breakdown voltage-2V under room temperature, the corresponding gain was 71. the breakdown voltage is 70V. good performance APDs were obtained. Further research is to optimize both device structure and processing to get good Geiger mode performance .

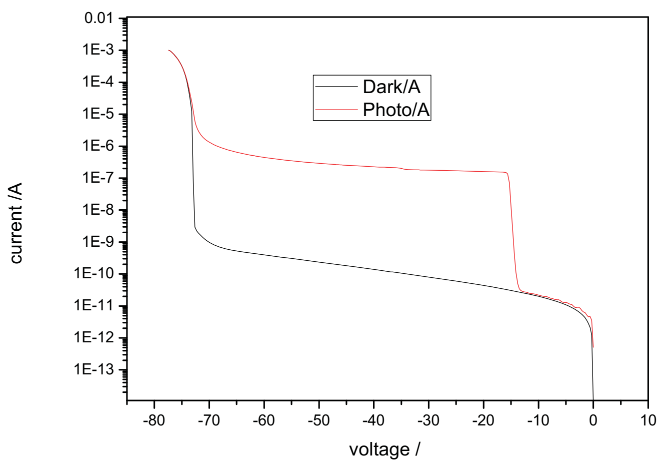


Fig. 1 measurement results of dark and photo-current under room temperature

# QuPAD – Waveguide Integrated Superconducting Nanowire Array for Ultra-Fast Parallelized Single-Photon Detection

**Martin A. Wolff[1,5], Fabian Beutel[1], Wladislaw Hartmann[1], Matthias Häußler[1] Robin Stegmüller[1], Nicolai Walter[1], Max Tillmann[2], Michael Wahl[2], Tino Röhlicke[2], Andreas Bülter[2], Doreen Wernicke[3], Nicolas Perlot[4], Jasper Rödiger[4], Wolfram H. P. Pernice[1,*], Carsten Schuck[1,*]**

[1]*University of Münster, Institute of Physics, Heisenbergstraße 11, 48149 Münster*

[2]*PicoQuant GmbH, Rudower Chaussee 29, 12489 Berlin*

[3]*Entropy GmbH, Gmunder Straße 37a, 81379 München*

[4]*Frauenhofer Heinrich Hertz Institute, Einsteinufer 37, 10587 Berlin*

[5]*martin.wolff@uni-muenster.de*, **wolfram.pernice@uni-muenster.de*, **carsten.schuck@uni-muenster.de*

Superconducting nanowire single-photon detectors (SNSPDs) have developed into a leading sensor technology for ultraviolet to mid-infrared light as they offer efficient photon-counting with high repetition rate, short timing jitter and low dark count rates [1]. The integration of these detectors with wideband transparent $Si_3N_4$ nanophotonic waveguides [2] allows for implementing state-of-the-art quantum optics experiments on silicon chips. However, many applications such as linear optical quantum computing (LOQC), light detection and ranging (LIDAR) and in particular quantum key distribution (QKD) would benefit from the parallelization of single-photon detection channels on a single device.

Here we present first steps towards a massively parallelized system for ultra-fast waveguide-integrated single-photon detection. We fabricate large numbers of SNSPDs on $Si_3N_4$ waveguides (Fig. 1a), each of which connects to a different fiber optic channel in an array. We demonstrate SNSPDs that exhibit near unity internal quantum efficiency over a wide plateau region (Fig. 1b), which are patterned from ultra-thin NbTiN films deposited in a room-temperature magnetron sputtering process. The detectors show low timing jitter of <50 ps and pulse decay times of ~2ns, thus enabling repetition rates of several hundred MHz.

Efficient interfaces between individual optical fibers in the array and nanophotonic waveguides on-chip are provided via wideband 3D coupling geometries fabricated with direct laser writing (Fig. 1c) [3]. Here we optimize such 3D coupling structures in finite difference time domain (FDTD) simulations for vertical incidence of light from a fiber and find less than 1dB insertion loss into nanophotonic waveguides. The combination of low-loss interfaces between optical fibers and state-of-the-art single-photon detectors enables high system detection efficiencies and therewith significantly widens the application space for waveguide-integrated SNSPDs, e.g. providing an attractive solution for high-bandwidth quantum key distribution.

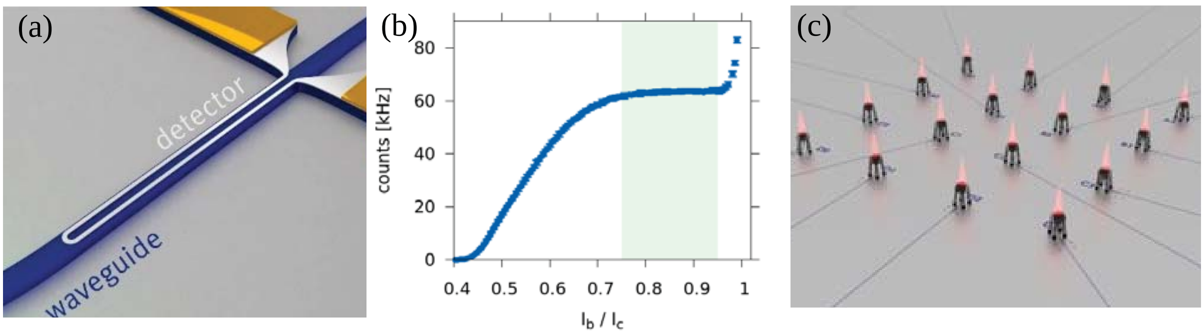


**Figure 1:** (a) U-shaped SNSPD on top of a nanophotonic waveguide; (b) rate of 1550 nm wavelength photons counted with a waveguide-integrated SNSPD made from NbTiN thin films. An extended plateau region at high bias currents is clearly visible; (c) 3D optical interfaces between a 2D fiber array (not shown) and nanophotonic waveguides.

**References**

[1] S. Ferrari et al., Nanophotonics, 7, 1725 (2018)

[2] C. Schuck et al., Appl. Phys. Lett., 102, 051101 (2013)

[3] H. Gehring et al. APL Photonics 4, 010801 (2019)

# State Readout of a Trapped Ion Qubit Using a Trap-integrated Superconducting Nanowire Detector

**S. L. Todaro[1], V. B. Verma[2], A. C. Wilson[1], R. P. Mirin[2], D. J. Wineland[1], S. W. Nam[2], D. Leibfried[1], D. H. Slichter[1]**

[1] *Time and Frequency Division, National Institute of Standards and Technology, 325 Broadway, Boulder, Colorado 80305, USA*

[2] *Electromagnetics Division, National Institute of Standards and Technology, 325 Broadway, Boulder, Colorado 80305, USA*

Superconducting nanowire single photon detectors (SNSPDs) are a versatile class of photon-counting detectors exhibiting near-unity detection efficiencies, fast response times, low timing jitter, and very low dark counts over a broad range of wavelengths. SNSPDs made from amorphous superconducting materials such as MoSi have enabled device fabrication without lattice-matched substrates [1] and with high yield, making it easier to integrate SNSPDs with other technologies. Our work focuses on integrating SNSPDs with surface-electrode rf ion traps, which are microfabricated devices for trapping atomic ions in vacuum; trapped atomic ions are an important technology for quantum information processing applications. Readout of the quantum state of a trapped ion qubit is accomplished by driving a state-selective optical cycling transition of the trapped ion and counting the resulting fluorescence photons; the presence or absence of fluorescence indicates the qubit state. These photons are traditionally collected with high-numerical-aperture bulk optics and detected with a camera or photomultiplier tube. By integrating SNSPDs directly into microfabricated surface-electrode ion traps, we can realize a scalable architecture for spatially-resolved, high-quantum-efficiency detection of fluorescence photons without the need for collection optics [2]. There are challenges with this approach, notably the presence of large rf voltages near the SNSPD (necessary for trapping the ions) and the requirement of operation at temperatures near 4 K.

Here we report the first readout of a trapped ion qubit with a trap-integrated SNSPD, using a single $^9Be^+$ ion in a cryogenic surface-electrode trap. Fluorescence photons with a wavelength of 313 nm are emitted by the ion and detected by the SNSPD, with count rates comparable to those achievable with traditional bulk collection optics, and very low dark counts. The SNSPD is operated in the presence of peak-to-peak rf voltages of 18 V at 68 MHz on nearby electrodes, at a temperature of 3.6 K. We use the known detector-ion geometry and saturated ion fluorescence rate to provide an absolute calibration of the photon flux and thus the quantum efficiency of the SNSPD. We report the impact of the detector on motional heating of the ion, as well as the photon crosstalk from a fluorescing ion in other regions of the trap not directly over the detector. This work is supported by IARPA and the NIST Quantum Information Program.

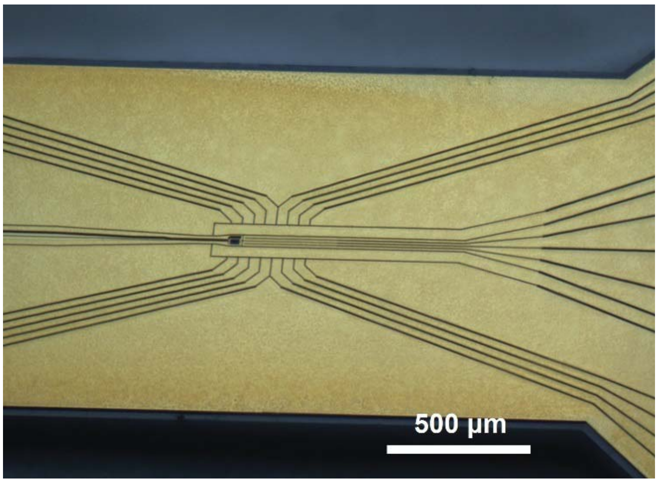


Fig. 1 Optical microscope image of a surface electrode ion trap with an integrated SNSPD. The trapping electrodes are made from electroplated gold, while the SNSPD, made from MoSi, can be seen at one end of the trapping region as a dark grey rectangle.

**References**

[1] V. B. Verma, B. Korzh, F. Bussières, R. D. Horansky, S. D. Dyer, A. E. Lita, I. Vayshenker, F. Marsili, M. D. Shaw, H. Zbinden, R. P. Mirin, and S. W. Nam, "High-efficiency superconducting nanowire single-photon detectors fabricated from MoSi thin-films", Opt. Express **23**, 33792 (2015).

[2] D. H. Slichter, V. B. Verma, D. Leibfried, R. P. Mirin, S. W. Nam, and D. J. Wineland, "UV-sensitive superconducting nanowire single photon detectors for integration in an ion trap", Opt. Express **25**, 8705 (2017).

# QuPAD – high bandwidth photon detection enabled by a massively parallelized system

Max Tillmann[1], Michael Wahl[1], Tino Röhlicke[1], Andreas Bülter[1], Doreen Wernicke[2], Martin Wolff[3], Matthias Häußler[3], Nicolai Walter[3], Robin Stegmüller[3], Fabian Beutel[3], Wolfram Pernice[3], Carsten Schuck[3], Nicolas Perlot[4]

*[1] PicoQuant GmbH, Rudower Chaussee 29, 12489 Berlin*
*[2] Entropy GmbH, Gmunder Str. 37a, 81379 München*
*[3] WWU Münster, Physikalisches Institut, CeNTech II, Heisenbergstr. 11, 48149 Münster*
*[4] Fraunhofer Heinrich-Hertz Institute, Einsteinufer 37, 10587 Berlin*

Single photons are ideal information carriers in many classical and quantum applications. One of the key challenges in transferring these applications from a laboratory environment 'into the field' are the limited count rates achievable with today's hardware. Individual photon detection units – comprised of a single detector element and its timing electronic – run against a physical limit if photons impinge too rapidly.
It is the scope of this project to develop key enabling components to push beyond the bandwidth-limit of single devices with a massively parallelized (x64) single-photon detection system. To this end, detector elements based on superconducting nanowires are optimized for lowest reset times and highest temporal resolution. Care is taken that the optical and electrical interfacing does not degrade the detection performance. To process the high data rates generated with such a system, the readout electronics need to be parallelized in a similar fashion. In particular, an on-chip (FPGA) data processing over all detector channels provides a viable solution to pre-process the initial data such that it can be transferred to a host computer via limited bandwidth links. Ultimately, the performance of this detection system will be evaluated in an applied scenario via a suitable QKD-scheme.

# Micron-wide, photolithographically-patterned SNSPDs with saturated internal detection efficiency at telecommunications wavelengths

**Jeff Chiles[1], Sonia M. Buckley[1], Varun B. Verma[1], Adriana E. Lita[1], Jason Allmaras[2], Boris Korzh[2], Emma Wollman[2], Matt D. Shaw[2], Jeffrey M. Shainline[1], Richard P. Mirin[1], Sae Woo Nam[1]**

[1]*National Institute of Standards and Technology, Boulder, CO, USA*

[2]*Jet Propulsion Laboratory, Pasadena, CA, USA*

Superconducting nanowire single-photon detectors (SNSPDs) have become invaluable in a broad range of applications thanks to their superior detection efficiency and low dark count rates [1,2]. Amorphous superconductors such as tungsten silicide (WSi) exhibit enhanced long-wavelength sensitivity (due to the smaller superconducting energy gap) and high material homogeneity (due to the absence of crystalline grain boundaries) allowing excellent yield and consistent performance across many devices, compared to other materials such as niobium nitride (NbN). This makes it possible to fabricate and yield large-area detectors and arrays with performance similar to their smaller-area counterparts with the same fundamental nanowire geometry (wire width, gap, *etc.*). However, since the typical nanowire width is in the range of 100-250 nm, devices are still time-consuming to fabricate with electron-beam lithography and are susceptible to small geometrical constrictions. Inspired by [3], we demonstrate micron-wide nanowire detectors patterned with a conventional i-line UV stepper. By reducing the film thickness to 2.2 nm and modifying the composition of the superconductor to be more silicon-rich, the energy sensitivity is improved and the free-carrier density is reduced [4], enabling efficient detection even at this extreme wire width.

The nanowires were fabricated by depositing 2.2 nm of WSi onto a silicon wafer with a silicon nitride insulating spacer layer on the surface, then patterning with photolithography and plasma etching. They were fabricated in an out-and-back geometry with a total wire length of 400 μm, using an on-chip meandered inductor to inhibit latching. The wire width is 980 nm with a gap of 800 nm. The devices were cooled to 750 mK, and the bias current was swept while infrared light flood-illuminated the chip. As shown in Fig. 1(c), a wide plateau region is observed, confirming saturated internal detection efficiency at $\lambda$ = 1550 nm. The device supports a critical current of 18 μA due to the wide cross-section and tolerance to small constrictions. Preliminary measurements with focused laser spot scans at several wavelengths indicate the detection efficiency to be highly uniform along the entire length of the wire and not a result of constrictions or current crowding at any feature such as the hairpin.

We further explore the limits of this material by fabricating meandered SNSPDs with an area of 3100 μm × 3100 μm (wire width of 900 nm, 50% fill factor, Fig. 1(d)). Out of 8 such devices tested at 780 mK, two exhibited critical currents ~ 0.8 times the nominal value expected for small (400 μm wire length) out-and-back devices of this wire width. This shows great promise for detectors capable of capturing collimated light sources directly. Measurements of photon counting in these large-area (9.6 mm$^2$) devices are underway.

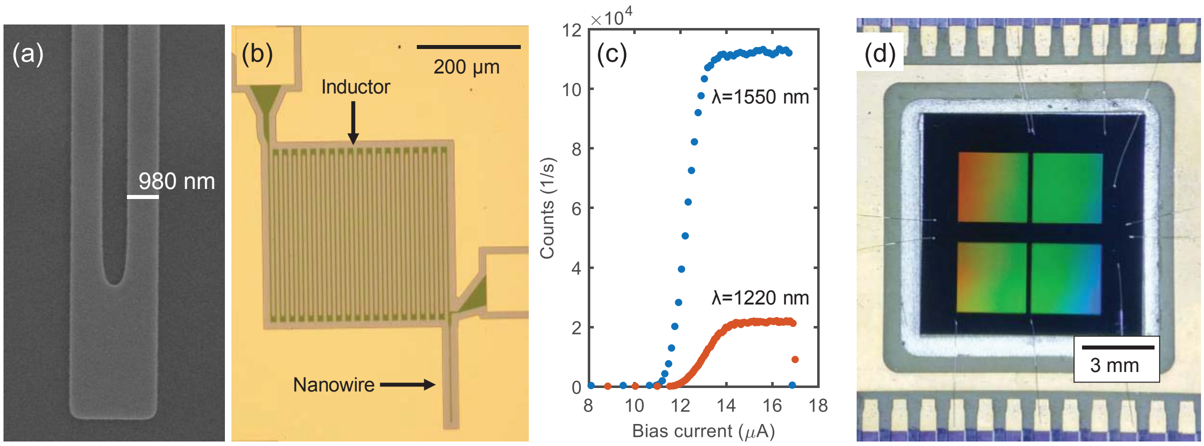


Fig. 1. (a) SEM top-view of the micron-wide nanowire at the hairpin section. (b) Optical micrograph of the device layout. (c) Counts vs. bias current when flood illuminating the micron-wide nanowire with 1550 nm and 1220 nm light. (d) Photograph of separate chip containing several 3100 μm × 3100 μm area meandered SNSPDs with 900 nm wire width and 50% fill factor.

## References

[1] F. Marsili et al., "Detecting single infrared photons with 93% system efficiency," Nature **7**, 210 (2013).
[2] Y. Hochberg et al., "Detecting Dark Matter with Superconducting Nanowires," arXiv:1903.05101 (2019).
[3] Y. Korneeva et al., "Optical Single-Photon Detection in Micrometer-Scale NbN Bridges," Physical Review Applied, **9**, 064037 (2018).
[4] V. B. Verma et al., "Towards single-photon spectroscopy in the mid-infrared using superconducting nanowire single photon detectors," Proc. SPIE 10978, 1097890N (2019).

# Intrinsically-limited timing jitter in molybdenum silicide superconducting nanowire single-photon detectors

**M. Caloz[1], B. Korzh[2], E. Ramirez[2], C. Schönenberger[3], R.J. Warburton[3], H. Zbinden[1], M.D. Shaw[2], F. Bussières[1]**

[1]*Group of Applied Physics, University of Geneva, Switzerland*

[2]*Jet Propulsion Laboratory, California Institute of Technology, Pasadena CA, USA*

[3]*Department of Physics, University of Basel, Switzerland*

Recent progress in the development of superconducting nanowire single-photon detectors (SNSPDs) has delivered excellent performances, and has had a great impact on a range of research fields. The timing jitter, which denotes the temporal resolution of the detection, is a crucial parameter for many applications. Despite extensive work since their apparition, the lowest jitter achievable with SNSPDs is still not clear, and the origin of the intrinsic limits is not fully understood. Understanding its intrinsic behaviour and limits is a mandatory step toward improvements.

We report intrinsically-limited timing jitter with MoSi SNSPDs [1]. To reach fundamental limits, we show that the kinetic inductance has to be minimized taking into account the latching current of the detector. We developed an experimental setup that minimizes every component of the system jitter and allows us to probe and quantify the intrinsic jitter [1, 2]. The energy-dependence is shown and points to a strong intrinsic jitter component for wavelengths longer than 1064 nm. Finally, we observed that the intrinsic jitter is higher for thicker devices and longer wavelengths. We obtained system timing jitter as low as 6.0 ps at 532 nm and 10.6 ps at 1550 nm photon wavelength.

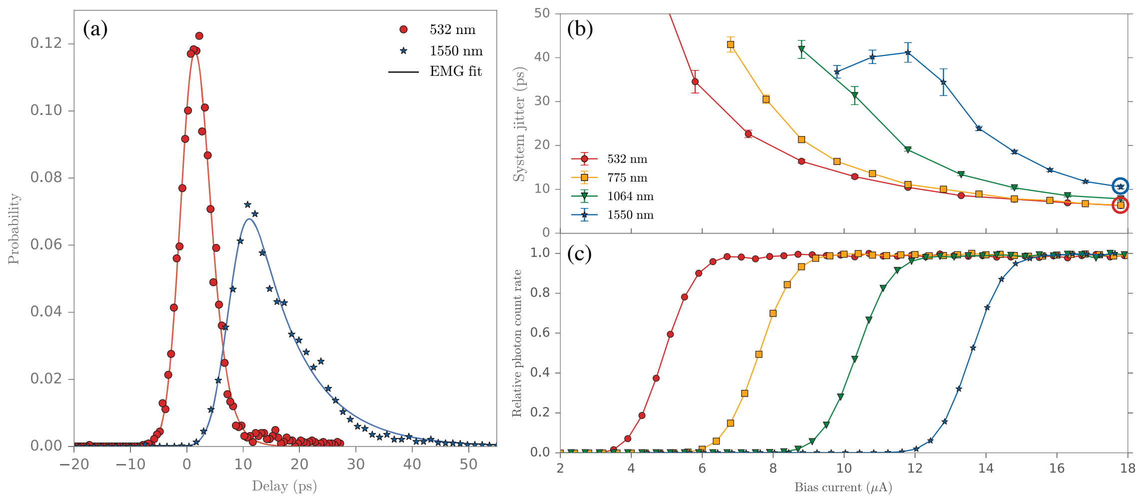


Fig. 1: Results for 7 nm-thick and 100 nm-wide device. (a) Jitter histogram at 532 and 1550 nm for a bias current of 17.9 μA, as indicated by the circles in (b). The lines represent the Exponentially Modified Gaussian fit. (b) Jitter FWHM as a function of the bias current, for different wavelengths. (c) Photon count rates for the same wavelengths as shown in (b).

## References

[1] M. Caloz et al., “Intrinsically-limited timing jitter in molybdenum silicide superconducting nanowire single-photon detector”, arXiv 1906.02073 (2019).

[2] B. Korzh et al., "Demonstrating sub-3 ps temporal resolution in a superconducting nanowire single-photon detector", arXiv 1804.06839 (2018).

# Waveguide-integrated SNSPDs from amorphous Molybdenum Silicide thin films

**M. Häußler[1], M. A. Wolff [1], M. Mikhailov[2], C. Schuck[1]**

[1] *Institute of Physics and Center for Nanotechnology, University of Münster, D-48149 Münster, Germany*

[2] *B. Verkin Institute for Low Temperature Physics & Engineering of the National Academy of Sciences of Ukraine, 61103 Kharkiv, Ukraine*

Superconducting nanowire single-photon detectors (SNSPDs) have developed into a superior sensing choice for a wide range of applications in modern quantum technology because they combine high detection efficiencies and low noise performance with high-speed operation and extremely accurate timing resolution [1]. While conventional SNSPDs are stand-alone devices that connect via optical fibers to experimental setups, waveguide-integrated SNSPDs are embedded in a scalable fashion with nanophotonic networks, realizing state-of-the-art quantum optics experiments on silicon chips [2]. Although superconducting nanowires made from amorphous material systems have shown very attractive performance characteristics in conventional SNSPD geometries [3], waveguide-integrated SNSPDs have so far predominantly relied on polycrystalline material systems, e.g. niobium nitride. Here we report on the fabrication and characterization of waveguide-integrated superconducting nanowire single-photon detectors made from amorphous molybdenum silicide (MoSi) thin films. The detectors are patterned in a travelling-wave geometry on silicon nitride waveguides. For 1550 nm wavelength photons traveling inside a nanophotonic waveguide we observe saturated detection efficiency of 46 ± 7 % at a temperature of 1.8 K for a detector made from a 4.2 nm thin MoSi film. We further find pulse decay times of 5.6 ns for 92 µm long nanowires and a timing jitter of 185 ps FWHM. These attractive performance characteristics demonstrate the potential of SNSPDs made from amorphous thin films embedded with photonic integrated circuit and significantly expand the choice of possible substrate/waveguide material systems, which limit implementations with lattice-matched polycrystalline superconducting thin films. MoSi thin films offer the additional benefit of allowing for operating SNSPDs at temperatures of up to 2 K, as shown here, without requiring technologically more demanding cryogenic solutions for sub-Kelvin operation as it is the case for other amorphous materials.

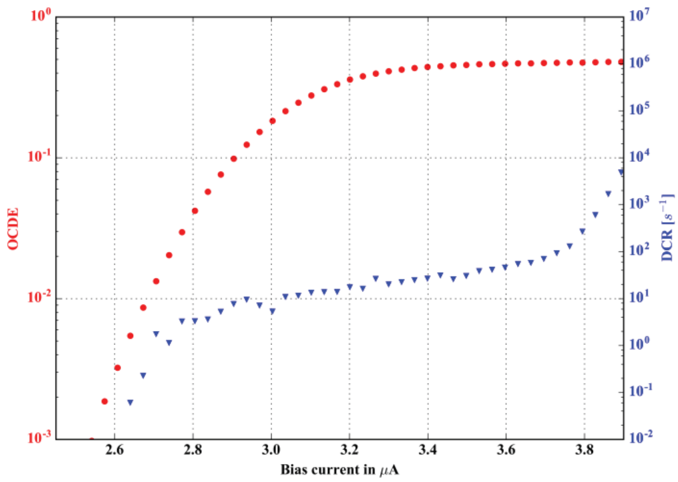


Figure 1: On-chip detection efficiency (OCDE) and dark count rate (DCR) of amorphous MoSi waveguide-integrated SNSPDs at 1.8 K. A plateau region for 1550 nm wavelength light is visible up to bias currents of 3.9 µA.

**References**

[1] B. Korzh, C. C. W. Lim, R. Houlmann, N. Gisin, M. J. Li, D. Nolan, B. San-guinetti, R. Thew, and H. Zbinden, “Provably secure and practical quantum key distribution over 307 km of optical fibre,” Nature Photonics 9, 163 (2015)

[2] S. Ferrari, C. Schuck, and W. Pernice, “Waveguide-integrated superconducting nanowire single-photon detectors,” Nanophotonics 7, 1725–1758 (2018).

[3] Y. P. Korneeva, M. Y. Mikhailov, Y. P. Pershin, N. Manova, A. Divochiy,Y. B. Vakhtomin, A. Korneev, K. Smirnov, A. Sivakov, A. Y. Devizenko,et al., “Superconducting single-photon detector made of MoSi film,” Superconductor Science and Technology 27, 095012 (2014)

# Incorporating micro-electronics with silicon nano-photonics to realise sub-mm$^2$, 1.5GHz homodyne detectors for scalable photonic quantum technology

**Joel F. Tasker[1], Jonathan Frazer[1,2], Giacamo Ferranti[1], Jonathan C. F. Matthews[1]**

[1]*Affiliation: Quantum Engineering Technology Labs, University of Bristol, United Kingdom*

[2]*Affiliation: Quantum Engineering Centre for Doctoral Training, University of Bristol, United Kingdom*

Homodyne detection finds use in a variety of tomography experiments in continuous-variable (CV) quantum optics as well as being an integral component of CV-implemented quantum technologies such as quantum random number generation (QRNG), quantum key distribution (QKD) and quantum computing. In order to characterise weak, single-photon level states in short time modes, low-noise, high bandwidth electronics are required to amplify the detector signal. To date, the bandwidth of most detectors has been limited by techniques using low-speed bulk optical photodiodes and op-amp based amplification. The total footprint per detector in these cases also limits their potential for large-scale fabrication and incorporation into experiments with many spatial modes. By wire bonding silicon microelectronics directly to an integrated silicon photonic circuit we have produced a two-chip homodyne detector with a higher bandwidth than previously reported whilst maintaining a quantum-classical noise ratio of 13dB. In addition, the device exhibits shot-noise limited performance to >8GHz and has a total footprint of less than 1 mm$^2$ per detector.

As well as enabling more complex homodyne and multiplexed heterodyne quantum optics experiments [1], high-bandwidth homodyne detection is a valuable resource for continuous-variable quantum key distribution and random number generation. In such applications, a high key rate and bit generation rate are desirable. These are typically set by the bandwidth of the amplifier electronics which is in turn primarily limited by the capacitances in the circuit [2]. Our device consists of a custom designed photonic chip fabricated by IMEC foundry services, along with a MAXIM MAX3277 transimpedance amplifier die. The photonic chip comprises a directional coupler based Mach-Zehnder interferometer and high efficiency, low capacitance photodiodes. By wire bonding the photonic chip directly to the amplifier, we minimise the parasitic input capacitance seen by the amplifier which is a crucial parameter determining the MAX3277 bandwidth and noise.

For quantum states generated on chip, the quantum-classical noise ratio of 13dB and 1.1A/W responsivity of the photodiodes combined with low-loss directional couplers gives an efficiency for state tomography of ~85% which is sufficient to observe, for example, negativity of the single photon Wigner function [4]. The broadband nature of the device would allow the characterisation of broadband quadrature squeezing and enables high speed quantum random number generation at a rate in excess of 15Gbps.

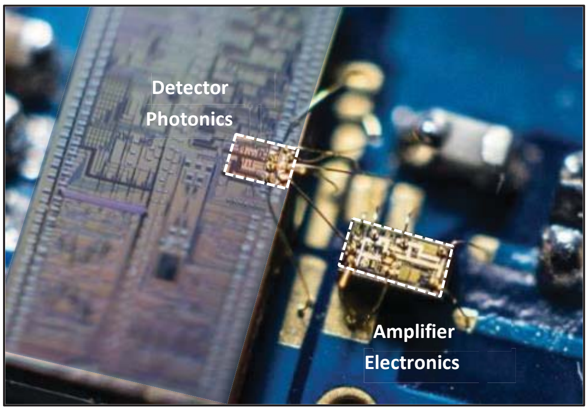


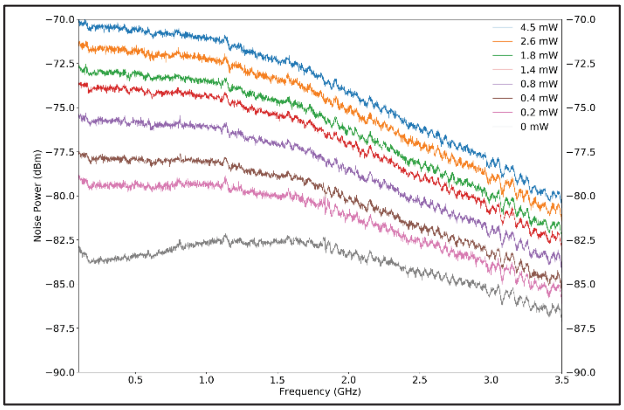


**Fig. 1 a)** The device: The photonic chip and amplifier die are both mounted on a custom PCB which contains the biasing circuitry **b)** Detector shot-noise frequency response with local oscillator power from 0.1-3.5GHz.

**References**

[1] Yoshikawa, J.-I et al. (2016, 9 1). *APL Photonics, 1*(6), 060801

[2] Masalov, A., Kuzhamuratov, A., Lvovsky, A., *Review of Scientific Instruments*, 88(11), (2017).

[3] Esposito, M., et al. (2016, 12 4). *EPJ Quantum Technology, 3*(1), 7.

# Characterizing integrated single photon detectors on lithium niobate waveguides

**Jan Philipp Höpker[1], Varun Verma[2], Thomas Gerrits[2], Adriana Lita[2], Harald Herrmann[1], Raimund Ricken[1], Viktor Quiring[1], Richard Mirin[2], Sae Woo Nam[2], Christine Silberhorn[1], Tim J. Bartley[1]**

[1]*Department of Physics, Paderborn University, Warburger Str. 100, 33098 Paderborn, Germany*

[2]*National Institute of Standards and Technology, 325 Broadway, Boulder, Colorado 80305, USA*

We report on the characterization of integrated superconducting nanowire single photon detectors (SNSPDs) and transition edge sensors (TESs), evanescently coupled to titanium in-diffused lithium niobate waveguides. We discuss the fabrication process of these on-chip detectors, characterization methods and single photon detection efficiency optimization.

Titanium in-diffused lithium niobate is an interesting platform for integrated quantum optics, due to its low-loss waveguiding of TE- and TM-polarization modes, electro-optic properties, and high second order susceptibility [1]. Many different tools for quantum optics applications have been realized using this platform, including single-photon sources, couplers, switches, and modulators [1]. In addition, due to an optimized mode overlap with the titanium in-diffused waveguides, high-efficiency fiber-coupling can be achieved by direct end-face pigtailing, a crucial element for quantum information applications requiring low loss. Integrated single photon detectors are also compatible with this platform [2, 3, 4, 5].

State-of-the-art single photon detectors at optical or telecommunication wavelengths use the breakdown of superconductivity and a resulting electric response to measure absorbed photons. These detectors provide outstanding quantum efficiency and low noise. On the other hand, they require cryogenic temperatures below 1K.

We fabricated WSi-SNSPDs and W-TESs on titanium in-diffused lithium niobate waveguides and characterized the evanescent coupling strength of the on-chip detectors. By comparing measurements of the response of multiple detectors per waveguide from illumination with different polarizations and from illumination for either end, we were able to clearly determine how many photons are coupled via evanescent coupling and from scattering. Furthermore, multiplexed detectors on one waveguide are interesting for new calibration schemes or complex state generation [6, 7].

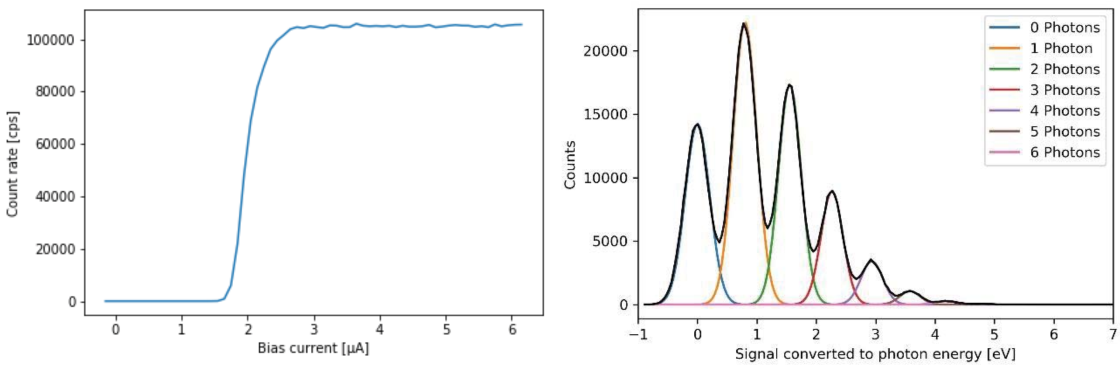


Fig. 1 (a) On-chip SNSPD response (countrate versus bias current) (b) Photon trace histogram of an on-chip TES

**References**

[1] P. R. Sharapova, K. H. Luo, H. Herrmann, M. Reichelt, T. Meier, and C. Silberhorn, New Journal of Physics 19, 123009 (2017).

[2] M. G. Tanner, L. San Emeterio Alvarez, W. Jiang, R. J. Warburton, Z. H. Barber, and R. H. Hadfield, Nanotechnology 27, 505201 (2012).

[3] J. P. Höpker, M. Bartnick, E. Meyer-Scott, F. Thiele, S. Krapick, N. Montaut, M. Santandrea, H. Herrmann, S. Lengeling, R. Ricken, V. Quiring, T. Meier, A. E. Lita, V. Verma, T. Gerrits, S. W. Nam, C. Silberhorn, and T. J. Bartley, Proceedings of SPIE: Quantum Photonic Devices 10358, 1035809 (2017).

[4] E. Smirnov, A. Golikov, P. Zolotov, V. Kovalyuk, M. Lobino, B. Voronov, A. Korneev, and G. Goltsman, Journal of Physics: Conference Series 1124, 051025 (2018).

[5] J. P. Höpker, T. Gerrits, A. Lita, S. Krapick, H. Herrmann, R. Ricken, V. Quiring, R. Mirin, S. W. Nam, C. Silberhorn, T. J. Bartley, Applied Physics Letters Photonics 4, 056103 (2019

[6] T. Gerrits, Journal of Optics 18, 054014 (2016)

[7] R.J. Leon-Montiel, O. S. Magana-Loaiza, A. Perez-Leija, A. U'ren, K. Busch, A. Lita, S. W. Nam, T. Gerrits, R. Mirin, Quantum Information and Measurement Conference Proceedings, OSA T5A.14 (2019)

# Relative time multiplexing of heralded single photon sources using switchable multi-path fiber delay lines

**Eunjoo Lee [1], Sang Min Lee [1] and Hee Su Park [1]**

[1] *Korea Research Institute of Standards and Science, Daejeon, South Korea*

Deterministic single photon sources (SPSs) are a key component of quantum information processing and quantum metrology. Multiplexing of randomly heralded single photons into a pre-determined single spatial/temporal mode has provided a promising solution to increase the single photon generation rate without increasing multi-photon contamination. Time-multiplexing increases the number of multiplexed modes without requiring an increased number of resources such as nonlinear crystals and trigger detectors. Time multiplexing can be achieved by actively delaying the heralded photons based on the which-channel information among the time-bins of interest for the generated photon pairs. Two methods can apply this kind of time delay: a storage cavity and switchable multi-path optical fiber delays. A storage cavity uses an electro-optic switch which stores and releases heralded photons to the pre-determined output time. A switchable multi-path delay line consists of fast optical switches and dual-rail single mode fiber (SMF) delay lines between them. Depending on the heralding times, proper amount of delays are introduced by active switching of paths. For large-scale (> 100 channels) multiplexing, the switchable multi-path method is more advantageous due to the potentially smaller optical loss through the delay unit. However, single mode fibers of extended length are required, which can reduce indistinguishability between output photons unless dispersion and temperature-dependence are properly managed.

Relative multiplexing [1] can be implemented to synchronize the single photons emitted from different photon pair sources. A previous work [2] uses two copies of an SPS and an active switching unit to make photons injected simultaneously into each input of the fiber Hong-Ou-Mandel interferometer (HOMI). We implement the relative multiplexing to measure HOMI between heralded photons in different time-bins from one SPS using a fiber-type asymmetric Mach-Zehnder interferometer. One arm of the interferometer includes the switchable multi-path delay lines which combine heralded photons within up to 32 time-bins. When two photons are triggered with a certain interval, the multi-path delay lines are switched to provide the same amount of time delay so that the photons can be synchronized after the interferometer. The delay between the synchronized photons is scanned using a fiber-pigtailed motorized delay line to measure coincidence with respect to the delay. Figure 1 shows the experimental result of HOMI. After subtracting the accidental counts due to higher-order photon pair generation and detector dark counts, the depth of Hong-Ou-Mandel dip was 0.88 ± 0.03 in good agreement with our theoretical estimation. We expect that highly indistinguishable single photons can be generated near-deterministically using large-scale time-multiplexing based on the switchable multi-path delay lines.

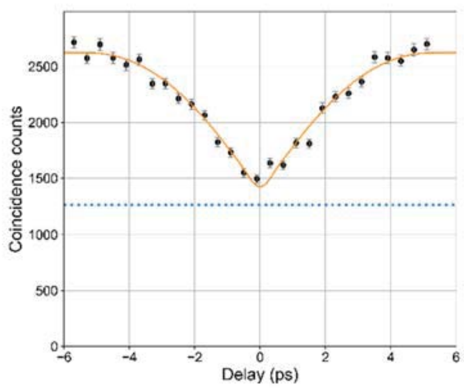


Fig. 1 Hong-Ou-Mandel interference fringe by relatively synchronized heralded photons. (blue dotted line : the total accidental counts).

**References**

[1] Rudolph, Terry. “Why I Am Optimistic about the Silicon-Photonic Route to Quantum Computing.” APL Photonics 2, no. 3 (2017): 030901.

[2] F. Kaneda, F. Xu, J. Chapman, and Paul G. Kwiat, "Quantum-memory-assisted multi-photon generation for efficient quantum information processing," Optica 4, 1034-1037 (2017)

# First realization of genuine time-bin entanglement

**F. Vedovato[1], C. Agnesi[1], M. Tomasin[1], M. Avesani[1], J.-Å. Larsson[2], G. Vallone[1], P. Villoresi[1]**

[1]*Dipartimento di Ingegneria dell'Informazione, Università di Padova, 35131 Padova, Italy*

[2]*Institutionen för systemteknik, Linköping Universitet, 581 83 Linköping, Sweden*

Time-bin entanglement [1] has been widely used for testing quantum non-locality via the violation of a Bell-like inequality, as well as for quantum cryptographic applications. However, all the realization of time-bin entanglement implemented to date are based on the interferometric scheme proposed by Franson [2] (sketched in the left panel of Fig. 1), which is actually affected by the so-called postselection loophole [3] undermining the faithfulness and the validity of the implementations. Indeed, to obtain a violation of the Bell-CHSH inequality it is necessary to discard half of the collected data by selecting only the detection events occurring within a coincidence window centered around the mid peak of the detection pattern. This procedure allows for a Local Hidden Variable model reproducing the prediction of quantum mechanics, thus invalidating the Bell's inequality as a test of local realism and enabling the hacking of the scheme when used with cryptographic purposes [4].

A proper violation of the Bell-CHSH inequality can be obtained with the active time-bin scheme we introduced and realized in Ref. [5] (right panel of Fig. 1). We replaced the first beam splitter of the measurement interferometer with an additional balanced Mach-Zehnder interferometer acting as a fast optical-switch synchronized with source. The deterministic recombination of the "short" and "long" pulses, that travelled the pump interferometer before impinging on the spontaneous-parametric-down-conversion (SPDC) crystal generating the entangled pair, allows to not discard any data, thus rendering the obtained time-bin entanglement "genuine", i.e., free of the postselection loophole. In Ref. [5] we first presented the detailed analysis of the passive and active time-bin entanglement schemes by describing the POVM realized by the interferometric measurements (with and without the postselection procedure), and then we showed the experimental realization which allowed us to obtain a Bell-CHSH inequality violation of more than 9 standard deviations.

Time-bin entanglement is more robust than polarization in long-distance fiber propagation. Hence, the capability to overcome the postselection loophole paves the way to the realization of a conclusive loophole-free Bell's test based on genuine time-bin entanglement. In fact, despite of genuine energy-time entanglement [6], which requires to stabilize two long interferometers whose extension is determined by the distance between the two measurement stations, our scheme requires imbalances that are much less demanding and much more achievable.

Furthermore, our scheme can be realized using commercial off-the-shelf fiber components and it can be made compatible with today's integrated photonics, making it attractive for realizations of device-independent secure communications between two parties [7]. Moreover, the capability of implementing fast optical-switches for time-bin encoding, as we showed, can be exploited to realize encoders and receivers for high-dimensional time-bin qudits, as proposed in [8].

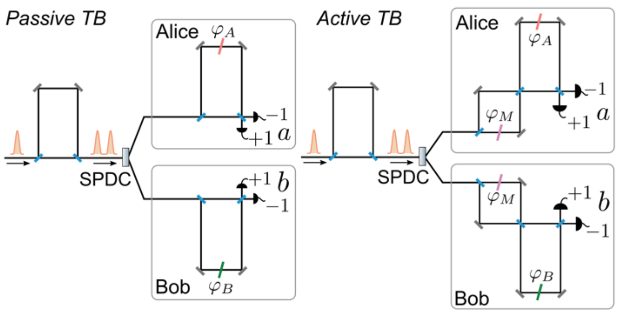


Fig. 1 The passive and active time-bin (TB) entanglement schemes.

## References

[1] J. Brendel *et al.*, Phys. Rev. Lett. **82**, 2594 (1999)
[2] J. D. Franson, Phys. Rev. Lett. **62**, 2205 (1989)
[3] S. Aerts *et al.*, Phys. Rev. Lett. **83**, 2872 (1999)
[4] J. Jogenfors *et al.*, Sci. Adv. **1**, e1500793 (2015)
[5] F. Vedovato *et al.*, Phys. Rev. Lett. **121**, 190401 (2018)
[6] A.Cabello *et al.*, Phys. Rev. Lett. **102**, 040401 (2009)
[7] A. Acin, N. Gisin, L. Masanes, Phys. Rev. Lett. **97**, 120405 (2006)
[8] J. M. Lukens *et al.*, Appl. Phys. Lett. **112**, 111102 (2018)

# Domain-engineered PPLN for generating polarization-entangled photon pairs

**Paulina S. Kuo[1], Varun B. Verma[2], Thomas Gerrits[2], and Sae Woo Nam[2]**

[1]*Information Technology Laboratory, National Institute of Standards and Technology, Gaithersburg, Maryland USA*

[2] *Physical Measurement Laboratory, National Institute of Standards and Technology, Boulder, Colorado USA*

Spontaneous parametric downconversion (SPDC) has become the mainstay for generating polarization-entangled photon pairs [1]. These pair sources are used in quantum networks to distribute entanglement, demonstrate quantum key distribution, quantum teleportation and in tests of local realism [2]. We recently developed a new SPDC source based on domain-engineered, periodically poled lithium niobate (PPLN) [3]. In non-degenerate downconversion, the $|Hs\rangle|Vi\rangle$ and $|Vs\rangle Hi\rangle$ processes are associated with two different phase-mismatches; that is, they are two separate downconversion processes. By engineering the PPLN domains using a phase-modulated design, both processes can be simultaneously phasematched in the same crystal [3]. Here, we describe the first observation of polarization entanglement using this domain-engineered PPLN crystal.

The 25-mm long, MgO-doped PPLN crystal was designed for type-II down-conversion of 775 nm $\rightarrow$ 1535 nm + 1570 nm. We characterized the down-conversion spectra using fiber-assisted single-photon spectroscopy [3]. The two downconversion processes became degenerate in wavelength at 143.6 °C. With a 774.8 nm pump, the signal and idler were observed at 1530.9 nm and 1568.8 nm, respectively. We separated the signal and idler using dichroic filters (marked Dic, F1, F2 in Fig. 1a). We used a temporal compensation (TC) crystal (12.5 mm long $MgO:LiNbO_3$) to compensate the birefringent walkoff in the PPLN. The TC crystal was rotated by 90° relative to the PPLN (swap the slow and fast birefringence axes) and erase temporal distinguishability.

To observe polarization entanglement, we set the polarization of the signal and rotated the idler polarization using a half-wave plate. The coincidence counts for different signal polarizations are shown in Fig. 1b. With temporal compensation, we observed very good visibility: 97% for horizontally polarized signal, and 94% and 93% for diagonal and anti-diagonal polarizations, respectively. In contrast, when we removed the TC crystal, the visibility for diagonally polarized signal dropped to 15% (see Fig. 1c).

In conclusion, we designed and fabricated an aperiodic PPLN crystal with phase-modulated domain structure. We determined the operating temperature where the wavelengths of the dual downconversion processes become matched. We showed very good polarization entanglement visibility between the signal and idler.

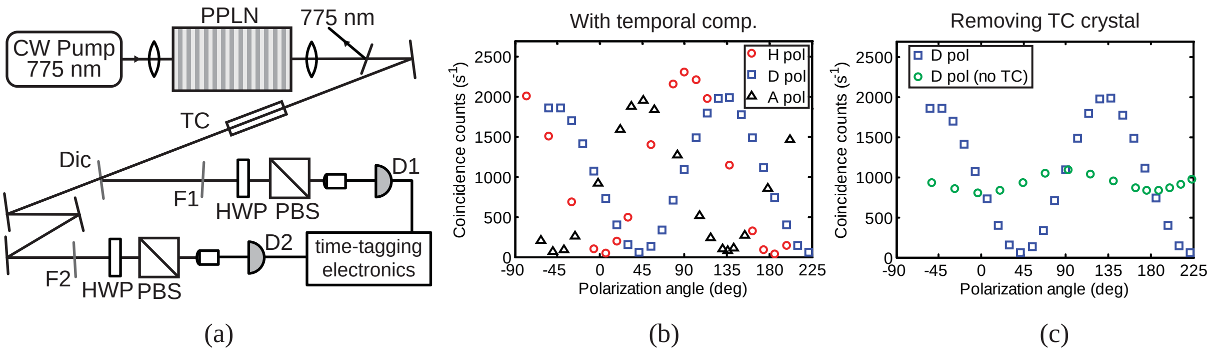


Fig. 1 (a) Experimental setup; TC, temporal compensation crystal; Dic, dichroic filter; HWP, half-wave plate; PBS, polarizing beam splitter; F1(2), filter 1(2); D1(2), detector 1(2). Measured coincidence counts at different signal polarizations (b) with temporal compensation and (c) with the temporal compensation crystal removed. With the temporal compensation, visibilities above 93% were observed, but when the TC crystal was removed, the visibility dropped to 15%.

## References

[1] P. G. Kwiat, K. Mattle, H. Weinfurter, and A. Zeilinger, "New High-Intensity Source of Polarization-Entangled Photon Pairs," Phys. Rev. Lett. **75**, 4337 (1995).

[2] L. K. Shalm, et al, "Strong Loophole-Free Test of Local Realism," Phys. Rev. Lett. **115**, 250402 (2015).

[3] P. S. Kuo, T. Gerrits, V. B. Verma, S. W. Nam, O. Slattery, L. Ma, and X. Tang, "Characterization of type-II spontaneous parametric down-conversion in domain-engineered PPLN," Proc. SPIE **9762**, 976211 (2016).

# Modeling Quantum Key Distribution with Continuous-Wave-Pumped Polarization Entangled Photon Sources

**Bo Liu, Sebastian Neumann, Rupert Ursin, Thomas Scheidl**

*Institute for Quantum Optics and Quantum Information, Vienna, Austria*

We show how to model entanglement-based quantum key distribution (QKD) schemes such as BBM92 [1] with continuous-wave (CW) pump lasers. Our model can predict final secure key rates and calculate loss budgets, based on experimentally accessible and easily assessable parameters. Furthermore, we present a software capable of analyzing and post-processing the classical data accumulated during real-world QKD in real-time.

The basic principle of QKD with polarization-entangled photon sources is as follows: An entangled two-photon state is created by pumping a non-linear crystal with high laser power, utilizing spontaneous parametric down-conversion (SPDC). One of the photons is sent to partner Alice (A) and the other to partner Bob (B). They measure their respective photon in one of two randomly chosen, mutually unbiased polarization bases. To identify which detection event corresponds to the same pair, they record time tags to find coincident photons. They publicly communicate these tags and their basis choices only and keep the corresponding (secret) results ("sifted key"). After error correction and privacy amplification, they share a secure key.

The first and most commonly used model for estimating key rates with BBM92 was done by Ma et al. in 2007 [2], however based on sources where SPDC is produced with a *pulsed* pump laser, the standard at the time. Recent developments especially in timing resolution of single-photon detectors have shown *CW-pumped* sources to have two crucial advantages in the context of long-distance communication. Firstly, due to the Poissonian pair emission statistics, a $g^{(2)}$ correlation can be carried out to find matching pairs, thus drastically lowering the requirements for timing synchronization of distant communication partners. Secondly, the spectrum of the entangled photons can be orders of magnitude narrower. This mitigates chromatic dispersion effects. It is also necessary to approach the narrow spectra required for writing to quantum memories. These differences to the pulsed scheme however also require different modelling of the expected quantum error bit rate (QBER) and key rates.

The first difference comes from the fact that the emission of uncorrelated multi-pairs, which degrade the fidelity of the measurement, follows different statistics. Due to approx. 6 orders of magnitude lower instantaneous pump powers, coherent multi-pair emission can be neglected in the CW case. Therefore, the emission of independent photon pairs within the same coincidence window is the only multi-pair effect, which follows Poissonian statistics. Secondly, the detectors for CW-pumped sources are free-running, i.e. only the detection of a photon at A (B) triggers a coincidence window of length $\tau_{CC}$ in which a partner photon is expected at B (A). Now if this partner photon is lost, either a noise count or a photon from a multi-pair emission can lead to a false coincidence ("accidental" count). Since all these events suffer from temporal (measurement) uncertainty, the actual accidental window $\tau_{acc}$ is larger than $\tau_{CC}$ (see fig. 1.)

Furthermore, in our model we elaborate on the effects of erroneous detection, especially in the case of multi-pairs. We thus arrive, to the best of our knowledge, at the first key rate estimation model for CW-pumped entanglement-based QKD protocols.

Additionally, we present a software that is capable to perform all computations necessary to extract a quantum secure key from our experimental set-up. This includes reading out the time tags of two detectors at remote locations, calculating their $g^{(2)}$ in real-time, reading out subsets of the detection events to estimate the QBER, and performing privacy amplification.

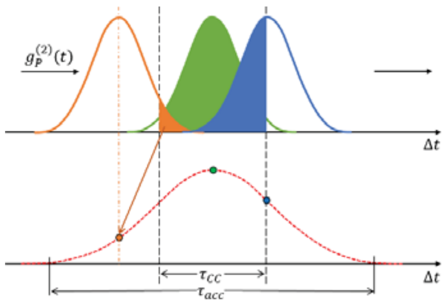


Fig. 1 Accidental window in CW-QKD: The coincidence window $\tau_{CC}$ has to be extended by convolution with temporal uncertainties originating from detector jitter and chromatic dispersion, thus leading to a larger accidental window $\tau_{acc}$.

## References

[1] Bennett, C. H. et al..: Quantum cryptography without Bell's theorem. *Phys. Rev. Lett., APS,* **1992**, *68*, 557
[2] Ma, X. et al.: Quantum key distribution with entangled photon sources. *Phys. Rev. A, APS,* **2007**, *76*, 012307

# High purity heralded single photons at telecommunications wavelengths using commercial birefringent optical fiber

**R.J.A. Francis-Jones[1], J. Lugani[1], J. Boutari[1], and I.A. Walmsley[1]**

[1]*Clarendon Laboratory, Department of Physics, University of Oxford, Oxford, UK.*

Single photon sources are one of the fundamental building blocks for quantum optics and quantum information processing experiments and applications [1]. Spontaneous non-linear optical processes, such as parametric downconversion and four-wave mixing (FWM) remain amongst the most commonly utilised methods for generating heralded single photons in pure spectral states. FWM in optical fibres is a particularly promising avenue as the dispersion of the guided mode can be tailored to achieve phasematching at particular desired wavelengths, but also the group velocities of the interacting fields can be appropriately matched to ensure a spectrally factorable two-photon state and hence a heralded photon in a single mode can be made possible[2]. Typically, this requires careful manipulation of the cladding structure of the fibre, such as in photonic crystal fibres, however imperfections in the manufacturing process lead to fluctuations in the dispersion of the fibre, and a move away from factorable conditions [3]. Here we present a heralded single photon source based on cross-polarised FWM in a commercial all solid birefringent fibre, which allows us to achieve high purity with a higher repeatability in a cost-effective way.

We use a 9cm commercial birefringent fibre PM980-XP, pumped with femtosecond pulses at 1um from an OPO to achieve the required phase- and group velocity matching required for pure state generation, see Fig.1. We match the bandwidth of the pump pulses, by spectral filtering, to the phasematching bandwidth of the fibre to achieve a factorable state. Signal and Idler photon-pairs at 810nm and 1310nm respectively were generated cross-polarised to pump. Broadband filtering was applied to reject the pump without imparting any filtering to the joint spectral amplitude. The generated photon-pairs were coupled to superconducting nanowire single photon detectors, and the singles, and coincident count rates of the source measured, we observe a maximum coincident count rate of ~30kC/s with a maximum observed Klyshko heralding efficiency of ~25%.

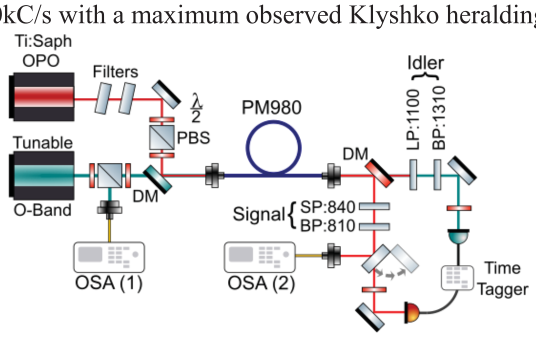


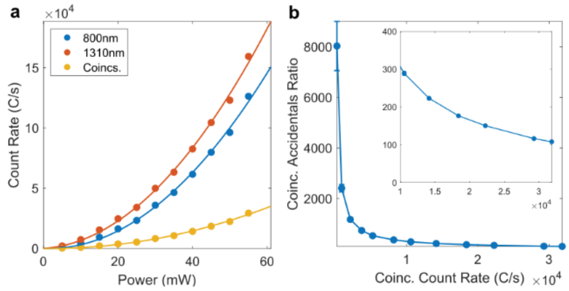


Fig. 1 (left) Schematic of the fibre photon-pair source. (right) a : single photon count rate for signal, idler and coincidences. b : coincidence-to-accidentals ratio never drops below 100.

We find that the Coincidence-to-Accidentals Ratio never drops below 100 over the full range of powers used here. This, together with the nearly pure quadratic dependence of the count rates indicate that we are largely free of noise such as spontaneous Raman scattering that typically plagues fibre-based single photon sources. This was made possible by exploiting the birefringent phasematching to generate photons far de-tuned from the pump wavelength. We performed a measurement of the heralded second order coherence with $g^{(2)}_{H}(0) < 0.02$, and the marginal second order coherence, a measure of the single photon purity, with a $g^{(2)}_{M}(0) \sim 1.71$ at 1310nm. Finally, we have also measured the joint spectral intensity of the source through stimulated emission tomography by seeding the FWM with a tunable laser at the idler wavelength and recording the signal mode on a spectrometer, we determine an upper bound on the purity to be $P$=75%. Further to this, we made measurements of the JSI over different lengths through a sample of the fibre, and found that the fibre remains uniform over at least 45cm, making it possible to build 4 nominally identical sources. The source is also tunable, and by changing the pump wavelength to 1100nm, signal and idler photon-pairs in a factorable state can be generated at 852nm and 1550nm. In Conclusion, we have demonstrated a low-noise source of heralded single photons with high purity based on FWM in a commercial birefringent optical fibre. The source can produce heralded single photons across the telecom. O-, and C-Band dependent on the choice of pump wavelength. The uniformity of the fibre allows one to build multiple, identical, source of single photons with high purity and brightness.

**References**

[1] Knill, et al. Nature **409**, 46-52 (2001).
[2] Cohen, et al. Phys. Rev. Lett. **102**, 123603 (2009)
[3] Francis-Jones, Mosley, Optics Express, **24**(22), 22836-24845

# Development and characterization of a waveguide SPDC source of highly-nondegenerate polarization-entangled photon pairs

**Kristina A. Meier[1], Fumihiro Kaneda[2], Paul G. Kwiat[1]**

[1]*University of Illinois at Urbana-Champaign, Department of Physics, Urbana, Illinois, USA*

[2]*Frontier Research Institute for Interdisciplinary Sciences, Tohoku University, Japan*

As benchtop quantum information protocols become increasingly more advanced and the distances over which these experiments are performed becomes significantly longer, integrated optics provide a small, robust, and practical alternative to traditional bulk optics. The development of quantum networks on mobile platforms well above ground level would allow long-distance transfer of photonic qubits [1]. Specifically, waveguide technology makes it possible to create bright single-photon sources that can be used on platforms where weight and stability requirements are limiting factors. For our goals, we are working on the characterization of a highly nondegenerate Spontaneous Parametric Down-Conversion (SPDC) waveguide source of polarization-entangled photon pairs on a periodically poled KTP (PPKTP) crystal [2]. Our current waveguide source uses type-II phase-matching at 532 nm to create collinear signal and idler photons at 1550 nm and 810 nm, respectively (Fig 1 a). Future iterations are in development with the goal of increasing the entanglement quality and efficiency of our source.

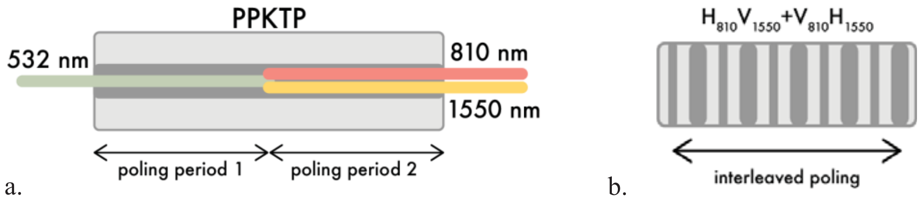


Fig. 1 a. A cartoon of our waveguide SPDC source. A 532-nm pump downconverts into signal and idler photons at 1550 nm and 810 nm, respectively. This figure shows a consecutive poling scheme where one process is created in the first half and the other is created in the second half. b. A simplified interleaved poling scheme is shown with the desired maximally entangled state.

To date, we have achieved a concurrence of 63% and a purity of 72% from a consecutively poled, free-space-coupled iteration of our source (Fig. 2a). Our current iteration features interleaved poling with a pigtailed input (Fig. 1b). Furthermore, we believe that several improvements will substantially improve the source quality. Using low-birefringence crystal wedges, such as quartz, we can finely tune the amount of temporal compensation in the downconversion beam paths to optimally account for the group velocity walk-off within the waveguide. In previous iterations of our waveguide source, free-space coupling the pump into the fundamental mode proved unreliable and therefore measuring the concurrence with respect to the amount of compensation was difficult. To overcome this modal drift within the waveguide, our current iteration has a pigtailed input using a single-mode fiber for our pump wavelength. Additionally, we can temperature tune our downconversion spectrum to find the operating temperature that yields the best overlap between the two processes. To do so, we couple a tunable seed laser at 810 nm into the pigtailed single-mode fiber and measure the counts on the 1550 nm detector. This stimulated downconversion process allows us to look at the downconversion spectrum and therefore pick the appropriate filters and waveguide temperature for maximizing the entanglement visibility of our source.

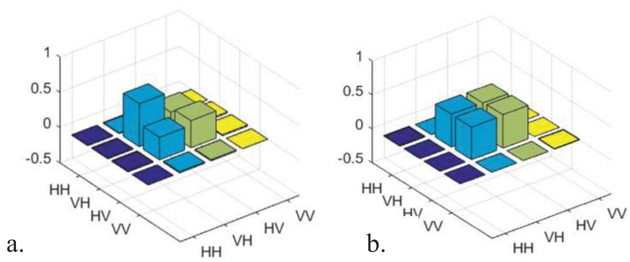


Fig 2 a. The absolute value of the density matrix of the measured entangled state. b. The theoretical density matrix of the desired maximally entangled state.

## References

[1] Proc. Free-Space Laser Communication and Atmospheric Propagation XXVIII, Vol. 9739 (SPIE 2016)
[2] AdvR-Inc, Bozeman, MT

# Efficient Coupling of an Ensemble of NV⁻ Center to the Resonance Mode of a High-Q, cross-bar $Si_3N_4$ Photonic Crystal Cavity

**Konstantin G. Fehler[1*], Anna P. Ovvyan[2*], Nico Gruhler[3], Wolfram H. P. Pernice[2], Alexander Kubanek[1]**

*[1]Institut für Quantenoptik and IQST, Universität Ulm, D-89081 Ulm, Germany*

*[2]Institute of Physics and Center for Nanotechnology, University of Münster, D-48149 Münster, Germany*

*[3]Karlsruhe Institute of Technology (KIT), Institute of Nanotechnology, D-76344 Eggenstein-Leopoldshafen, Germany*

*[*]Both authors contributed equally to this work.*

Integrated nanophotonics based on $Si_3N_4$ platform due to low-loss broadband optical transparency has high potential for quantum technology applications. While individual negatively charged nitrogen vacancy center in diamond ($NV^-$) [1] can be employed as photostable with no evidence of photobleaching single photon emitter, however the main obstruction is low Debye-Waller factor ≈ 3% coherent emission into zero phonon line. The solution is integration $NV^-$ center into cavity to enhance emission by means of the Purcell-effect.

Thus, in this work we evanescently coupled ensemble of $NV^-$ centers located in Nanodiamond (ND) into new design freestanding $Si_3N_4$ cross-bar Photonic Crystal (PhC) cavity on chip (Fig.1 a)). A cross-bar architecture allows to couple the optical transition of $NV^-$ centers, placed on top of the cavity, into high-Q PhC modes, where enhanced light is coupled out through waveguide which consists PhC cavity, while on-chip excitation of the source is provided through crossed waveguide. Thus, developed cross-bar PhC cavity design allows spectral and spatial separation enhanced emitted light and pump light ensuring filtration of excitation light (20 dB) and sufficient suppression of background fluorescence.

Designed cross-bar PhC cavity consists of two modulated Bragg mirrors with cavity region in between where ND with incorporated ensemble of $NV^-$ centers was positioned. Parameters of the cavity were optimized via 3D FDTD simulations [2] and transmission measurements. The simulation and measurements results are in agreement leading to highest measured Quality factor $Q = 47 * 10^3$ (simulated $Q = 51 * 10^3$) for cross-bar PhC cavity with optimal cavity length [3]. Determination of optimized position of source on the cavity region was performed via Local Density of States (LDOS) simulations leading to LDOS enhancement spatial map [3].

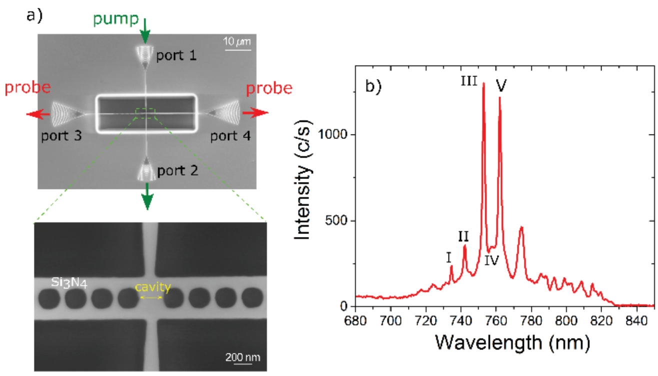


Fig. 1. High-*Q* $Si_3N_4$ PhC cavity. a) SEM image of the freestanding cross-bar PhC cavity. b) Detected at ports 3,4 emission of an ensemble of $NV^-$ centers coupled into resonance modes of PhC cavity. The resonance modes are indicated as I-V.

Experimentally ND with incorporated $NV^-$ centers was selected by confocal scan and placed on the cavity region of PhC during postprocessing step by combination of coating and pick-and-place AFM technique. The ensemble of $NV^-$ was excited via crossed waveguide (port 1), while optical transition fed the cavity modes and was detected via ports 3,4, detected spectrum is shown in Fig. 1 b). On-resonance fluorescence signal experiences more than 13-fold increase in comparison with background signal under the same on-chip excitation via crossed waveguide [3]. Thus, ensemble of $NV^-$ was successfully coupled into V-order cavity mode achieving measured on-resonance efficiency of $\beta_\lambda = 71\%$ in agreement with simulated value $\beta_\lambda = 75\%$ [3].

## References

[1] F. Jelezko, J. Wrachtrup. Single Defect Centres in Diamond: *A Review. Phys. Status Solidi* A 2006, 203, 3207−3225.
[2] A. F. Oskooi, D. Roundy, M. Ibanescu, P. Bermel, J. D. Joannopoulos, S. G. Johnson. MEEP: A Flexible Free-Software Package for Electromagnetic Simulations by the FDTD Method. *Comput. Phys. Commun. 2010*, 181, 687−702.
[3] K. G. Fehler, A. P. Ovvyan, N. Gruhler, W. H. P. Pernice, A. Kubanek. Efficient Coupling of an Ensemble of Nitrogen Vacancy Center to the Mode of a High-Q, $Si_3N_4$ Photonic Crystal Cavity. *ACS Nano 2019*, 13, 6891−6898

# The angular-dependent emission characteristics of NV-centers in nanodiamonds near dielectric interfaces

**Justus Christinck, Beatrice Rodiek, Marco López, Hristina Georgieva, Helmuth Hofer, Stefan Kück**
*Physikalisch-Technische Bundesanstalt (PTB), Braunschweig, Germany*

Nowadays, a lot of attention is being paid to the development of stable and reliable single photon sources. PTB absolutely characterized a single photon emitting NV-center in a nanodiamond using a confocal microscope setup. Its absolute optical radiant flux and spectral power distribution are traceable to the national standards via an unbroken traceability chain [1]. Consequently, we now aim to achieve a better understanding of the angular-dependent emission of the NV-centers in our setup to optimize the collection efficiency and to understand losses within the fluorescence light path. The NV-centers are localized at a dielectric interface, namely a microscope cover glass, which interacts with the near field of the emitting dipoles. This results in refraction of evanescent waves into the cover glass and a highly directional emission of photons.
A model of the angular distribution of the emitted light is presented. First, the orientation of the transition dipole moments of NV-centers in the crystal with respect to the laboratory frame of reference is investigated. Second, using a model of the light emission by dipoles [2], the radiation patterns of an arbitrary oriented NV-center are calculated. With this, a theoretical back focal plane image (Fig. 1) and the collection efficiency of the setup can be computed.
Furthermore, a sample consisting of spin-coated, NV-center doped nanodiamonds on a cover glass was studied. The NV-centers were characterized spectroscopically and by measurement of the 2$^{nd}$ order correlation function in a Hanbury Brown and Twiss interferometer. Images of the back focal plane of the NV-center emission were taken using a sCMOS camera. The calculated and measured angular-dependent emission patterns of NV-centers are compared (Fig. 1). Furthermore, the possibility to obtain the orientation of the NV-centers from measurements of their back focal plane image is evaluated.

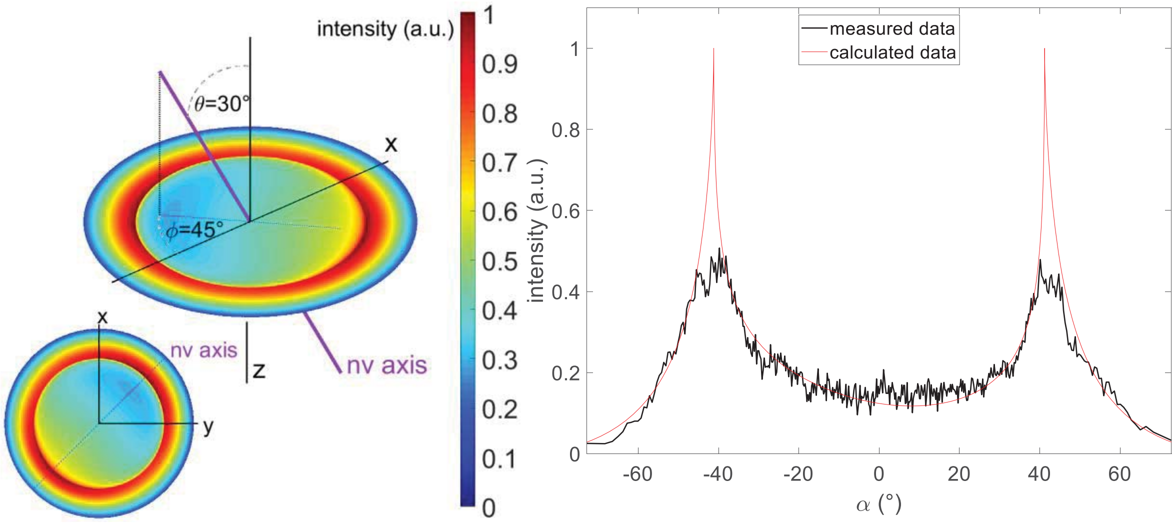


Fig. 1 : Back Focal Plane image and NV-center symmetry axis (left) and comparison of the measured and calculated angular emission of a NV-center (right).

**Acknowledgement**
The work reported on this paper was funded by the Deutsche Forschungsgemeinschaft (DFG, German Research Foundation) under Germany's Excellence Strategy – EXC-2123/1 and by project EMPIR 17FUN06 SIQUST. This project received funding from the EMPIR programme co-financed by the Participating States and from the European Union Horizon 2020 research and innovation programme.

**References**
[1] B. Rodiek et al., Experimental realization of an absolute single-photon source based on a single nitrogen vacancy center in a nanodiamond, Optica 4 (1), 71-76, 2017.
[2] W. Lukosz, Light emission by magnetic and electric dipoles close to a plane dielectric interface. {III}. Radiation patterns of dipoles with arbitrary orientation, Journal of the Optical Society of America 69, 1195-1503, 1979.

# One photon per pulse emission from NV centers in diamond under electrical excitation at high repetition rates

**Igor A. Khramtsov and Dmitry Yu. Fedyanin**

*Moscow Institute of Physics and Technology, Dolgoprudny, Russian Federation*

Color centers in diamond recently emerged as promising candidates for true single-photon sources (SPSs) [1]. They demonstrate bright, stable, non-bleaching and non-blinking photoluminescence and long spin coherence times at room temperature, which make them extremely attractive for practical applications. These point defects in the crystal lattice of diamond have been intensively studied under optical pumping for the past two decades. However, the possibility of their electrical excitation, which is highly desirable for practical devices, was open to question for a long time, mainly because diamond is a unique material at the interface between solid-state and semiconductor physics. Nevertheless, single-photon electroluminescence of nitrogen-vacancy (NV) centers in diamond p-i-n diode (Fig. 1a) has been recently demonstrated [2,3] and explained [4,5]. However, all theoretical and experimental studies of color center single-photon electroluminescence dealt only with the steady-state regime. At the same time, for practical applications, it is important to generate single photons on demand, i.e., produce single-photons with near-unity probability within a very short time interval, which can be achieved only under pulsed excitation.

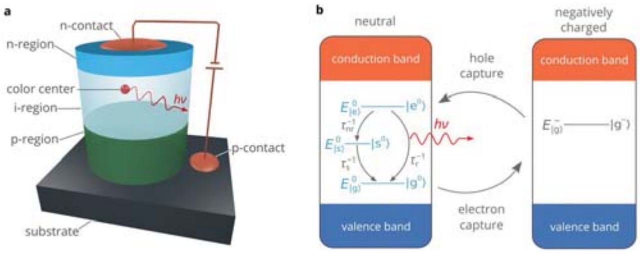


Fig. 1. (a) Schematic illustration of the electrical SPS based on a single color center in a diamond p-i-n diode. (b) Diagram of the single-photon electroluminescence process for the NV center in diamond [4,5].

Here, we study for the first time electrical excitation of color centers in the pulsed mode and investigate the possibility of generation of true single-photon pulses on demand. We found that the process of color center electroluminescence is remarkably different from their photoluminescence process and the electroluminescence process of quantum dots [4,5] (Fig. 1b). Apart from transitions between the ground and excited states, it involves structural transformations of the center due to the electron and hole captures and releases. Despite that diamond single-photon emitting diodes (SPEDs) based on p-i-n structures can show attractive characteristics in the steady state [4-6], we show that their photon statistics cannot approach that of an ideal SPS (Fig. 2a-c). Even if the quantum efficiency of the color center $\eta$ equals 1, we observe either a very high probability of pulses without photons (Fig. 1b) or a high probability of producing a pulse with 2 or more photons (Fig. 2c). We emphasize that it is fundamentally impossible to find a compromise between these two regimes. To improve the ideality of the diamond on-demand SPS, we have reconsidered the design principles and found that the photon statistics can be dramatically improved by locating the NV-like color center in the n-type region of the optimized p-n diode (Fig. 2d). The self-consistent numerical simulations demonstrate that the probability of producing exactly 1 photon in the optical pulse approaches 99% in the optimized device at a repetition rate of 0.1 MHz ($\eta$ = 1). These results lay the foundation for the development of high single-photon purity SPS based on color centers in diamond.

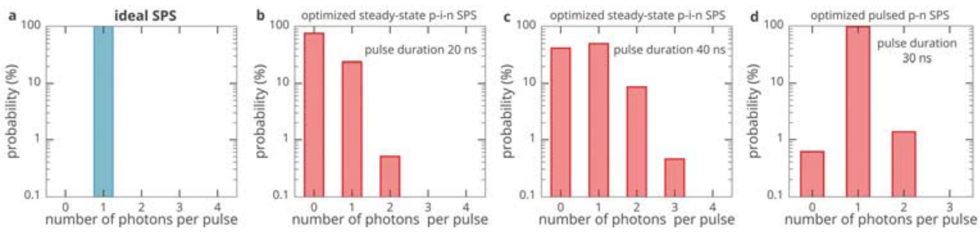


Fig. 2. Probability distribution of the photon number per pulse for the ideal pulsed SPS (a), for the optimized steady-state p-i-n SPED operating in the pulsed mode (b,c), and for the optimized p-n SPED (d). $\eta$ is assumed to be equal to 1, other parameters of the color center are the same as that of the NV center, the pulse repetition rate is 0.1 MHz.

## References

[1] I. Aharonovich et al., Rep. Prog. Phys. **74**, 076501 (2011).
[2] N. Mizuochi et al., Nat. Photonics **6**, 299 (2012).
[3] A. Lohrmann et al., Appl. Phys. Lett. **99**, 251106 (2011).
[4] D.Y. Fedyanin and M. Agio, New J. Phys. **18**, 073012 (2016).
[5] I. A. Khramtsov, M. Agio, and D. Y. Fedyanin, Phys. Rev. Applied **8**, 024031 (2017).
[6] I.A. Khramtsov and D.Y. Fedyanin, Semicond. Sci. Technol. **34**, 03LT03 (2019).

# Single silicon vacancy centers in diamond generated by femtosecond laser illumination

**Youying Rong[1], Zhiping Ju[1], Chengda Pan[1], Qiang Ma[1], Shikang Liu[1], Si Shen[1], Botao Wu[1], and E Wu[1,2,3]**

*1 State Key Laboratory of Precision Spectroscopy, East China Normal University, Shanghai 200062, China*

*2 Collaborative Innovation Center of Extreme Optics, Shanxi University, Taiyuan, Shanxi 030006, China*

*3 Joint Institute of Advanced Science and Technology, East China Normal University, Shanghai 200062, China*

Single photon source based on silicon vacancy (SiV) center in diamond is greatly promising for applications in quantum technologies due to its remarkable optical properties, such as strong and narrow zero-phonon line (ZPL) emission and short excited-state lifetime [1]. Generally, SiV centers are fabricated by ion implantation or chemical vapor deposition technique to implant ionized Si atoms into diamond or dope Si impurities during the diamond growth [2]. Here, we report an easy and flexible method to fabricate single SiV centers in diamond coated with a layer of Si nanoballs by femtosecond laser irradiation. Besides the creation of vacancies, external Si elements were implanted into diamond. After annealing, single SiV centers could be detected around the illuminated spot.

The diamond used here was an ultrapure single crystal with nitrogen impurities < 5 ppb. The water solution containing Si nanoballs with average diameter of 46 µm was spin-coated on the diamond. After the water vaporing naturally, the nanoballs layer was > 1 µm thick. Subsequently, a pulsed laser at 800 nm with 50 fs pulse duration and 1 kHz repetition rate was focused on the coated diamond. The pulse number was 50. At the focus point, the average power and fluence of the laser pulses were 10 mW and 1.6 J/cm$^2$, respectively. Finally, the sample was annealed at 850 ºC in vacuum for 1 h. Fluorescence from emitters in diamond was characterized by a confocal microscope. Excitation was performed by a continuous-wave laser at 662 nm focused by a 1.4 NA oil objective. The fluorescence collected by the same objective was either guided into a spectrometer for spectral measurements or detected by two single photon detectors after splitting by a polarized beam splitter. The two detectors were then connected to a time-correlated single photon counter for second-order autocorrelation function $g^2(t)$ measurements.

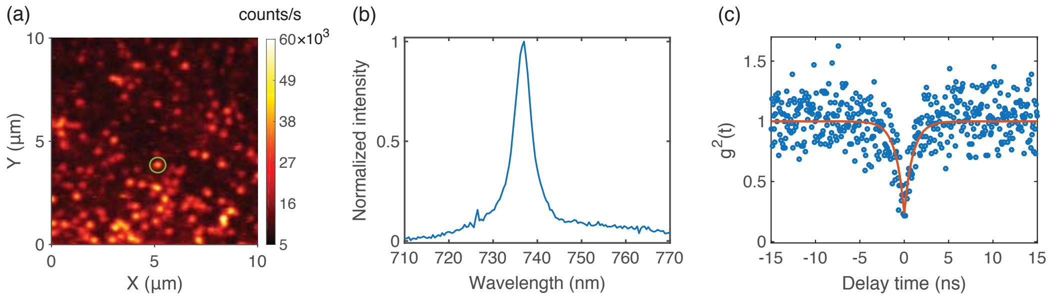


Fig. 1 Characterisation of single SiV center in diamond produced by femtosecond laser technique. (a) Fluorescence image of the area around the irradiated crater. (b) Spectrum and (c) $g^2(t)$ curve of the emitter marked by green circle in (a).

Figure 1 (a) shows the fluorescence image of the area 22.7 µm away from the irradiated crater center at excitation power of 8.2 mW. Lots of bright emitters are visible in this area, which were identified to be SiV centers by spectral measurements. Figure 1 (b) displays spectrum of the emitter marked by the green circle in Fig. 1 (a). The strong ZPL peak is located at 737 nm with linewidth of ~ 4.9 nm, characteristic of a SiV center. The $g^2(t)$ function for the SiV center was measured as presented in Fig. 1 (c). The value of $g^2(0)$ is ~ 0.24, revealing a single SiV center. The results demonstrate the method can effectively and rapidly create single SiV center in diamond.

The formation of the SiV centers can be depicted as follows. When the high-fluence laser pulses was focused on the Si nanoballs, electrons absorbed photon energy and ejected fast from the irradiated area. Thus, $Si^+$ ions would accumulate in the irradiated area, and Coulomb repulsive force among them would become more and more intense until it broke bonds among $Si^+$ ions, triggering Coulomb explosion of Si and leading to fast ejection of $Si^+$ ions out of the nanoballs in all directions [3]. A part of $Si^+$ ions with high kinetic energy impinged into diamond, creating vacancies simultaneously. After annealing, the vacancies diffused to Si impurities forming SiV centers.

This work is funded by National Natural Science Foundation of China (11722431, 11674099, 11621404); Program of Introducing Talents of Discipline to Universities (B12024); Shanghai International Cooperation Project (16520710600); Natural Science Foundation of Shanghai (16ZR1409400); Shuguang Program (15SG22) by Shanghai Education Development Foundation and Shanghai Municipal Education Commission.

## References

[1] I. Aharonovich *et al.*, "Diamond-based single-photon emitters", Rep. Prog. Phys. **74**, 076501 (2011).
[2] J.O. Orwa *et al.*, "Fabrication of single optical centres in diamond—a review", J. Lumin. **130**, 1646–1654 (2010).
[3] H. Dachraoui *et al.*, "Ultra-short laser ablation of metals and semiconductors: evidence of ultra-fast Coulomb explosion", Appl. Phys. A **83**, 333 (2006).

# Fabrication of diamond-based quantum emitters upon ion implantation

**J. Forneris[1], S. Ditalia Tchernij[2,1], P. Traina[3], E. Moreva[3], I. P. Degiovanni[3], T. Lühmann[4], T. Herzig[4], S. Pezzagna[4], J. Meijer[4], M. Jakšić[5], M. Genovese[3], P. Olivero[2,1,3]**

[1] *Istituto Nazionale di Fisica Nucleare (INFN) - Sez. Torino, Italy*
[2] *Physics Department and "NIS" inter-departmental centre, University of Torino, Italy*
[3] *Istituto Nazionale di Ricerca Metrologica (INRiM), Torino, Italy*
[4] *Department of Nuclear Solid State Physics, Leipzig University*
[5] *Laboratory for Ion Beam Interactions, Ruđer Bošković Institute, Zagreb, Croatia*

Color centers in diamond are systems with appealing photo-physical properties for the development of quantum technologies. The ever-growing interest in these systems is motivated by their operation at room temperature, together with an ease of access and manipulation in a solid state system characterized by high transparency and structural stability, with applications as bright and stable single-photon sources or individual spin systems with optical readout, with record performances even at room temperature. Despite literally hundreds of optically active color centers in diamond have been reported in the past decades, only a handful of them can be consistently fabricated by means of a reproducible process such as ion implantation.

In this contribution, the ongoing efforts towards a systematic investigation in the formation of novel single-photon sources based on optically-active defects in diamond will be discussed. Particularly, recent results will be presented on the fabrication by means of ion implantation and subsequent photo-physical characterization of novel classes of single-photon sources upon the implantation of Sn and Pb ions and subsequent thermal annealing at 950 °C [1,2]. The discovery of such classes of emitters represent a significant step toward completing the interpretational framework on the optical activity of diamond defects related to group IV impurities.

Furthermore the perspective of producing single-photon through the introduction of He ions [3] as well as other light elements in diamond will also be discussed on the basis of ensemble spectral characterizations and confocal microscopy imaging.

**References**

1. S. Ditalia Tchernij et al., "Single-photon-emitting optical centers in diamond fabricated upon Sn implantation", ACS Photonics 4, 2580 (2017)..
2. S. Ditalia Tchernij et al., "Single-Photon Emitters in Lead-Implanted Single-Crystal Diamond ", ACS Photonics 5, 4864 (2018).
3. J. Forneris et al., "Creation and characterization of He-related color centers in diamond", J. Lumin. 179 (2016) 59.

# International joint pilot study on g(2) measurement for single-photon sources in the visible and telecom spectral ranges

**P. Traina[1], E. Moreva[1], F. Piacentini[1], E. Rebufello[1], M. López[2], R. A. Kirkwood[3], I. Ruo-Berchera[1], M. Gramegna[1], G. Brida[1], S. Kück[2], C. J. Chunnilall[3], J. Forneris[4], S. Ditalia Tchernij[5], F. Picollo[5], P. Olivero[5], M. Genovese[1] and I. P. Degiovanni[1]**

[1] *Istituto Nazionale di Ricerca Metrologica (INRIM), Torino, Italy*

[2]*Physikalisch-Technische Bundesanstalt (PTB), Braunschweig, Germany*

[3]*National Physical Laboratory (NPL), Teddington, United Kingdom*

[4]*Istituto Nazionale di Fisica Nucleare (INFN) Sez. Torino, Torino, Italy*

[5]*Physics Department and NIS Inter-Departmental Centre, University of Torino, Torino, Italy*

With the aim of establishing standard techniques in single-photon metrology, device-independent and reproducible methods for source characterization are needed. Measurement of the $g^{(2)}(0)$ parameter is of utmost importance in characterising and understanding single-photon emission. In this talk I will report on the pilot studies, performed by INRIM, NPL and PTB, on the measurement of $g^{(2)}(0)$ parameter on test single-photon sources (SPSs) in two different spectral ranges and regimes: 1) a SPS based on a single Nitrogen Vacancy center in pulsed excitation emitting in the visible; 2) an heralded SPS realized by the process of parametric down-conversion emitting at Telecom wavelength.

# Enhancing the brightness of room-temperature electrically driven single-photon sources using color centers in silicon carbide

**Igor A. Khramtsov, Andrey A. Vyshnevyy, and Dmitry Yu. Fedyanin**
*Moscow Institute of Physics and Technology, Dolgoprudny, Russian Federation*

Practical implementation of unconditionally secure communication lines and other quantum information technologies suffers from the lack of bright and efficient single-photon sources that can operate under ambient conditions. In spite of intense research in this area, it is still a challenge to obtain bright and stable single-photon emission at room temperature, especially under electrical excitation, which is highly desirable for practical applications. Currently, point defects in the crystal lattice of diamond known as color centers are considered as the most promising room-temperature single-photon emitters [1]. However, diamond is a material at the interface between insulators and semiconductors, and therefore, electrical excitation of color centers in diamond is challenging [2]. The maximum demonstrated single-photon electroluminescence rate is about 50 kcps [3,4], while recent theoretical studies show that it can hardly exceed 2 Mcps at room temperature [2,5], which is not sufficient for high-performance quantum information devices.

In this work, we focus on color centers in silicon carbide, which have recently emerged as a potential alternative to color centers in diamond [6], and demonstrate that these emitters can be far superior to any other quantum system under electrical control at room temperature [7]. The greatest advantage of SiC over diamond and many other materials that can host color centers, such as the newly emerged 2D materials, is its excellent semiconducting properties, which give the possibility to efficiently pump color centers electrically [8]. Here, we reveal the physics behind the process of single-photon emission from color centers in 4H-SiC p-i-n diodes under electrical excitation and perform a rigorous study of the silicon antisite-stacking fault ($Si_C$-SF) defect in the 4H-SiC p-i-n diode. The results of our self-consistent numerical simulations accurately reproduce and interpret experimental observations on an existing device [8] (Fig. 1a-b) [7]. Moreover, we show that by optimizing the parameters of the single-photon emitting diode and decreasing the lifetime of the excited state of the color center (which can be achieved with an optical cavity or a nanoantenna, or choosing a proper color center), it is possible to increase the single-photon electroluminescence rate well above 1 Gcps at room temperature (Fig. 1c) [7], which is significantly higher than what can be achieved with any other electrically driven quantum emitter under ambient conditions. These findings lay the foundation for the development of practical single-photon sources which can be produced in a well-developed CMOS compatible process flow.

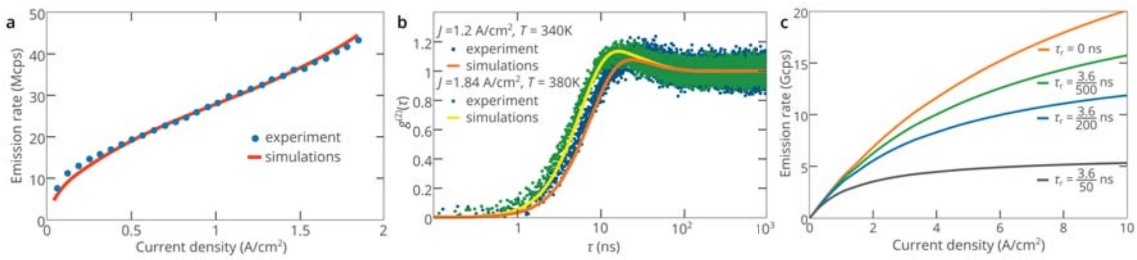


Fig. 1. (a,b) Input-output characteristics (a) and the second-order autocorrelation function (b) retrieved from the experiment and predicted by our numerical simulations. (c) Simulated maximum single-photon emission rate from the properly designed SiC single-photon emitting diode as a function of the pump current for different lifetimes of the excited state of the color center at room temperature. For details, see Ref. [7].

## References

[1] I. Aharonovich, D. Englund, and M. Toth, Nat. Photonics **10**, 631 (2016).
[2] D.Y. Fedyanin and M. Agio, New J. Phys. **18**, 073012 (2016).
[3] N. Mizuochi et al., Nat. Photonics **6**, 299 (2012).
[4] A. Lohrmann et al., Applied Physics Letters **99**, 251106 (2011).
[5] I.A. Khramtsov and D.Y. Fedyanin, Semicond. Sci. Technol. **34**, 03LT03 (2019).
[6] A. Lohrmann, B.C. Johnson, J.C. McCallum, and S. Castelletto, Rep. Prog. Phys. **80**, 034502 (2017).
[7] I.A. Khramtsov, A.A. Vyshnevyy, and D.Y. Fedyanin, npj Quantum Inf. **4**, 15 (2018).
[8] A. Lohrmann et al., Nat. Commun. **6**, 7783 (2015).

# Coupling organic molecules to nanophotonic bullseye cavities

**Salahuddin Nur, Dominika Bogusz, Ross C. Schofield, Sebastien Boissier, Kyle D. Major, E. A. Hinds, and Alex S. Clark***

*Centre for Cold Matter, Imperial College London, UK*
**contact: alex.clark@imperial.ac.uk*

Cryogenically cooled organic dye molecules are excellent sources of indistinguishable photons [1]. They can, however, be drastically improved through the use of optical cavities [2]. Integrated nano-cavities are inherently stable, as they are in the solid state, and have small mode volumes comparable with the wavelength of light. When a quantum emitter, such as a dibenzoterrylene (DBT) molecule, shown in Fig. 1(a), is placed at the correct position within such a cavity the emitter will preferentially emit photons into a single spatial-spectral-polarisation mode, and can also do so at a much faster rate than it would have done outside the cavity – known as Purcell enhancement. I will present our recent work using bullseye grating cavities to capture and enhance emission from DBT.

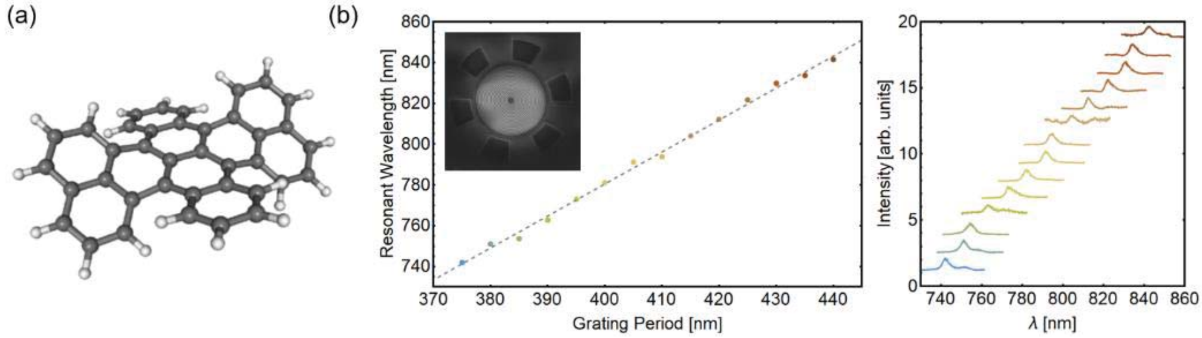


Figure 1: (a) Dibenzoterrylene. (b) Resonant wavelength of bullseye grating cavities with changing grating period (left) found from reflection spectra (right). A scanning electron microscope image of a bullseye grating cavity is inset.

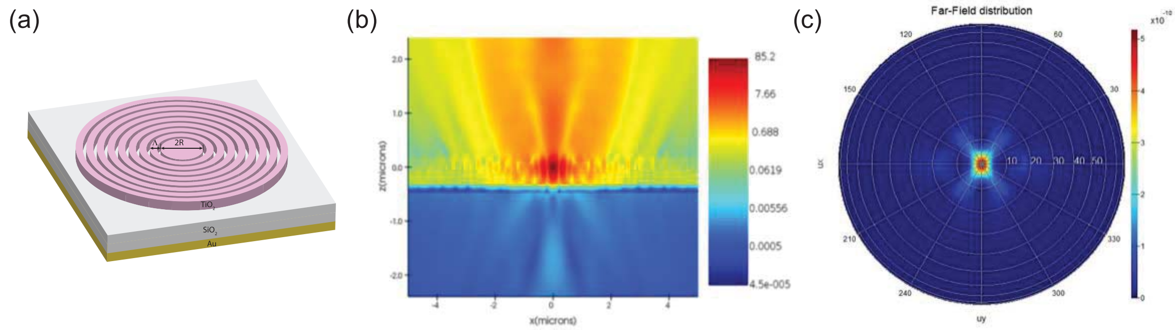


Figure 2: (a) Schematic of a bullseye grating cavity with Au back-reflector. (b) E-field distribution of the fundamental mode at XZ plane. (c) Far-field distribution of the fundamental mode.

Our cavities were designed in Lumerical FDTD and fabricated in titanium dioxide ($TiO_2$) thin films on silica-on-silicon substrates using electron beam lithography. The cavity is a solid central disk of $TiO_2$, surrounded by concentric rings with a period of ~ $\lambda_{cav}/n_{eff}$, where $\lambda_{cav}$ is the resonant wavelength of the cavity and $n_{eff}$ is the effective index of the $TiO_2$ film [3, 4]. They have a predicted quality factor of ~400, and a mode-volume of order $2(\lambda_{cav}/n)^3$. These non-suspended bullseye grating cavities can provide a collection efficiency around 40%. By illuminating them with white light and monitoring reflection, we were able to measure the variation in $\lambda_{cav}$ and quality factor versus the period of the grating (Fig. 1(b) & (c)). We have deposited DBT-doped nanocrystals of anthracene [5] on these devices, and we are now characterising them at both room and liquid helium temperatures. I will present analysis of this emission including collection efficiency, saturation, molecular excited state lifetime, and anti-bunching, and will describe the planned addition of a back-reflector [6] as shown in Fig. 2. The addition of an effective back-reflector can further improve the collection efficiency up to around 80%.

**References**

[1] S. Grandi et al., Phys. Rev. A **94**, 063839 (2016).
[2] M. Trupke et al., Appl. Phys. Lett. **87**, 211106 (2005).
[3] M. Davanço et al., Appl. Phys. Lett. **99**, 041102 (2011).
[4] N.M.H. Duong et al., ACS Photonics **5**, 3950 (2018).
[5] S. Pazzagli et al., ACS Nano **12**, 4295-4303 (2018).
[6] J. Liu et al., Nat. Nanotech. **14**, 586 (2019).

# Pure Photon Generation From Domain Engineered Crystals

A. Pickston,[1] F. Graffitti,[1] P. Barrow,[1] M. Proietti,[1] D. Kundys,[1] J. Ho,[1] A. M. Brańczyk,[2] and A. Fedrizzi[1]

[1] *Institute of Photonics and Quantum Sciences, School of Engineering and Physical Sciences, Heriot-Watt University, Edinburgh EH14 4AS, UK*

[2] *Perimeter Institute for Theoretical Physics, Waterloo, Ontario, Canada, N2L 2Y5*

Scalable photonic quantum technologies require pure single photons created on demand. Photon sources based on probabilistic parametric down-conversion can be multiplexed to achieve pseudo determinism, they achieve high heralding efficiency, and the spectrum can be engineered to achieve high purity and thus high quality multi-photon interference. Here, we develop upon previous work [1–3] based on domain engineering of periodically poled KTP crystals (ppKTP). Using a mode-locked with a sech$^2$-shaped intensity envelope, we generated photon pairs at telecommunications wavelength with single photon purities of 95.3% without spectral filtering—a record for domain engineered crystals at that time. We have further improved on these results by fine-tuning crystal design parameters which trade off non-linearity with photon purity. Our new designed crystals are capable of even higher photon purity, 98.6%, the highest achieved through domain engineering alone.

Crystal domain engineering allows a level of control to be gained over the phase matching function (PMF), which governs the spectral response of the non-linear interaction. The ferroelectric domains of a commonly employed periodically poled crystal can be varied in width and orientation to generate a targeted PMF. The ideal target function, a Gaussian, results in the production of photon pairs that possess a separable joint spectral amplitude (JSA) and high purity. The domain engineering algorithms we reported in [2] exploited sub-coherence length domain structures, which improved upon all previous algorithms in that high purities can be achieved even for short crystals matched to femtosecond pump pulses. The benefits of removing purity degrading spectral correlations is best highlighted when comparing the JSA (or joint spectral intensity (JSI)) of a commonly utilised non-linear crystal, ppKTP, that suffer these correlations due to their sinc shaped PMF, with our custom crystals in Fig.1. The domain engineering technique we deploy is fast, can be readily implemented commercially and can target more complex field amplitudes which allows for exploration into more exotic cases, such as the generation of an anti-symmetric PDC joint spectra.

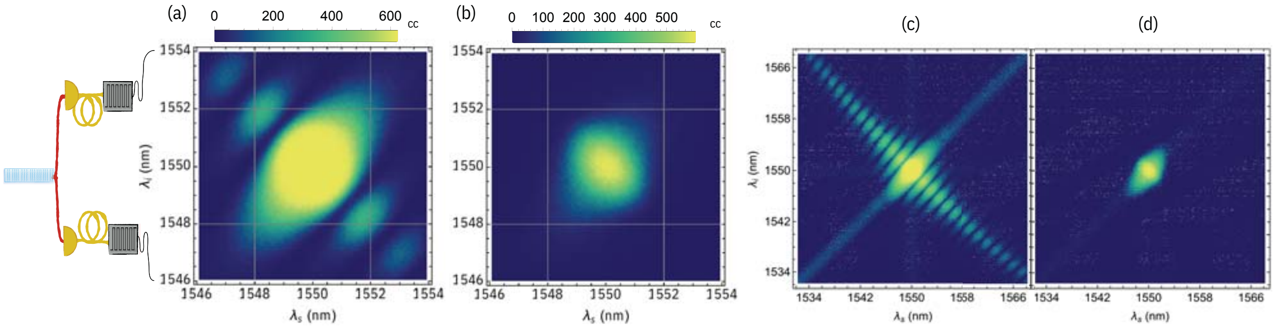


FIG. 1. A reconstruction of the joint spectral intensities for both ppKTP **(a)** and our custom crystals **(b)** was made possible by recording 6234989 and 1759158 single photons respectively, detected by SNSPD's which operate with < 50ps jitter, < 25ns dead time and with < 200Hz dark count rate and then processed via a Picoquant HydraHarp. We also show a logarithmic plot of a larger wavelength range for better visualisation of the difference in a ppKTP crystals JSI **(c)** and the JSI of our custom crystals **(d)**.

The results we report include a comprehensive benchmark and comparison between photons created in standard ppKTP, and our new, custom apodised crystal (aKTP). To experimentally characterise the performance of the crystals, we carried out high-precision measurements of multi-photon interference between two independent PDC sources. Along with this, we performed an in-depth discussion of extrapolated spectral purity as measured by the independent two-photon interference measurements with highly resolved and image post-processed joint spectral intensity (JSI) measurements; a required discussion, as only the singular valued decomposition of the JSA can yield the actual photon purity and many use the JSI, the $\sqrt{\text{JSA}}$ or the extrapolated two-photon interference visibility to conclude on measured photon purities.

[1] F. Graffitti, D. Kundys, D. T. Reid, A. M. Brańczyk, and A. Fedrizzi, Quantum Science and Technology **2**, 035001 (2017).
[2] F. Graffitti, P. Barrow, M. Proietti, D. Kundys, and A. Fedrizzi, Optica **5**, 514 (2018).
[3] F. Graffitti, J. Kelly-Massicotte, A. Fedrizzi, and A. M. Brańczyk, Physical Review A **98**, 053811 (2018).

# List of authors

Carlos Abellán (ICFO-Institut de Ciencies Fotoniques)

Julie Abergel (CEA-Leti)

Hamza Abudayyeh (Hebrew University of Jerusalem)

Giulia Acconcia (Politecnico di Milano)

Fabio Acerbi (FBK)

Jeremy Adcock (University of Bristol)

Viatcheslav Agafonov (GREMAN, UMR CNRS-7347, Université F. Rabelais)

Costantino Agnesi (University of Padova)

Benito Alén (IMN-CNM, Instituto de Micro y Nanotecnologia, CSIC)

Mohammad Alhejji (National Institute of Standards and Technologies)

Alessia Allevi (Universiti of Insubria - Department of Science and High Tecnology)

Jason Allmaras (JPL)

Norah Almutairi (King's College London)

Yoann Altmann (Heriot-Watt University)

Maria Amanti (Université de Paris)

Giampiero Amato (Istituto Nazionale di Ricerca Metrologica (INRiM), Italy)

Emna Amri (ID Quantique / University of Geneva)

Chengwu An (National Metrology Centre, A*STAR)

Matthew Anderson (Toshiba Research Europe Ltd)

Carlos Antón (CNRS C2N)

Carlos Anton Solanas (C2N, Center of Nanosciences and Nanotechnology, Universite Paris-Saclay)

Juan Miguel Arrazola (Centre for Quantum Technologies)

Simon Arridge (University College London, Department of Computer Science)

Alberto Artioli (Univ. Grenoble Alpes, CEA, IRIG, PHELIQS, "Nanophysique et semiconducteurs" group)

Asimina Arvanitaki (Perimeter Institute for Theoretical Physics)

Simone Atzeni (Istituto di Fotonica e Nanotecnologie - Consiglio Nazionale delle Ricerche (IFN-CNR))

Alexia Auffeves (Institut Neel)

Etiennette Auffray (CERN)

Brian Aull (MIT Lincoln Laboratory)

Claire Autebert (ID Quantique / University of Geneva)

Alessio Avella (Istituto Nazionale di Ricerca Metrologica (INRiM))

Marco Avesani (University of Padova)

Stefano Azzini (University of Trento)

Florent Baboux (Université de Paris)

Davide Bacco (CoE SPOC, Dep. Photonics Eng., Technical University of Denmark)

Emmanuel Bacher (French-German Research Institute of Saint-Louis)

In-Ho Bae (KRISS)

Soohyun Baek (Wooriro)

Bing Bai (University of Science and Technology of China)

Daniele Bajoni (Università degli Studi di Pavia)

Laurent Balet (CSEM)

Philippe Ballet (CEA-Leti)

Rex H.S. Bannerman (University of Southampton)

Jorge Barreto (University of Bristol)

Peter Barro (Heriot-Watt University)

Peter Barrow (Heriot-Watt University)

Tim Bartley (Paderborn University)

Tim J. Bartley (University of Paderborn)

Masha Baryakhtar (NYU)

Abdella Battou (NIST)

Christoph Becher (Universität des Saarlandes)

Anurag Behera (Politecnico di Milano, Dipartimento di Fisica)

Anthony Bennett (Cardiff University)

Oliver Benson (Humboldt Universität zu Berlin)

Karl Berggren (MIT)

Ettore Bernardi (Istituto Nazionale di Ricerca Metrologica)

Bänz Bessire (Institute of Applied Physics, University of Bern)

Fabian Beutel (WWU Münster)

Jörn Beyer (Physikalisch-Technische Bundesanstalt Berlin)

Roberto Bez (LFoundry)

Narayan Bhusal (Louisiana State University)

Paolo Bianchini (Istituto Italiano di Tecnologia)

Joshua Bienfang (National Institute of Standards and Technology)

Peter Bierhorst (University of New Orleans)

Sam Bishop (Cardiff University)

Sébastien Bize (LNE-SYRTE, Observatoire de Paris)

Josef Blazej (Czech Technical University in Prague)

Joël Bleuse (CEA)

Pierre Bluet (CEA-Leti)

Luca Boarino (Istituto Nazionale di Ricerca Metrologica (INRiM), Italy)

Dominika Bogusz (Imperial College London)

Jonas Böhm (TU Berlin)

Dmitri Boiko (CSEM)

Sebastien Boissier (Imperial College London)

S. Bounouar (nstitute of Solid-State Physics, Technische Universität Berlin)

Maria Bondani (CNR - Institute for Photonics and Nanotechnologies)
Joseph Steven Borbely (MSL)
Massimo Borghi (SM Optics)
Frédéric Bouchard (Department of physics, University of Ottawa)
Pierre Boulenc (imec)
Joelle Boutari (University of Oxford)
Allan Bracker (US Naval Research Lab)
Agata Branczyk (Perimeter Institute)
Florian Brandt (IQOQI Vienna)
Benjamin Brecht (University of Paderborn)
Giorgio Brida (Istituto Nazionale di Ricerca Metrologica)
Werner Brockherde (Fraunhofer Institute for Microelectronic Circuits and Systems IMS)
Alex Browning (NPL)
Sonia Buckley (NIST)
Lukas Bulla (IQOQI Vienna)
Gerald Buller (Heriot-Watt University)
Andreas Bülter (PicoQuant GmbH)
Ivan Burenkov (Joint Quantum Institute at NIST)
S. Burger (Zuse Institut Berlin)
Félix Bussières (ID Quantique / University of Geneva)
Mauro Buttafava (Politecnico di Milano)
Gustavo C. Amaral (Delft University of Technology)
Davide Calonico (INRIM)
Misael Caloz (University of Geneva)
Andrew Cameron (University of Waterloo)
Charles H. Camp Jr. (National Institute of Standards and Technology)
Robin Camphausen (ICFO – The Institute of Photonic Sciences)
Yuan Cao (University of Science and Technology of China)
Massimo Capasso (FBK)
Valentina Carabelli (Universita' degli studi di Torino)
Samuel Carter (U.S. Naval Research Lab)
Gonzalo Carvacho (Dipartimento di Fisica, Sapienza Universitá di Roma)
Marco Castello (Istituto Italiano di Tecnologia)
Francesco Ceccarelli (Istituto di Fotonica e Nanotecnologie - Consiglio Nazionale delle Ricerche (IFN-CNR))
Robert Cernansky (Department of Physics and Astronomy, University of Southampton, Southampton SO17 1BJ, UK)
Poompong Chaiwongkhot (University of Waterloo)
Stanley Chan (Purdue University)
Joseph C. Chapman (Department of Physics, University of Illinois at Urbana-Champaign)
Ilya Charaev (MIT)
Edoardo Charbon (EPFL)
Yu-Ao Chen (University of Science and Technology of China)
Giovanni Chesi (University of Insubria - Department of Science and High Technology)
Fabio Chiarello (Istituto di Fotonica e Nanotecnologie-CNR)
Jeffrey T. Chiles (NIST)
Fumihiro China (National Institute of Information and Communications Technology)
Seok-Beom Cho (ID Quantique)
Sungwan Cho (Electronics and Telecommunications Research Institute)
Justus Christinck (Physikalisch-Technische Bundesanstalt)
Frank Christnacher (The French-German Research Institute of Saint-Louis (ISL))
Joaquin Chung (Argonne National Laboratory)
Christopher J. Chunnilall (National Physical Laboratory)
Marcus Cicerone (National Institute of Standards and Technology)
Alex S Clark (Imperial College London)
Alex S. Clark (Imperial College London)
Chloe Clear (University of Bristol)
Eliahu Cohen (Bar Ilan University)
Marco Colangelo (MIT)
M. Colautti (NR-INO and LENS, Istituto Nazionale di Ottica)
Enrico Conca (Politecnico di Milano)
Peter Connolly (Heriot-Watt University)
Amy Conover (Quantum Opus LLC)
Davide Contini (Politecnico di Milano, Dipartimento di Fisica)
Guillaume Coppola (C2N, Center of Nanosciences and Nanotechnology, Universite Paris-Saclay)
David Cory (University of Waterloo)
Daniele Cozzolino (CoE SPOC, Dep. Photonics Eng., Technical University of Denmark)
Andrea Crespi (IFN-CNR)
Alvaro Cuevas (ICFO – The Institute of Photonic Sciences)
David Cumming (Glasgow University)
Beatrice Da Lio (Technical University of Denmark)
Jibo Dai (A*STAR Institute of Materials Research and Engineering)
Dan Dalacu (National Reseach Council Canada)
Alberto Dalla Mora (Politecnico di Milano, Dipartimento di Fisica)
Andrew Dane (MIT)

Alexandre Dauphin (ICFO – The Institute of Photonic Sciences)
Marcelo Davanco (National Institute of Standards and Technology)
Jacob H. Davidson (Delft University of Technology)
Valery Davydov (L.F. Vereshchagin Institute for High Pressure Physics of RAS)
Eleni Diamanti (Sorbonne Université)
Innocenzo De Marco (Toshiba Research Europe Limited)
Hugues de Riedmatten (ICFO)
Lorenzo De Santis (CNRS C2N)
Muriel de Souza (INMETRO)
Ivo P. Degiovanni (Istituto Nazionale di Ricerca Metrologica (INRiM))
Laura Di Sieno (Politecnico di Milano, Dipartimento di Fisica)
Alberto Diaspro (Istituto Italiano di Tecnologia)
Yunhong Ding (Technical University of Denmark)
Jean-Marc Dinten (CEA-LETI)
Sviatoslav Ditalia Tchernij (University of Torino)
Sergiy M. Dobrovolsky (Single Quantum B.V.)
Philip Dolan (National Physical Laboratory)
Timo Dönsberg (Teknologian tutkimuskeskus)
Jonathan Dowling (Louisiana State University)
Christian Drago (University of Toronto)
Jan Henning Drewes (Fraunhofer Institute for Microelectronic Circuits and Systems IMS)
Sara Ducci (Université de Paris)
A Ducuara (University of Bristol)
Luc Duempelmann (ICFO – The Institute of Photonic Sciences)
Erik Duerr (MIT Lincoln Laboratory)
James Dunphy (Waymo LLC)
Ivan Dyakonov (Quantum Technology Center & Faculty of Physics, M.V. Lomonosov Moscow State University)
James Dynes (Toshiba Research Europe Limited)
Jan Dziewior (Max-Planck-Institut für Quantenoptik, Ludwig-Maximilians-Universität)
Susan K Earles (Florida Institute of Technology)
Sebastian Ecker (IQOQI Vienna)
Satoru Efumi (Tokyo University of Science)
Omar Elgendy (Gigajot Technology)
Ricky Elwell (University of California, Los Angeles)
Stefan Enoch (Aix Marseille Univ., CNRS, Centrale Marseille, Institut Fresnel)
Emanuele Enrico (Istituto Nazionale di Ricerca Metrologica (INRiM), Italy)
Kleanthis Erotokritou (University of Glasgow)
Robin Essling (PTB)
Nicolas Fabre (Université de Paris)
Daniele Faccio (University of Glasgow)
Mohsen Falamarzi Askarani (Delft University of Technology)
Paolo Falferi (CNR-FBK and INFN)
Jingyun Fan (University of Science and Technology of China)
Jingyun Fan (Southern University of Science and Technology)
Yu-Qiang Fang (University of Science and Technology of China)
Andrea Farina (Consiglio Nazionale delle Ricerche, Istituto di Fotonica e Nanotecnologie)
Ian Farrer (The University of Sheffield)
Renato Federico (Politecnico di Milano)
Alessandro Fedrizzi (Heriot-Watt University)
Dmitry Fedyanin (Moscow Institute of Physics and Technology)
Konstantin Fehler (Institut für Quantenoptik and IQST (Universität Ulm))
Yue-Yang Fei (University of Science and Technology of China)
Qilai Fei (University of Shanghai for Science and Technology)
Matthew Feldman (Vanderbilt University)
Edoardo Ferocino (Politecnico di Milano, Dipartimento di Fisica)
Giacomo Ferranti (University of Bristol)
Robert Fickler (IQOQI Vienna & Photonics Laboratory, Physics Unit, Tampere University)
Donald Figer (Center for Detectors, RIT)
Eden Figueroa (Stony Brook University)
Sarah Fischbach (TU Berlin)
Mael Flament (Stony Brook University)
Suren Fldjan (Quantum Technology Center & Faculty of Physics, M.V. Lomonosov Moscow State University)
Valerie Fleischauer (Center for Detectors, RIT)
Alexander Flocke (iC-Haus)
Giulio Foletto (Dipartimento di Ingegneria dell'Informazione, Università degli Studi di Padova)
Giorgio Fontana (University of Trento)
Jacopo Forneris (Istituto Nazionale di Fisica Nucleare (INFN) Sez. Torino)
Eric Fossum (Thayer School of Engineering at Dartmouth)
Saverio Francesconi (Université de Paris)
Robert J.A. Francis-Jones (University of Oxford)
Jonathan Frazer (University of Bristol)
Jonathan Frechette (MIT Lincoln Laboratory)
Philipp Fuchs (Universität des Saarlandes)

David Fuster (IMN-CNM, Instituto de Micro y Nanotecnologia, CSIC)
Alessandro Gaggero (Istituto di Fotonica e Nanotecnologie-CNR)
Justin Gallagher (Center for Detectors, RIT)
Matteo Galli (Università degli Studi di Pavia)
Daniel Gammon (U.S. Naval Research Lab)
Angela Gamouras (National Research Council Canada)
Alagappan Gandhi (A*STAR Institute of High Performance Computing)
Leonardo Gasparini (FBK)
James C. Gates (University of Southampton)
Bruno Gayral (CEA)
Nathan Gemmell (University of Sussex)
Stephane Gendron (Canadian Space Agency)
Marco Genovese (Istituto Nazionale di Ricerca Metrologica (INRiM))
Hristina Georgieva (Physikalisch-Technische Bundesanstalt)
Sonali Gera (Stony Brook University)
Jean-Michel Gérard (CEA)
Thomas Gerrits (National Institute of Standards and Technology)
Massimo Ghioni (Politecnico di Milano)
Andrew Gibson (Canadian Space Agency)
Maria Gieysztor (Nicolaus Copernicus University)
Andrea Giudice (Micro Photon Devices Srl)
Cristina E Giusca (National Physical Laboratory)
Scott Glancy (National Institute of Standards and Technology)
René Glazenborg (Photonis Netherlands BV)
Eric Gloutnay (Canadian Space Agency)
Abhiram Gnanasambandam (Purdue University)
Alberto Gola (FBK)
Dominique Golanski (STM)
E.A. Goldshmidt (Army Research Laboratory)
Yolanda González (IMN-CNM, Instituto de Micro y Nanotecnologia, CSIC)
Peter Gordebeke (European Institute for Biomedical Imaging Research)
Stephan Götzinger (Friedrich-Alexander-Universität Erlangen – Nürnberg)
Sylvain Gout (CEA-Leti)
Paul C. Gow (University of Southampton)
Francesco Graffitti (Heriot-Watt University)
Marco Gramegna (Istituto Nazionale di Ricerca Metrologica)
Samuele Grandi (ICFO)
Gaëtan Gras (ID Quantique / University of Geneva)
Aikaterini Gratsea (ICFO (Institute of Photonic Sciences), Okinawa Institute of Science and Technology (OIST))
James Grieve (Centre for Quantum Technologies)
Joel Grim (US Naval Research Lab)
Marcel.Li Grimau Puigibert (University of Basel)
Simon Grosse (Fraunhofer)
Dragan Grubisic (Laser Components DG, Inc.)
Nico Gruhler (Center for Nanotechnology, University of Münster)
Jan Grygar (Palacký University)
Manuel Gschrey (TU Berlin)
Angelo Gulinatti (Politecnico di Milano)
Stefan Gundacker (CERN, University of Milano-Bicocca)
Ke Guo (University of York & National Physical Laboratory)
Mohit Gupta (University of Wisconsin-Madison)
Anant Gupta (University of Wisconsin-Madison)
Yelena Guryanova (IQOQI Vienna)
Geraldine Haack (Group of applied physics, University of Geneva)
John Hadden (Cardiff University)
Robert Hadfield (University of Glasgow)
Sofiane Haffouz (National Research Council of Canada)
Abderrahim Halimi (Heriot-Watt University)
Klemens Hammerer (University Hannover)
Ling Hao (National Physical Laboratory)
Abdelmounaim Harouri (C2N, Center of Nanosciences and Nanotechnology, Universite Paris-Saclay)
Wladislaw Hartmann (University of Münster)
Karim Hassan (CEA-LETI)
Matthias Häußler (WWU Münster)
Jon Heffernan (The University of Sheffield)
Tobias Heindel (TU Berlin)
Robert Henderson (The University of Edinburgh)
Harald Herrmann (Paderborn University)
Tobias Herzig (Leipzig University)
Xu Hesong (AMS)
Brendon Higgins (University of Waterloo)
Paul Hilaire (C2N)
E A Hinds (Imperial College London)
Ed Hinds (Imperial College London)
Jakob Hinney (Vienna University of Technology)
Thomas Hird (University of Oxford)
Liisa Hirvonen (King's College London)
Josef Hloušek (Palacký University)
Joseph Ho (Heriot-Watt University)
Michael Hofbauer (Institute of Electrodynamics, Microwave and Circuit Engineering, TU Wien)

Helmuth Hofer (Physikalisch-Technische Bundesanstalt)

Sven Höfling (Julius-Maximilians-Universität Würzburg)

Jennifer Hollingsworth (Los Alamos National Laboratory)

Rebecca Holmes (Los Alamos National Laboratory)

T. Höhne (Zuse Institut Berlin)

Kee-Suk Hong (Korea Research Institute of Standards and Science (KRISS))

Jan Philipp Höpker (Paderborn University)

El Dirani Houssein (CEA-LETI)

Gregory Howland (Center for Detectors, RIT)

Ting Hu (A*STAR Institute of Microelectronics)

Yi Hu (University of Science and Technology of China)

Xin Huang (University of Science and Technology of China)

Kun Huang (University of Shanghai for Science and Technology, East China Normal University)

Junwu Huang (Perimeter Institute for Theoretical Physics)

Hannes Hübel (AIT - Austrian Institute of Technology)

Marcus Huber (IQOQI Vienna)

Tobias Huber (Joint Quantum Institute)

Eric Hudson (University of California, Los Angeles)

Diana Huffaker (Cardiff University)

Jan Huwer (Toshiba Research Europe Ltd)

Michael Hynes (University College London)

Erkki Ikonen (Aalto University and VTT Technical Research Centre of Finland Ltd)

Jake Iles-Smith (The University of Sheffield)

Hans Ingelberts (Vrije Universiteit Brussel)

Atul Ingle (University of Wisconsin-Madison)

Massimo Inguscio (I.N.Ri.M.—Istituto Nazionale di Ricerca Metrologica, Turin)

Jun Ishihara (Tokyo University of Science)

M.V. Jabir (NIST)

Milko Jakšić (Ruder Boskovic Institute)

Justin Jeet (University of California, Los Angeles)

John Jeffers (University of Strathclyde)

Gobinath Jegannathan (Vrije Universiteit Brussel)

Thomas Jennewein (University of Waterloo)

Bora Jeon (Wooriro)

Hyunseok Jeong (Seoul National University)

Kwang-Yong Jeong (Department of Physics, Korea University)

Michael Jetter (Institut für Halbleiteroptik und Funktionelle Grenzflächen, University of Stuttgart)

Miroslav Ježek (Palacký University)

Xiao Jiang (University of Science and Technology of China)

Ralph Jimenez (JILA, University of Colorado)

Weijie Jin (University of Science and Technology of China)

Lin Jin (WWU Muenster)

Jeongwan Jin (National Research Council Canada)

Zhiping Ju (East China Normal University)

Arsenty Kaganskiy (Institut für Festkörperphysik, Technische Universität Berlin)

Dmitry Kalashnikov (A*STAR Institute of Materials Research and Engineering)

Alexander Kalinkin (Quantum Technology Center & Faculty of Physics, M.V. Lomonosov Moscow State University)

Martin Kamp (University of Würzburg)

Fumihiro Kaneda (Department of Physics, University of Illinois at Urbana-Champaign)

Connor Kapahi (University of Waterloo)

Gautam Kavuri (NIST)

Emilie Kernen (Photonis Netherlands BV)

Rajkumar Kettimuthu (Argonne National Laboratory)

Igor Khramtsov (Moscow Institute of Physics and Technology)

Mijin Kim (KeyW Corporation)

Chul Soo Kim (U.S. Naval Research Lab)

Youngshin Kim (Stony Brook University)

Jung-Hyun Kim (Wooriro)

Robert Kirkwood (National Physical Laboratory)

L Kling (University of Bristol)

Manny Knill (National Institute of Standards and Technology)

Emanuel Knill (National Institute of Standards and Tech)

Felix Koberling (PicoQuant GmbH)

Jan Kodet (Czech Technical University in Prague)

Siddarth Koduru Joshi (Institute for Quantum Optics and Quantum Information (IQOQI))

Sami Koho (Istituto Italiano di Tecnologia)

Oskar Kohout (IQOQI Vienna)

Alexander Kolar (Northwestern University)

Sylwia Kolenderska (The Dodd-Walls Centre for Photonic and Quantum Technologies, The Department of Physics, The University of Auckland)

Piotr Kolenderski (Nicolaus Copernicus University)

Steven Kolthammer (Imperial College)

Alex Komjati (Consultant)

Ilya Kondratjev (Quantum Technologies Center, Lomonosov Moscow State University)

Frank Koppens (ICFO)

Alexander Korneev (Moscow State Pedagogical University)

Yuliya Korneeva (Moscow State Pedagogical University)
Boris Korzh (JPL)
Alexander Koujelev (Canadian Space Agency)
Alexander Kozen (U.S. Naval Research Lab)
Benedikt Krämer (PicoQuant GmbH)
Olivier Krebs (CNRS C2N)
Leonid Krivitskiy (A*STAR Institute of Materials Research and Engineering)
Andrey Krysa (Sheffield University)
Alexander Kubanek (Institut fu¨r Quantenoptik and IQST, Universita¨t Ulm)
Toomas Kübarsepp (AS Metrosert)
Stefan Kück (Physikalisch-Technische Bundesanstalt)
Maarten Kuijk (Vrije Universiteit Brussel)
Sergei Kulik (Quantum Technology Center & Faculty of Physics, M.V. Lomonosov Moscow State University)
Dmytro Kundys (Heriot-Watt University)
Katanya Kuntz (University of Waterloo)
Paulina S. Kuo (NIST)
Timm Kupko (TU Berlin)
Christian Kurtsiefer (Centre for Quantum Technologies)
Astghik Kuzanyan (Institute for Physical Research NAS of Armenia)
Armen Kuzanyan (Institute for Physical Research NAS of Armenia)
Paul G. Kwiat (Department of Physics, University of Illinois at Urbana-Champaign)
Paul Kwiat (University of Illinois at Urbana-Champaign)
Michele Lacerenza (Politecnico di Milano (Dip. Fisica))
Dario Lago-Rivera (ICFO)
Elizabeth Laier-English (National Physical Laboratory)
Kaisa Laiho (TU Berlin)
Loïc Lanco (Université Paris Diderot)
Loïc Lanco (C2N)
Radek Lapkiewicz (University of Warsaw, Faculty of Physics)
Jean Lapointe (National Research Council of Canada)
Jan-Ake Larsson (Linköping Universitet)
Robert Lasenby (Stanford University)
Mikolaj Lasota (Nicolaus Copernicus University)
Mikael Lassen (Danmarks Nationale Metrologiinstitut)
Martin Laurenzis (The French-German Research Institute of Saint-Louis (ISL))
Benjamin Lawrie (Oak Ridge National Laboratory)
Paul Lecoq (CERN)
Patrick Ledingham (University of Oxford)
Sang Min Lee (Korea Research Institute of Standards and Science)
Seung-Woo Lee (Korea Institute for Advanced Study)
Eunjoo Lee (Korea Research Institute of Standards and Science (KRISS))
Bumsu Lee (U.S. Naval Research Lab)
Hee Jung Lee (Korea Research Institute of Standards and Science)
Dong-Hoon Lee (KRISS)
Pascal Lefebvre (University of Calgary)
John Lehman (National Institute of Standards and Technology)
Dietrich Leibfried (NIST)
Chris Leitz (MIT Lincoln Laboratory)
Aristide Lemaitre (CNRS C2N)
Aristide Lemaître (C2N, Center of Nanosciences and Nanotechnology, Universite Paris-Saclay)
Nicolo Leone (University of Trento)
Victor Leong (A*STAR Institute of Materials Research and Engineering)
Roberto Leoni (Istituto di Fotonica e Nanotecnologie-CNR)
Jérôme Le Perchec (CEA-Leti)
Zachary Levine (National Institute of Standards and Technology)
Maciej Lewenstein (ICFO – The Institute of Photonic Sciences)
Hao Li (Shanghai Institute of Microsystem and Information Technology, Chinese Academy of Sciences (SIMIT, CAS))
Yu-Huai Li (University of Science and Technology of China)
Zheng-Ping Li (University of Science and Technology of China)
Minghan Li (University of Science and Technology of China)
Zheng-Da Li (University of Science and Technology of China)
Longyue Liang (Jinan Institue of Quantum Technology)
Junsheng Liang (Shandong Institute of Quantum Science and Technology Co., Ltd.)
Yan Liang (University of Shanghai for Science and Technology)
Abigail Licht (MIT Lincoln Laboratory)
Hee-Jin Lim (Korea Research Institute of Standards and Science (KRISS))
David Lindell (Stanford University)
Tobias Lindstrom (National Physical Laboratory)
Alexander Ling (Centre for Quantum Technologies)
Adriana Lita (National Institute of Standards and Technology)
Wei Liu (University of Science and Technology of China)

Yang Liu (University of Science and Technology of China)

Bo Liu (Institute for Quantum Optics and Quantum Information)

Wenzhao Liu (University of Science and Technology of China)

Li-Zheng Liu (University of Science and Technology of China)

Shikang Liu (East China Normal University)

Daniel Llewellyn (University of Bristol)

José M. Llorens (IMN-CNM, Instituto de Micro y Nanotecnologia, CSIC)

T Loke (University of Western Australia)

Pietro Lombardi (Istituto Nazionale di Ottica)

Marco Antonio López Ordonez (Physikalisch-Technische Bundesanstalt)

Juan Carlos Loredo (C2N, Center of Nanosciences and Nanotechnology, Universite Paris-Saclay,)

Johannes W. N. Los (Single Quantum B.V.)

Elena Losero (INRIM)

Chao-Yang Lu (University of Science and Technology of China)

Colin P. Lualdi (Department of Physics, University of Illinois at Urbana-Champaign)

Boaz Lubotzky (Hebrew University of Jerusalem)

Marco Lucamarini (Toshiba Research Europe Ltd)

Marco Toliman Lucchini (Princeton University)

Jasleen Lugani (University of Oxford)

Tobias Lühmann (Leipzig University)

Daniel J. Lum (National Institute of Standards and Technology)

Rudi Lussana (Politecnico di Milno)

Thomas Lutz (ETH)

Ashley Lyons (University of Glasgow)

Lijun Ma (National Institute of Standards and Technology)

Xiongfeng Ma (Tsinghua University)

Jiaju Ma (Gigajot Technology)

Qiang Ma (East China Normal University)

Aurora Maccarone (Heriot-Watt University)

Eugene Machusky (National Technical University of Ukraine "Kyiv Polytechnic Institute")

Jean-Philippe MacLean (University of Waterloo)

Omar Magana-Loaiza (Louisiana State University)

Sahand Mahmoodian (University Hannover)

Ilse Maillette (C2N)

Kyle D Major (Imperial College London)

Kyle D. Major (Imperial College London)

Somak Majumder (Los Alamos National Laboratory)

Mehul Malik (IQOQI Vienna & Institute of Photonic and Quantum Sciences (IPaQS), Heriot-Watt University)

Bastien Mamdy (STM)

Farshid Manoocheri (Aalto-korkeakoulusäätiö sr)

Jean-Robert Manouvrier (STMicroelectronics)

Nadezhda Manova (Moscow State Pedagogical University)

Ya-Li Mao (Center for Quantum Computing, Peng Cheng Laboratory)

Davide G. Marangon (Toshiba Cambridge Research Laboratories)

Giovanni Margutti (LFoundry)

Chiara Marletto (University of Oxford; Fondazione ISI; National University of Singapore)

G Marshall (University of Bristol)

Francesco Martini (Istituto di Fotonica e Nanotecnologie-CNR)

Claire Marvinney (Oak Ridge National Laboratory)

Saleh Masoodian (Gigajot Technology)

Nicola Massari (Fondazione Bruno Kessler)

Lydie Mathieu (CEA-Leti)

Jonathan Matthews (University of Bristol)

Francesco Mattioli (Istituto di Fotonica e Nanotecnologie-CNR)

Francesco Mattioli Della Rocca (The University of Edinburgh)

Michael D. Mazurek (National Institute of Standards and Technology)

Luca Mazzarella (University of Strathclyde)

Alberto Mazzi (FBK)

Aongus McCarthy (Heriot-Watt University)

Adam N. McCaughan (NIST)

Dara McCutcheon (University of Bristol)

Kenneth McEwan (The Defence Science and Technology Laboratory (Dstl))

Alex McIntosh (MIT Lincoln Laboratory)

Joe McKee (National Research Council of Canada)

Stephen McLaughlin (Heriot-Watt University)

Alice Meda (INRIM)

Kristina Meier (University of Illinois at Urbana-Champaign)

Jan Meijer (Leipzig University)

Paolo Mennea (University of Southampton)

Evan Meyer-Scott (University of Paderborn)

Peter Michler (Institut für Halbleiteroptik und Funktionelle Grenzflächen, University of Stuttgart)

Alan Migdall (National Institute of Standards and Technology)

Mikhail Mikhailov (B. Verkin Institute for Low Temp. Physics & Engineering of the National Academy of Sciences of Ukraine)

Alexander Mikhaylov (JILA, University of Colorado)

Shigehito Miki (National Institute of Information and Communications Technology)
Aaron Miller (Quantum Opus LLC)
Clement Millet (CNRS C2N)
Perola Milman (Université de Paris)
Mariella Minder (University of Cambridge)
Richard P. Mirin (National Institute of Standards and Technology)
Sergei Mironov (Institute for Nuclear Research of the Russian Academy of Sciences)
Marta Misiaszek (Nicolaus Copernicus University)
Morgan Mitchell (ICFO-Institut de Ciencies Fotoniques)
Valentin Mitev (CSEM)
Kensuke Miyajima (Tokyo University of Science)
Shigeyuki Miyajima (National Institute of Information and Communications Technology)
Jerome Mlack (U.S. Naval Research Lab)
Khaled Mnaymneh (National Research Council of Canada)
Manuel Moreno Garcia (FBK)
Ekaterina Moreva (Istituto Nazionale di Ricerca Metrologica (INRiM))
Samuel Morley-Short (University of Bristol)
Dmitry Morozov (University of Glasgow)
Tina Müller (Toshiba Research Europe Ltd)
Markus Müller (Joint Quantum Institute)
Joseph Munns (Imperial College London)
Alberto Mura (INRIM)
Gabriella Musarra (University of Glasgow)
Sae Woo Nam (National Institute of Standards and Technology)
Mehdi Namazi (Stony Brook University)
Jakub Nedbal (King's College London)
Sebastian Philipp Neumann (Institute for Quantum Optics and Quantum Information)
Jean-Alain Nicolas (CEA-Leti)
Vahan Nikoghosyan (Institute for Physical Research NAS of Armenia)
Niko Nikolay (Humboldt Universität zu Berlin)
David Northeast (National Research Council of Canada)
Joshua Nunn (University of Bath)
Salahuddin Nur (Imperial College London)
Daniel Oblak (University of Calgary)
J O'Brien (University of Bristol)
S O'Gara (University of Bristol)
Stefano Olivares (University of Milan - Department of Physics)
Paolo Olivero (University of Torino)
Segolene Olivier (CEA-LETI)
Hélène Ollivier (C2N, Center of Nanosciences and Nanotechnology, Universite Paris-Saclay)
Helene Ollivier (CNRS C2N)
Caner Onal (Waymo LLC)
Galen O'Neil (NIST)
Paolo Organtini (LFoundry)
Dmitry Orlov (Photonis Netherlands BV)
Roberto Osellame (National Research Council (CNR))
Matthew O'Toole (Carnegie Mellon University)
Rupert Oulton (Blackett Laboratory, Department of Physics, Imperial College London)
Yassine Oussaiti (STMicroelectronics)
Anna Ovvyan (Center for Nanotechnology, University of Münster)
Leif Katsuo Oxenløwe (CoE SPOC, Dep. Photonics Eng., Technical University of Denmark)
Stefano Paesani (University of Bristol)
Marco Paganoni (University of Milano-Bicocca)
Mano Rahul K Pakalapati (Florida Institute of Technology)
Mano Varun K Pakalapati (Florida Institute of Technology)
Marco Pala (Centre de Nanosciences et de Nanotechnologies)
Jian-Wei Pan (University of Science and Technology of China)
Chengda Pan (East China Normal University)
Lucio Pancheri (University of Trento)
Pietro Panizza (Scientific Institute (IRCCS) Ospedale S. Raffaele-Breast Imaging Unit)
Taofiq Paraiso (Toshiba Research Europe Limited)
Matteo G. A. Paris (University of Milan - Department of Physics)
Matteo Paris (University of Milan)
Hee Su Park (Korea Research Institute of Standards and Science)
Seongchong Park (Korea Research Institute of Standards and Science (KRISS))
Chan-Yong Park (WOORIRO)
Chulwoo Park (ID Quantique)
Jae Park (National Institute of Standards and Technology)
Luca Parmesan (FBK)
Kristen M. Parzuchowski (JILA, University of Colorado)
Raj B. Patel (University of Oxford)
Giovanni Paternoster (FBK)
Anna Paterova (Institute of Materials Research and Engineering, A*STAR)
Lorenzo Pavesi (University of Trento)
Emma Pearce (Blackett Laboratory, Department of Physics, Imperial College London)

Francesco Pellegatta (Istituto di Fotonica e Nanotecnologie - Consiglio Nazionale delle Ricerche (IFN-CNR))
Cheng-Zhi Peng (University of Science and Technology of China)
Franck Pereira Dos Santos (LNE-SYRTE, Observatoire de Paris)
Matteo Perenzoni (FBK)
Nicolas Perlot (Fraunhofer Heinrich-Hertz Institute)
Wolfram H. P. Pernice (Institute of Physics and Center for Nanotechnology, University of Mu¨nster)
Matthieu Perrenoud (University of Geneva)
Mathieu Perriollat (CEA-LETI)
Salvatore Pes (CEA-Leti)
Sébastien Pezzagna (Leipzig University)
David S. Phillips (University of Oxford)
Fabrizio Piacentini (Istituto Nazionale di Ricerca Metrologica (INRiM))
Alexander Pickston (Heriot-Watt University)
Federico Picollo (University of Torino)
Antonio Pifferi (Politecnico di Milano, Dipartimento di Fisica)
Mirko Pittaluga (Toshiba CRL)
Hou Shun Poh (Centre for Quantum Technologies)
Emanuele Polino (Dipartimento di Fisica, Sapienza Universitá di Roma)
Alberto Politi (Department of Physics and Astronomy, University of Southampton)
Sergey Polyakov (NIST)
Margaret Polyakova (National Research University Higher School of Economics)
Philip Poole (National Research Council of Canada)
Santeri Porrasmaa (Aalto University)
Geiland Porrovecchio (Czech Metrology Institute)
Simone L. Portalupi (Institut für Halbleiteroptik und Funktionelle Grenzflächen, University of Stuttgart)
Adarsh Prasad (Vienna University of Technology)
Enrico Prati (Consiglio Nazionale delle Ricerche)
Ivan Prochazka (Czech Technical University in Prague)
Massimiliano Proietti (Heriot-Watt University)
Valerio Pruneri (ICFO – The Institute of Photonic Sciences)
Geoff Pryde (Griffith University)
Dmitry Pushin (University of Waterloo)
X Qiang (National Innovation Institute of Defense Technology)
Victor Quiring (Paderborn University)
Jelena Rakonjac (ICFO)
T Ralph (The University of Queensland)
Tim Rambo (Quantum Opus LLC)
Edward Ramirez (Jet Propulsion Laboratory)
Ronen Rapaport (Hebrew University of Jerusalem)
John Rarity (University of Bristol)
Markus Rau (Ludwig Maximilian University of Munich)
Sebastian Raupach (PTB)
Arno Rauschenbeutel (HU Berlin)
Arnault Raymond (Université de Paris)
Enrico Rebufello (Politecnico di Torino; Istituto Nazionale di Ricerca Metrologica (INRiM))
Ivan Rech (Politecnico di Milano)
Dileep Reddy (National Institute of Standards and Technology)
Stephan Reitzenstein (TU Berlin)
Jelmer Renema (University of Twente)
Sebastien Renet (CEA-Leti)
Marco Renna (Politecnico di Milano (DEIB))
Kevin Resch (University of Waterloo)
Alessandro Restelli (Joint Quantum Institute; University of Maryland and the National Institute of Standards and Technology)
Bogdan Reznychenko (Institut Neel)
Raouia Rhazi (CEA)
Raimund Ricken (Paderborn University)
Lucas Rickert (TU Berlin)
Denis Rideau (STM)
Samuel Rind (Vienna University of Technology)
David Ritchie (University of Cambridge)
George Roberts (Toshiba)
Beatrice Rodiek (Physikalisch-Technische Bundesanstalt)
Jasper Rödiger (Fraunhofer)
Sven Rodt (TU Berlin)
Thomas Roger (Toshiba Research Europe Limited)
Sumeet Rohilla (PicoQuant GmbH)
Tino Röhlicke (PicoQuant GmbH)
Youying Rong (East China Normal University)
Bogdan Rosinski (Vermon SA)
Maarten Rosmeulen (imec)
Alessandro Rossetta (Istituto Italiano di Tecnologia)
Jean-Pierre Rostaing (CEA-Leti)
Johan Rothman (CEA-Leti)
Karsten Rottwitt (Technical University of Denmark)
Alessandro Ruggeri (Micro Photon Devices Srl)
Ivano Ruo-Berchera (Istituto Nazionale di Ricerca Metrologica)
Konstantin Rusakov (University of Warsaw, Faculty of Physics)
Jennifer Ruskowski (Fraunhofer Institute for Microelectronic Circuits and Systems IMS)
Kevin Ryu (MIT Lincoln Laboratory)
Frederico Sabattoli (Università degli Studi di Pavia)

Isabelle Sagnes (C2N, Center of Nanosciences and Nanotechnology, Universite Paris-Saclay)
Steven Sagona-Stophel (Stony Brook University)
Döndü Sahin (University of Bristol)
Matteo Salomoni (University of Milano-Bicocca, CERN)
Barry Sanders (University of Calgary)
Raffaele Santagati (University of Bristol)
R Santagati (University of Bristol)
Jean-Louis Santailler (CEA-Leti)
Mirko Sanzaro (Toshiba Research Europe Limited)
Dusan Sarenac (University of Waterloo)
Dylan Saunders (University of Oxford)
David Savéry (Supersonic Imagine, S.A.)
Mikhail Saygin (Quantum Technology Center & Faculty of Physics, M.V. Lomonosov Moscow State University)
J. Schall (Institute of Solid-State Physics, Technische Universität Berlin)
Thomas Scheidl (Institute for Quantum Optics and Quantum Information)
Andreas Schell (Physikalisch Technische Bundesanstalt (PTB), Institut für Festkörperphysik, Leibniz Universität Hannover)
Hansjörg Scherer (Physikalisch-Technische Bundesanstalt)
Stephane Schertzer (French-German Research Institute of Saint-Louis)
Alexander Schlehahn (TU Berlin)
Marco Schmidt (TU Berlin)
Peter Schnauber (Institut für Festkörperphysik, Technische Universität Berlin)
Philipp Schneeweiss (HU Berlin)
Christian Schneider (Julius-Maximilians-Universität Würzburg)
Christian Schneider (University of California, Los Angeles)
Kerstin Schneider-Hornstein (Institute of Electrodynamics, Microwave and Circuit Engineering, TU Wien)
Ross C. Schofield (Imperial College London)
Christian Schönenberger (University of Basel)
Felicien Schopfer (Laboratoire national de métrologie et d'essais)
Carsten Schuck (WWU Münster)
Daniel Schuette (MIT Lincoln Laboratory)
Jan-Hindrik Schulze (TU Berlin)
Sacha Schwarz (University of Waterloo)
Corrado Sciancalepore (CEA-Leti)
Fabio Sciarrino (Sapienza University of Rome)
Alessia Scriminich (University of Padova)
Karolina Sedziak-Kacprowicz (Nicolaus Copernicus University)
Hiroya Seki (The University of Electro-Communications)
Santiago Sempere-Llagostena (Imperial College London)
Pascale Senellart (Center of Nanosciences and Nanotechnology - CNRS, Univ. Paris-Saclay)
Alessandro Seri (ICFO)
Vincenzo Sesta (Politecnico di Milano- Dip. di Elettronica, Informazione e Bioingegneria)
Fabio Severini (Politecnico di Milano)
Yash Shah (Glasgow University)
Jeffrey M. Shainline (NIST)
Lynden K. Shalm (NIST)
Matthew Shaw (JPL)
Si Shen (East China Normal University)
Yicheng Shi (Center for Quantum Technologies)
Yanli Shi (yunnan university)
Andrew Shields (Toshiba Research Europe Ltd)
Ryosuke Shimizu (The University of Electro-Communications)
Takahiro Shinada (Tohoku University)
Yichen Shuai (Joint Quantum Institute)
Christine Silberhorn (Paderborn University)
Josh Silverstone (University of Bristol)
Alastair Sinclair (National Physical Laboratory)
A. Singh (National Institute of Standards and Technology, Gaithersburg)
John Sipe (University of Toronto)
K. Sirinvasan (National Institute of Standards and Technology, Gaithersburg)
Joanna Skiba-Szymanska (Toshiba Research Europe Ltd)
P Skrzypczyk (University of Bristol)
Natko Skukan (Ruđer Boskovic Institute)
Benjamin Slater (University of Bristol)
Oliver Slattery (National Institute of Standards and Technology)
Eli Slenders (Istituto Italiano di Tecnologia)
Daniel Slichter (NIST)
Karolina Słowik (Institute of Physics, Nicolaus Copernicus University in Toruń)
Marek Smid (Czech Metrology Instittue)
Marek Smid (Ceský Metrologický Institut)
Eugeny Smirnov (Moscow State Pedagogical University)
Devin Hugh Smith (University of Southampton)
Peter G.R. Smith (University of Southampton)
Philip Soan (The Defence Science and Technology Laboratory (Dstl))
Glenn Solomon (Joint Quantum Institute)

Niccolo Somaschi (Quandela, SAS)
Kwang Yong Song (Chung-Ang University)
J.D. Song (Center for Opto-Electronic Convergence Systems, KIST)
Anders Sørensen (University of Copenhagen)
Andrea Sosso (Istituto Nazionale di Ricerca Metrologica)
Nicoló Spagnolo (Dipartimento di Fisica, Sapienza Universitá di Roma)
Julia Spina (University of Illinois at Urbana-Champaign)
Jolene Splett (National Institute of Standards and Technology)
Hélène Spourtouche (Supersonic Imagine, S.A.)
Kartik Srinivasan (NIST/University of Maryland)
Andrea Stanco (University of Padova)
Dakota Starkey (Gigajot Technology)
Robert Starkwood (National Physical Laboratory)
Ilya Starshynov (University of Glasgow)
André Stefanov (Institute of Applied Physics, University of Bern)
Robin Stegmüller (WWU Münster)
Bernhard Steindl (Institute of Electrodynamics, Microwave and Circuit Engineering, TU Wien)
Fabian Steinlechner (IQOQI Vienna & Fraunhofer Institute for Applied Optics and Precision Engineering IOF Jena)
Martin J. Stevens (National Institute of Standards and Technology)
Mark Stevenson (Toshiba Research Europe Ltd)
Ivo Straka (Palacký University)
Stanislav Straupe (Quantum Technology Center & Faculty of Physics, M.V. Lomonosov Moscow State University)
André Strittmatter (Technische Universität Berlin, Otto-von-Guericke Universität Magdeburg)
Stephen Sturzenbaum (King's College London)
Ersoy Subasi (Florida Institute of Technology)
Martin Suchara (Argonne National Laboratory)
Holger Suchomel (University of Würzburg)
Klaus Suhling (King's College London)
Qi-Chao Sun (University of Science and Technology of China)
Vyshnavi Suntharalingam (MIT Lincoln Laboratory)
Andreas Süss (OmniVision Technologies)
Jakub Szlachetka (Institute of Physics, Nicolaus Copernicus University in Toruń)
Jerzy Szuniewicz (University of Warsaw, Faculty of Physics)
Dmitry Tabakaev (Group of applied physics, University of Geneva)
Julián Tachella (Heriot-Watt University)
Alex N. Tait (NIST)
Takahiro Takumi (The University of Electro-Communications)
Jian-Shun Tang (University of Science and Technology of China)
Xiao Tang (National Institute of Standards and Technology)
Takashi Tanii (Waseda University)
Paola Taroni (Politecnico di Milano- Dip. di Fisica)
Joel Tasker (University of Bristol)
Gioan Tatsi (University of Strathclyde)
Gregor Taylor (University of Glasgow)
Hamid Tebyanian (University of Padova)
Hirotaka Terai (National Institute of Information and Communications Technology)
Roland Terborg (ICFO – The Institute of Photonic Sciences)
Robert Thew (Group of applied physics, University of Geneva)
Sarah Thomas (Imperial College London C2N)
Mark Thompson (University of Bristol)
Johannes Tiedau (University of Paderborn)
Max Tillmann (PicoQuant GmbH)
Simone Tisa (Micro Photon Devices Srl)
Nora Tischler (Griffith University)
Wolfgang Tittel (Delft University of Technology)
Rachael Tobin (Heriot-Watt University)
Susanna Todaro (NIST)
Marco Tomasin (University of Padova)
Costanza Toninelli (Istituto Nazionale di Ottica)
Nicolas Torcheboeuf (CSEM)
Alessandro Torricelli (Politecnico di Milano, Dipartimento di Fisica)
Giorgio Tortarolo (Istituto Italiano di Tecnologia)
Alberto Tosi (Politecnico di Milano)
Paolo Traina (Istituto Nazionale di Ricerca Metrologica (INRiM))
Alex Turpin (University of Glasgow)
Yuta Uchihori (Tokyo University of Science)
Manuel Unternährer (Institute of Applied Physics, University of Bern)
Rupert Ursin (IQOQI Vienna)
Lev Vaidman (Tel Aviv University)
Mauro Valeri (Dipartimento di Fisica, Sapienza Universitá di Roma)
Giuseppe Vallone (University of Padova)
Rene van der Molen (Single Quantum)
Joscelyn van der Veen (University of Waterloo)
Chris Van Hoof (imec)
Edward Van Sieleghem (imec)

Ken Van Tillburg (NYU and Institute for Advanced Studies)

Frédérique Vanholsbeeck (The Dodd-Walls Centre for Photonic and Quantum Technologies, The Department of Physics, The University of Auckland)

Anthony Vaquero-Stainer (University of York)

Igor Vayshenker (National Institute of Standards and Technology)

Francesco Vedovato (University of Padova)

Vlatko Vedral (University of Oxford; Fondazione ISI; National University of Singapore)

Andreas Velten (University of Wisconsin-Madison)

Elena Venturini (Scientific Institute (IRCCS) Ospedale S. Raffaele-Breast Imaging Unit)

Simon Verghese (Waymo LLC)

Varun B. Verma (National Institute of Standards and Technology)

Marijn A. M. Versteegh (Department of Applied Physics, Royal Institute of Technology (KTH), Stockholm)

Giuseppe Vicidomini (Istituto Italiano di Tecnologia)

Michelle Victora (University of Illinois at Urbana-Champaign)

Niko Viggianiello (University of Rome, La Sapienza)

Caterina Vigliar (University of Bristol)

Federica Villa (Politecnico di Milano)

Paolo Villoresi (University of Padova)

Salvatore Virzì (Università di Torino, Istituto Nazionale di Ricerca Metrologica (INRiM))

Denis Vodolazov (Institute for Physics for Microstructures, Russian Academy of Sciences)

Jürgen Volz (HU Berlin)

Martin von. Helversen (TU Berlin)

Andrey Vyshnevyy (Moscow Institute of Physics and Technology)

Michael Wahl (PicoQuant GmbH)

Ian A. Walmsley (University of Oxford)

Nicolai Walter (WWU Münster)

Yi-Tao Wang (University of Science and Technology of China)

Zhen Wang (Shanghai Institute of Microsystem and Information Technology, Chinese Academy of Sciences)

Bin Wang (University of Science and Technology of China)

Bing Wang (University of Science and Technology of China)

Hui Wang (University of Science and Technology of China)

Jack Wang (National Institute of Standards and Technology)

Jianwei Wang (Peking University)

Eugene Wang (Argonne National Laboratory)

J Wang (University of Bristol)

J Wang (University of Western Australia)

Frances Wang (University of Illinois at Urbana-Champaign)

Richard Warburton (University of Basel)

Martin B. Ward (Toshiba Research Europe Ltd)

Michael Wayne (Joint Quantum Institute / National Institute of Standards and Technology)

John Weber (National Research Council of Canada)

Helene Wehbe Alause (STM)

Kejin Wei (USTC&GXU)

Gregor Weihs (University of Innsbruck)

Stephen Wein (IQST and department of Physics and Astronomy)

Harald Weinfurter (Ludwig Maximilian University of Munich)

Sören Wengerowsky (Institute for Quantum Optics and Quantum Information Vienna)

Doreen Wernicke (Entropy GmbH)

Gordon Wetzstein (Stanford University)

Andrew White (The University of Queensland)

C Wilkes (University of Bristol)

Robin Williams (National Reseach Council Canada)

Andrew Wilson (NIST)

David Wineland (NIST)

Martin Wolff (WWU Münster)

Emma Wollman (JPL)

Sabine Wollmann (University of Bristol)

Adrian Wonfor (University of Cambridge)

E Wu (East China Normal University)

Botao Wu (East China Normal University)

Xiaoliang Wu (Illinois Institute of Technology)

Zi-Heng Xiang (University of Cambridge/Toshiba Cambridge Research Laboratory)

Xiuping Xie (Jinan Institue of Quantum Technology)

Feihu Xu (University of Science and Technology of China)

Ruoxuan Xu (University of Waterloo)

André Xuereb (University of Malta)

Masahiro Yabuno (National Institute of Information and Communications Technology)

Michael Yakes (U.S. Naval Research Lab)

Hongzhi Yang (Institute of Materials Research and Engineering, A*STAR)

Seung-Chul Yang (Wooriro)

Quan Yao (Jinan institute of quantum technology)

Xu-Fei Yin (University of Science and Technology of China)

Lixing You (Shanghai Institute of Microsystem and Information Technology, Chinese Academy of Sciences (SIMIT, CAS))

Chenglong You (Louisiana State University)

Jae Hyeong Youn (Chung-Ang University)

Richard Younger (MIT Lincoln Laboratory)

Chao Yu (University of Science and Technology of China)

Zhiliang Yuan (Toshiba Reseach Europe Limited)

Maxim Zalalutdinov (US Naval Research Lab)

Franco Zappa (Politecnico di Milano (DEIB))

Majid Zarghami (FBK)

Hugo Zbinden (University of Geneva)

Anton Zeilinger (Institute for Quantum Optics and Quantum Information, AAS)

Heping Zeng (University of Shanghai for Science and Technology, East China Normal University)

Weijun Zhang (Shanghai Institute of Microsystem and Information Technology, Chinese Academy of Sciences (SIMIT, CAS))

Qiang Zhang (University of Science and Technology of China

Jinan Institue of Quantum Technology)"

Jun Zhang (University of Science and Technology of China)

Jun Zhang (yunnan university)

Xingjian Zhang (Tsinghua University)

Rui Zhang (University of Science and Technology of China)

Jun Zhang (University of Calgary)

Yanbao Zhang (NTT)

Si-Ran Zhao (University of Science and Technology of China)

Qi Zhao (Tsinghua University)

Ming-Yang Zheng (Jinan Institue of Quantum Technology)

Tian Zhong (University of Chicago)

X Zhou (Sun Yat-sen University)

Hongxia Zhu (yunnan university)

Julien R. Zichi (Department of Applied Physics, Royal Institute of Technology (KTH), Stockholm)

Antonin Zimmer (STM)

Horst Zimmermann (Institute of Electrodynamics, Microwave and Circuit Engineering, TU Wien)

Pamela Zolda (European Institute for Biomedical Imaging Research)

Nicola Zorzi (FBK)

Val Zwiller (KTH Royal Institute of Technology)

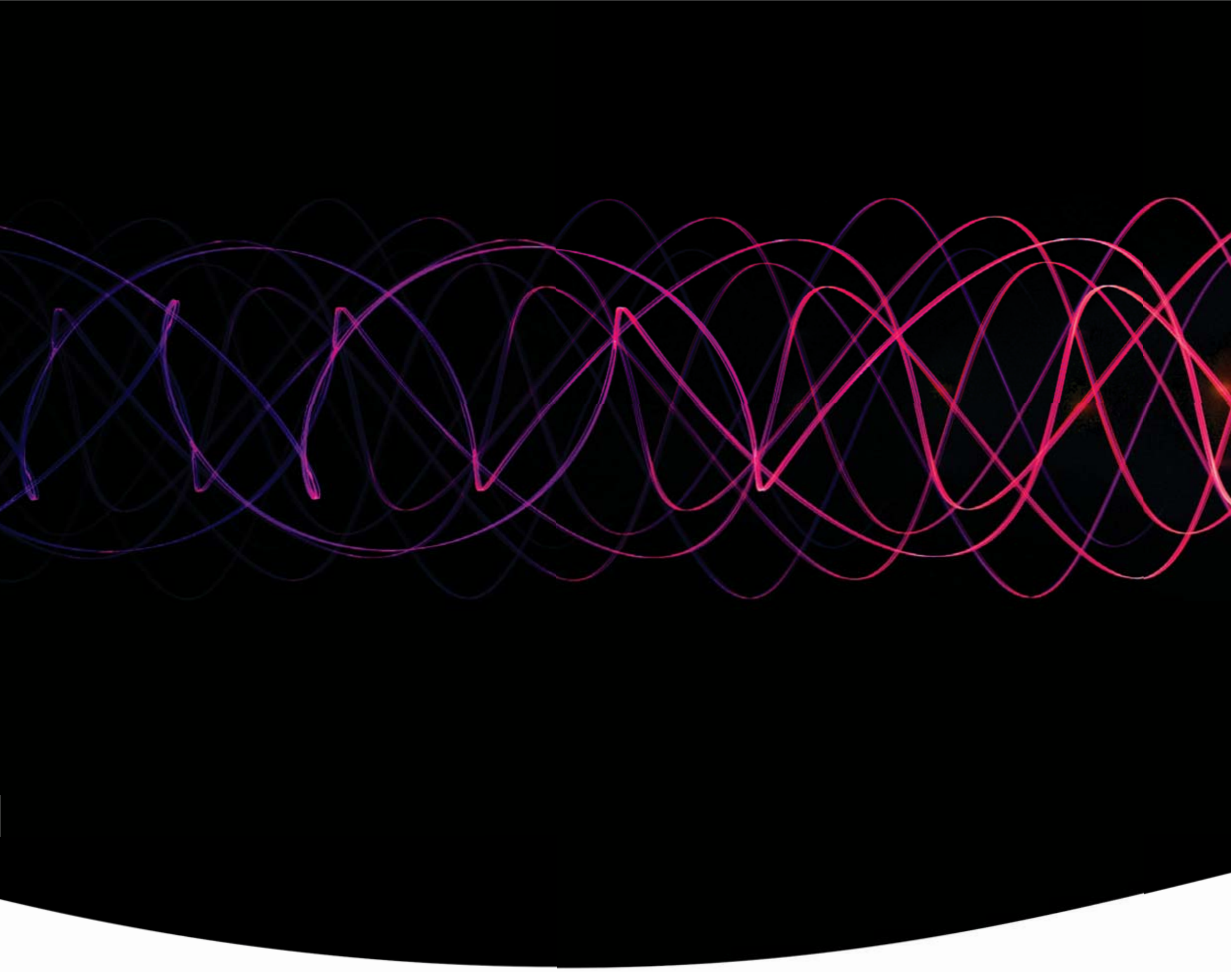

Single Photon Workshop 2019 is the ninth installment in a series of workshops on **SINGLE-PHOTON TECHNOLOGIES AND APPLICATIONS.** SPW 2019 is intended to bring together a broad range of people with interests in single-photon sources, single-photon detectors, photon entanglement, and their use in scientific and industrial applications. It is an exciting opportunity for those interested in these technologies to learn about the state of the art and to foster continuing partnerships with others seeking to advance the capabilities of such technologies.